

Vol I

NASA-CR-61180

# VOLUME I - MISSION & SYSTEM STUDY

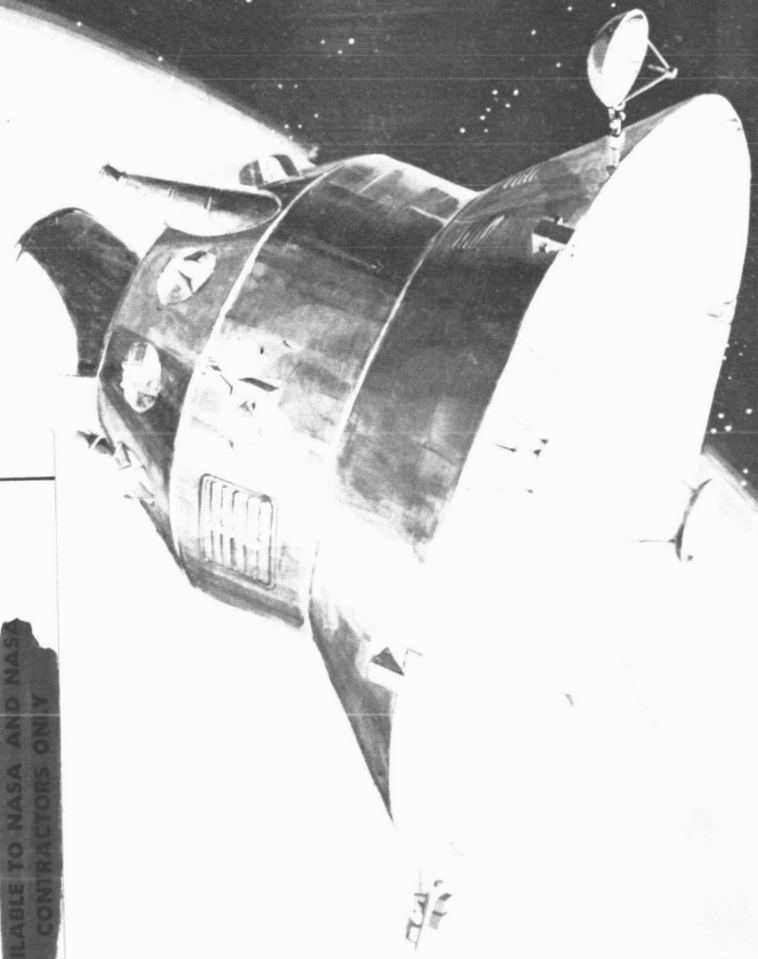
AUGUST 1967

PREPARED UNDER  
NASA AUBURN ALABAMA  
SUMMER FACULTY FELLOWSHIP PROGRAM  
IN ENGINEERING SYSTEMS DESIGN

NASA CONTRACT NSR 01-003-025

REPORT NO. CR-61180

# J O V E



FF No. 602(B)

N68-10887  
(ACCESSION NUMBER)

399  
(PAGES)

cc# 61180  
(NASA CR OR TMX OR AD NUMBER)

1  
(THRU)

31  
(CODE)

(CATEGORY)

AVAILABLE TO NASA AND NASA CONTRACTORS ONLY

SCHOOL OF ENGINEERING  
AUBURN UNIVERSITY  
AUBURN, ALABAMA

# JOVE

## JUPITER ORBITING VEHICLE FOR EXPLORATION

VOLUME I

MISSION and SYSTEM STUDY

prepared under

CONTRACT NSR 01-003-025  
UNIVERSITY AFFAIRS OFFICE  
HEADQUARTERS

NATIONAL AERONAUTICS AND SPACE ADMINISTRATION

with the cooperation of

THE

ADVANCED SYSTEMS OFFICE  
GEORGE C. MARSHALL SPACE FLIGHT CENTER  
NATIONAL AERONAUTICS AND SPACE ADMINISTRATION

by

AUBURN-ALABAMA ENGINEERING SYSTEMS DESIGN  
SUMMER FACULTY FELLOWS

AUGUST, 1967

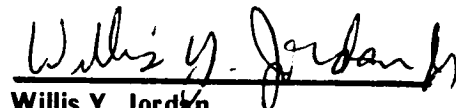
APPROVED:



Reginald L. Vachon, Ph.D.  
Alumni Professor, Auburn Univ.  
Co-Director

Gordon W. Breland, Ph.D.  
Asst. Professor, Auburn Univ.  
Associate Director

Ross M. McDonald, Ph.D.  
Asst. Professor, University of Tulsa  
Associate Director



Willis Y. Jordan  
MSFC Advanced Systems Office  
Co-Director

Alfred M. Leppert  
Asst. Professor, Auburn Univ.  
Associate Director

# PREFACE

## Objective

Systems engineering or systems engineering design has become an accepted term to describe the multidisciplinary or interdisciplinary character of the "systematic design" of any large engineering system. It emphasizes and attempts to systematize, through the availability of modern techniques, the design of modern, complex, multidisciplinary engineering systems. The term seems to have originated in the aerospace field where the complexity of modern aerospace systems demanded a systematically controlled approach to design to insure that all factors of all subsystems, representing many disciplines, were carefully integrated into the final system. The importance of the multidisciplinary systems approach has been recognized by the National Aeronautics and Space Administration to the extent that they now support three engineering systems design summer programs for engineering faculty fellows.

This report summarizes the results of one of these programs. This study was conducted by 19 faculty members, representing some 14 engineering colleges throughout the United States. The program was conducted by Auburn University and University of Alabama at the Marshall Space Flight Center in Huntsville, Alabama. The group received a great deal of technical assistance from the Marshall Space Flight Center and from the many contractors that assist the Center. The technical data contained in this report, however, do not reflect the views or policy of the George C. Marshall Space Flight Center, nor those of any other government agency or private corporation.

The Acknowledgments section lists individuals and companies to whom we are especially indebted.

The University Affairs Office, National Aeronautics and Space Administration, Headquarters, Washington, D. C., funded the project with the primary objective of allowing the participants to obtain actual design experience as members of a multidisciplinary design team. The engineering educational world is indebted to NASA for this farsighted assistance to engineering educational programs of this country.

## Organization

Very early in the program, the participants were briefed on the main objectives, both technical and educational. They selected an interplanetary orbiting vehicle as the primary design objective, then organized themselves into groups and assigned tasks, according to the background of each faculty fellow. Originally, there were four groups: Mission Profile, Spacecraft Configuration, Telecommunications, and Experiments. Spacecraft Configuration eventually split itself into several groups because of its size, and the final actual grouping was more like the chapter headings in this report. The participants and their educational backgrounds are listed in the next section.

The program had three phases. The first was an educational one during which time the group organized itself, listened to extensive briefings by the Marshall people and representatives of their associated contractors, and developed background material pertinent to the solution of the problems. This phase covered approximately three weeks.

The next five weeks were spent evaluating alternate solutions to the problems as they developed, effecting trade-offs, and in preliminary design studies and analysis. The last two weeks were occupied with the organization of the material for the oral presentation and for the written material that appears in this report.

The participants of this program sincerely hope that this report of their ten weeks effort at the Marshall Space Flight Center will be of interest and value to the Marshall Space Flight Center and to the space effort of the United States. Any such benefit would be a real bonus since, as has already been pointed out, the primary purpose of the program was to give a group of college professors a feel for, and experience with, systems engineering. Comments, criticisms, suggestions and questions will be answered as promptly as possible if they are directed to the attention of Dr. R. I. Vachon, Alumni Professor of Mechanical Engineering, Auburn University, Auburn, Alabama 36830.

This final report of JOVE (Jupiter Orbiting Vehicle for Exploration) is broken into two volumes for convenience: Volume I, Mission and System Study, and Volume II, Appendixes. It should be understood that both volumes represent an integral part of the results of this program and both must be studied to obtain the full story of the JOVE mission. The format selected by the fellows was to keep the technical description directly related to the mission in Volume I, and to place supporting engineering and scientific data in Volume II.



- |     |   |   |
|-----|---|---|
| 8.  | Robert Grant Golden, Jr.<br>Ass't. Prof. of Engr. Graphics &<br>Design<br>Newark College of Engineering | A. B. , Little Rock College, 1951<br>B.S.M.E. , Newark College of<br>Engineering, 1956<br>A.M. , Seton Hall University, 1961<br>Mission Profile Group Leader                |
| 9.  | John Wesley Herring, Jr.<br>Assoc. Prof. of Elect. Engr.<br>Mississippi State University                | B.S. E. E. , Mississippi State Univ. ,<br>1950<br>M. S. E. E. , Univ. of Arizona, 1960<br>Ph.D. , Univ. of Arizona, 1967<br>Electronics Group Leader                        |
| 10. | Martin Theophilus Jasper<br>Ass't. Prof. of Mech. Engr.<br>Mississippi State University                 | B. S. , Mississippi State Univ. , 1955<br>M. S. , Mississippi State Univ. , 1962<br>Ph. D. , Univ. of Alabama, 1967<br>Spacecraft Configuration Group                       |
| 11. | Murray I. Lieb<br>Instructor of Mathematics<br>Newark College of Engineering                            | B.S. E. E. , Newark College of Engr. ,<br>1961<br>M. S. E. E. , Newark College of Engr. ,<br>1963<br>M. S. (Math), New York University,<br>1965<br>Experiments Group Leader |
| 12. | Philip Arthur Loretan<br>Ass't. Prof. of Nuclear Engr.<br>Iowa State University                         | B.S. , University of Notre Dame, 1961<br>M. S. , Iowa State University, 1963<br>Ph.D. , Iowa State University, 1965<br>Spacecraft Configuration Group                       |
| 13. | Frank Stanley Moore, Jr.<br>Ass't. Prof. Physics<br>Pfeiffer College                                    | B. S. , Hampden Sydney College, 1957<br>M. S. , Univ. of Michigan, 1959<br>Experiments Group Leader   |
| 14. | Jacob Monroe Schmidt<br>Assoc. Prof. Mech. Engr. and<br>Physics<br>Chico State College                  | A. B. Physics, Phillips Univ. , 1932<br>M. S. Physics, Univ. of Oklahoma,<br>1932<br>Ph. D. , Univ. of Southern Calif. , 1944<br>Experiments Group Leader                   |

## LIST OF PARTICIPANTS

- |  |   |
|--|---|
| 1. Fayette Johnson Brown<br>Ass't Prof. of Mech. Engr.<br>Chico State College                      | B. S. , Ohio University, 1952<br>M. S. M. E. , Univ. of Washington, 1956<br><br>Spacecraft Configuration Group  |
| 2. Ward Ervin Bullock<br>Assoc. Prof. in Mech. Engr.<br>State University of New York at<br>Buffalo | M. E. , Univ. of Cincinnati, 1928<br><br>Spacecraft Configuration Group   |
| 3. James J. Carlson<br>Assoc. Prof. of Mech. Engr.<br>University of Nevada                         | B. S. M. E. , Univ. of Nevada, 1955<br>M. S. M. E. , Univ. of California<br>(Berkeley) 1959<br>Engineer, Stanford University, 1965<br><br>Spacecraft Configuration Group  |
| 4. John E. Dimatteo, Sr.<br>Assoc. Prof. of Engr. Graphics<br>Newark College of Engineering        | B. S. M. E. , Cooper Union, 1931<br>M. S. M. E. , Stevens Inst. of<br>Tech. , 1950<br><br>Spacecraft Configuration Group  |
| 5. James Edward Dupree<br>Instructor of Electrical Engr.<br>Auburn University                      | B. E. E. , Auburn University, 1960<br>M. S. E. E. , Auburn University, 1963<br><br>Electronics Group Leader   |
| 6. Donnel Wayne Dutton<br>Prof. of Aerospace Engr.<br>Georgia Institute of Technology              | B. S. M. E. , Univ. of Missouri<br>School of Mines and Metalurgy, 1935<br>M. S. A. E. , Georgia Inst. of Tech. ,<br>1940<br>M. E. (Honorary), Univ. of Missouri<br>at Rolla, 1959<br><br>Spacecraft Configuration Group Leader<br>Project Leader<br>JOVE Editor |
| 7. Norman Jay Gleicher<br>Assistant Professor<br>State Univ. of New York                           | B. E. E. , City College of New York,<br>1962<br>M. E. E. , New York University, 1964<br><br>Electronics Group Leader  |

- |   |   |
|---|---|
| <p>15. Leverne Kenneth Seversike<br/>         Ass't. Prof. of Aerospace Engr.<br/>         Iowa State University</p>      | <p>B. S. , Iowa State University, 1958<br/>         M. S. , Iowa State University, 1961<br/>         Ph. D. , Iowa State University, 1964</p> <p>Mission Profile Group Leader<br/>         Project Leader</p> |
| <p>16. David W. C. Shen<br/>         Prof. of Elect. Engr.<br/>         Moore School of Electrical Engr.</p>              | <p>B.Sc. National Tsing Hua Univ. , 1938<br/>         Ph. D. , University of London, 1948</p> <p>Electronics Group</p>  |
| <p>17. Kenneth Alva Stead<br/>         Instructor, Civil Engr.<br/>         University of So. Carolina</p>                | <p>B. C. E. , Univ. of Louisville, 1953<br/>         M. S. , Univ. of Missouri, 1961</p> <p>Spacecraft Configuration Group</p>  |
| <p>18. Harold Francis Trent<br/>         Assoc. Prof. of Industrial Engr.<br/>         Virginia Polytechnic Institute</p> | <p>B. S. , Roanoke College, 1941<br/>         M. S. , Virginia Polytechnic Inst. 1958</p> <p>Spacecraft Configuration Group</p>   |
| <p>19. Jesse H. Wilder<br/>         Professor of Mech. Engr.<br/>         University of Dayton</p>                        | <p>B. S. M. E. , Duke University, 1947<br/>         M. S. , State University of Iowa, 1949</p> <p>Spacecraft Configuration Group Leader<br/>         Project Leader</p>                                       |

## ACKNOWLEDGMENTS

The successful completion of Project JOVE would not have been possible without the enthusiastic cooperation of the offices and personnel of the Marshall Space Flight Center, their supporting contractors, and many individuals. It is a distinct pleasure for the directors and participants of the 1967-Auburn-Alabama-MSFC Engineering Systems Design Program to acknowledge their efforts and support.

The number of persons and organizations deserving recognition would defy any attempt at a complete listing. We feel, however, that we would be remiss if several key contributors to Project JOVE were not specifically recognized.

We are particularly indebted to Mr. F. L. Williams, Director of the Advanced Systems Office, and his fine staff; Mr. H. F. Thomae, Aero-Astroynamics Laboratory; Mr. A. G. Orillion, Propulsion & Vehicle Engineering Laboratory; and Mr. Fred Digesu, Astrionics Laboratory. A giant share of the credit for the success of Project JOVE must go to the Program Co-Director, Mr. W. Y. Jordan of the Voyager Definition Task Group. Mr. Jordan's organizational efforts and his continuing advice and encouragement were dominant factors in the realization of a noteworthy systems engineering program. We also wish to specifically thank Mr. W. R. Payne of the Advanced Systems Office for his continuing support of the program. Mr. Payne's efforts in the publication of the final reports, preparation of audio-visual aids for the oral presentation on JOVE, and in obtaining special equipment and services necessary for completion of the systems engineering project have been indispensable.

Mr. David Newby, Assistant to the Center Director for Scientific and Technical Analysis, and Center Management both deserve special recognition for their guidance and assistance in lending the full support of the Marshall Space Flight Center to this project.

It is a pleasure to acknowledge the support of Mr. Pat R. Odom, of the Northrop Space Laboratories. The assistance of Mr. Odom was invaluable, both during the formative stages of the project, and during the technical studies in the latter phases of Project JOVE.

Finally, all of us associated with Project JOVE wish to express our sincere thanks to Mrs. Betty Mayo, our good friend and secretary for the duration of the project. It is a pleasure to acknowledge this support, and it is certain that without Mrs. Mayo, the probability of project success would have been small indeed.

## ABSTRACT

JOVE (Jupiter Orbiting Vehicle for Exploration) is the preliminary design of a Voyager-class space vehicle. The design has been integrated with the present Voyager concepts in an attempt to utilize many basic components in both vehicles. JOVE is a natural sequence to Voyager with a proposed launch date in the late 1970's or early 1980's. Studies and trade-offs of complete systems were made, and layouts are presented for a recommended configuration and an alternate configuration. JOVE utilizes a standard Saturn V launch vehicle and attaches to a special short shroud just above the Instrument Unit. The total weight injected in the heliocentric transfer to Jupiter is approximately 19 500 pounds, with a total Jupiter orbiting weight of approximately 8000 pounds.

A number of unique features of the JOVE vehicle are:

1. An extended mission time of approximately 800 - 900 days in transit, with at least 100 working days in orbit around Jupiter.
2. Complete dependence upon eight radioisotope thermoelectric generators for power over this extended period of time.
3. A fixed 20 foot high-gain antenna as opposed to the usual gimballed antenna present on a 3-axis stabilized spacecraft.
4. A gimballed attitude control reference-axis system (Sun and Canopus sensors).
5. A modular concept that allows the basic structure to be used for other missions including use on uprated Saturn V boosters.

The unknown radiation environment near Jupiter dictated another unique feature, a two orbit concept. It is proposed that the vehicle enter a highly elliptical orbit with a perijove of 7 or 8 Jupiter radii, test the Jovian magnetic and radiation environment and, if it is found tolerable, to retrofire to a lower perijove of 4 or 5 Jovian radii.

The main spacecraft structural body, the midcourse engines, the Apollo descent engine, the experimental packages, and the experiments and instrument platform are quite similar to those presently proposed for Voyager. The spacecraft is considered to be a simpler vehicle than either Voyager or the Apollo Lunar Landing Vehicle, and it is pointed out that its simplicity helps

overcome reliability problems that are associated with the long mission time. Extensive micrometeoroid protection is applied in the structure of the vehicle and it is completely insulated from outer space environment. It is anticipated that heat rejected from the RTG units will be utilized as required for thermal control within the spacecraft body. An extensive discussion of JOVE's science packages is presented, including instruments such as TV which will be used only while in orbit around Jupiter. Several recommendations on the value of the mission are included, particularly as pertains to the unknown environment around Jupiter and its effect on Jupiter Flyby missions.



# TABLE OF CONTENTS

	Page
Preface . . . . .	iii
List of Participants . . . . .	v
Acknowledgments . . . . .	viii
Abstract . . . . .	ix

## CHAPTER I. INTRODUCTION

Mission Selection and Objectives . . . . .	1-1
Summary . . . . .	1-3
Integration with Other Space Programs . . . . .	1-5
Recommendations . . . . .	1-6

## CHAPTER II. MISSION ANALYSIS

Definition of Symbols . . . . .	2-1
Mission Description . . . . .	2-3
Mission Concept . . . . .	2-4
Trajectory Analysis . . . . .	2-7
Summary of Mission Studies . . . . .	2-49
Bibliography . . . . .	2-53

## CHAPTER III. SCIENTIFIC SYSTEMS

Definition of Symbols . . . . .	3-1
Introduction . . . . .	3-2
Interplanetary Measurements and Instruments . . . . .	3-7
Uniquely Orbital Measurements and Instruments . . . . .	3-34
References . . . . .	3-47
Bibliography . . . . .	3-50

## CHAPTER IV. TELECOMMUNICATION SYSTEM

Definition of Symbols . . . . .	4-1
Introduction . . . . .	4-5
Functional Description . . . . .	4-5
Communication System Design Constraints . . . . .	4-5
Earth-Based System-DSN . . . . .	4-7
Transmission Environment . . . . .	4-18
JOVE Radio Subsystem . . . . .	4-27

## TABLE OF CONTENTS (Continued)

	Page
CHAPTER IV. (Continued)	
Telemetry Subsystem .....	4-40
Command Subsystem .....	4-65
References .....	4-73
Bibliography .....	4-75
CHAPTER V. SPACECRAFT MECHANICAL DESIGN	
Definition of Symbols .....	5-1
Concept Development .....	5-3
Systems Definitions and Weights .....	5-17
Special Design Considerations .....	5-21
Structural Design .....	5-26
Materials Evaluation .....	5-30
Thermal Control .....	5-35
References .....	5-47
Bibliography .....	5-49
CHAPTER VI. SPACECRAFT PROPULSION SYSTEMS	
Definition of Symbols .....	6-1
Introduction .....	6-3
Primary On-Board Propulsion Requirements .....	6-3
Retropropulsion Subsystem Calculations .....	6-11
Trajectory Correction/Orbit Trim (TC/OT) Propulsion Subsystem Design .....	6-17
Attitude Control Propulsion Subsystem Calculations .....	6-21
Summary .....	6-25
References .....	6-27
Bibliography .....	6-27
CHAPTER VII. GUIDANCE AND CONTROL	
Definition of Symbols .....	7-1
Introduction .....	7-2
Guidance System .....	7-3
Attitude Control System .....	7-4

## TABLE OF CONTENTS (Concluded)

	Page
CHAPTER VII. (Continued)	
Articulation . . . . .	7-17
Summary . . . . .	7-18
References . . . . .	7-19
Bibliography . . . . .	7-20

### CHAPTER VIII. POWER SUPPLY SYSTEM

Definition of Symbols . . . . .	8-1
Introduction . . . . .	8-4
Mission Power Requirements and Power Allotment . . . . .	8-4
Comparison of Power Supplies . . . . .	8-5
SNAP Systems Available . . . . .	8-11
RTG Fuel Considerations . . . . .	8-12
Nuclear Safety with an RTG Power Supply . . . . .	8-21
Description of the RTG Unit . . . . .	8-22
Radiation Levels Caused by the RTG Units . . . . .	8-36
Ground Operations for the RTG Power Supply . . . . .	8-38
RTG Temperatures during Flight Phases . . . . .	8-41
Cost Estimates for the Power Supply System . . . . .	8-42
References . . . . .	8-44
Bibliography . . . . .	8-46

### CHAPTER IX. COST AND RELIABILITY

Definition of Symbols . . . . .	9-1
Spacecraft Program and Cost Estimating Relationships . . . . .	9-2
Allocation of Subsystem Weights to Cost Categories . . . . .	9-4
Cost of the JOVE Planetary Vehicle . . . . .	9-7
Discussion . . . . .	9-7
Reliability . . . . .	9-31
Bibliography . . . . .	9-38

# LIST OF ILLUSTRATIONS

FIGURE	TITLE	PAGE
II-1	Mission Schematic . . . . .	2-6
II-2	Declination of the Launch Azimuth Limitations . . . . .	2-9
II-3	Declination of the Launch Azimuth - 1978 . . . . .	2-10
II-4	Declination of the Launch Azimuth - 1980 . . . . .	2-11
II-5	Saturn V Launch Capabilities . . . . .	2-13
II-6	Injection Energy Requirements - Type I Minimum Energy Trajectory . . . . .	2-15
II-7	Injection Energy Requirements - 1978 . . . . .	2-16
II-8	Hyperbolic Excess Velocity at Arrival - 1978 . . . . .	2-17
II-9	Injection Energy Requirements - 1980 . . . . .	2-18
II-10	Hyperbolic Excess Velocity at Arrival - 1980 . . . . .	2-19
II-11	Capture Orbit Schematic . . . . .	2-21
II-12	Velocity Increment Required for Jovian Capture Maneuver - $n = 5$ . . . . .	2-22
II-13	Velocity Increment Required for Jovian Capture Maneuver - $n = 10$ . . . . .	2-23
II-14	Velocity Increment Required for Jovian Capture Maneuver - $n = 15$ . . . . .	2-24
II-15	Velocity Increment Required for Jovian Capture Maneuver - $n = 20$ . . . . .	2-25
II-16	Effect of Apisidal Ratio on Braking Requirement . . . . .	2-26
II-17	Mass Fraction Variation with Braking Impulse . . . . .	2-27
II-18	Parametric Capture Braking Performance - $r_p = 5R_4$ , $n = 15$ . . . . .	2-28
II-19	Parametric Capture Braking Performance - $r_p = 5R_4$ , $n = 20$ . . . . .	2-29
II-20	Parametric Capture Braking Performance - $r_p = 7R_4$ , $n = 10$ . . . . .	2-30
II-21	Parametric Capture Braking Performance - $r_p = 7R_4$ , $n = 15$ . . . . .	2-31
II-22	Parametric Capture Braking Performance - $r_{p2} = 5R_4$ , $n_2 = 14$ . . . . .	2-33
II-23	Parametric Capture Braking Performance - $r_{p1} = 7R_4$ , $n_1 = 14.28$ and $r_{p2} = 5R_4$ , $n_2 = 20$ . . . . .	2-34
II-24	Parametric Capture Braking Performance - $r_{p1} = 8R_4$ , $n_1 = 10$ and $r_{p2} = 5R_4$ , $n_2 = 16$ . . . . .	2-35

## LIST OF ILLUSTRATIONS (Continued)

FIGURE	TITLE	PAGE
II-25	Parametric Capture Braking Performance - $r_p = 8R_4$ , $n_1 = 12.5$ and $r_{p_2} = 5R_4$ , $n_2 = 20$ . . . . . $p_1$ . . . . .	2-36
II-26	Jovian Capture Orbit Period as a Function of Apsidal Ratio . . . . .	2-37
II-27	Mission Analysis Block Diagram . . . . .	2-39
II-28	Parametric Mission Analysis Diagram . . . . .	2-40
II-29	Effect of Trip Time on Gross Capture Weight - Single Orbit - 1978 . . . . .	2-41
II-30	Effect of Trip Time on Gross Capture Weight - Single Orbit - 1980 . . . . .	2-42
II-31	Effect of Trip Time on Gross Capture Weight - Dual Orbit - 1978 . . . . .	2-43
II-32	Effect of Trip Time on Gross Capture Weight - Dual Orbit - 1980 . . . . .	2-44
II-33	Travel Angle and Position Time History - 800 Day 1980 . . . . .	2-46
II-34	800 Day Mission Trajectory . . . . .	2-47
II-35	Sun-Spacecraft-Earth Angle Time History - 800 Day 1980 . . . . .	2-48
III-1	Flux Gate Magnetometer Schematic . . . . .	3-8
III-2	Flux Gate Magnetometer Hysteresis Loop . . . . .	3-9
III-3	Flux Gate Magnetometer Functional Block Diagram . . . . .	3-11
III-4	Rubidium - 87 Energy-Level Diagram . . . . .	3-12
III-5	Dual Cell Self Oscillating Magnetometer . . . . .	3-13
III-6	Trapped Radiation Detector . . . . .	3-16
III-7	Electrostatic Analyzer . . . . .	3-18
III-8	Positive Ion Energy Resolution . . . . .	3-19
III-9	Geometry-Faraday Cup Probe . . . . .	3-20
III-10	Cosmic Ray Telescope Block Diagram . . . . .	3-24
III-11	Energy Loss in $D_1$ Detector . . . . .	3-25
III-12	Schematic-Scintillator Assembly . . . . .	3-27
III-13	Energy Relations for Various Particles . . . . .	3-29
III-14	Micrometeoroid Mass Distribution . . . . .	3-31
III-15	Micrometeoroid Detector . . . . .	3-32
III-16	Mariner-4 Micrometeoroid Circuit . . . . .	3-33
III-17	Block Diagram - Typical Ultraviolet Photometer . . . . .	3-36
III-18	Block Diagram - Mariner-2 Infrared Radiometer . . . . .	3-37
III-19	Component Arrangement - Mariner-2 Infrared Radiometer . . . . .	3-38

## LIST OF ILLUSTRATIONS (Continued)

FIGURE	TITLE	PAGE
III-20	Mariner-2 Microwave Radiometer-Dish . . . . .	3-40
III-21	Block Diagram - Mariner-2 Microwave Radiometer . . . . .	3-42
III-22	Diagram of Infrared Spectrometer . . . . .	3-45
IV-1	JOVE Telecommunications System . . . . .	4-9
IV-2	DSS Block Diagram . . . . .	4-12
IV-3	Bit Error Probability vs. $\beta$ . . . . .	4-20
IV-4	Free Space Path-Loss vs. Distance . . . . .	4-24
IV-5	Antenna Temperature, $T_A$ , vs. Distance from Sun, AU . . . . .	4-28
IV-6	Antenna Temperature, $T_A$ , ( $^{\circ}$ K). Due to Jupiter . . . . .	4-29
IV-7	JOVE Radio Subsystem Block Diagram . . . . .	4-31
IV-8	20 Foot Antenna Parameters . . . . .	4-33
IV-9	Transponder Block Diagram . . . . .	4-35
IV-10	Bit Rate vs. Distance . . . . .	4-45
IV-11	Spacecraft Telemetry Subsystem . . . . .	4-47
IV-12	Real Time Data Transmission Formats . . . . .	4-52
IV-13	Non-Scan Science Minor Frame . . . . .	4-53
IV-14	Data Word and Bit Sync Generation . . . . .	4-56
IV-15	Bit Error Probabilities . . . . .	4-58
IV-16	Receiving Sync System for Generation of Coherent Data . . . . .	4-59
IV-17	Coherent Demodulation and Matched Filter Detection . . . . .	4-62
IV-18	Power Spectral Density . . . . .	4-64
IV-19	Schematic of Command Subsystem . . . . .	4-67
IV-20	Command Detection System . . . . .	4-69
IV-21	Coherent Demodulation System . . . . .	4-70
IV-22	Quadrature Detector . . . . .	4-71
V-1	JOVE Spacecraft Layout . . . . .	5-5
V-2	First Alternate Spacecraft Layout . . . . .	5-7
V-3	Preliminary Configuration Studies . . . . .	5-9
V-4	Antenna and Sun Sensor Coupling . . . . .	5-12
V-5	Boost Support Structure . . . . .	5-27
V-6	Spacecraft Bus . . . . .	5-29
V-7	Schematic of JOVE Thermal Control Subsystem . . . . .	5-37



## LIST OF ILLUSTRATIONS (Continued)

FIGURE	TITLE	PAGE
V-8	Temperature vs. Distance from Sun for an Insulated Flat Plate Facing Sun . . . . .	5-39
V-9	Equilibrium Temperature for Flat Plate Normal to Sun for Varying $\alpha/\epsilon$ . . . . .	5-40
V-10	Equilibrium Skin Temperature versus Heat Rejected to Black Space . . . . .	5-41
VI-1	Propellant Classifications . . . . .	6-5
VI-2	Propulsion Design Chart . . . . .	6-7
VI-3	Propellant Requirements - Tank Sizing Analysis . . . . .	6-13
VII-1	Pitch or Yaw Acquisition and Cruise Modes - Simplified Block Diagram . . . . .	7-8
VII-2	Variation of Earth-Spacecraft-Sun Angle with Elapsed Mission . . . . .	7-12
VII-3	On-Board Control System . . . . .	7-14
VII-4	Arrangement of Attitude Control Nozzles . . . . .	7-16
VIII-1	Isotopic Power Variation with Time . . . . .	8-16
VIII-2	Production of Pu <sup>238</sup> . . . . .	8-19
VIII-3	Flowsheet for Production of Pu <sup>238</sup> . . . . .	8-20
VIII-4	JOVE Mission Power Supply . . . . .	8-26
VIII-5	80 W <sub>e</sub> RTG Pictorial View. . . . .	8-27
VIII-6	Schematic View - JOVE's 80 W <sub>e</sub> RTG . . . . .	8-28
VIII-7	Fuel Body Cross Section . . . . .	8-30
VIII-8	RTG Fuel Cost . . . . .	8-43
IX-1	Planetary Vehicle Structure Design/Development Costs . . .	9-11
IX-2	Planetary Vehicle Structure First Unit Cost . . . . .	9-12
IX-3	Propulsion Module Structure Design/Development Cost . . .	9-13
IX-4	Propulsion Module Structure First Unit Cost . . . . .	9-14
IX-5	Propulsion Module Engine (Liquid Propellant) Design-Development Cost . . . . .	9-15
IX-6	Propulsion Unit Engine First Unit Cost . . . . .	9-16
IX-7	Navigation and Guidance Design/Development Cost Versus Weight . . . . .	9-17

## LIST OF ILLUSTRATIONS (Concluded)

FIGURE	TITLE	PAGE
IX-8	Navigation and Guidance First Unit Cost . . . . .	9-18
IX-9	Stabilization and Control Systems Design/Development Cost . . . . .	9-19
IX-10	Stabilization and Control First Unit Cost . . . . .	9-20
IX-11	Communications Design/Development Cost . . . . .	9-21
IX-12	Communications First Unit Cost . . . . .	9-22
IX-13	Data Management Design/Development Cost . . . . .	9-23
IX-14	Data Management First Unit Cost . . . . .	9-24
IX-15	Radioisotope Thermoelectric Generator Power Supply Design/Development Cost . . . . .	9-25
IX-16	Radioisotope Thermoelectric Generator Power Supply First Unit Cost . . . . .	9-26
IX-17	Scientific Instruments (Experimental and Mission Sensors) Design/Development Cost . . . . .	9-27
IX-18	Scientific Instruments First Unit Cost Payload (Experiments and Mission Sensors) . . . . .	9-28
IX-19	Cost of Age, Tooling, and Special Test Equipment . . . . .	9-29
IX-20	Cost of Systems Integration . . . . .	9-30
IX-21	Comparison of Reliabilities for Entire System Replacement (Method X) and Subsystem Replacement (Method Y) for a System Containing Four Subsystems . . . . .	9-36
IX-22	Ratio of $P_y$ to $P_x$ vs. $p$ . . . . .	9-37

## LIST OF TABLES

TABLE	TITLE	PAGE
II-1	Summary 1978 Launch . . . . .	2-50
II-2	Summary 1980 Launch . . . . .	2-51
III-1	Recommended Measurements . . . . .	3-3
III-2	Experiments . . . . .	3-4
III-3	Summary - Experiment Packages . . . . .	3-5
III-4	Summary - Television Experiment . . . . .	3-4
IV-1	Summary of Deep Space Instrumentation Facility (DSIF) . . .	4-10
IV-2	Antenna Mechanical Characteristics . . . . .	4-13
IV-3	Doppler Tracking System Summary . . . . .	4-14
IV-4	Microwave and Antenna Performance . . . . .	4-17
IV-5	Telecommunication Parameters . . . . .	4-21
IV-6	Characteristics of 20 Watt TWT . . . . .	4-38
IV-7	Telecommunication Design Control (Telemetry) . . . . .	4-41
IV-8	Telecommunication Design Control (Command) . . . . .	4-43
IV-9	Summary of Engineering Data . . . . .	4-50
V-1	Detailed Weight Statement . . . . .	5-13
V-2	Weight Summary for the JOVE Vehicle . . . . .	5-18
V-3	Summary of Weights for Mariner, Voyager and JOVE . . . .	5-19
V-4	Fuel Tank Data . . . . .	5-28
V-5	Radiation Damage to Components . . . . .	5-31
V-6	Number of Estimated Orbits to Indicated Total Absorbed Dose . . . . .	5-32
V-7	Radiation Levels that Produce Appreciable Property Changes . . . . .	5-34
V-8	Properties of Coatings . . . . .	5-38
VII-1	Factors Considered in Determining Desired Orientation of the Spacecraft . . . . .	7-11
VIII-1	Power Allotment . . . . .	8-6
VIII-2	Parametric Comparison of Several Power Systems . . . . .	8-8
VIII-3	Systems for Nuclear Auxiliary Power (SNAP) Units (Typical Space Application Units) . . . . .	8-13
VIII-4	Characteristics of Attractive Radioisotopic Heat Sources . .	8-14
VIII-5	Pu <sup>238</sup> Fuel Forms . . . . .	8-15
VIII-6	Production of Np <sup>237</sup> in Specific Reactors . . . . .	8-18
VIII-7	Properties of Thermoelectric Elements . . . . .	8-33
VIII-8	Activity of an 80 W <sub>e</sub> RTG . . . . .	8-37

## LIST OF TABLES (Concluded)

TABLE	TITLE	PAGE
VIII-9	Isotopic Composition of Pu in PuO <sub>2</sub> . . . . .	8-38
IX-1	Distribution of JOVE Mission Weights to Cost Categories, Planetary Vehicle Weights . . . . .	9-5
IX-2	Distribution of JOVE Mission Weights to Cost Categories, Propulsion Module . . . . .	9-6
IX-3	Planetary Vehicle Cost . . . . .	9-8
IX-4	Planetary Vehicle Propulsion Module Cost . . . . .	9-9
IX-5	Planetary Vehicle Total Program Cost (P/V TPC) . . . . .	9-10

**CHAPTER 1**  
**INTRODUCTION**

# CHAPTER I. INTRODUCTION

## MISSION SELECTION AND OBJECTIVES

### Motivation and Justification

Jupiter occupies a unique position in any planned exploration of the solar system, including a search for its origin and the origins of life. It is a pivotal planet in that its large gravitational field can be used to assist the boosting of exploratory vehicles to any other place in the solar system through the now well-known swingby concept. Jupiter is of interest, then, for at least the following three reasons:

Jupiter Swingby. Many advanced mission studies have already been conducted by NASA and several private contractors. The results of these studies clearly indicate that the energy requirements for missions to the outer planets, and particularly to the sun, are significantly reduced if the spacecraft could swingby Jupiter, thus utilizing Jupiter's strong gravitational field and orbital momentum to modify the velocity vector to the desired direction.

Planetology. Perhaps the most enticing aspect about Jupiter is its very low mean atmospheric density, approximately one quarter that of Earth with an average molecular weight less than helium. Occultation experiments between spacecraft and Earth have been included in order to probe the atmospheric composition of Jupiter.

Jovian Life. In the past it was generally accepted that the Jovian environment was too hostile to support any form of life. A recent report, July 1967, indicates that a U. S. physiologist, Dr. Sanford Siegel, conducted an experiment in which he took a small spot of soil from an ancient open air urinal, incubated it in a hostile ammonia atmosphere, and fed it with a nutrient broth. Within weeks a strange umbrella shaped microorganism appeared. Shortly thereafter a Harvard paleontologist, Elso S. Barnhorn, reported finding two billion year old microfossils in western Ontario. The microfossils he found bore no resemblance to anything living but were very difficult to distinguish when placed side by side with Dr. Siegel's discovery. The belief that Jupiter's ammonia atmosphere has undergone little change since its formation leads one to believe not only in the existence of Jovian life forms, but also that Dr. Siegel's microorganisms might well be the ancestors to all life everywhere in the solar system.



## Mission Statement

A tentative mission statement first adopted was, "To determine what modifications or changes in the design of Voyager, as presently conceived, will be necessary to accomplish a similar (to Mars and Venus) exploration of Jupiter and what, if any, bonuses can be realized with a narrowing of the objective or mission later, if it appears wise. This does not preclude the consideration of other propulsion systems or potential future advances."

Not all of the objectives outlined in this statement were realized. The result is JOVE, a preliminary design study of a Jupiter orbiting vehicle designed to conduct experiments during the trip through interplanetary space (including the Asteroid Belt) and then to orbit around Jupiter.

## Mission Scientific Objectives

JOVE will return to Earth information about the solar atmosphere, and about Jupiter's atmospheric and magnetic environment, its topographic features, gravitational field, temperature distribution, and any Van Allen type Radiation.

Several particles and fields measurements will be made in route. Interplanetary data pertaining to the Asteroid Belt and solar flares, which should be in abundance because of heavy solar activity anticipated during the selected launch window of 1978-1980, are of particular interest. A planet scan platform contains infrared, ultra-violet and television scanning instruments for use at Jupiter. The high resolution television camera will have a resolution of 36 kilometers at the first perijove distance of 7 Jovian radii\*. Jupiter's strong magnetic field and hazardous trapped radiation particles, which might well be 100 times as intense as the earth's Van Allen belt, dictates the high orbit. A primary objective of JOVE is to map the intensities of these particles and fields.

## Mission Constraints

Four general constraints were recognized as the study of JOVE progressed. The first three are firm engineering constraints, while the fourth is

---

\* JOVE's polar orbit will enable the TV, ir, and uv instruments to get a good look at the Great Red Spot, latitudinal color bands, and prevailing cloud patterns.

a restraint of convenience. Nevertheless, it too is based on sound engineering judgment.

a. The long transit and total mission time forces an extended exposure to the micrometeoroid flux, the solar plasma, the hard vacuum, and the low temperature of space (as well as a relatively high radiation dosage from JOVE's RTG's). This presents a difficult reliability problem. It is felt that the simplicity of the vehicle and careful design will help overcome this constraint.

b. The suspected strong radiation field around Jupiter dictated the orbit size and the nearest approach to Jupiter, approximately 5 Jupiter radii during the second orbit.

c. The communication distance between Earth and the spacecraft orbiting around Jupiter will vary from about 400 million miles to approximately 500 million miles. This places severe constraints on the communication, guidance and control, and command systems and is highlighted by the fact that it will take 45 minutes for a command or radio signal to travel from the transmitters on Earth to the receivers on the spacecraft orbiting Jupiter. Thus, it would be 1 1/2 hours after commanding the spacecraft to perform a certain function before one would know if the spacecraft had properly carried out the instructions. During this time JOVE will have moved in its orbit around Jupiter perijove approximately 60 000 miles.

d. No sterilization or quarantine constraints were imposed on the vehicle other than normal cleanliness because it is felt that it would be impossible for the vehicle to impact Jupiter. It might, however, after a long period of time impact one of the moons of Jupiter.

## SUMMARY

The JOVE spacecraft is a large interplanetary unmanned vehicle. Its total weight at heliocentric injection is approximately 19 500 pounds, with a Jupiter orbiting weight of approximately 8000 pounds. Most of the weight difference represented by these two figures is expended in attaining a highly elliptical orbit about Jupiter. JOVE is proposed for launch in either the 1978 or 1980 opportunity. The heliocentric transfer phase will take approximately 825 days. Following this time, a 90- to 100-day scientific investigative period in orbit around Jupiter is planned. The suspected strong radiation field about Jupiter will dictate a very cautious approach. JOVE will follow a two-orbit

concept, i. e. , the first orbit periapsis will be at approximately an altitude of 7 planet radii above the Jupiter surface. Then if radiation environment tests prove the Van Allen type radiation is not as large as anticipated, the second orbit will be moved in to a lower periapsis with an expected altitude of about 4 planet radii.

JOVE is completely dependent upon eight radioisotope thermal electric generators for supplying electrical power over this extended mission time. These eight RTG's are designed to supply  $80 W_e$  from the radioactive decay of plutonium. Each RTG is an independent entity, making a redundant power supply possible. The RTG's are cooled by passive fins using radiative heat transfer only. A fixed 20 foot diameter high-gain antenna, along with location of the RTG's, proved to be the dominant factor in determining the configuration of the spacecraft. This huge fixed antenna was required for acceptable transmission rates from the tremendous distance of Jupiter. Theoretical transmission rates from Jupiter, to the average distance of Earth, are approximately 3800 bits/sec. This transmission rate will allow many television pictures to be transmitted while JOVE orbits near Jovian periapsis. The large fixed antenna is backed up with a smaller, gimballed (3-foot diameter) antenna. The small antenna will be used for transmission during the first 270 days of the heliocentric transfer. After approximately 270 days in transit, the craft will be rotated to point the large antenna at Earth, and it will be used for communications during the remainder of the trip.

The large fixed antenna, while optimum for structural and transmission reasons, puts some unique restraints on the attitude control system. These restraints were resolved by adopting a gimballed attitude control reference axis system (Sun and Canopus sensors). Such a system has apparently never been flown, but there are no engineering reasons why it could not be developed over the next ten years. Missions to outer planets may require large antennas for communications, and it is apparent that it is much easier to fix these antennas to the spacecraft, thereby requiring a gimballed attitude control reference system.

The thermal control system of JOVE is essentially passive in nature. The main thermal control is accomplished for the most part with three schemes:

1. Controlling the spacecraft surface absorbtivity and emissivity,
2. Utilizing louvers, and
3. Controlling heat rejected from the RTG units (as required).

Many of the subsystems of JOVE are common to currently accepted Voyager concepts. The main spacecraft structural body, the midcourse engines, The Apollo descent engine with its associated tankage, the experiment packages, parts of the television experiment, and the experiment platforms are quite similar to current Voyager concepts. JOVE, however, requires a unique micro-meteorite protective structure that the Voyager need not have. Absence of the Lander Capsule and sterilization restraints have made JOVE a simpler, more reliable vehicle than Voyager concepts.

## INTEGRATION WITH OTHER SPACE PROGRAMS

Study of the interplanetary exploratory mission to Jupiter fits appropriately into the present long range plans of our space program, and follows the recommendation of the Space Science Board. In July 1965, this Board said, "We recommend planetary exploration as the most rewarding scientific objective for the 1970-1985 period." The Pioneer and Explorer series of spacecraft have yielded information about the space between Venus and Mars, and the Mariner projects to Mars and Venus are continuing to yield useful data. The Apollo Program starts its flight phase this year and will be nearing completion sometime in the middle 1970's. Scientific and engineering talent should very soon then be available for post Apollo and interplanetary space projects planned in the late 70's and early 80's. These projects include the Voyager Program designed to orbit twin vehicles about Mars and Venus, and to land probes on each planet during the middle 1970's.

Long range advanced planning for outer planetary missions is extremely important because it takes almost three years after launch for the information to be returned for analysis and use on Earth. The trip time from Earth to Jupiter, for example, is a very sensitive function of the injection velocity (hence payload weight), but reasonable minimum trip times that might be obtained with nuclear upper stages are still larger than 500 days. These large trip times dictate that outer planetary investigations be fully integrated programs rather than single-mission oriented.

JOVE is an interplanetary vehicle designed to extend our knowledge of the environment of the solar system between 1 AU and 5.5 AU. Its unique mission indicates that it could well establish several scientific and engineering "firsts." Among these "first" accomplishments are: the first orbital mission to an outer planet, the first penetration of the Asteroid Belt, the first extremely long (planned) controlled flight, the first interplanetary craft depending completely upon a nuclear power source, and the first planetary craft designed to investigate Jupiter, one of the gas giants.

Since Jupiter is a pivotal planet, it would be possible to realize many bonuses from a project such as JOVE. Appendix C, for example, deals with a single vehicle radio occultation experiment. A two vehicle occultation experiment (the so-called "mother-daughter" concept) was not included because of the communications problems related thereto. Study of the daughter vehicle revealed the possibility that JOVE could carry additional payload packages when launched during ideal launch opportunities. These packages could be probes to outer planets or toward the sun that would utilize the Jupiter swingby technique for velocity vector correction.

## RECOMMENDATIONS

The studies and trade-offs that were made as the design of JOVE progressed indicated the need for additional research and development in many areas. These are described below:

1. Since RTG's appear to be the only feasible power sources for missions beyond Mars, the development of more reliable and efficient medium sized electric power sources and associated shielding should be accelerated.
2. While missions to the outer planets using the Jupiter swingby techniques are possible with the present Saturn V, the development of a nuclear NERVA third stage would greatly enhance these missions and allow considerably more freedom with the selection of launch time and launch windows.
3. It is recommended that probes or flybys of Jupiter be launched within the next four to seven years, so that the data collected could be utilized in the final design of JOVE. Interplanetary space travel and the design of spacecraft to effect this travel requires careful long range planning and systems engineering of the highest caliber.
4. Extremely large communications distances required for exploration of the outer planets place a premium upon developing subsystems which interface with the communications problem. A few of these subsystems, or components, which need additional research include:
  - a. Large deployable antennas,
  - b. High power ( $\geq 100$  watts) transmitting devices,
  - c. Gimballed attitude control reference sensors,
  - d. Laser communication systems.

5. Materials problems associated with long time exposures to the environment of outer space must be investigated. Nonmetallic materials, transistors, for example, should be made less susceptible to radiation damage and outgassing effects.



CHAPTER II  
MISSION ANALYSIS



## CHAPTER II. MISSION ANALYSIS

### DEFINITION OF SYMBOLS

a	Semi-major axis
$A_z$	Launch azimuth angle from north
c	Chord length
$C_3$	Injection energy ( $C_3 = V_{HD}^2$ )
DLA	Declination of the launch outgoing heliocentric asymptote with respect to the ecliptic plane
$I_{sp}$	Specific impulse
GM	Gravitational parameter
	For Earth $3.9860 \times 10^5 \text{ km}^3/\text{sec}^2$
	For Jupiter $1.2671 \times 10^8 \text{ km}^3/\text{sec}^2$
	For Sun $1.3272 \times 10^{11} \text{ km}^3/\text{sec}^2$
MR	Mass ratio $\left( \frac{\text{weight before rocket burn}}{\text{weight after rocket burn}} \right)$
n	Apsidal ratio $\left( n = \frac{r_a}{r_p} \right)$
p	Orbital period
r	Magnitude of the radius vector
$r_a$	Apoapsis distance
$r_p$	Periapsis distance

## DEFINITION OF SYMBOLS (CONTINUED)

$R_4$	Jupiter radius ( $7.14 \times 10^4$ km)
t	Time
V	Velocity
$V_{es}$	Escape velocity
$V_{HD}$	Hyperbolic excess velocity at departure
$V_{HP}$	Hyperbolic excess velocity at arrival
$\Delta V_{a_1}$	Retro impulse velocity at apoapsis
$\Delta V_B$	Capture orbit braking impulse velocity at periapsis
$\alpha$	Sun-Spacecraft-Earth angle
$\lambda$	Launch site latitude

Subscripts:

$( )_1$	Initial capture orbit
$( )_2$	Final capture orbit

## MISSION DESCRIPTION

The primary purpose of the JOVE mission is to place an unmanned scientific payload into an orbit around the planet Jupiter so as to gather the maximum amount of scientific data compatible with the design of the spacecraft and the constraints imposed on the mission definition. To accomplish such a mission, it is necessary to examine the interrelationships between the flight mechanical and Jovian capture maneuver parameters consistent with launch vehicle capabilities, orbit insertion limitations, communications, spacecraft design, and scientific experiment requirements. This type of study permits a systematic design of the spacecraft and mission which will insure a high degree of probability of success.

For a Jupiter mission, launch opportunities occur about every thirteen months, so that during the time period under consideration, 1975-1980, there are six opportunities. Prime consideration is given to the 1978 and 1980 launch opportunities. A 1978 launch has rather stringent requirements based upon the trajectory injection energy, whereas the 1980 launch represents a fairly typical opportunity for the time interval being considered. Examination of these two mission conditions permits a certain degree of flexibility from the standpoint of mission planning which can be realized through the appropriate selection of trip time and Jovian capture orbit characteristics.

Selection of the interplanetary transfer trajectory is largely dependent upon the capabilities of the launch vehicle to insert the vehicle onto the trajectory and the trip time involved. A short trip time requires more injection energy as well as more energy to perform the capture orbit maneuver, but it improves the reliability of the system. Hence, it was decided to keep the trip time to a minimum, consistent with the capabilities of the propulsion systems and the communication limitations. This means that only Type I (transfer angle  $< 180^\circ$ ) trajectories were considered. In this connection, a parametric study was made to determine the trip time which would place the maximum gross weight in a capture orbit, still keeping the trip time relatively short.

The energy requirements for a retropropulsion system to place a vehicle into an orbit around Jupiter necessitate that a highly elliptical capture orbit be established. Another constraint on the orbit selection arises because of the large trapped radiation belts which appear to be present around Jupiter. From the standpoint of useful lifetime of the scientific and communications equipment, the periapses of several Jupiter radii were, therefore, given primary consideration in this study.

Once the vehicle has been placed in a capture orbit and the radiation levels have been assessed, it may be possible to alter the capture orbit size. If analysis of the data indicates that a lower orbit with small periapsis distance would not seriously endanger the mission objectives, then the retropropulsion system would be activated at the apoapsis to accomplish this maneuver. Such a procedure would permit an enlarged scope of scientific data to be gathered. This technique of establishing a dual capture orbit was then carried throughout the mission planning.

In the following sections, a summary of the parametric study of mission performance will be presented along with a detailed description of the analysis of each trajectory phase.

## MISSION CONCEPT

### Vehicle Concept

The spacecraft, designed around the retropropulsion system and the fixed twenty foot high-gain antenna, is attached to a short cylindrical shroud by means of a circular support ring. The three-stage Saturn V employing the S-IVB as the third stage will be used as the launch vehicle.

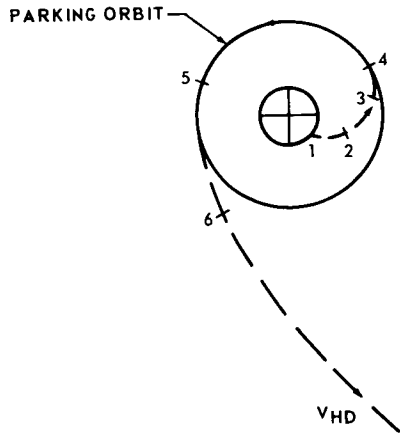
### Mission Profile

The vehicle is to be launched from Cape Kennedy along the AMR using a variable launch azimuth consistent with range safety considerations. It will follow a nominal two-dimensional ascent trajectory into a 185 km altitude circular Earth parking orbit. The vehicle will remain in this parking orbit until the desired position relative to the outgoing geocentric asymptote is attained, at which time the S-IVB will be reignited to inject the vehicle on a 700-900 day heliocentric transfer trajectory. Scientific measurements will be taken during the interplanetary coast phase, recorded, and transmitted to Earth on command. In addition, attitude control will be maintained throughout the coast phase and either two or three mid-course corrections (as required) will be made during this phase. The final mid-course correction will ensure that the approach asymptote is properly oriented for the Jovian capture orbit maneuver. This capture is accomplished by a retro maneuver employing the retropropulsion system for braking at the periapsis position. Scientific data will then

be gathered and transmitted to Earth at planned intervals in the capture orbit. Proper attitude control of the spacecraft, antenna, and scan platform must be maintained throughout the duration of the mission. An estimated useful lifetime of about 90 days in the capture orbit is planned based on component reliability, attitude control propellants, and radiation damage.

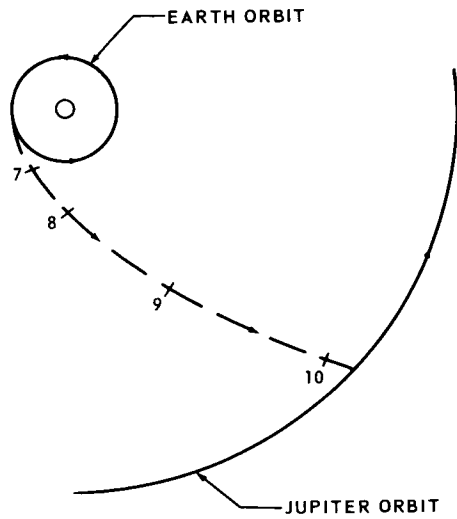
## Mission Sequence of Events (Figure II - 1)

- a. Launch from Cape Kennedy along AMR with Saturn V launch vehicle.
- b. First stage S-IC cut-off and staging. Second stage S-II ignites after staging. Nose fairing shroud is jettisoned during S-II burn at 350 000 feet altitude.
- c. S-II cut-off and staging. Third stage S-IVB ignition to boost into 185 km circular Earth parking orbit.
- d. Parking orbit established and on-board systems checkout initiated.
- e. Coast in parking orbit until favorable position relative to outgoing geocentric asymptote is attained. S-IVB engine reignited to insert onto heliocentric transfer trajectory.
- f. S-IVB cut-off. Jettison S-IVB stage, spacecraft adapter, and IU. Initiate search and acquisition mode for Earth and star sensors and trackers.
- g. First mid-course correction executed.
- h. Second mid-course correction executed, if necessary.
- i. Scientific data collection, recording, and transmission during the interplanetary coast phase.
- j. Third mid-course correction executed just before entry into the Jovian sphere of influence. This establishes the orientation of the Jovian capture orbit.
- k. Retropropulsion system activated to perform the Jovian capture orbit maneuver. Tracking from Earth verifies capture orbit.
- l. Experiment mode is activated.



1. LAUNCH FROM CAPE KENNEDY.
2. S-IC CUT-OFF AND STAGING; S-II IGNITION.
3. S-II CUT-OFF AND STAGING; JETTISON SHROUD; S-IVB IGNITION.
4. INJECTION INTO 185 Km CIRCULAR PARKING ORBIT.
5. RE-IGNITE S-IVB ENGINE TO INJECT ONTO HELIOCENTRIC TRANSFER.
6. JETTISON S-IVB STAGE, I.U., AND SPACECRAFT ADAPTER.

7. 1ST MID-COURSE CORRECTION.
8. 2ND MID-COURSE CORRECTION.
9. COLLECTION AND TRANSMISSION OF SCIENTIFIC AND ENGINEERING DATA AT SELECTED INTERVALS.
10. 3RD MID-COURSE CORRECTION PRIOR TO ENTRY INTO JOVIAN SPHERE OF INFLUENCE.



11. ACTIVATE THE RETROPROPULSION SYSTEM FOR JOVIAN CAPTURE ORBIT MANEUVER.
12. INITIATE EXPERIMENT MODE.
13. DATA COLLECTION AND TRANSMISSION WHILE IN CAPTURE ORBIT.
14. ACTIVATE THE RETROPROPULSION SYSTEM FOR RETRO MANEUVER TO ESTABLISH LOWER PERIAPSIS ORBIT.
15. DATA COLLECTION AND TRANSMISSION WHILE IN NEW ORBIT.

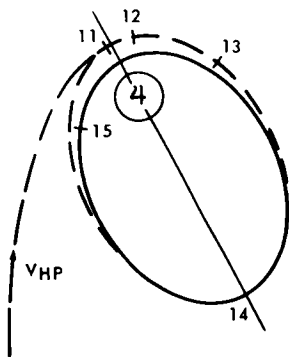


FIGURE II-1. MISSION SCHEMATIC

m. Vehicle remains in capture orbit, alternately collecting data and transmitting data to Earth until system failure.

NOTE

For the alternate mission plan of establishing a dual capture orbit, the following sequence would then proceed.

n. After data analysis indicates that a lower periapsis is possible without severe radiation damage, the retropropulsion system is reactivated at the apoapsis of the first orbit to retro into a lower periapsis orbit.

o. Vehicle remains in new capture orbit, alternately collecting and transmitting data to Earth.

## TRAJECTORY ANALYSIS

The Earth-Jupiter trajectory can be separated into three distinct phases. Each of these phases may in turn be sub-divided and analyzed from fundamental two-body mechanics concepts. These phases are as follows: Launch and Earth parking orbit; Heliocentric transfer trajectory; and Jovian capture orbit. The entire mission depends upon the careful mating of each of these phases since they influence one another to some degree. Each will be discussed further.

### Launch and Earth Parking Orbit Characteristics

The capabilities of the launch vehicle to place a vehicle into a 185 km circular Earth parking orbit determines to a large extent the weight of the spacecraft which can be injected onto the outgoing geocentric asymptote. The declination of this asymptote with respect to the ecliptic plane (DLA) cannot exceed the maximum inclination to the parking orbit with respect to the ecliptic plane. The factors which influence the maximum allowable DLA are the launch azimuth, the launch site latitude, and the parking orbit coast time. Assuming a parking orbit of one complete orbit or more, the maximum DLA is given by the following relationship.



$$\cos (\text{DLA})_{\text{max.}} = \sin A_z \cos \lambda \quad (1),$$

where  $A_z$  - launch azimuth measured from north

$\lambda$  - launch site latitude.

This is shown in Figure II-2 for launch from Cape Kennedy.

The required DLA as a function of launch data for constant trip times for the 1978 and 1980 launch opportunities are shown in Figures II-3 and II-4. Upon comparing these results, the launch azimuth for the Jovian mission will be constrained to 60° to 115°.

## Heliocentric Transfer Trajectories

The heliocentric/transfer trajectory phase can be further divided into three separate two-body mechanics problems:

- a. Geocentric hyperbolic escape maneuver.
- b. Heliocentric elliptical coast.
- c. Planetocentric hyperbolic motion during Jupiter encounter and before capture maneuver.

This method of analysis is referred to as the patched conic technique since the three phases are matched at the boundaries of the spheres of influence of the Earth, Sun, and Jupiter, respectively. The two-body problem for the motion of a particle in a central force field is completely described by the well-known results from Kepler's Laws.

For a vehicle to leave the Earth's sphere of influence it is necessary for it to acquire sufficient velocity to escape the Earth's gravitational field. The velocity which will just permit this is parabolic or escape velocity,  $V_{es} = \sqrt{\frac{2GM}{r}}$ .

The velocity at any point on a hyperbolic trajectory is given by the expression

$$V = \left[ \frac{u}{a} + \frac{2u}{r} \right]^{1/2} = \left[ \frac{u}{a} + V_{es}^2 \right]^{1/2} \quad (2)$$

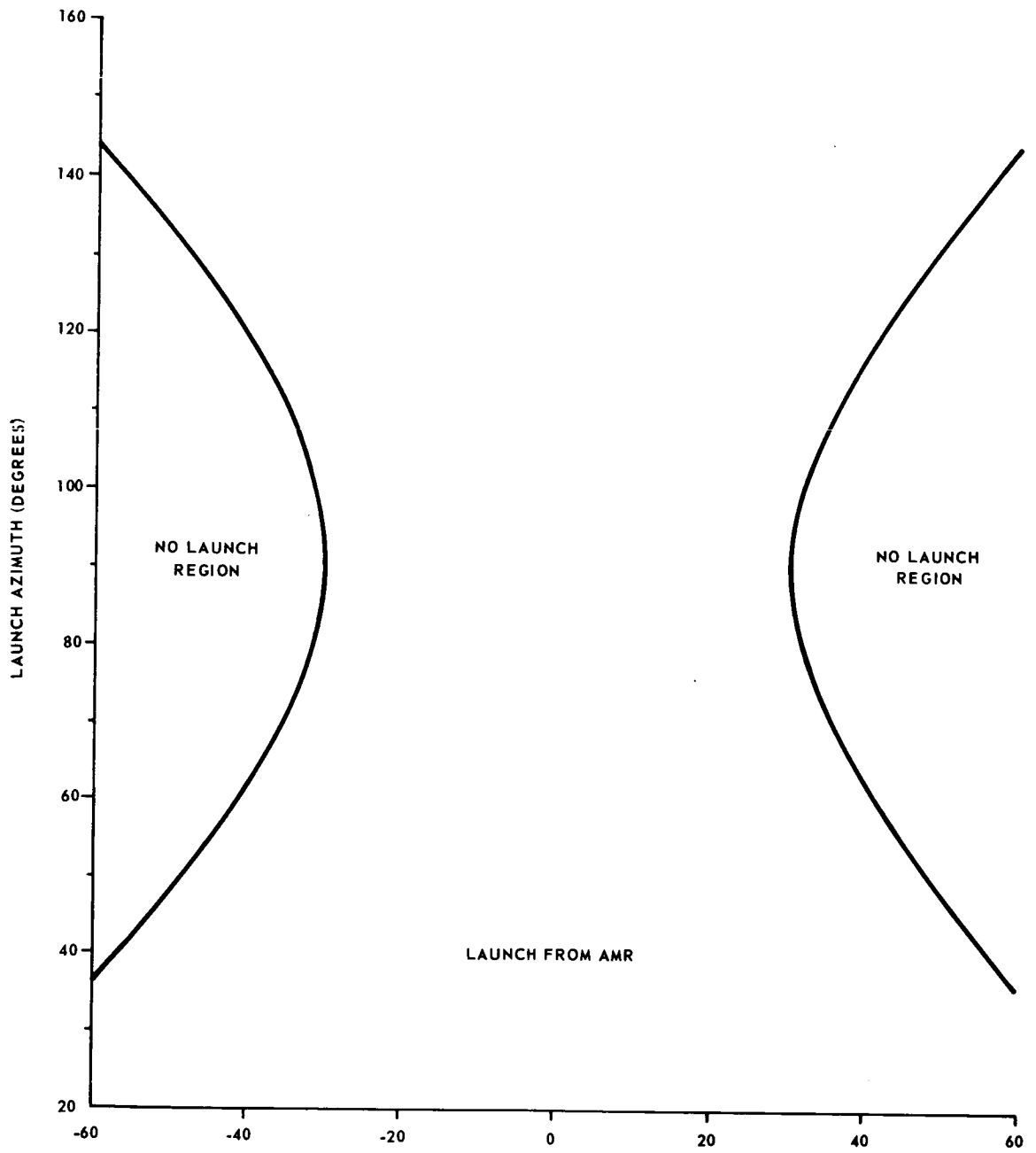


FIGURE II-2. DECLINATION OF THE LAUNCH AZIMUTH LIMITATIONS

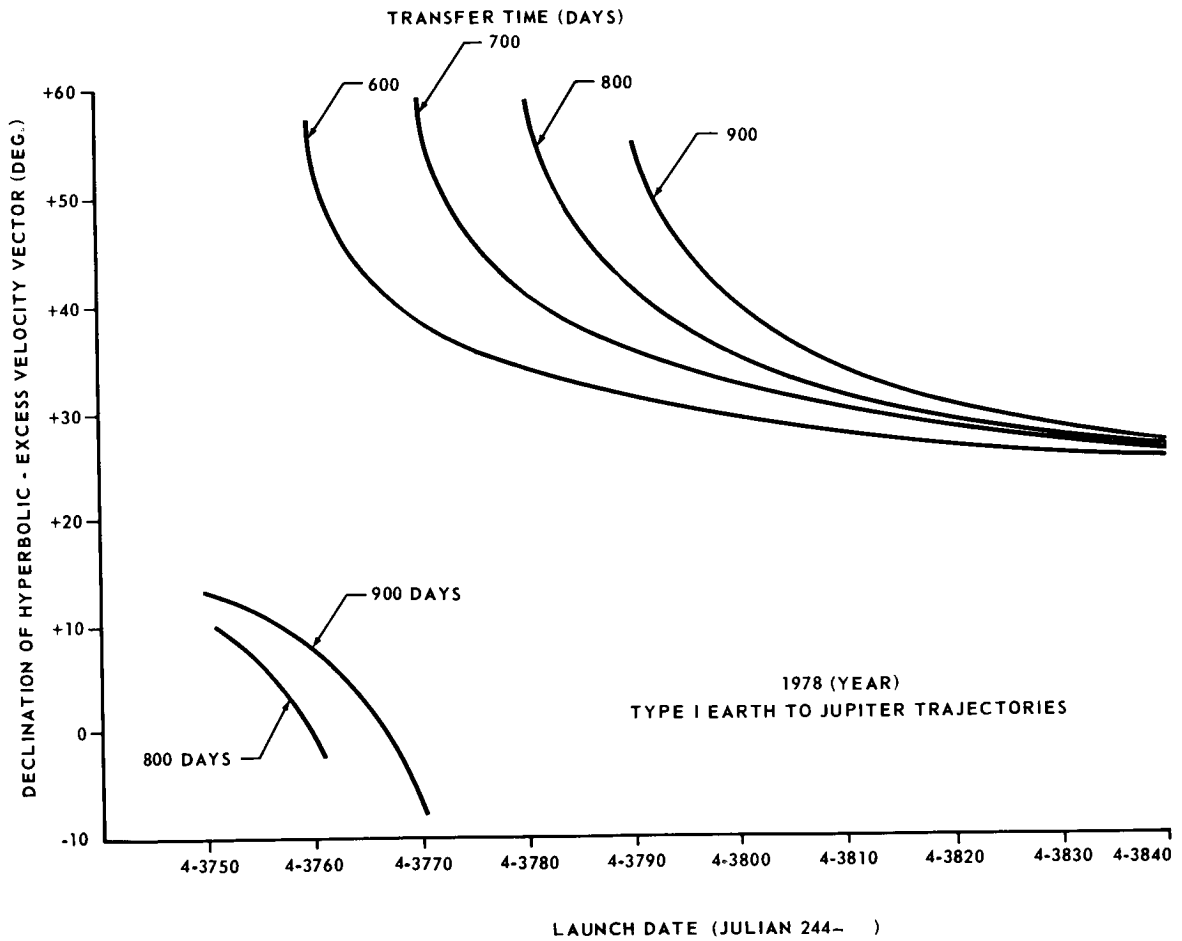


FIGURE II-3. DECLINATION OF THE LAUNCH AZIMUTH - 1978

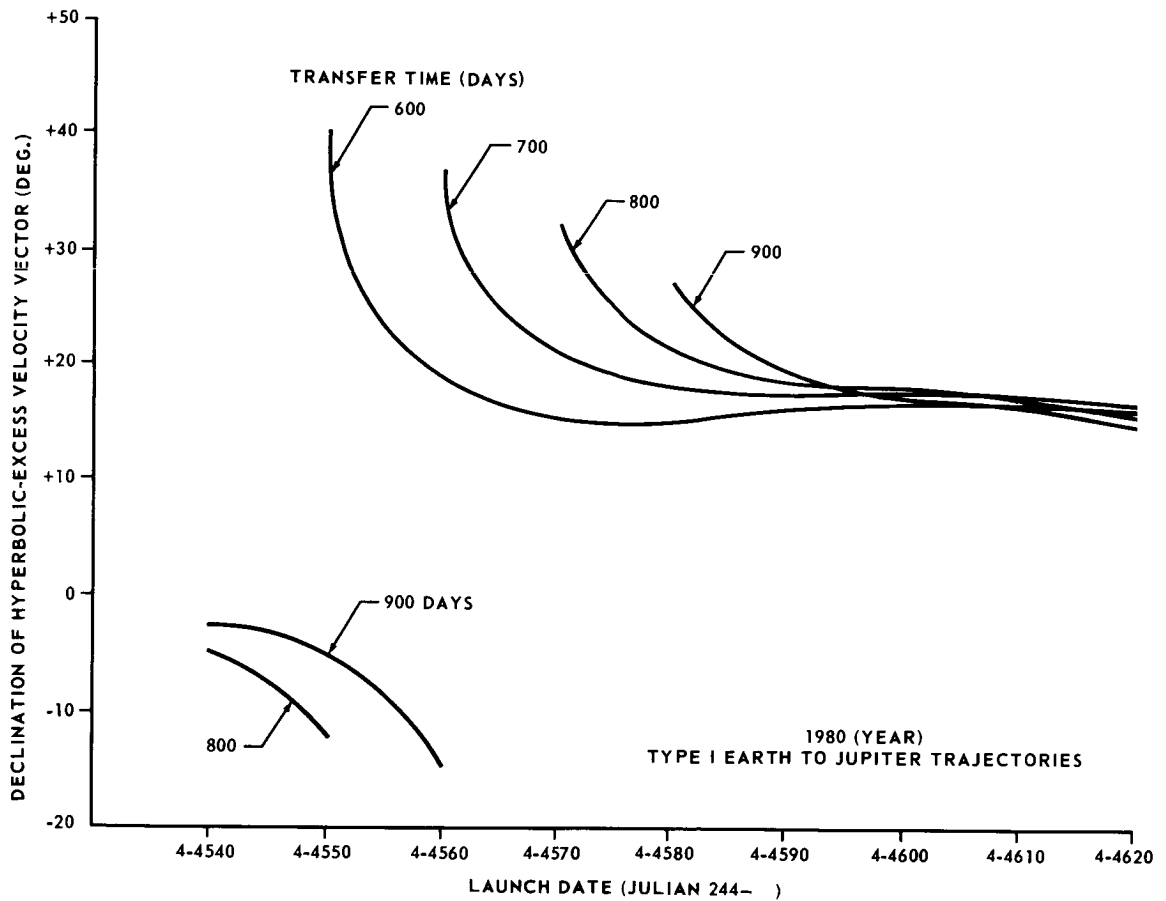


FIGURE II-4. DECLINATION OF THE LAUNCH AZIMUTH - 1980

The hyperbolic excess velocity at departure is then given by the expression

$$V_{HD} = \sqrt{\frac{u}{a}} . \quad (3)$$

A measure of the injection energy is then given by

$$C_3 = V_{HD}^2 . \quad (4)$$

A plot of the performance capabilities of the three stage Saturn V (third stage S-IVB) is given in Figure II-5 as a function of  $C_3$ .

The heliocentric elliptical coast phase takes into account the three-dimensional effects caused by the inclination and ellipticity of the planets' orbits. For mission planning purposes it is desirable to determine the necessary transfer trajectory required to go from a given planet departure date to a given planet arrival date. By specifying these two dates the departure planet and the arrival planet positions are determined as well as the trip time. Also the central angle along the transfer trajectory is known. The method of Gauss is then used to determine the characteristics of the transfer trajectory. This method is based on Lambert's theorem which states that the time required by a body in a central force field to pass through an arc section of any orbit depends only upon the radial distance from the attracting source to the two terminal points of the arc, the length of the chord connecting the terminals, and the semi-major axis of the orbit, i.e. ,

$$t = t(r_1, r_2, c, a) . \quad (5)$$

Hence, in the above relationship the only unknown is the semi-major axis, once the two dates are specified. Through an iterative process the semi-major axis can be determined along with the eccentricity of the transfer trajectory. With these it is then possible to determine all of the transfer orbit characteristics along with the departure and arrival velocity vectors. These velocities when coupled with the geocentric and planetocentric phases determine the energy requirements for the hyperbolic escape and Jovian capture maneuvers. These data have been computed and collected for various launch dates for Jupiter missions in Reference II-1.

In considering the various transfer trajectories, several types have been identified. These are:

Type I      Transfer angle < 180°

Type II      Transfer angle > 180°

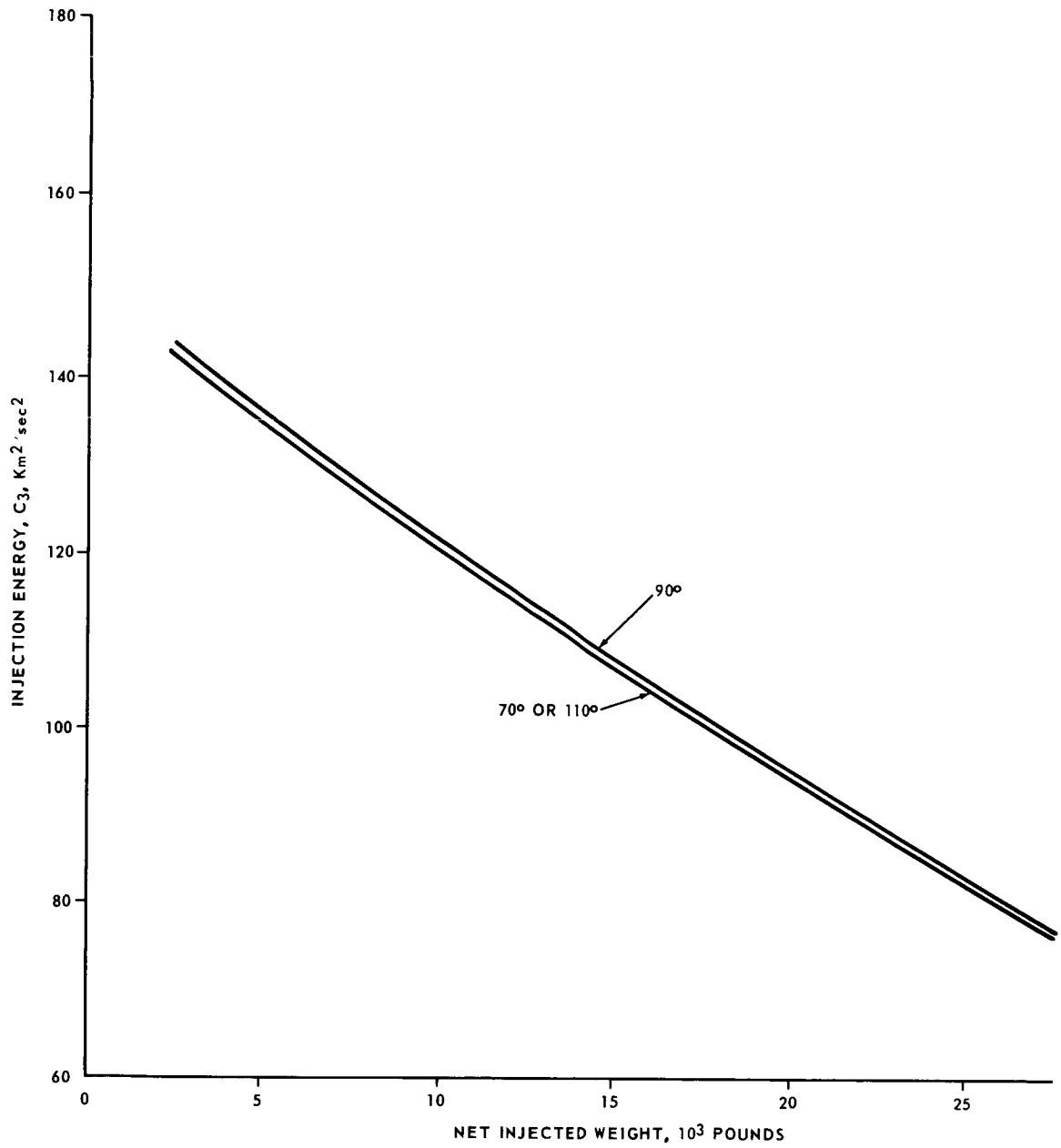


FIGURE II-5. SATURN V LAUNCH CAPABILITIES

- Class I     Target encounter before aphelion
- Class II    Target encounter after aphelion

In general, Type I/Class I has the shortest trip time and Type II/Class II has the longest trip time. A number of trade-offs on departure energy, arrival energy, trip time, communication distances, departure geometry, and arrival geometry must be made in selecting a suitable mission trajectory plan. For the purposes of this study it was decided to examine only Type I trajectories because of the reliability advantages afforded by the shorter trip times.

A launch opportunity for a Jupiter mission occurs about every thirteen months or once each synodic period which is 399 days. During this interval the launch energy requirements,  $C_3$ , reach their lowest values. Typically there is one launch date during each launch opportunity when  $C_3$  reaches a minimum. This is termed the minimum energy trajectory. It is also possible to determine the minimum value of  $C_3$  for a specified launch window. In Figure II-6 the values of  $C_3$  for a twenty-day launch window, minimum energy trajectory are shown for launch opportunities in the 1970-1980 time period. Note that the departure energy requirements are generally higher in the last half of this decade than in the first half. As previously indicated, the 1978 launch has the most severe requirement and the 1980 launch represents a more typical condition during the 1975-1980 interval being examined.

One method used in mission planning is that of studying the effects of various parameters which influence the mission performance while holding the trip time constant. This usually places more severe requirements on the departure and arrival energies than some other methods. It permits, however, greater flexibility in mission planning and presents a conservative estimate of the performance capabilities of the flight vehicle. This is the method which will be utilized in the present study.

Hence, the injection energy and hyperbolic excess velocity at arrival are shown for constant trip times for the 1978 and 1980 launch opportunities in Figures II-7 through II-10. The arrival velocities are specified as a fraction of the Earth mean orbital speed (EMOS), which is 29.78 km/sec.

## Jovian Capture Orbit Maneuver

To place a vehicle in a capture orbit around Jupiter it is necessary to determine the velocity impulse required of the retropropulsion system to reduce

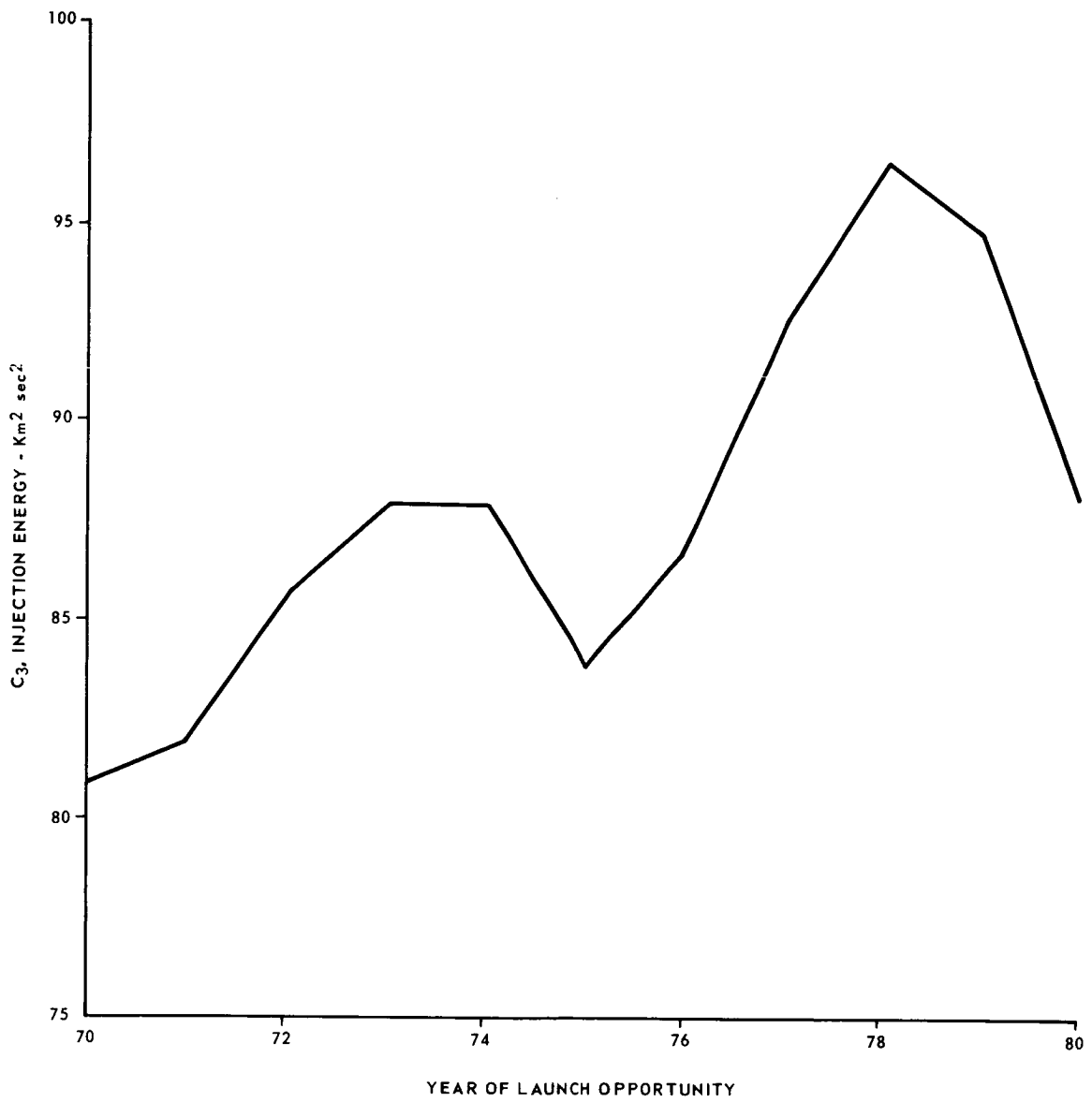


FIGURE II-6. INJECTION ENERGY REQUIREMENTS - TYPE I  
MINIMUM ENERGY TRAJECTORY



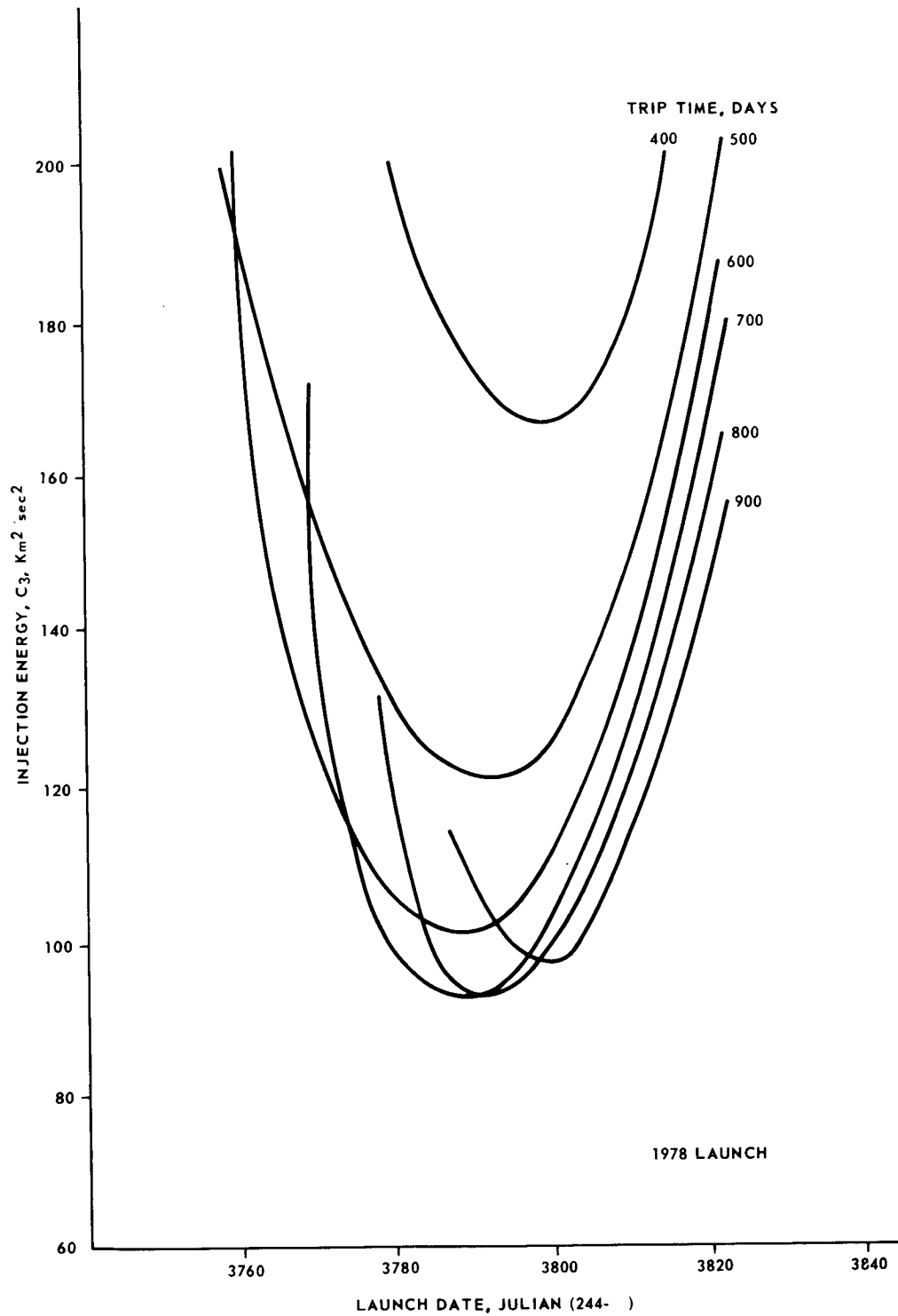


FIGURE II-7. INJECTION ENERGY REQUIREMENTS - 1978

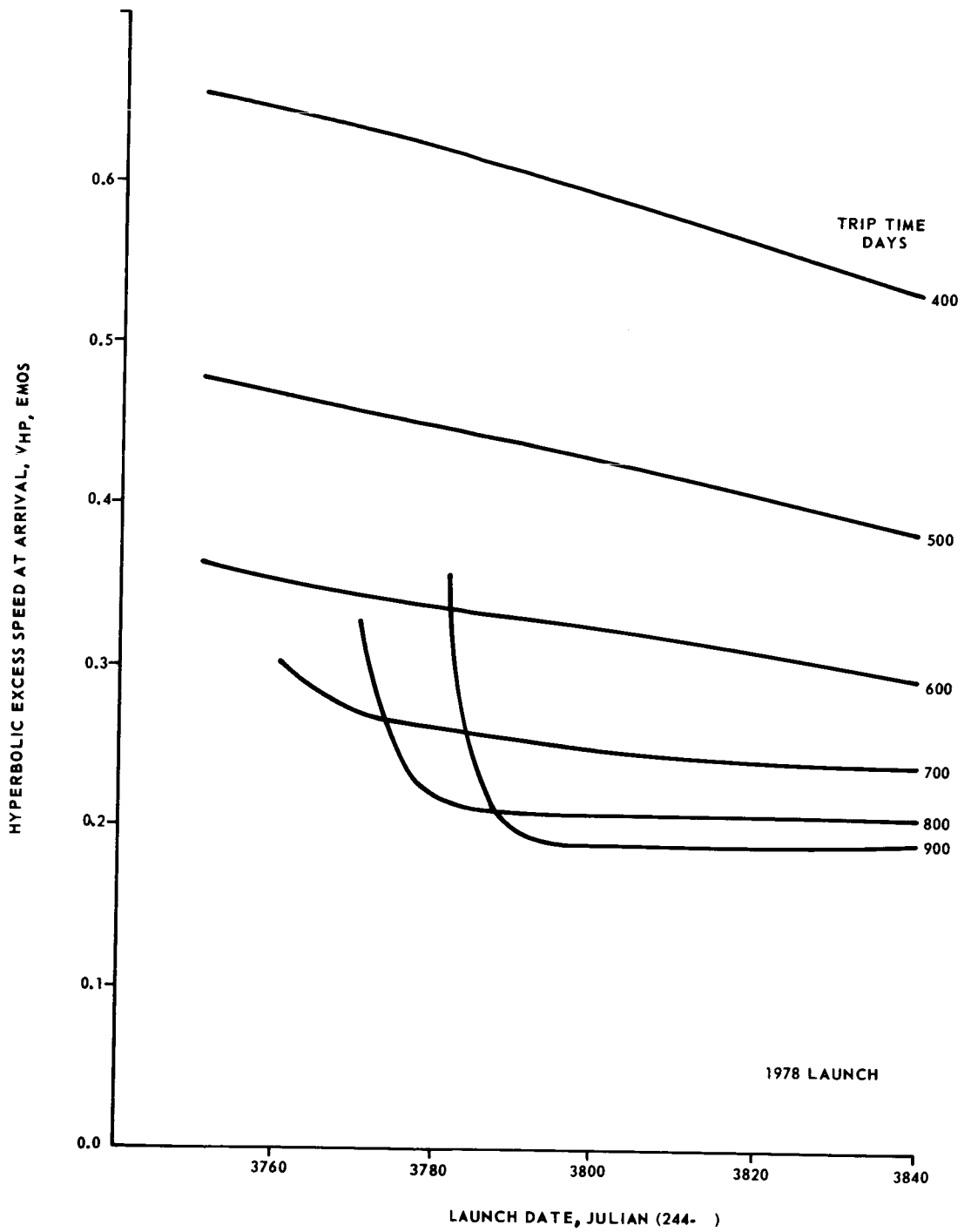


FIGURE II-8. HYPERBOLIC EXCESS VELOCITY AT ARRIVAL - 1978

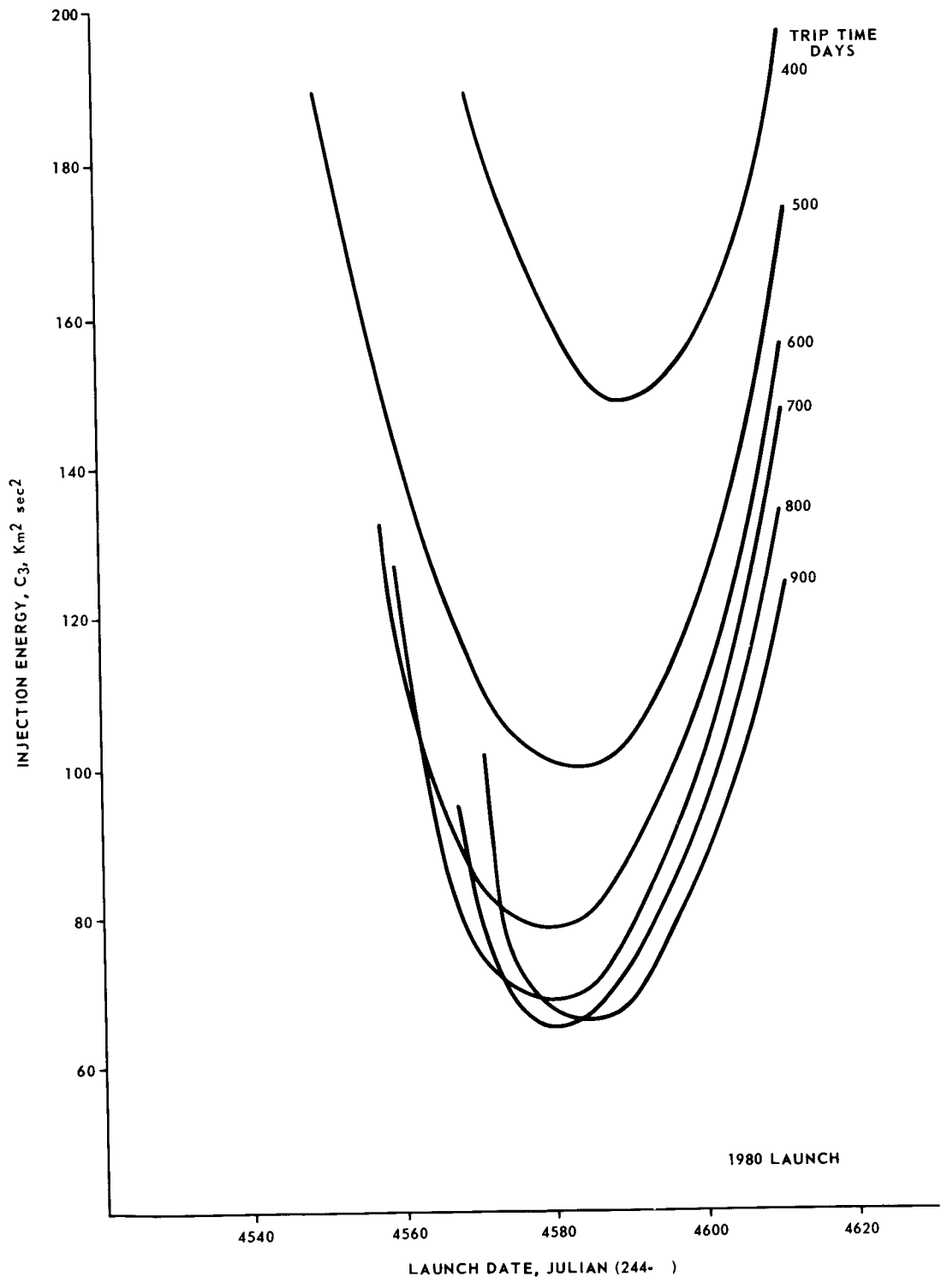


FIGURE II-9. INJECTION ENERGY REQUIREMENTS - 1980

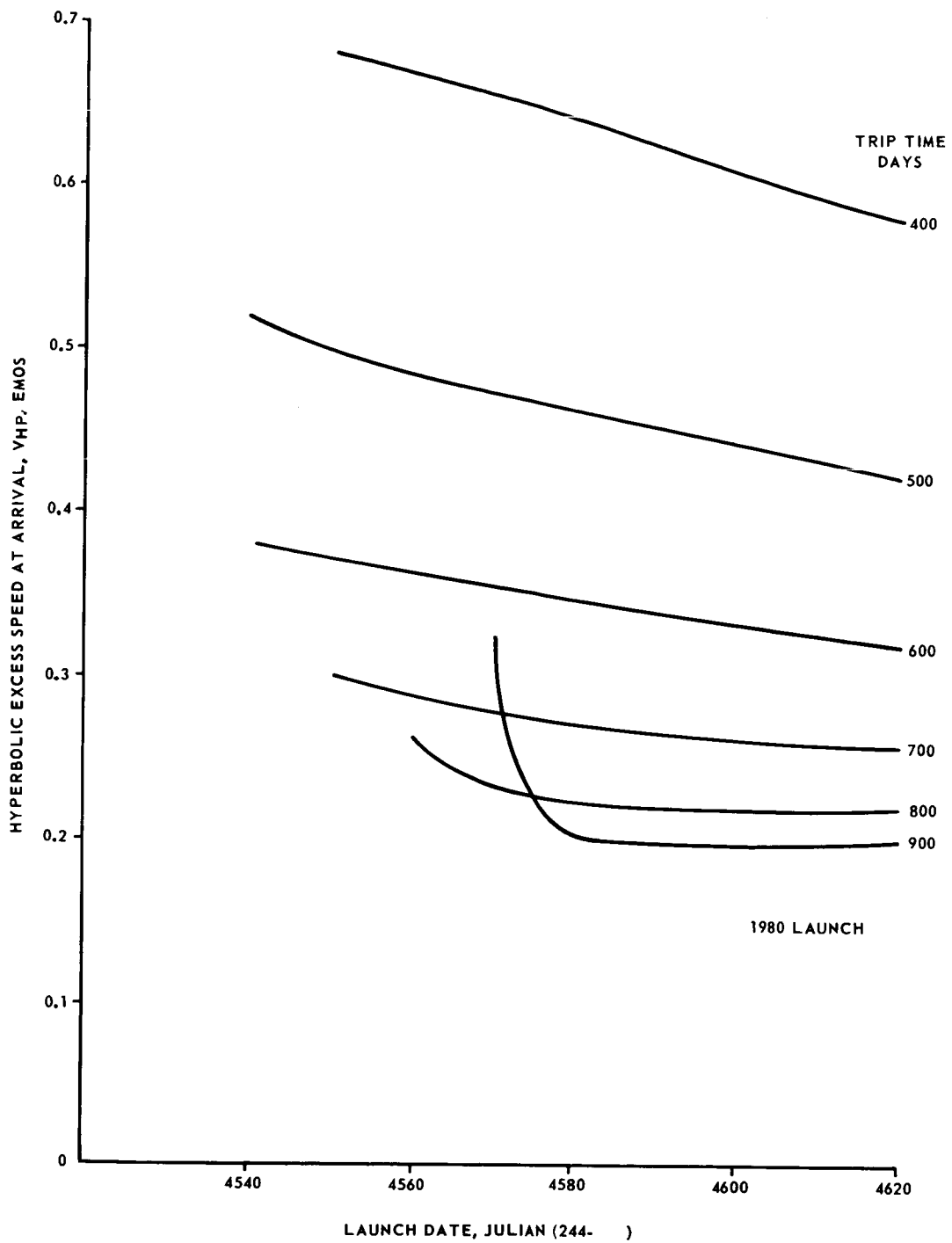


FIGURE II-10. HYPERBOLIC EXCESS VELOCITY AT ARRIVAL - 1980

the hyperbolic approach velocity to the orbital velocity. The minimum impulse is obtained when the retro maneuver is accomplished at the periapsis point as illustrated in Figure II-11. The required braking impulse is given by the following expression

$$\Delta V_B = \sqrt{V_{HP}^2 + \frac{2GM_p}{r_p}} - \sqrt{\frac{GM_p}{r_p} \left( \frac{2}{n+1} \right)} \quad (6)$$

The results from this expression are shown in Figures II-12 through II-15 for a range of values of the periapsis distance,  $r_p$ , and the apsidal ratio,  $n = ra/r_p$ .

The effect of decreasing the apsidal ratio, i. e. , making the orbit more nearly circular, is shown in Figure II-16. This emphasizes the fact that to establish a tighter orbit requires considerably more braking energy.

The velocity impulse capability of the retropropulsion rocket engine is given by

$$\Delta V_B = g I_{sp} \ln MR \quad (7)$$

where  $I_{sp}$  is the specific impulse and

MR the mass ratio given by the ratio of the weight at arrival to the gross capture weight.

The reciprocal of the mass ratio indicates the mass fraction of the spacecraft which will be placed in the capture orbit. Figure II-17 shows the effect of the capture braking requirements on the mass fraction. Using the material from Figures II-12 through II-17 it is then possible to make a parametric study of the gross capture weight versus the hyperbolic excess velocity at arrival with the weight at arrival as a parameter for each specified capture orbit. A selected group of these studies is illustrated in Figures II-18 through II-21. These graphs can be readily used in the parametric mission analysis study which is described in the next section.

The dual capture orbit can be established with a minimum expenditure of fuel from the retropropulsion system by applying the velocity impulse at the apoapsis point as shown in Figure II-11. The velocity impulse required to perform this maneuver is given by

$$\Delta V_{a1} = \sqrt{\frac{GM_p}{r_a}} \left\{ \left[ \frac{2}{n_1+1} \right]^{1/2} - \left[ \frac{2}{n_2+1} \right]^{1/2} \right\} \quad (8)$$

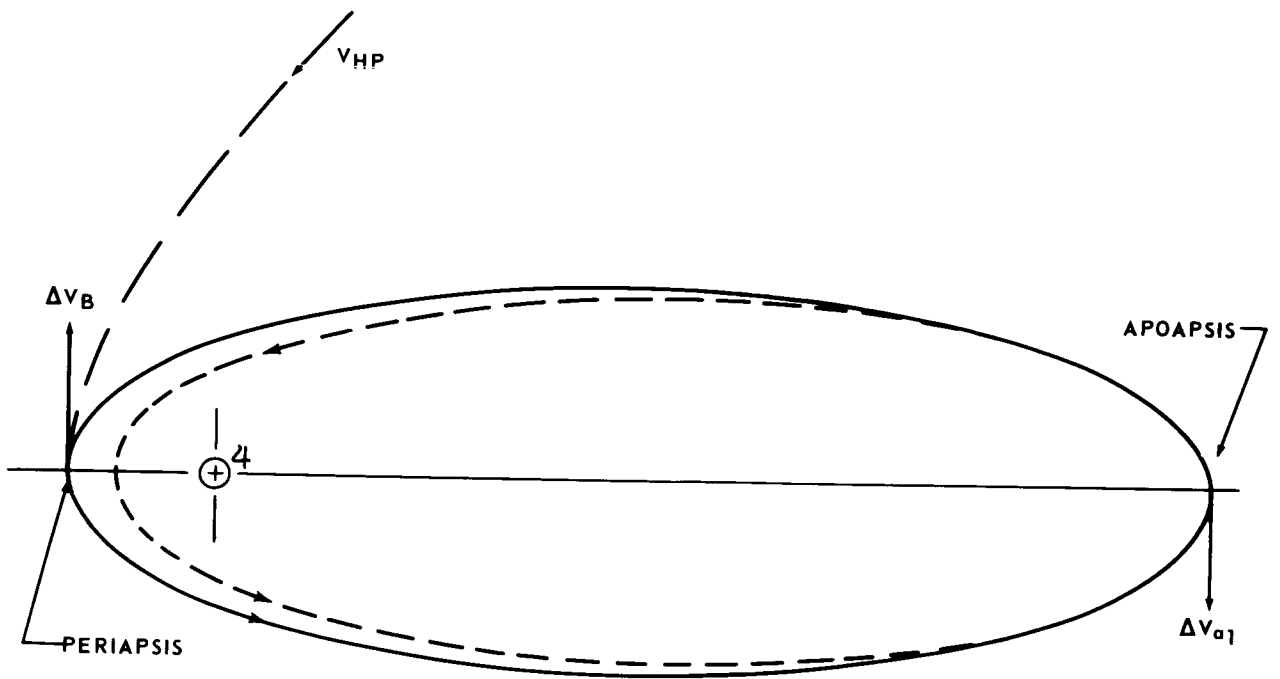


FIGURE II-11. CAPTURE ORBIT SCHEMATIC

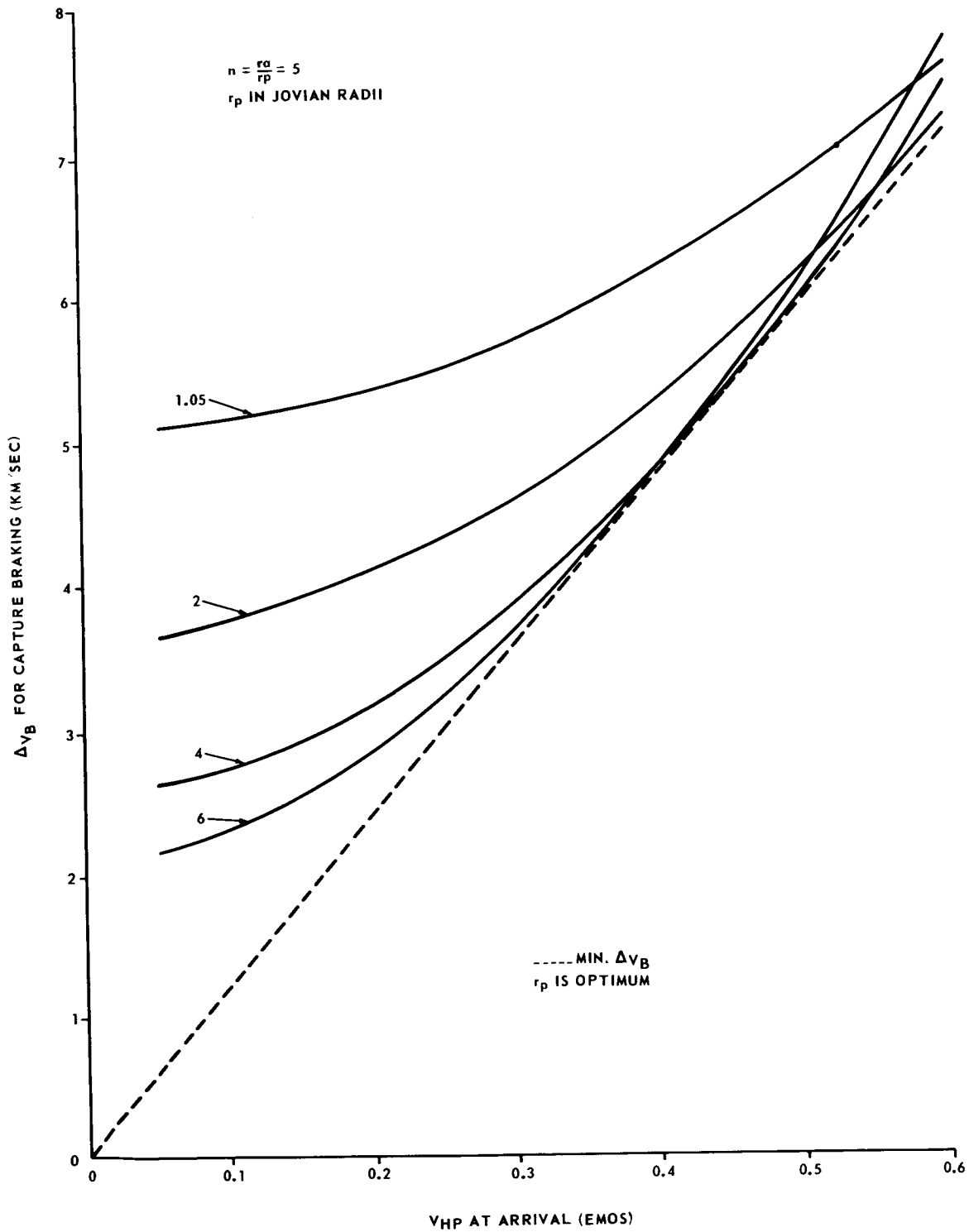


FIGURE II-12. VELOCITY INCREMENT REQUIRED FOR JOVIAN  
 CAPTURE MANEUVER -  $n = 5$

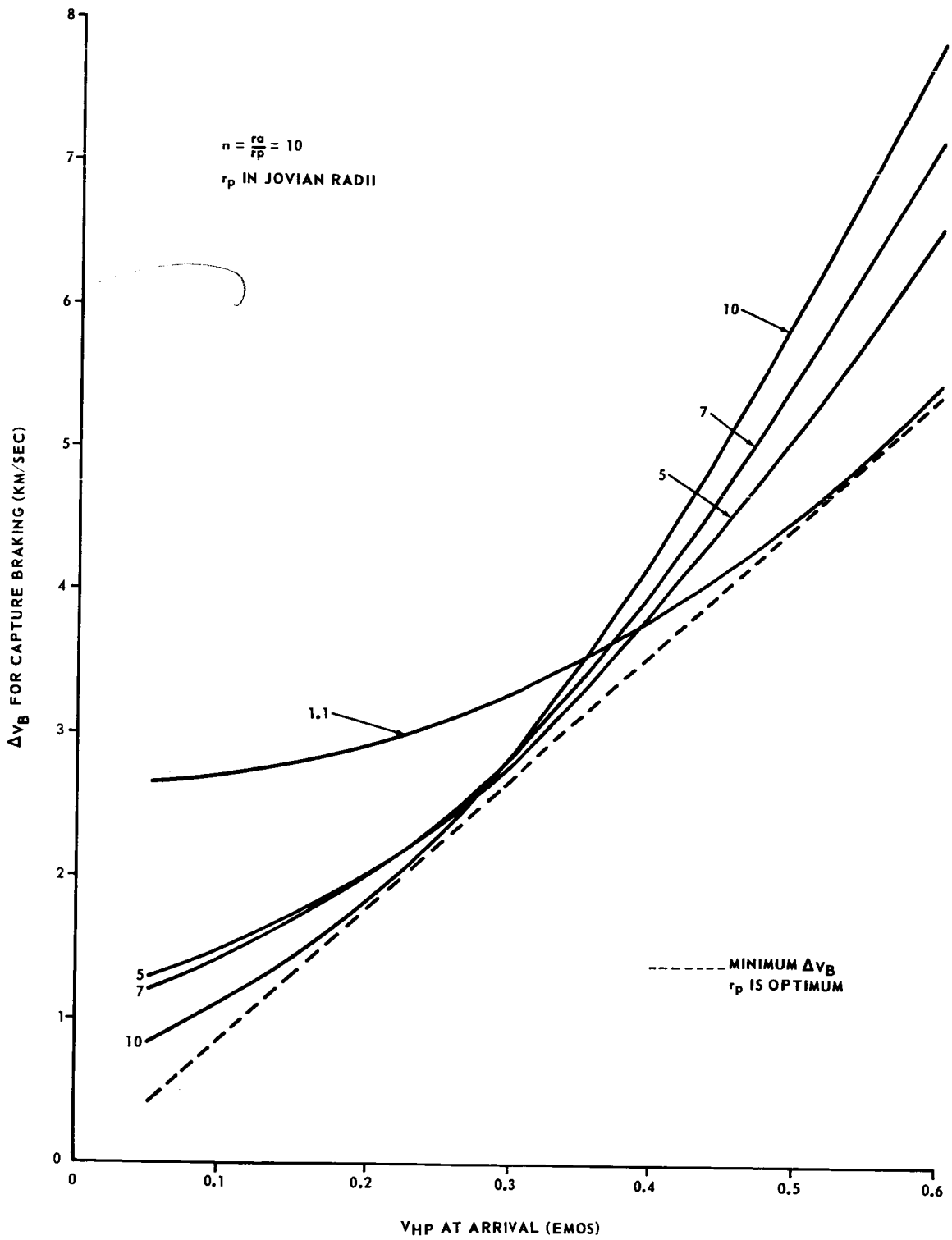


FIGURE II-13. VELOCITY INCREMENT REQUIRED FOR JOVIAN  
 CAPTURE MANEUVER -  $n = 10$



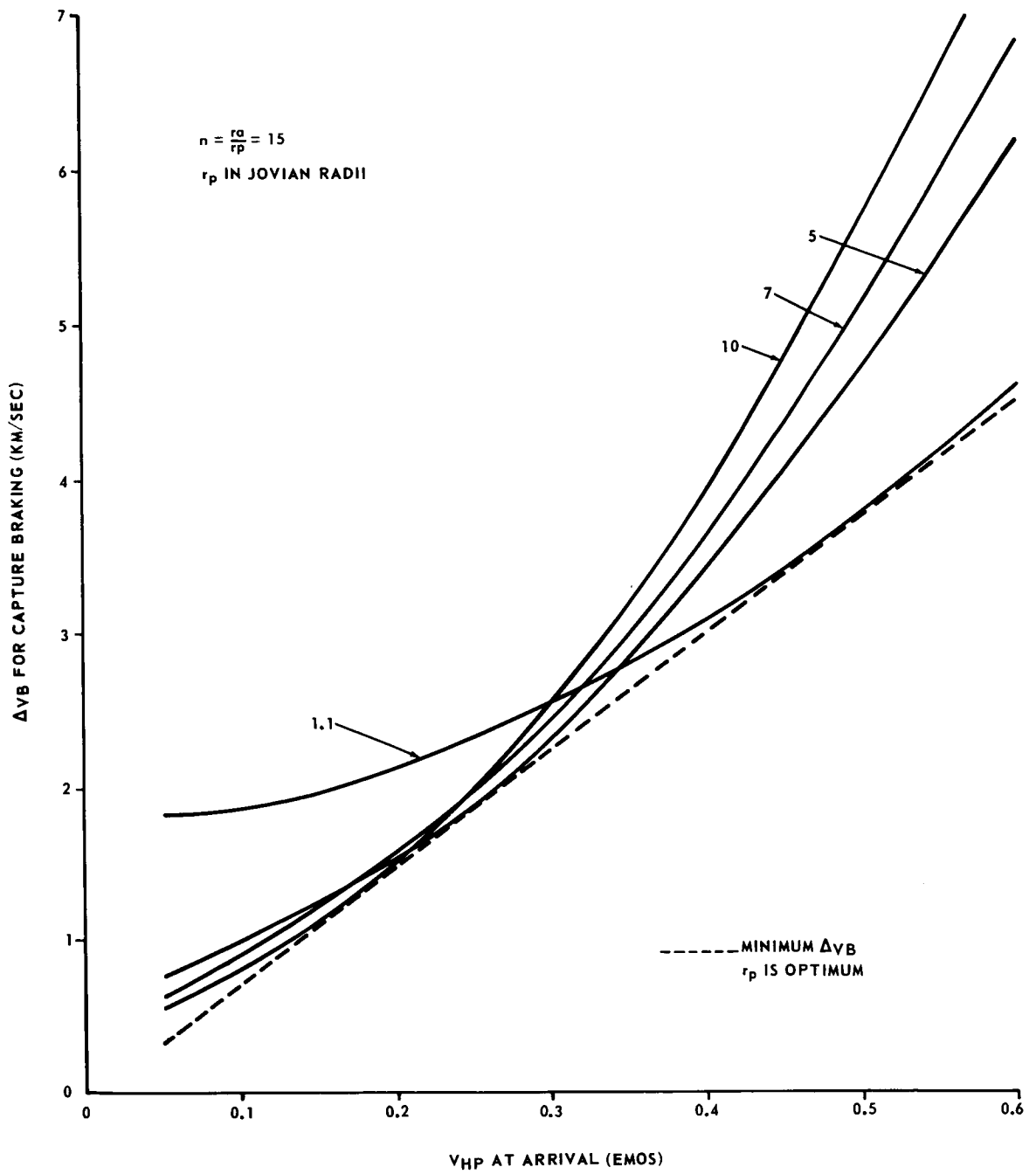


FIGURE II-14. VELOCITY INCREMENT REQUIRED FOR JOVIAN CAPTURE MANEUVER -  $n = 15$

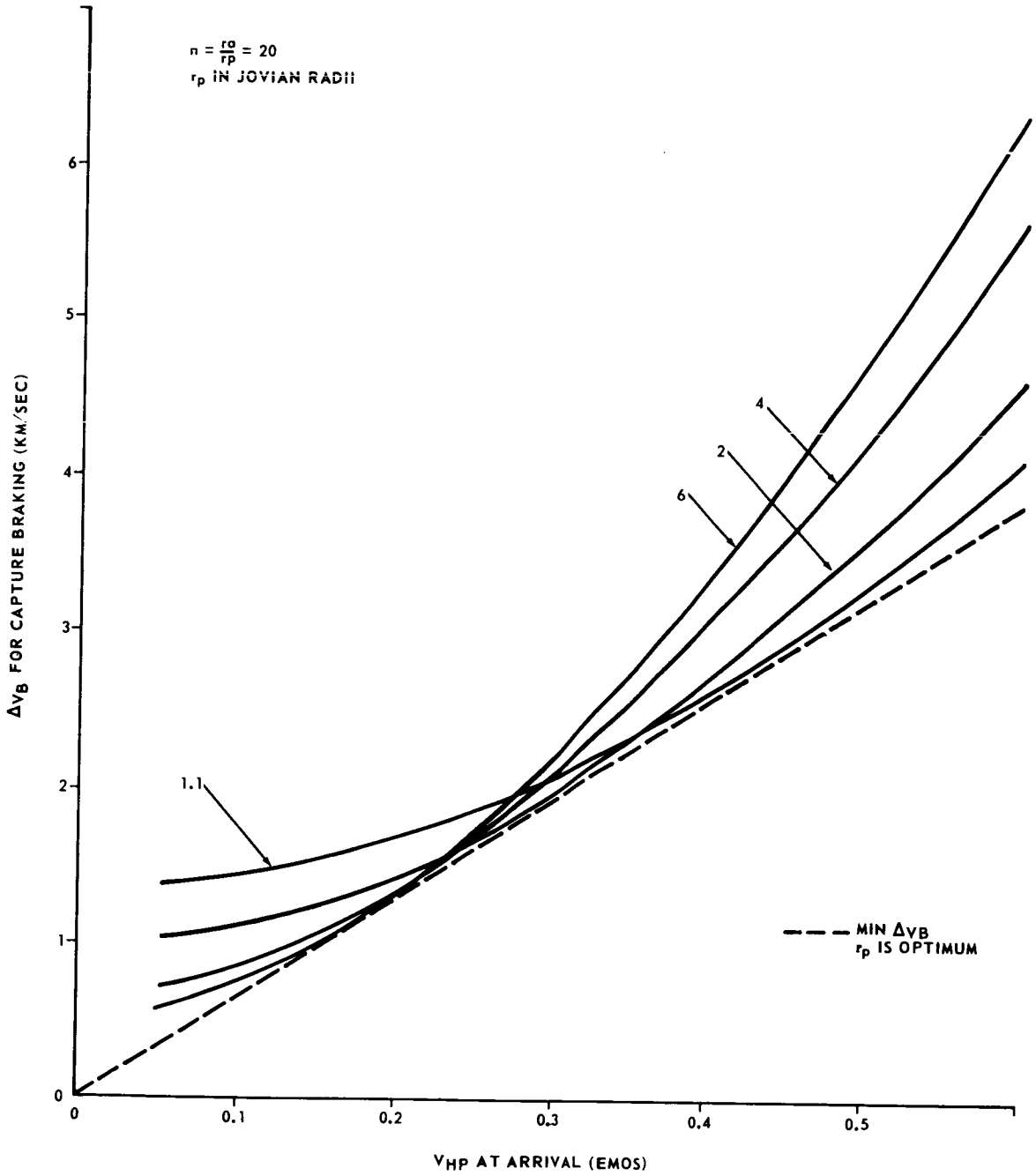


FIGURE II-15. VELOCITY INCREMENT REQUIRED FOR JOVIAN CAPTURE MANEUVER -  $n = 20$

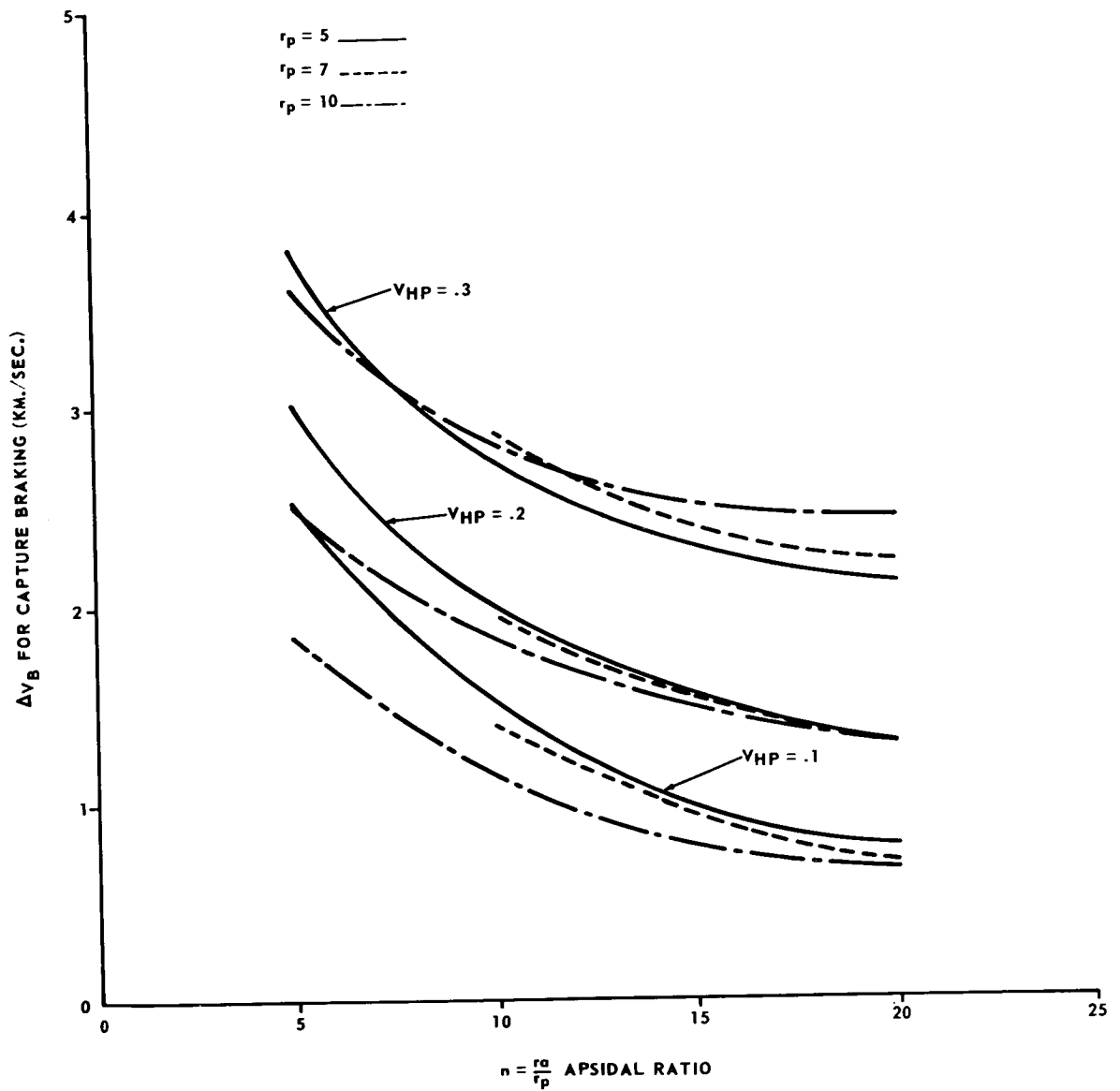


FIGURE II-16. EFFECT OF APSIDAL RATIO ON BRAKING REQUIREMENT

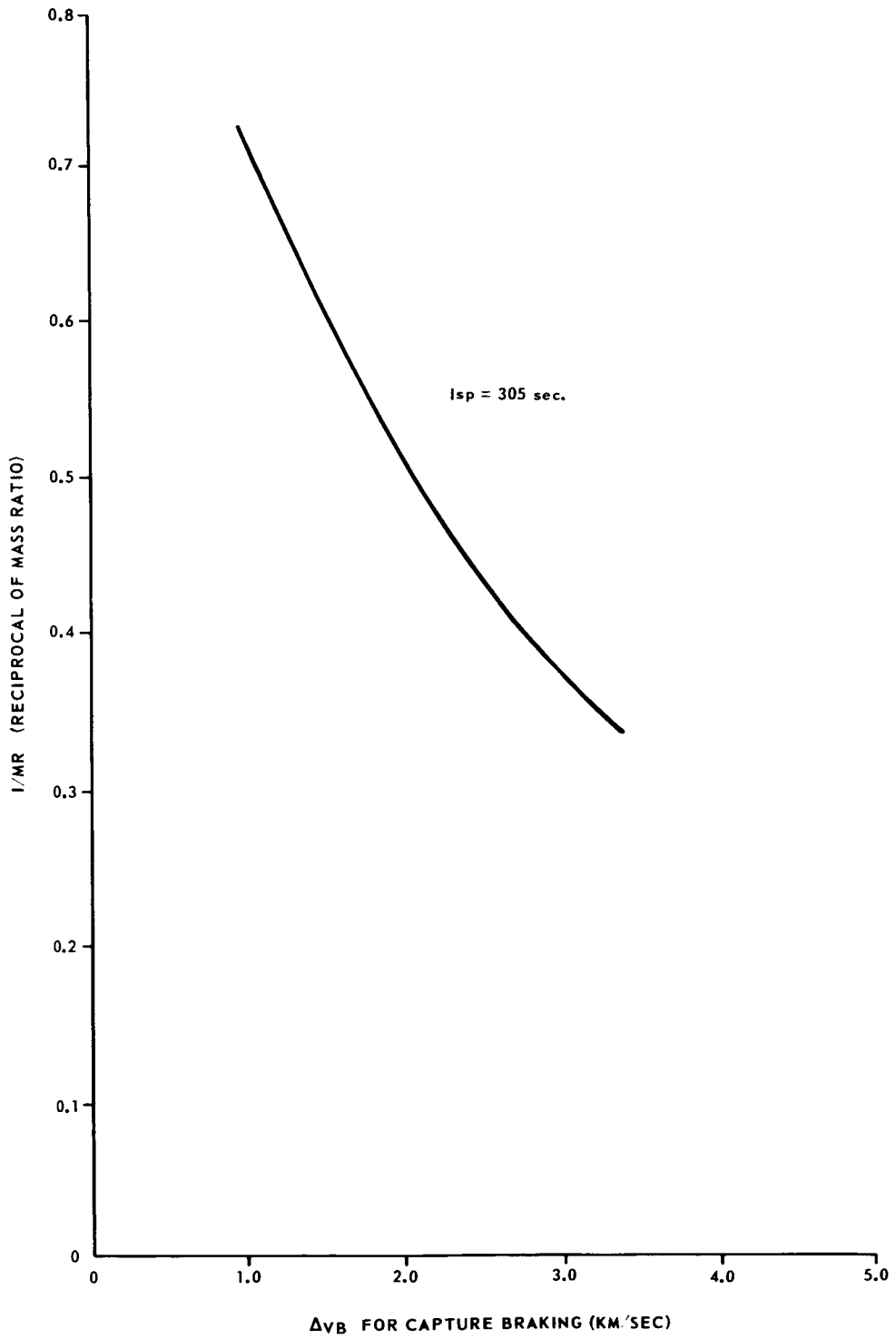


FIGURE II-17. MASS FRACTION VARIATION WITH BRAKING IMPULSE

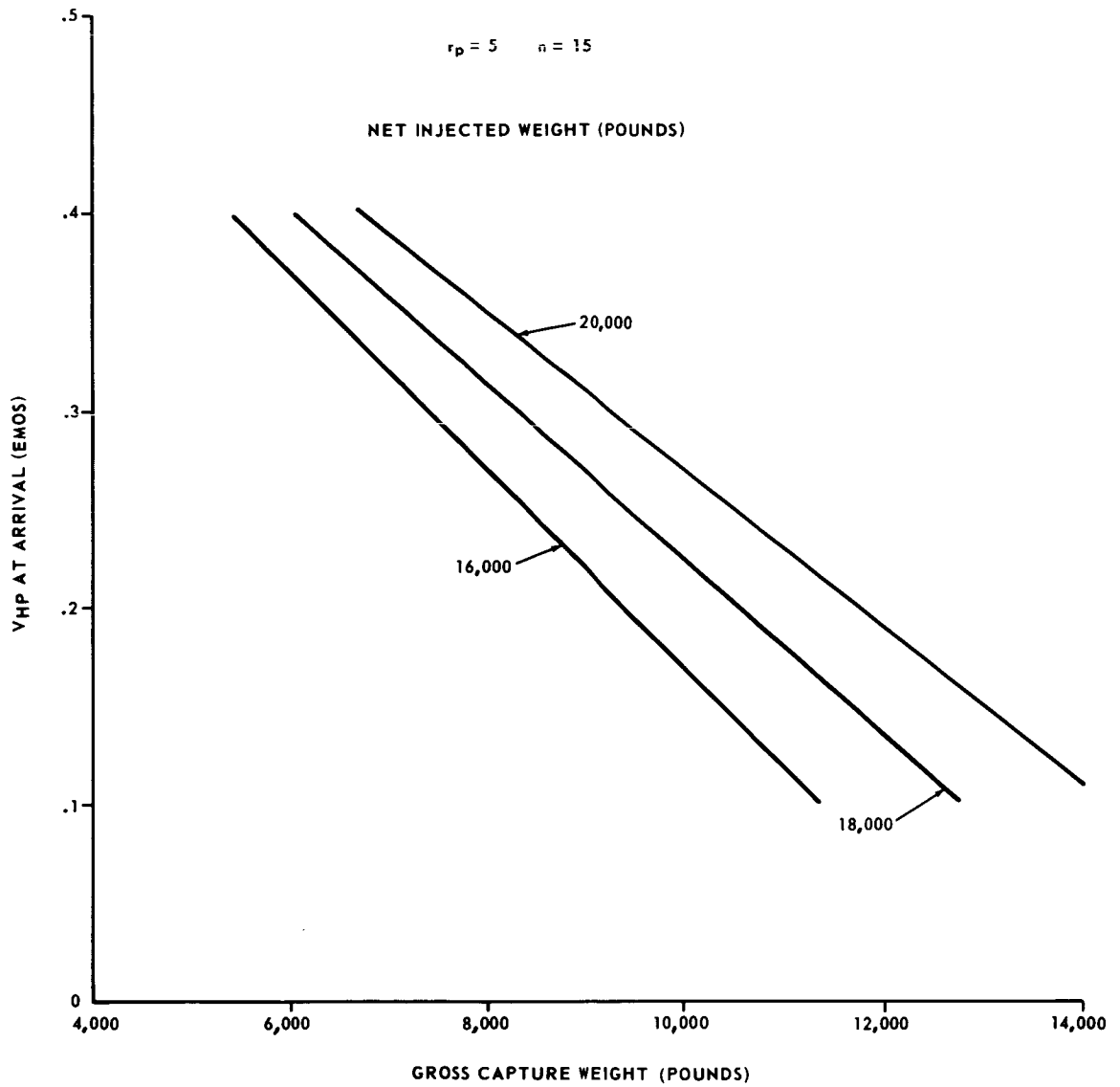


FIGURE II-18. PARAMETRIC CAPTURE BRAKING PERFORMANCE -  
 $r_p = 5R_4$ ,  $n = 15$

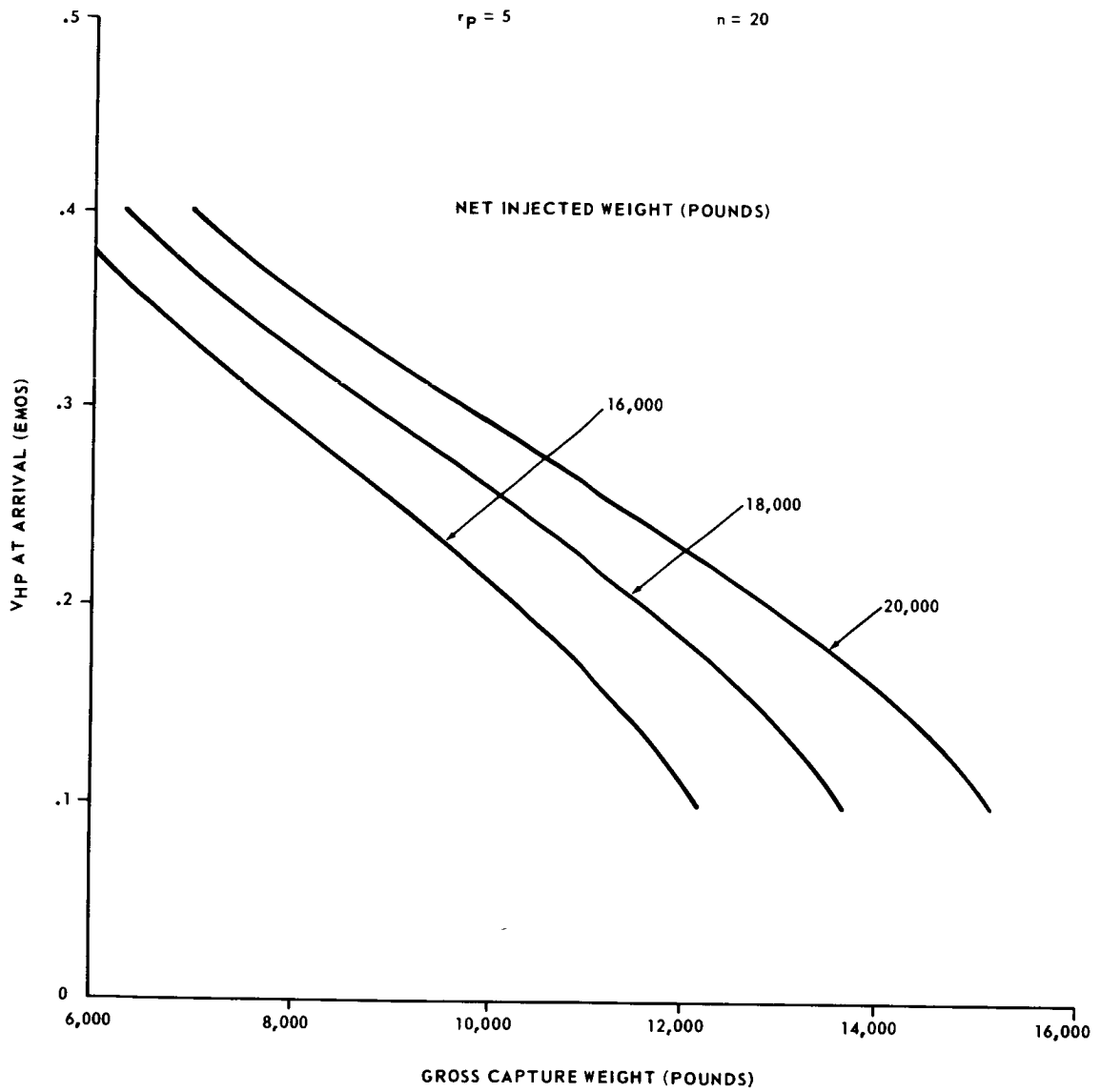


FIGURE II-19. PARAMETRIC CAPTURE BRAKING PERFORMANCE -  
 $r_p = 5R_4, n = 20$

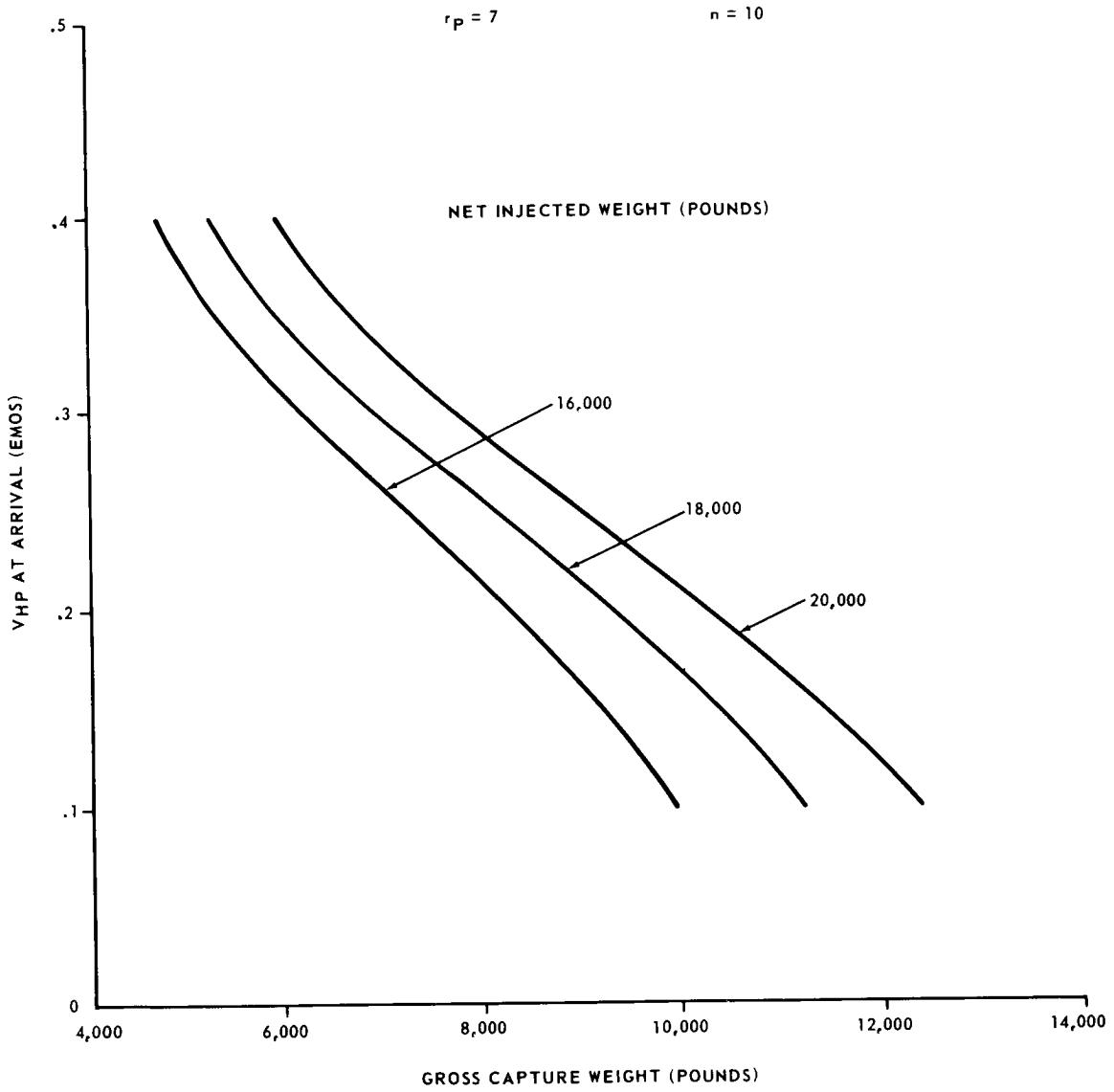


FIGURE II-20. PARAMETRIC CAPTURE BRAKING PERFORMANCE -  
 $r_p = 7R_4$ ,  $n = 10$

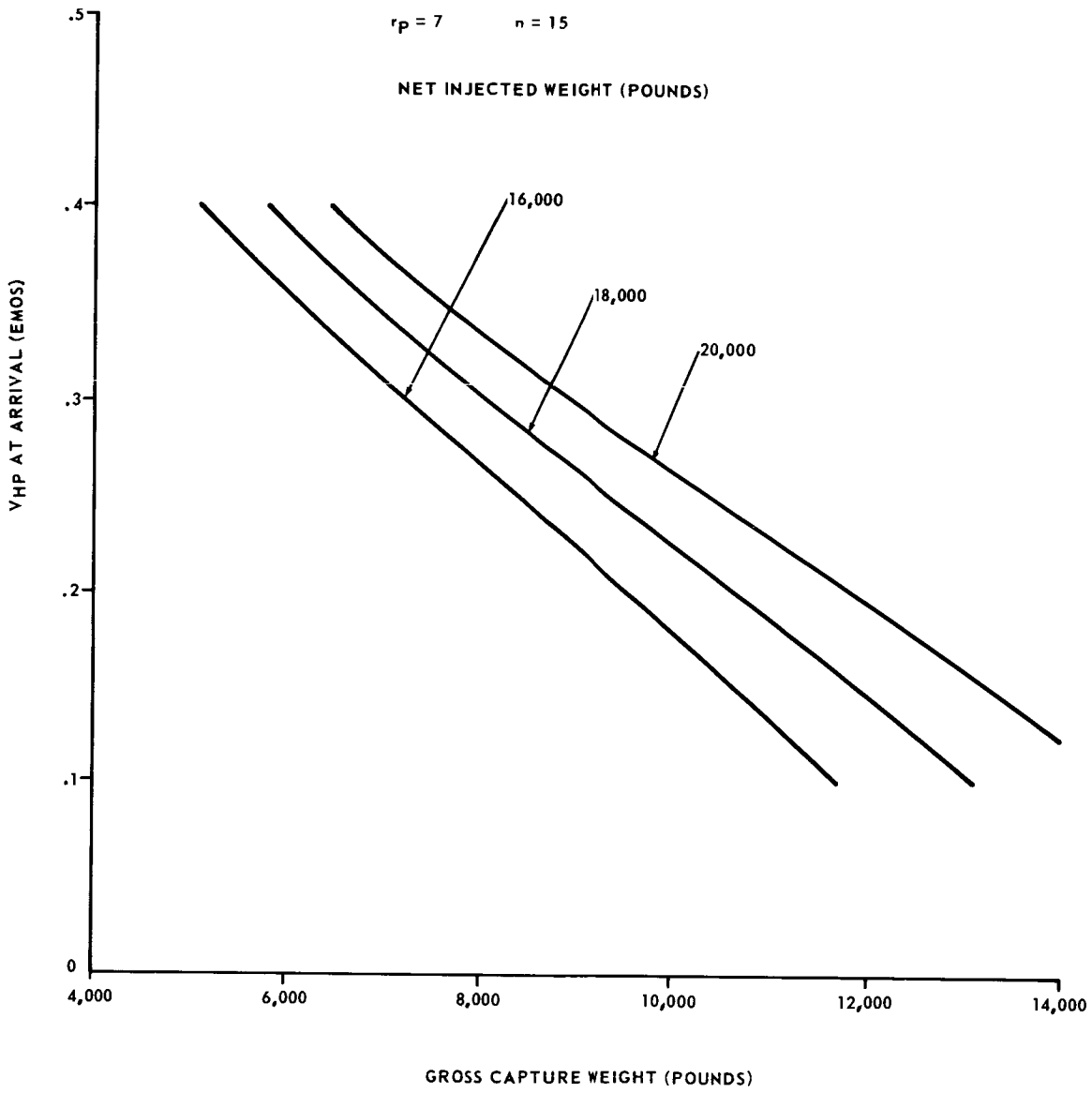


FIGURE II-21. PARAMETRIC CAPTURE BRAKING PERFORMANCE -  
 $r_p = 7R_4$ ,  $n = 15$



$$\text{where } n_1 = \frac{ra}{r_{p1}} \quad (9)$$

$$n_2 = \frac{ra}{r_{p2}} \quad (10)$$

The total velocity impulse required to establish the dual capture orbit is therefore

$$\Delta V_{\text{total}} = \Delta V_B + \Delta V_{a_1} \quad (11)$$

Hence, the retropropulsion engine needs to provide

$$\Delta V_{\text{total}} = g I_{sp} \ln [(\text{MR})_1 (\text{MR})_2] \quad (12)$$

where

$$(\text{MR})_1 = \frac{\text{Weight at arrival}}{\text{Gross capture weight in orbit 1}} \quad (13)$$

$$(\text{MR})_2 = \frac{\text{Gross capture weight in orbit 1}}{\text{Gross capture weight in orbit 2}} \quad (14)$$

$$\text{Thus, } (\text{MR})_1 (\text{MR})_2 = \frac{\text{Weight at arrival}}{\text{Gross capture weight in orbit 2}} \quad (15)$$

As a result, a parametric study similar to the one examined for the single capture orbit mission was made and is shown in Figures II-22 through II-25 for a selected number of dual orbit maneuvers.

The orbital period for the vehicle in the capture orbit is given by the following expression

$$P = \frac{2\pi}{\sqrt{GM}} \left[ \frac{r_p}{2} (n+1) \right]^{3/2} \quad (16)$$

This is plotted in Figure II-26.

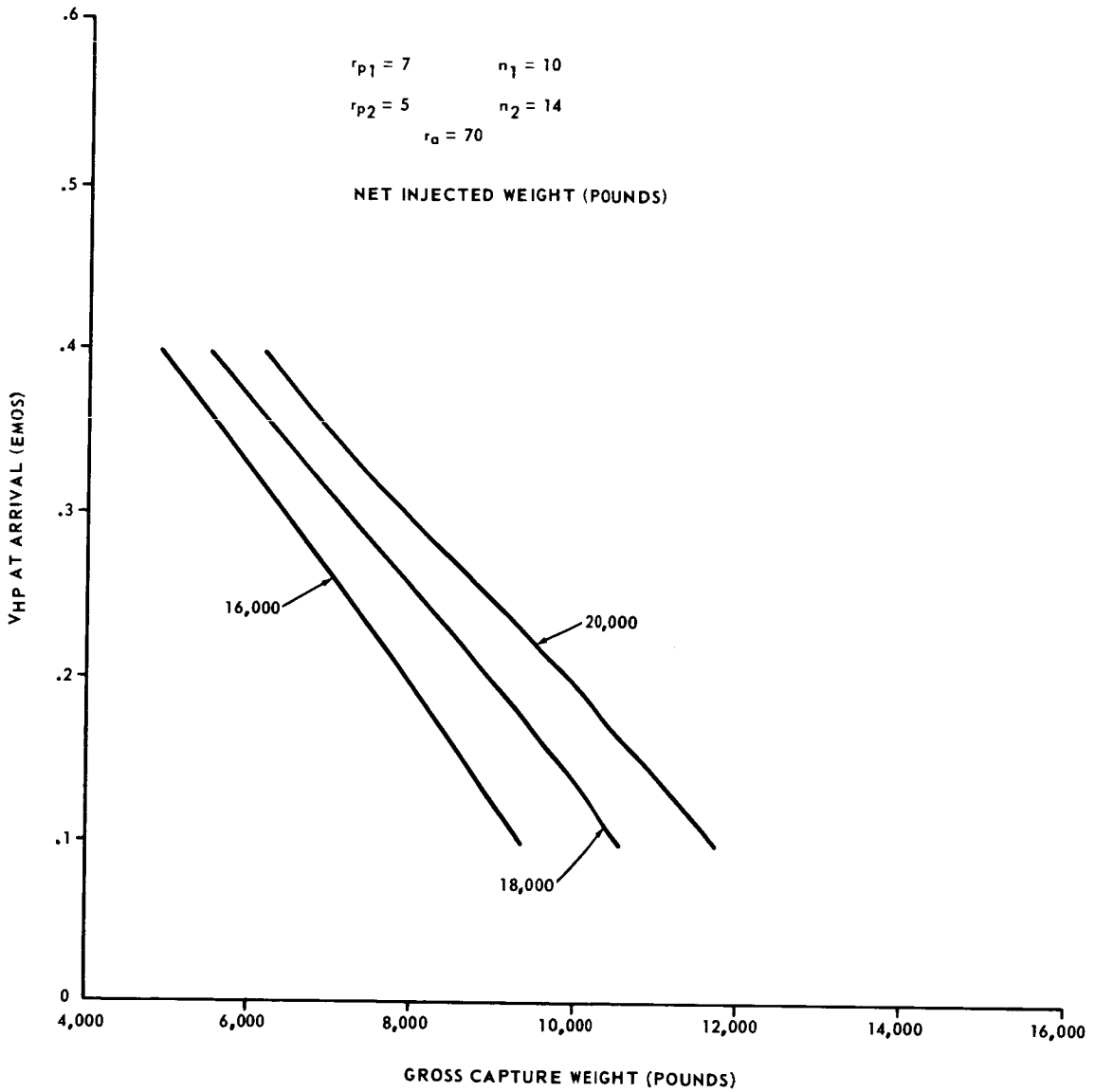


FIGURE II-22. PARAMETRIC CAPTURE BRAKING PERFORMANCE -  
 $r_{p2} = 5R_4$  ,  $n_2 = 14$

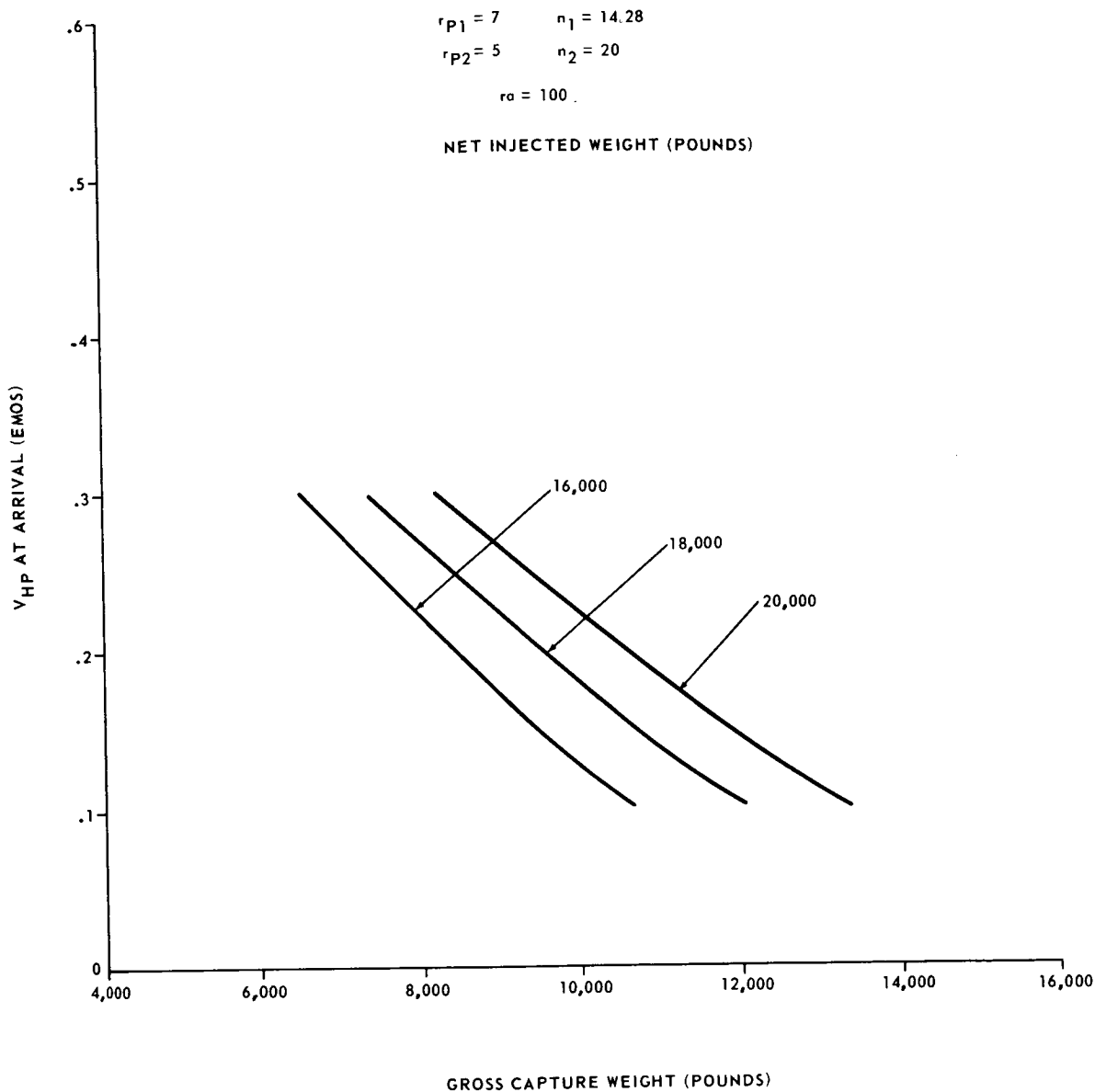


FIGURE II-23. PARAMETRIC CAPTURE BRAKING PERFORMANCE -  
 $r_{p1} = 7R_4$  ,  $n_1 = 14.28$  and  $r_{p2} = 5R_4$  ,  $n_2 = 20$

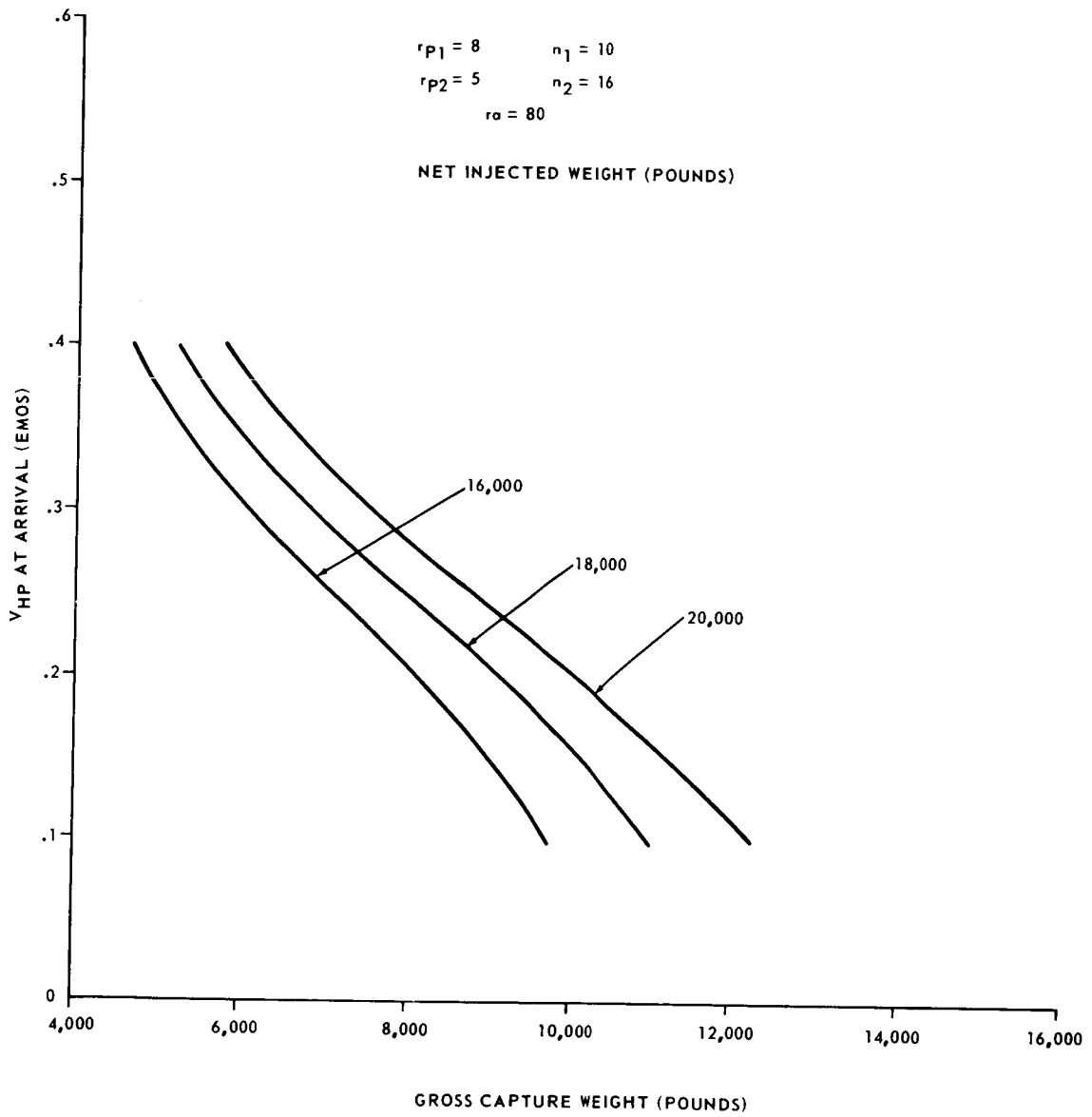


FIGURE II-24. PARAMETRIC CAPTURE BRAKING PERFORMANCE -  
 $r_{p1} = 8R_4$  ,  $n_1 = 10$  and  $r_{p2} = 5R_4$  ,  $n_2 = 16$

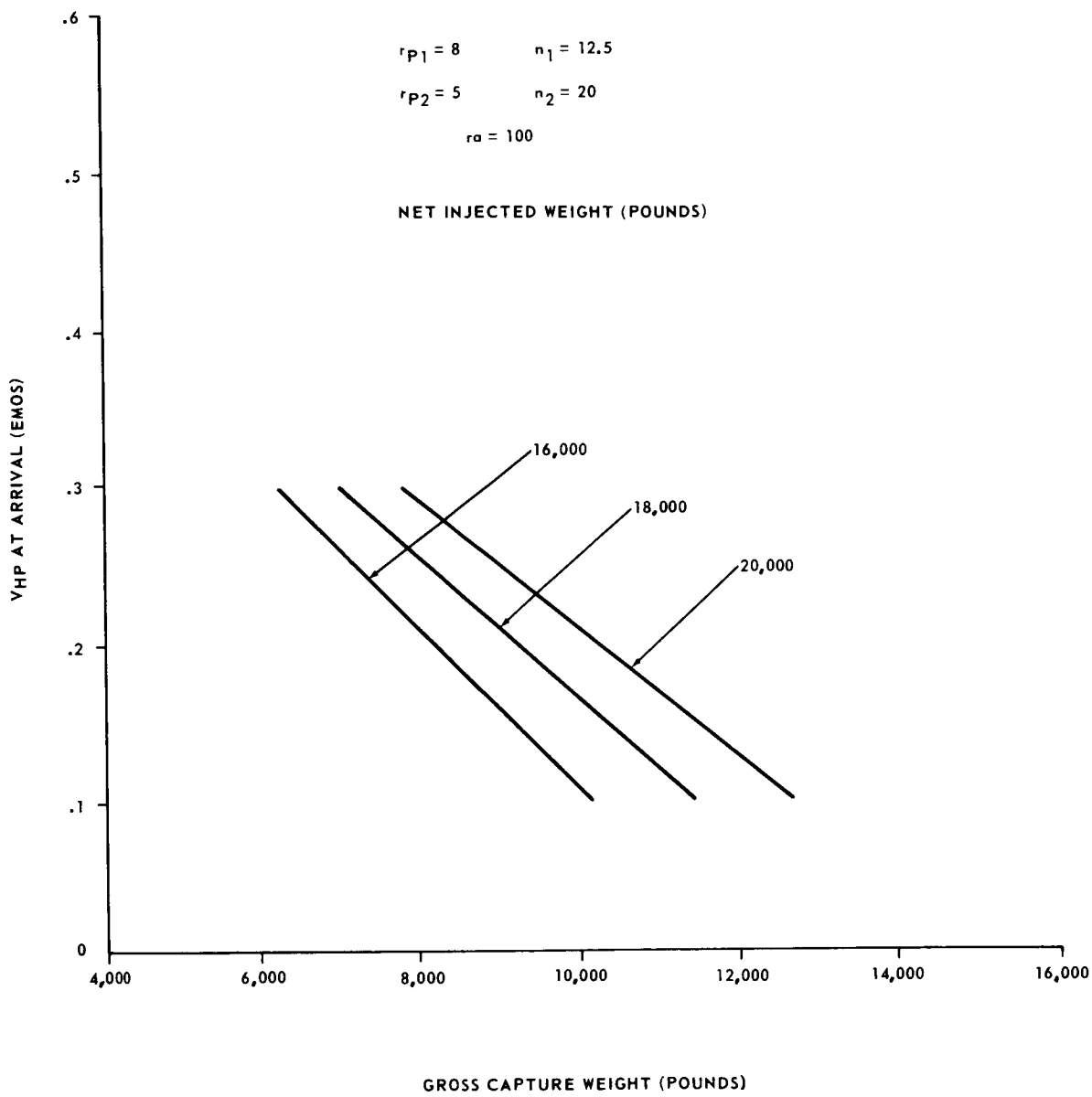


FIGURE II-25. PARAMETRIC CAPTURE BRAKING PERFORMANCE -  
 $r_{p1} = 8R_4$  ,  $n_1 = 12.5$  and  $r_{p2} = 5R_4$  ,  $n_2 = 20$

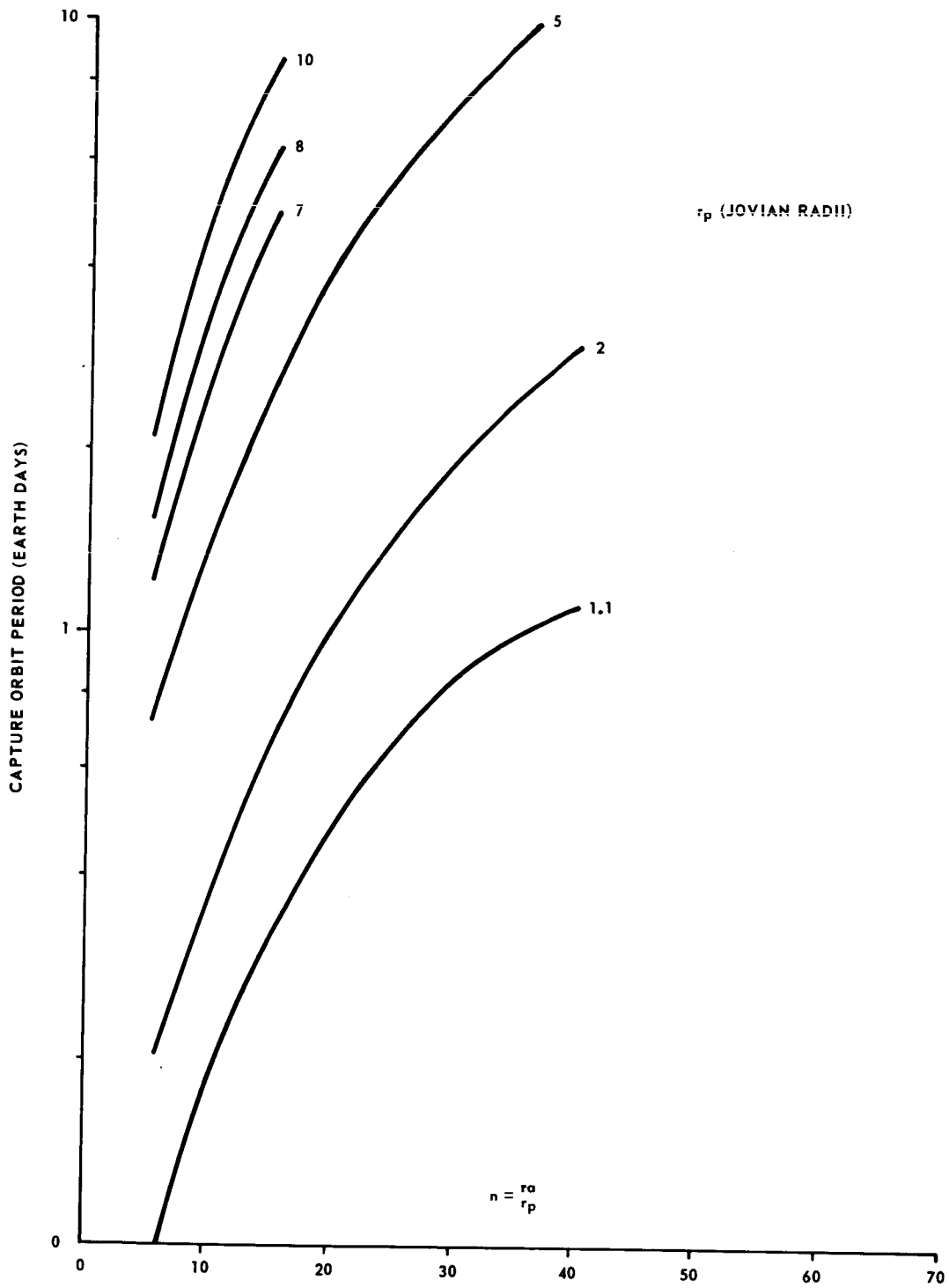


FIGURE II-26. JOVIAN CAPTURE ORBIT PERIOD AS A FUNCTION OF APSIDAL RATIO

## Mission Parametric Study

The material presented in the previous sections on launch capabilities, transfer trajectories, and capture orbit conditions is brought together in this section to analyze the overall mission performance. This analysis concentrates on the 1978 and 1980 launch opportunities as representative of the 1975-1980 time period of prime interest.

A block diagram illustrating the interrelationship among the three trajectory phases is shown in Figure II-27. The launch conditions determine the net injected weight onto the transfer trajectory and the arrival conditions coupled with the specified capture orbit determine the necessary braking velocity impulse. When this information is tied into the retropropulsion system performance, the gross weight in the capture orbit is obtained and ultimately the useful payload remains.

A parametric study for a wide variety of launch and capture orbit conditions can be made using a schematic as shown in Figure II-28. Curves of  $C_3$  ( $C_3 = V_{HD}^2$ ) and hyperbolic excess velocity at arrival,  $V_{HP}$ , versus launch date with trip time as a parameter for each launch opportunity are required and shown as graphs (1) and (2), respectively.

For a given launch window and trip time the required  $C_3$  is obtained along with the  $V_{HP}$  at arrival. From a plot of the Saturn V capabilities, illustrated in graph 3, the net injected weight for the corresponding  $C_3$  is available. For a given capture orbit,  $r_p$  and  $n$  specified, and the  $V_{HP}$  and weight at arrival obtained from the above steps, the gross capture weight can be read from graph (4). The difference between the net injected weight and the weight at arrival is the weight required for mid-course corrections and attitude control during the coast phase. Subtracting the spacecraft inert weight from the gross capture weight leaves the weight for the useful payload in orbit.

This type of analysis permits a great deal of flexibility in examining a large number of launch conditions, trip times, and capture orbits. This permits a number of trade-off analyses to be made, continuing to recognize that a short trip time improves reliability and enhances the probability of mission success.

Such a parametric study was conducted to analyze the JOVE mission. One of the items of primary interest was the maximum gross weight which could be placed in a Jovian capture orbit. The effect of trip time on this was examined for some selected capture orbits using the parametric method. The results of this study are shown in Figures II-29 through II-32. In general, the gross

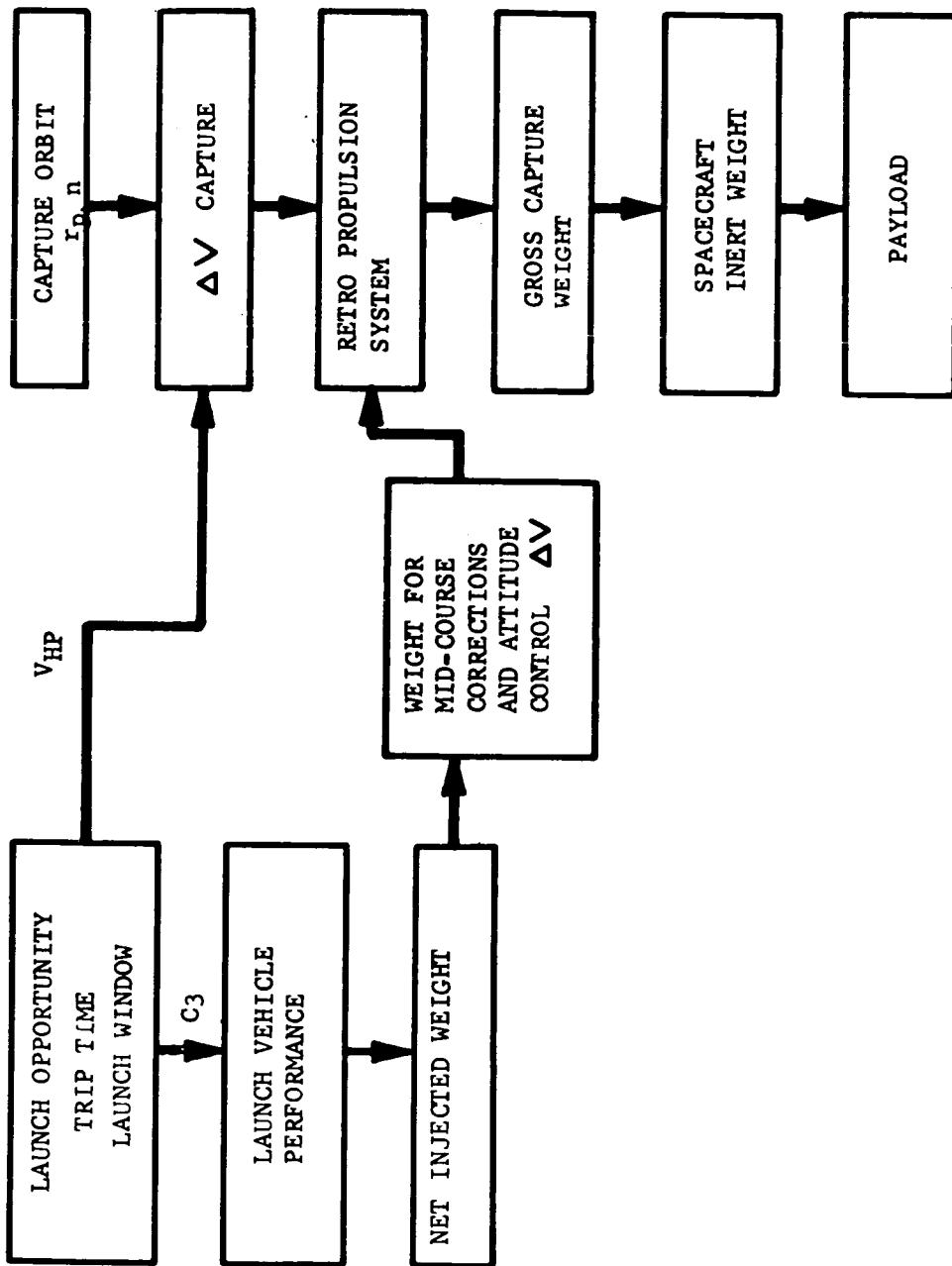


FIGURE II-27. MISSION ANALYSIS BLOCK DIAGRAM



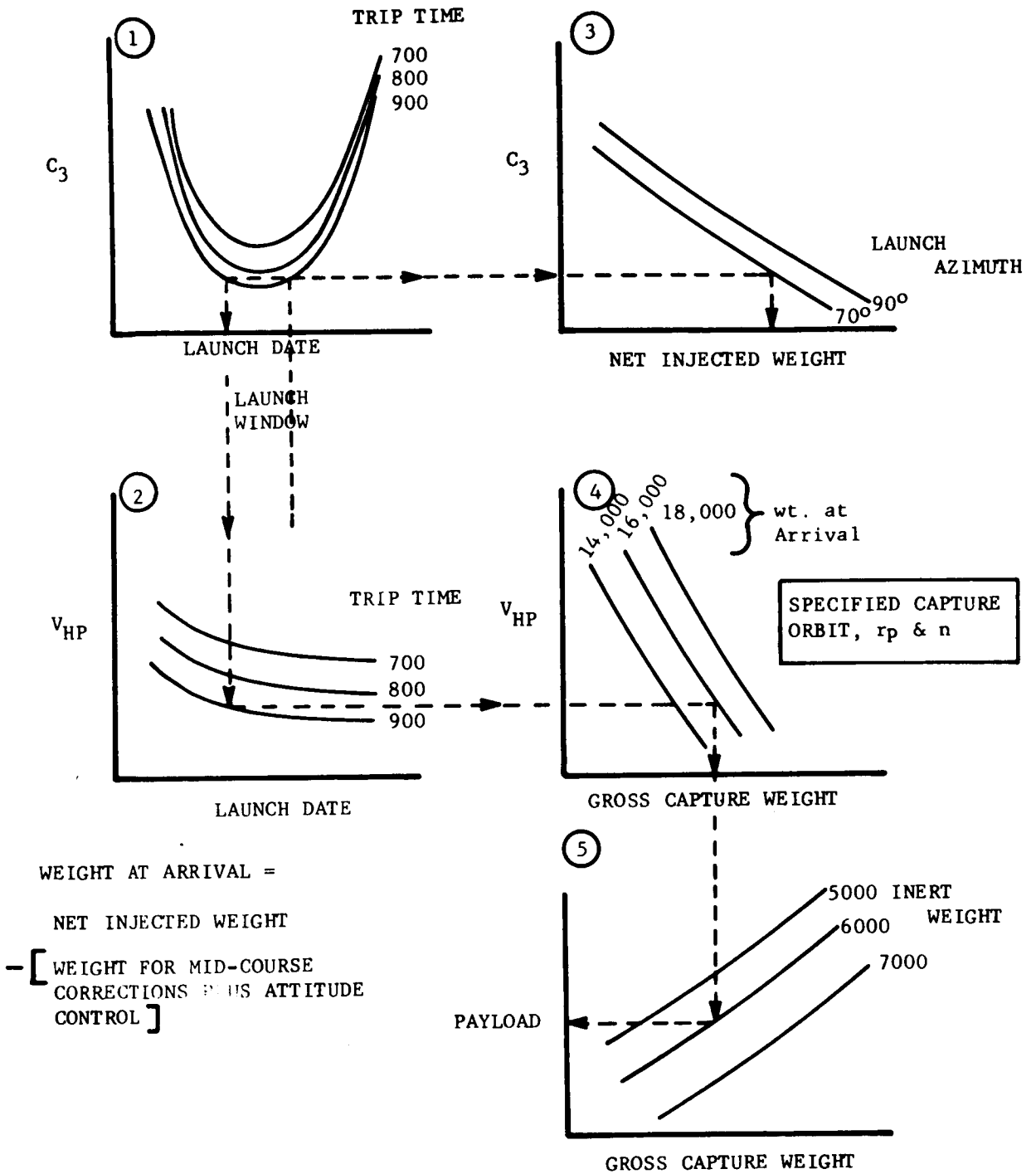


FIGURE II-28. PARAMETRIC MISSION ANALYSIS DIAGRAM

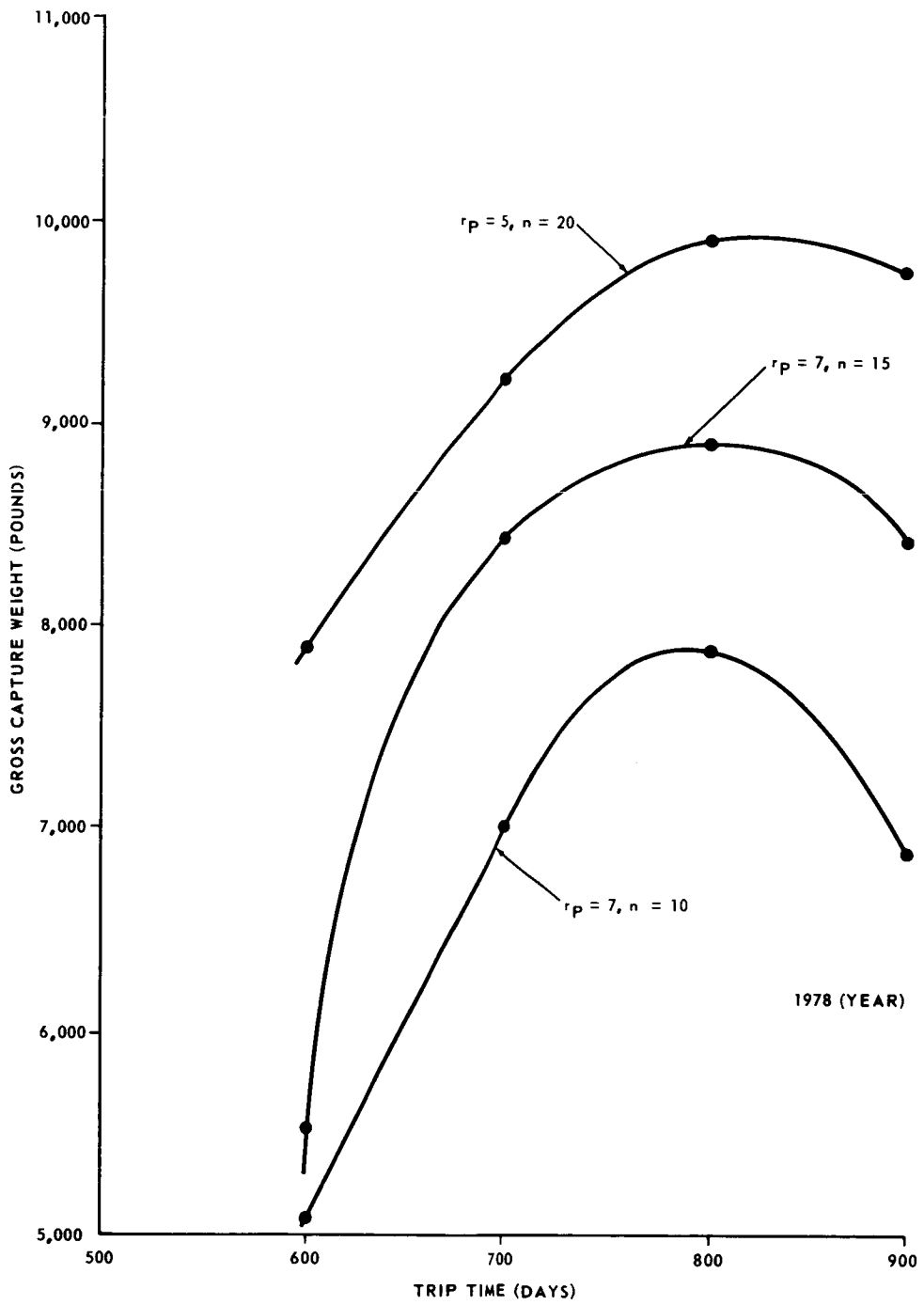


FIGURE II-29. EFFECT OF TRIP TIME ON GROSS CAPTURE WEIGHT - SINGLE ORBIT - 1978

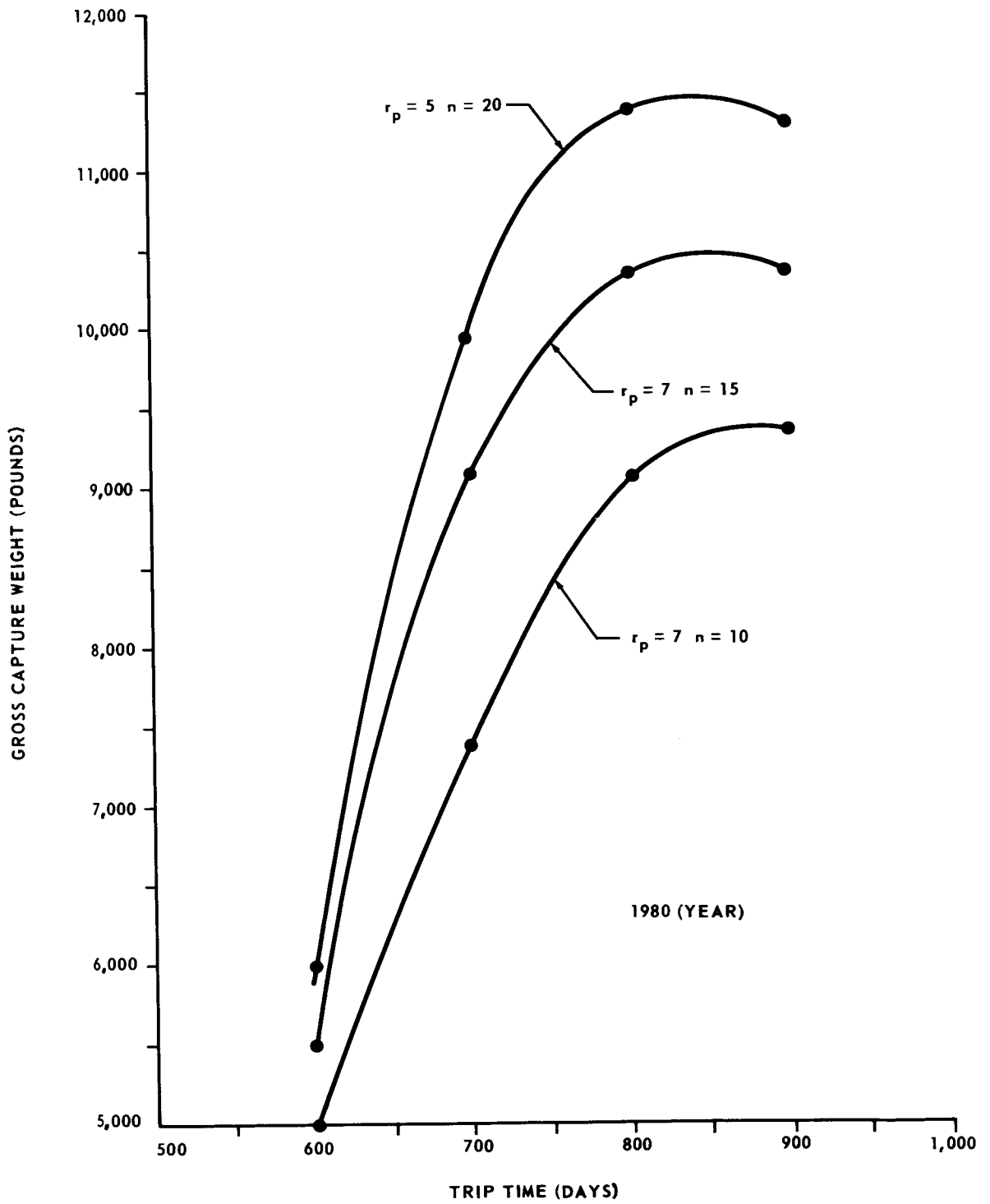


FIGURE II-30. EFFECT OF TRIP TIME ON GROSS CAPTURE WEIGHT - SINGLE ORBIT - 1980

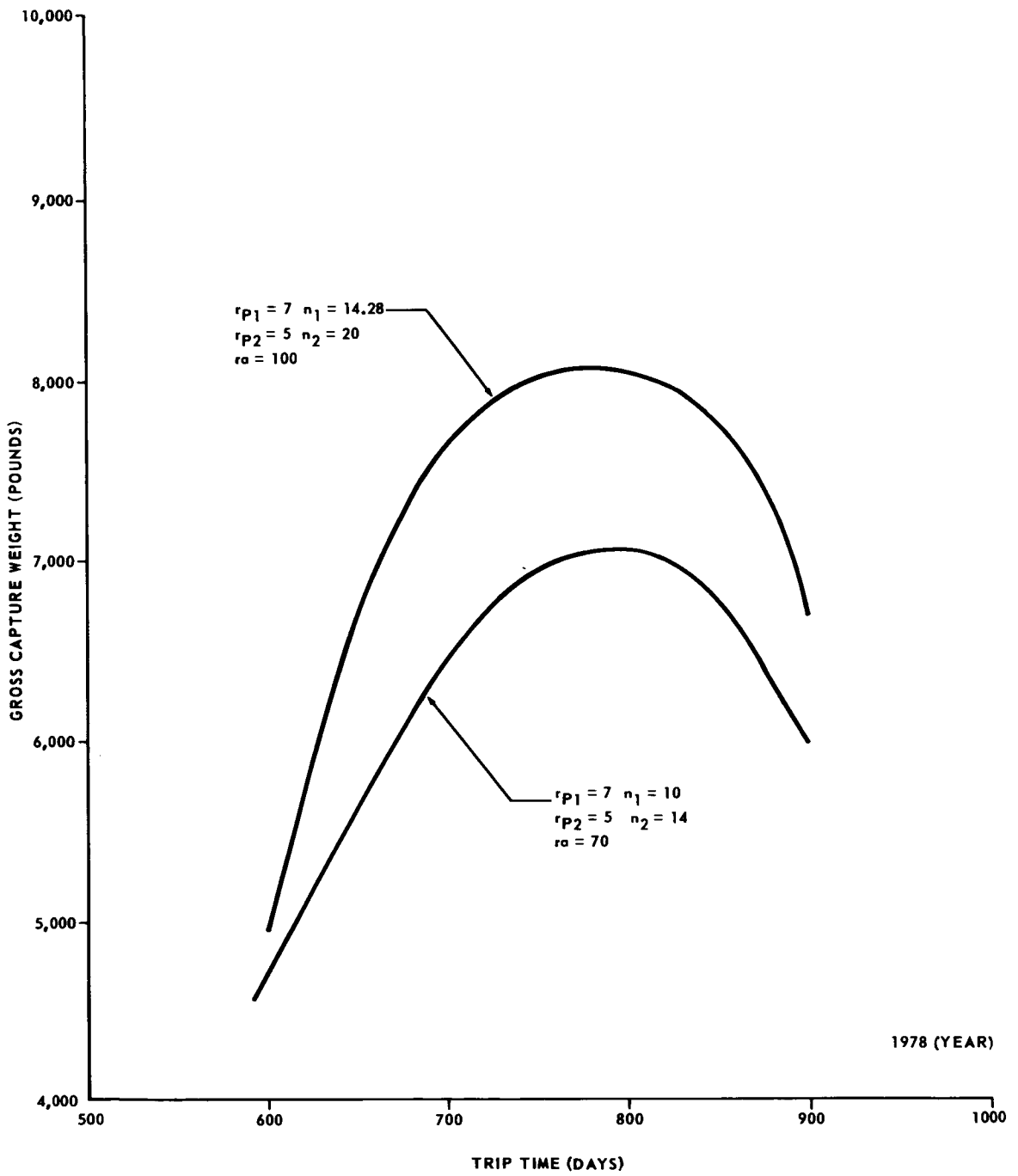


FIGURE II-31. EFFECT OF TRIP TIME ON GROSS CAPTURE WEIGHT - DUAL ORBIT - 1978

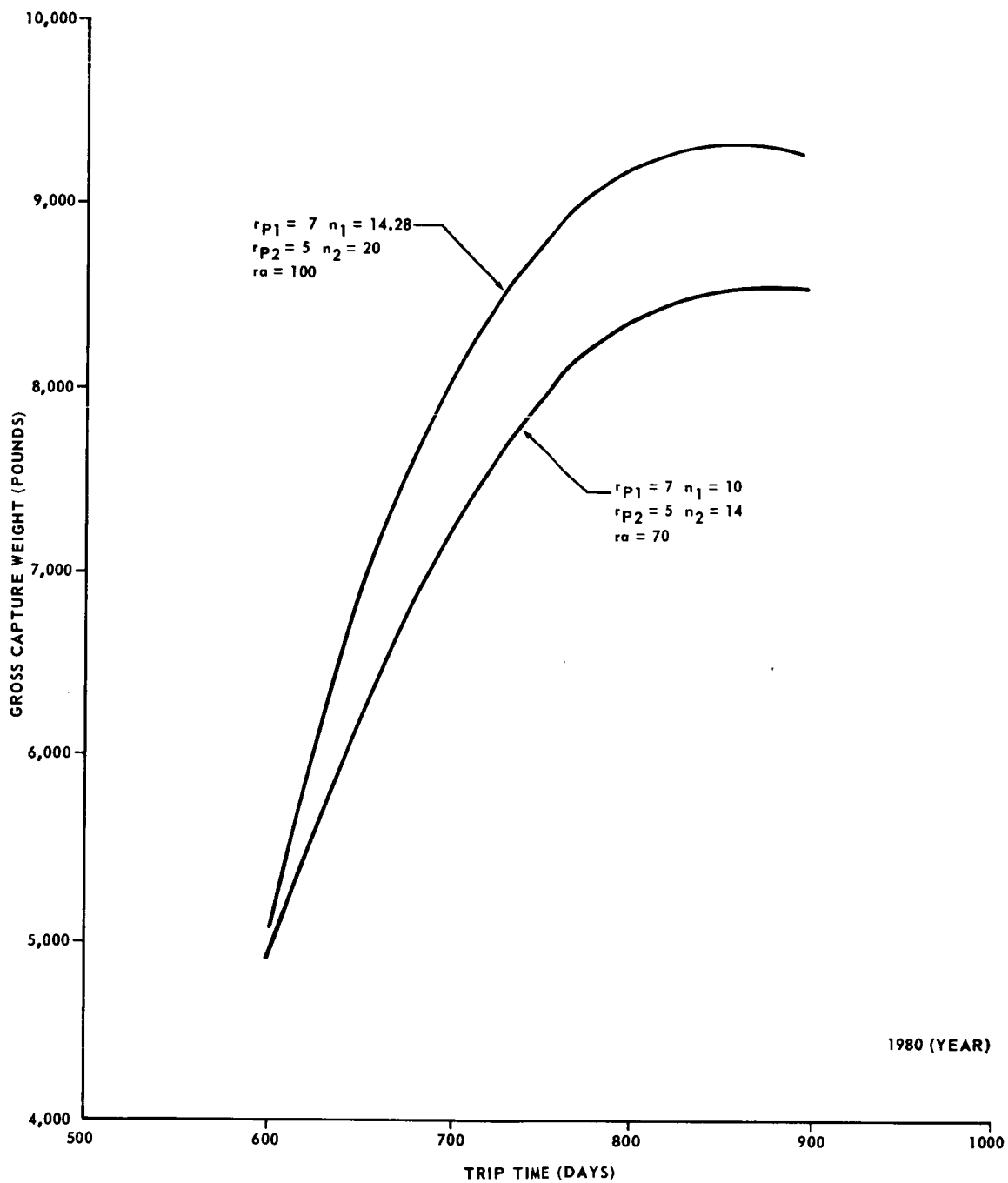


FIGURE II-32. EFFECT OF TRIP TIME ON GROSS CAPTURE WEIGHT - DUAL ORBIT - 1980

capture weight increases with increasing trip time, reaching a maximum near an 800 day trip time. Hence, it was decided to examine the details of an 800 day trip for JOVE more thoroughly.

The above mentioned graphs can be used in several other ways. If the gross capture weight is specified, then the trip time corresponding to the desired capture orbit can be obtained. Or, if the trip time and gross capture weight are specified, then the capture orbit apsidal ratio can be estimated quite accurately. The effect of decreasing the apsidal ratio is readily seen from these figures.

One item to be concerned with in mission planning is the relative positions of the Earth, spacecraft, Sun, and Jupiter throughout the expected mission lifetime. This plays a large role in determining communication capabilities, attitude control requirements, and spacecraft thermal control. These constellations were calculated for an 800 day trip during the 1980 launch opportunity. To perform such calculations it is necessary to know the semi-major axis and eccentricity of the transfer trajectory as well as the orientation of the transfer trajectory. This information is available for a particular mission in NASA SP-35, Volume 3, Part 5, "Space Flight Handbook," 1966. Using this information together with Kepler's equation relating position and time, and the polar form of the orbit equation, the variation of the angular position and the magnitude of the radius vector with travel time can be plotted as in Figure II-33. From this information, a diagram illustrates the relative positions of the Earth, Jupiter, and the spacecraft JOVE throughout the mission (Fig. II-34). Two items are of significance for this 800 day mission.

a. The Sun-Spacecraft-Earth angle,  $\alpha$ , is quite large at arrival and the communication distance is about average. This is further illustrated in Figure II-35.

b. During the expected orbital lifetime of JOVE, about 90 days, the angle  $\alpha$  does not become zero and the communication distance continually decreases.

Both of these points are important from a communication standpoint. When  $\alpha$  becomes zero either there is a Sun occultation by the Earth or an Earth occultation by the Sun. The latter means that the Earth-spacecraft communication is degraded to some extent. Both of these conditions are undesirable at arrival and during the orbital lifetime. Figure II-35 indicates that there will be two Sun occultations, one at about 80 days after launch and one at about 535 days. Also, there are two Earth occultations at 320 days and at 720 days after launch. On this figure, the distance of the spacecraft from the Sun is shown and below it the communication distance.

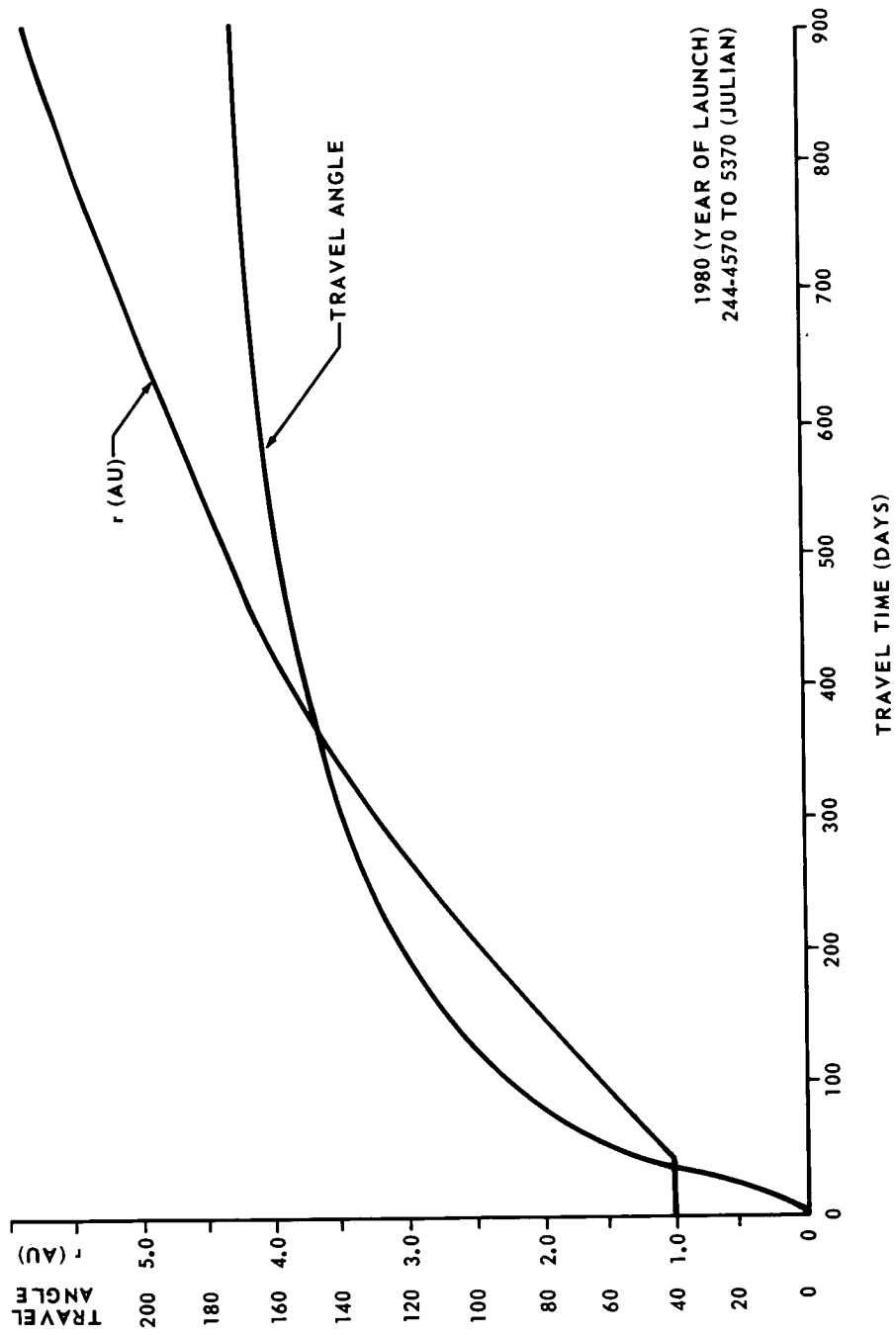


FIGURE II-33. TRAVEL ANGLE AND POSITION TIME HISTORY -  
800 DAY 1980

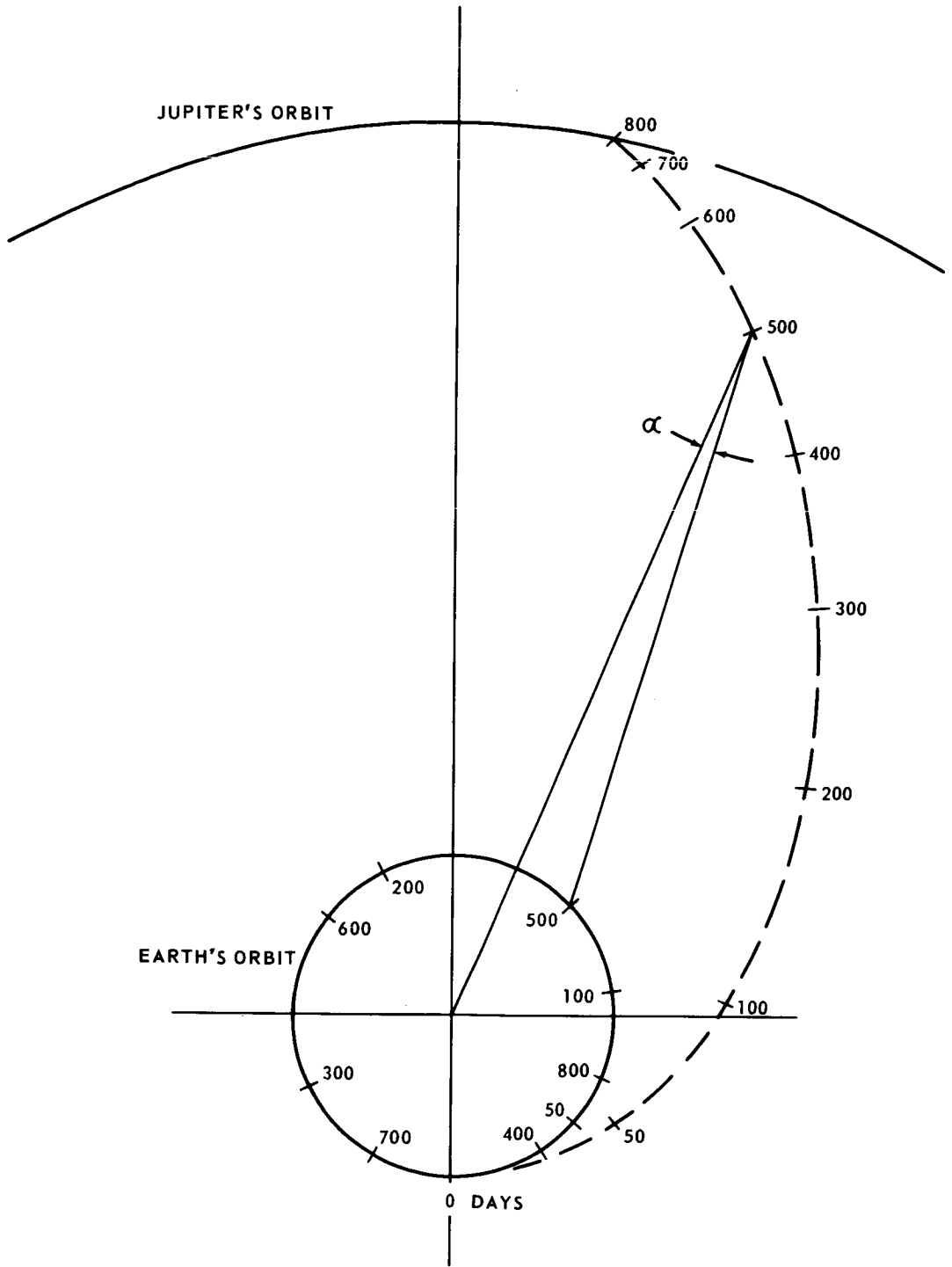


FIGURE II-34. 800 DAY MISSION TRAJECTORY



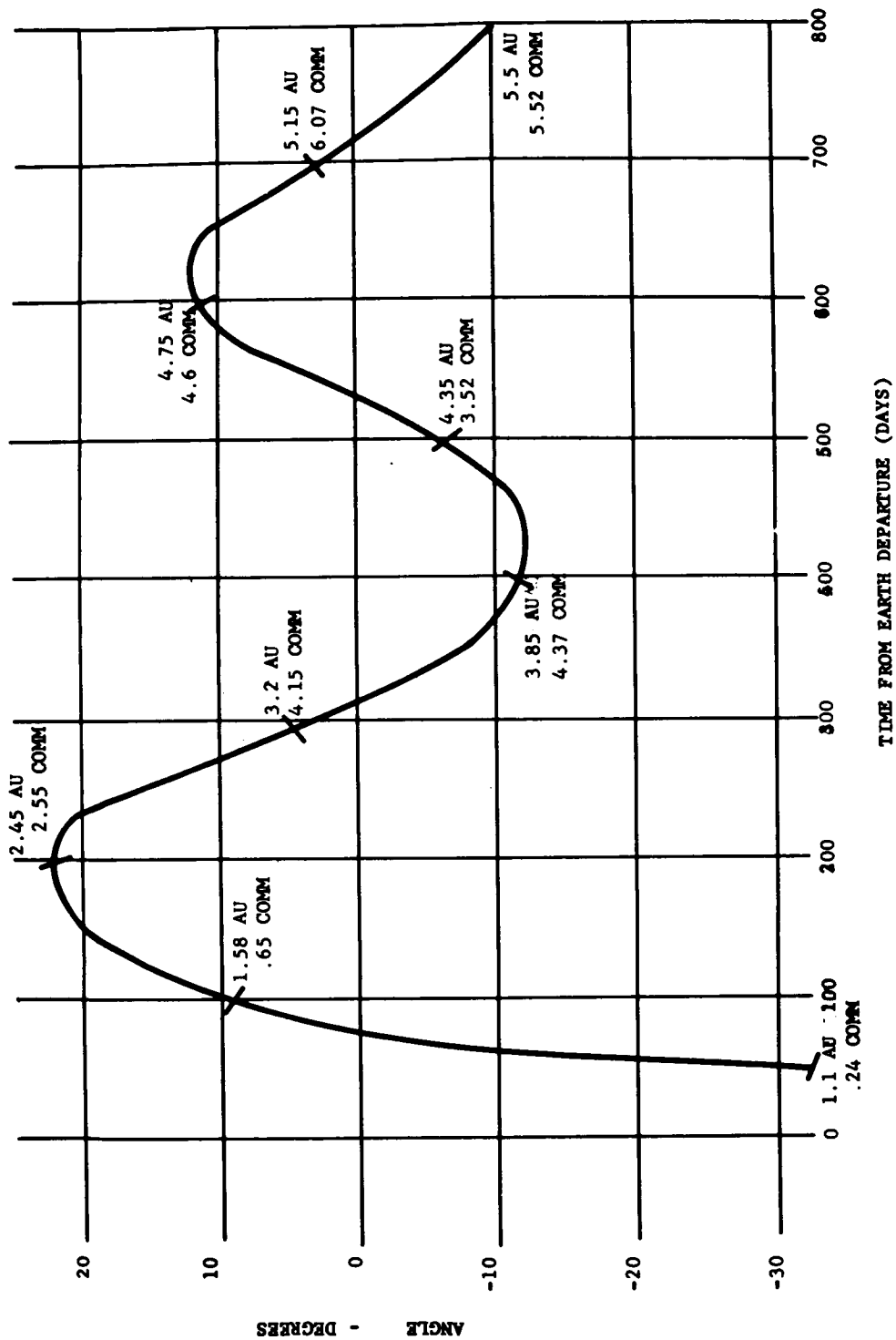


FIGURE II-35. SUN - SPACECRAFT - EARTH ANGLE TIME HISTORY - 800 DAY 1980

The mid-course corrections must also be planned so as to avoid the occultation points so that good tracking data will be available.

## Planet Approach and Targeting

The orientation of the capture orbit will depend primarily upon the hyperbolic excess approach asymptote. The plan for the JOVE mission is to place the vehicle into a near polar orbit with the periapsis region near the terminator of the planet. This orientation of the orbit will permit good coverage of the planet from the planetary scientific instruments. Also, since the orbit is highly elliptical, the magnetosphere of the planet on the backside of the planet will be covered quite thoroughly. The orbits of the moons of Jupiter lie primarily in the orbit plane of Jupiter, hence, the possibility of encountering one accidentally is quite remote. The perturbing effect of the moons on the motion of the spacecraft could be significant, however.

The pointing of the approach asymptote by the final mid-course correction will permit nearly any orbit orientation desired.

## SUMMARY OF MISSION STUDIES

The material presented in the previous sections on mission analysis permits a great deal of flexibility in planning a JOVE mission which will carry out the scientific and engineering objectives. Many analyses of the effects of any number of parameters on the overall mission performance could be conducted and were examined to some extent in this study. Of particular interest were the effects of trip time and apsidal ratio on the gross capture weight in a Jovian orbit. One item that must constantly be kept in mind, however, is the systems reliability associated with a long trip time. Hence, it was desirable to keep the trip time as short as possible consistent with the overall mission operation.

A number of missions were examined and some of the results are summarized in the following tables. Table II-1 is for an 800 day mission during the 1978 launch opportunity and Table II-2 shows the results for a similar mission during the 1980 launch opportunity. The first four cases are single capture orbit missions and the last two cases are dual capture orbit missions.

TABLE II-1. SUMMARY 1978 LAUNCH

Launch beginning 244-3782 (October 1, 1978)

20 day launch window

$$C_3 = 104 \text{ km}^2/\text{sec}^2$$

800 day trip time

$$V_{HP} = 6.75 \text{ km/sec}$$

Communication distance 5.4 A. U.

Net Injected Weight 15 700 lb

	Case 1	Case 2	Case 3	Case 4	Case 5	Case 6
Initial periapsis (Jovian radii)	5	5	7	7	7	7
Initial apoapsis ratio	15	20	10	15	10	14.28
Final periapsis (Jovian radii)	-	-	-	-	5	5
Final apoapsis ratio	-	-	-	-	14	20
$\Delta V_{\text{total}}$ (km/sec)	1.75	1.50	2.06	1.70	2.40	2.00
Gross capture weight (lb)	8700	9900	7900	8900	7050	8050
Orbit period (days)	27	44	30	52	24	44

TABLE II-2. SUMMARY 1980 LAUNCH

Launch beginning 244-4572 (November 29, 1980)

20 day launch window

$$C_3 = 96 \text{ km}^2/\text{sec}^2$$

800 day trip time

$$V_{HP} = 6.88 \text{ km/sec}$$

Communication distance 5.5 A. U.

Net Injected Weight 18 500 lb

	Case 1	Case 2	Case 3	Case 4	Case 5	Case 6
Initial periapsis (Jovian radii)	5	5	7	7	7	7
Initial apoapsis ratio	15	20	10	15	10	14.28
Final periapsis (Jovian radii)	-	-	-	-	5	5
Final apoapsis ratio	-	-	-	-	14	20
$\Delta V_{total}$ (km/sec)	1.80	1.45	2.08	1.70	2.35	2.05
Gross capture weight (lb)	10 100	11 400	9100	10 400	8400	9200
Orbit period (days)	27	44	30	52	24	44

Several general observations can be made concerning a mission.

1. The shorter the trip time, the greater the injection energy and the orbit capture braking requirements, hence, the smaller the gross capture weight in orbit.

2. The tighter the capture orbit, i. e. , smaller apsidal ratio, the greater the orbit capture braking requirement, hence, less gross capture weight in orbit.

3. The longer the launch window, the greater the injection energy and capture orbit braking requirements.

4. The dual capture orbit maneuver requires more energy than the single capture orbit for the same size final capture orbit, hence, less gross capture weight in orbit for the dual capture orbit maneuver.

The results of this study show that the JOVE mission can be accomplished using the three-stage Saturn V launch vehicle throughout the 1975-1980 time period being considered. There is sufficient flexibility between the selection of a mission trip time and the capture orbit size to permit a mission to be flown even during the most demanding 1978 launch opportunity. The precise mission selection and planning will depend upon a more detailed analysis of the JOVE spacecraft and how it relates to the mission performance capabilities.

For most of the missions it will be necessary to "off-load" the fuel for the retropropulsion system in order to meet the limitations on the weight that can be injected onto the transfer trajectory. This will permit a greater variety of missions to be flown as the Saturn V launch vehicle is updated.

## BIBLIOGRAPHY

- Advanced Planetary Probe Study - Final Technical Report prepared for the Jet Propulsion Laboratory under Contract 951 311, Volume 2, Spin-Stabilized Spacecraft for the Basic Mission. TRW Systems, Redondo Beach, California, 27 July 1966.
- Baker, Robert M. L., Jr. and Makemson, Maud W.: An introduction to Astrodynamics. Academic Press, Inc., New York and London, 1960.
- Battin, Richard H.: Astronautical Guidance. McGraw-Hill Book Company, New York and San Francisco-Toronto-London, 1964.
- Ehrlicke, Kraft A.: Space Flight. Volume II: Dynamics - Principles of Guided Missile Design, Grayson Merrill, Captain, U. S. M. (Ret.), ed. D. Van Nostrand, Inc., Princeton, N. J., 1962.
- Escobal, Pedro Ramon: Methods of Orbit Determination. John Wiley and Sons, Inc., New York-London-Sydney, 1965.
- Haviland, R. P. and House, C. M.: Handbook of Satellites and Space Vehicles - Principles of Guided Missile Design, Grayson Merrill, Captain, U. S. M. (Ret.), ed. D. Van Nostrand, Inc., Princeton, N. J., 1965.
- Hunter, Maxwell W. II: Unmanned Scientific Exploration Throughout the Solar System. Space Science Reviews, 6 March 1967, pp. 601-654.
- Kendrick, J. B., ed.: TRW Space Data, Third Edition, TRW Systems Group, TRW, Inc., 1967.
- Odom, Pat R.: Application of Saturn/Apollo Hardware to Unmanned Scientific Exploration of the Solar System, Northrop Space Laboratories, TR-292/3-6-003, April 1966.
- Odom, Pat R.; Hill, A. S.; Brown, B. G.; Thadani, M. C. and MacKensie, C. M.: Application of the Saturn V Launch Vehicle to Unmanned Scientific Exploration of the Solar System. Jupiter Orbiter/Solar Probe Mission Study Advanced Mission Investigations. TR-292/3-6-075, Northrop Space Laboratories, September 1965.
- Roy, Archie E.: The Foundations of Astrodynamics. The MacMillian Company, New York, 1965.

## BIBLIOGRAPHY (CONTINUED)

Stewart, Robert L. : Single-Impulse Requirements for Planetary Capture.  
Northrop Space Laboratories, Huntsville, Alabama, May 1967.

**CHAPTER III**  
**SCIENTIFIC SYSTEMS**





## CHAPTER III. SCIENTIFIC SYSTEMS

### DEFINITION OF SYMBOLS

$\gamma$	=	Intensity of magnetic field (1 gauss = $10^5$ gamma)
$\theta$	=	Solid angle subtended by the objective of an optical instrument (steradians)
$\text{\AA}$	=	Angstrom unit = $10^{-8}$ cm
G	=	$10^9$
M	=	$10^6$
K	=	$10^3$
AU	=	Astronomical units
$\omega$	=	Angular frequency
H	=	Intensity of magnetic field
B	=	Magnetic induction
e	=	Electronic charge
m	=	Electronic mass, also magnetic moment
c	=	Speed of light
g	=	Lande' factor for atomic species
$F_L$	=	Larmor frequency
M	=	Mass of charged particle
V	=	Velocity of charged particle
R	=	Radius of circular path of charged particle
Q	=	Charge of particle
E	=	Electrostatic field strength
Z	=	Atomic number
$I(\alpha)$	=	Intensity at angle = $\alpha^\circ$
$I(0)$	=	Intensity at angle = $0^\circ$

# INTRODUCTION

The experiments for the JOVE mission were selected for two primary objectives. First, to study the temperature of various zones of the face of Jupiter, as well as the composition of its upper atmosphere and to measure the magnetic fields, the trapped radiation belts, and the micrometeoroid environments of the planet; and the second, to take advantage of the long travel time to make a detailed study of the solar plasma, interplanetary magnetic field, galactic cosmic rays, and micrometeoroid environments in the range of 1 AU to 5 AU.

Therefore, the experiments on this mission may be divided into two groups. The first group consists of the experiments performed during the interplanetary or cruise part of the mission. The instruments used will be the magnetometers, solar plasma detector, cosmic ray detector, micrometeoroid detector, and charged particle detector. These instruments will be activated immediately after injection into the transfer trajectory and will be used for the remainder of the mission.

The second group of instruments will consist of television cameras, infrared and ultraviolet spectrometers, a photometer, and infrared and microwave radiometers. These instruments will be turned on after an orbit of Jupiter is achieved.

The experiments recommended [ Ref. III-1, III-2, III-3, III-4, III-5] for an early Jovian mission are summarized in Table III-1. Many of these experiments will be carried by JOVE, but some must be left behind.

The anticipated first periapsis of JOVE is 7 R<sub>j</sub>. This may be lowered to 5 R<sub>j</sub> if the radiation conditions encountered indicate the feasibility of a lower orbit. This large periapsis eliminates a topside sounder because all currently envisioned sounders have a maximum range of 40 000 km [ Ref III-6, III-7, III-8] which is slightly more than 1/2 R<sub>j</sub>. Additionally, a recommended search for a trapped proton belt will not be made because the required periapsis distance of 3 R<sub>j</sub> will not be achieved.

In Table III-2 is found a detailed list of the instruments to be carried by JOVE, and it shows their sizes and characteristics as well. A more detailed discussion of each instrument will follow. Table III-3 is a summary of the experiment packages, giving the time of operation, package weights, and location of each category of experiment.

TABLE III-1. RECOMMENDED MEASUREMENTS  
[ Ref. III-1 ]

Measurements	Range	Possible Instrument	Max. Closest Approach for Useful Data (Rj)
1. Magnetic Field	0.5 $\gamma$ to 1 gauss	Magnetometer	40
2. Trapped Energetic Electron Flux	$10^6$ to $10^8/cm^2$ sec	Counter	7
3. Trapped Proton Flux	$10^8$ to $10^{11}/cm^2$ sec	Counter	3
4. Atmospheric & Ionospheric Scale Heights		Occultation of Telemetry	40
5. Ionospheric Electron Density		Topside Sounder	3
6. Ultraviolet Emission Lines	1000 - 7000 $\text{\AA}$	U. V. Spectrometer	40
7. H, He, Ne Lines and Reflected Brightness	1216 $\text{\AA}$ (H) 3880 $\text{\AA}$ (He) 6402 $\text{\AA}$ (Ne)	U. V. Photometer	7
8. High Atmospheric Temperature	10 u to 13 u	I. R. Radiometer	7
9. Polarization of Reflected Sunlight		Polarimeter	40

TABLE III-2. EXPERIMENTS

INSTRUMENTS	No.	SIZE (in.)	WEIGHT (lb)	POWER (watts)	ENVIRONMENT RESTRICTIONS	NOTES
INTERPLANETARY MEASUREMENTS						
1. Magnetometer (Rb)	1	8x8x6 Cup 3 Dia x $\frac{1}{2}$	2.2	7.0	Sensor 25-45°C Low Mag. Field	
2. Fluxgate Magnetometer	1	3 Dia x 6 Long 6x6x4 (Ele)	4.4	6.0		3 Detectors - mutually at right angles. One on spin axis
3. Trapped Rad. Det.	2	6x6x4	8.8	2.0		Clear view of outside
4. Curved Surface Plasma Anal.	1	12x12x5	4.8	1.5		Orient towards Sun
5. Faraday Cup Plasma Anal.	1	6x6x6 Cup 3 Dia x 1.5	2.7	0.5		Orient towards Sun
6. Cosmic Ray Telescope	1	9x9x6	2.6	0.6		Orient away from Sun
7. Cosmic Ray Charge & Mass Det.	1	4x4x5.5 8x8x8	10.5	1.7		Orient away Sun
8. Solar Flare Det.	1	4x4x5.5 8x8x8	10.5	1.7		Orient towards Sun
9. Micrometeoroid Det.	3	9x9x $\frac{1}{4}$ 2x9x4	7.5	0.6		Spaced equal distant around craft
UNIQUELY ORBITAL MEASUREMENTS						
10. Visible & U. V. Photometer	1	4x5x6	6.0	5.0	No Sunlight can enter	Filters and Polarizers
11. I. R. Radiometer	1	4x6x6	5.0	3.0	"	
12. Microwave Radiometer	1	60 Dia Ant. 6 Depth	22.0	10.0	"	Needs own antenna
13. T. V. System	1	5x7x14	30.0	20.0	"	400 lines - 1° 1000 lines - 10°
14. I. R. Spectrometer	1	10x12x14	16.0	5.0	Detector 25° K	
15. Visible & U. V. Spectrometer	1	10x13x16	20.0	10.0		

TABLE III-3. SUMMARY - EXPERIMENT PACKAGES

EXPERIMENT	OPERATION		PACKAGE WEIGHTS	LOCATION
	TRANSIT	ORBIT		
SOLAR WIND AND SOLAR FLARE DETECTORS	X	X	31 lb	SOLAR SCAN PLATFORM
COSMIC RADIATION DETECTORS	X	X		ON
MICROMETEOROID DETECTORS	X	X	23 lb	SPACECRAFT
MAGNETOMETERS	X	X		
TRAPPED RADIATION DETECTORS	X	X		
PHOTOMETER AND RADIOMETERS		X		PLANET
SPECTROGRAPHS		X	99 lb	SCAN
TELEVISION		X		PLATFORM

TABLE III-4. SUMMARY - TELEVISION EXPERIMENT

Distance from Center-Rj	Distance from Surface-km	Area Covered - km on a side	Maximum Theoretical Spatial Resolution-km
Camera #1 - 10° view			
11.0	700 000	114 000	230
7.0	420 000	73 000	150
5.0	280 000	49 000	100
4.0	210 000	36 000	70
3.0	140 000	25 000	50
Camera #2 - 1° view			
11.0	700 000	12 000	60
7.0	420 000	7300	35
5.0	280 000	5000	25
4.0	210 000	3700	18
3.0	140 000	2400	12
<p>Size: 5 in. x 7 in. x 14 in.</p> <p>Weight: 30 lb</p> <p>Power: 20 watts</p> <p>Bits: 10<sub>6</sub>/rdg (1000 lines) 0.4 x 10<sup>6</sup>/rdg (400 lines)</p> <p>Frequency of rdg = 4/orbit for 1000 line camera = 41/orbit for 400 line camera</p>			

# INTERPLANETARY MEASUREMENTS AND INSTRUMENTS

## Magnetometers

Introduction. Radioastronomical measurements of the decimeter radiation from Jupiter have provided estimates of the Jovian magnetic field [ Ref. III-9]. If this radiation is synchrotron radiation from relativistic electrons, the field strength at 3 R<sub>J</sub> would lie in the range of 0.1 to 10 gauss. Measurement of this field is most essential as its magnitude and extent will control the intensity and energy of the trapped radiation belt around Jupiter. For this reason, the measurement of the magnetic field is considered the most important experiment in any Jupiter mission. Further, the greater than two year transit time of the mission provides an unequalled opportunity for measuring interplanetary magnetic field in the region of 1 AU to 5 AU, whose magnitude probably lies in the range of 0.1 to 10 gammas [ 1 gamma = 10<sup>5</sup> gauss]. The period 1977 through 1980 covers the peak of a sunspot cycle. Hence, the possibility of seeing one or more solar flares during the flight, with the resulting changes in the solar magnetic field, will be excellent. Because of the wide dynamic range of measurement and the importance of the measurement, two magnetometers will be carried. One, a flux gate magnetometer, will be optimized for low field measurements in the range of 0 to 300 gammas, but it will operate in higher magnetic fields with reduced accuracy. The other, a rubidium vapor magnetometer, with a range of 3 to 10<sup>4</sup> gammas will be used for high field measurements and in calibration of the flux gate magnetometer.

Flux Gate Magnetometer. This magnetometer consists of three independent orthogonal elements, one oriented along the spacecraft roll axis, the other two perpendicular to one another in a plane orthogonal to the roll axis. Each element provides an output proportional to the intensity of the magnetic field and its direction.

Each sensor of the flux gate magnetometer consists of a torodial core to which two windings are applied (Fig. III-1). One, the primary winding, is fed by a driving oscillator at a frequency  $\omega$ . The other, the secondary winding, feeds an output filter whose frequency is  $2\omega$ . The ambient field to be measured,  $H_1$ , and the field provided by the driving oscillator,  $H \sin \omega t$  are both applied to the core. The value of  $H$  is chosen to be large enough to drive the core to saturation at its maximum value (Fig. III-2). The magnetic induction of the core is modified by the saturability of the core. During the peaks of the gating field,  $H \sin \omega t$ , the toroidal cores are saturated at a value  $\pm B$  and the ambient field is gated. Between the peaks the value of the magnetic induction is given by

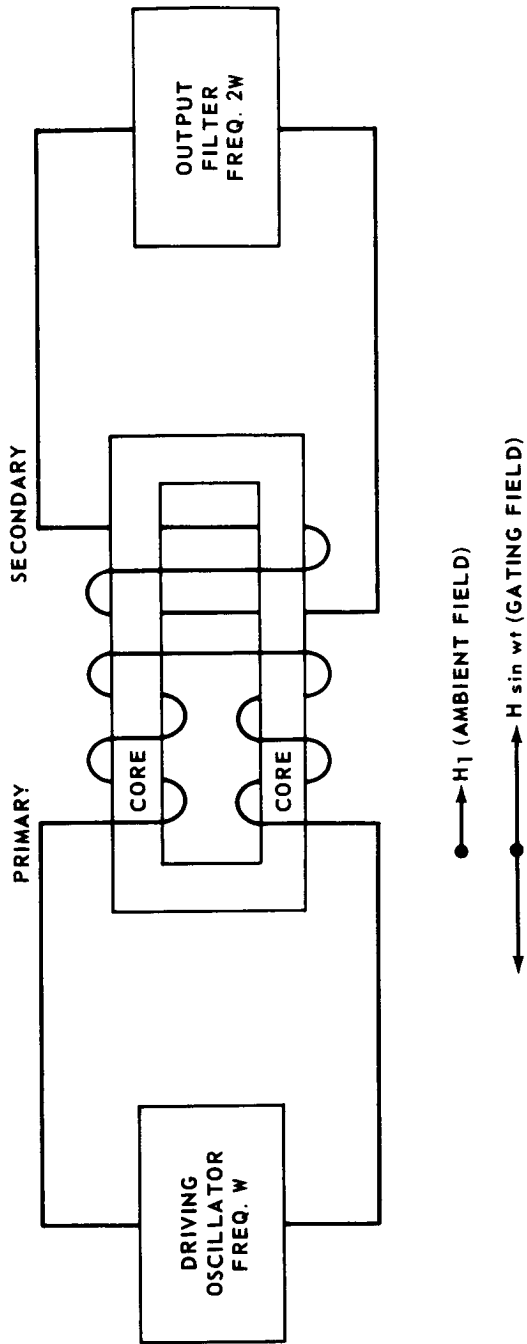


FIGURE III-1. FLUX GATE MAGNETOMETER SCHEMATIC



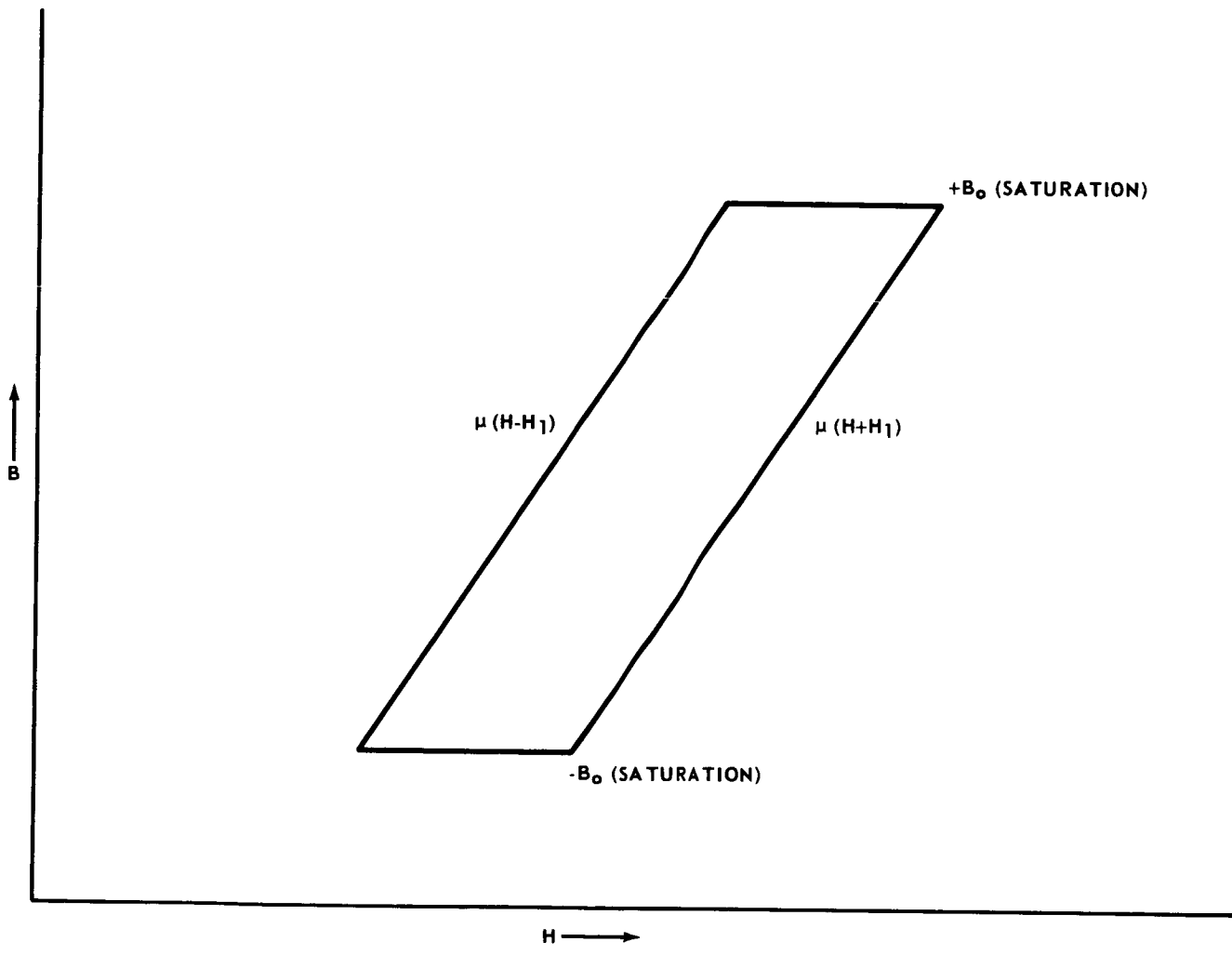


FIGURE III-2. FLUX GATE MAGNETOMETER HYSTERESIS LOOP

$$B = \mu [ H \sin \omega t \pm H_1 ].$$

The ambient field,  $H_1$ , therefore, introduces an asymmetry into the induction cycle. If the total induction is expanded in a Fourier series

$$B = a_0 + \sum a_n \cos n\omega t + \sum b_n \sin n\omega t$$

it may be shown that the source of this asymmetry, the ambient field  $H_1$ , also gives rise to the even harmonics in the Fourier series expansion [ Ref. III-10]. Therefore, the filter at  $2\omega$ , which is fed by the secondary coil, selects the second harmonic which is proportional to the ambient field. A block diagram of the flux gate magnetometer to be flown is shown in Figure III-3. An auxiliary coil is used in this experiment to allow the nulling out of the spacecraft's magnetic field and also the application of a known calibration magnetic field to the coil during the mission.

Rubidium Vapor Magnetometer. The second magnetometer will be a rubidium vapor magnetometer. This device depends upon the Zeeman effects, or in other words, upon magnetically split atomic energy states for its operation (Fig. III-4). Its output depends only upon the magnitude of the magnetic field and thus, although it gives no directional information, it gives us the absolute value of the magnetic field. The operation of this device is shown in Figure III-5. The interference filter transmits only the  $D_1$  line of the rubidium spectrum into the rubidium vapor cell and through the circular polarizer. Because of the circular polarization of the light, the magnetic quantum number,  $m$ , must change by  $+1$ . Hence, the atoms are pumped into  $^2S_{1/2}$ ,  $m = 2$  (Fig. III-4), metastable state. During this process, the cell absorbs the  $D_1$  light and the output of the photocell is low. When the process is completed the cell becomes transparent to the  $D_1$  line and the output of the photocell rises.

If, at this point, radiofrequency radiation at the Larmor frequency,

$$F_L = g \frac{eH}{4\pi^2 mc}$$

is applied to the cell, the atoms will redistribute themselves to all the sub-levels and the cell's transmission of the  $D_1$  light is again reduced as it is now capable of absorbing the radiation and repumping itself to the metastable state [ Ref. III-11, III-12, III-13].

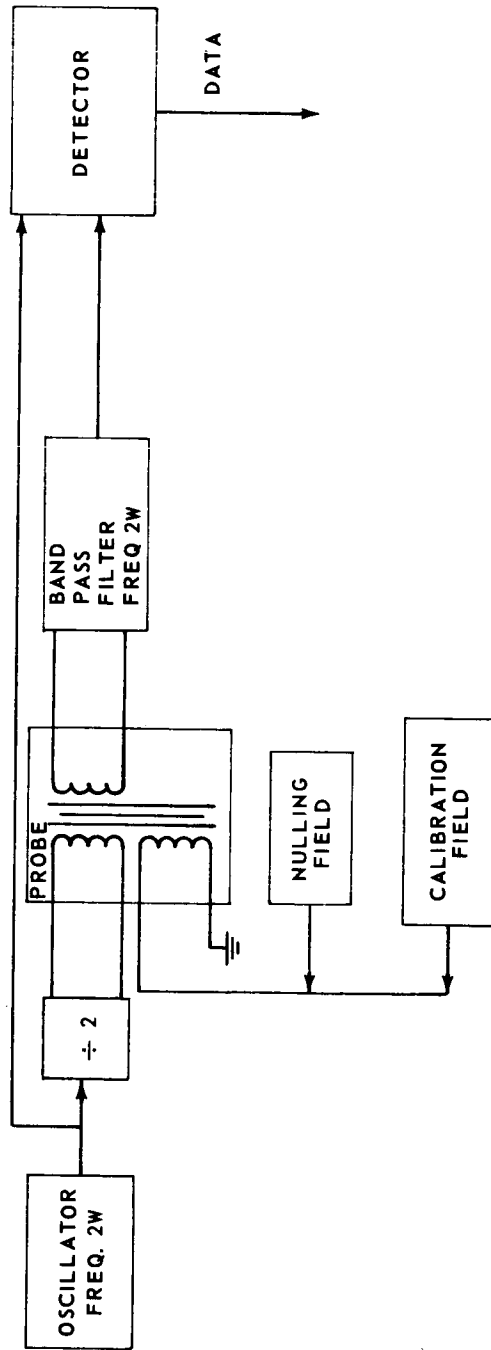


FIGURE III-3. FLUX GATE MAGNETOMETER, FUNCTIONAL BLOCK DIAGRAM

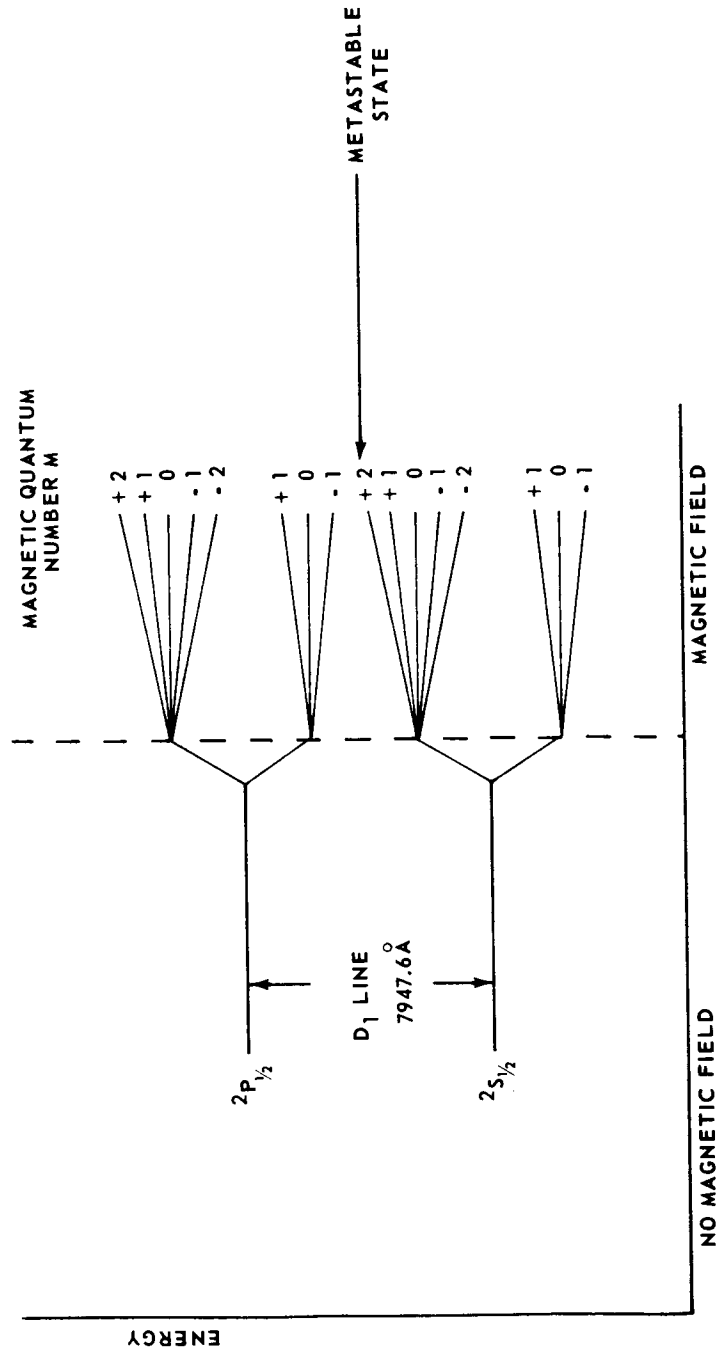


FIGURE III-4. RUBIDIUM - 87 ENERGY - LEVEL DIAGRAM

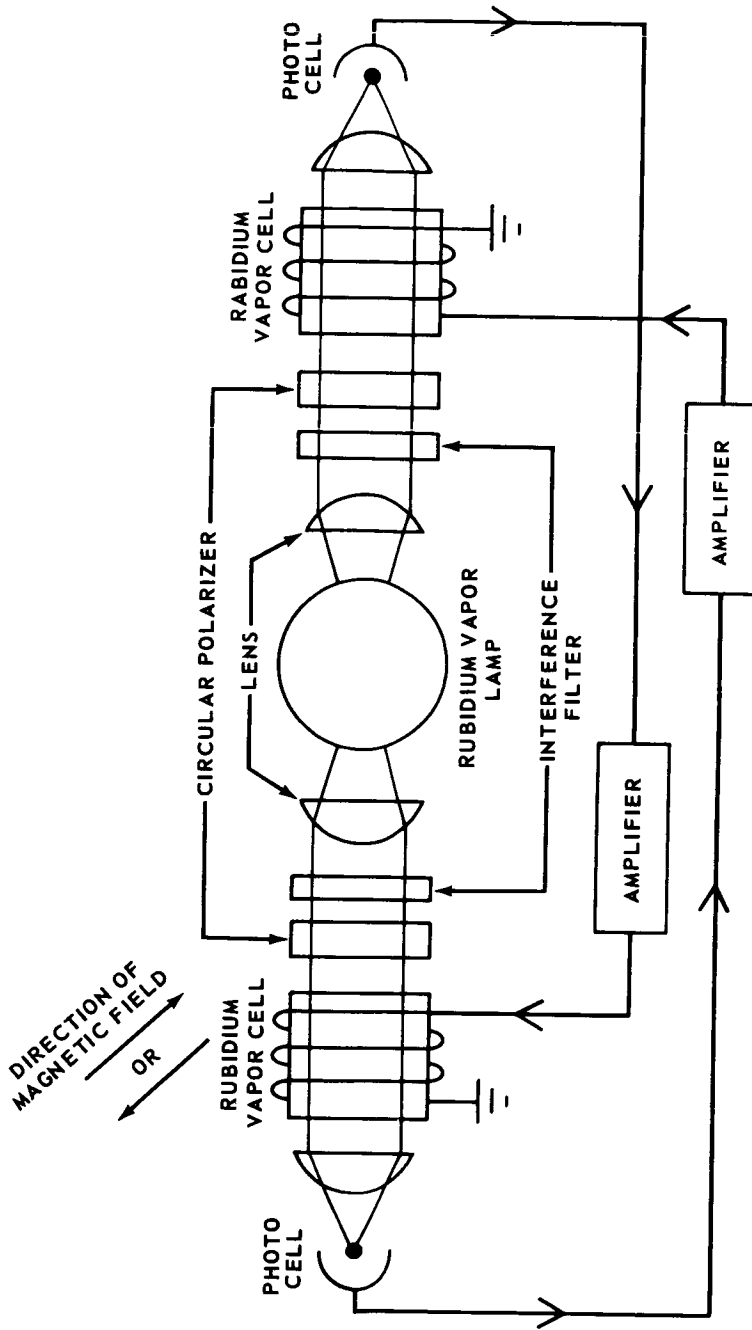


FIGURE III-5. DUAL CELL SELF OSCILLATING MAGNETOMETER

Such a cell may be made self-oscillating at the Larmor frequency and if two cells and a central lamp are used (Fig. III-5) the oscillations in light output seen by one photocell are of the correct phase to de-excite the other Rubidium vapor cell and the whole system will then oscillate at the Larmor frequency. From the above equation for the Larmor frequency it may be seen that the measured frequency, and, hence, the field strength are related by known atomic constants. Therefore, the absolute value of the field may be determined. These magnetometers have been constructed and flown (Explorer X) for magnetic field of  $3 \gamma$  to  $10^4 \gamma$ .

A magnetometer of this type will not yield useful signals if it is within  $\pm 12^\circ$  of an orientation parallel to the field or  $\pm 7^\circ$  of perpendicular to the field. Additionally, the rubidium vapor cell must be maintained between the temperature limits of 25-45°C. Using the two magnetometers permits calibrating the flux gate magnetometer with the rubidium vapor magnetometer, and using the flux gate magnetometer if the rubidium vapor magnetometer is inoperative because of its orientation. In order to obtain valid results with either magnetometer the magnetic field of the spacecraft in the vicinity of the magnetometer must be kept as low as possible (close to 1 gamma or less). The output of each element of the flux gate magnetometer is a voltage proportional to the intensity of the magnetic field. The output of the rubidium vapor magnetometer is an alternating voltage whose frequency is equal to the Larmor frequency. Vital statistics of both magnetometers are summarized below:

Weight:	2 kg (4.4 lb)
Power:	6 watts
Data:	(bits/scan) 30 (10 each axis)
Size:	Sensor: cylinder 3 in. diameter by 6 in. long Electronics: one box 6 in. x 6 in. x 4 in.

Rubidium vapor:

Weight:	1 kg (2.2 lb)
Power:	5.5 watts
Data:	10 bits/sample
Size:	Sensor: cylinder 3 in. diameter by 12 in long Electronics: one box 8 in. x 8 in. x 6 in.

# Trapped Radiation Detectors

Introduction. Based on astronomical studies of its radio emission, Jupiter is believed to have an intense trapped radiation belt [ Ref. III-14, III-15]. Planned future missions to other planets have proposed the use of a Jupiter swingby trajectory to obtain the required energy without sacrificing payload. Since the amount of energy which may be added depends upon the closest approach to the planet and since, therefore, future Jovian missions will desire a close approach to the planet, it is imperative that experiments be carried out to measure the extent of the Jovian radiation belt.

Instrumentation. The trapped radiation detector to be carried will be similar to that in the Mariner-Mars experiment [ Ref. III-16] , and will consist of three Geiger-Mueller tubes and a solid state detector. A functional block diagram of the apparatus is given in Figure III-6. Detectors a, b, and c are end window Geiger-Mueller tubes (G-M tubes) having energy thresholds of 40 keV for electrons and 500 keV for protons. They are shielded so that particles of low and medium energies may enter only through the windows. High energy particles may enter only through the side. Detector b has been shielded to increase its threshold to 130 keV for electrons and 3 meV for protons. Detector c has been shielded to increase its threshold to 1 meV for electrons and 20 meV for protons. This permits one to obtain a coarse energy discrimination of the charged particles found in the radiation belts. Detector d, a solid state detector, is designed to measure the proton flux, thus permitting an analysis of the proton and electron components in the trapped radiation belt. The two discriminators provide energy resolution in the ranges of 500 keV to 11 keV to 4 meV. Data from the five outputs is sent to the SDS where it is accumulated in five 10-bit registers until time for readout for transmission to Earth. Readout of the accumulated counts in each 10-bit register is accomplished once each data frame. There will be two complete detector systems carried because of the importance of the experiment. The SDS will store data from each system in the accumulators alternately so that, although trapped radiation data will be readout each data frame, it will be supplied by system 1 and system 2 in alternate frames. Vital statistics of the trapped radiation detector are summarized below:

Mass:	1 kg (2.2 lb)
Power:	0.4 watts
Data:	10 bits/sensor (5 sensors)
Size:	box 6 in. x 6 in. x 4 in. with 4 sensors,

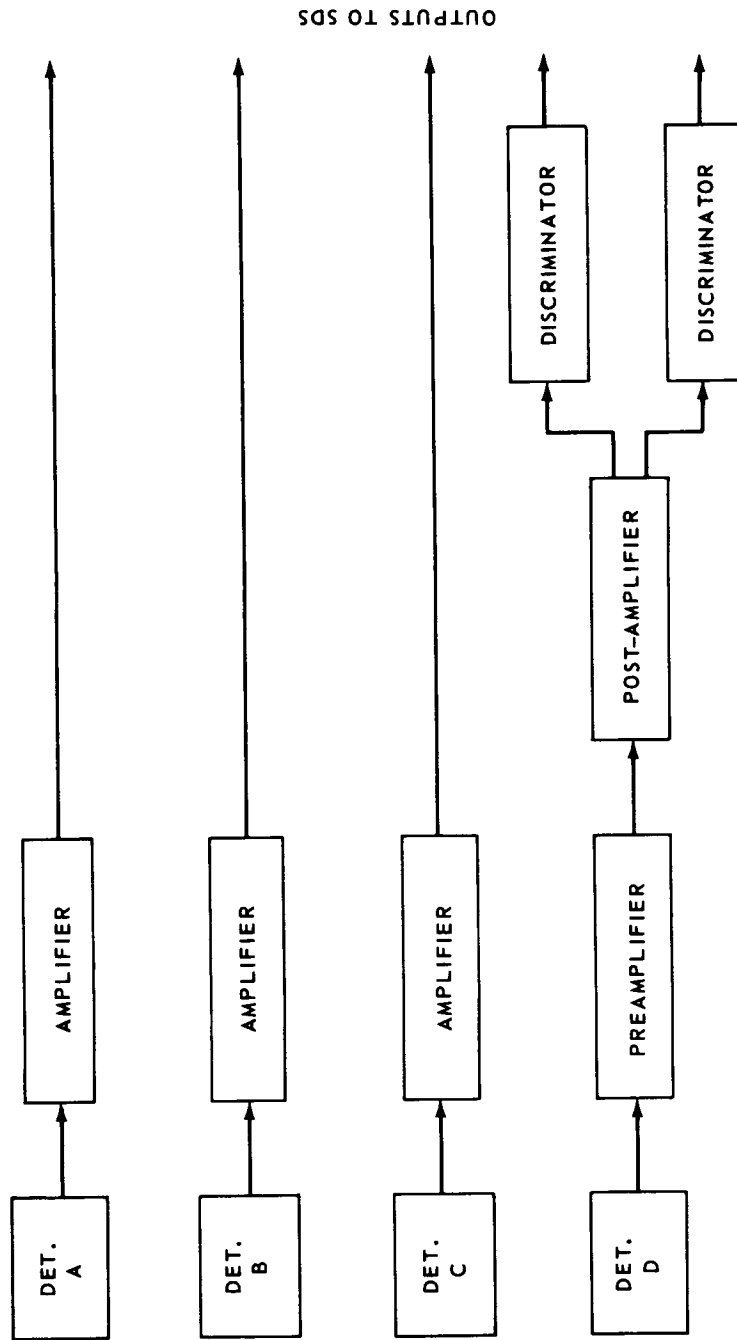


FIGURE III-6. TRAPPED RADIATION DETECTOR



1 in. diameter x 4 in. long extending  
from 6 in. x 4 in. side

## Plasma Probes

Introduction. The majority of the matter in the universe is found in the plasma state [ Ref. III-17]. The JOVE mission will spend over two years in this medium during its transit from Earth to Jupiter and thus, it will provide long term observations of the solar wind, solar flares and galactic cosmic ray flux in a region of space from 1 AU to 5 AU which, up to now, have not been explored. Additionally, the eccentricity of the orbit chosen about Jupiter will permit a study of the interaction of the solar wind with the magnetic field of the planet and the resulting hydromagnetic shock waves and the creation of a magnetosphere containing the magnetic field of the planet.

The need for more data on solar flares and the Forbush decrease in cosmic ray intensity during solar flares plus the possible hazards to manned missions resulting from solar flares combine to make analysis of the solar plasma an experiment of extreme importance, perhaps second only to the magnetometer and trapped radiation experiments in importance. The launch period from 1977 through 1980 covers a peak of a sunspot cycle. The solar flare cycle has been shown to correlate with the sunspot cycle. Hence, there is a high probability of seeing one or more solar flares during the mission. Three plasma probes will be carried on the spacecraft. Two of them will be low energy devices to study the solar wind and to do an energy analysis of the low energy protons which make up the majority of the solar wind and to attempt to measure the proton-alpha ratio. The third detector will be a cosmic ray detector sensitive to high energy particles to study the energy distribution of the high energy protons from solar flares which may have energies as high as  $10^3$  MeV and which have large numbers of particles with energies of over 20 MeV.

Curved Surface Plasma Detector. This is an electrostatic analyzer [ Ref. III-1B, III-19] whose principle of operation is shown in Figure III-7. By equating the electrical and centrifugal forces one obtains:

$$\frac{MV^2}{R} = QE$$

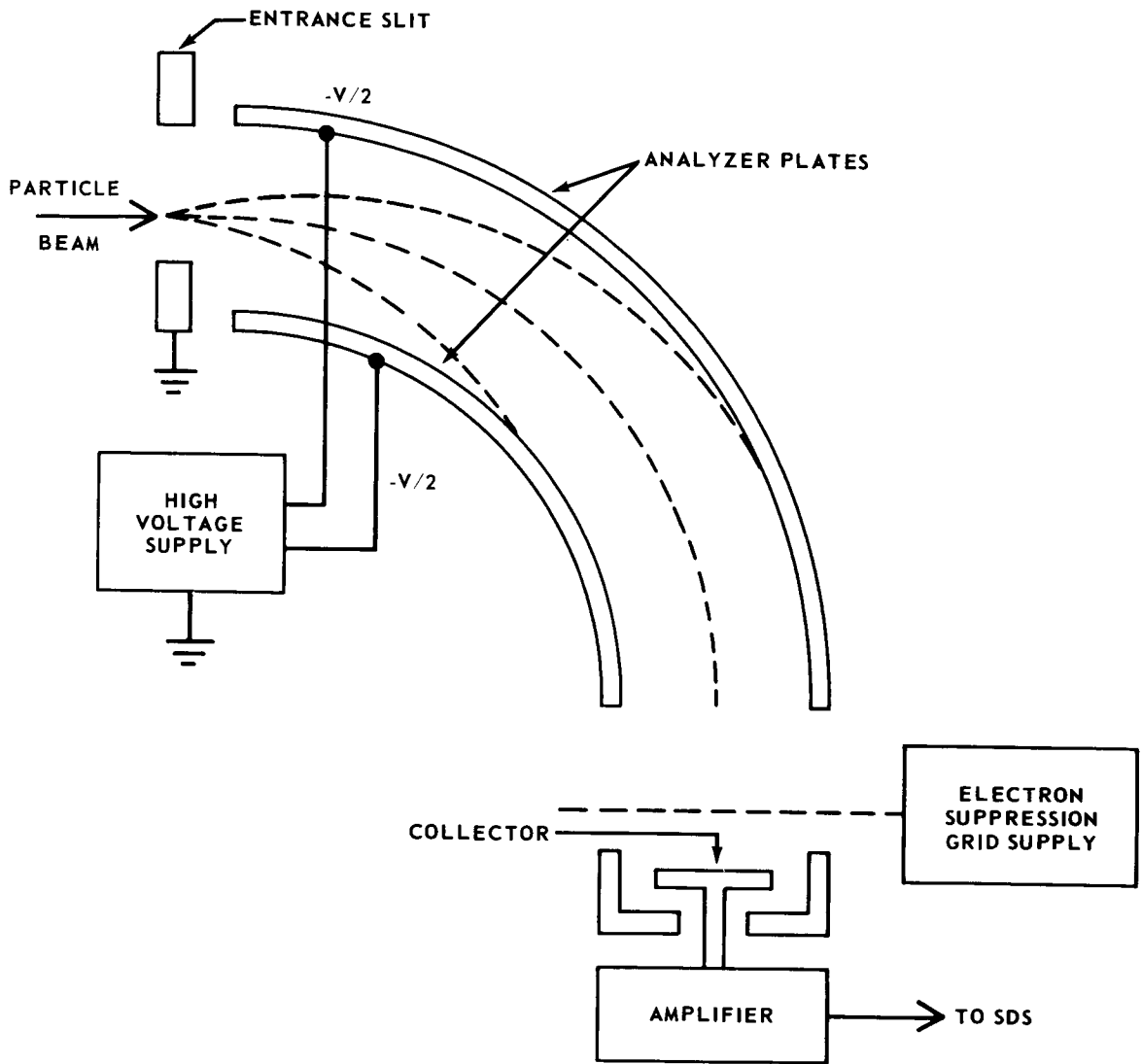


FIGURE III-7. ELECTROSTATIC ANALYZER

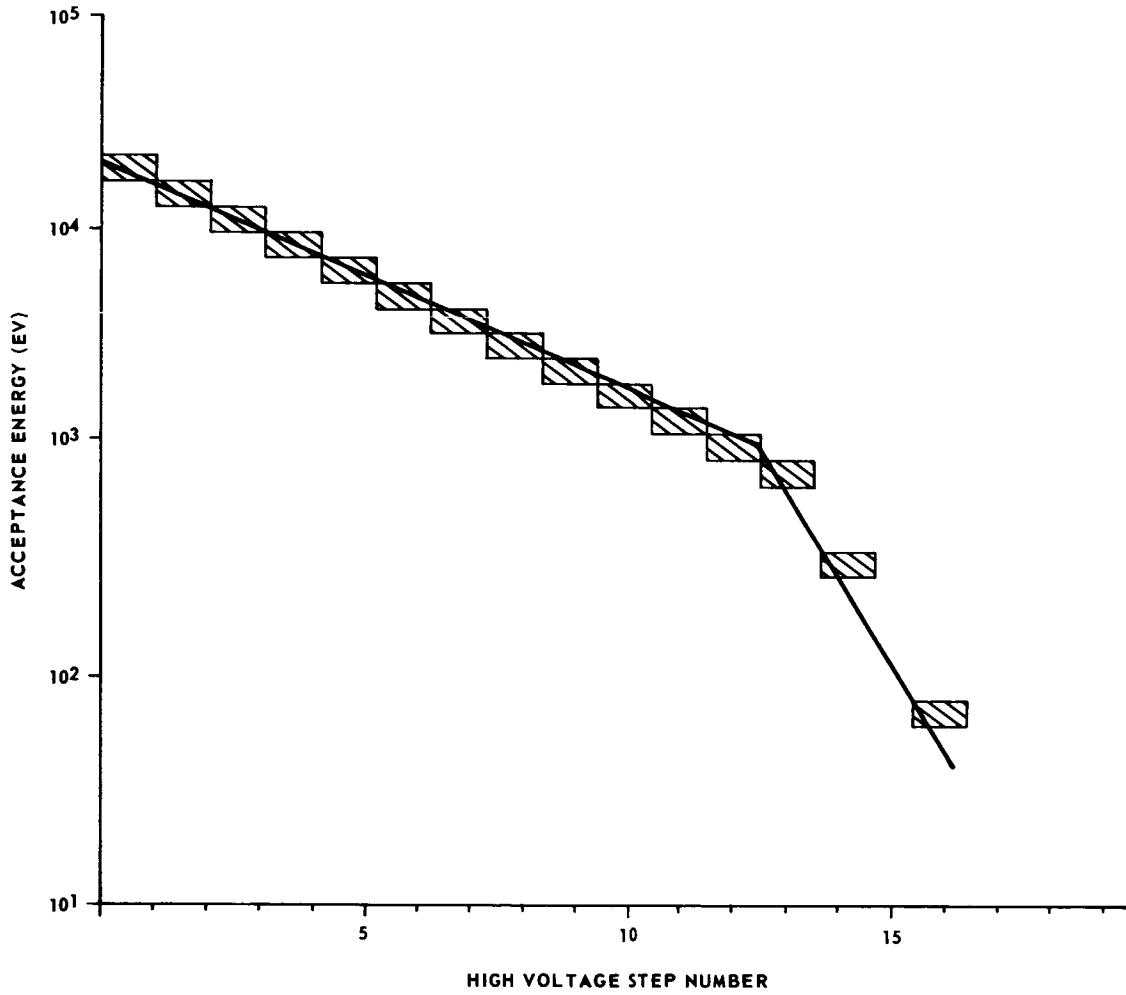
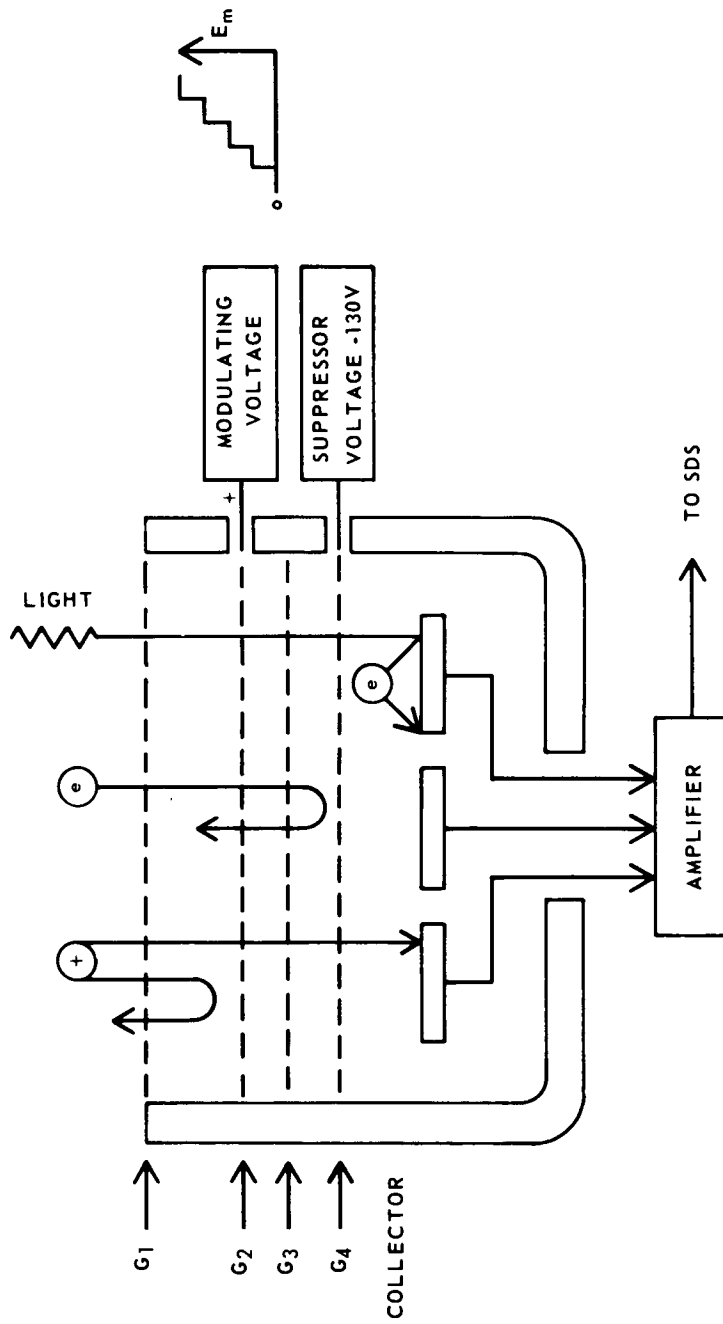


FIGURE III-8. POSITIVE ION ENERGY RESOLUTION



FIGUER III-9. GEOMETRY - FARRADY CUP PROBE

where  $M$  = particle mass

$V$  = particle velocity

$R$  = the radius of the circular path of the particle

$Q$  = the particle's electronic charge

$E$  = the electrostatic field between the plates (this is determined by the voltage and the geometry of the plates)

Hence, for a given  $E$  only particles for the specified  $\frac{MV^2}{QR}$  will be collected.

Therefore, this detector provides a differential energy spectrum the energy resolution of which is determined by the number and size of the voltage steps applied to the deflecting plates (Figure III-8). This type of detector is excellent for the range of proton energies from  $10^2$  to  $10^4$  electron volts.

Faraday Cup Probe. The Faraday Cup Probe will be used to measure the low energy component of the solar plasma [ Ref. III-19, III-20, III-16]. It will measure the plasma density in the energy range of 10 to 1000 eV. The geometry of the probe is shown in Figure III-9. In this figure  $G_1$  is grounded to the spacecraft.  $G_2$  is a modulating grid to which positive voltage steps are applied for energy discrimination of the incident particles.  $G_3$  is a grounded shield grid and  $G_4$  is used to suppress photoelectrons. The detector to be flown will be similar to the Mariner-Mars detector. It will have a split collector. The collector will be split into three sections which will permit a coarse angular discrimination of the incoming flux since the side walls of the detector will shadow the sections of the collector by differing amounts. In addition, the modulating voltage will have sixteen steps. This will permit sixteen energy windows. The analysis will be as follows:

(1) All three sections of the collector will be analyzed together and the sixteen voltage steps applied to give an energy spectrum without angular discrimination. This will total sixteen measurements.

(2) Sequentially the left side, center and right side of the collector will be analyzed for the sixteen voltage steps giving an additional forty-eight individual measurements. Eight other measurements for timing and calibration yield a grand total of 72 measurements per complete scan of the instrument.

(3) In each data frame only one measurement will be read out. Therefore, 72 data frames will be required to give a complete scan of the instrument. The scientific data system will give the stepping signal to the modulating voltage source and therefore, time the entire procedure. This device collects all protons whose energies are greater than the modulating voltage. Therefore, it produces an integral energy spectrum.

Solar Flare Detector. This detector will be flown expressly to observe the high energy particles from the solar flares expected during the mission. It will also measure the high energy component of the solar wind. It will be identical to the scintillation counter telescope to be flown for charge and mass identification of primary cosmic rays, except that it will lack the scale changing capability of this instrument, and will operate in the electron, hydrogen, and helium analysis mode only. A detailed description of this device will be given in the section on cosmic ray experiments. It will provide flux measurements in the energy range of 10 to  $5 \times 10^2$  MeV.

Instruments should be mounted in such a manner that they are oriented toward the Sun while they are taking data. The cosmic ray experiments, on the other hand, should be mounted pointing away from the Sun so that they will see the galactic cosmic ray contribution and not the solar cosmic radiation. Therefore, the cosmic ray experiments and the solar flare detectors will be mounted on a small platform called the Solar Scan Platform. The solar flare detectors will be mounted on the end of this platform which faces the Sun, while the cosmic ray detectors will be mounted on the opposite end facing away from the Sun.

Important characteristics of the plasma probe detectors are summarized below:

Curved Surface Detector:

Mass: 2.2 kg (4.8 lb)  
Power: 1.5 watts  
Data: (bits/sample) 10  
Size: one box 12 in. x 12 in. x 5 in.

Faraday Cup Detector:

Mass: 1.3 kg (2.7 lb)  
Power: 0.5 watts  
Data: 10 bits/sample, 72 samples/scan  
Size: Sensor: cup 3 in. diameter x 1.5 in. deep  
Electronics: 6 in. x 6 in. x 6 in.

### Solar Flare Detector:

Mass:	4.5 kg (10.5 lb)
Power:	1.7 watts
Bits:	20 bits/sample
Size:	Sensor: 4 in. x 4 in. x 5 in. Electronics: 8 in. x 8 in. x 8 in.

## Cosmic Ray Experiments

Introduction. Cosmic rays are energetic particles originating outside Earth's atmosphere [ Ref. III-21]. Primary cosmic rays, that is, energetic particles unmodified by Earth's atmosphere, may be divided into two categories: solar cosmic rays originating in solar flares and characterized by transient high intensity bursts of radiation lasting only a few days, and galactic cosmic rays presumably originating within our galaxy. The solar cosmic rays are primarily protons and helium nuclei with a maximum observed energy of 20 to 30 Gev, while galactic cosmic rays may have energies as high as  $10^{11}$  Gev. Solar cosmic rays are detected by the solar flare detector. Hence, this discussion is limited to those detectors to be flown to study the galactic cosmic ray flux from 1 AU to 5 AU. They will measure the energy of the primary cosmic ray particles and the isotopic distribution of these particles and look for the Forbush decrease during solar flares.

Cosmic Ray Telescope. The cosmic ray telescope is designed to measure the absolute flux levels and energy spectrum of the two main components of the primary cosmic radiation - protons and helium nuclei in the energy range of 1 to 170 MeV per nucleon [ Ref. III-16].

It will also identify cosmic rays with energies greater than 170 MeV per nucleon. It consists of three silicon surface barrier detectors separated by absorbers to produce a telescope with an acceptance cone having a half-angle of  $20^\circ$  (Fig. III-10). To penetrate the window and produce a count in detector,  $D_1$ , the particle must have a minimum energy of 1 MeV per nucleon. To penetrate to  $D_2$ , requires 15 MeV per nucleon, and to penetrate to  $D_3$ , at least 70 MeV per nucleon. Figure III-11 shows the energy loss in the  $D_1$  detector as a function of the particle energy. Particles penetrating the  $D_1$  detector completely deposit less and less energy in the  $D_1$  detector as their energy increases because of the decreasing rate of energy loss with the increasing energy, until the minimum ionizing particle level is reached [ Ref. III-22, III-23].

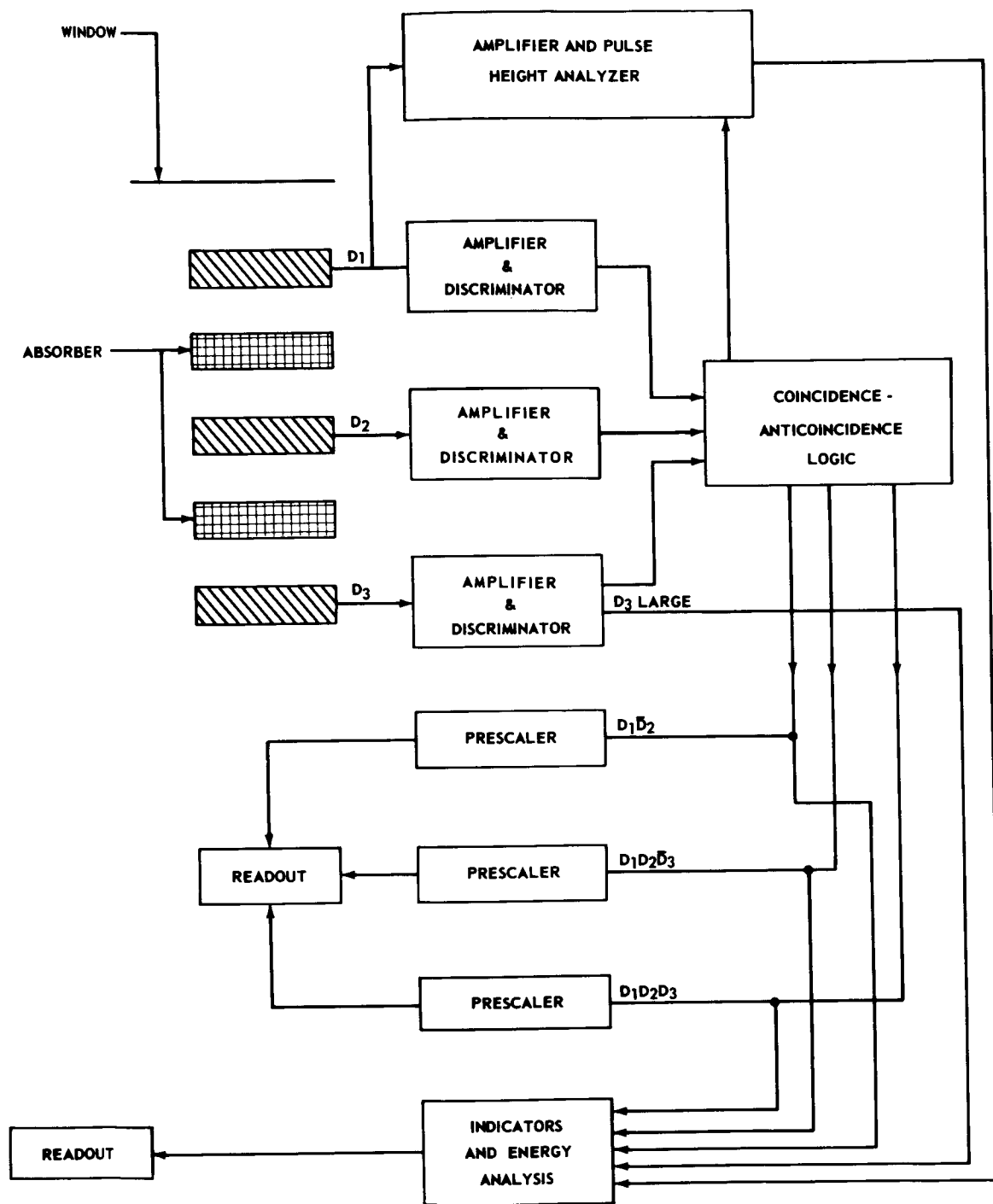


FIGURE III-10. COSMIC RAY TELESCOPE BLOCK DIAGRAM



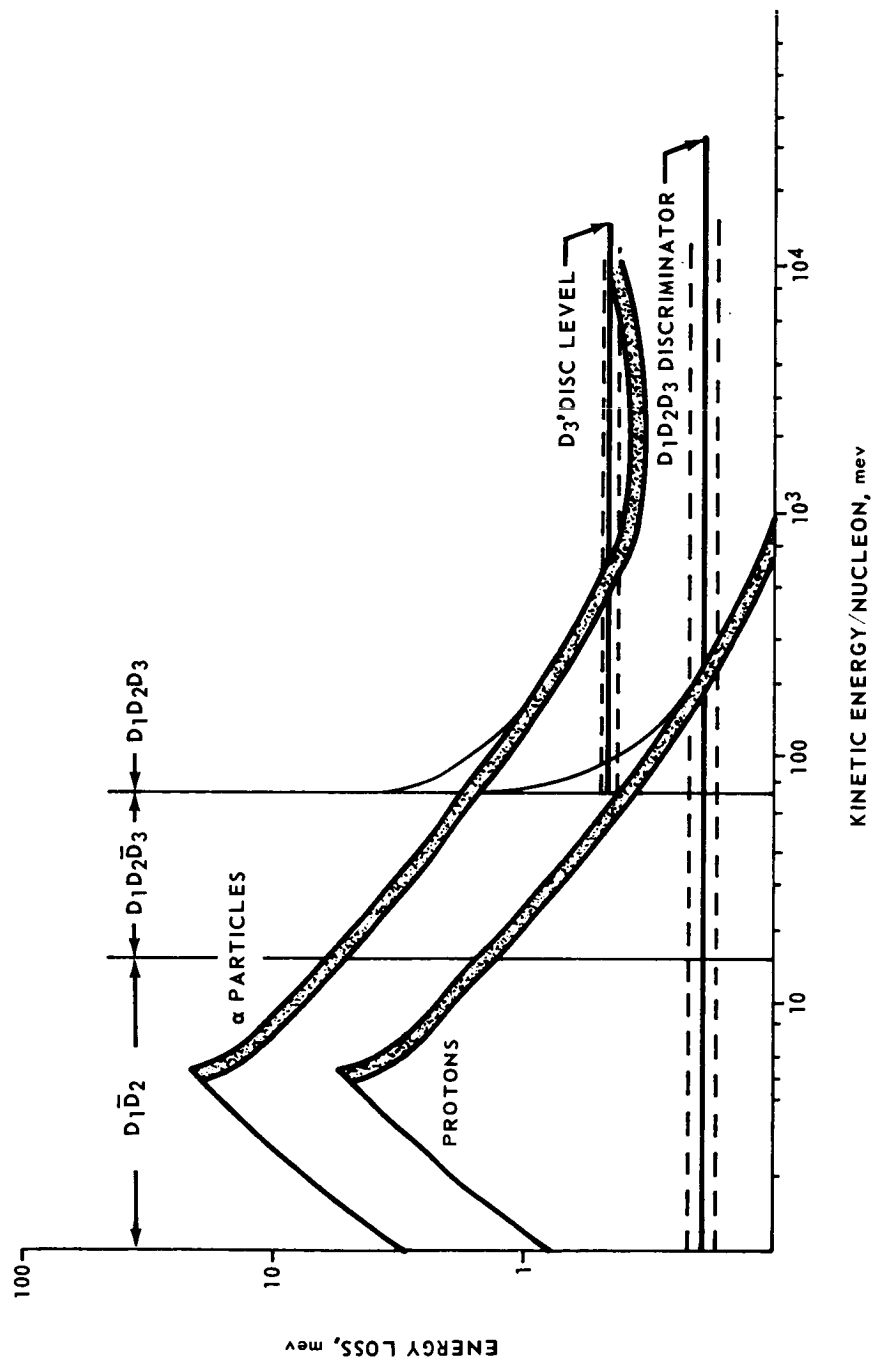


FIGURE III-11. ENERGY LOSS IN  $D_1$  DETECTOR

In the case of the proton, the ionization drops below a measurable value at about 170 MeV. Since the rate of energy loss is proportional to  $Z^2$ , the helium nuclei are separated from the hydrogen nuclei by their energy loss in the 15- to 70-MeV range, and for helium nuclei there is no limit for detection above 170 MeV because even as minimum ionizing particles, they still leave measurable amounts of energy in  $D_1$ . Coincidence circuitry is fed by the outputs of discriminators which are fed from the detectors. This coincidence-anticoincidence circuitry produces as its output three counting rates corresponding to the previously mentioned energy ranges: the  $D_1$  singles counting rate given by the  $D_1D_2$  ( $D_1$  and  $D_2$  coincidences), the  $D_1D_2D_3$  counting rate, and  $D_1D_2D_3$ . The data for the three count rates is prescaled and stored in a single 10-bit register. The energy lost in the  $D_1$  detector is analyzed for  $D_1D_2$  and  $D_1D_2D_3$  events by recording the pulse height for the first  $D_1D_2$  event after each readout. In addition, indicator bits record whether this event was a double or a triple coincidence, and whether the energy loss in  $D_3$  was large or small. This information permits distinguishing the particles and discriminates against those entering the rear of the telescope.

Charge and Mass Identification Telescope. This instrument, minus the mode switching for analysis of heavy ions is used as a solar flare analyzer and since the operation of both devices is otherwise identical, both are discussed here. This instrument will determine the relative abundances of nuclei of  $Z$  from 1 through 8 (oxygen) and measure their energy spectrum over a range of 10 to 20 MeV per nucleon [ Ref. III-24, III-25]. A thin cesium iodide scintillator (Fig. III-12) measures  $\frac{dE}{dx}$  and the remainder of the energy is deposited in the E scintillator. A particle passing completely through the E scintillator will cause a scintillator in the guard scintillator which is operated in anticoincidence to discriminate against incomplete energy deposition in the E scintillator and against particles entering from the rear. Normally the system operates in a high gain mode, but if either the  $\frac{dE}{dx}$  or E pulses is greater than a pre-set amplitude the gain of both the  $\frac{dE}{dx}$  and E amplifiers is automatically reduced to shift to the heavy particle mode. The  $\frac{dE}{dx}$  and E measurements are analyzed separately to 128 energy increments and stored in separate 10-bit registers with an indication when the analyzer is in the heavy particle mode. Hence, the analyzer can handle only one analysis per scan. A third 10-bit register will record the total number of  $\frac{dE}{dx}$  and E but not counter coincidences to indicate the total number of events detected in the measurement interval. This last 10-bit register is read out only once for every third reading of  $\frac{dE}{dx}$  and E. Figure III-13 [ Ref. III-24] indicates how the data may be analyzed to obtain Z and E information for cosmic radiation.

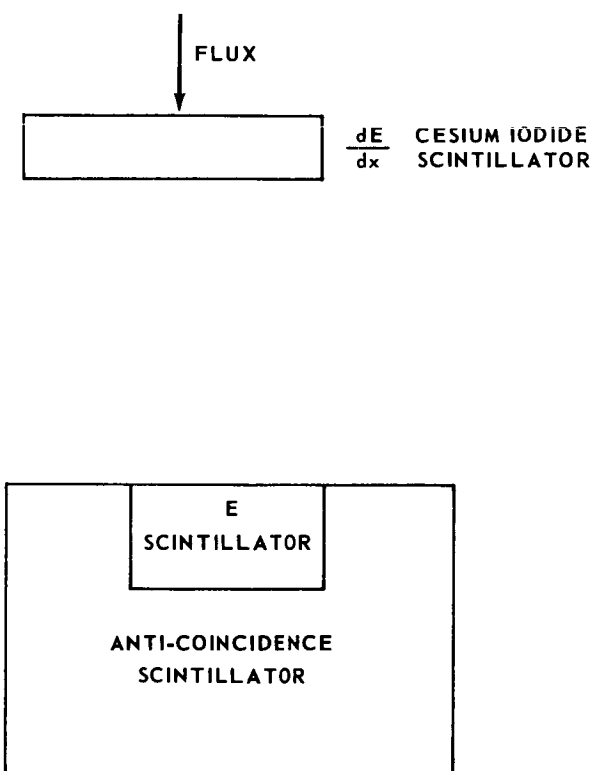


FIGURE III-12. SCHEMATIC-SCINTILLATOR ASSEMBLY

Important characteristics of cosmic ray experiments are outlined below:

#### Cosmic Ray Telescope:

Mass: 1.1 kg (2.4 lb)  
Power: 0.6 watts  
Data: 20 bits/sample  
Size: 9 in. x 9 in. x 6 in.

#### Charge and Mass Telescope:

Mass: 4.5 kg (10.5 lb)  
Power: 1.7 watts  
Data: 30 bits/sample  
Size: Sensor: 4 in. x 4 in. x 5.5 in.  
Electronics: 8 in. x 8 in. x 8 in.

## Micrometeoroids

Introduction. Ever since man has studied the heavens, it has been known that the solar region is occupied by a large number of small particles in addition to the Sun, planets and their moons, and asteroids. These particles, smaller than 1 mm in diameter, are arbitrarily called micrometeoroids. These particles are too small to be burned up when they enter Earth's atmosphere. A large number of such particles are found in the space occupied by our solar system. A space vehicle traveling in this region may encounter and collide with some of these particles. These particles have a finite mass and a fairly high velocity relative to the spacecraft and may either penetrate the craft or cause erosion of various parts of its structure. Those particles having sufficient momentum or kinetic energy to puncture pressurized chambers of the spacecraft or the fuel system are dangerous to the mission. If the number of particles is large and even though the momentum of each particle is insufficient for penetration, erosion of the various members of the spacecraft may result. Such erosion could either weaken the structure or cause a change in the thermal property of the radiators or the performance of the energy absorbers. In this way, the performance of the craft may be degraded and the mission may fail.

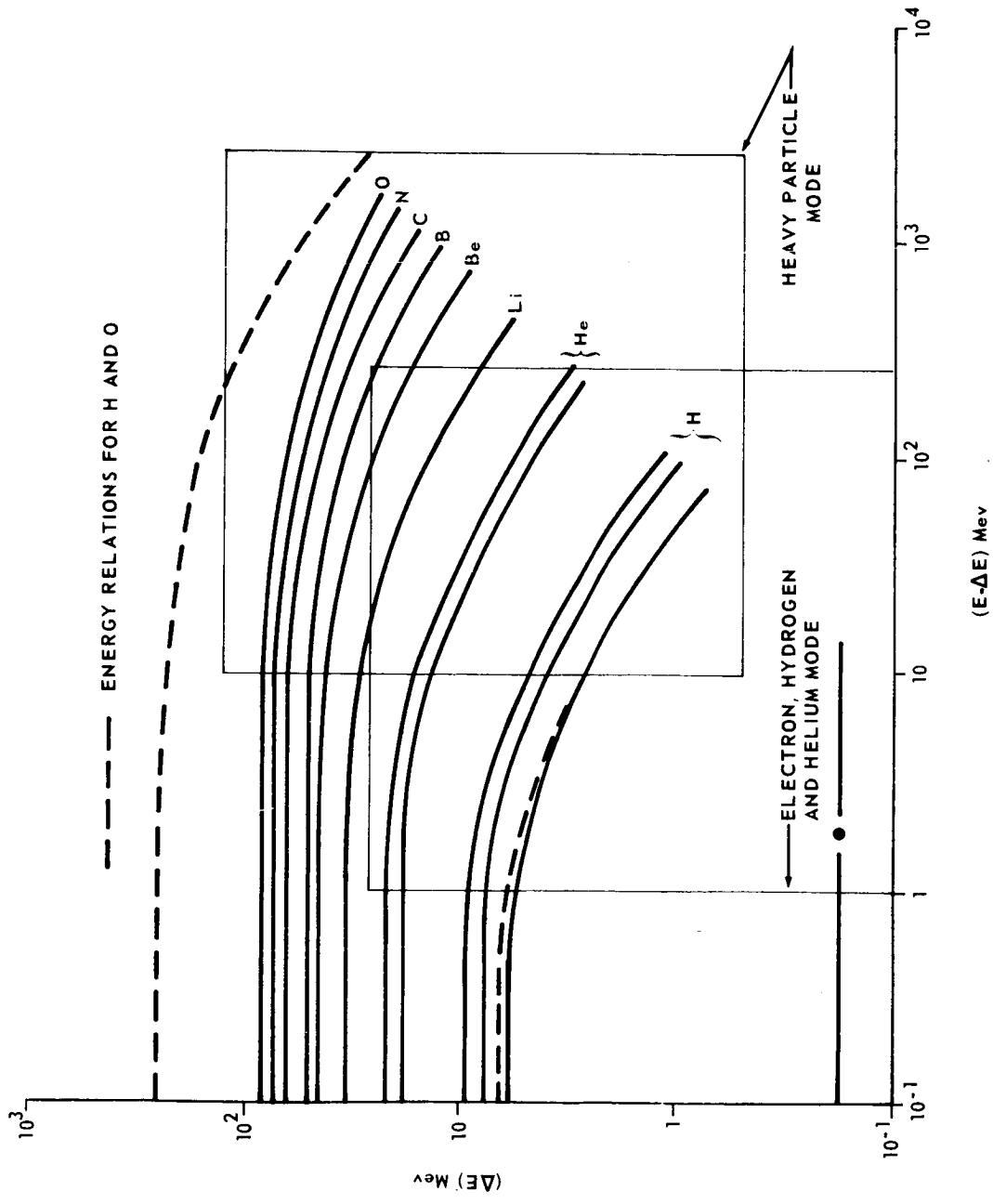


FIGURE III-13. ENERGY RELATIONS FOR VARIOUS PARTICLES

The designers of space vehicles should be aware of the probability of penetration and the extent of erosion caused by micrometeoroids. Erosion caused by micrometeoroids may not be important on short missions, but in missions extending over a long period of time, erosion may become very serious [ Ref. III-26].

The micrometeoroid flux in cislunar space has been measured and is fairly well understood. Such earlier satellites as Vanguard, Explorers and Pioneers carried micrometeoroid detectors. Most of these detectors could measure only the number of impacts and the momentum of the particles. The velocity of the particles and/or their mass was undetermined. The cumulative mass-distribution curve obtained in various earlier satellite flights in the vicinity of the Earth is shown in Figure III-14 [ Ref. III-10]. The masses of the particles were obtained by assuming a constant mean velocity of the micrometeoroids.

Now that travel to the outer planets is anticipated, a knowledge of the micrometeoroid population in this part of the solar system becomes important. Even though the probability of penetration may be small, penetration becomes an important factor when the time of flight becomes great. Also even though the erosion rate may be small, the times involved in travel to the outer planets are large enough that the total depth of erosion may be significant. So a knowledge of the micrometeoroid flux in this region of outer space is important to the designer of future spacecraft planned for the exploration of the outer planets.

Micrometeoroid Measurements on JOVE. JOVE is planned to traverse the space between Earth and Jupiter and then to orbit Jupiter. This vehicle will carry detectors to measure the number and penetrating power of the micrometeoroids in this region. Such information will be of interest for the cosmologists and will aid the designers of future space vehicles planned for use in this region of the solar system.

The micrometeoroid detectors utilized on JOVE will be similar to those used by JPL on the Mariner-Mars spacecraft. These detectors consist of aluminum plates 22 cm by 22 cm to which is fastened a crystal acoustical transducer. Whenever a micrometeoroid strikes the plate, the crystal will emit an electrical pulse. Each side of the aluminum plate is covered with an insulating and a conducting film thus forming a capacitor type of detector. A potential is placed across this type of capacitor detector and when a micrometeoroid punctures the insulation of the capacitor an electrical discharge occurs. Such capacitor detectors are self healing. It is, therefore, good for

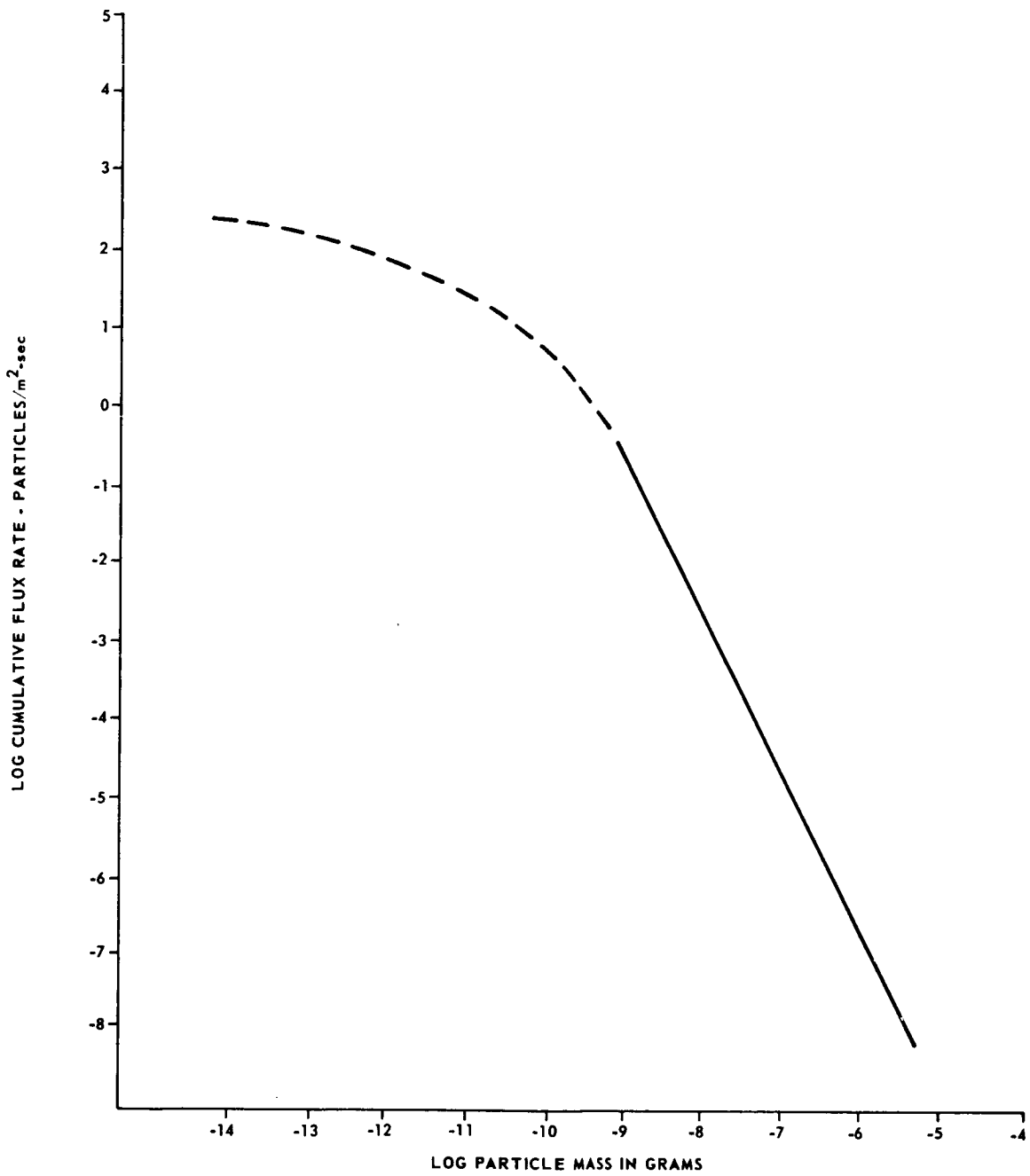
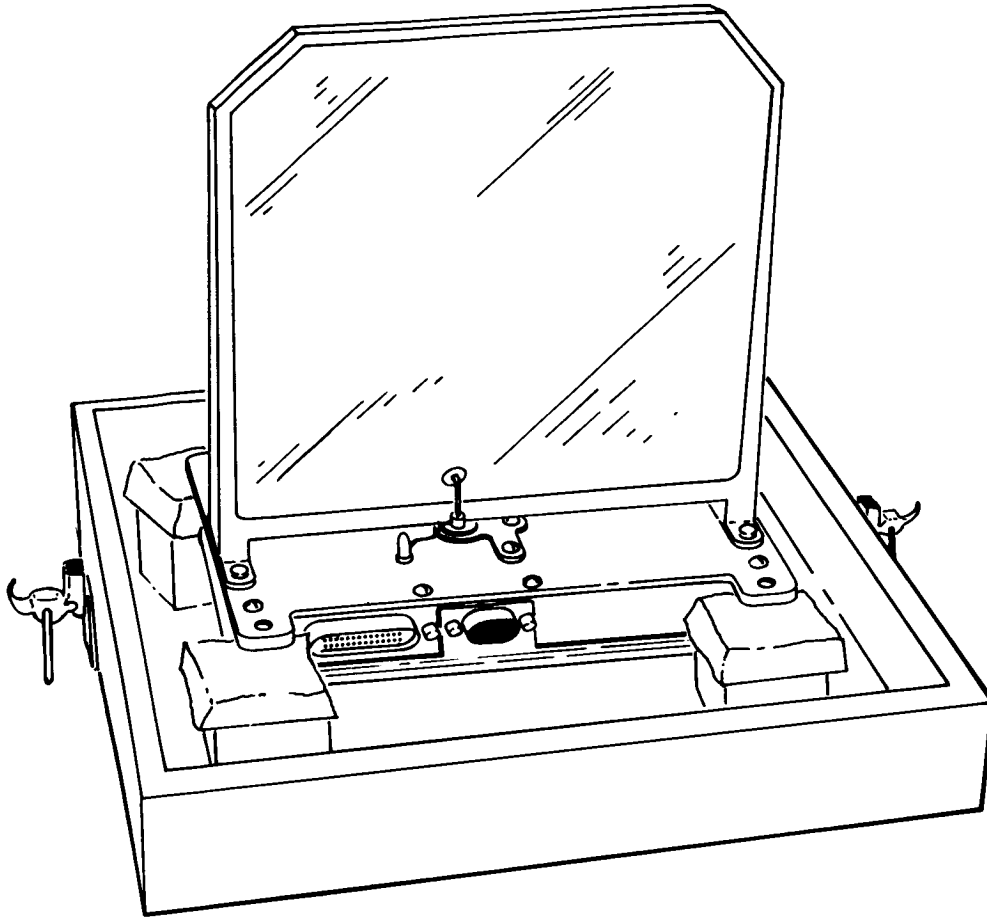


FIGURE III-14. MICROMETEOROID MASS DISTRIBUTION



<b>SIZE:</b>	<b>PLATES OF DETECTOR = 9" X 9" X 1/4"</b>
	<b>ELECTRONICS = 2" X 9" X 4"</b>
	<b>ANTENNA = 60" DIA.</b>
<b>WEIGHT:</b>	<b>2.5 LB.</b>
<b>POWER:</b>	<b>0.2 WATTS</b>
<b>BITS/RDG:</b>	<b>10</b>

**FIGURE III-15. MICROMETEOROID DETECTOR**



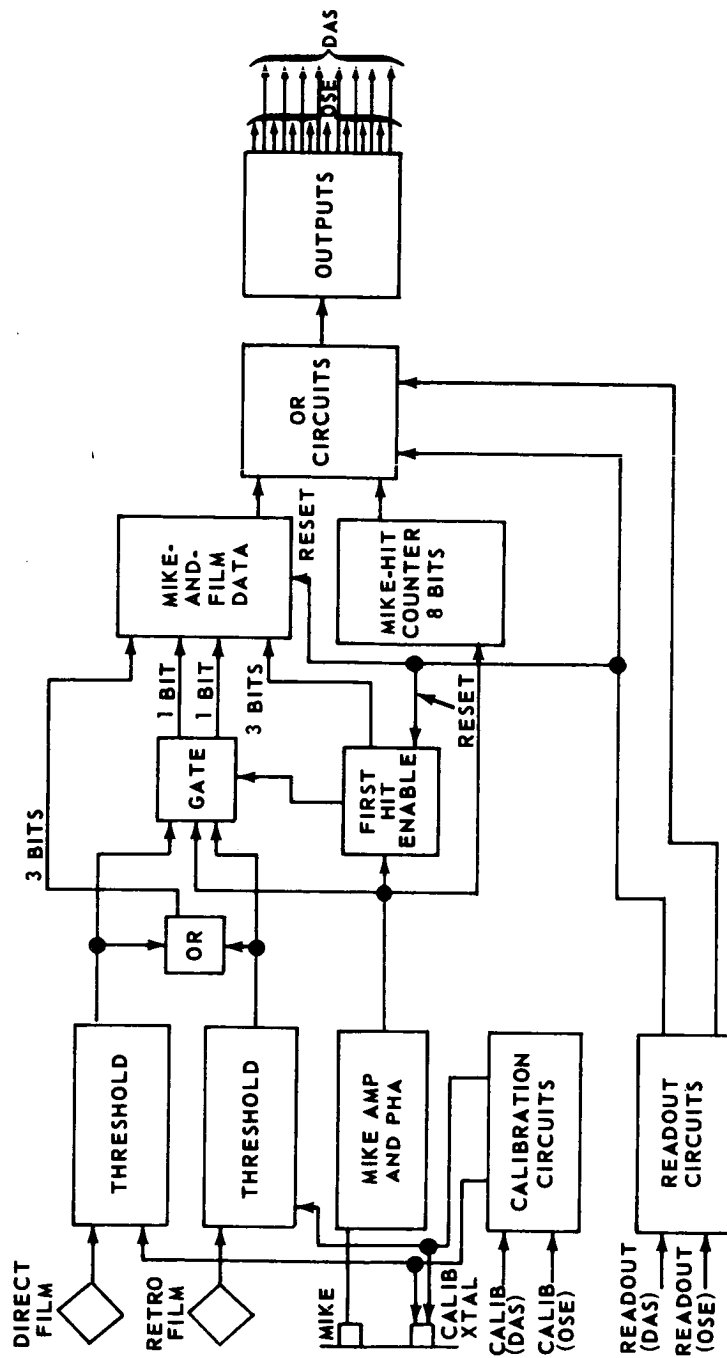


FIGURE III-16. MARINER-4 MICROMETEOROID CIRCUIT

repeated use. When the output of the acoustic detector is in coincidence with one or the other capacitor detector outputs, the direction of the micrometeoroid can be determined. Three of these detectors will be mounted with equal spacing around the outside of the spacecraft.

Detectors giving the velocity as well as the momentum should be carried on this mission but since such detectors are as yet not available, presently available detectors will be carried. If new micrometeoroid detectors are available by the time JOVE is scheduled they will be carried in place of or in addition to those described above.

The detector described is shown in Figure III-15 [ Ref. III-16 ], and the corresponding electronic circuit is shown in Figure III-16 [ Ref. III-10 ].

## UNIQUELY ORBITAL MEASUREMENTS AND INSTRUMENTS

### Photometers (Visible and Ultraviolet)

A photometer will be used to measure reflected brightness at various phase angles allowing for a determination of the planet's phase function

$$\phi(\alpha) = \frac{I(\alpha)}{I(0)}$$
. A filter wheel giving transmission at 1216, 3888, and 6402 Å will be used. The narrow band photometry above will be used to look for hydrogen, helium, and neon, respectively.

Combined photometric and polarization measurements will give an unambiguous fit of a model atmosphere. This is possible because the polarization caused by Rayleigh scattering dust particles, thin clouds and reflected light from the planet can be separated and a model constructed that fits the measured polarization. The polarization cannot be determined by viewing in one direction and is therefore not possible from Earth because the phase angle is never greater than eleven degrees. A polarimeter will also give data on particle size and distribution in the atmosphere and will aid in determining albedo.

In-flight calibration will be accomplished by injecting a standardized calibration current into the input amplifier or looking at a standard brightness source. This instrument is mounted on the scan platform and must be shielded from direct or reflected sunlight.

A block diagram of a typical ultraviolet photometer is shown in Figure III-17. Other specifications are summarized below:

Weight:	6 lb
Size:	4 in. x 5 in. x 6 in.
Power:	5 watts
Bits/rdg.	120
Scan frequency:	maximum - one/min

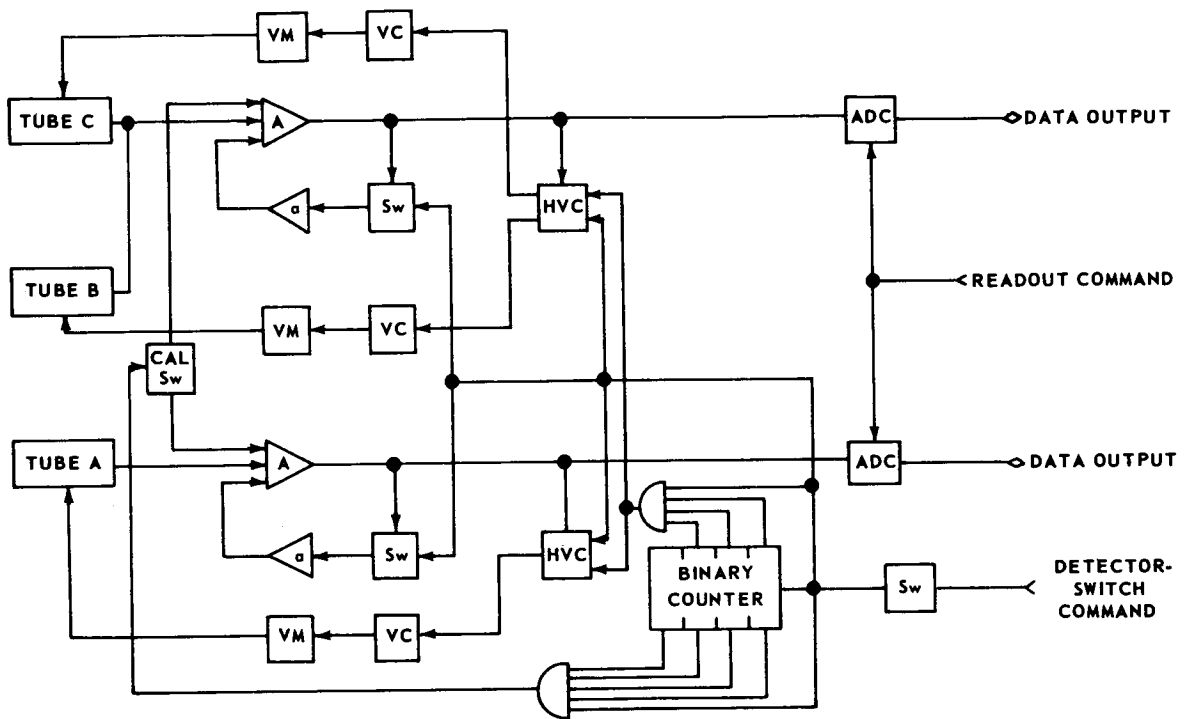
## Radiometers

Infrared. This will measure radiation flux in the infrared region of the spectrum to allow for a temperature map of the clouds or surface when it is visible. The device, similar to the one used in Mariner II (Fig. III-18, III-19) contains two optical sensors, each with a focal length of 3 inches and an f number of 2.4. One of the sensors is used to scan the planet, the other one to obtain internal reference readings. Radiation enters the optics, passing through a rotating disk with two apertures positioned so that the two sensors can see their respective targets. The light beam is chopped at 20 cycles per second. The beam is then split by a dichroic filter into two components polarized at right angles. These two beams fall upon thermister bolometers. The temperature of the sensors is proportioned to the intensity of the incident radiation. By selecting suitable filters any infrared wavelength can be studied. These filters will transmit the 1 through 9  $\mu$ , the 9 through 13  $\mu$ , and the 13 through 16  $\mu$  (micron) bands.

Use of a broad band flux measurement will determine whether Jupiter radiates more energy than it receives. Scanning with this instrument will give the wavelength dependence of the atmospheric opacity and its variation over the disk of the planet. These measurements cannot be made from Earth with anywhere near the resolution obtainable from an orbit of Jupiter.

Some characteristics of the device are shown below:

Weight	5 lb
Size:	4 in. x 6 in. x 6 in.
Power:	3 watts
Bits/rdg.	20
Scan frequency	max. one/min



CAL. SW: CALIB. SWITCH (SOLID STATE)  
 Sw: SWITCH (SOLID STATE)  
 A: INPUT AMPLIFIER  
 a: DRIFT CORRECTION AMPLIFIER  
 HVC: HIGH VOLTAGE CONTROL  
 VC: HIGH VOLTAGE CONVERTER  
 VM: VOLTAGE MULTIPLIER  
 ADC: ANALOG TO DIGITAL CONVERTER  
 PS: POWER SUPPLY  
 CL: CURRENT LIMITER

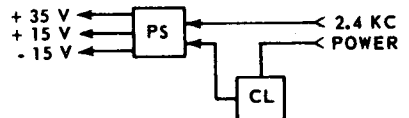


FIGURE III-17. BLOCK DIAGRAM - TYPICAL ULTRAVIOLET PHOTOMETER

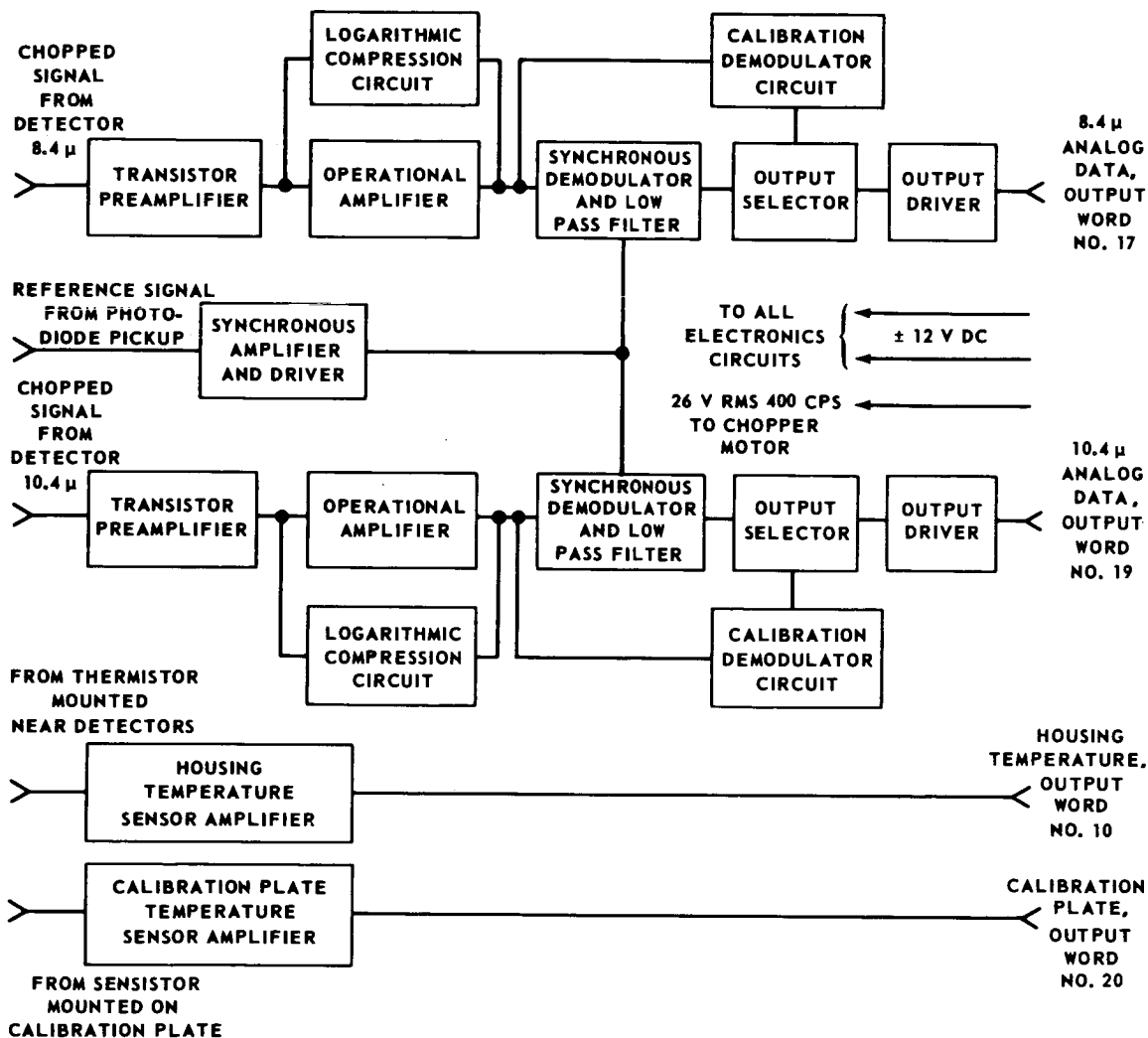


FIGURE III-18. BLOCK DIAGRAM - MARINER-2 INFRARED RADIOMETER

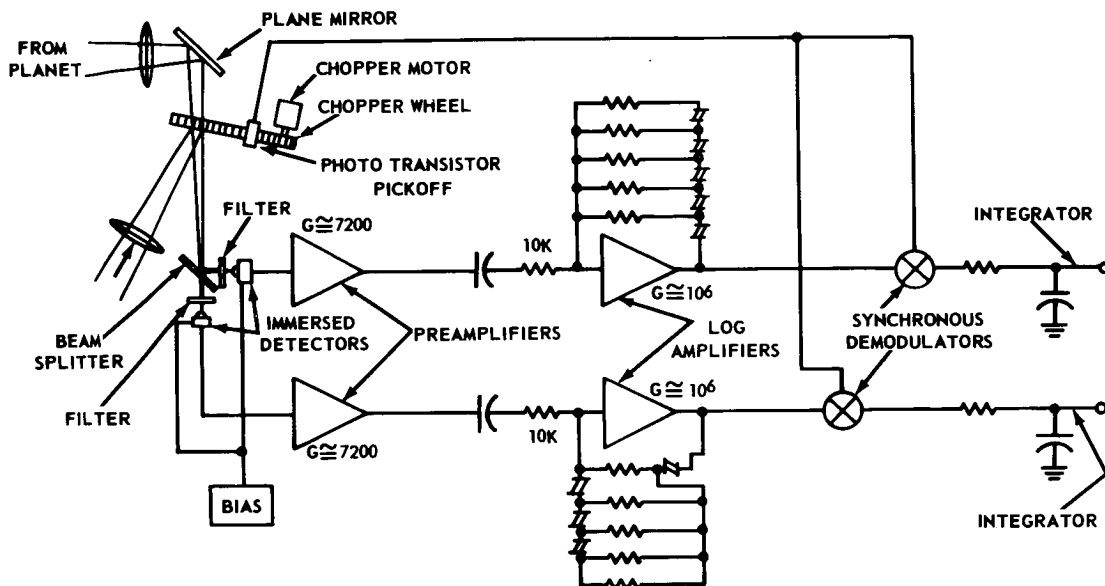


FIGURE III-19. COMPONENT ARRANGEMENT - MARINER-2 INFRARED RADIOMETER

Microwave. Two types of microwave radiation are emanating from the planet Jupiter; thermal radiation and non-thermal radiation.

The thermal radiation is in the millimeter and low centimeter region and the non-thermal radiation is in the decimeter and decameter region.

The non-thermal signals seem to come from accelerated electrons in the magnetic field of Jupiter. The radiation in the decimeter range apparently comes from synchrotron electrons.

Measurements of the radio signals from Jupiter have been made from the earth. Thus it has been possible to map the surface of Jupiter of the side facing the earth. However, it has not been possible to map the region facing away from the earth for this type of radiation. Therefore, it seems highly desirable to carry instrumentation for this type of measurement on a Jupiter orbiting spacecraft.

For measurements of the microwave signals from Jupiter, a microwave radiometer similar to the one used on Mariner II will be carried on JOVE. This radiometer will also be a fixed frequency radio receiver picking up signals in two frequency regions: 3 cm and 30 cm. In all other respects a microwave radiometer similar to the one used on Mariner II will be carried. This instrument is shown in Figure III-20.

The radio signals emanating from the side of Jupiter which faces the earth can be measured more accurately from the earth than from a spacecraft. It is suggested therefore, that the microwave radiometer not be turned on during the time of flight of the vehicle from the Earth to Jupiter, but that it be operative just before the spacecraft begins its orbital path around Jupiter.

The signals in the 3 cm region will be used to measure the temperature of various regions of Jupiter. In view of this, the measurements taken by the microwave radiometer should be taken at the same time and in the same region as the measurements taken by the infrared radiometer. The microwave radiometer should be mounted on the same gimballed platform as the infrared and ultraviolet radiometers.

The microwave radiometer will be about 22 pounds in weight and will use 10 watts of power. The information is read out at the rate of 20 bits/reading. The diameter of the antenna used by the microwave radiometer is about 5 feet.

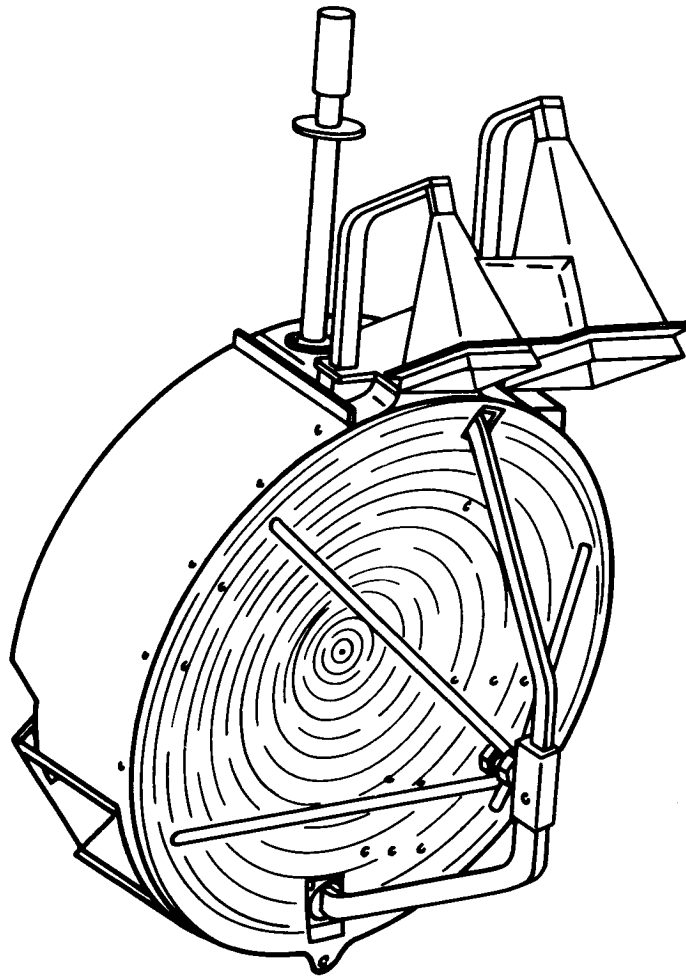


FIGURE III-20. MARINER-2 MICROWAVE RADIOMETER-DISH



The resolution of the microwave radiometer [ Ref. III-27, III-28] , is given by the relation:

$$\text{Resolution} = \frac{\text{Beamwidth} \times \text{Distance}}{57.3}$$

For wavelength of 3 cm

$$\text{B. W.} = 1.5^\circ$$

$$\text{Res.} = 12\,000 \text{ km.}$$

For wavelength of 30 cm

$$\text{B. W.} = 15^\circ$$

$$\text{Res.} = 120\,000 \text{ km.}$$

Figure III-21 shows the electronic circuits associated with the microwave antenna.

## Television

Introduction. Direct visual pictures of Jupiter can best be obtained through the use of a television system. Photography is ruled out because of the sensitivity of photographic emulsions to the radiation that will be encountered in space, near Jupiter, and from the RTG units on the spacecraft itself.

The use of television greatly increases the data storage problem but this is justified by the greater resolution that is obtainable over Earth-based telescopes, as well as the favorable public relations effect of "pictures" of Jupiter. The best resolution as seen from Earth is on the order of one thousand kilometers allowing us to see only the grossest features such as the red spot and the latitude banding. Telescopes in orbit about Earth could give a resolution of two hundred kilometers but there is no plan at present to orbit such a telescope. While it is not absolutely clear what the higher resolution will show, it is believed that there are many things that are now on the border of this higher resolution that appear to be very interesting.

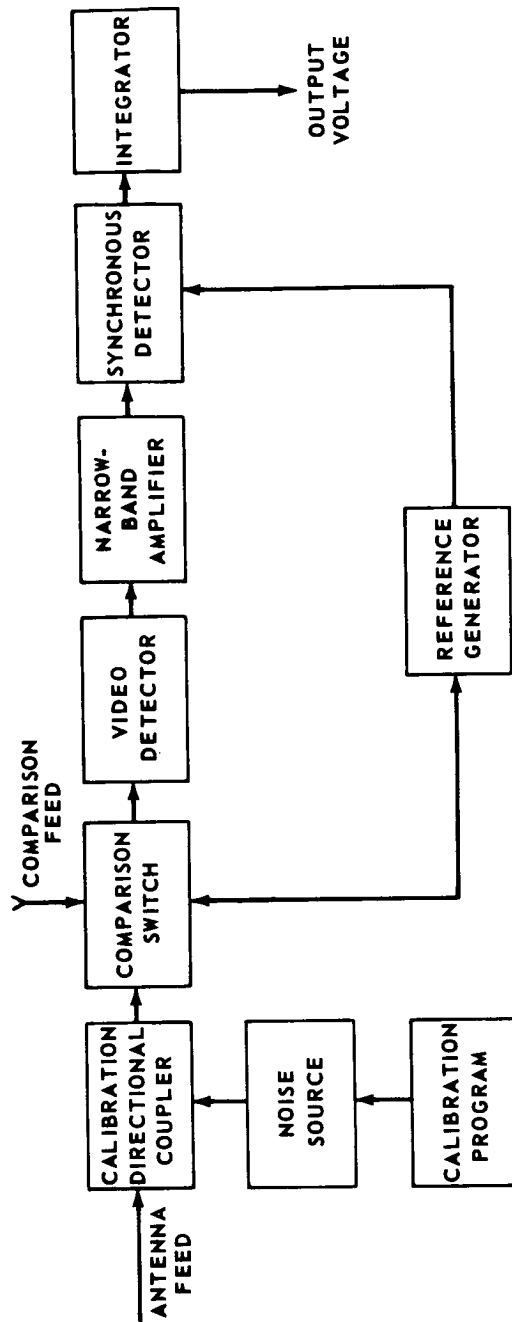


FIGURE III-21. BLOCK DIAGRAM - MARINER-2 MICROWAVE RADIOMETER

Instrumentation. Resolution on the order of 60-70 kilometers will allow observation of some structure in the red spot, boundaries between the latitude bands, and behavior of the general circulation around the edges of the red spot. The TV cameras will also get information regarding the meteorology of the outer Jovian atmosphere. On the dark side of the planet, the TV experiment will show lightning flashes and near the limb aurora effects will be shown, especially within  $10^{\circ}$  -  $30^{\circ}$  of the magnetic poles.

The television system will be mounted on a scan platform such that it never sees direct sunlight or scattered light reflected from the spacecraft lest the sensitive phosphors be damaged by this intense light. Three spectrally separated filters will be mounted on a shutter wheel to look at the color components separately. These filters will be stable in the space environment. An electrostatic type vidicon tube will be used because of its simplicity, weight, size, ruggedness, and ability to operate itself. The image will be stored on the face of the tube for 20-30 seconds with negligible degradation while it is being read out and converted to a digital output. The picture is erased by flooding the phosphors with electrons, preparing for the next picture. Only a few wide angle pictures for orientation will be taken, but many narrow angle pictures for detail will be available.

The optical system will be made of materials that minimize focal shifts and distortions caused by thermal expansion and radiation. To keep lens transmission loss less than ten percent an optically flat piece of radiation resistant fused quartz will be used as a lens cover. This cover will be several tenths of an inch thick and will also serve as thermal protection for the system.

The television system will consist of two cameras: (1) a 1000 line system with a  $10^{\circ}$  view and (2) a 400 line system with a  $1^{\circ}$  view.

The spatial resolution of the two cameras is shown in Table III-4 for various distances from the center of the planet Jupiter. Pertinent physical parameters for both cameras are included.

## Spectrometers

Infrared. At present the energy balance of Jupiter is not understood. Jupiter absorbs radiation from the sun and emits infrared radiation largely between 10 and 50 microns. Ammonia, a known constituent of Jupiter's atmosphere is an absorption band in the region of 9 to 13 microns. It is

suspected that there are other infrared absorbing constituents in the atmosphere of this planet since its surface temperature is higher than would be the case if more of the emitted infrared escaped into outer space.

An infrared spectrometer is needed to scan the planet at wavelengths from 5 to 30 microns with sufficient resolution (about 1 micron) to detect infrared active constituents in its atmosphere. From these data one can determine the presence and concentration of infrared active gases. It will also be possible to measure atmospheric temperature for thermal wavelength regions and get an indication of surface conditions at the poles, which are relatively free of clouds. Scientists have not been able to obtain these measurements from Earth because of atmospheric and energy considerations.

This instrument can also detect some of the Sinton bands between five and sixteen microns that will be indicative of organic molecules on the surface. Carbon dioxide and water can also be detected with a slightly extended range instrument (Fig. III-22).

Dispersion is obtained with a diffraction grating but detection in these wavelengths is limited to a Golay gas cell or a germanium-zinc semiconductor, the latter of which will be used.

If the angle of view is  $2^\circ$ , the solid angle subtended is  $\theta = 4 \times 10^{-2}$  steradians. At  $N R_j$  distance, the percent of surface area covered is about  $\frac{N^2\theta}{2\pi}$  or about  $0.01N^2$  percent per degree of view. Using Stefan's law the power received at the probe is  $\frac{10^{-2}}{N^2} \frac{\text{watts}}{\text{CM}^2}$  for a planet temperature of  $150^\circ \text{K}$ .

Some important characteristics of the instrument are given below:

Weight:	16 lb
Power:	5 watts
Size:	10 in. x 12 in. x 14 in.
Bits/rdg:	5000
Scan:	once every thirty minutes (maximum)

This instrument will be mounted on the scan platform and the detector will be kept at a temperature near  $25^\circ \text{K}$ .

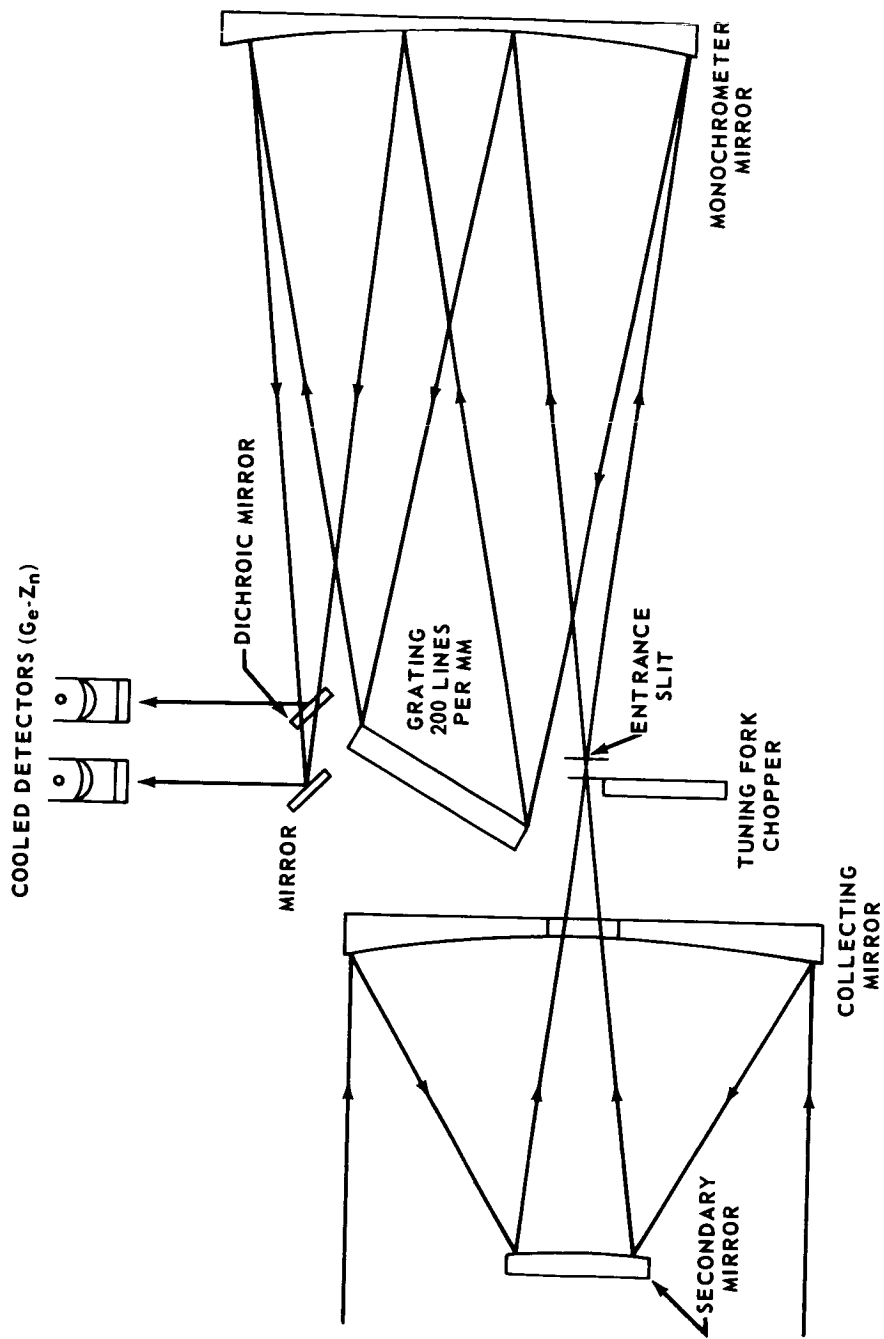


FIGURE III-22. DIAGRAM OF INFRARED SPECTROMETER

Visible and Ultraviolet. An instrument with a 1000 - 5000 Å resolution (and sufficient spatial resolution to determine limb and terminator effects) will be used to examine the cloud cover and surface obtaining information about the constituents, pressure, and temperature. This close spectroscopic examination is to identify constituents whose absorption bands are either too weak to be observed on Earth or are below the atmospheric cutoff. These data can lead to estimates of pressure, temperature, and abundance of gases which will aid in formulating a model of the Jovian atmosphere.

Identification of C-N-H compounds will aid in explaining the periodic color changes observed in the clouds and will help to describe the history and internal composition of Jupiter. Scanning the red spot may give useful data. A scan of the limb will give a pressure measurement, while a scan over the terminator will give atmospheric absorption and aurora information.

This instrument must be mounted on the scan platform and no direct or scattered sunlight can be allowed to impinge on the detector. Characteristics are given below:

Weight:	20 lb
Size:	10 in. x 13 in. x 16 in.
Power:	10 watts
Bits/rdg:	10 000
Scan:	once every 30 min
Calibration:	internal

## REFERENCES

1. Witting, J. M; Cann, M. W. P and Owen, T. C.: Critical Measurements on Early Missions to Jupiter. IITRI Report P-10, December 1965.
2. Davies, W. O.; Norin, F.; Roberts, D. L.; Schmidt, L. A.; Scholz, L. C.; Store, C. A. and Vickers, R.: Survey of a Jovian Mission. IITRI Report M-1, September 1963.
3. Space Science Board, Space Research Direction for the Future, Parts I and II, National Academy of sciences, January 1966.
4. Sodek, B. A. and Redmond, J. C.: Jupiter: Review and Space Probe Measurements, FZM-4677, General Dynamics, Fort Worth Division, August 1966.
5. Hill, A. S. and Lucas, W. C.: Survey of Experiments for a Jupiter Orbiter/Close Solar Probe, TM-293-6-049, Northrop Space Laboratories, Huntsville, Alabama.
6. Mohr, B.; Poznonski, Z.; Luganski, D.; Kraft, G and Gross, S. H.: Investigation of Planetary Ionospheres, NASA CR-689, May 1967.
7. Flattau, T. and Donegan, R.: Final Report for Study of Topside Sounder for Mars and Venus Ionospheres from Mariner Spacecraft, NASA CR-52731, October 1963.
8. Corliss, W. R.: Space Probes and Planetary Exploration. D. Van Nostrand, 1965, p. 420.
9. Handbook of the Physical Properties of the Planet Jupiter. NASA SP-3031, 1967.
10. Corliss, W. R.: Space Probes and Planetary Exploration. D. Van Nostrand, Princeton, 1965.
11. Ruddock, K. A.: Optically Pumped Rubidium Vapor Magnetometer for Space Experiments in Space Research III, W. Priester, ed., Interscience, New York, 1963.

## REFERENCES (Continued)

12. Slocum, R. E. and Reilly, F. N.: Low Field Magnetometer for Space Applications. IEEE Transactions on Nuclear NS-10, 165-171.
13. Green, A. E. S. and Wyatt, P. J.: Atomic and Space Physics. Addison Wesley, 1965, Chapter 12.
14. Significant Achievements in Particles and Fields 1958-1964. NASA SP-97, 1966.
15. Handbook of the Physical Properties of the Planet Jupiter. NASA SP-3031, 1967.
16. Schultz, F. L., et al.: Mariner-Mars Science Subsystem. JPL Technical Report Number 32-813, August 15, 1966.
17. Corliss, W. R.: Space Probes and Planetary Exploration. D. Van Nostrand, Princeton, 1965, Chapter 3.
18. Baden, M.; Fryer, T. B. and Witteborn, F. C.: Two Instruments for Measuring Distributions of Low Energy Charged Particles in Space. NASA Technical Note D-1035, July 1961.
19. LeGalley, D. P. and Rosen, A.: Space Physics. John Wiley & Sons, New York, 1964, Chapter 11.
20. Corliss, W. R.: Space Probes and Planetary Exploration. D. Van Nostrand, Princeton, 1965, Chapter 13.
21. LeGalley, D. P. and Rosen, A.: Space Physics. John Wiley & Sons, New York, 1964, Chapter 17.
22. Price, W. J.: Nuclear Radiation Detection Second Edition. McGraw-Hill, 1964, Chapter 1.
23. Friedland, S. S.; Ziembra, F. P.; Olson, R. M and DeLyser, H.: Application of Nuclear Semiconductor Detectors for Space Spectrometry. IRE Transactions of Nuclear Science, N. S. -9 pp. 391-399.



## REFERENCES (Concluded)

24. Bryant, D. A.; Ludwig, G. H. and McDonald, F. B.: A Scintillation Counter Telescope for Charge and Mass Identification of Primary Cosmic Rays. NASA Technical Note D-1757, August 1963.
25. Ludwig, G. H. and McDonald, F. B.: Cosmic Ray Experiments for Explorer XII and the Orbiting Geophysical Observatory in Space Research III, W. Priester, ed. Interscience, New York, 1963.
26. LeGalley, D. P. and Rosen, A.: Space Physics. John Wiley & Sons, New York, 1964, Chapter 8, pp. 270-296.
27. International Telephone and Telegraph Corporation: Reference Data for Radio Engineers, Fourth ed., p. 803.
28. Steinberg, J. L. and Lequeux, J.: Radio Astronomy. McGraw-Hill, 1963.

## BIBLIOGRAPHY

Astro Science Center - I. I. T. Research Institute: Summary of Flight Mission to Jupiter, NASr-65 (06).

Brown and Lovell,: The Exploration of Space by Radio. John Wiley & Sons.

D'Aiutolo,: The Micrometeoroid Satellite Explorer XIII (1961CHI). Langley Research Center NASA TND-2468.

Hayes and Miller: Effects of 1.2 and 3.0 MeV Electrons on the Optical Transmission Properties of Several Transparent Materials, NASA TN D-2620.

Kobren, L: Effect of Electron Radiation on TV Lens Components. NASA TN D-2919.

Lewis Research Center: Micrometeoroid Satellite (Explorer XIII) Stainless Steel Penetration Rate Experiment NASA TN D-1986.

McFarling, J. L.: Survey of Instrumentation and Instrumental Techniques for Scientific Exploration of the Moon. Battelle Memorial Institute. Redstone Arsenal Contract Number DA-01-021-AMC-203 (Z).

Northrop: Survey of Experiments for a Jupiter Orbiter/Close Solar Probe. TM-293-6-049, July 1, 1966.

Odom, P. R.: Applications of Saturn/Apollo Hardware to Unmanned Scientific Exploration of the Solar System. TR-292/3-6-003, April 1966.

Research Triangle Institute. Study on the Electron Irradiation Effects on Capacitor-Type Micrometeoroid Detectors. Contract NAS 1-3892, NASA Cr-312.

Smith, and Carr: Radio Exploration of Planetary System. D. Van Nostrand.

Smith and Vaughan, Jr.: Space Environment Criteria Guidelines for Use in Space Vehicle Development. 1937 Revision NASA TMX-53521, February 1, 1967.

## BIBLIOGRAPHY (Concluded)

Sodek, B. A. and Redmond, J. C.: Jupiter Review and Space Probe Measurements.

Wyckoff, R. C.: Scientific Experiments for Mariner R-1 and R-2. JPL TR 32-315.

**CHAPTER IV**  
**TELECOMMUNICATION SYSTEM**



# CHAPTER IV. TELECOMMUNICATION SYSTEM

## DEFINITION OF SYMBOLS

$P_r$	=	received signal power, watts
$P_t$	=	transmitted signal power, watts
$G_t$	=	transmitting antenna gain
$G$	=	antenna gain
$G_r$	=	receiving antenna gain
$L_f$	=	free space path loss
$L_a$	=	system loss
$\beta$	=	communications efficiency
$E_{\min}$	=	minimum energy/bit
$\epsilon^2$	=	noise power spectral density
$\frac{S_i}{N_i}$	=	predetection signal-to-noise ratio
$B$	=	predetection signal bandwidth
$\frac{S}{N}$	=	postdetection signal-to-noise ratio
$H$	=	message bandwidth
$P_{\min}$	=	minimum received power, watts
$k$	=	Boltzmann's constant, $1.38 \times 10^{-23}$ Joules/ $K^\circ$
$T$	=	effective noise temperature $^\circ K$

## DEFINITION OF SYMBOLS (Continued)

$\lambda$	=	wavelength, meters
$A_{em}$	=	maximum effective aperture, square meters
$A_{phys.}$	=	physical aperture, square meters
$D$	=	reflector diameter, meters
$D_{\lambda}$	=	reflector diameter, wavelengths
$R$	=	range
$\theta$	=	angle
$F(r)$	=	aperture field distribution
$r$	=	plane-projected radial distance from vertex to point on the paraboloidal surface
$R(\theta)$	=	radiation field intensity
$BW$	=	beamwidth, degrees
$K_p$	=	polarization loss
$A_t$	=	transmitting antenna axial ratio
$A_r$	=	receiving antenna axial ratio
$T_a$	=	antenna noise temperature, °K
$T_s(\theta, \phi)$	=	source brightness temperature
$G(\theta, \phi)$	=	antenna gain
$\Omega_s$	=	solid angle subtended by source at the point of observation
$\bar{T}_s$	=	average source temperatures

## DEFINITION OF SYMBOLS (Continued)

$\theta_s$	=	plane angle subtended by the source
$\theta_b$	=	plane angle 3 dB antenna beamwidth
S	=	flux density, watts/m <sup>2</sup> cps
df	=	frequency interval
Pe <sup>b</sup>	=	bit error probability
Pd	=	bit period
bps	=	bits per second
Fc	=	clock frequency supplied to PN generators
D	=	command bit
$\oplus$	=	half addition, or modulo 2 addition
L	=	length of PN code
N/B	=	noise spectral density per cycle/second
N	=	number of bits per word
Pi	=	probability density function
PN	=	pseudorandom
S	=	signal power
Pe <sup>w</sup>	=	word error probability
A/D	=	analog to digital converter
CC&S	=	central computer and sequencer

## DEFINITION OF SYMBOLS (Concluded)

DSIF = deep space instrumentation facility

DSN = deep space network

EDE = engineering data encoder

MTR = magnetic tape recorder

NRT = non-real time

PSK = phase shift key

PCM = pulse code modulation

SDS = science data system



## INTRODUCTION

The purpose of the JOVE telecommunications system is to provide a means of information transfer and control of sufficient quality to accomplish the mission of unmanned reconnaissance of Jupiter. In order to achieve the stated purpose efficiently, it is necessary to rely upon the existing and/or planned capabilities of the NASA-JPL Deep Space Network for the Earth-based portion of the telecommunication system. However, the emphasis in this section will be mainly on the transmission medium and the spacecraft portion of the telecommunication system. An understanding of capabilities and constraints of the existing Earth-based system, however, is essential for effective system integration.

## FUNCTIONAL DESCRIPTION OF THE TELECOMMUNICATION SYSTEM

The telecommunication system performs four basic functions on unmanned interplanetary spacecraft: tracking, data acquisition, command, and control. Tracking is the function of locating the spacecraft, calculating its distance, velocity vector, and position, and following its course in order to correctly interpret scientific data. Data acquisition consists of the recovery of information from the spacecraft in the form of telemetry of the recorded measurements of the condition of the spacecraft and of the scientific data obtained by the spacecraft. The command function involves the sending of signals to the spacecraft to guide it in its flight and to operate scientific and engineering equipment on board the spacecraft. Control refers to making command decisions from a central facility and to the overall direction of flight operations during a mission. The manner in which each of the functions is performed will be developed in the following sections.

## COMMUNICATION SYSTEM DESIGN CONSTRAINTS

The communication system design must provide for telemetering of engineering and scientific data on the downlink from the spacecraft to DSIF stations in a reliable yet flexible manner. The JOVE telemetry system will

have the capability of adding or deleting measurements as a function of specific flight phase. An example is that of the mid-course correction maneuver phase, when extensive measurements must be made on the mid-course motor but are not required at any other time during flight.

In addition to telemetry, the communication system must provide an Earth-to-spacecraft command-link for the initiation and modification of various spacecraft functions. The data rate for the command system is very low, but the requirements on accuracy are severe. Since the command system must be used for correcting possible malfunctions in the attitude control system of the spacecraft, the spacecraft command system's receivers must be accessible in any spacecraft attitude. This requires omnidirectional antenna coverage. The system must also provide two-way Doppler information for the purpose of accurate trajectory determination and allow automatic angle tracking of the spacecraft at the receiving sites as well.

The study of possible Earth-Jupiter trajectories revealed early in the design process that the communication system must be capable of operating over a distance of  $825 \times 10^6$  km ( $500 \times 10^6$  mile). This enormous communication distance causes a great attenuation (278.7 dB) of the radio waves from the spacecraft, as well as from the Earth-based communication stations. Since radio waves travel at a finite velocity ( $3 \times 10^8$  meters per second), the round trip communication delay time (92 minutes) makes real-time control of the spacecraft out of the question. Thus, command signals for the control of the spacecraft must be sent well in advance of the time of execution, or stored as pre-programmed instructions in the spacecraft computer and sequencer.

One of the major elements of the spacecraft system design is a three-axis attitude stabilization system. Sun-seeking devices will first orient the longitudinal axis of the spacecraft in the direction of the sun, establishing two-axis stabilization, and a star seeking system will orient the third axis toward the star Canopus, thereby achieving third axis control. After acquisition, a gimballed medium-gain antenna may then be pointed at the Earth during early phases of the mission. During later phases of the mission, the Sun sensors will be gimballed, and a high-gain parabolic antenna will be pointed toward the Earth. However, at launch and until such time as attitude control is achieved, communications must depend upon a nearly omnidirectional antenna system.

The lifetime of the mission, 850 to 900 days of heliocentric coast, places severe requirements upon components of the communication system. Choice of power amplifiers, for example, is predicated upon the lifetime of the devices. Also, the expected radiation environment in the vicinity of Jupiter rapidly degrades semiconductor performance.

Because of the spacecraft-sun-Earth relationship during the extended cruise to Jupiter, there will be periods when communications with the spacecraft will not be possible. The times of critical maneuvers during the spacecraft flight will be chosen to occur when there is communication with the spacecraft. If this is not possible, then instructions for the maneuver will be pre-programmed or transmitted via the command link well in advance of the execution time for the maneuver.

A spacecraft which is dependent upon solar cells for power would be severely limited in a cruise to Jupiter, since the solar flux and temperature decrease rapidly with increasing distance from the sun. The decision to use RTG's for spacecraft power means that the available power is almost constant throughout the cruise and is independent of the spacecraft orientation. However, since the RTG emits radiation which is damaging to semiconducting materials, the presence of the RTG on the spacecraft imposes a design constraint on the placement of electronic equipment.

A further important constraint imposed upon the communication system is that it must be compatible with, and use to the fullest extent possible, the existing NASA-JPL Deep Space Network (DSN) [ Ref. IV-1, IV-2]. A discussion of the capability and constraints imposed by the DSN is the subject of the next section.

## EARTH-BASED SYSTEM - DSN

This section contains a summary of the capabilities of the Deep Space Network (DSN) which is a facility of the National Aeronautics and Space Administration (NASA). The DSN is managed by the Jet Propulsion Laboratory (JPL) under contract to NASA for research, development, operation, and maintenance of the DSN stations.

### DSN Description

The Deep Space Network is a precision tracking, communications and data handling system which is used to support deep-space missions at Earth-referenced distances of more than 10 000 miles (16 090 km) and within  $\pm 30$  degrees Earth latitude. The Deep Space Network (Figure IV-1) comprises three major elements:

- 1 The Deep Space Instrumentation Facility (DSIF)
- 2 The DSN Ground Communications Facility (DSN)
- 3 The JPL Space Flight Operations Facility (SFOF)

DSIF Description. The DSIF is a worldwide chain of Deep Space Stations (DSS) that provide radio contact with the spacecraft. The DSIF for JOVE will probably consist of the space communication complexes and Deep Space Stations (DSS) shown in Table IV-1. To maintain continuous mission coverage, the stations are located approximately 120 degrees apart in longitude around the Earth, so that the spacecraft is always within the field of view at least one of the ground stations.

Radio contact with JOVE begins when it is poised on the launch pad at Cape Kennedy and, except for intervals during the sun's occultation of JOVE, is maintained throughout the mission. The Cape Kennedy Station supports the final checkout before launch, verifies the compatibility between the DSN and JOVE, measures JOVE frequencies during the countdown and provides limited telemetry reception during and immediately after launch. Later in the launch trajectory, while JOVE is relatively low in altitude, the signal is picked-up by the 30-foot diameter antenna at Ascension Island. Once JOVE is in orbit, the Deep Space Stations, with large antennas, low-noise phase-lock receiving systems, and high-power transmitters take over radio communications and follow JOVE to its destination. These stations obtain angular position (two angular coordinates), velocity (Doppler), and distance (range) data for JOVE and provide command control (up-link) at 2113 MHz and data reception (down-link) at 2295 MHz for JOVE. The standard 85-foot diameter antennas in use at the Deep Space Stations have gains of 53 dB at 2295 MHz, permitting the receipt of significant data at distances as far as Mars (1.5 AU). An improved data rate and distance capability are provided by a 210-foot diameter antenna having a gain of  $61.81 \pm 0.32$  dB at 2295 MHz which has been built at DSS 14. Two additional antennas of this size are planned for installation by 1971, at DSS 43 and DSS 63. In the present configuration, all stations listed in Table IV-1 are full S-band.

Deep Space Network/Ground Communication System (DSN/GCS). The DSN/GCS is an integrated communications network linking the various stations of the DSN when supporting spaceflight operation and mission test. It includes voice, teletype, and high-speed data links between the DSIF stations and the SFOF. The functions of the GCS are:

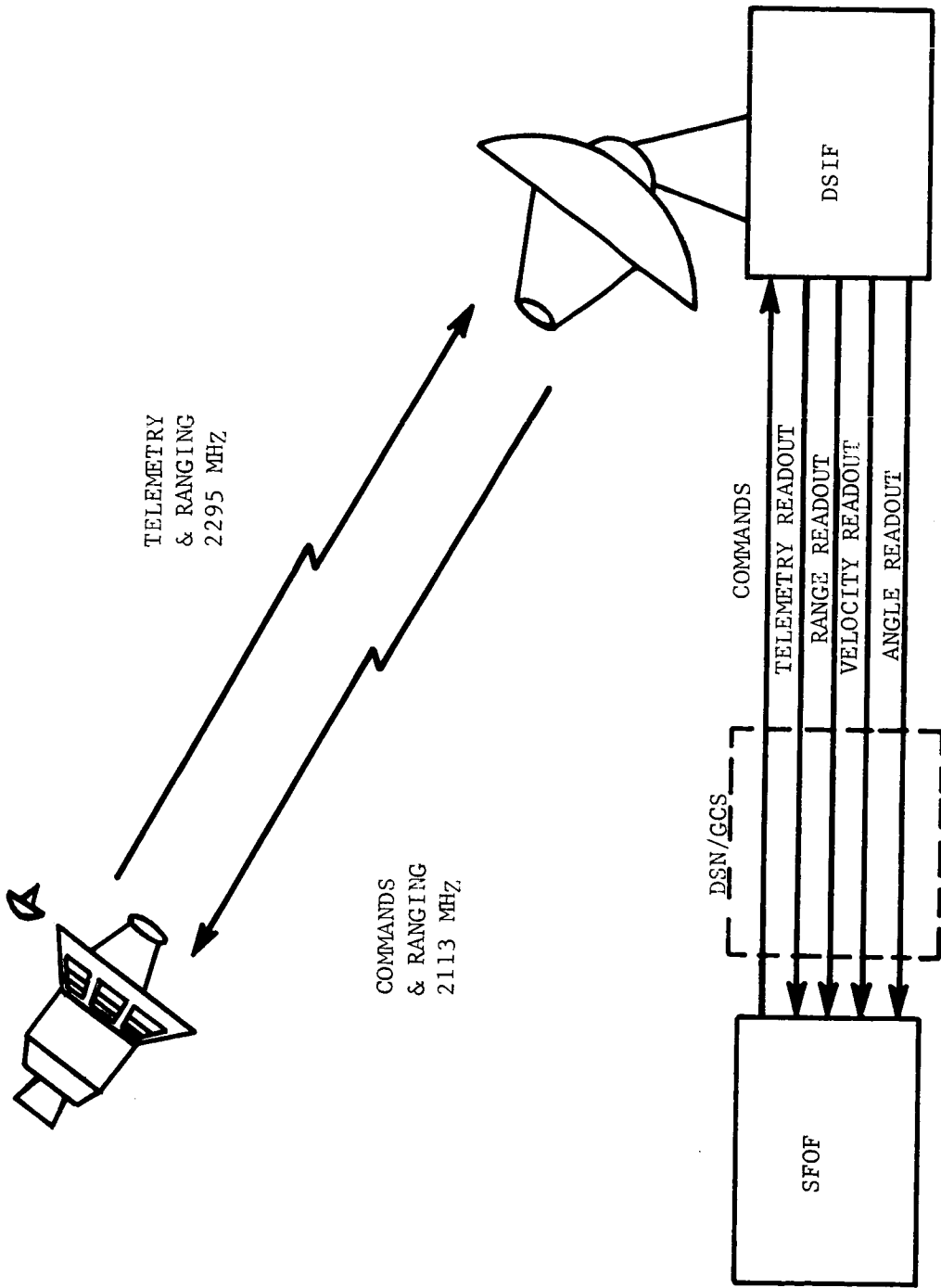


FIGURE IV-1. JOVE TELECOMMUNICATIONS SYSTEM

TABLE IV-1. SUMMARY OF DEEP SPACE INSTRUMENTATION FACILITY (DSIF)

<u>DEEP SPACE COMMUNICATION COMPLEX (DSCC)</u>	<u>DEEP SPACE STATION (DSS)</u>	<u>DSS SERIAL DESIGNATION</u>	<u>GEODETTIC LONGITUDE, DEG.</u>
Goldstone	Echo	12	243.2E
	Mars	14	243.1E
Canberra	Booroomba <sup>A</sup>	43	-
Madrid	Rio Corfio <sup>B</sup>	63	-
	Cape Kennedy (Spacecraft Monitoring)	71	279.4E
	Ascension Island (Spacecraft Guidance and Command)	72	345.7E

<sup>A</sup> Station not yet authorized - Geodetic longitude will be approximately 149E.

<sup>B</sup> Station not yet authorized - Geodetic longitude will be approximately 356E.

- to relay data and information received by the DSIF to the SFOF;
- to relay status information, operational instructions, and JOVE commands originating in the SFOF to the DSIF.

SFOF Description. The SFOF, located at the Jet Propulsion Laboratory in Pasadena, California, contains the central control and data operations complex, providing the means by which mission, flight, and DSN control may be exercised during the conduct and execution of spaceflight operations. Selected manned space flight network stations or ships may also be used for early orbit coverage.

## Data System Description [Ref. IV-2]

A block diagram of a Deep Space Station (DSS) is shown in Figure IV-2.

Automatic angle tracking using a simultaneous lobing technique is provided on both the 85-foot and 210-foot DSIF antennas. In addition, the antennas will be capable of being pointed with an antenna-pointing computer, using predictions generated at the SFOF. Automatic angle tracking is available only in the coherent mode; that is, when the received carrier is locked with a phase-lock loop. A wide angle, low-gain acquisition antenna is employed for initial acquisition with 85-foot antennas. Tracking is transferred to the 85-foot high-gain antennas as soon as practicable. The acquisition feed is mounted on the 85-foot reflector structure and hence has the same rate and acceleration limitations. The mechanical characteristics of DSIF station antennas are listed in Table IV-2.

Angle data is not an extremely useful orbit determination parameter for slant ranges much in excess of 100 000 miles ( $1.6 \times 10^5$  km); the primary value of angle tracking is to provide convenient antenna pointing in the absence of accurate angle predictions. Angle data is digitally encoded directly from antenna shaft positions on the 85-foot antennas, and from a master equatorial unit which is optically locked to the antenna structure on the 210-foot antenna.

One-way and two-way Doppler measurement capability will be available at all stations in the DSIF. Two-way Doppler data is presently the most valuable tracking parameter for orbit determination purposes. The technique involves transmitting a precision carrier to JOVE where it is coherently shifted and sent back via the down-link. The ground receiver then compares the phase of the received carrier with that of the transmitted carrier to extract the Doppler data. The distance at which the DSIF stations can obtain Doppler data is, of course, dependent on the sensitivity of JOVE's receiver and the power output

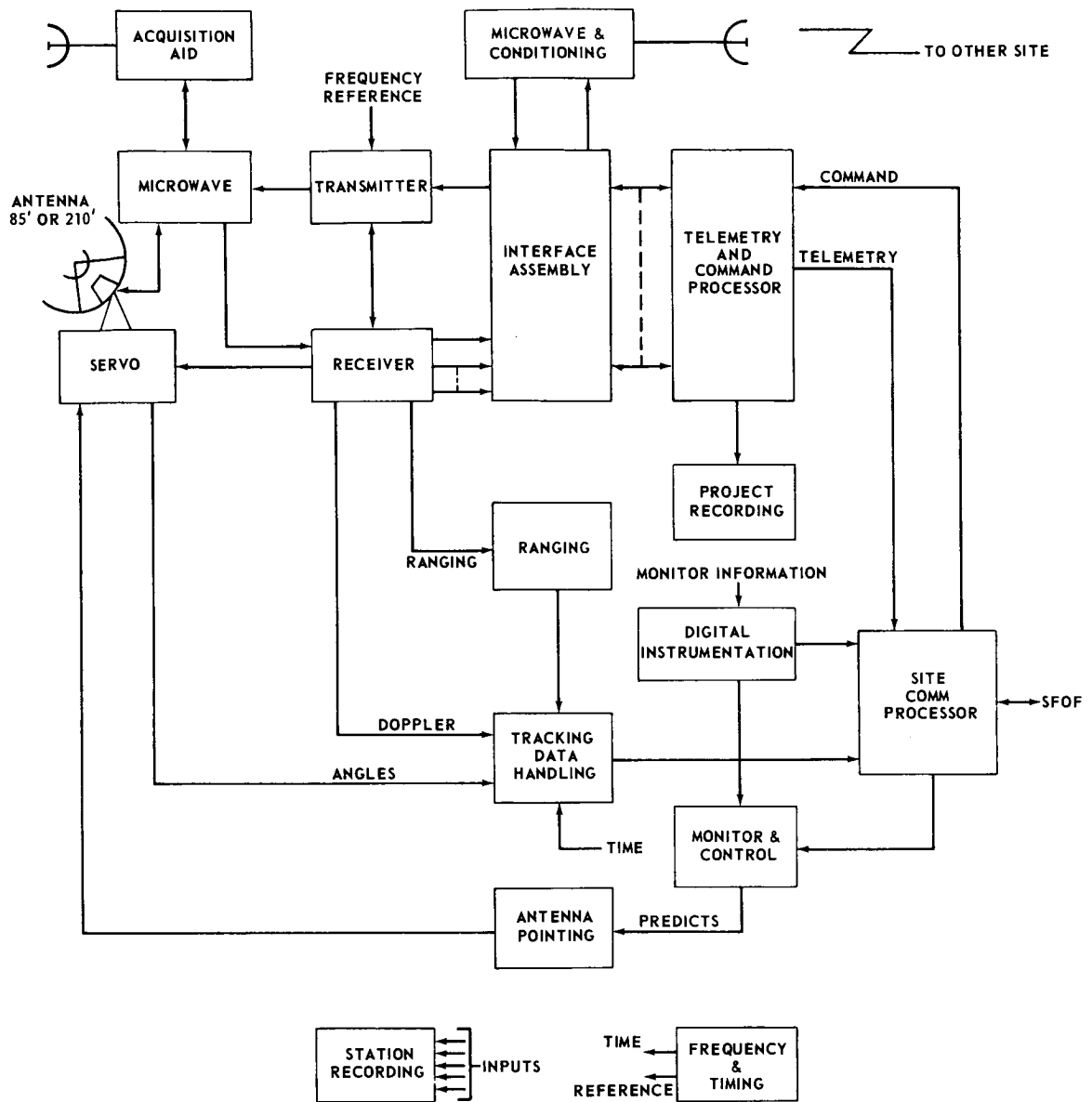


FIGURE IV-2. DSS BLOCK DIAGRAM



TABLE IV-2. ANTENNA MECHANICAL CHARACTERISTICS  
[ Ref. IV-2]

	85-Foot Antenna	Acquisition Aid	210-Foot Antenna	30-Foot Antenna DSS-72
Mount	HA-DEC	On 85 ft Antenna	ALT-AZI	AZ-EL
Auto Track <sup>1</sup>	Yes	Yes	Yes	Yes
Maximum Track Rate (Each Axis)	0.85°/Sec	0.85°/Sec	0.2°/Sec	6°/Sec-AZ 3°/Sec-EL
Maximum Accel. Rate (Each Axis)	0.6°/Sec <sup>2</sup>	0.6°/Sec <sup>2</sup>	0.1° Sec <sup>2</sup>	5°/Sec <sup>2</sup>
Pointing Error Max. <sup>2</sup>	0.02° rms	0.02° rms	0.02° rms	0.01° rms

<sup>1</sup>Can also be pointed by computer according to predictions.

<sup>2</sup>During the periods in which angle tracking accuracy is most significant (e.g., when data for an initial ephemeris calculation are required), when strong signal levels are available. The rms tracking error at receiver threshold increases to approximately 0.05 degrees.

of JOVE's transponder; if the carrier can be locked, Doppler can be made available. Two-way radio-frequency lock is not attempted until one-way lock has been achieved and requires an additional 1 to 3 minutes when the round-trip transmission time is short. At the communication distance of Jupiter, the round-trip transmission time is the controlling factor.

One-way Doppler is available by merely locking the receiver to the down-link carrier. However, the accuracy of one-way Doppler data is limited primarily because of unknown spacecraft auxiliary oscillator drift and has limited use for precision orbit determination purposes. The one-way Doppler is usually

no more accurate than  $\pm 30$  meters/sec. (In the two-way system, the frequency control is maintained by the ground transmitter exciter and is known precisely.) After angle acquisition, radio-frequency lock to the spacecraft auxiliary oscillator signal is achieved in 1 to 2 minutes. A priori information about the expected received frequency considerably reduces the time required to lock the carrier. It is usually necessary that the signal level be 3 to 6 dB above the receiver threshold in order to establish carrier lock. The absolute threshold for maintaining lock is usually taken to be 0 dB signal-to-noise ratio in the noise bandwidth.

Doppler tracking rate capability is dependent on the signal level and on the receiver bandwidth setting. The phase-locked loop included a limiter; hence, in any one bandwidth position, the bandwidth is a function of predetection signal-to-noise ratio. Table IV-3 [Ref. IV-2] is a listing of the strong signal and threshold loop bandwidths of the Doppler tracking system and the equivalent maximum frequency rate capability ( $30^\circ$  phase error) at strong signal.

TABLE IV-3. DOPPLER TRACKING SYSTEM SUMMARY  
[ Ref. IV-2]

Threshold Noise Bandwidth, Hz	Strong Signal Noise Bandwidth, Hz	f Maximum
5	50	25 Hz/sec
12	120	150 Hz/sec
48	255	1200 Hz/sec
152	500	7000 Hz/sec

The Doppler tracking range will be approximately  $\pm 70$  KHz/sec, ( $\Delta V = \pm 45$  km/sec) from nominal center frequency before a change in center frequency is required.

Precision ranging capability is also available at each station. The range measurement is related to the time difference between two identical, separately generated, pseudo-random signals, one generated at the transmitter and the other generated at and synchronized by the receiver for correlation detection. The spacecraft transponder will use a correlation technique for bit synchronization to reconstruct the code sequence before retransmission to Earth, or may use a simple turn-around system for the up-link range code modulation.

The present ranging system has a maximum unambiguous code length of 800 000 km. It is designed mainly for mid-course maneuver orbit pre-determination and lunar orbit and landing purposes. The present lunar ranging system in the DSIF has a resolution of 0.007  $\mu$  sec round-trip time, corresponding to a range uncertainty of  $\pm 2.1$  meters. Worst-case range error estimate, because of unknown system delays, including transponder delay, is approximately  $\pm 15$  meters, one way. It is planned that the planetary ranging system will have comparable accuracy at ranges out to about  $10^8$  km. This unambiguous code length would accommodate Voyager-Mars and Venus missions adequately. Some additional "bookkeeping" would be required to resolve range ambiguities in JOVE's mission to Jupiter unless the code length is increased further.

The precision ranging detection system is operable as long as carrier phase coherence is maintained in the two-way system. The ranging signal is phase-modulated on the RF carrier. The modulation input is direct-coupled and has a maximum bandwidth (3dB) of 2 MHz. The general mode of operation for the ranging system will be to initiate range modulation, establish range-lock, and then to remove range modulation and count carrier Doppler cycles to maintain the range tally.

Planetary ranging equipment with a noncoherent clock will be available at the 210-foot stations. A noncoherent clock allows a ranging fix without first locking the Doppler system.

The tracking data handling system (Figure IV-2) processes all tracking data for transmission to the SFOF by way of the GCS. Processing includes formatting the data, adding quality bits, and also time tags.

A command system data processing and transmitter phase modulation capability will be provided by the DSN at each DSS. A command verification technique will be used whereby the incoming command message is verified and translated by the Telemetry and Command Processor into the proper spacecraft language, and is then transmitted. During transmission, a bit-by-bit comparison is made for final verification or for command inhibit in case of error.

The basic design of the DSIF telemetry receiver provides for phase detection of the telemetry spectrum. In addition, interface equipment and general purpose computers will provide bit and work detection, special correlations, or other project requirements for special demodulation

The Telemetry and Command Data Processing (TCP) subsystem provides on-site data processing capability for digital commands and telemetry. Some limited A/D capability for handling analog signals is planned, but significant analog processing (such as analog TV, for example) is not foreseen for the Voyager era, and probably will not be required for JOVE.

The basic deep space frequencies now used by the DSIF are 2290-2300 MHz for receive and 2110-2120 MHz for transmit. The present Doppler system is designed for a receive-transmit frequency ratio of 240/221.

## Hardware System Design

Microwave and Antenna Performance. Performance data are shown in Table IV-4. The microwave equipment is designed to operate in a duplexed mode, transmitting at high power, while simultaneously receiving at low noise temperatures. Both 85-foot and 210-foot antennas will be equipped with a primary and a backup maser for low-noise reception. A parametric amplifier is presently used with the acquisition antenna, and with the 30-foot antenna. DSS-72.

Receiver Performance. The DSIF stations incorporate extremely sensitive and stable receivers that are designed to track the phase of the received RF carrier and to detect both amplitude and phase modulation. The receiver consists of a low-noise preamplifier, mixer, carrier, and sideband IF amplifiers, detectors, and a voltage-controlled local oscillator, the combination of which constitutes a double conversion superheterodyne automatic-phase-tracking receiver. Doppler-data are derived from the local oscillator signal, telemetry data from separate detection channels, angle error data from separate angle-error detection channels, and range data from a ranging receiver.

At present each station has two reference receiver channels and two angle error detection channels. The 85-foot antennas have two additional angle channels for the acquisition aid antenna. A coherent AGC system is used which provides gain control for the receiver and an indication of received signal level.

Transmitter Performance. The DSIF transmitters, operating with the antenna and receiver subsystem, perform the function of transmitting RF carrier frequency, range code modulation, and command information to the spacecraft. Planned capability of the DSIF transmitters is 100 kW per channel on two channels simultaneously, and 400 kW on a single channel

TABLE IV-4. MICROWAVE AND ANTENNA PERFORMANCE [ Ref. IV-2 ]

	85-Foot Antenna	Acquisition Aid	210-Foot Antenna	30-Foot Antenna DSS-72
Antenna Gain (DB Relative to Isotropic, Matched Polarization)				
Transmit (2110-2120 MHz)	51 +1.0 -0.5	19.1 ±1	60.0 ±0.8	42 ±0.5
Receive (2290-2300 NHZ)	53 +1.0 -0.5	22 ±1	61.0 ±1.0	42.5 ±0.5
Polarization Ellipticity (DB Peak-to-Peak)	RCP/LCP	RCP/LCP	RCP/LCP	RCP
Transmit	1.0 ±0.5	1.0 ±0.5	---	0.8 ± 0.2
Receive	0.7 Max.	0.7 Max.	0.8 Max.	0.5 = 0.2
Beamwidth (Half-Power)				
Transmit	0.36 ±0.03 Deg	18 Deg ±1	0.145 Deg	1.04 ±0.2 Deg
Receive	0.33 ±0.03 Deg	16 Deg ±1	0.135 Deg	0.98 ± .02 Deg
System Temperature, diplexed* (Mean for useful elevation)	55 ±10° K w/Maser	270 ±50° K w/Paramp	45 ±10° K w/Maser	250 ±50° K w/Paramp

\* 10 kw transmitter power; low-noise reception with high power (100-400 kW) is still under development.

## TRANSMISSION ENVIRONMENT

The design of the telecommunication system for JOVE involves trade-offs between transmitting power, transmitting antenna gain, and receiving antenna gain, with modulation and encoding techniques, operating frequency, path link and other factors in the transmission environment playing important roles. The influence of these factors on the required effective radiated power can be seen by examining the communication equation [ Ref. IV-3]

$$P_r = P_t \frac{G_t G_r}{L_f L_a} \quad (1)$$

where  $G_t$  and  $G_r$  are the transmitter and receiver antenna gains respectively.  $L_f$  is the free space loss,  $L_f = (4\pi R/\lambda)^2$ , where  $R$  is the communication distance in meters and  $\lambda$  is the operating wavelength in meters.  $L_a$  is the system loss and  $P_t$  is the transmitter power in watts. The effective radiated power is the product  $P_t G_t$ .

The effect of various modulation and encoding schemes can be introduced into the communications equation by defining a quantity  $\beta$  called the communications efficiency.

$$\beta = \frac{E \min}{c^2} \quad (2)$$

A plot of  $\beta$  versus bit error probability is shown in Figure IV-3. A comparison of several modulation methods by Sanders [ Ref. IV-4] shows that in many cases the trade-off between signal-to-noise ratio and bandwidth can be expressed as

$$\left(\frac{S_i}{N_i}\right) B = \left(\frac{S}{N}\right) \Pi \quad (3)$$

where  $\left(\frac{S_i}{N_i}\right)$  is the predetection signal-to-noise ratio,  $B$  is the predetection bandwidth,  $\left(\frac{S}{N}\right)$  is the post-detection bandwidth, and  $\Pi$  is the message bandwidth. Then equation (2) can be expressed as

$$\beta = \frac{P_{\min}}{\epsilon^2 H} = \frac{P_{\min}}{kTH} \quad (4)$$

Solving (4) for  $P_{\min}$ , substituting into (1) and solving for H gives the bit rate

$$H = \left( \frac{S}{N} \right) \frac{B}{\beta} = \frac{P_t G_t G_r}{kT\beta L_f L_a} \quad (5)$$

For the case of parabolic reflector antennas, the gain of the antenna is given by

$$G = \frac{4\pi}{\lambda^2} A_{em} \approx [0.55 A_{phys.}] \frac{4\pi}{\lambda^2} = 0.55 \left( \frac{\pi D}{\lambda} \right)^2 \quad (6)$$

where  $A_{em} \approx 0.55 A_{phys.}$

Introducing the expression for gain of a parabolic antenna into equation (5) and fixing certain parameters results in a relation between bit rate, antenna diameter, and range of the form

$$H = KP_t \left( \frac{D}{R} \right)^2 \quad (7)$$

The constant, K, can conveniently be chosen so that  $P_t$  is in watts. D is in feet, and R is in astronomical units. Equation (7) can be used conveniently to extrapolate the communications parameters for a Voyager mission to Mars to the distances of Jupiter in order to get an idea of the increased requirements for these distances. Typical communications parameters for Voyager-Mars are listed in Table IV-5. For comparison, the corresponding quantities for a Voyager-Jupiter mission are also listed in Table IV-5. To keep the same telemetry bit rate, without an increase in transmitter power, requires that the antenna diameter be increased. From equation (6), it can be seen that the ratio of the antenna diameters for the two missions will be equal to the ratio of the communications distances in astronomical units. This means that the 7-1/2 foot antenna for a Voyager-Mars mission would be increased to 25.3 feet for the JOVE-Jupiter mission. This antenna diameter, however, is larger than the allowable shroud dimension for the launch vehicle. Therefore, the antenna diameter is necessarily limited to 20 feet. In order to maintain the

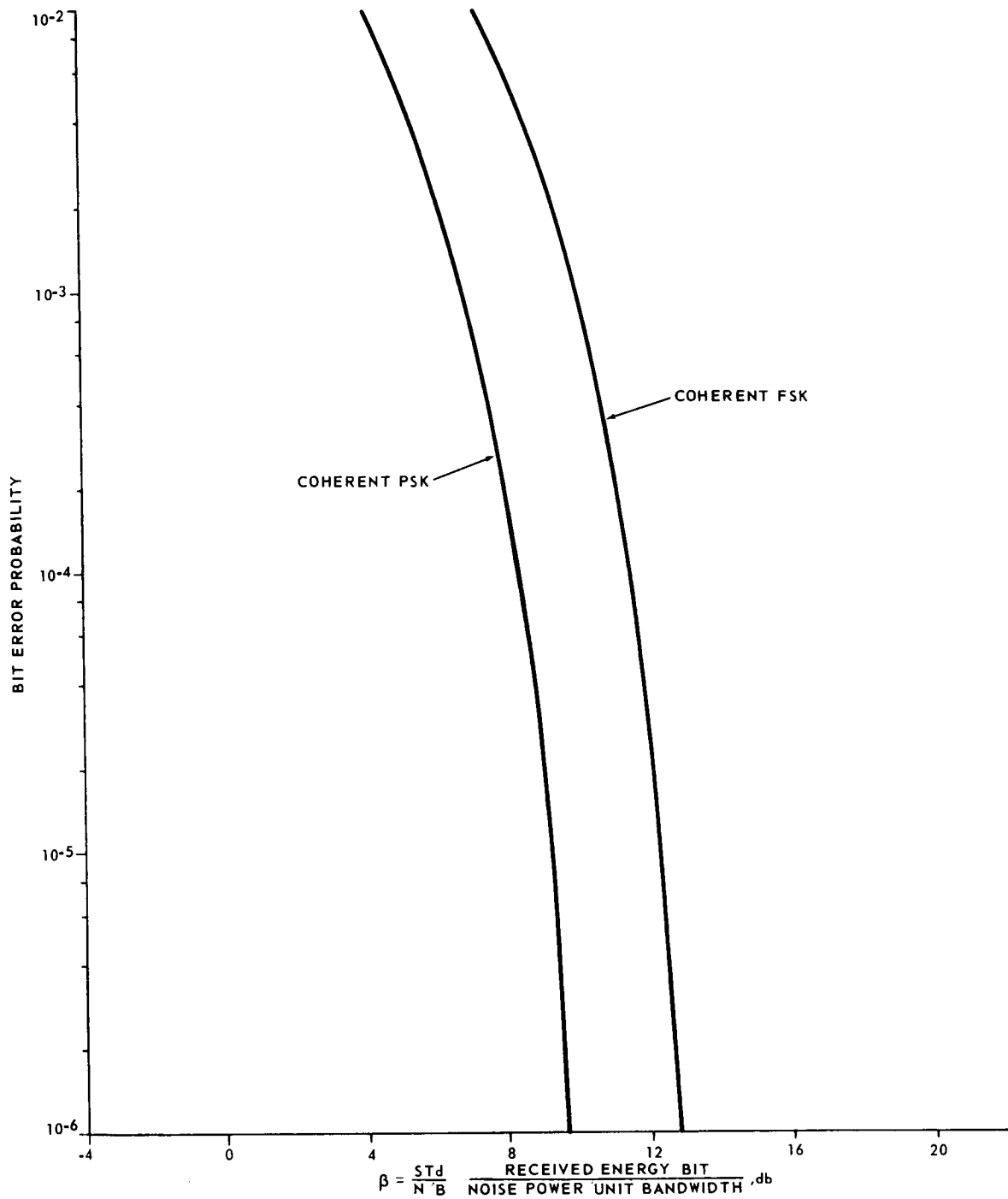


FIGURE IV-3. BIT ERROR PROBABILITY VS.  $\beta$



TABLE IV-5. TELECOMMUNICATION PARAMETERS

A. Voyager-Mars [Ref. IV-6]

Telemetry data rate	15 kb/sec
Command data rate	1 bit/sec
Range at encounter	1.63 AU
Space attenuation	266.5 dB
Radio Delay	27.2 min
Antenna	7-1/2 ft

---

B. JOVE-Jupiter

Telemetry data rate	15 kb/sec
Command data rate	1 bit/sec
Range at encounter	5.5 AU
Space attenuation	278.7 dB
Radio delay	92 min
Antenna diameter	25.3 ft

same bit rate in the communication system, an increase in transmitted power from 50 watts (Mars) to 74 watts (Jupiter) is required. Thus, it can be seen that with comparable experiments for the two distances, a reasonable increase in both transmitter power and antenna gain are required for communication over the longer distances.

For an intelligent application of equation (5), the factors in the right hand side of the equation must be examined in detail. The transmitting antenna gain, in general, is a function of the aperture size and the frequency. Also, in general, higher antenna gains result in narrower beamwidths with the concomitant difficulty of stringent requirements on attitude control. The most efficient antenna type for a given aperture size is the parabolic reflector antenna. For this antenna, the transmitting antenna gain is given [Ref. IV-7] by the equation

$$G = 0.55 \pi^2 D_\lambda^2 \quad (8)$$

and the beamwidth is given by

$$\theta = \frac{58}{D_\lambda} \text{ degrees.} \quad (9)$$

Since the attitude control system in a 3-axis stabilized spacecraft will not maintain the spacecraft pointed exactly in the desired direction, the question arises as to what is an allowable dead-band bandwidth for the attitude control system from the standpoint of transmitting antenna pointing loss resulting from misalignment of the antenna. This question cannot be answered exactly without a detailed knowledge of the transmitting antenna radiation pattern which is not unique to the parabolic reflector type of antenna. The radiation pattern of the parabolic reflector antenna depends upon the way in which the reflector is illuminated by the feed system. Here, only typical results can be stated. One of the earliest cases to be studied [Ref. IV-8, IV-9] is that in which the aperture field distribution is of the form

$$F(r) = (1 - r^2)^P, \quad P=1, 2, 3, \dots \quad (10)$$

For this case, the half-power beamwidth will be approximately

$$BW_{\text{deg}} \approx \frac{46}{D_\lambda} \quad (11)$$

and the radiation field will be given

$$R(\theta) = \frac{1}{2} e^{-v^2 \theta^2} \quad (12)$$

where

$$\nu = \frac{70}{\text{BW}} \text{deg} \quad (13)$$

and  $\theta$ , in radians, has been assumed to be small. Calculations for a 20-foot (6.1 meter) diameter antenna using these equations shows that dead bandwidth would be approximately  $0.2^\circ$  for a 1 dB loss.

Balakrishnan [Ref. IV-10] states that, as a rule of thumb, the antenna design requires attitude stability good to at least one-tenth of the antenna beamwidth in order not to lose more than about 1 dB of signal strength. Using formulas (8) and (9) for the transmitting antenna gain and beamwidth, and applying this rule of thumb shows that for a 1 dB pointing loss, the dead band bandwidth of the attitude control system would be in the order of  $0.15^\circ$ . Also, on page 166, Balakrishnan shows a figure which indicates the pointing accuracy for 0.25 dB loss vs. gain. Extrapolation of this figure shows that a 40-dB gain antenna would have a pointing loss of about 0.25 dB with an attitude control system dead band bandwidth of around  $0.25^\circ$ . These calculations indicate that the dead band bandwidth for the high gain antenna will be of the order of a few tenths of a degree. On the other hand, the dead band bandwidth for the medium gain antenna would be on the order of  $1^\circ$  to  $2^\circ$ .

A space loss is incurred which is caused by the spreading out of waves from the source. The space loss (Figure IV-4) is given by the equation  $L_f = (4\pi R/\lambda)^2$ . The free space transmission loss over a distance of 5.5 AU is 278.7 decibels.

Faraday rotation is the rotation of a plane polarized wave by virtue of its interaction with the ionosphere. Theoretically, infinite attenuation, corresponding to complete cross-polarization, could occur if the receiving station had only one plane polarized antenna. If two orthogonal antennas and diversity reception are used, or one circularly polarized antenna, the maximum loss is 3 decibels. Faraday rotation is inversely proportional to the square of the frequency, but in the worst case, does not become negligible dropping below  $10^\circ$  until about 10 GHz is reached. Under average conditions, it is negligible at 5 GHz but cannot be neglected at 2 GHz. For two circularly polarized antennas with the same sense of polarization the Faraday rotation would be  $0^\circ$ . It is extremely difficult, however, to synthesize and maintain complete circular polarization. The antennas of the DSS are elliptically polarized, and if the spacecraft antennas are designed with the same sense of elliptical polarization, then the polarization loss between the spacecraft and ground station antennas can be computed [Ref. IV-1] as

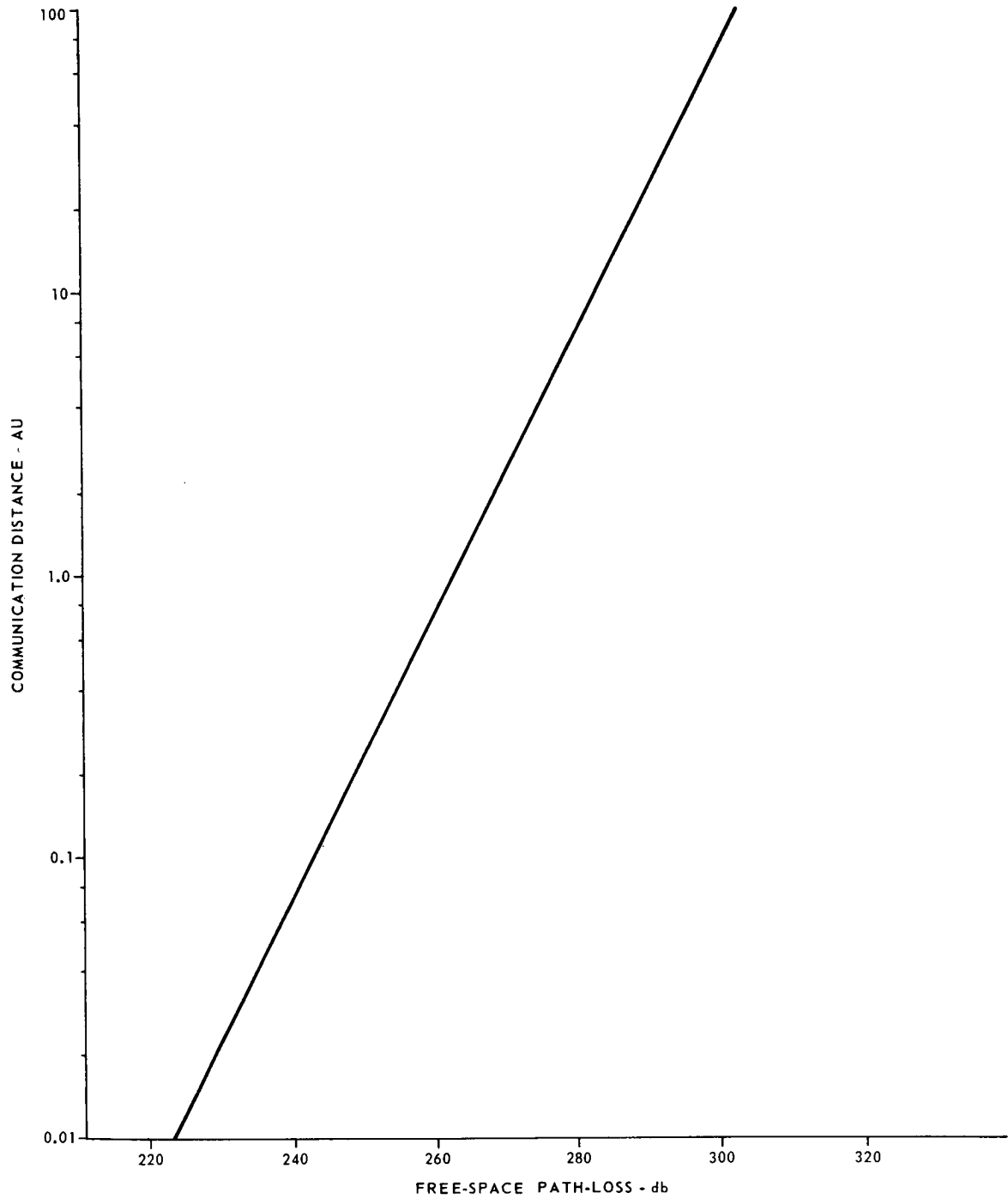


FIGURE IV-4. FREE SPACE PATH-LOSS VS. DISTANCE

$$K_p \approx \frac{1}{2} \left[ 1 \pm \frac{4 A_t A_r + (1 - A_t^2) (1 - A_r^2) \cos 2\theta}{(1 + A_t^2) (1 + A_r^2)} \right] \quad (14)$$

( $\theta$  equals the orientation angle between polarization ellipses, and  $\pm$  indicates same and opposite sense polarization respectively.)

A sample calculation will clarify the use of equation (14). It is assumed in the following example that  $\theta = 90^\circ$ , and that the same sense of polarization prevails.

$$K_p \approx \frac{1}{2} \left[ 1 + \frac{4 A_t A_r + (1 - A_t^2) (1 - A_r^2) \cos 180^\circ}{(1 + A_t^2) (1 + A_r^2)} \right]$$

$$A_t = 1.0 \pm 1.0 \text{ dB} \quad A_r = 0.8 \text{ dB max.}$$

$$\therefore A_t = 0.9 \text{ or } \left| \begin{array}{c} 1 \\ .8 \end{array} \right| \quad \therefore A_r = 0.93 \text{ max.}$$

$$K_p \approx \frac{1}{2} \left[ 1 + \frac{4 (0.9) (.93) + (1 - 0.9^2) (1 - 0.93^2) (-1)}{(1 + 0.9^2) (1 + 0.93^2)} \right]$$

$$K_p \approx 0.05 \text{ dB} \quad \begin{array}{l} + 0.01 \text{ dB} \\ - 0.17 \text{ dB} \end{array}$$

The characteristics [ Ref. IV-2] of the DSS antennas are shown in Table IV-4.

One of the parameters that determine telecommunications system performance is the system noise temperature, or the noise spectral density. In turn, the noise spectral density depends on the antenna temperature and the equivalent noise temperature of the receiving devices. The measured contributions to the antenna temperature will be thermal noise intercepted by the side-lobes of the ground antenna, and noise caused by the ground or spacecraft antenna pointed at the sun or Jupiter. If the sun appears in the beam width of the spacecraft or ground antennas, its effect will be to increase the total receiving system temperature. Considering the antenna to be a generator of noise power for the rest of the system, it can be considered a resistor, the value of which

is the radiation resistance of the antenna at temperature T. This temperature is defined as that which a resistor must have to produce noise power equal in amount to the antenna noise power. Computer trajectories indicate that the sun-spacecraft-Earth angles at certain instances will be approximately 0°. This means that the spacecraft antenna and the DSIF antenna, during these periods, will be pointed at the sun. When the spacecraft is in the vicinity of the target, the DSIF antenna may be pointed directly at Jupiter for a short period of time. Again, when the probe gets behind Jupiter, the planet may be in the spacecraft antenna beam. Since the sun and Jupiter radiate a considerable amount of noise in the range 2100 to 2300 MHz, this noise will increase antenna noise temperature and degrade system performance somewhat. The amount of radiation from Saturn, Neptune and Uranus is much smaller than that from Jupiter and will not degrade system performance.

If the antenna is in thermal equilibrium with its surroundings, its equivalent temperature can be expressed (Ref. IV-9) as

$$T_a = \frac{1}{4\pi} \int \int_{\Omega_s} G(\theta, \phi) T_s(\theta, \phi) d\Omega_s. \quad (15)$$

Assuming that the source is directly on the antenna beam axis for the case when antenna beam solid angle  $\Omega_b$  is much smaller than  $\Omega_s$ ,  $T_a$  can be approximated by

$$T_a = \bar{T}_s \left( \frac{\theta_s}{\theta_b} \right)^2. \quad (16)$$

In the other extreme, when the source is much larger than the antenna beam width,  $T_a$  is approximately equal to  $\bar{T}_s$ . The average source temperature can be computed from the measured flux densities using the expression

$$\bar{T}_s = \frac{S \lambda^2}{2k\Omega_s} \quad (17)$$

where

$$S = \frac{2k\Omega_s \bar{T}_s}{\lambda^2}. \quad (18)$$

For small solid angles  $\Omega_s$  can be accurately approximated by  $\Omega_s \approx \frac{\pi}{4} \theta_s^2$ .

This last relation expresses the total noise radiation power density, randomly polarized, emitted from a black body at a temperature T within a frequency band df. Only half of this energy can be received by a single given antenna.

An antenna can be sensitive, however, to only one of any two possible orthogonal polarization modes [Ref. IV-12]. That is, an antenna cannot be simultaneously right and left hand circularly polarized, or simultaneously vertically and horizontally polarized. Thus, in terms of the power density available per polarization mode, we have

$$S_{df} = \frac{kT}{\lambda^2} df. \quad (19)$$

At 2.3 GHz, the planet Jupiter represents a black body source of temperature 1000° K [Ref. IV-13] while the quiet sun represents a black body source of temperature 100 000° K [Ref. IV-14]. The disturbed sun temperature is approximately 200 times greater.

An analysis of the antenna temperature contributions caused by the sun and Jupiter was made and the results (Figs. IV-5 and IV-6) indicate that for distance of 3 AU or less, the increase in antenna temperature of a 20-foot parabolic antenna looking at the sun will be appreciable. Also, the increase in antenna temperature caused by the DSIF station looking at the sun will be overpowering. The increase in antenna temperature of a medium gain parabolic antenna would probably be considered negligible in comparison to the inherent noise of the receiving system for the spacecraft at distances from the sun of 1 to 2 AU.

If the planet Jupiter appears in the beamwidth of the DSIF station during the encounter, the increase in antenna temperature will be only approximately 5° K which would be considered a negligible increase. On the other hand, during orbital operations at the planet Jupiter, the planet would subtend the beam width of the 20-foot parabolic antenna, and in those attitudes in which the spacecraft looks directly at the planet, the increase in antenna temperature would be 1000° K. This would approximately double the noise power in the receiver, assuming a crystal mixer RF front end.

## JOVE RADIO SYSTEM

The JOVE radio subsystem is similar to the radio subsystem envisioned for Voyager class vehicles. Designed to be compatible with the existing DSIF, the radio subsystem must perform the functions of telemetry modulation and transmission during all phases of the JOVE mission, command reception and demodulation, and turn-around frequency translation and transmission over the ranging channel.

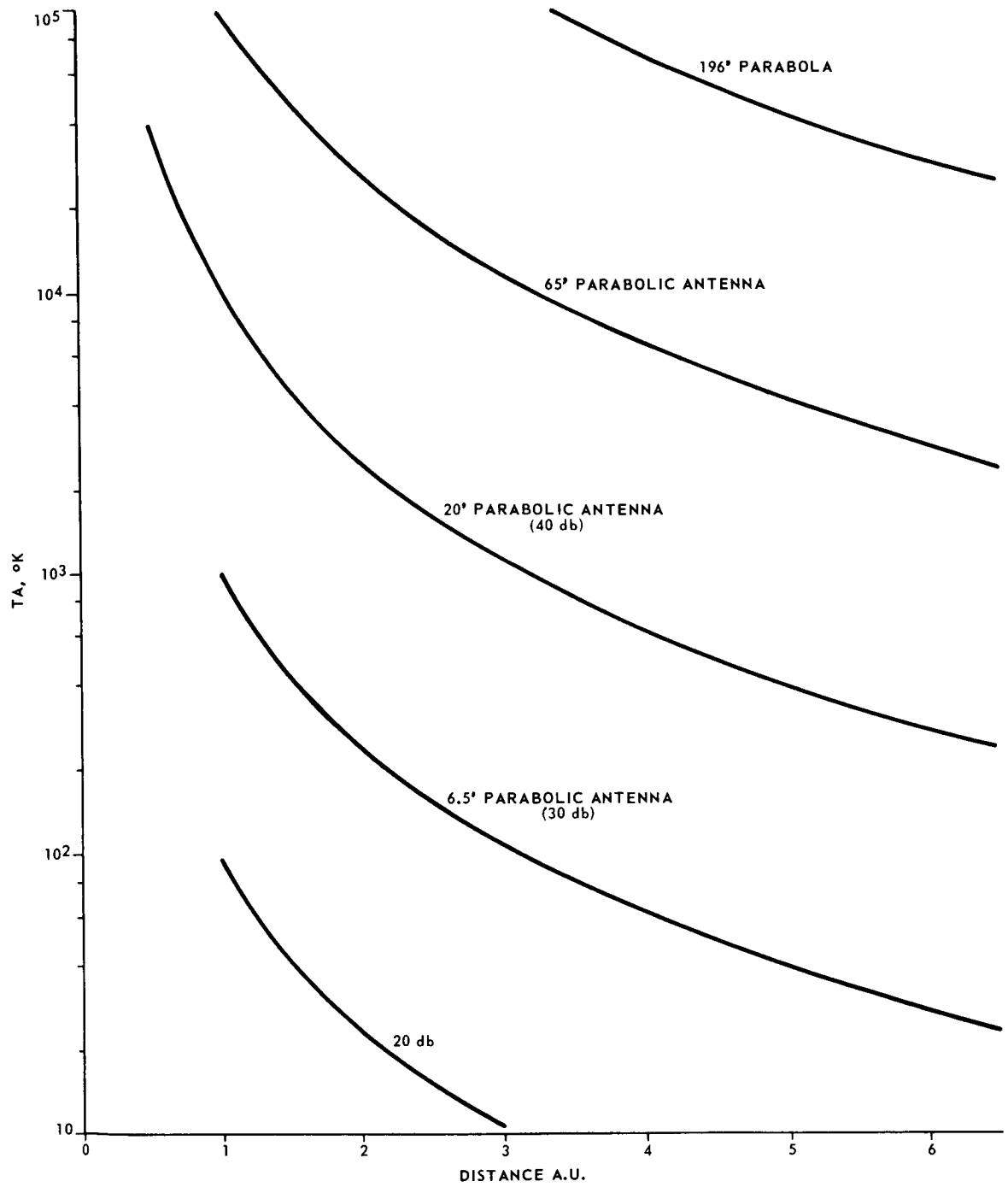


FIGURE IV-5. ANTENNA TEMPERATURE,  $T_A$ , VS. DISTANCE FROM SUN, AU



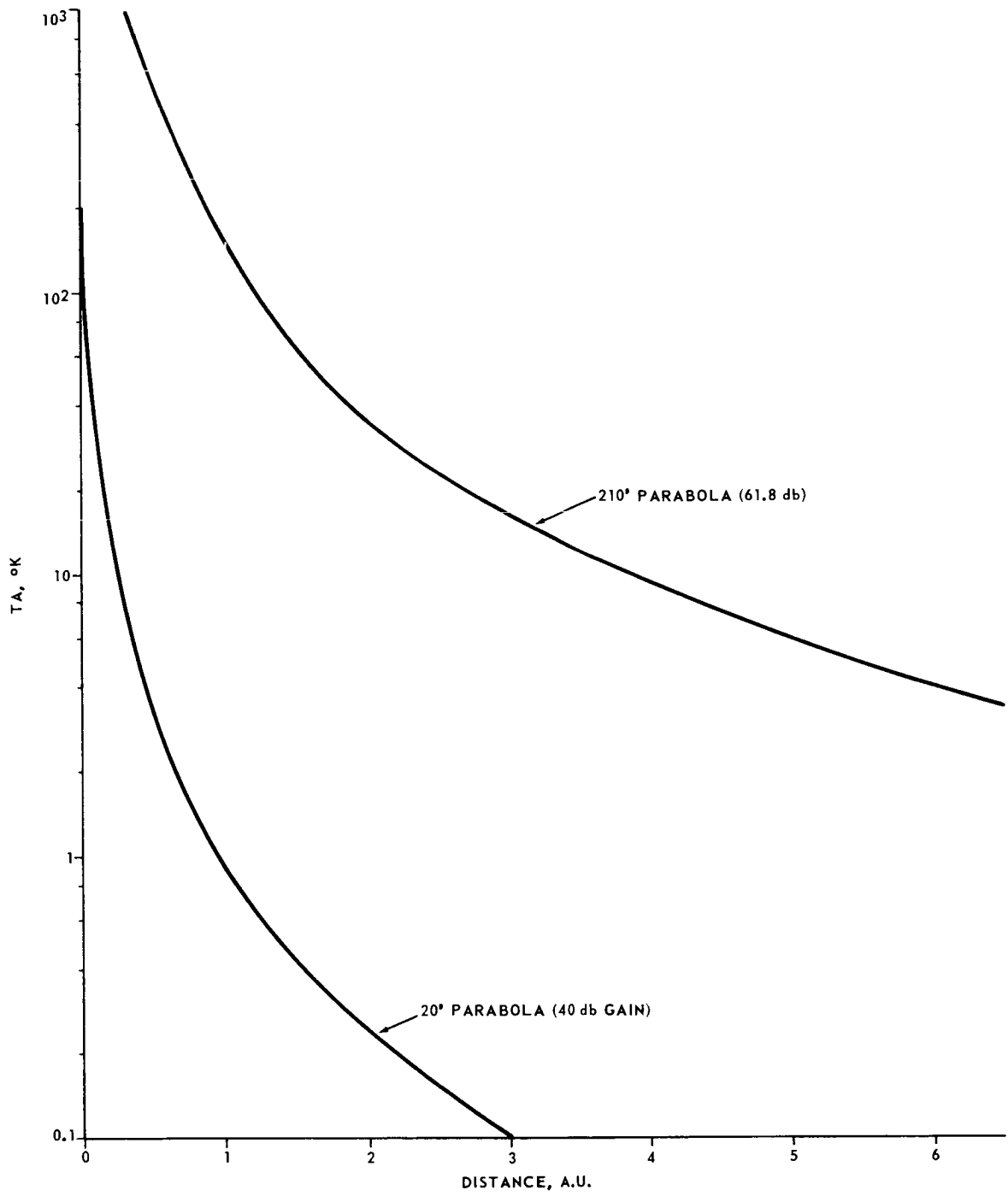


FIGURE IV-6. ANTENNA TEMPERATURE,  $T_A$ , (°K).  
DUE TO JUPITER

## Block Diagram

A block diagram of the JOVE radio subsystem Figure IV-7 shows that the system combines three transmitters and three receivers in a redundant fashion. Some of the general considerations of this design are:

a. No single failure of the radio subsystem will result in a failure to achieve mission objectives.

b. Three traveling wave tubes (TWT) amplifiers are used and are connected such that the two 50-watt amplifiers can be operated separately or in parallel. The reasons for choosing to use two amplifiers in this connection are thermal control and reliability. A single high power high wave tube concentrates a great deal of thermal energy in one location. It becomes difficult to reject the dissipated heat with thermal control louvers of a standard size. By using the lower power devices in a parallel approach the 100-watt range of RF power can be obtained, and if one of the TWT's quits working there is a modest degradation of power, not the complete outage that would result if a single high power tube failed. Also, the lower power tubes are likely to be more reliable since higher powered tubes require higher voltages, high cathode current densities, and temperatures. This means they have shorter operating lifetimes. There is no information currently available on the lifetimes of high powered devices, but available data indicated that relatively low powered tubes, up to 20 to 30 watts, can be expected to last at least five years, and perhaps as long as ten years. Presumably, by the time JOVE is launched, 50 watt traveling wave tube amplifiers will have reached the same level of reliability.

c. Any of the three exciters shown may be used for any one of the three power amplifiers, or for the two 50-watt amplifiers in parallel.

d. Switching and diplexing will be arranged so that it is possible to call up the receivers through any antenna, and to transmit through a selected antenna.

e. A receiver selector gate will inhibit receiver outputs to the command and ranging units unless the receiver is in phase lock. If more than one receiver is in phase lock, receiver outputs will be selected with a priority in one of two modes, a maximum coverage mode or a maximum gain mode. Telemetry information is applied to all exciters in parallel.

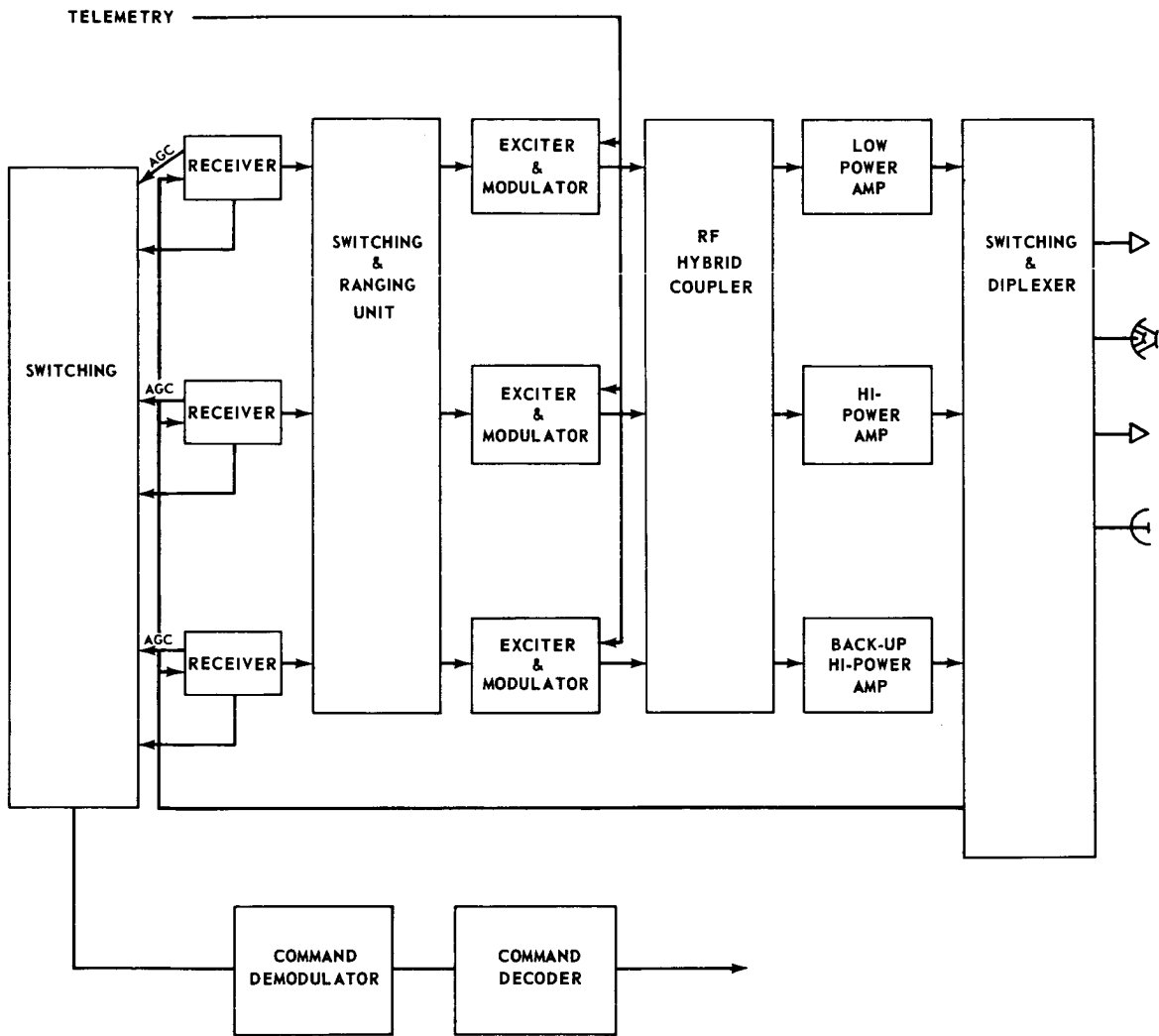


FIGURE IV-7. JOVE RADIO SUBSYSTEM BLOCK DIAGRAM

Referring to the functional block diagram of the JOVE spacecraft portion of the communication system (Figure IV-7) the major subsystems will now be described.

## Antennas

The high gain parabolic antenna will be used for transmission at 2295 MHz and for reception at 2113 MHz. It will be 20 feet (6.1 meters) in diameter, with a maximum gain, at 2295 MHz, of 40 dB above isotropic, and a beam width of about 1.5 degrees full cone angle. The ratio of focal length to diameter is 0.4. In its presently conceived mechanization, the feed assembly is a Cassegrainian type [ Ref. IV-12, IV-15, IV-16] with a hyperboloidal subreflector located with its focus at the paraboloidal focus and an S-band microwave horn located at the other focus of the hyperboloid. The hyperboloidal surface has the property that it is the locus of points such that the difference in distances to the two foci is a constant. Thus, radiowaves emanating from the microwave horn and reflected from the hyperboloidal subreflector reach the paraboloid with the same relative phase relationship they would have had if they had originated at the focus of the paraboloid. This results in a collimated radio beam from the antenna which is desirable from the standpoint of gain, and at the same time, it simplifies the location and support of the horn feed. There is, of course, some aperture blocking by the subreflector but experimental optimization of the feed system can result in antenna efficiencies at least as high as those obtained with conventional feed systems.

The use of a large fixed parabolic antenna imposes severe requirements on the attitude control system. The entire spacecraft must be oriented in order to point the antenna in the desired direction. In order to keep the pointing loss or loss because of misorientation of the antenna below about 1 dB, it is necessary to maintain the pointing accuracy to within 1/10 of a beam width. This means (Fig. IV-8) that the pointing accuracy must be within 0.15 degrees. A study of the cold gas requirements for attitude control to this accuracy in a cruise to Jupiter has shown that it is feasible to maintain this pointing accuracy. A survey of attitude control sensors has shown that it is feasible to maintain the spacecraft attitude to within this accuracy.

A study of the communication circuit for this mission shows that a medium gain antenna can be used for telemetry and command communication during the early phases of the flight. A two-axis gimballed 36-inch diameter parabolic reflector antenna is used for the medium gain antenna. This antenna is mounted

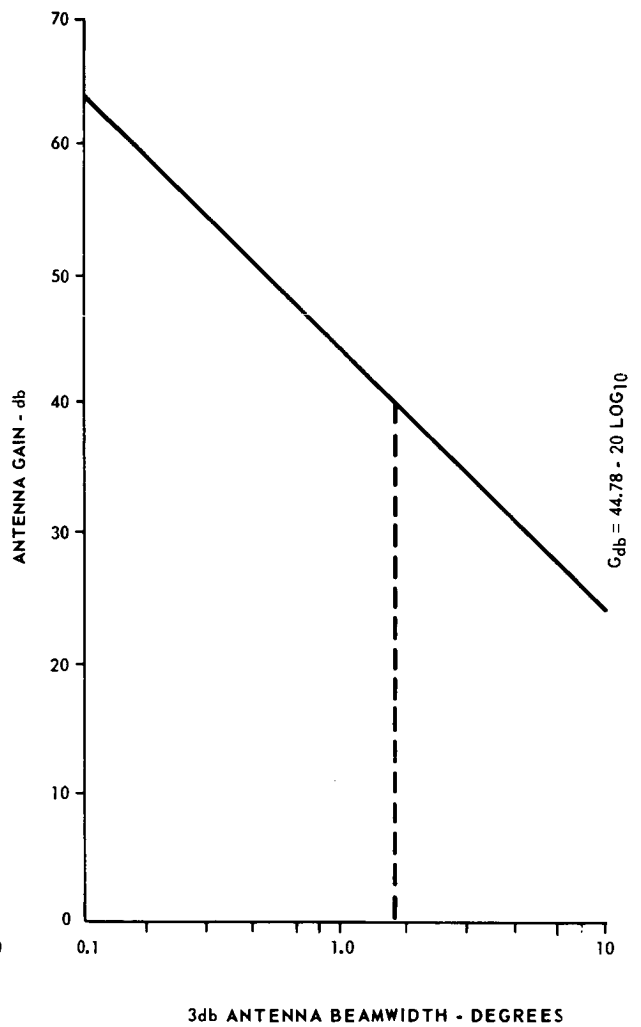
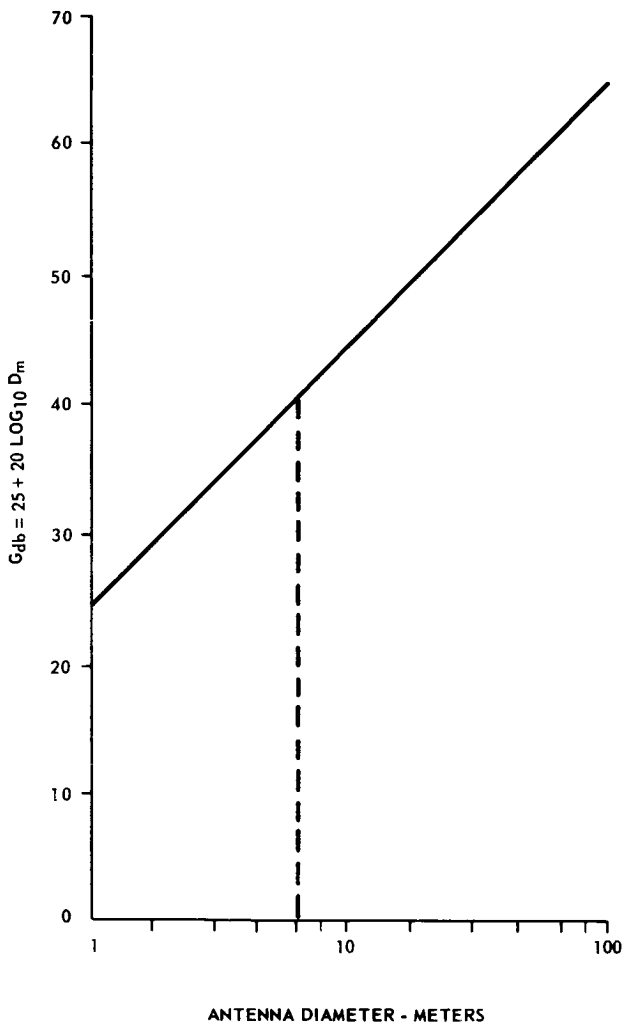


FIGURE IV-8. 20 FOOT ANTENNA PARAMETERS

on a boom, is stowed during the spacecraft launch, and is deployed after injection into the heliocentric cruise. The feed system for the medium gain antenna is a pyramidal cone. The medium gain antenna has a variety of uses. It can be used as a backup system for the high gain antenna, and it can be used as the primary telemetry antenna during the early phases of the heliocentric cruise phase.

## Transponder

This section contains a discussion of the transponder, Figure IV-9. The transponder selected for the JOVE mission is similar to the Mariner transponder, a reliable design which is comparable with the DSIF requirements. The operation of the transponder is described below.

The transponder is designed to receive the uplink signal consisting of a carrier phase modulated by the ranging and command information. A synchronous detector controlled in phase by a phase lock loop separates the composite command signal and PRN range code from the carrier, and sends the composite command signal to the command demodulator. The PRN range code is transferred to a downlink phase modulator. The downlink consists of a 2295 MHz carrier phase modulated by the PRN range code, and a phase modulated telemetry subcarrier. The transponder itself comprises a triple conversion superheterodyne receiver, and a phase-modulated transmitter. The phase of all local oscillators is controlled by means of an automatic phase control loop which is locked to the uplink signal. Frequency and phase information for the first and second detectors of the transponder is obtained by means of harmonic frequency multiplication of the VCO signal.

The frequency acquisition procedure for the spacecraft transponder is as follows. If the spacecraft receiver is not in phase lock, the transmitter frequency is derived from a crystal controlled auxiliary oscillator. For a spacecraft frequency of 2295 MHz, the frequency of the auxiliary oscillator would be 19.125 MHz. The frequency of this auxiliary oscillator is multiplied by 240 to the frequency 2295 MHz and transmitted by means of the spacecraft antenna to one of the DSIF stations. When the DSIF antennas are pointing in the proper direction, they receive the downlink signal from the spacecraft and the uplink signal derived from the DSIF frequency standard by means of a frequency synthesizer is transmitted to the spacecraft on a frequency of 2113 MHz. When this signal is acquired by the spacecraft phase lock receiver, a transfer command from the spacecraft AGC system, this connects the auxiliary oscillator and the exciter frequency is derived from the lock loop voltage controlled

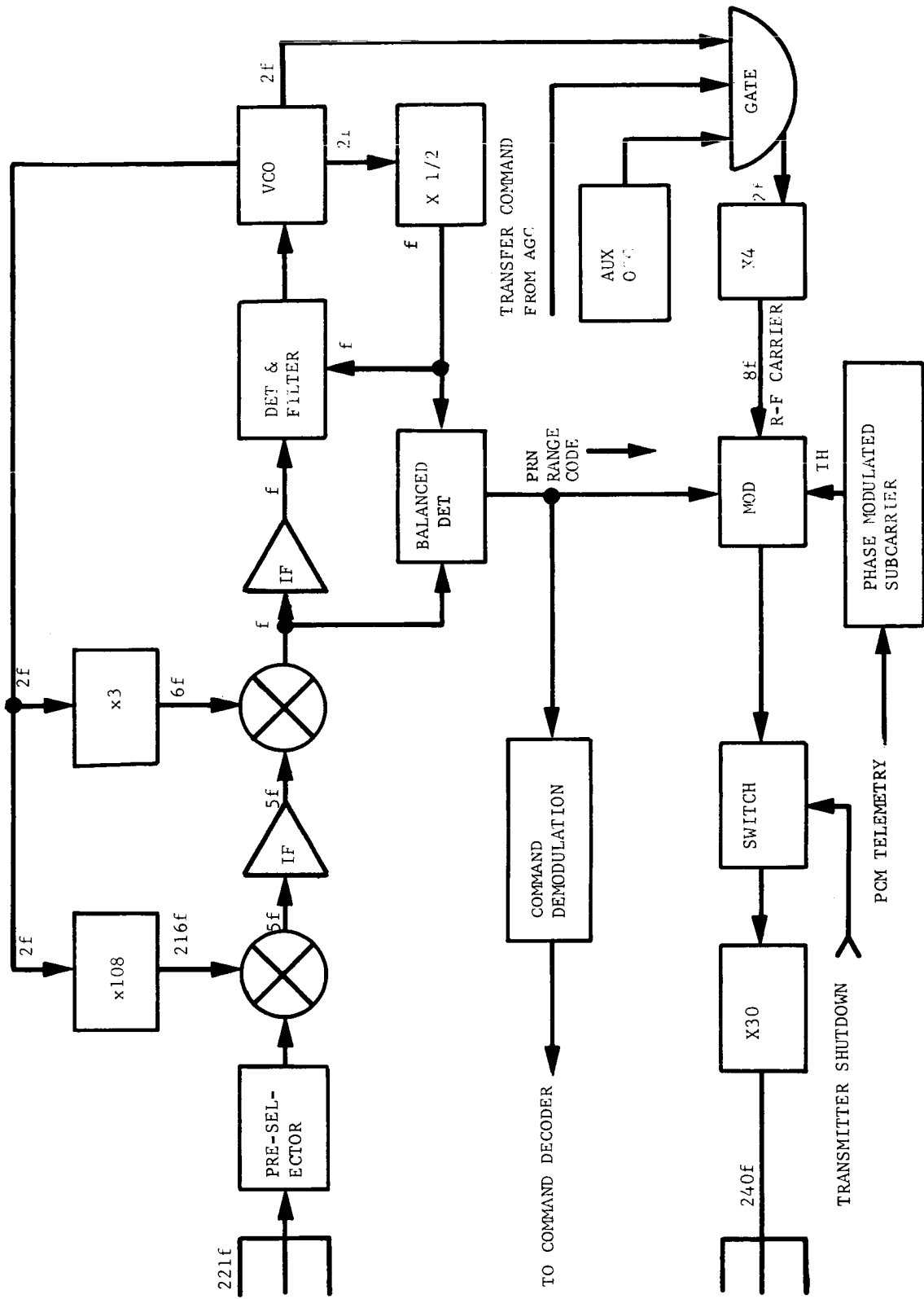


FIGURE IV-9. TRANSPONDER BLOCK DIAGRAM

oscillator (VCO). The VCO signal is then multiplied, amplified, and transmitted by means of the spacecraft antennas (downlink) to the DSIF. At this time, two-way Doppler tracking and automatic angle tracking become available.

## Power Amplifiers [Ref. IV-5, IV-18]

Successful communication from the spacecraft at the distances involved in this mission depends, to a great extent, on the devices generating the output signal. A large array of devices present themselves for possible application. Among these devices are: tunnel diodes, bulk effect devices, transistors, diode multipliers, parametric up converters, vacuum triodes, klystrons, amplitrons, and traveling wave tubes.

The power levels of solid state devices at present is less than a few watts, thus ruling out these devices in a Jovian mission. We are, therefore, constrained to the use of vacuum tube sources, among which are: triodes, voltage tunable magnetrons, klystrons, amplitrons, and traveling wave tubes. The voltage tunable magnetron has the advantage of simplicity in some applications, since it is essentially a power oscillator which can be directly frequency modulated by varying the anode voltage. Frequency stability and noise characteristics, however, present a problem in an interplanetary mission, since good frequency stability is important. Triode cavity amplifiers can supply power levels of 20 watts at 2 GHz. The lifetime of tubes operating at high power levels is around 10 000 hours. Electrostatically focused klystron amplifiers (ESFK) are available for high-power, narrow-band applications. Prototype models of 50 watt ESFK power amplifiers now exist. They are basically 20-watt versions operated at higher supply voltages. Some developmental work would be necessary in order to develop a flight-qualified Electrostatically Focused Klystron amplifier. Efficiency would probably run around 25 percent and weight for a 20-watt unit would be around 2 pounds with 3-1/4 inches diameter. Bandwidth for the klystron amplifier would be in the neighborhood of 0.1 to 0.3 percent. The expected life would be in the order of 50 000 hours.

Amplitrons (crossed field backward wave amplifiers) present an attractive advantage in that redundant amplifiers can be provided without RF switching. With amplitrons, series connection is used and the deactivated unit presents about 0.5 dB insertion loss. Further problems with the amplitron tube, however, such as the requirement for a complex high-voltage power supply mated to the individual tubes characteristics, lifetimes in the neighborhood of 10 000 hours, sensitivity to loading and to power supply voltages make the amplitron unattractive, at the present, for the JOVE mission.



Traveling wave tube (TWT) amplifier flight experience is extensive. Telestar, Relay, Syncom, Surveyor and Pioneer 6 are some examples. Tests on a WJ-274 indicate that an overall efficiency of 35 percent can be expected by careful selection and matching of the tube and power supply. Tests also indicate that the 20-watt tube can be operated at a 50-watt level, with 40 percent efficiency, by changing the power supply voltages. No information was found on the WJ-274 lifetime operated at the higher power level. Traveling wave tubes have demonstrated typical lifetimes of around 30 000 hours, and life is predicted to reach as high as 90 000 hours for some low-power units in development. Wide bandwidth, about 50 percent, is commonplace, eliminating temperature effects on center frequency, common with cavity loaded triodes and klystrons. It seems reasonable that in the time period of the JOVE mission, 50-watt traveling wave tubes, with high efficiency and reliability, will have been developed and space qualified.

There seems to be no need at present to consider power levels higher than about 50 watts, because of thermal control problems and reliability. If two 50-watt amplifiers are operated in parallel, the total power output is 100 watts. A single high-power traveling wave tube would concentrate a great deal of thermal energy in one location. It would then become difficult to reject the dissipated heat with thermal control louvers of reasonable size. By using two lower power devices in parallel, the 100-watt range of RF power can be obtained, and if one of the TWT's quits working, there is a modest degradation of power, 3 dB, not the complete outage would result if a single high-power tube failed. Also, the lower power tubes are likely to be more reliable, since higher power tubes require higher voltages, high cathode current densities, and temperatures. This means that they have shorter operating lifetimes. Therefore, a combination of two 50-watt traveling wave tubes and one 20-watt traveling wave tube was chosen for the power amplifier section of the JOVE spacecraft.

Switching is to be arranged so that the two 50-watt traveling wave tubes can be operated separately, or in parallel for high power requirements. A 20-watt WJ-274 traveling wave tube (Table IV-6) [Ref. IV-24] is provided as a back-up amplifier and can be used at the shorter distances where the high power levels are not required. The WJ-274 has its own power supply which provides all required voltages, high voltage time delay function, telemetry signal conditioning of important currents and voltages, and RFI suppression when mounted in the appropriate enclosure. The tube and power supply are in a common housing with conduction through the bottom surface to a heat sink.

TABLE IV-6. CHARACTERISTICS OF 20 WATT TWT

A. WJ-274 Characteristics

Performance:

Frequency Range	2.2 - 2.4 GHz
Minimum power output	22 watts
R-F input	+22 dbm
Overall efficiency (including heater)	35% minimum
Total D-C power input (including heater)	64 watts maximum
Cooling	Conduction only
Focusing means	PPM

Electrical:

Heater voltage	3.0 volts
Heater current	0.95
Anode voltage	+100 volts
Anode current	1.2 ma
Helix voltage	Ground potential
Collector voltage	-520 volts
Collector current	44 ma
Cathode voltage	-1610 volts
Cathode current	52.2 ma

TABLE IV-6. CHARACTERISTICS OF 20 WATT TWT  
(Continued)

Mechanical:

Length	8.7 inches
Cross section (excluding connectors)	0.90x0.95 in. max.
Weight	12 ounces
D-C connector	Fly leads
R-F connectors	TNC female

B. WJ-274 Power Supply Characteristics

Electrical:

Power supply efficiency (dc-dc) including telemetry and time delay, at worst case conditions (high line voltage and high temperature)	85 percent
Regulation caused by time and temperature	0.07 percent
Temperature Range	-40 to +85°C
Power input for 63 watt D-C output	74 watts

Mechanical:

Dimensions	$5 \times 8\frac{1}{2} \times 1\frac{3}{8}$ in.
Volume	58.5 cu in.
Weight	3.5 lb
Cooling	Conduction only

## Telecommunications Design Control Tables

The telecommunication design control tables for the JOVE spacecraft/DSIF telemetry link and the DSIF/JOVE spacecraft command link are given in Tables IV-7 and IV-8. In the telemetry link calculations, it is assumed that the spacecraft is transmitting 100 watts power, using the 20-foot diameter antenna (40 dB gain), and that the 210-foot diameter DSIF and low noise receiver are used. Elliptical polarization of both the spacecraft and DSIF antennas is assumed.

In the command link calculations, it is assumed that the DSIF transmitter output power is 400 kW, that a 210-foot diameter DSIF antenna (61 dB gain) is used, and that a 5-dB gain spacecraft antenna is used. Both the transmitting and receiving antennas are assumed to be elliptically polarized, with the same polarization loss as assumed in the telemetry link calculations.

The bit rate varies inversely as the square of the distance. Thus, the bit rate is diminished by a factor of four when the distance is doubled (Fig. IV-10). The telecommunications system for JOVE has significant growth potential and as currently configured will provide significant telemetry rates at the greater distances of the outermost planets of the solar system

### TELEMETRY SUBSYSTEM

#### Function

The principal functions of the telemetry subsystem on the spacecraft are to time multiplex engineering and scientific data samples and to encode them for efficient modulation of the spacecraft to Earth RF carrier. The subsystem is specifically required to perform the following tasks:

- a. Transduce engineering parameters into electrical signals.
- b. Time multiplex engineering and scientific measurement signals.
- c. Convert engineering data samples to binary words.

TABLE IV-7. TELECOMMUNICATION DESIGN CONTROL  
(TELEMETRY)

PROJECT: JOVE

CHANNEL: SC/DSIF Telemetry

MODE: 100w/ 20 ft Ant./210 ft Ant.

NO.	PARAMETER	VALUE	TOLERANCE	SOURCE
1	Total Transmitter Power	50 dbm		Assumed
2	Transmitting Circuit Loss	-3.00 dB	-1.00 dB +3.00 dB	Assumed
3	Transmitting Antenna Gain	40.00 dB	±1.00 dB	Assumed
4	Transmitting Antenna Pointing Loss	-1.5 dB	+1.50 dB -0.50 dB	Assumed
5	Space Loss	-278.7 dB	±0 -2.00	Calculated
6	Polarization Loss	-0.05 dB	+0.01 -0.17	Calculated
7	Receiving Antenna Gain	61.0	±1.00	EPD-283
8	Receiving Antenna Pointing Loss	0	Included in 7	Included in 7
9	Receiving Circuit Loss	0	Unknown	Assumed
10	Net Circuit Loss	-182.25	+6.51 -5.67	Calculated
11	Total Received Power	-132.25 dbm	+6.51 -5.67	Calculated
12	Receiver Noise Spectral Density (N/B)	-182.12 dbm	+0.92 -1.04	Calculated
	T System = 50°K			EPD-283
13	Carrier Modulation Loss	-3.00	Unknown	Assumed
14	Received Carrier Power	-132.25 dbm	+6.51 -5.67	
15	Carrier APC Noise BW ( $2B_{LO} = 24$ Hz)	13.8	+0.0 -0.0	EPD-283
	<u>CARRIER PERFORMANCE - TRACKING</u> (One-way)			
16	Threshold SNR in $2B_{LO}$ ( $2B_{LO} = 24$ Hz)	0.00	-	Assumed
17	Threshold Carrier Power	-168.32 dbm	+7.43 -6.71	
18	Performance Margin	+33.07	+7.43 -6.71	Calculated
	<u>CARRIER PERFORMANCE-TRACKING</u> (Two-way)			
19	Threshold SNR in $2B_{LO}$ ( $2B_{LO} = 24$ Hz)	2.00	-	Assumed
20	Threshold Carrier Power	-166.32	+7.43 -6.71	Calculated
21	Performance Margin	+31.07	+7.43 -6.71	Calculated

TABLE IV-7. TELECOMMUNICATION DESIGN CONTROL  
(TELEMETRY) (Continued)

PROJECT: JOVE

CHANNEL: SC/DSIF/Telemetry

MODE: 100 w/20 ft Ant./210 ft Ant.

NO.	PARAMETER	VALUE	TOLERANCE	SOURCE
	<u>CARRIER PERFORMANCE</u>			
22	Threshold SNR in $2B_{LO}$ ( $2B_{LO} = 24 \text{ Hz}$ )	6.00 dB	-	Assumed
23	Threshold Carrier Power	-162.32 dbm	+7.43 dB -6.71 dB	Calculated
24	Performance Margin	+27.07 dB	+7.43 dB -6.71 dB	Calculated
	<u>DATA CHANNEL</u>			
25	Modulation Loss	4.50 dB	-	Assumed
26	Received Data Subcarrier Power	-139.75 dbm	+6.51 -5.67	Calculated
27	Bit Rate (Bit Rate = 3740 BPS)	35.73 dB	-	Assumed
28	Required ST/N/B ( $P_b^e = 1 \times 10^{-3}$ )	7.00 dB	-	Fig. IV-3
29	Threshold Subcarrier Power	-145.12 dbm	+7.43 dB -6.71 dB	Calculated
30	Performance Margin	0	+7.43 dB -6.71 dB	Calculated
	<u>SYNC CHANNEL</u>			
31	Modulation Loss	-4.50	-	Assumed
32	Receiver SYNC Subcarrier Power	-139.75	+6.51 -5.67	Calculated
33	SYNC APC Noise BW ( $2B_{LO} = 1.00 \text{ Hz}$ )	0	-	Assumed
34	Threshold SNR in $2B_{LO}$	24 dB	-	Assumed
35	Threshold Subcarrier Power	-158.12		Calculated
36	Performance Margin	+18.37	+7.43 dB -6.71 dB	Calculated

**TABLE IV-8. TELECOMMUNICATION DESIGN CONTROL  
(COMMAND)**

PROJECT: JOVE

CHANNEL: DSIF/SC/-Command

MODE: 400 kw/210 ft Antenna/5 dB Antenna

NO.	PARAMETER	VALUE	TOLERANCE	SOURCE
1	Total Transmitter Power	86 dbm	-	JPL EPD-2E3
2	Transmitting Circuit Loss	-0.5 dB	+0.50 -1.00	Assumed
3	Transmitting Antenna Gain	60.0	±0.8 dB	JPL EPD-283
4	Transmitting Antenna Pointing Loss	0	Included in 4	Assumed
5	Space Loss	-278.7 dB	+0.00 dB -2.00 dB	Calculated
6	Polarization Loss	-0.05 dB	+0.01 dB -0.17 dB	Assumed
7	Receiving Antenna Gain	5.00 dB	Unknown	Assumed
8	Receiving Antenna Pointing Loss	-1.50 dB	-	Assumed
9	Receiving Circuit Loss	-3.00 dB	+1.00 dB -1.00 dB	Assumed
10	Net Circuit Loss	-218.75	+2.31 dB -4.97 dB	Calculated
11	Total Received Power	-132.75 dbm	+2.31 -4.97 dB	Calculated
12	Receiver Noise Spectral Density (N/B)	-166.45 dbm/cps	Unknown	Calculated
	T System = 2600° K (10 dB N-F)		Unknown	Assumed
13	Carrier Modulation Loss	-3.00 dB	-	Assumed
14	Received Carrier Power	-135.75 dbm	+2.31 dB -4.97 dB	Calculated
15	Carrier APC Noise BW ( $2B_{LO} = 24 \text{ Hz}$ )	13.8	-	EPD-283
	<u>CARRIER PERFORMANCE-TRACKING</u> (One-way)			
16	Threshold SNR in $2B_{LO}$ ( $2B_{LO} = 24 \text{ Hz}$ )	0.00	-	Assumed
17	Threshold Carrier Power	-152.65		Calculated
18	Performance Margin	-16.90	-2.31 -4.97	Calculated
	<u>CARRIER PERFORMANCE-TRACKING</u> (Two-way)			
19	Threshold SNR in $2B_{LO}$ ( $2B_{LO} = 24 \text{ Hz}$ )	2.00	-	Assumed
20	Threshold Carrier Power	-150.65 dbm		Calculated
21	Performance Margin	+14.90	+2.31 -4.97	Calculated

TABLE IV-8. TELECOMMUNICATION DESIGN CONTROL  
(COMMAND) (Continued)

PROJECT: JOVE

CHANNEL: DSIF/SC - COMMAND

MODE: 400 kw/210 ft Antenna/5 dB Antenna

NO.	PARAMETER	VALUE	TOLERANCE	SOURCE
	<u>CARRIER PERFORMANCE</u>			
22	Threshold SNR in $2B_{LO}$ ( $2B_{LO} = 24 \text{ Hz}$ )	6.00	-	Assumed
23	Threshold Carried Power	-146.65 dbm	+2.31 -4.97	Calculated
24	Performance Margin	+10.90	+2.31 -4.97	Calculated
	<u>DATA CHANNEL</u>			
25	Modulation Loss	-4.50	-	Assumed
26	Received Data Subcarrier Power	-137.25	+2.31 -4.97	Calculated
27	Bit Rate (B.R. = 1 BPS)	0 dB	-	Calculated
28	Required $ST/N/B P_b^e = 1 \times 10^{-6}$	9.5 dB	-	Fig. IV-3
29	Threshold Subcarrier Power	-156.95	+2.31 -4.97	Calculated
30	Performance Margin	19.70 dB	+2.31 -4.97	Calculated
	<u>SYNC CHANNEL</u>			
31	Modulation Loss	-4.50	-	Assumed
32	Receiver SYNC Subcarrier Power	-137.25	+2.31 -4.97	Calculated
33	SYNC APC Noise BW ( $2B_{LO} = 1 \text{ Hz}$ )	0 dB	-	Calculated
34	Threshold SNR in $2B_{LO}$	24 dB	-	Calculated
35	Threshold Subcarrier Power	-142.45	+2.31 -4.97	Calculated
36	Performance Margin	5.20	+2.31 -4.97	Calculated



CHANNEL: SC DSIF TELEMETRY RATE  
MODE: 100 WATTS 210' DIA. ANTENNA

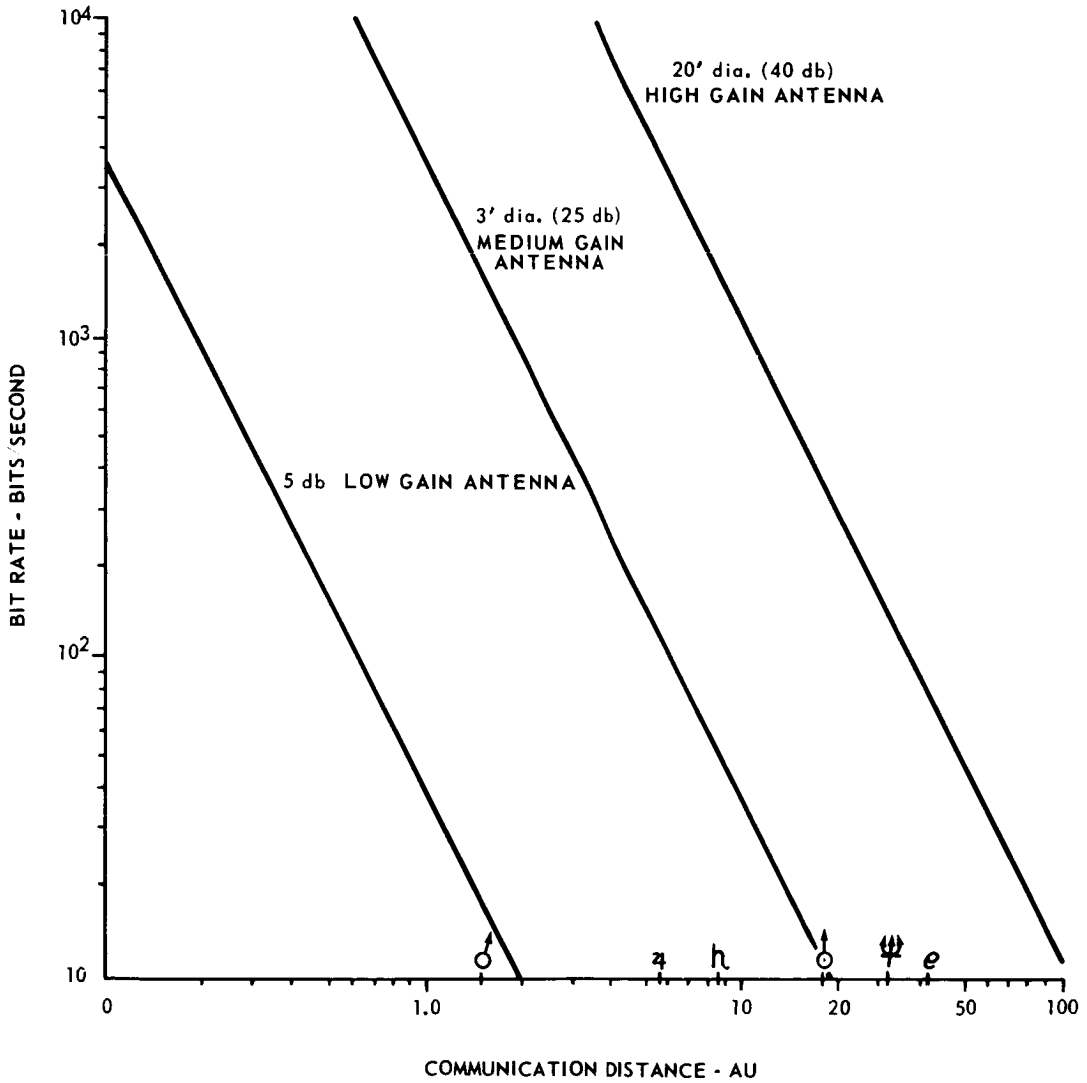


FIGURE IV-10. BIT RATE VS. DISTANCE

- d. Store digitally encoded video data if required.
- e. Phase shift key a subcarrier with a binary signal.
- f. Generate a cyclic binary pseudorandom sequence for use in synchronizing the encoding and decoding of the telemetry data.
- g. Phase shift key a second subcarrier with the sync code.
- h. Combine the two subcarriers into a composite telemetry signal. A block diagram of the entire telemetry subsystem, including external commands and synchronization, is shown in Figure IV-11.

## Multiple Transmission Modes

Justification. The intent of multiple modes of transmission is to assure maximum return of information. Four of the primary factors which influence the return of information thereby necessitating definition of distinct transmission modes are:

1. Data priority: During different phases of the mission certain sources of information are of greater importance than others. This necessitates design of multiple data formats and transmission rates during different phases of the mission.

2. Allowable bit rates: Some factors which influence bit rates are:

- Distance between the spacecraft and Earth,
- Instability during power maneuvers and periods of acquisition require use of omni directional antennas which result in lower available bit rates,
- Periods of occultation, and
- Possible antenna failure.

3. Dynamic range and rates of change of raw data: It is desirable to separate the engineering and science data as completely as possible. The reason for this is that engineering measurements lend themselves readily to

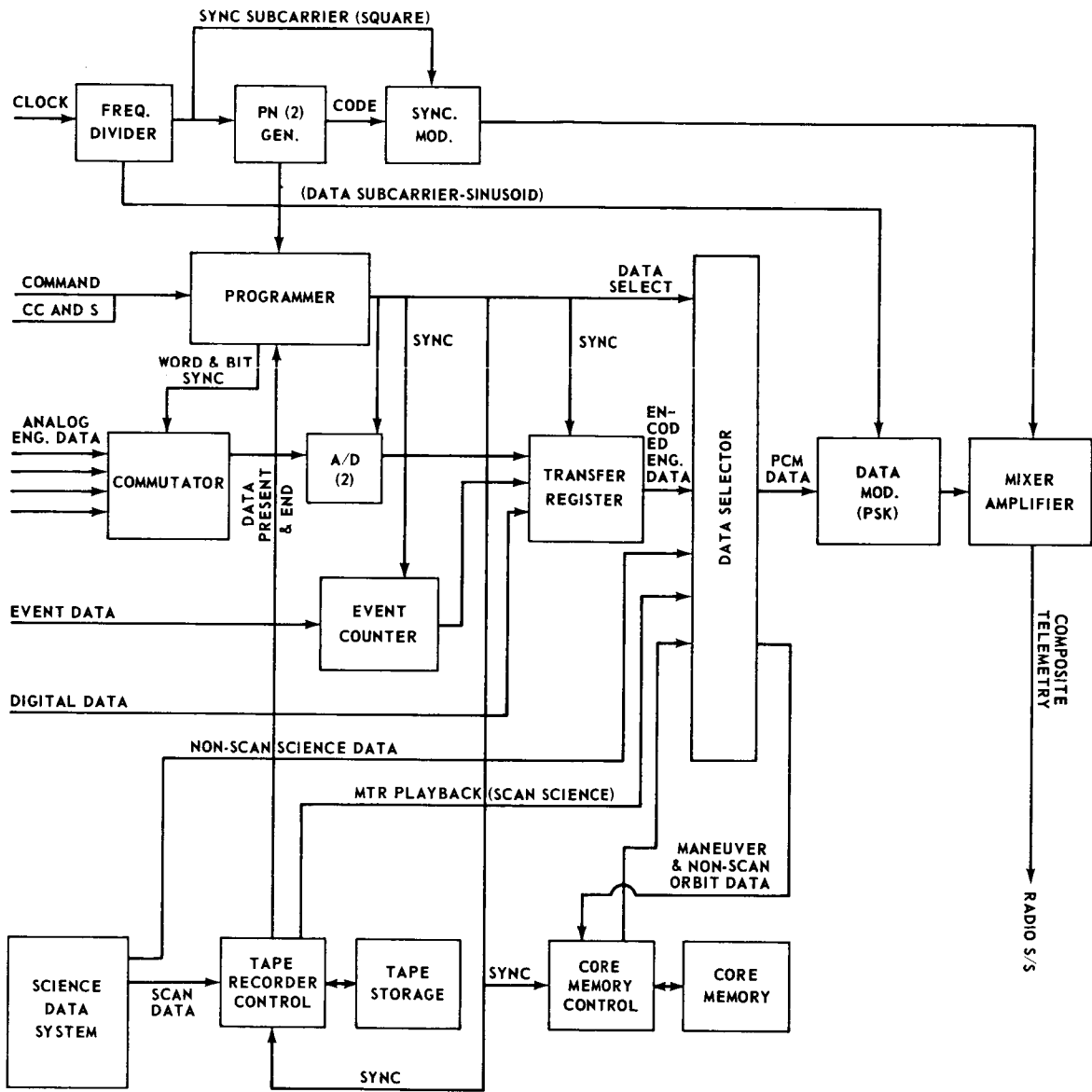


FIGURE IV-11. SPACECRAFT TELEMETRY SUBSYSTEM

fixed sampling rates. On the other hand, scientific experiments, by their very nature, may yield data orders of magnitude different from that anticipated. For this reason employment of multiple data formats and varied transmission rates are mandatory.

4. Data storage requirements: Particular mission phases require data storage. This requires generation of several command and synchronization pulses to assure that record and playback information can be accurately detected at the DSIF ground station.

Transmission Mode. The overall mission to orbit a spacecraft about Jupiter has been broken up into seven (7) transmission modes. Three modes have been defined between launch and orbit insertion. The other modes which have been defined are two orbital modes, one occultation mode and one backup mode in case the high gain antenna configuration should fail. The seven transmission modes are:

1. Acquisition mode
2. Normal cruise mode
3. Maneuvers mode
4. Periapsis mode
5. Apoapsis mode
6. Occultation mode
7. Backup mode

## Data Handling

### Data Sources

Engineering Housekeeping Data. It is anticipated that there will nominally be some three hundred engineering channels to monitor during the mission. Typical

engineering measurements to be handled by the engineering data encoder are temperatures of antennas, electronic packages, batteries, RTG, and cold gas storage bottles; also sun sensor outputs, mode switch positions, cold gas storage pressure, power system voltages and currents, and TWT voltage. The amount of engineering data collected and transmitted during each phase of the mission is given in Table IV-9. The number of engineering data channels selected were arrived at by comparison with the Mariner IV mission. The engineering data provided for in JOVE exceeds the Mariner IV mission by a factor of 3. This amount of data is required primarily because of the increased complexity of the JOVE spacecraft. The particular bit rate selected was the most easily mechanized figure which came closest to the desirable bit rate.

Non Scan Science Data. The following instruments were selected by the Experiments Group to provide scientific information during the total mission:

- Cosmic ray telescope,
- Cosmic ray detector,
- Microwave radiometer,
- Curved surface plasma analyzer,
- Faraday cup analyzer,
- Trapped radiation detector,
- Three axis fluxgate magnetometer, and
- Micrometeoroid detectors.

Planet Scan Data: The following instruments will be carried on the spacecraft in order to make visible and infrared measurements while orbiting the planet:

- Visible and ultra-violet photometer,
- Infrared radiometer,
- High resolution television system,

TABLE IV-9. SUMMARY OF ENGINEERING DATA

Transmission Mode	Worst Case Available Bit Rate (bps)	Selected Bit Rate (bps)	Storage Requirements
1. Acquisition (< .25 AU)	400 - omni antenna	100	Eng. Data temporarily stored in Mag. core memory
2. Normal Cruise	3740 - high gain antenna	800	None
3. Maneuvers (> .25 AU)	118 - med. gain antenna	50	Eng. Data temporarily stored in magnetic core memory
4. Periapsis	3740 - high gain antenna	800	About $2.2 \times 10^7$ bits of scan data stored on magnetic tape
5. Apoapsis	3740 - high gain antenna	800	Non-scan science data temporarily stored during scan data playback
6. Backup	118 - medium gain antenna	50	None
7. Occultation	---	---	All data temporarily stored in magnetic core memory

- Wide angle TV system,
- Infrared spectrometer, and
- Visible and ultra-violet spectrometer.

### Science Data System (SDS)

**Function.** The science data system contains two independent subsystems. A realtime science data system (RT-SDS) automatically controls and synchronizes the data gathering sequence of the cruise or nonscan data from launch to end of mission. The RT-SDS also processes and formats all the diversified science data into a single stream of binary data for the telemetry system. The non-real-time or NRT-SDS controls the encounter sequence and puts all planet scan data into formats for recording and subsequent transmission back to Earth. The NRT-SDS is not energized until approximately 800 days after launch.

RT-SDS - Data Format (Figures IV-12 and IV-13). Two RT science data formats have been defined. There are:

a. Cruise format - nonscan science data is collected in 36 word blocks with 10 bits per word, approximately every 7 seconds, using engineering data encoder bit sync, and

b. Orbital format - in the realtime periapsis transmission mode non-scan data will be collected and put into formats of two blocks with 36 words of 10 bits each, spaced at 40-word intervals. The intervening 40 words are engineering identification data. During apoapsis transmission mode, when the NRT-SDS is in operation, realtime data is temporarily stored in 108 minor word frames on magnetic core memories while blocks of planet scan data are played back from the tape recorders and transmitted back to Earth.

NRT-SDS - Data Format. Planet scan data sampled at nominally 50 000 bits per second during the periapsis transmission mode is stored on magnetic tape recorders at the same rate. The data will be recorded in frames of  $10^6$  bits upon command from the SDS. A total of  $2.1 \times 10^7$  bits/orbit of planet scan data is anticipated. Three tape recorders are provided which in series provide a maximum storage capacity of  $6 \times 10^8$  bits or 600 frames.

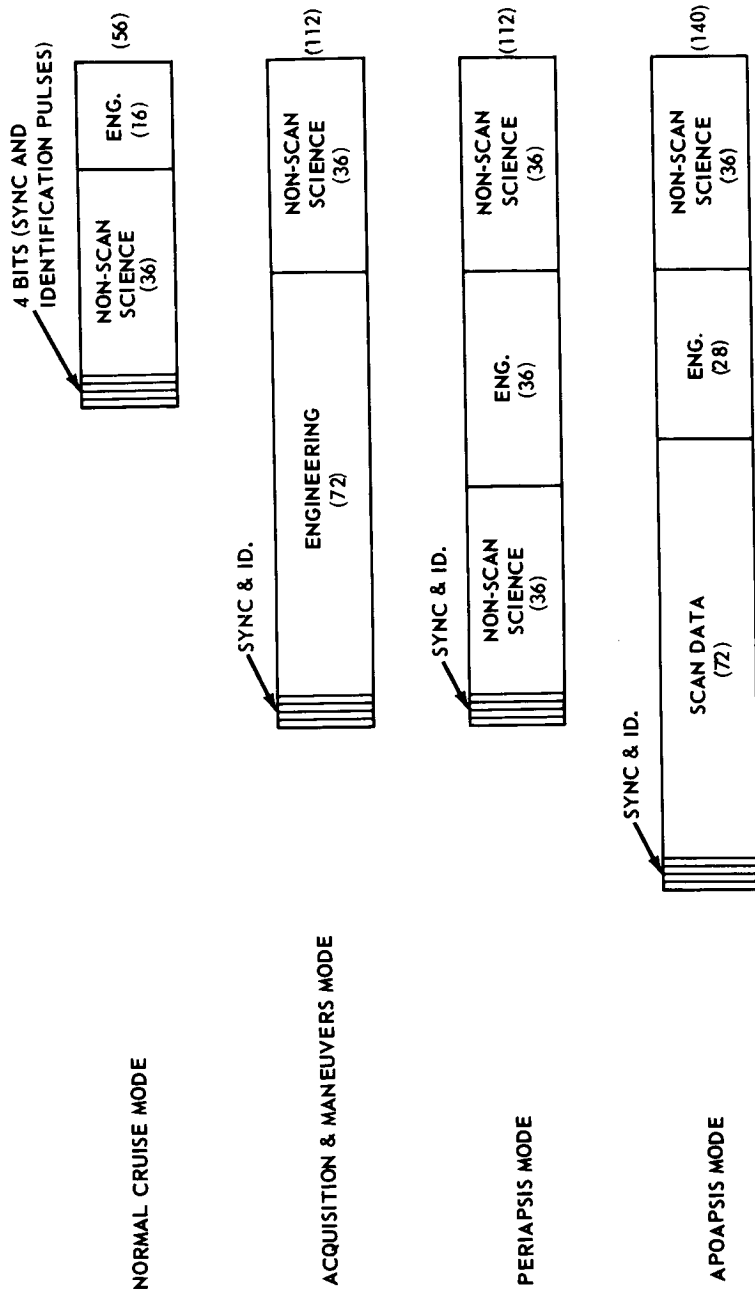


FIGURE IV-12. REAL TIME DATA TRANSMISSION FORMATS



FGM 1,2,3
RVM
CSD
FCD
SFD 1,2
CMT 1,2
FGM 1,2,3
SFD 1,2
CRT 1,2
CMT 1,2
FGM 1,2,3
SFD 1,2,3
CMT 1,2,3
MMD 1,2,3
TRD 1,2,3,4,5

(36)\*

\*10 BITS PER SCIENCE WORD - 36 WORDS

- FGM - FLUX GATE MAGNETOMETER
- RVM - RUBIDIUM VAPOR MAGNETOMETER
- CSD - CURVED SPACE PLASMA DETECTOR
- FCD - FARADAY CUP DETECTOR
- CRT - COSMIC RAY TELESCOPE
- CMT - CHARGE & MASS TELESCOPE
- SFD - SOLAR FLARE DETECTOR
- TRD - TRAPPED RADIATION DETECTOR
- MMD - MICROMETEROID DETECTOR

FIGURE IV-13. NON-SCAN SCIENCE MINOR FRAME

## Engineering Data Encoder (EDE)

**Function.** The function of the Engineering Data Encoder is to sample, encode and commutate all engineering data. Each data sample will be quantized into a seven bit binary word. Data words will be encoded into one of three fixed data formats by the transfer register depending on which transmission mode is in use. Ultimately all engineering and science data will be time shared in order to phase shift key a single subcarrier oscillator. Generation of necessary word and bit synchronization pulses are discussed in detail in a subsequent section.

**Engineering Data Format.** Data priority considerations, in addition to a desire to maintain a minimum level of complexity, led to the choice of four data formats (Fig. IV-12). Selection of, and rate of sampling, of each of the formats depends on selection of a given transmission mode. Each of the formats will contain frame synchronization as well as mode and format identification pulses. The four formats selected were:

- a. **Cruise format:** Nominally 250 cruise channels are formatted into 36 word blocks and transmitted serially through high gain antenna in real time at 800 bits per second.
- b. **Acquisition and Maneuver format:** Nominally 100 maneuver channels are formatted into 72-word blocks to be simultaneously stored and transmitted through either the med. gain antenna or omni antenna at the preselected bit rate for each transmission mode.
- c. **Orbit formats:** There are separate formats depending upon orbit location, i. e. , periapsis and apoapsis. Nominally 300 orbital channels are put into formats with 36-word blocks and either transmitted in real time during the periapsis transmission mode or temporarily stored in blocks of 108-word minor frames to be later transmitted along with playback of planet scan data through the high gain antenna at 800 bits per second.

### Synchronization

**Requirements.** Two types of synchronization are required. They are:

- a. Word and bit sync pulses which includes stepping of the commutators, analog to digital converters, readout of data from the science data systems, readout of the event registers and timers, and playback of stored video or maneuver data.

b. Precise indication of the phase of the unmodulated data carrier. This is absolutely necessary for coherent demodulation at the ground receiver station.

### Mechanization

After much consideration a design evolved with which all synchronization is accomplished with one system (Fig. IV-14). The basic timing for the sub-system is derived from a clock frequency (14.4 kHz) on the spacecraft which is divided down to provide two subcarrier frequencies, one for data and one for synchronization. Synchronization pulses are generated with the use of a redundant pair of pseudorandom (PN) generators which generate maximal length cyclic codes. The advantages of pseudorandom codes are twofold.

- a. PN codes have two level bi-polar auto correlation functions, and
- b. PN codes are easily mechanized using shift register generators and module two adders in the feedback loop.

Word sync pulses occur once per cycle of the code while the data sync bit pulses occur once every 9 PN code bits. The result is 7 data bit sync pulses for every cycle of the PN code. Thus, by selecting the appropriate frequency divider to drive the PN code generators, data bit sync timing pulses at a rate of 50, 100 or 800 bits per second are generated. A particular data rate is selected by command from the programmer depending on which transmission mode is in use. One engineering data word pulse is generated each cycle of the PN code and an external decode counter is used to supply one science data word pulse for every 10 data bit sync pulses.

Based on Mariner IV a data word error of  $10^{-2}$  was selected. For an uncoded coherent PSK communication system the corresponding required bit error probability is

$$Pe^b = 1 - (1 - Pe^w)^{1/n}$$

which can be expanded in series form and approximated by

$$Pe^b \approx Pe^w/n$$

Thus for science data where  $n = 10$

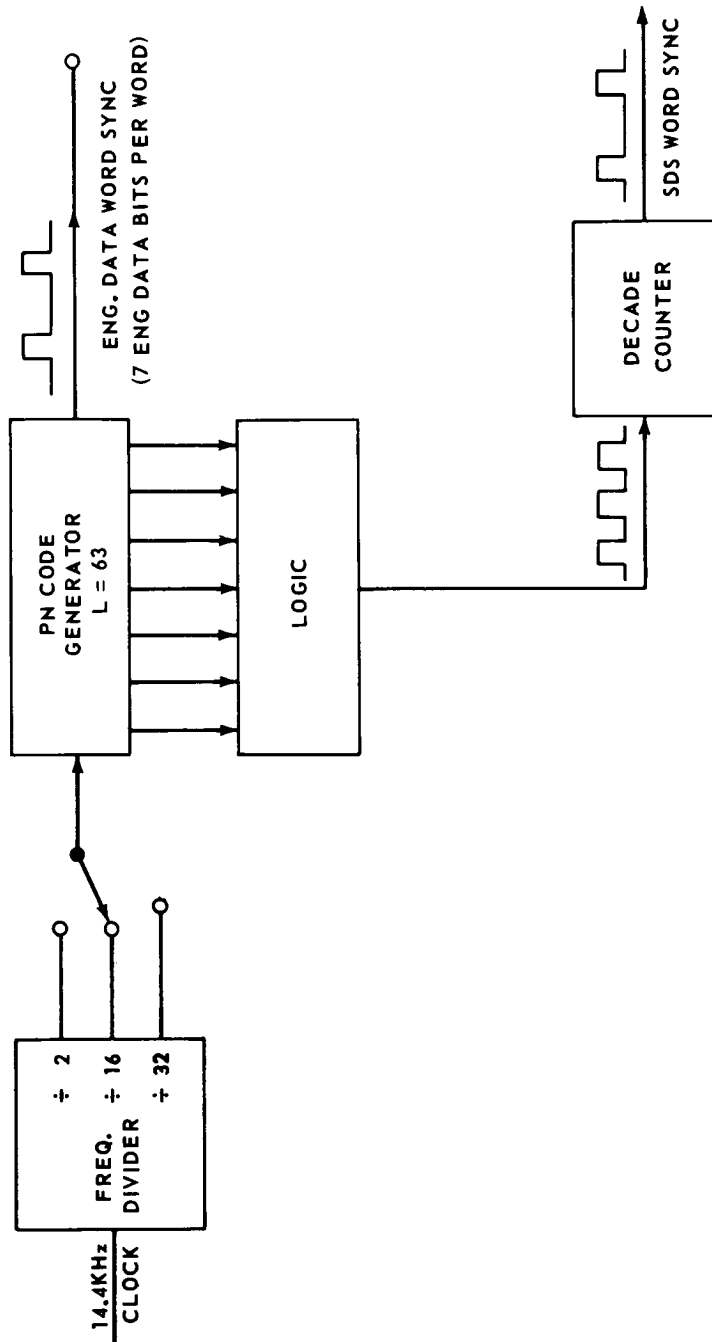


FIGURE IV-14. DATA WORD AND BIT SYNC GENERATION

$$P_e^b \text{ (science)} = \frac{10^{-2}}{10} = 10^{-3}$$

and for engineering data  $n = 7$

$$P_e^b \text{ (eng.)} = \frac{10^{-2}}{7} = 1.43 \times 10^{-3}$$

These required bit error probabilities dictate a certain communication efficiency or received signal to noise ratio (Fig. IV-15) which, coupled with transmission losses, circuit losses, antenna gains and noise sources dictate the allowable data transmission rates (bps).

In order to convey the bits and word sync timing to the ground stations for use in synchronous demodulation of the telemetry subcarrier, the code also phase shift keys the synchronization subcarrier. The output of the telemetry system to the spacecraft transponder RF phase modulator is thus a composite signal composed of modulated telemetry and synchronization subcarriers. These subcarriers are linearly mixed to form the composite telemetry signal. This composite signal contains all the information necessary for demodulation and decommutation of the telemetry data by the ground telemetry sub-system. At the ground station a local model of the PN code is phase locked to the received code. Word gates identical to those in the spacecraft then produce accurate word and bit sync pulse trains (Fig. IV-16).

## Telemetry Data Transmission

Modulation. A study of various modulation methods was conducted with two main considerations in mind: communication efficiency, and compatibility with the DSN ground station.

It has been quite conclusively proved that the biorthogonal channel with a conveyance of information in the state of one of two mutually opposed phase states, that is  $0^\circ$  and  $180^\circ$  or  $\pm 90^\circ$  of a carrier frequency is the simplest and perhaps best mechanization of such an orthogonal system. This modulation technique is often called phase-shift keying, or PSK modulation.

The design of such a system is characterized by a specification of bit error probability, i. e. , the likelihood that a decision device will make an error because of the additive noise and is usually presented as a function of received signal to noise ratio. It is convenient that systems of this type can readily be

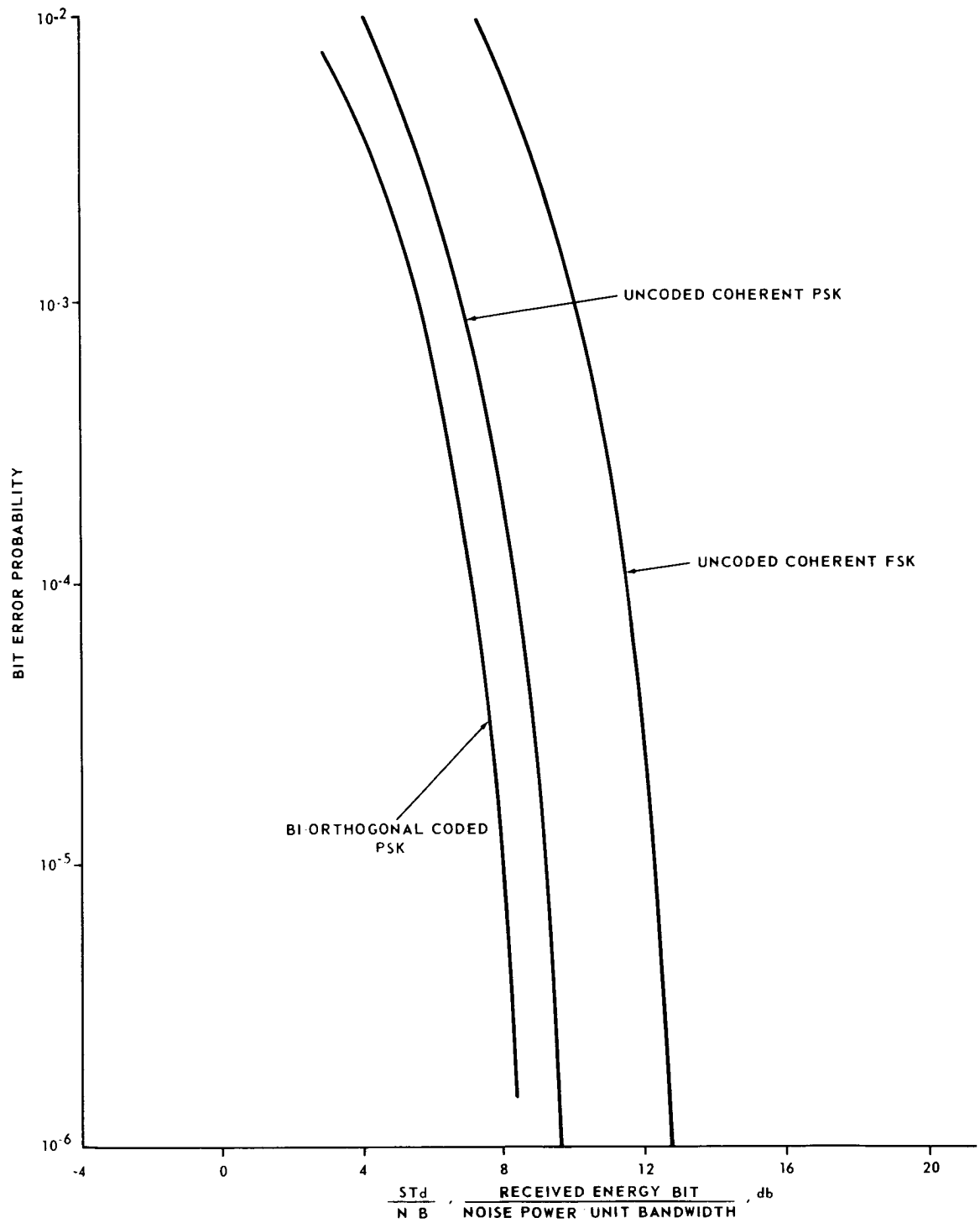


FIGURE IV-15. BIT ERROR PROBABILITIES

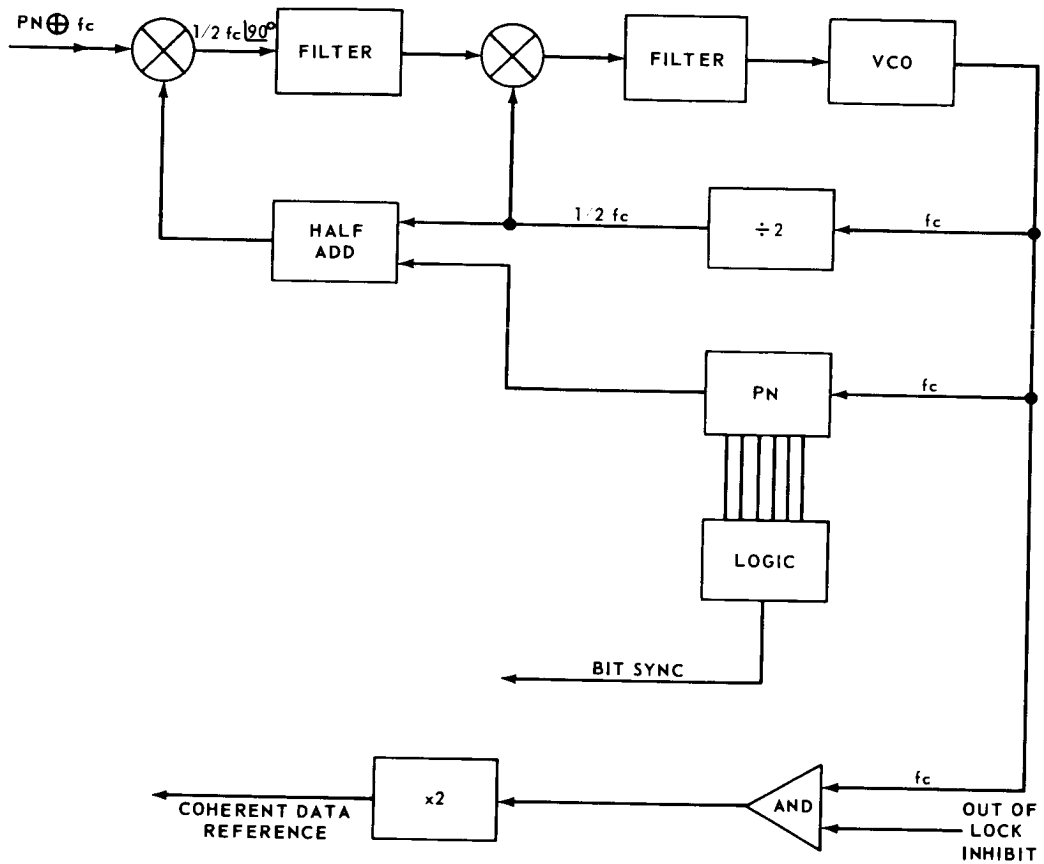


FIGURE IV-16. RECEIVING SYNC SYSTEM FOR GENERATION OF COHERENT DATA

analyzed and that their performance is only a function of the received signal energy per bit over which the channel designer has control, and the system noise power spectral density  $N/B$  which (hopefully) is known. Except for second order effects, the performance is independent of band width considerations. Figure IV-15 shows the comparative bit error performance of three types of binary system. Note that matched filter detection has been assumed in all cases. A coherent PSK system is apparently 3 dB better than its nearest competitor, coherent FSK.

The modulation scheme selected, therefore, was to encode and multiplex the raw data into a stream of binary bits which phase shift keys or biphase modulates a subcarrier oscillator, which in turn phase modulates the RF carrier.

Such a system is normally abbreviated as a PCM/PSK/PM modulation system. The use of subcarrier techniques is necessary to keep the telemetry system compatible with the DSIF receiving systems and the command system compatible with the spacecraft transponder receiver.

Demodulation. Coherent demodulation was selected consistent with the DSIF capability. Coherent demodulation of a biphase modulated carrier requires knowledge of the exact phase of the unmodulated carrier at the receiving station. This is accomplished by locking on to a PN sequence transmitted on a synchronization subcarrier by the spacecraft. The ground station generates an exact replica of the incoming PN code, and with phase-locked loop techniques, locks on to the incoming synchronization signal (Fig. IV-16). The synchronization system provides a phase coherent clock frequency at 7200 Hz in the form of a local oscillator in the loop. This signal when frequency multiplied by 2 provides a simply derived coherent reference for the demodulation of this data subcarrier located precisely at 14 400 Hz. Phase coherent demodulation is an inherently non-linear process, and only about 50 percent of the total transmitted power can be put into the usable carrier side bands. This 3 dB penalty is, however, more than offset by the advantages of phase-locked detection of the RF carrier.

Detection. Following the demodulation process, the noise corrupted binary wave form must be detected and it has been shown that the optimum detector for systems corrupted by additive gaussian noise is the matched filter (Fig. IV-17). This detector will always maximize the output signal to noise ratio, and is characterized by an impulse response which is the inverse time function of the wave form to be detected. Necessary synchronization for the matched filter detector is available as explained above.



Error Control Coding. If the information in such a system is conveyed in a single state, that is 1 or 0, the system is often referred to as an uncoded binary system, and the detection technique required on the ground is called bit by bit detection. By using a combination of two phase states, literally a coded phase word to represent a single information state, the modulation efficiency of such a system can be increased. The coded systems are also referred to as redundant, since more than one phase state is used to represent a single information state, and the corresponding detection technique in the ground system is often called word detection. Specific attention was given to the use of bi-orthogonal codes. Analysis of code performance was based on maximizing the ratio  $\frac{ST_d}{N/B}$  for a given probability of error. Figure IV-15

shows the merits of bi-orthogonal codes compared with the uncoded binary word. Results of the study indicate that, if error control codes were to be used, the choice based on efficiency would be the bi-orthogonal code, with an improvement of 1.76 dB at the required  $1.43 \times 10^{-3}$  bit error rate. This marginal gain in efficiency, higher development and production cost, increased system complexity (encoder and decoder) and lower MTBF rates suggest use of the uncoded word for telemetry link. The resulting bit probability error for the uncoded word is given by

$$P_e^b = \frac{1}{2} \left[ 1 - \operatorname{erf} \sqrt{\frac{ST_d}{N/B}} \right]$$

### Transmission Rates

1. Available Data Rates - The principal parameters of the spacecraft system which affect the transmission capability (Fig. IV-11) are antenna gains, transmitter power, and bulk storage capacity.

- High gain antenna: The upper bound for our telecommunications system is set by the selection of a 20-foot parabolic antenna and a 100-watt power amplifier. These parameters in conjunction with transmission and system losses yield a nominal data rate of 3740 bits per second.

- Medium Gain Antenna: Communication with the medium gain antenna during maneuvers beyond 0.25 AU as well as in the backup transmission mode, yields a nominal data rate of about 118 bps.

- Omni-directional antenna array: During early maneuvers (less than 0.25 AU) and periods of acquisition, communication is limited to use of omni-directional antennas with a resultant available bit rate of about 400 bps.

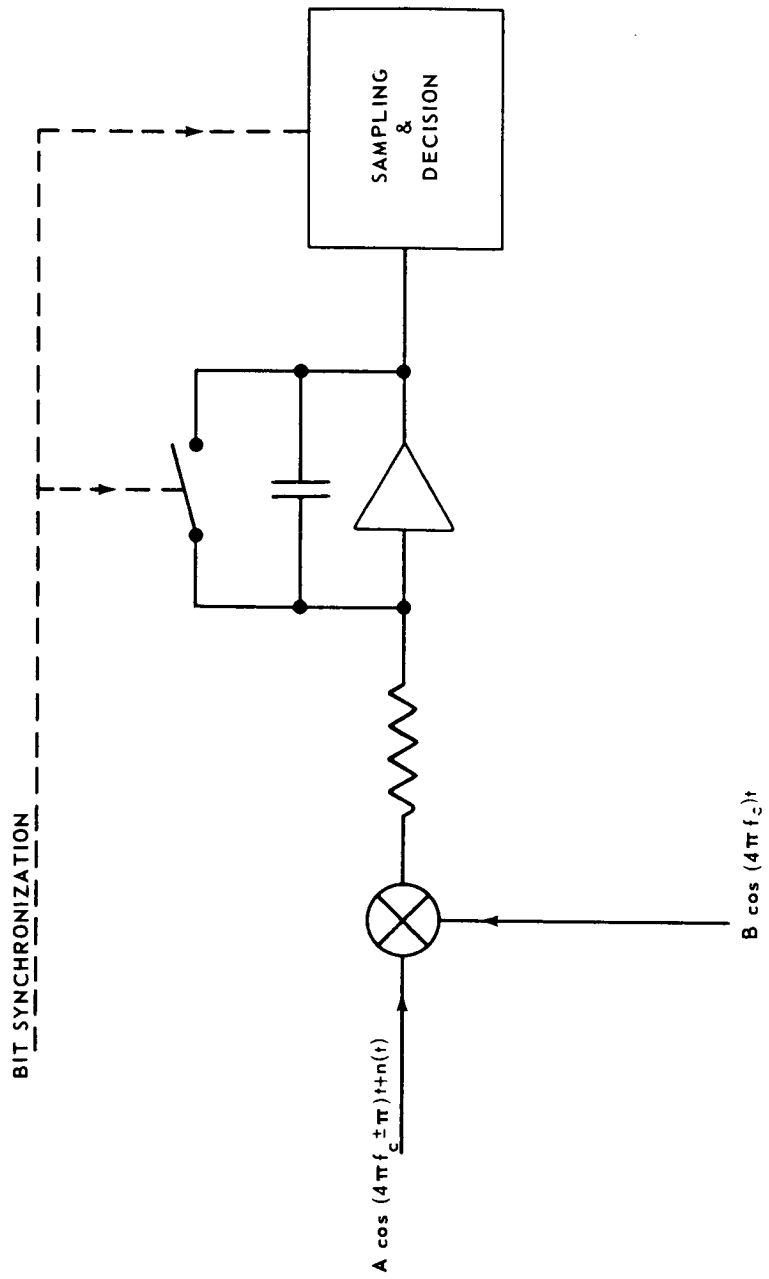


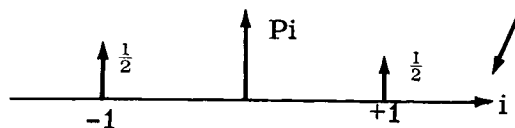
FIGURE IV-17. COHERENT DEMODULATION AND MATCHED FILTER DETECTION

2. Mechanization - In the interest of minimizing system complexity, a set of multiple fixed transmission rates was selected. The data rate selected was on a worst case basis for a given transmission mode (Fig. IV-11).

Bandwidth Considerations. The power spectrum of the PN modulated subcarrier is derived as follows: The output of the sync modulator is a modulo 2 addition of the PN code and the square wave clock (PN  $\oplus$   $f_c$ ). By treating the PN code as a random process with two equally probable states the weighted Fourier transform in each of the switching intervals, in this case  $1/f_c$  is:

$$G(f) = \sum_{n=1}^2 P_i \left| H_i(f) \right|^2$$

The probability density function  $P_i$  is given by



and

$$H_i(f) = f_c \int_0^{1/2f_c} (+1) e^{-j\omega t} dt + f_c \int_{1/2f_c}^{1/f_c} (-1) e^{-j\omega t} dt .$$

Therefore

$$G(f) = 2f_c \left| H_i(f) \right|^2 = \frac{2}{f_c} \frac{\sin^4(\pi f / \pi f_c)}{(\pi f / 2f_c)^2} .$$

It can be seen (Fig. IV-18) that the power spectrum of the PN modulated subcarrier contains broad nulls at 2 and 4 times the clock frequency of 7.2 KHz. While the occurrence of spectral nulls is inherent in the process of biphase modulation, the fact that they occur where they do is a result of choosing the sync subcarrier to be a square wave. It can be shown that a sinusoidal sync subcarrier would produce narrow nodes at 1.5 and 3 times the clock frequency. The unmodulated data subcarrier is conveniently located in the broad null at 14.4 KHz as shown. It was decided to make the data subcarrier a sinusoid since a square wave would create an overall spectrum too wide to be accommodated by the predetection filters of the TRAC(E) receiving system at the DSIF ground station.

Summary. The telemetry system employs two subcarriers related in frequency by a ratio of 2 to 1. The upper or data subcarrier frequency is

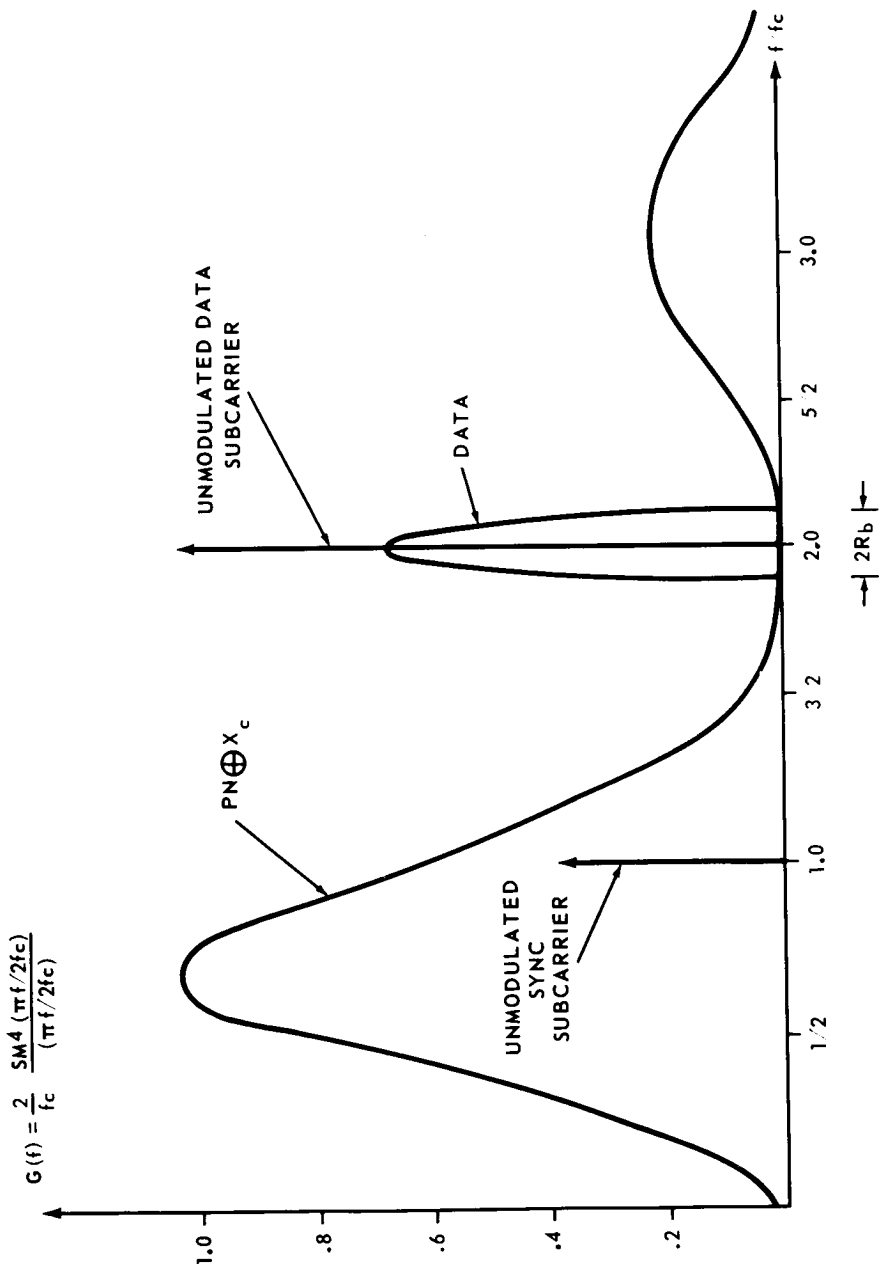


FIGURE IV-18. POWER SPECTRAL DENSITY

biphase modulated in accordance with the state of the binary data information, and the lower synchronization subcarrier is biphased modulated by a cyclic pseudorandom code. At the receiving end, the sync subcarrier is essentially reconstructed and in the process, generates bit sync information. This clock frequency then locks a phase coherent loop, the local oscillator of which is multiplied by 2 to provide a coherent reference for the demodulation of the data subcarrier. A matched filter then detects the demodulated binary waveform to complete the mechanization of the coherent PSK system. The scheme selected thus simultaneously provides necessary word and bit synchronization and generation of a coherent reference for synchronous detection.

## COMMAND SUBSYSTEM

### Introduction

Command guidance in the space vehicle involves three events. These are:

- a. Sensing the parameters involved,
- b. Computation of the appropriate correction,
- c. Communication of the command signal.

Command guidance involves external tracking which is done by radio and may be accomplished by inertial mechanisms, radio, or combination of these two. Radio systems provide continuous measurements of position, and velocity and do not suffer from the drift errors of gyroscopes although they may require a rather long averaging period.

In the Jet Propulsion Laboratory DSIF, a stable carrier signal  $2115 \pm 5$  MHz is transmitted to the spacecraft. There it is received by a phase-lock-loop, filtered, frequency multiplied by the exact ratio of  $240/221$  and retransmitted to the ground. At the ground station, the return carrier is received by the reference phase-lock-loop, filtered and then compared with the transmittal signal, approximately multiplied, to determine the Doppler shift. The command at the ground station is fed into the command modulator, whose function is to synchronize both the command word bits properly and to modulate the command subcarrier with both command and synchronizing information. The RF carrier is phase modulated by the output of the command modulator and the resultant signal is transmitted by the 210-foot antenna to the spacecraft.

The command subsystem on the spacecraft is shown in the block diagram of Figure IV-19.

The command detector function is threefold:

- a. Lock to the received synchronizing signals,
- b. Demodulate the command subcarrier to recover the command word bits, and
- c. Supply the command decoder with synchronizing and timing signals.

The decoder performs essentially the following two functions:

- a. Identifying through its address which command has been received and supplying synchronizing signals to proper spacecraft systems, and
- b. Providing input to the computer sequencer programmer according to the command information which includes simple switching for selection of scientific and telemetry modes, as well as complicated re-programming of spacecraft computer.

## PSK for Command Detection

The following two signals are required for PSK detection:

- a. A coherent reference for phase detection, and
- b. Bit synchronization for timing of matched-filter sampling and discharge.

The ground station modulates the PN code by commands to give the resultant modulator output

$$D \oplus PN \oplus 2 fs$$

where D is the command bit,  $2 fs$  represents the code clock having the form of a square wave and  $\oplus$  denotes half-addition. Assuming the duration of each command bit is equal to one cycle of the PN code, it follows that

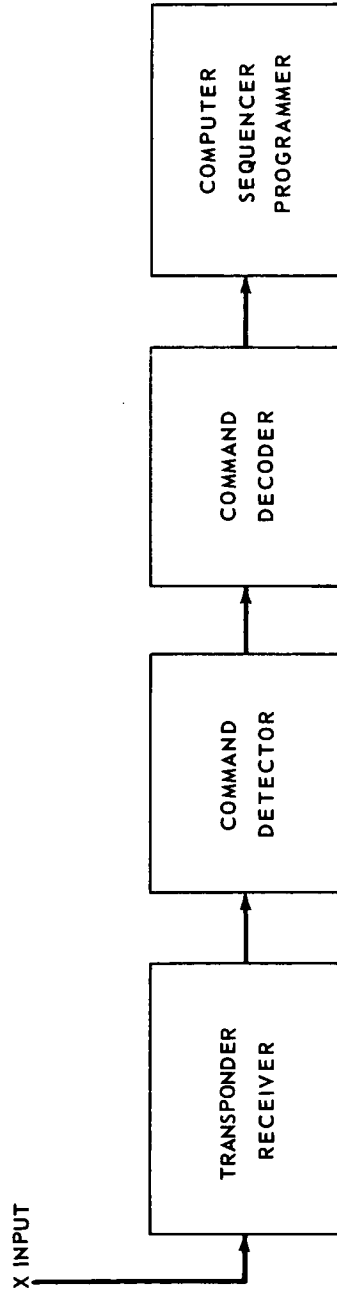


FIGURE IV-19. SCHEMATIC OF COMMAND SUBSYSTEM

$D \oplus PN \oplus 2 fs = + PN \oplus 2 fs$  if a "1" is sent,  
 and that  $D \oplus PN \oplus 2 fs = - PN \oplus 2 fs$  if a "0" is sent.

Figure IV-20 shows that the received  $D \oplus PN \oplus 2 fs$  is multiplied by the locally generated  $PN \oplus fs$  and  $PN$  codes to produce  $D \oplus fs \underline{90^\circ}$  and  $D \oplus 2 fs$  respectively. After passing through band pass filters,  $D \oplus 2 fs$  and  $D \oplus fs \underline{90^\circ}$  are multiplied together to eliminate the command-data component  $D$  resulting in an  $fs$  signal to the Phase-lock-loop (PLL). Then  $fs$  is multiplied by the local  $fs \underline{90^\circ}$ , the output forms the error signal for PLL which is closed through the loop filter and the voltage-controlled oscillator (VCO). The VCO then supplies the necessary  $2 fs$  and  $fs$  signals for the receiver operation.

Should there be a difference between the modulator  $f_2s$  and the detector  $f_2s$  when the loop is opened, the transmitted and local  $PN$  codes drift with respect to each other and the output of the PLL multiplier is their correlation function. Code lock and phase lock are obtained by closing the loop and adjusting by means of a  $2 fs$  difference to obtain the well known S curve which is the desired loop error function.

## Command Bit Detection

The bit synchronizing signals are provided by the detection of any one of the  $(2^n - 1)$  states of the  $PN$  generators. The signal  $D \oplus fs \underline{90^\circ}$  (Fig., IV-20), after passing through a band pass limiter, is coherently demodulated by multiplying with the VCO generated signal  $fs \underline{90^\circ}$ . The output of the demodulator is passed through a matched filter, where the signal is integrated and the noise components averaged over a bit period, so that the probability of making the correct decision as to which bit was transmitted is maximized. The decision required at the matched-filter is whether the sample is less than or greater than zero. Figure IV-21 shows the scheme of coherent demodulation and matched-filter detection.

## Quadrature Detector

The quadrature detector indicates when the PLL is locked and serves to inform the command decoder when to accept command information. The scheme is similar to Figure IV-21 except that the input is  $fs$ . Figure IV-22 is a block diagram of the scheme.



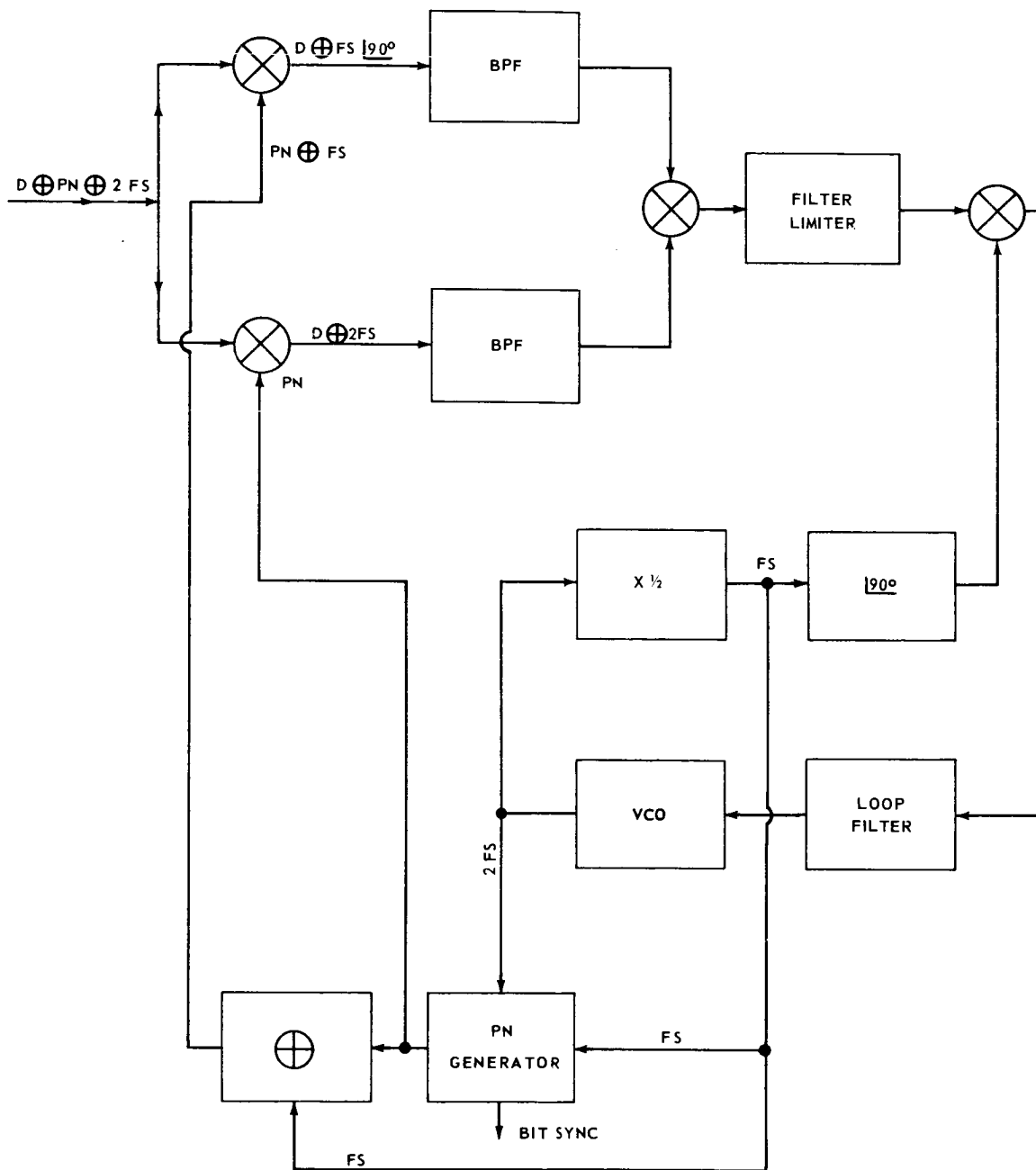


FIGURE IV-20. COMMAND DETECTION SYSTEM

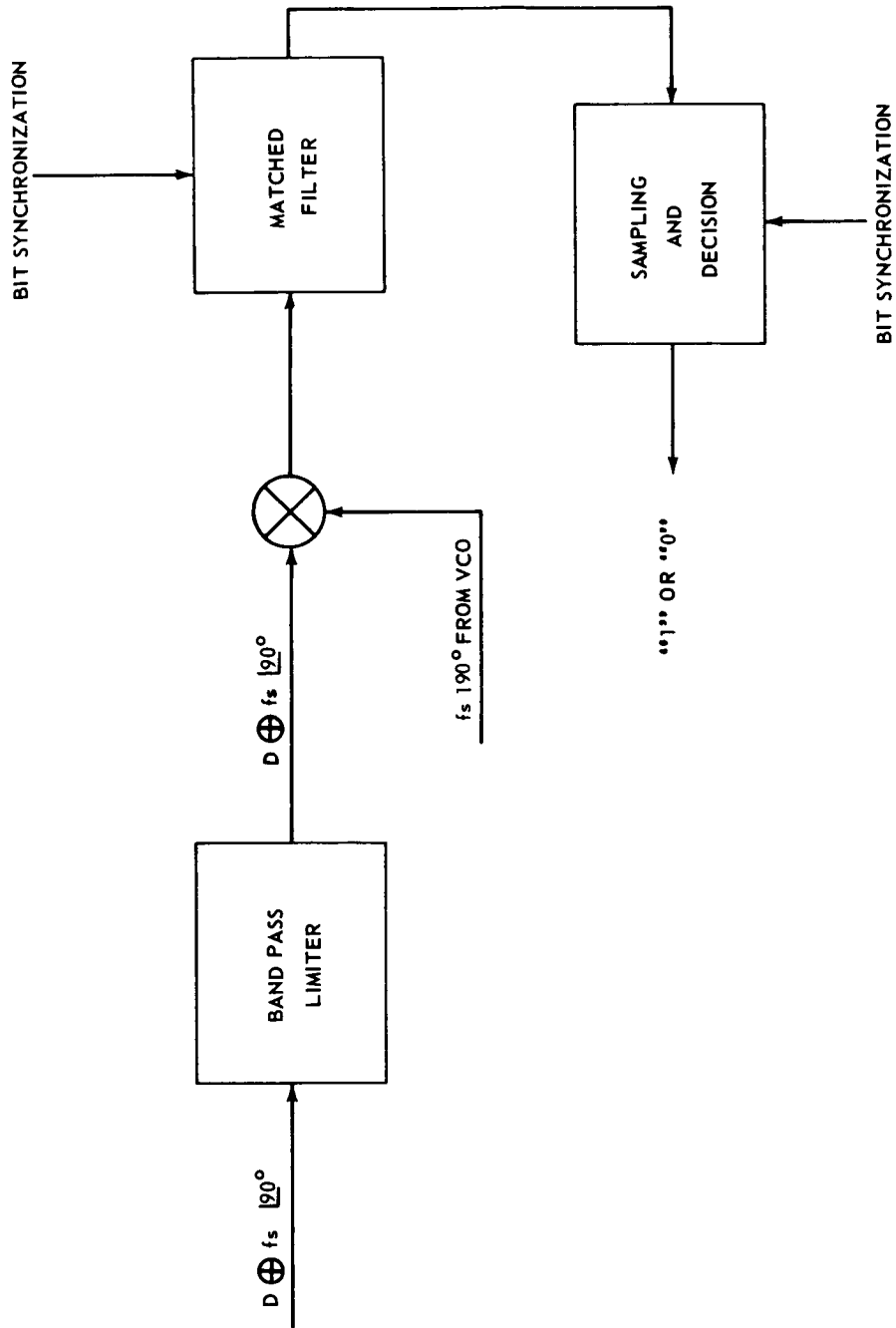


FIGURE IV-21. COHERENT DEMODULATION SYSTEM

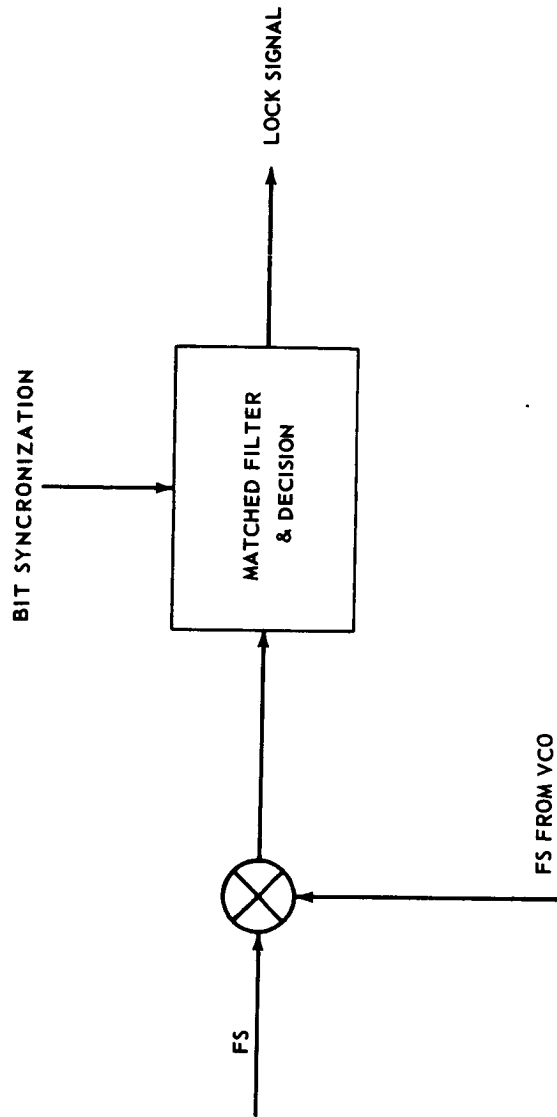


FIGURE IV-22. QUADRATURE DETECTOR

## Program Sequencer

Programmers control all timing and logic operations. The data programmer also adds synchronization to data frames. A spacecraft clock is used to provide the various frequencies and pulse rates for generating various codes and timing signals.

Inputs to the sequencer include program modification from the command detector. Outputs furnished by the sequencer in response to these inputs include (a) command reception verification, (b) position program sequences to the medium gain antenna, (c) event initiation commands to altitude, mid-course, and encounter maneuvers, as well as scientific experiments, and (d) timing references to the data encoder and power subsystem.

In the sequencing of JOVE maneuvers, an address matrix and encoder logic direct command data to the proper registers or flip-flops. When the correct data have been stored, the maneuver sequence starts by turning on the gyro power in the attitude control subsystem. After certain interval, a roll turn sequence is initiated. The roll stops until the roll register overflows. The Retro-Thrust register is pulsed in sequence in a similar manner. After a velocity correction, and the cruise mode has been reestablished, the inertial sensors are turned off.

## REFERENCES

1. Jet Propulsion Laboratory: System Capabilities and Development Schedule of the Deep Space Instrumentation Facility 1963-1967. Pasadena, JPL, March 1962.
2. Gatz, E. C., and Hartley, R. B.: Planned Capabilities of the DSN for VOYAGER 1973, Engineering Planning Document No. 283, Revision 2. Pasadena, JPL, January 1967.
3. Kendrick, J. B., ed.: TRW Space Data, Third ed. Redondo Beach, California, TRW Systems Group, TRW Inc., 1967.
4. Sanders, R. W.: Communication Efficiency Comparison of Several Communications Systems. Proceedings of the IRE, April 1960, pp. 575-588.
5. Charyulu, Varada P.: ICARUS. Stanford-NASA Space Systems Project, August 1966, pp. 34-69.
6. Presentation to Auburn University-NASA Summer Faculty Fellowship Design Program by T. A. Barr, R-ASTR-IR.
7. Kraus: Antennas. New York, McGraw-Hill Book Company.
8. Silver, S.: Microwave Antenna Theory and Design. M. I. T. Radiation Laboratory Series, vol. 12, 1949, pp. 192-195.
9. TRW Systems. Advanced Planetary Probe Study, Final Technical Report, vol. 4, Appendix G, JPL Contract 951311, July 27, 1966.
10. Balakrishnan, A. V.: Space Communications. New York, McGraw-Hill Book Company, 1965, p. 26.
11. General Electric Company. Telecommunications, VOYAGER Spacecraft System Preliminary Design. Flight Spacecraft Preferred Design, vol. A, book 2 of 4, JPL Contract 951112, July 30, 1965.
12. Potter, P. D.: Antennas. Chapter 9 of Space Communications, A. V. Balakrishnan, ed.

## REFERENCES (Concluded)

13. Michaux, C. M.: Handbook of the Physical Properties of the Planet Jupiter. Douglas Aircraft Company, Inc., Santa Monica, California, NASA SP-3031, 1967.
14. Hogg, David C.: The Effective Noise Temperature of the Sky. Microwave Journal, March 1960, pp. 80-84.
15. Reed, H. H.: Communication Satellite Ground Station Antennas. Microwave Journal, June 1967.
16. Williams, H. Paul: Antenna Theory and Design, vol. 2, Second ed., London, Sir Isaac Pitman and Sons Ltd., 1965, pp. 258-357.
17. TRW Systems: TRW Phase 1A, Voyager Spacecraft, vol. 5, Alternate Designs, Appendix II.
18. Roberts, Lester A.: The Design and Performance of a High-Efficiency Traveling-Wave Tube, The WJ-274, Final Report, Phase 1, Palo Alto, California. NASA Contract No. NAS1-3766, July 1965.
19. Martin, B. D.: The Mariner Planetary Communications System. JPL Report No. 33-38, 1960.
20. Springett, James C.: Pseudo-Kandora Coding for Bit and Word Synchronization of PSK Data Transmission Systems, International Telemetry Conference, London 1963.

## BIBLIOGRAPHY

Becker, H. D. and Lawton, J. G.: Theoretical Comparison of Binary Data Transmission Systems. Cornell Aeronautical Laboratory Report No. CA-1172-S-1, May 1958.

Bickmore, R. W.: A Note on the Effective Aperture of Electrically Scanned Arrays. Transactions IRE, vol. AP-6, April 1958, pp. 194-196.

Charles, F. J. and Lindsey, W. C.: Some Analytical and Experimental Phase-Locked Loop Results for Low Signal-to-Noise Ratios. Proceedings of the IEEE. Vol. 54, no. 9, September 1966, pp. 1152-1166.

Cuccia, Louis C.: Lightweight Very-Wide-Band Integral Package TWT's. Microwave Journal. July 1960, pp. 47-57.

Develet, Jean A., Jr.: A Threshold Criterion for Phase-Lock Demodulation. Proceedings of the IEEE, February 1963, pp. 349-356.

Dimond, Robert H.: Interplanetary Telemetry. Proceedings of the IRE. April 1960, pp. 679-685.

Easterling, Mahlon: A Long-Range Precision Ranging System. JPL TR 32-80. July 1961.

General Electric Spacecraft Department: Voyager Spacecraft System Preliminary Design, vol. B (Book 2 of 3) VB 233AA105.

Gilchrist, C. E.: Application of the Phase-Locked Loop to Telemetry as a Discriminator or Tracking Filter. IRE Transactions on Telemetry and Remote Control. June 1958, pp. 20-35.

Golomb, et al.: Digital Communications with Space Applications. Prentice Hall, Inc., Englewood Cliffs, New Jersey, 1964.

Golomb, Solomon W., ed.; Baumert, L. D.; Easterling, M. F.; Stiffler, J. J. and Viterbi, A. J.: Digital Communications with Space Applications. Englewood Cliffs, New Jersey, Prentice-Hall, 1964.

## BIBLIOGRAPHY (Continued)

Heitchue, R. D.: Space Age Fundamentals. Douglas Report SM-47656, Douglas Aircraft Company, Inc., 1964.

Hunter, John A.: Mariner Mars 1964 Telecommunication System. JPL TR 32-836, December 1, 1965.

Jaffe, R. and Rehtin, E.: Design and Performance of Phase-Lock Circuits Capable of Near-Optimum Performance Over a Wide Range of Input Signal and Noise Levels. IRE Transactions - Information Theory, March 1955, pp. 66-76.

Jet Propulsion Laboratory: Report from Mars, Mariner IV 1964-1965. Jet Propulsion Laboratory, California Institute of Technology. NASA Contract No. NAS 7-100, NASA Document EP-39.

Keenan, R. K. and Mannex, R. K.: Spacecraft Communications Systems, Space/Aeronautics, Part II, November 1962.

Korvin, William and Chadwick, George G.: Latest Word in Space Talk: It Can Come from Anywhere. Electronics, May 30, 1966, pp. 117-126.

Ksienski, A.: Signal Processing Antennas. Microwave Journal. October 1961, pp. 77-85.

Kummer, W. H. and Birgenheier, R. A.: Spacecraft Antenna Systems, Final Engineering Report. Hughes Aircraft Company, Culver City, California. NASA Contract No. NAS 5-3545, 1966.

Mathison, Richard P.: Mariner Mars 1964 Telemetry and Command System. JPL TR 32-684, June 1965.

Mueller, George E.: A Pragmatic Approach to Space Communication. Proceedings of the IRE. April 1960, pp. 557-566.

Northrop Space Laboratory: Application of SATURN/APOLLO Hardware to Unmanned Scientific Exploration of the Solar System. TR-292/3-6-003, NASA (MSFC) Contract No. NAS8-20082, April 1966.



## BIBLIOGRAPHY (Concluded)

- Odom, P. R., et al.: Northrop Space Laboratories. SATURN/APOLLO Hardware to Unmanned Scientific Exploration of the Solar System, 1966.
- Rochelle, R. W.: Signal to Noise Considerations for a Space Telemetry System. Proceedings of the IRE. April 1960, pp. 691-693.
- Shnitkin, Ho: Survey of Electronically Scanned Antennas. Microwave Journal, December 1960.
- Siegman, A. E.: Thermal Noise in Microwave Systems. Microwave Journal, March 1961.
- Smith, A. G.: Extraterrestrial Noise a Factor in Space Communications. Proceedings of the IRE. April 1960, pp. 593-599.
- Springett, J. C.: Command Techniques for the Remote Control of Interplanetary Spacecraft. JPL TR 32-314, August 1962.
- Springett, J. C.: Telemetry and Command Techniques for Planetary Spacecraft. JPL TR 32-495, January 15, 1965.
- Viterbi, A. J.: On Coded Phase-Coherent Communications. JPL TR 32-25. August 1960.
- Viterbi, A. J.: Phase-Locked Loop Dynamics in the Presence of Noise by Fokker-Planck Techniques. Proceedings of the IEEE, December 1963, pp. 1737-1753.
- Viterbi, A. J.: Phase-Lock-Loop Systems. Chapter 8, Space Communications. A. V. Balakrishnan, ed., New York, McGraw-Hill Book Company, Inc., 1965.
- Vogelman, Joseph H.: Propagation and Communications Problems in Space. Proceedings of the IRE, April 1960, pp. 567-569.
- Wilker, Leonard B.: Requirements for the Design of a Jupiter Precursory Spacecraft Data Transmission. Supplement to IEEE Transactions on Aerospace and Electronic Systems, vol. AES-2, no. 4, July 1966, pp. 442-448.

**CHAPTER V**  
**SPACECRAFT MECHANICAL DESIGN**



# CHAPTER V. SPACECRAFT MECHANICAL DESIGN

## DEFINITION OF SYMBOLS

$q$	Thermal Energy	Btu
$q_{sr}$	Radiation, solar reflected	Btu/hr
$q_p$	Solar radiation, direct from planet	Btu/hr
$q_{ob}$	Thermal energy released on-board as function of time	Btu/hr
$\sigma$	Stefan-Boltzmann Constant ( $0.1714 \times 10^{-8}$ )	Btu/hr-ft <sup>2</sup> -° R <sup>4</sup>
$\bar{h}_c$	Average coefficient of convection	Btu/hr-ft <sup>2</sup> -° R
$F$	Configuration factor	
$F_{c-s}$	Configuration factor, Craft-Sun	
$F_{c-p}$	Configuration factor, Craft-Planet	
$K$	Thermal conductivity	Btu/hr-° F ft <sup>2</sup> -° R
$\epsilon$	Emissivity	
$\epsilon_c$	Emissivity of craft	
$\tau$	Time, seconds and hours	
$T$	Temperature	°K, °R or °F
$\alpha$	Absorptivity	
$\alpha_s$	Absorptivity of surface for direct solar radiation	
$\alpha_{sr}$	Absorptivity of surface for reflected solar energy	

## DEFINITION OF SYMBOLS (CONTINUED)

$\alpha_p$	Absorptivity of surface for direct planet radiation	
$q_{ob}$	Heat energy generated on-board the craft as a function of time, $q(\tau)$	
$r$	Fraction of solar energy reflected	
$S$	Solar constant	Btu/ft <sup>2</sup> -hr

# CONCEPT DEVELOPMENT

## Introduction and Configuration Selection

The principal constraints to the mechanical and structural design of the JOVE spacecraft were the required interfacing with the Saturn V Launch Vehicle at the Instrument Unit, the envelope defined by the "standard" conical nose shroud and the desirability of designing a basic vehicle that could possibly with minor modification be suitable for the Voyager mission.

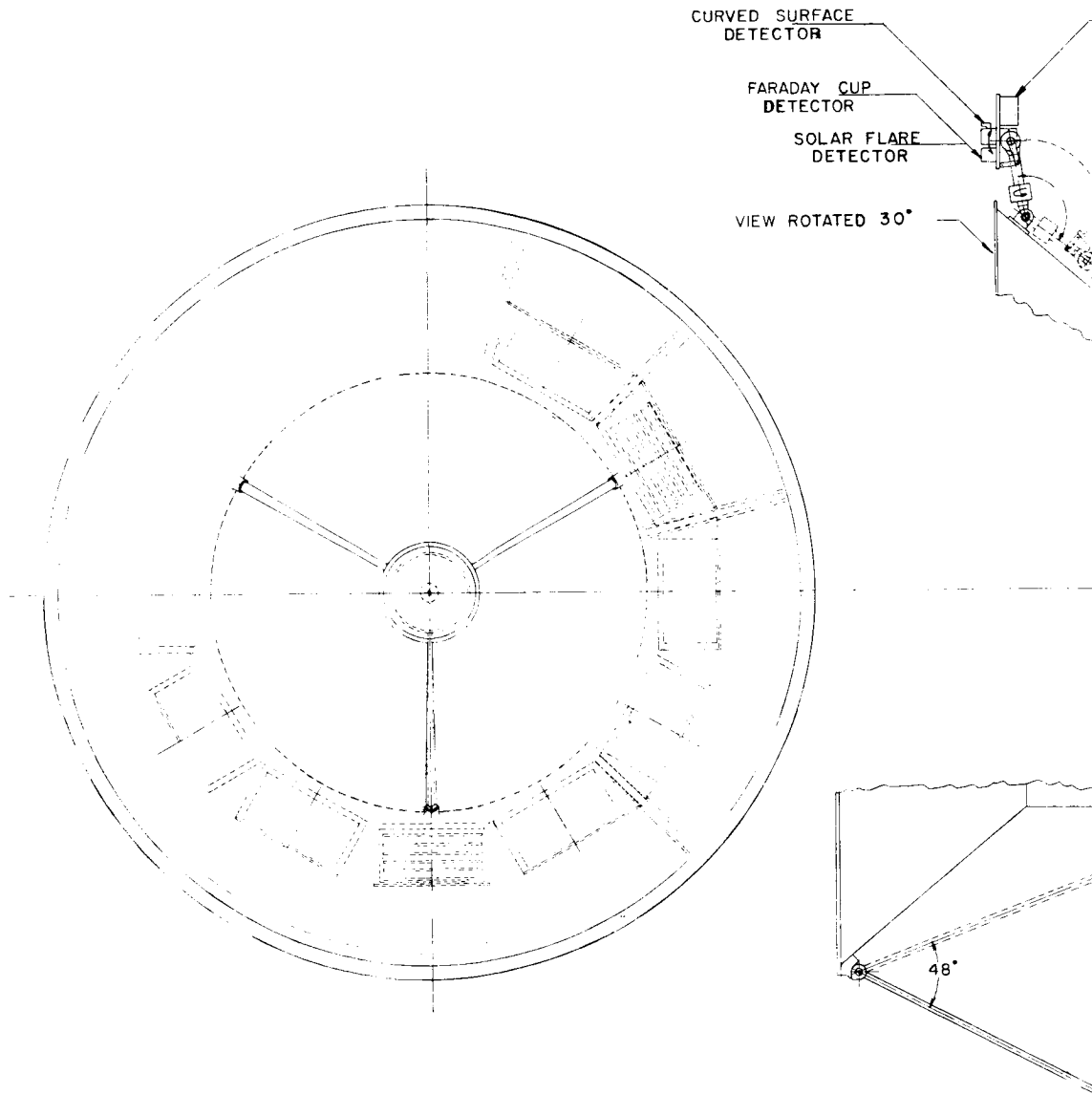
The spacecraft that evolved, Figure V-1, is suitable "with modifications" for the Voyager mission. (The first alternate configuration is shown in Figure V-2). There are many constraints on JOVE, however, that are not necessary nor required on Voyager, such as:

- a. The approximately 900-day mission life requiring new concepts of reliability or redundancy,
- b. Passage through the Asteroid Belt requiring additional micrometeoroid protection,
- c. Communication distances of approximately 500 000 000 statute miles requiring larger and heavier antennas.
- d. Complete dependence upon RTG's for power during the unusually long mission requiring that special consideration be given to radiation shielding and displacement of components.

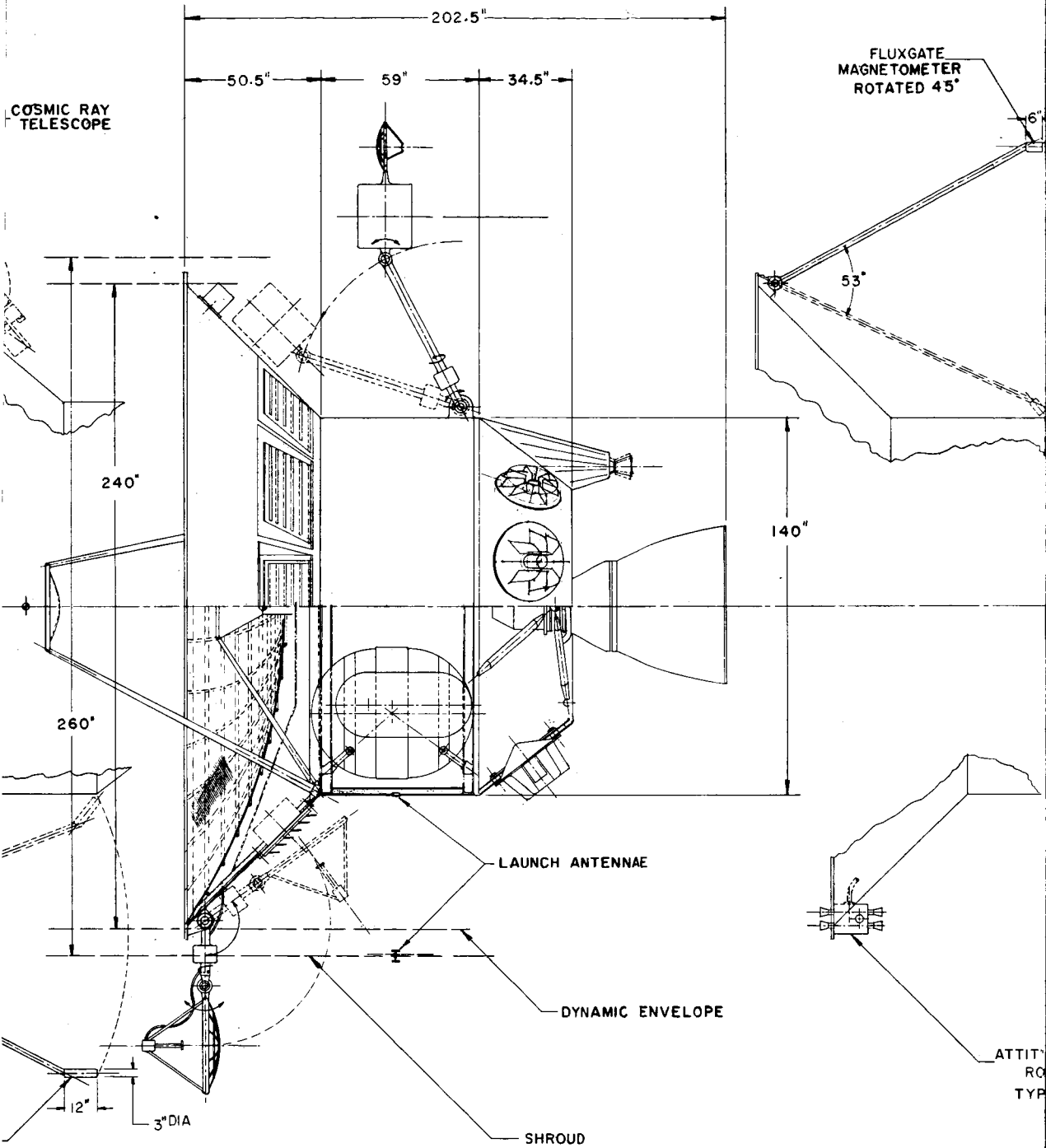
Configuration 4 of Figure V-3 illustrates the fit of the JOVE spacecraft within the "standard" conical nose shroud and the 55-inch long structural shroud. The result is a lower silhouette (only 36.7 feet above the Saturn V) than either the Apollo (82 feet) or the Voyager (73 feet).

Throughout the design studies simplicity of structure as a factor affecting reliability and lightweight was considered to be important parameter. Simplicity included keeping the number of extendable and/or articulated components to a minimum since the approximately 900-day total mission life will demand a high degree of reliability of all operating mechanisms.

The use of the LEM bus vehicle was discarded early in the study because it is designed to withstand the lunar landing loads and thus is designed to higher



RUBIDIUM VAPOR  
 MAGNETOMETER



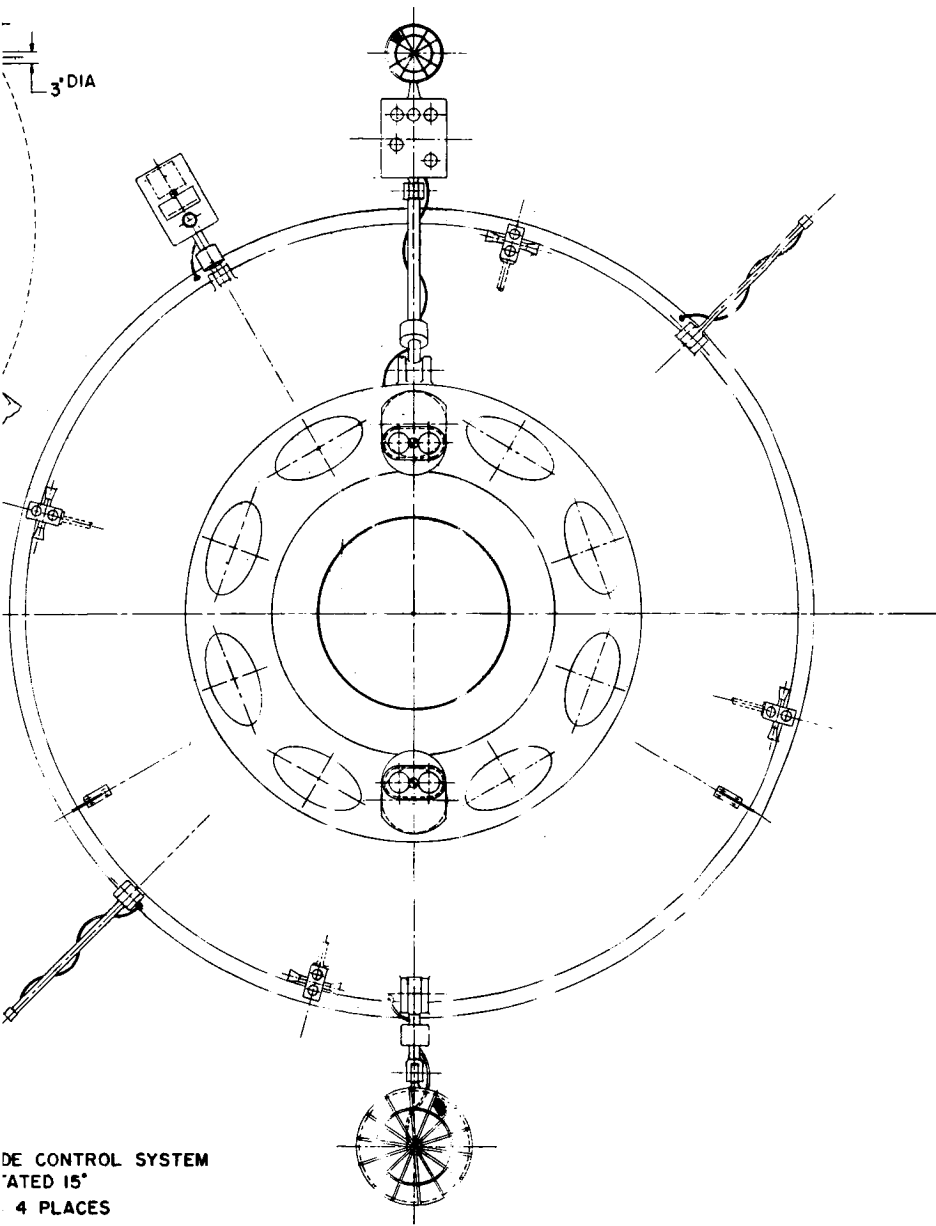
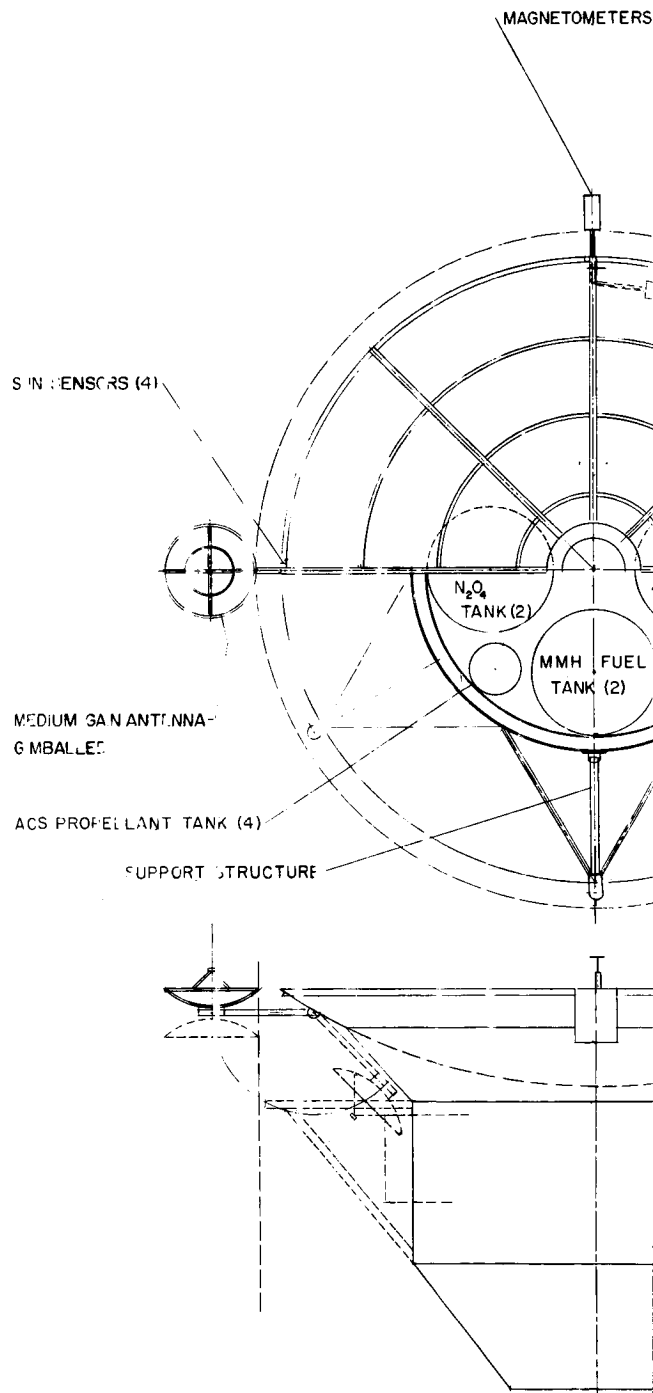
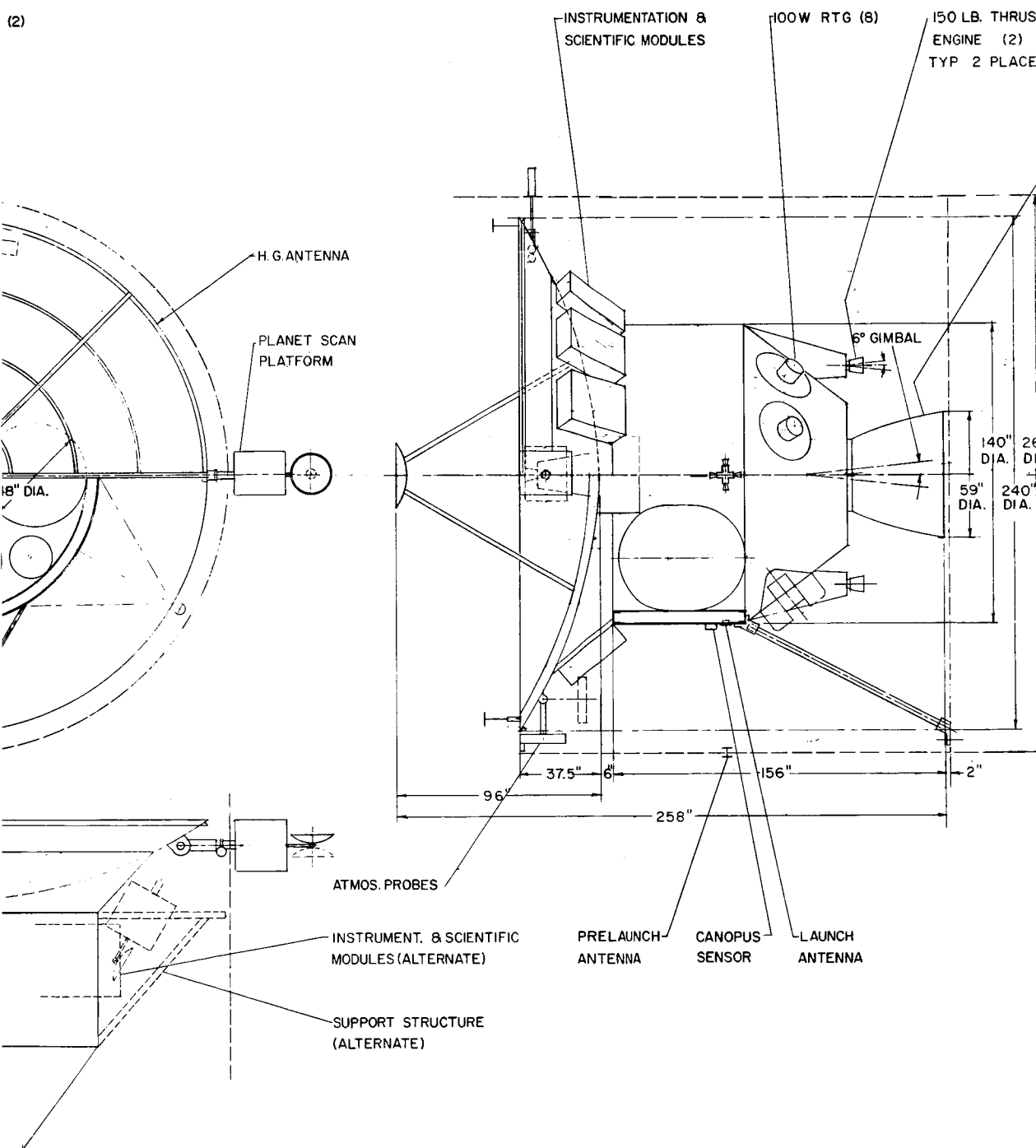


FIGURE V-1. JOVE SPACECRAFT LAYOUT





(2)



185

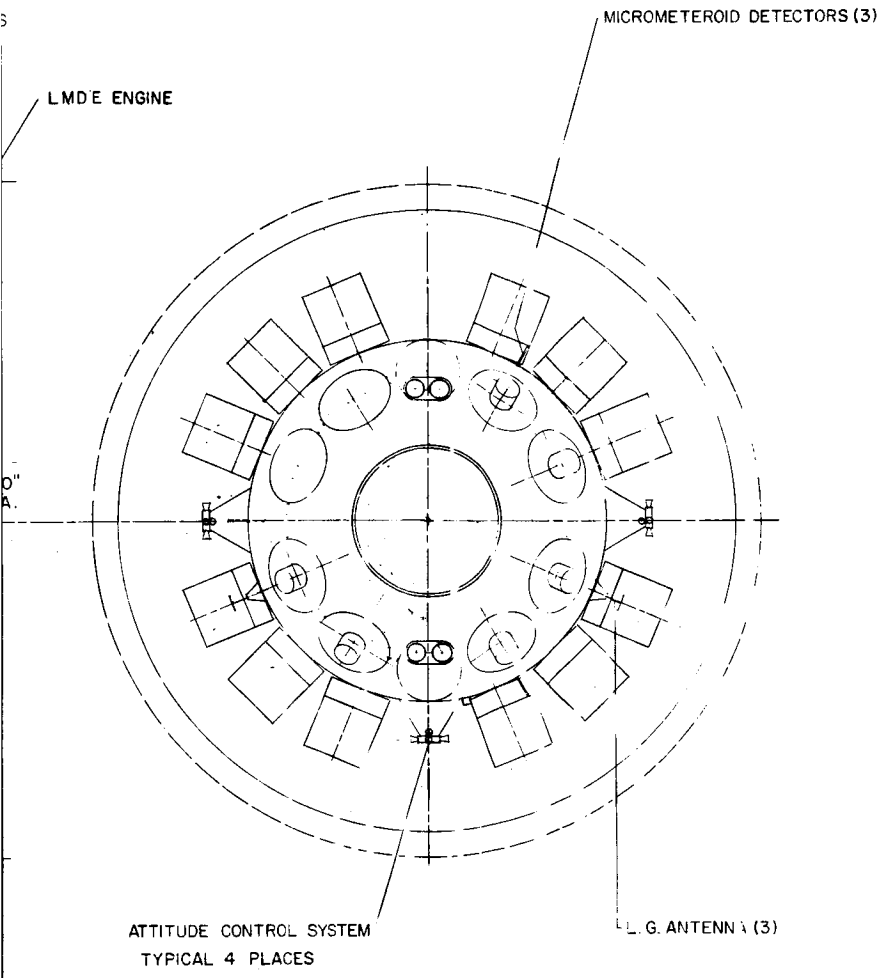
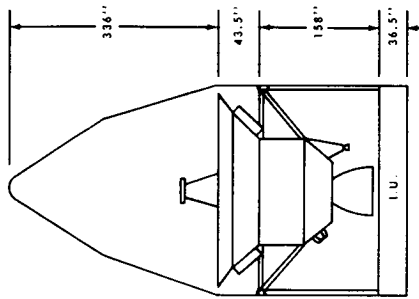
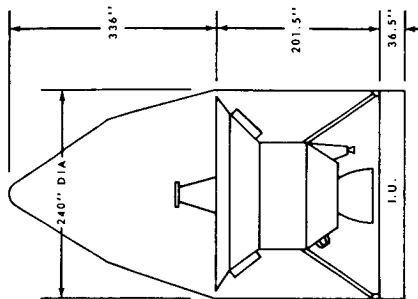


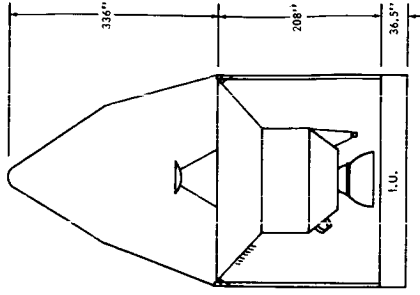
FIGURE V-2. FIRST ALTERNATE SPACECRAFT LAYOUT



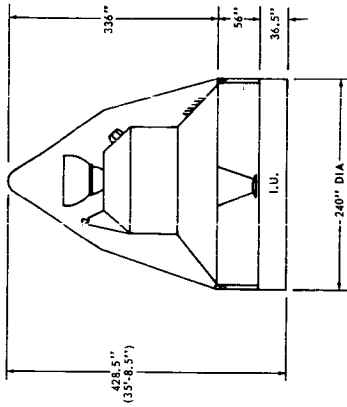
CONFIGURATION 1  
 ENGINE DOWN DURING LAUNCH  
 VOYAGER TYPE TRUSS  
 STRUCTURAL SHROUD - LONG  
 RTG'S ARE SHIELDED UNTIL SPACECRAFT HAS BEEN  
 INSERTED INTO HELIOCENTRIC TRAJECTORY



CONFIGURATION 2  
 ENGINE DOWN DURING LAUNCH  
 INVERTED TRUSS  
 NON-STRUCTURAL SHROUD  
 RTG'S PARTIALLY SHIELDED BY I.U.



CONFIGURATION 3  
 ENGINE DOWN DURING LAUNCH  
 STRUCTURAL ANTENNA  
 LONG STRUCTURAL SHROUD  
 RTG'S SHIELDED AS IN CONFIGURATION 1



CONFIGURATION 4 (LOVE)  
 ENGINE UP DURING LAUNCH  
 STRUCTURAL ANTENNA  
 SHORT STRUCTURAL SHROUD  
 RTG'S UNSHIELDED

FIGURE V-3. PRELIMINARY CONFIGURATION STUDIES

load factors that are necessary for a Jupiter orbiter mission. A thin sheet shell structure has been selected rather than the tubular type structure that is used in the LEM lander and several of the Voyager configurations. The structure itself is adaptable to the proposed Voyager configurations with minor modifications. Figure V-2 and Configuration 1 of Figure V-3 illustrate an alternate design concept that uses a truss mounting to the same attachment points and lower shroud support proposed for Voyager. This commonality would result in a net weight penalty since the structural shroud is 102 inches longer on Configuration 1 than on Configuration 4.

The spacecraft is designed to accommodate payloads and fuel loads corresponding to a launch year with average capabilities during the period 1975-1980. Off loading of payload or longer trip time would result during the worse year of 1978 and slightly additional payload, shorter trip times, or more optimum orbits are then possible in the most favorable year of 1975 for example.

## Layout Development and Interfacing

Two basic configurations were studied: One with the retro-engine (LEMDE) exhaust pointing upward at launch and the other with the engine pointing downward. These configurations are shown in Figures V-1, V-2 and V-3. Basically, the two concepts differ only in the design of the fixed 20-foot, high-gain antenna support and the booster interfacing structure. Other minor differences exist in packaging and location of experiments and subsystems.

The configuration with obvious advantages is the upward pointing engine primarily because of convenience and possible weight savings realized through the use of an integrated spacecraft-booster interfacing and antenna support structure, and the lower silhouette mentioned above. Upon selection of the preferred configuration (Fig. V-1), development of details of the less desirable configuration was stopped. The preliminary design calls for jettisoning of the nose cone as soon as possible during S-II burn.

Several factors were important to the packaging and layout of the spacecraft. Optimum location of scientific experiments took precedence over all other considerations, and their protection against hostile environments including thermal and nuclear radiation entered into the optimization.

Electronic components and radiation sensitive experiments were located as far as practicable from the RTG power units. Moreover, whenever possible

propellant tanks and other insensitive massive elements were positioned between the RTG units and radiative sensitive elements.

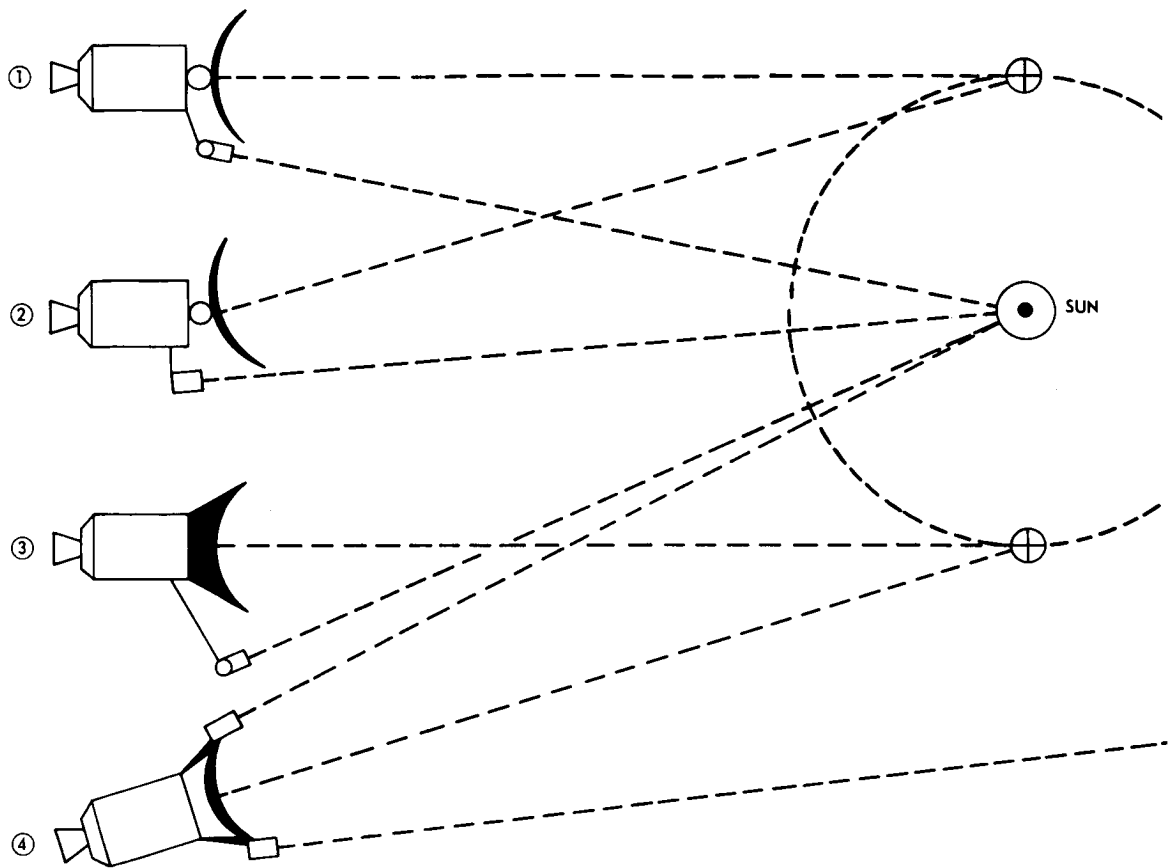
In the interest of heat energy management, the RTG's were strategically located in fixed positions rather than being deployed on booms. Preliminary investigations indicated that there may be periods in the mission during which heat from the RTG's will be required to maintain desired temperature levels in the basic spacecraft. At other times heat rejection over and above the RTG waste will be required. A passive thermal control system was adopted. Detailed energy balances, however, may prove the necessity for cold plates in electronic compartments with the accompanying pumps and plumbing. Super insulation is provided over most of the spacecraft with louvers being located in critical areas for heat rejection.

Figure V-1 points up some of the more significant aspects of the spacecraft. Two of the more prominent members associated with the telecommunications and control systems are the 20-foot diameter, fixed, high-gain antenna, and the 3.0 foot diameter, gimballed, medium-gain antenna.

The designers adopted the philosophy that whenever feasible hardware from other space systems would be incorporated into the Jupiter mission vehicle to improve its reliability without going into long time development programs. Consequently, they have drawn freely from the Apollo system and subsystems concepts as well as from earlier generation systems that have successfully flown.

The fixed antenna and articulated "fine" sun sensors represent a departure from present practice where the sun sensors are attached rigidly to the main body of the spacecraft and antenna is articulated. Four methods were examined and are illustrated in Figure V-4. Method 3 was selected as optimum and is the one detailed in Figure V-1. Two sun sensors are provided for redundancy.

A weight summary for the recommended design is included in Table V-I. The resulting total injected weight works out to 19 846 pounds. The following pages contain outlines of the reasoning behind the locations selected for the instruments and experiments packages and discussions in some detail of the structural details and analysis. There are reviews of the materials and propellants used and indications of the affects of the environment on them. Finally, there is a presentation of the thermal control problem and an analysis of some of the more important considerations.



METHOD 1 - ARTICULATED ANTENNA AND ARTICULATED SUN SENSORS.  
 METHOD 2 - ARTICULATED ANTENNA AND FIXED SUN SENSOR.  
 METHOD 3 - FIXED ANTENNA AND ARTICULATED SUN SENSOR. (JOVE)  
 METHOD 4 - FIXED ANTENNA AND "MANY" FIXED SENSORS SET AT VARIOUS  
 ANGLES TO ACCOMMODATE ANGLE BETWEEN ANTENNA AND SUN  
 SENSOR LINE.

FIGURE V-4. ANTENNA AND SUN SENSOR COUPLING

TABLE V-1. DETAILED WEIGHT STATEMENT - PLANETARY VEHICLE,  
 PLANETARY VEHICLE PROPULSION, PLANETARY VEHICLE ADAPTER  
 (WEIGHT IN POUNDS)

PLANETARY VEHICLE

Structural and Mechanical		1383
Basic Structure	855	
Fittings	57	
Equipment Modules	100	
Mounting Panels for Equipment Modules	20	
Micrometeoroid Protection	345	
Miscellaneous Attachments	6	
Pyrotechnics		24
Explosives, Mechanisms, and Controls	24	
Temperature Control		260
Heaters	5	
Thermostats	5	
Insulation and Coatings	125	
Louvers	25	
Cold Plates	80	
Miscellaneous Attachments	20	
Radio		
S-Band Transponders	40	
Power Amplifiers	17	
High Gain Antenna	150	
Medium Gain Antenna	40	
Low Gain Antenna	20	
Antenna Switches	1	
Diplexer	2	
Hybrid RF Coupler	1	
Directional Coupler	1	
Data Storage		52
Playback Sequencer Controls	1	
Central Logic Module	2	
Redundant Power Supply	4	
Tape Transport Modules	45	



TABLE V-1. DETAILED WEIGHT STATEMENT - PLANETARY VEHICLE,  
 PLANETARY VEHICLE PROPULSION, PLANETARY VEHICLE ADAPTER  
 (WEIGHT IN POUNDS) (CONTINUED)

Telemetry		16
Encoders, Control Electronics and Power Supply	16	
Command		15
Command Detector	5	
Command Decoder	6	
Transformer Rectifier	4	
Computing and Sequencing		35
Digital Computer	35	
Cabling		200
Electrical Wiring and Harnesses	200	
Power		645
Radioisotope Thermoelectric Generators	580	
Power Conditioning Equipment	65	
Guidance and Control		430
Attitude Control	(31)	
Star sensors	12	
Sun sensors	4	
Earth detector and other sensors	3	
Gimbals	12	
Autopilot	(59)	
Gyro-package	40	
Electronic signal processors	6	
Electrical wiring, frame, and hardware	13	
Cold Gas Jets	(340)	
Tanks	205	
Propellant	105	
Hardware	30	

TABLE V-1. DETAILED WEIGHT STATEMENT - PLANETARY VEHICLE,  
 PLANETARY VEHICLE PROPULSION, PLANETARY VEHICLE ADAPTER  
 (WEIGHT IN POUNDS) (CONTINUED)

Science Instruments		150
Visible and Ultraviolet Photometer	6	
Infrared Radiometer	5	
Television Systems	30	
Infrared Spectrometer	16	
Visible and Ultraviolet Spectrometer	20	
Micrometeoroid Detector	8	
Rubidium Magnetometer	2	
Trapped Radiation Detector	9	
Curved Surface Plasma Analyzer	5	
Faraday Cup Plasma Analyser	3	
Microwave Radiometer	22	
Cosmic Ray Telescope	3	
Cosmic Ray Detector	11	
Solar Flare Detector	10	
 PLANETARY VEHICLE PROPULSION		 15 194
Dryweights	(2086)	
Tanks	1190	
Lunar Excursion Module Descent Engine	406	
Trajectory Correction/Orbit Trim Propulsion Subsystem	43	
Tank and Engine Supports	197	
Valves, Lines and Other Fittings	250	
Inert Fluids	(508)	
Trapped Fluids	474	
Helium	34	
Consummable Propellants	(12 600)	
Hydrazine	3270	
Unsymmetrical Dimethyl Hydrazine	1870	
Nitrogen Tetroxide	7460	

TABLE V-1. DETAILED WEIGHT STATEMENT - PLANETARY VEHICLE,  
PLANETARY VEHICLE PROPULSION, PLANETARY VEHICLE ADAPTER  
(WEIGHT IN POUNDS) (CONTINUED)

PLANETARY VEHICLE ADAPTER

Structure, Hardware and Cabling 520

TOTAL PLANETARY VEHICLE WEIGHT 19 846

## Booster Interfacing

The spacecraft is attached to the instrument unit atop the Saturn V boost vehicle by means of a structural shroud or adapter. This shroud is 56 inches long, supports the nose cone as well as the spacecraft, and is jettisoned with the I. U. and the S-IVB stage after the spacecraft has been inserted into heliocentric transfer trajectory. The choice of twelve attachment or hard points was based on the number of equipment boxes. Eight attachment points were favored until it became apparent that ten equipment boxes were required, whereupon a 12-point attach system was adopted, leaving 2 equipment bays empty, but equipped with thermal louvers.

The spacecraft is designed to launch engine foremost through a conical boost support structure that performs the triple tasks of main boost support, antenna support, and equipment box support.

Four launch configurations were considered (Fig. V-3). The chosen configuration, number 4, has the following salient advantages:

a. The RTG radiators face dark space within 4 minutes after initial boost since the conical nose shroud serves only as an aerodynamic shield. Configurations 1 and 3 of Figure V-3 present severe thermal control problems during Earth parking orbit since the shroud is structural and must remain in place until after third stage firing has placed the spacecraft in its heliocentric trajectory.

b. The conical boost support structure is multipurpose as noted above and, being internal, does not interfere with the field of view of any instruments.

c. The length of structural shroud is only 56 inches.

d. The spacecraft projects into the conical nose shroud, thus reducing the overall height and weight.

Since the configuration selected requires a structural support shroud, it may not be the lightest of the four studied. However, 88 percent of the weight of the spacecraft is dictated by the micrometeoroid protection requirements. Thus, the difference in structural weights between all configurations (Fig. V-3) is negligible.

## SYSTEMS DEFINITION AND WEIGHTS

A brief definitive description of the JOVE planetary vehicle subsystems will be given in this section. Figure V-1 illustrates the basic geometry of the JOVE planetary vehicle. Inside the structure and around the outside of the planetary vehicle is housed all instrumentation which will gather from interplanetary space during the heliocentric phase, and from the planetary environment of Jupiter after arrival, the engineering and scientific data for transmission back to Earth.

A clean demarcation of the weights between the various subsystems cannot be made because of the overlapping functions sometimes performed. Table V-1 is a detailed weight statement which gives an estimated weight breakdown of the subsystems into component parts wherever applicable. Table V-2 is a simplified weight summary. The total estimated weight of the planetary vehicle, including the planetary vehicle adapter, is 19 846 pounds. Table V-3 is a summary of the actual weights for the Mariner planetary vehicles launched to date and estimated weights of other unmanned planetary missions under consideration.

The major planetary vehicle subsystems are described by listing the components contained within it and, in some instances, by additional functional information:

1. Structural and Mechanical - consists of the basic structure; fittings such as latches, hinges and miscellaneous supports; equipment modules; mounting panels for equipment modules; micrometeoroid protection and miscellaneous attachments. Total weight 1383 pounds.
2. Pyrotechnics - consists of the explosives, mechanisms, and controls used to initiate the release and deployment of nonrecurring incidents. The function of releasing the planetary vehicle from the launch vehicle is performed by this subsystem. Midcourse correction control and orbit insertion firing of the propulsion system is a part of this subsystem's function. Total weight 24 pounds.

TABLE V-2. WEIGHT SUMMARY FOR THE JOVE VEHICLE

PLANETARY VEHICLE

Structural and Mechanical	1383
Pyrotechnics	24
Temperature Control	260
Radio	272
Data Storage	52
Telemetry	16
Command	15
Computing and Sequencing	35
Cabling	200
Power	645
Guidance and Control	430
Science Instruments	150
Contingency	650
PLANETARY VEHICLE PROPULSION	15 194
PLANETARY VEHICLE ADAPTER	520
TOTAL PLANETARY VEHICLE WEIGHT - pounds	19 846

3. Temperature Control - consists of the heaters, thermostats, insulation and coatings, louvers, cold plates, and miscellaneous attachments to the planetary vehicle and/or to instruments aboard the planetary vehicle. Total weight 260 pounds.

4. Radio - consists of the S-band transponders and the power amplifiers. Includes the high-gain, medium-gain, and low-gain antennas with switches and any structural support arms they may have. Also, the diplex, the hybrid RF coupler package, and the directional coupler package. Total weight 272 pounds.

5. Data Storage - consists of the playback sequencer controls; control logic module which controls record and playback; redundant power supply; and the tape transport modules. Total weight 52 pounds.

TABLE V-3. SUMMARY OF WEIGHTS FOR MARINER, VOYAGER AND JOVE

	M A R I N E R					V O Y A G E R					J O V E	
	VENUS 62 *	MARS 64 *	VENUS 67 *	MARS 69	JPL 71	JPL 73	BOEING	GENERAL ELECTRIC	TRW SYSTEMS	MSFC	AUB. DESIGN STUDY	
PLANETARY VEHICLE												
Structural and Mechanical	82.3	78.4	69.3	82.1	745	365	408.5	457.0	777	1390	1383	
Pyrotechnics	4.3	12.2	8.5	12.1	36	32	34.9	11.9	51	50	24	
Temperature Control	10.1	15.5	17.3	22.3	75	150	80.1	144.8	111	150	260	
Radio	39.0	41.8	47.5	46.7	124	146	162.5	188.3	151	172	272	
Data Storage	13.6	16.9	18.9	38.0	100	120	107.7	115.6	72	185	52	
Telemetry	8.8	22.4	23.4	21.9	173	54	57.3	16.6	8	125	16	
Command	11.2	10.1	10.4	10.0	19	19	31.4	29.9	11	28	15	
Computing and Sequencing	11.4	11.4	13.1	18.0	37	22	45.0	35.0	36	70	35	
Cabling	37.8	45.7	44.0	55.8	181	225	184.0	117.4	229	200	200	
Power	105.3	150.0	130.8	150.5	648	544	541.6	473.2	522	875	645	
Guidance and Control	53.3	63.3	57.4	57.3	682	222	266.4	313.5	268	375	430	
Approach Guidance			6.0	6.0								
Science Data	9.1	11.8	14.6	16.5	100	35	400.0	400.0	400	500	150	
Science Instruments	40.4	47.2	34.8	117.6	300	215						
Devices for Measurements	4.7			42.4								
Contingency				44.2								
PLANETARY VEHICLE				45.2	15 000	13 000	15 000.0	15 000.0	14 714	13 914	15 194	
PROPULSION	33.9	47.6	47.2									
FLIGHT CAPSULE AND ADAPTER					2730	4000	2000.0	3000.0	3000	5000		
PLANETARY VEHICLE ADAPTER	49.0	58.0	60.0	61.7	1500	1500	850.0	1500.0	1500		520	
TOTAL PLANETARY VEHICLE WEIGHT-POUNDS	502.8	632.3	597.2	853.3	22 450	21 000	20 350.0	22 000.0	22 000	23 094	19 846	

\* Actual Weights

6. Telemetry - consists of real-time data encoder, stored data encoder, control electronics, and power supplies. Total weight 16 pounds.

7. Command - consists of command detector, command decoder, and transformer-rectifier. Total weight 15 pounds.

8. Computing and Sequencing - consists of a cycled digital computer which includes timer, data register, switching network, logic network, and maneuver matrix. Total weight 35 pounds.

9. Cabling - consists of the necessary electrical wiring and/or harnesses for electrically interconnecting the planetary vehicle subassemblies. Total weight 200 pounds.

10. Power - consists of the Radioisotope Thermoelectric Generating (RTG) units and the necessary power conditioning equipment. Also, contains the controls for activation and/or deactivation of the numerous loads. Total weight 645 pounds.

11. Guidance and Control - consists of the attitude control assembly with the Earth detector, star sensors, and gimballed sun sensors. Consists of the autopilot assembly with gyroscopes, accelerometer, electronic signal processors, electrical wiring, frame and miscellaneous hardware. Consists of the cold gas jet assembly with tanks, propellant, and miscellaneous hardware. Total weight 430 pounds.

12. Science Instruments - consists of visible and ultraviolet photometer, infrared radiometer, television systems, infrared spectrometer, visible and ultraviolet spectrometer, micrometeoroid detector, rubidium magnetometer, trapped radiation detector, curved surface plasma analyzer, microwave radiometer, cosmic ray telescope, cosmic ray detector, and solar flare detector. Total weight 150 pounds.

13. Contingency - consists of subsystem weights not allocated elsewhere. Total weight 650 pounds.

The planetary vehicle propulsion subsystems are defined as follows:

1. Dryweights - consists of the propellant tanks, Lunar Excursion Module Descent Engines (LEMDE), Trajectory Correction/Orbit Trim Propulsion Subsystem (TC/OT), tank and engine supports, valves, lines, and miscellaneous fittings. Total weight 2086 pounds.

2. Inert Fluids - consists of the trapped fluids and helium. Total weight 508 pounds.

3. Consummable Propellants - consists of hydrazine and unsymmetrical dimethyl hydrazine (UDMH) and nitrogen tetroxide. Total weight 12 600 pounds.

The planetary vehicle adapter consists of the structure between the planetary vehicle and the launch vehicle interface. Inside the planetary vehicle adapter is located the associated hardware and cabling necessary for the inflight separation of the planetary vehicle and the launch vehicle. Total weight 520 pounds.

## SPECIAL DESIGN CONSIDERATIONS

### Location of Experiments

The scientific instruments can be divided into two groups according to their operating regime and are so listed below:

Group One - used for measurements during the interplanetary flight phase as well as the orbital phase:

- a. Rubidium Magnetometer
- b. Fluxgate Magnetometer
- c. Trapped Radiation Detector
- d. Curved Surface Plasma Analyzer
- e. Faraday Cup Plasma Analyzer
- f. Cosmic Ray Telescope
- g. Cosmic Ray Charge and Mass Detector
- h. Solar Flare Detector
- i. Micrometeoroid Detector

Group Two - used for measurements only during the orbital phase about Jupiter:

- a. Visible and Ultra Violet Photometer
- b. Infrared Radiometer



- c. Microwave Radiometer
- d. Television No. 1
- e. Television No. 2
- f. Infrared Spectrometer
- g. Visible and Ultra Violet Spectrometer

In the design of the space vehicle, it was necessary to consider the proper locations for all of these instruments. Additionally, certain of the instruments must be articulated. Each instrument is discussed individually below, listing the specific requirements which must be satisfied in the design.

Rubidium Magnetometer. The important portion of this magnetometer is the sensor, a device 3 inches in diameter and 12 inches long. It should operate in a low magnetic field as far from the body of the spacecraft as practicable and is therefore mounted at the end of a 9-foot boom. Before deployment, the boom and magnetometer are folded close to the body of the spacecraft and may be extended as desired to the limit of the boom or approximately 18 feet from the center line of the spacecraft. Location around the periphery of the spacecraft is immaterial.

Fluxgate Magnetometer. The sensor of this instrument is a cylinder 3 inches in diameter and 6 inches long. It is located in exactly the same fashion as the Rubidium Magnetometer but on the opposite side of the spaceship, for purpose of symmetry. When completely deployed, the long axis of the sensor should be parallel to the spacecraft axis. This requirement follows from the nature of the magnetometer.

Trapped Radiation Detector. No particular location requirements are indicated for this instrument beyond the fact that its sensors should have a clear and unobstructed view of space. There are two such instruments located at convenient and symmetrical positions on the body of the spacecraft.

Curved Surface Plasma Analyzer. This instrument must have a clear and unobstructed view of the sun at all times. Since the 20-foot antenna is, in general, oriented towards Earth, the analyzer is mounted on a Solar Scan Platform which swings outward from the antenna rim and is oriented in a direction parallel to the antenna axis. The Solar Scan Platform is also articulated to insure that the analyzer sensor **sees the sun at all times**. Radial location of the analyzer is immaterial and consequently only a matter of convenience.

Faraday Cup Plasma Analyzer. Statements made for the Curved Surface Plasma Analyzer are equally valid for the Faraday Cup Analyzer. For convenience and compactness, it is also mounted on the Solar Scan Platform.

Cosmic Ray Telescope. The most important requirement for this instrument is that it must, at all times, point away from the sun. Since the two instruments described in the preceding two sections must, at all times, be oriented toward the sun, the Cosmic Ray Telescope is logically mounted on the same Solar Scan Platform as the other two instruments but oriented in the opposite direction, thus insuring that it never sees the sun.

Cosmic Ray Charge and Mass Detector. This sensor must also, at all times, be oriented away from the sun. Consequently this instrument is also mounted on the articulated Solar Scan Platform and it looks in the same direction as the Cosmic Ray Telescope - away from the sun.

Solar Flare Detector. It is not essential that this sensor be mounted on the deployable and articulated Solar Scan Platform. It has been placed there, however, adjacent to the Faraday Cup Analyzer and, like the Analyzer, is always oriented toward the sun.

Micrometeoroid Detector. This instrument consists essentially of a very thin aluminum plate, about 8 inches by 8 inches, mounted in a base containing instrumentation which must be shielded from the sun. Furthermore, a view through 360 degrees in planes perpendicular to the spacecraft axis should be possible. On the basis of these requirements, three such plate detectors are attached to the conical surface of the spacecraft and directly behind the 20-foot antenna which then serves as an umbrella against the sun. Spacing of the detectors is at 120-degree intervals.

The seven instruments in the Orbital Measurement Group are mounted on a deployable and articulated platform controlled and oriented in such a way as to cause the instruments to always scan the planet Jupiter. This platform is referred to as the Planet Scan Platform. It is essential that no sunlight, direct or reflected, enter the sensors.

## Navigation, Guidance, and Control Sensors

The instruments involved in these categories are discussed below:

Coarse Sun Sensor. During sun acquisition, the coarse sun sensors must have a 360-degree field of view in order to acquire the sun, regardless of the initial orientation of the spacecraft. Consequently they are mounted on the rim of the 20-foot antenna in such a fashion as to look either forward or backward. Four such sensors have been recommended: two looking forward and two looking backward. Each of the two pairs is symmetrically placed for balance.

Fine Sun Sensor. As the name implies, this sensor must be arranged to sight accurately on the sun. Its view must be completely unobstructed and it must be articulated in order to maintain a sun fix. The mechanism required for this single instrument platform is lightweight and relatively small and is located on a fixed boom which extends through the mesh of the 20-foot antenna. The articulated platform carrying the sensor is located at the outer end of the boom.

Canopus Sensor. In JOVE the sun and the star Canopus which has a declination of approximately minus 76° from the plane of the ecliptic provides a satisfactory reference set for attitude determination. The Canopus Sensor is therefore located on the side of the spacecraft looking outwards at right angles to the spacecraft longitudinal axis. Since the fine sun sensor is articulated, it will then be possible to maintain accurate attitude control of the vehicle using the sun and Canopus as references.

Earth Sensor. This sensor is used primarily during the early part of the mission in order to verify Canopus acquisition. It is, of course, logical that it should always look toward Earth and consequently it is located on the rim of the 20-foot antenna.

Gyro Package. This instrument, a completely gimballed device, is to be found in the central portion of the body of the vehicle, protected as completely as possible by fuel tanks and other structural elements. Available drawings of the spacecraft are not sufficiently detailed to show this package.

Launch and Omni-Directional Antennae. The titles of these antennae are somewhat self-explanatory. The launch antennae must provide for communication with the spacecraft while the vehicle is still enclosed within the shroud. Thus, a dual system is used - one component being located in the surface of the body of the vehicle and the mating component extending through the shroud. These mating components are located opposite one another. Omni-directional antennae are located in various convenient positions on the spacecraft so that communication with the craft will be possible regardless of the orientation of the vehicle.

## Articulated Members

The components of the space vehicle which are to be articulated are:

- a. LMDE
- b. Two 150-pound Thrust Mid-course Maneuver Jets

- c. 36-inch Antenna
- d. Planetary Scanning Instrument Package
- e. Solar Scan Platform
- f. Fine Sun Sensor
- g. Two Magnetometer Booms

The LMDE and the Mid-Course Maneuver Jets are gimbaled, i.e., each may be moved through a total angle of 6 degrees in any desired direction in order to achieve required corrections.

The 36-inch antenna, the Planetary Scanning Instrument Package, the Solar Scan Platform and the Magnetometer booms are all folded adjacent to the body of the spacecraft until after it has been detached from the third stage of the Saturn V rocket. Once the spacecraft is free of the boosters these units can be deployed to their operating positions.

The 36-inch antenna must be able to look in any direction. Consequently, once deployed, its boom may rotate through  $360^\circ$ ; also, the antenna itself can rotate through  $360^\circ$  relative to and in a plane at right angles to the boom. A portion of the required motion could be accomplished by the deployment action alone but the motion achieved here is inadequate. Deployment is accomplished by spring action which is automatically initiated, the boom being permanently locked in its deployed position. Rotations of the antenna boom and of the antenna head relative to the boom are provided by means of individual servomotors which are powered from the RTG units. The individual activation of the two main portions of the antenna insure that definite and precise control can be attained.

The general arrangement of both the Planetary Scanning Instrument Package and the Solar Scan Platform is similar to that described for the 36-inch antenna in that a  $360^\circ$  rotatable instrument platform is involved and, as before, these motions are produced by action of individually controlled servomotors. Because of the sensitivity of these instruments and to their somewhat greater weight, the platforms are deployed by means of hydraulic (or pneumatic) actuators. Once fully deployed, the booms are locked in place and their capability to be rotated provides the proper orientation.

The boom carrying the Fine Sun Sensor is fixed. The mechanism at the end of the boom provides for full articulation of the sensor itself.

The Magnetometer Booms require initial deployment only and this is accomplished by spring action after which the booms are permanently locked in place.

## Nose Cone and Shroud Details

The configuration of the spacecraft and its orientation with the LEM forward during launch resulted in a substantial saving in shroud weight. It was also possible to house the entire vehicle within the standard nose cone. Thus, to clear the way for the separation of the vehicle from the adapter above the third stage of the rocket, only the nose cone need be jettisoned. The nose cone is 21 feet 8 inches in diameter and 28 feet in length. It was deemed preferable to split the nose cone into three sections, at 120°, rather than into two halves. Standard locking and jettisoning hardware can be used but modifications in the support structure of the jettisoning elements will be required because of the decision to use a three rather than a two-section nose cone.

Locking hardware consists essentially of a bolt connecting two flanges, facing each other and attached, respectively, to the edges of adjacent sections of the nose cone. Explosive-type bolts are used and immediately before jettison a time charge is detonated fracturing the bolts. A series of such connections are located along the lengths of the three 120° splits in the nose cone.

Jettisoning of the three sections of the nose cone will be initiated by the action of spring-loaded catapults. These devices are located in the forward portion of the nose cone and are cocked against the petal segments. Within a few seconds after the locking devices have been released, explosive charges in the cocking mechanism of the catapults are detonated and the three sections of the nose cone are forcibly separated from one another and swing outward into space, each petal segment rotating about a pivot near its base. The design of the pivots is such that, after the nose cone sections have rotated through a specified angle relative to the axis of the vehicle, they automatically disengage from the pivots and spiral away from the spacecraft.

## STRUCTURAL DESIGN

### Primary Structure

The structure is designed for limit boost loads of six Earth gravities along the longitudinal axis of the boost vehicle, one gravity laterally, and an arbitrary torque around the longitudinal axis of the boost vehicle of 12 000 000 in.-lb. Complete analysis would consider maneuver and ground loads plus vibration analyses, but time did not permit this. A factor of safety on ultimate strength of 1.25 was applied.

Boost loads are carried from the boost vehicle to the bus by twelve 3 in. by 2-1/2 in. I-sections (Fig. V-5) of 7075-T6 aluminum. These sections have strong axis moments of inertia of 1.99 in.<sup>4</sup> and areas of 1.75 sq. in. The design torque of 12 000 000 in.-lb is

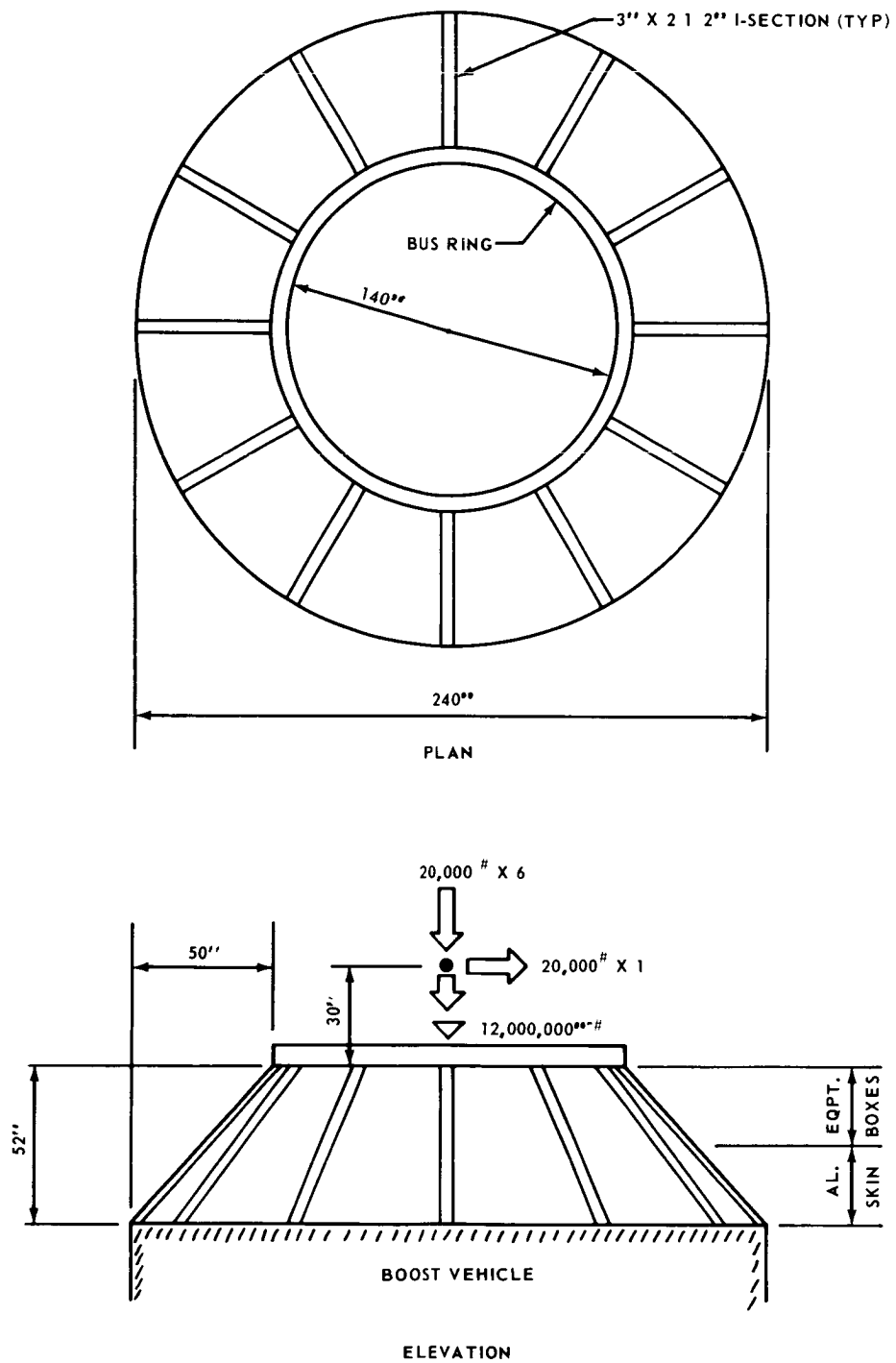


FIGURE V-5. BOOST SUPPORT STRUCTURE

carried by a 0.03 in. aluminum skin around the twelve I-sections. In the area of equipment boxes, the torque is carried by them, as they are intended to fit continuously and attach directly to the I-sections.

The spacecraft bus (Fig. V-6) is a cylindrical sandwich shell of 0.06 in. aluminum faces separated by 2 in. of lightweight foam. The shell design is controlled by micro-meteoroid protection requirements rather than strength requirements. Even so, it is expected that in the asteroid belt, two micrometeoroids will penetrate the shell (but not the equipment inside).

At either end of the cylindrical bus is a bus ring. These rings are 3 in. by 2 1/2 in. I-sections of 7075-T6 aluminum, having strong axis moments of inertia of 2.07 in.<sup>4</sup> and areas of 2.00 sq. in. They weigh 86.5 lb each. The engine end ring is taken as the same section as the antenna end ring, but could be a lighter section. Tanks and engines are supported directly by the rings. The antenna end ring carries loads from the twelve boost support members and half the tankage. The engine end ring supports the remaining half of the tankage and the engines.

Another sandwich shell, attached to the engine and end bus ring, carries the RTG's and acts as a micrometeoroid barrier. This shell has 0.03 inch faces separated by one inch of lightweight foam.

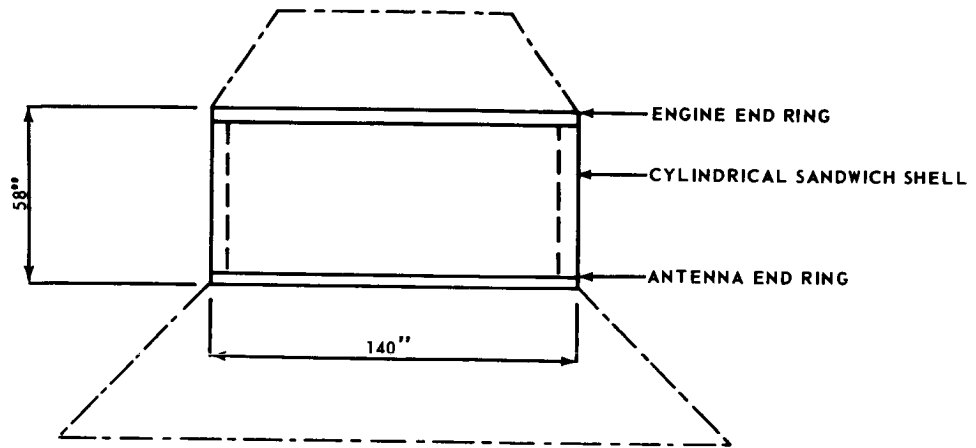
Calculations showing loads, moments of inertia, weights, etc., for all major pieces of structure are in Appendix F, Volume II.

## Tanks

All tanks are designed for 6Al-4V titanium. Table V-4 summarizes the tank design. Detail calculations which verify the data shown in Table V-4 are also shown in Appendix F, Volume II. The calculations show relations involving tank pressures, volumes, thicknesses, weights, etc.

TABLE V-4. FUEL TANK DATA

FLUID	Number of Tanks	Wall Thickness (in.)	Diameter (in.)	Length (in.)	Capacity (ft) <sup>3</sup>
50/50 UDMH/N <sub>2</sub> H <sub>4</sub>	2	0.1	48	54	39.6
N <sub>2</sub> O <sub>4</sub>	2	0.1	48	60	45.9
N <sub>2</sub> H <sub>4</sub>	2	0.05	24	51	11.26
He <sub>2</sub>	2	0.66	24	56	12.55
N <sub>2</sub>	2	0.35	12	12	3.6



SPACECRAFT BUS

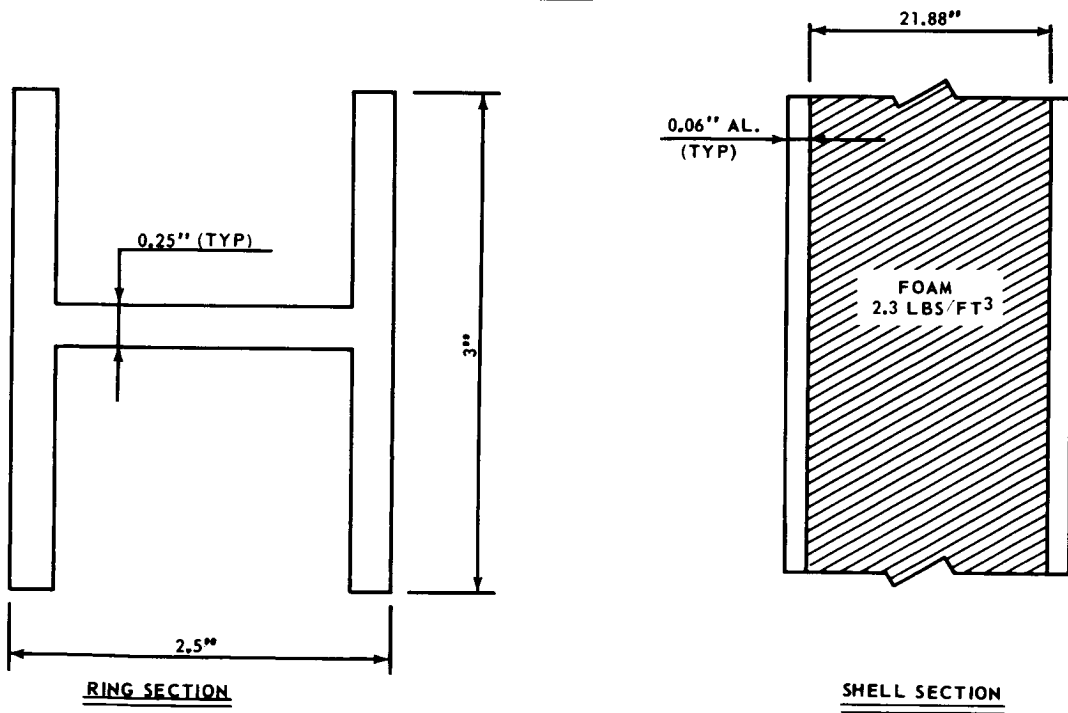


FIGURE V-6. SPACECRAFT BUS



# MATERIALS EVALUATION

## Radiation Environment

During the mission, the spacecraft will be subjected to several radiation fields. First it must pass through Earth's trapped radiation belts. During the entire time of flight, it will be irradiated by the protons of the solar plasma and bursts of energetic particles from any solar flares which might occur. Finally, at Jupiter, it will be traveling within the Jovian trapped radiation belts for a portion of each orbit, and for the entire mission it will be irradiated by neutrons from its own RTG's.

In this analysis, the effects of Earth's radiation belts have been ignored as the spacecraft will penetrate them in too short a time to accumulate a significant dose. Further, the solar plasma is made up principally of low energy protons which will be stopped by the outer structure of the spacecraft, and hence their damage will be limited to surface effects. The contribution to the radiation from solar flares has also been neglected since the number and intensity of solar flares is not known.

A large amount of information on radiation effects to various components and materials exists; however, the type of radiation used (neutron, proton, gamma, electron), the energy of the radiation, and the dosages differ, as do the units used in reporting them. Although exact conversion factors for converting the dose of one radiation into the equivalent dose of another do not, and probably will not, exist. A table of approximate conversions taken from RSIC-151 [Ref. V-1] has been used to convert the irradiation data to total absorbed dose units of ergs/gram.

Table V-5 lists some of the more radiation sensitive components. From an examination of this table, it may be seen that with some selection of components, a total absorbed dose of  $10^5$  ergs/gm is a threshold below which there is no degradation of performance.

Further, in many cases, irradiation results in a gradual degradation of performance, not catastrophic failure. Hence, the permissible total dose is that for which the system performance degrades below an acceptable value.

Radiation from the 8 RTG's to be employed would, over the  $10^3$  day mission lifetime used as the baseline, total from  $5 \times 10^3$  ergs/gm to  $1 \times 10^4$  ergs/gm, depending upon the shielding effects of the spacecraft structure. This is 10 percent or less of the threshold dose, and hence is not a constraint on the mission.

The solar proton flux is estimated to be approximately  $10^8$  protons/cm<sup>2</sup>/sec. (Appendix B, Volume II). This will yield  $8.6 \times 10^{15}$  protons/cm<sup>2</sup> over the  $10^3$  day mission. Since these are low energy particles with an average energy of 1 keV, the energy of these particles will be absorbed by the surface of the spacecraft and provide no hazard

to interior components. Studies show, however, that many thermal control paints show an increase in absorbance at total fluxes of  $10^{13}$  to  $10^{15}$  protons/cm<sup>2</sup> [Ref. V-8] and this must be considered in selecting these coatings.

TABLE V-5. RADIATION DAMAGE TO COMPONENTS

Component	Damage Threshold* (ergs/gm)	Inoperable (ergs/gm)
Piezoelectric crystals	$10^6$	$10^{11}$
Organic insulators and seals	$3 \times 10^3 \rightarrow 3 \times 10^7$	$3 \times 10^7 \rightarrow 3 \times 10^{10}$
Inorganic insulators	$3 \times 10^7 \rightarrow 3 \times 10^{11}$	$3 \times 10^9 \rightarrow 3 \times 10^{14}$
Semiconductors		
Diodes	$10^5$	$3 \times 10^8$
Tunnel diodes		$10^9 \rightarrow 10^{10}$
SCR	$2 \times 10^2$	$3 \times 10^6$
Transistors	$3 \times 10^2 \rightarrow 3 \times 10^4$	$3 \times 10^5 \rightarrow 3 \times 10^7$
UJT		$\sim 10^5$
FET		$10^7 \rightarrow 10^8$
Infrared detectors		
Pb S	$10^7$	$10^8$
Pb Se	$10^7$	$10^8$
Pb Te high output units failed at	$10^8$	
In Sb high output units failed at	$10^9$	
Optical glas (discoloration)	$10^6 \rightarrow 10^{10}$	

\*References V-1, V-2, V-3, V-4, V-5, V-6, V-7 and V-9.

Table V-6 gives the estimated number of orbits to reach three total absorbed radiation doses: I =  $1 \times 10^5$  ergs/gram (threshold, no degradation of performance); II =  $5 \times 10^5$  ergs/gm (some performance degradation); and III =  $1 \times 10^6$  ergs/gm (some possible component or system failures), caused by the Jovian trapped radiation belts. The data is presented for Jovian orbit periapsis of 5, 6, and 7 R<sub>J</sub> and for two models of the Jovian radiation belts. (Radiation model A corresponds to the model of Figure A-4 in Appendix A, Volume II, and model B to Figure A-5.) It may be seen from this graph that the Jovian trapped radiation strongly constrained the orbit choice.

TABLE V-6. NUMBER OF ESTIMATED ORBITS TO INDICATED TOTAL ABSORBED DOSE

Orbit Periapsis (Units of Jovian Radius)	Dose I		Dose II		Dose III	
	Radiation Model		Radiation Model		Radiation Model	
	A	B	A	B	A	B
5	1/3	2/3	1	2 1/3	3	6.1
6	1	1 1/3	3 1/3	4 2/3	8 1/3	11
7	2 1/2	7	8 2/3	23	21	61

Total Absorbed Dose

I =  $1 \times 10^5$  ergs/gm (threshold, no degradation of performance expected)

II =  $5 \times 10^5$  ergs/gm (some degradation)

III =  $1 \times 10^6$  ergs/gm (some possible component or system failures)

## Space Environmental Effects

The launching of a Voyager type spacecraft for an extensive mission opens a broad new spectrum for the study of effects on materials. A mission of this type which involves approximately  $10^3$  days in deep space, places extreme requirements on materials. These have not been experienced on previous space flights and thus the definite effects of temperature, radiation, and high vacuum encountered during this mission may be considered to be beyond the present day knowledge of some of the involved materials. Radiation and vacuum effects are of prime concern.

## Radiation Damage

Radiation effects from the space radiation environment and RTG's will threaten damage to both the metallic and nonmetallic components in the duration of the proposed  $10^3$  day mission.

By far, metals have demonstrated the greater resistance to nuclear type damage as compared to organic and semi-conductor materials. For this reason, no particular concern is given to the possible damage to the main metallic structural components of the vehicle. There is, however, some concern in the metallic applications involving delicate, sensitive instruments where high accuracy is of major consideration including instruments of telemetry or control nature. Radiation environment could conceivably affect the physical properties from a dimensional-stability viewpoint.

Studies of radiation effects on metals including aluminum, copper, gold, iron, nickel, molybdenum, silver, titanium, and zinc are outlined in Reference V-10.

The non-metallic materials conversely show significant effects from space radiation. The radiation damage to these materials is usually more dependent on the total dose rather than the type of radiation and the dose rate. The non-metallic materials used for potting, insulation, sealants, elastomers, lubricants, coatings, and various electronic components show varying degrees of resistance to radiation damage. In general, the radiation effects of these materials must be considered as serious and extreme caution must be exercised in the location and extent of their usage throughout the space vehicle.

Table V-7, taken from Reference V-1, illustrates property changes effects on some classifications of materials. References V-1 and V-10, and the bibliographies, contain more extensive information concerning radiation effects on materials.

Because of the proximity of the RTG's to the propellant tanks on JOVE it is desirable to know the long term effects of radiation on retropropulsion and midcourse correction fuels. These fuels were located close to the RTG's to help act as a shield for other components on JOVE which might be severely affected by nuclear radiation from the  $\text{Pu}^{238}$  and the  $\text{O}^{18}$ . This is a proper procedure provided the nuclear radiation does not then damage the fuel. Little research has been carried out on the problem. That which has been done indicates that a threshold of greater than  $10^{15}$  effective neutrons/cm<sup>2</sup> or  $10^7$  roentgens of  $\gamma$  radiation [Ref. V-11, V-12] is required to do primary damage to hydrazine ( $\text{N}_2\text{H}_4$ ),  $\text{N}_2\text{O}_4$  or 50-50 UDM Hydrazine. On the basis of this information the RTG nuclear radiation would not damage the fuel.

TABLE V-7. RADIATION LEVELS THAT PRODUCE APPRECIABLE PROPERTY CHANGES [REF. V-1]

<u>MATERIAL</u>	<u>IONIZATION</u> <u>ergs/gm</u>
<b>CERAMICS</b>	
Glass	$10^5 - 10^{10}$
Fused Silica	$10^7 - 10^{11}$
Crystalline Ceramics	$10^5 - 10^{11}$
<b>ELASTOMERS</b>	$10^8 - 10^{10}$
<b>METALS</b>	---
<b>OILS AND GREASES</b>	$10^9 - 10^{12}$
<b>PLASTICS</b>	
Tetrafluoroethylene	$10^6 - 10^7$
Other Plastics	$10^6 - 10^{11}$
<b>SEMICONDUCTOR MATERIALS</b>	---

## High Vacuum Effects

In deep space, the vacuum level is expected to be in the order of  $10^{-12} - 10^{-14}$  mm of Hg. Vacuums of this level can cause varying degrees of outgassing and sublimation, depending on temperature of the environment. For most metals, these effects are slight; however, severe damage is probable to many of the non-metallic materials. These effects to elastomers, plastics, coatings, structural adhesives, electrical insulation, laminates, potting compounds, and sealing materials are outlined in RSIC-150 [Ref. V-10].

## Materials Selection

It is anticipated that the Saturn V launch vehicle and related sections will be used and thus any presently existing materials deficiencies will have been corrected by the JOVE launch date. With this reasoning, no particular considerations are given this area.

It is anticipated that the JOVE spacecraft configuration will involve primary support members of aluminum or magnesium. The possibility of extensive use of titanium or beryllium alloys should not be ruled out because of their increasing use in space applications and increasing research developments with these materials. Shielding in the various locations will include aluminum or newer super types of non-metallics presently in use or in stages of development. Stored hydrazine fuel will be contained in metallic-rubber lined containers.

In a space vehicle of this type, it is obvious that non-metallics will be used extensively for sealants, lubrications, shielding, and components of structural, electronic, and various other assemblies. As forementioned, the vacuum environment in the order of  $10^{-12}$  to  $10^{-14}$  mm Hg and radiation fields can cause serious damage to many of these materials. Outgassing and sublimation may well prove to limit the use and selections of many of the presently used non-metallics. It is with hope and anticipation that progress in research and development of new materials will develop at a pace to make possible the construction and launching of vehicles for missions of this magnitude during the next decade.

## THERMAL CONTROL

### Overall Requirements

The phases of the Jupiter orbiter mission are pre-launch, launch and ascent, Earth parking orbit, transfer trajectory, and Jupiter orbit. Each phase presents thermal control problems that are more complex than a near-Earth satellite. First, during the pre-launch and launch and ascent phases, the RTG power producing units present unusual cooling problems. Secondly, because of the great distance travelled from the Earth, the overall energy balance varies considerably along the transfer trajectory and during the Jupiter orbit.

Jupiter, being at a nominal distance of five astronomical units (AU) from the sun, appreciates a solar constant of approximately four percent of Earth's. The solar constant varies as the inverse square of the distance between the sun and the subject planet, and by definition the semi-major axis of Earth's orbit about the sun is one AU which is:

1.  $49599 \pm 0.0004 \times 10^8$  km, or approx. 93 000 000 miles.

The numerical value of the solar constant at Earth is 1400 watts per square meter, and at Jupiter it is down to 52 watts per square meter (Table B-5, Appendix B, Volume II).

In spite of the widely varying thermal environment, there existed rather rigid requirements for maintaining temperatures throughout the spacecraft within specified bounds. Storable liquid fuels and oxidizers will be maintained between 20 and 70° F. ,

while electronic compartments for best reliability of components will be maintained at a temperature near 65° F. In the gross analysis, an average temperature of 60° F. for the entire spacecraft was assumed.

To accomplish the control desired, a thermal control subsystem was devised. In the broadest sense, it encompasses the entire spacecraft system. In the sense used herein, it consists only of the members devised or designed specifically for thermal control purposes such as louvers, radiation shields and insulation, conduction members, surface coatings, and electrical resistance elements and associated relays and thermostats. Not included as a part of the spacecraft thermal control subsystem are other subsystems required for pre-launch and launch phases of the mission. They are ground handling devices that normally serve more than one mission.

The overall configuration was, in great measure, dictated by thermal and nuclear effects. Other design factors influenced by temperature control requirements included packaging, placement of components and subsystems, surface finishes, and methods of attachment.

## General Approach

Thermal control became an integral part of the spacecraft configuration. The chosen configuration was amenable to thermal control through judicious placement of subsystems and the use of insulation louvers, and a minimum of electrical energy. The schematic of the system, Figure V-7 indicates the more significant heat flow directions but not their magnitudes.

As shown, the craft is flying in the sun pointing attitude desired for the first 270 days of a nominal 800-day trip time. At the end of the 270-day period, the craft will be approximately three AU (Fig. II-35) from the sun, and use of the high-gain antenna is required. Flying with a sun pointing antenna does not preclude in-transit maneuvers and possible reorienting of the spacecraft to bring the actual thermal profile in line with the nominal. A sun pointing antenna has the advantage that the electronic packages and the RTG's are pointing toward black space and for the most part are shaded by the antenna backed structural skirt. The antenna and spacecraft will be Earth pointing during the remaining 530 days of the trip.

It is seen that the insulation pattern divides the spacecraft into two compartments. The lower compartment houses the electronic equipment, propellant tanks, their associated pressurant tanks, cold gas tankage, and miscellaneous plumbing, etc. The upper compartment is a dead space which houses the retro-engine and its supports. It provides the supporting surface for the RTG's, mid-course, and orbit trim engines. Inasmuch as the back or support side of the RTG's may be designed for any reasonable desired temperature, it is assumed that it is 300° K and that heat flows through that side in an

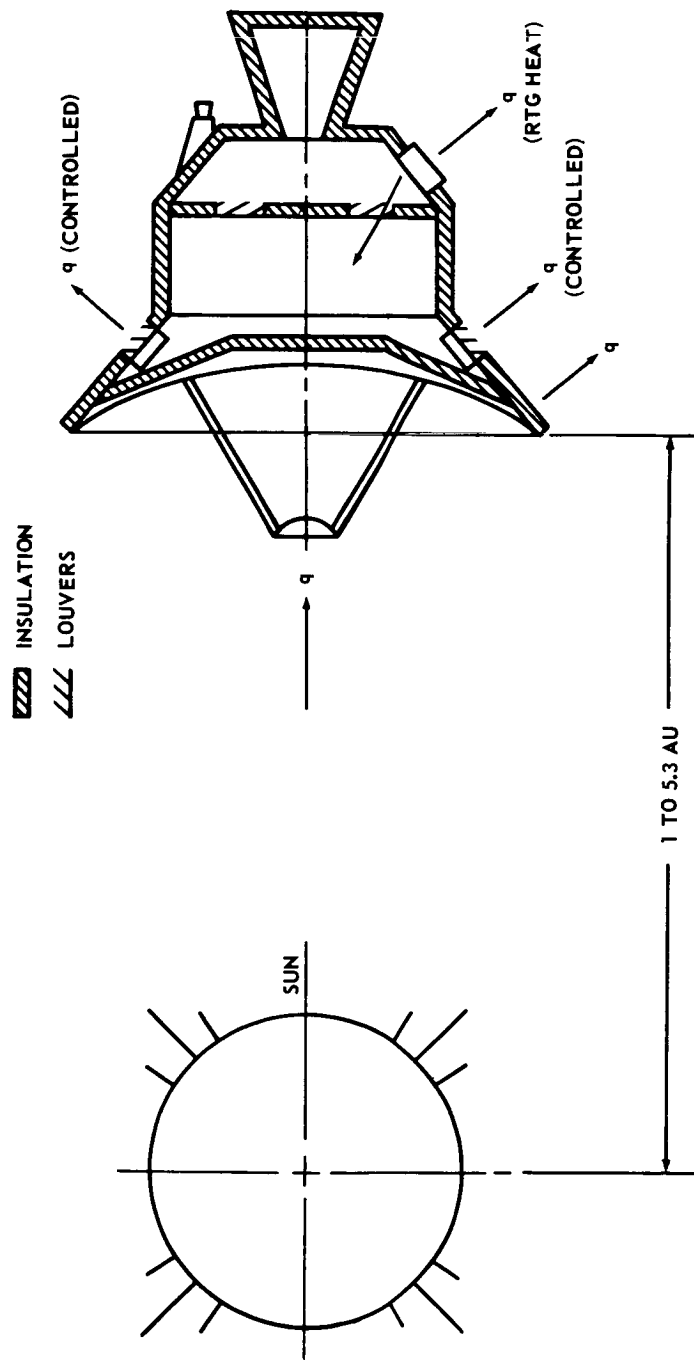


FIGURE V-7. SCHEMATIC OF JOVE THERMAL CONTROL SUBSYSTEM



amount necessary (only a few watts) to maintain an average temperature of 295°K (70° F) in the dead space. The dead space average temperature will drop slightly after the engine insulating cap is jettisoned just before the retro orbit insertion maneuver at Jupiter. However, 20 watts of electrical resistance heat is provided at the engine and thermostatically controlled to prevent temperature falling below the acceptable value of 20° F at the time of start of propellant flow. After final orbit trims are performed and all propellants are expended, no further need exists for controlling engine temperatures.

At the lower end of the electronics - propellant compartment in ten standard modules are located the heat producing electrical subsystems. The heat produced by the electrical subsystem is rejected to space through louvers. Two additional standard louvers are provided for general heat rejection purposes. To facilitate thermal coupling between members the interior surfaces are painted with Cat-a-lac black paint or its equivalent. Thus, the general approach is one of playing two warm ends of the spacecraft against an inert thermal fly-wheel in the middle. The middle has an initial approximate thermal capacity of 5000 BTU per ° F rise in temperature.

## Parametric Studies

Since neither time nor detail of system design was available for complete thermal control subsystem analyses, parametric studies and gross radiation data resulted in a readily usable form. From Table V-8, typical values of properties of coatings may be selected for use with Figures V-8, V-9, and V-10. Except for the Cat-a-lac black paint properties, the data of Table V-8 came from Reference V-14. Also, Figures V-8, V-9, and V-10 are similar to those of Reference V-14.

TABLE V-8. PROPERTIES OF COATINGS

	Absorptivity $\alpha$	Emissivity $\epsilon$	$\alpha/\epsilon$
Evaporated Gold	0.19	0.02	9.5
Evaporated Aluminum	0.08	0.025	3.2
White Paint	0.15 - 0.30	0.85	0.177 - 0.353
Black Paint (Cat-a-lac)	0.90 ± 0.05	0.90 ± 0.03	1.0
Evaporated SiO <sub>2</sub> on Evaporated Aluminum	0.12 - 0.18	0.10 - 0.60	1.2 - 3.0
Polished Aluminum	0.15 - 0.25	0.03 - 0.05	5.0

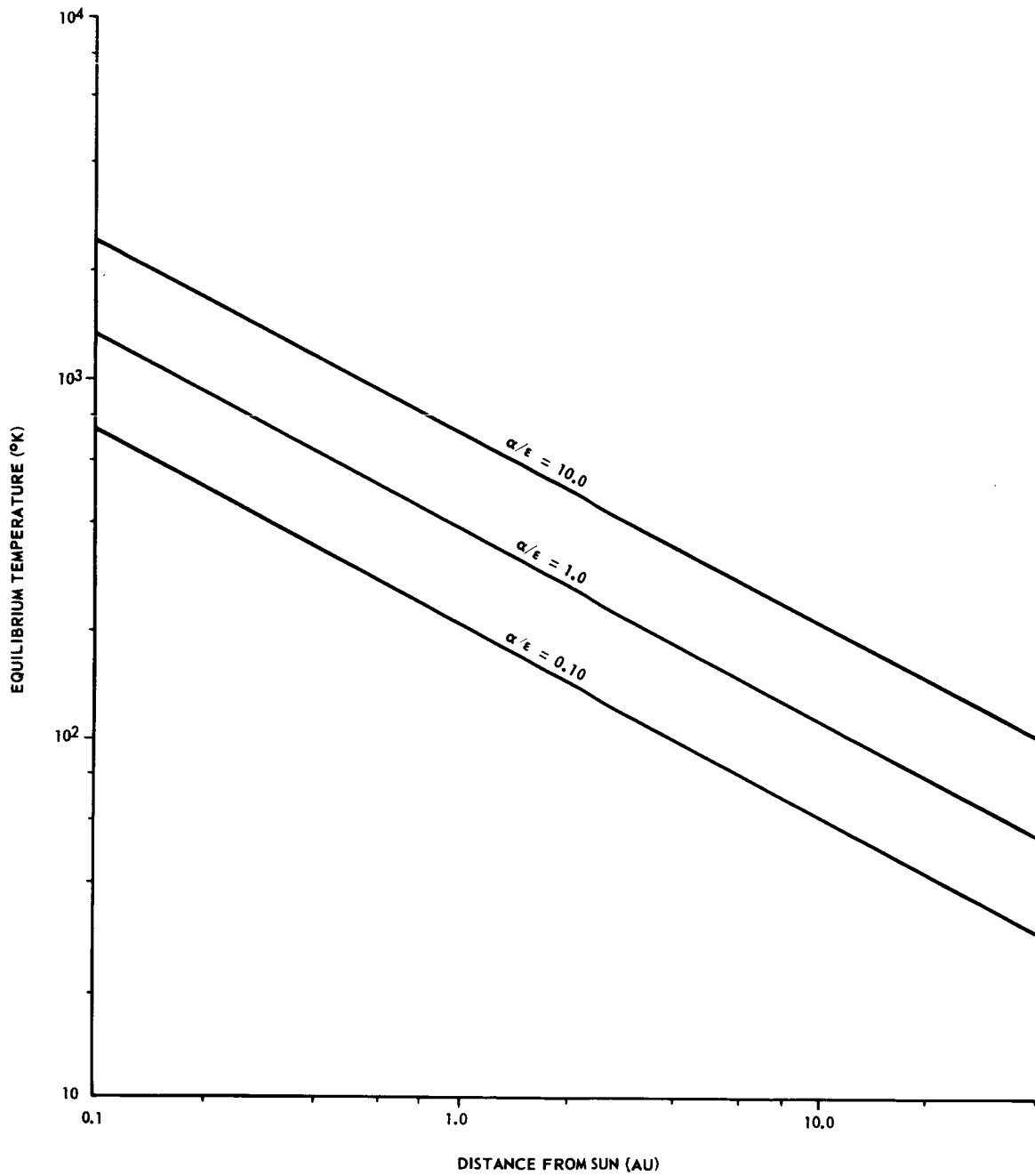


FIGURE V-8. TEMPERATURE VERSUS DISTANCE FROM SUN FOR AN INSULATED FLAT PLATE FACING SUN

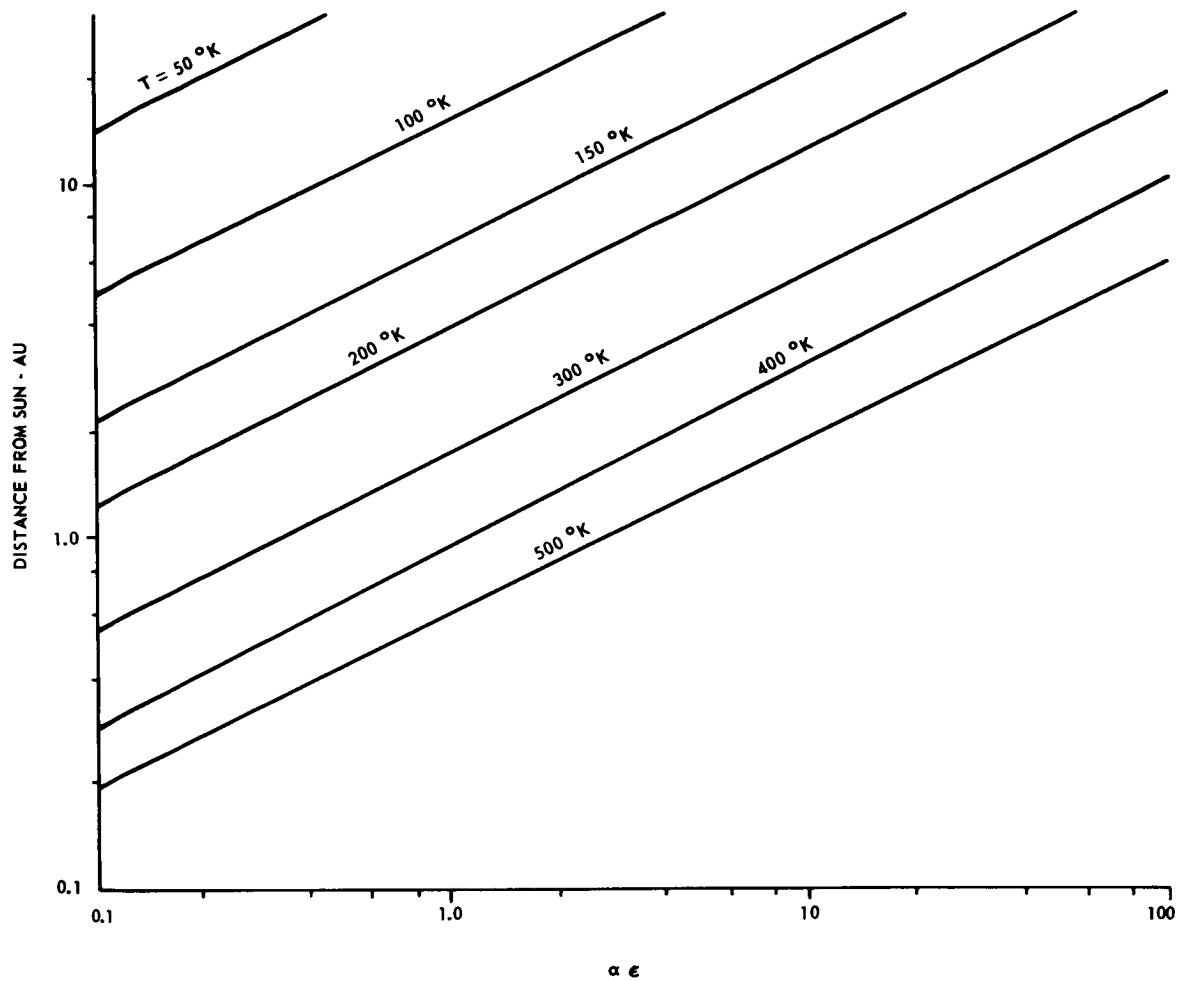


FIGURE V-9. EQUILIBRIUM TEMPERATURE FOR FLAT PLATE NORMAL TO SUN FOR VARYING  $\gamma/\epsilon$

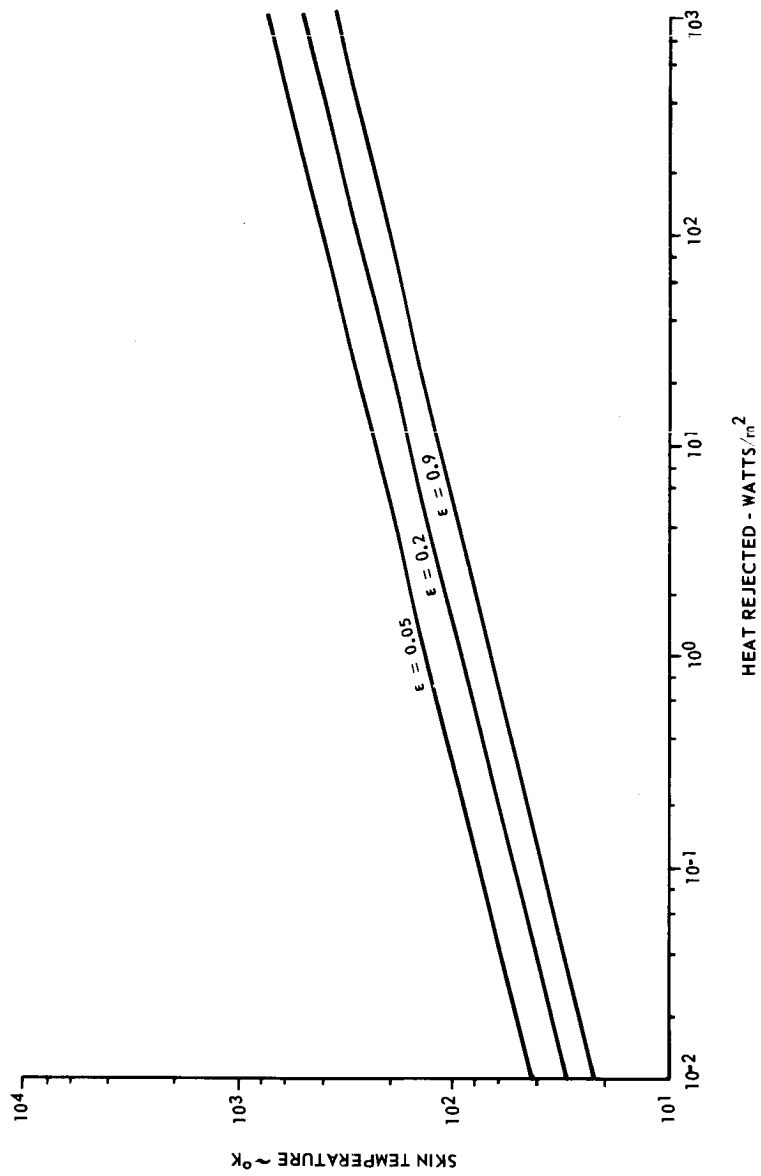


FIGURE V-10. EQUILIBRIUM SKIN TEMPERATURE VERSUS HEAT REJECTED TO BLACK SPACE

## Some Mission Phase Oriented Thermal Considerations

Each of the mission phases has thermal considerations and in some cases control features that differs from the others. Brief comments and/or analyses for the phases are presented herein, although detailed calculations are omitted in most cases.

Pre-launch Phase. Cooling of the RTG's was considered to be a ground handling problem and only feasibility studies were attempted. Final technique selection and the design will be the responsibility of those responsible for the RTG development, installation, and checkout.

The cooling devices may be portable transport casks, with built-in refrigeration, suitable for use through checkout and up until a few minutes before launch.

It is more probable that the cooling will be accomplished by forced convection with refrigerated air being the coolant. It is assumed that the electrical energy may be easily dissipated into the structure and cooling air, and that only the waste RTG heat need be considered here. Therefore, for a 640-watt electrical system with an efficiency of 4.5 percent, 48 500 Btu per hour of waste heat must be removed. From

$$\dot{q} = \dot{m}C_p \Delta T$$

the mass of cooling air required is 168 pounds per minute for a 20° F rise in temperature. For the nominal RTG's surface area of 160 ft<sup>2</sup>, and a surface conductance  $\bar{h}_c$ , of 6.0 Btu/° F - Ft<sup>2</sup> - hr, from

$$q = \bar{h}_c A \Delta T$$

Therefore

$$\Delta T = \frac{48\,500}{6(160)} = 50.7^\circ \text{ F.}$$

Considering the mean temperature of the coolant to be near 50° F, results in an RTG average temperature of about 100° F.

The majority of the mass of the spacecraft will be maintained near 50° F temperatures during checkout to serve as a heat sink during the launch phase.

Launch. No attempt was made at controlling the temperature during launch and the first few minutes of flight beyond cooling of the entire mass before launch. It is important that the nose cone and any shroud that shield the RTG's and electronics compartments from space be jettisoned early in the mission, preferably during the first few minutes. The following analysis arbitrarily used 30 minutes for the shielding time from

time of coolant flow stoppage. Each RTG has a mass of 80 pounds and an assumed average specific heat of  $0.2 \text{ Btu/Lb}_m \text{ } ^\circ\text{F}$ . From

$$mC_p \Delta T = \dot{q} \Delta \tau$$

the RTG temperature rise,  $\Delta T$ , of  $190^\circ\text{F}$ , is computed for the assumed 30-minute period ( $\Delta \tau$ ). The resulting final RTG temperature of  $290^\circ\text{F}$  is well below the design temperature and is acceptable. Heat produced by the electrical load will be absorbed by the spacecraft mass. Electrical power consumption will be held to a minimum.

Planet Orbits and Transfer Trajectory. Ideally, the spacecraft temperature will remain constant at  $60^\circ\text{F}$  throughout these phases of the mission except for the transient conditions encountered during maneuver set-ups. Ideal conditions cannot be achieved. The approach selected for solution of the problems involved, however, required the use of several proven techniques. They were:

1. Control of heat rejection to space through variable area louvers.
2. Control of heat transfer from one major compartment to the other through variable area louvers.
3. Control of energy distribution within compartments through conduction members and surface coatings of high emissivities and absorptivities, and
4. Control of heat leaks through careful design of attachments, and holding the loss through the surface to a negligible quantity by insulating with "super-insulation."

To determine skin temperatures and compute gross energy balances, the controlling terms of the following expression [Ref. V-16] were used

$$m c_p \frac{dT}{d\tau} = \alpha_s A_c F_{c-s} S + \alpha_{sr} A_c F_{c-p} S r_p + \alpha_p A_c F_{c-p} \frac{(1-r_p)}{4} S + q(\tau) - \epsilon_c \sigma A_c T_c^4$$

where the direct solar energy absorbed,  $q_s = \alpha_s A_c F_{c-s} S$  (a)

the solar energy reflected from a planet that is absorbed

$$q_{sr} = \alpha_{sr} A_c F_{c-p} S r_p$$
 (b)

the energy radiated from the planet that is absorbed,

$$q_p = \alpha_p A_c F_{c-p} \frac{(1-r_p)}{4} S$$
 (c)

the energy radiated away from the craft,

$$q_c = \epsilon_c \sigma A_c T_c^4 \quad (d)$$

and the heat generated on board,  $q_{ob} = q(\tau)$  (e)

Also, to derive Figures V-8 and V-9, the stored energy term  $mc_p dT/d\tau$  was set equal to zero and terms (a) and (d) considered dominant since the plate was assumed to be normal to the sun. Further, the solar energy absorbed was considered equal to the energy emitted by the flat plate (i. e., insulated plate).

Terms (b) and (c) were omitted throughout the analyses, since they exert appreciable influence only during periods during which the spacecraft is close to the planet. For JOVE, they do not strongly influence the thermal balance.

The RTG produced energy that remains on board, both electrical and thermal, and periodic release of chemical energy during engine burns are considered to be in  $q(\tau)$ .

## Surface Features

Surface coatings. All exterior surfaces, except for the RTG's, will be painted with black paint (Cat-a-lac or equal) with emissivity and absorptivity values of approximately 0.90. From Figure V-8 it is seen that initial equilibrium temperatures of those surfaces facing the sun will be 400°K at 1 AU and 175°K at 5 AU. The RTG surface will be painted with white paint whose emissivity is 0.85 - 0.90 and absorptivity is about 0.20.

Black was chosen to:

1. Give surfaces with predictable characteristics, and
2. Prevent accumulation of solar energy at the focal point of the antennas, thus producing a solar furnace.

A white surface with the characteristics cited above was selected to cover the RTG's to facilitate their cooling.

All interior surfaces are painted black for thermal coupling effect and the resulting near constancy of temperature throughout the spacecraft.

Insulation. Crinkled aluminized mylar was selected for insulating all exterior surfaces and the surface separating the two major compartments. Their thicknesses are 0.6 inch and 0.3 inch, respectively. The weight per 100 square feet of area for the 0.6 inch is estimated at 12.4 pounds, and it is comprised of 30 layers. Fifteen layers at 6.2 pounds per 100 square feet makes up the 0.3 inch layer between compartments. Very little heat is expected to flow through the compartment divider and it will flow, for the most part, through the variable area louvers. Total insulation weight is estimated at 125 pounds. All cold gas lines and instrument containers carried externally to the spacecraft are also wrapped with insulation of the same quality as crinkled aluminized mylar.

Thermal conductivity of the super-insulation is expected to vary from very high values before leaving Earth's surface down to  $2.0 \times 10^{-5}$  Btu/ft-°R-hr with  $10^{-4}$  Btu/ft-°R-hr representing a practical value experienced shortly after leaving Earth's heavier atmosphere. It will decrease steadily thereafter until the lower value is reached [Ref. V-16].

Heat loss through properly installed super-insulation for the entire spacecraft surface while in the colder regimes is estimated to be between 40 and 90 watts. Leaks through interfacing structure and other pass-throughs is expected to equal that lost through the insulation. Obviously, care must be exercised in final design of attachments and in locating and installing insulation.

Louvers. Variable area louvers with highly polished surfaces both inside and outside were selected for cooling the electrical equipment modules. Knowledge of thermal load distribution is not complete; however, the total is a nominal 640 watts. If this load is equally distributed between 10 modules, the load per module is 64 watts.

A reasonable sight factor of 0.75 and emissivity of 0.9 for the cold plates gives a cooling capacity of 27 watts per square foot and 108 watts for a nominal 4-square foot unit.

Since there are 10 electrical compartments and two standard louvered units for general thermal control (a total of 12 units), the total heat rejection capability is near 1296 watts. This is a comfortable total and the maximum load for any unit is estimated not to exceed 98 watts, an acceptable value.

Based upon a louver surface emissivity of 0.07 (polished aluminum) the minimum heat dissipation through closed louvers is computed to be 126 watts.

With two standard four square foot louvers placed in the compartment divider, a heat inflow to the lower compartment of up to 65 watts of RTG waste is realized. This could be very useful after the retro-engine insulating cap is jettisoned upon arrival at Jupiter.



## Summary

It appears that the following may be descriptive of possible energy transfers:

<u>Device</u>	<u>Louvers Closed</u>		<u>Louvers Open</u>
	<u>Low Minimum</u> (Watts)	<u>High Minimum</u> (Watts)	<u>Maximum Anticipated</u> (Watts)
Louvers	126	126	1296
Skin losses	40	90	90
Attach losses	<u>40</u>	<u>90</u>	<u>90</u>
	206	306	1476

A constant 640 electrical watts is available for continuous consumption and dissipation, with another 65 watts of waste heat on tap for a total of 705 watts. Approximately 50 of the electrical watts are available for localized heating purposes, 20 of which may be used near the retro-engine and its feed lines. A few of the thermal control watts are also devoted to heating and cooling of scientific packages.

Overall the thermal control for JOVE appears adequate. A more detailed analysis will be performed along with final design. Thermal analyzer computer programs would be employed to obtain subsystem optimization. Reference is made to Table V-1 for a breakdown of the 260-pound weight of the thermal subsystem.

## REFERENCES

1. Space Environmental Effects on Materials and Components, Volume II, Electronic and Mechanical Components, RSIC-151, April 1964.
2. Fleischer, H. L. and Szymkowiack, E. A. : Effects of Electron Radiation on Unijunction Transistors. NASA CR-526, July 1966.
3. Kobren, L. : Effects of Electronic Radiation on TV Lens Components. NASA TN D-2919, September 1965.
4. Hyanes, G. A. and Miller, W. E. : Effects of 1.2 and 3.0 MeV Electrons on the Optical Transmission Properties of Several Transparent Materials. NASA TN D-2620, March 1965.
5. Proton and Electron Permanent Damage in Silicon Semiconductor Devices. The Boeing Company, Document Number D2-90570, 1964.
6. Leach, E. R. ; Fairand, B. P. and Bettenhausen, L. H. : The Space Radiation Environment and Its Interactions with Matter. REIC Report Number 37. Radiation Effects Information Center, Battelle Memorial Institute, 1965.
7. The Effect of Nuclear Radiation on Electronic Components, including Semiconductors. REIC Report Number 36, 1964.
8. A Study of Jupiter Flyby Missions Final Technical Report. General Dynamics, Fort Worth Division, FZM-4625, May 1966.
9. Radiation Effects State-of-the-Art 1964-1965. REIC Report Number 38, 1965.
10. Space Environmental Effects on Materials and Components, vol. I, Elastomeric and Plastic Materials. RSIC-150, 1964.
11. Yasui, G. : RIFT Radiation Effects Program Irradiation No. 2, Liquid Propellants. NSP-63-80, July 15, 1963.
12. Plank, H. F. : RIFT Radiation Effects Program Irradiation No. 9, Monomethyl Hydrazine. NASP-64-10, February 15, 1964.
13. TRW Space Data, Third ed. , by TRW Systems Group, TRW, Inc.
14. Applications of Saturn/Apollo Hardware to Unmanned Scientific Exploration of the Solar System. Northrop Space Laboratories, NASA TR-292/3-6-003.

## REFERENCES (CONTINUED)

15. Krieth: Principles of Heat Transfer, Second ed. , International Textbook Company, 1965.
16. Grafton, J. C. and Nordwall, H. L. : Radiation Heat Transfer Analysis for Space Vehicles.

## BIBLIOGRAPHY

- Corliss, William R. : Spaceprobes and Planetary Exploration. D. Van Nostrand Company, Inc., NASA, 1965.
- JPL Voyager Spacecraft Presentations at MSFC February 8 and 9, 1967, with reference to Current Estimates of '71 and '73 Spacecrafts, by R. A. Neilson.
- Mariner Mars 1964 Project Report. Technical Report Number 32-740, JPL, 1966.
- Mariner Mission to Venus. McGraw-Hill Book Co., Inc., 1963.
- Mariner-Venus 1962 - Final Project Report. NASA SP-59-1965.
- Patlee, H. E. and Monroe, R. E. : Adhesion in the Space Environment, RSIC-607, 1966.
- Report from Mars - Mariner IV - 1964-65. Government Printing Office.
- Space Log. TRW vol. 14, no. 4, Winter 1964-65.
- Voyager Spacecraft System. Final Technical Reports, Task B, The Boeing Company, January 1966.
- Voyager Spacecraft System. Final Technical Reports, Task B, TRW Systems Group, January 1966.
- Voyager Spacecraft System. Preliminary Design, Task B, General Electric Company, January 1966.
- Westrom, J. L. and Anthony, D. C. : Design Guidelines for Circuitry in a Nuclear Reactor PROPELLED Spacecraft, Lockheed Missiles and Space Company, Huntsville, Alabama, October 1965.

**CHAPTER VI**

**SPACECRAFT PROPULSION SYSTEMS**



# CHAPTER VI. SPACECRAFT PROPULSION SYSTEMS

## DEFINITION OF SYMBOLS

$R$	Gas constant
$T$	Torque
$M$	Micrometeoroid mass
$\bar{V}$	Micrometeoroid velocity relative to spacecraft
$b$	Distance from C. G. to point of micrometeoroid impact
$I$	Moment of inertia
$\theta_F$	Excursion angle following collision
$(\Delta t/t)$	Dimensionless pulse width
$F_T$	Thrust level
$l$	Center-to-center distance AC/S jets
$\theta_E$	Deadband angle
$\dot{\theta}_E$	Angular rate
$\Delta I$	Unit impulse
$\Delta t$	Pulse width (also called thrust duration)
$t_1$	Pulse spacing
$I_T$	Total impulse
$P$	Mission length
$W_{N_2}$	High-pressure $N_2$ storage weight
$\beta_p$	Redundant storage factor

## DEFINITION OF SYMBOLS (CONTINUED)

$I_{sp}$	Specific impulse
$\alpha_p$	Specific impulse degradation factor
P	Pressure
T	Temperature
$V_{N_2}$	High-pressure $N_2$ storage volume
R	Oxydizer/fuel ratio
$\mathcal{J}$	Impulse per axis
$\Delta V$	Velocity increment
r	Mass ratio, tank radius (depending on use)
W	Weight
$m_f$	Gross capture weight
$m_o$	Net injection weight
V	Volume
$\rho$	Density
$V^*$	Dimensionless storage factor
k	Ratio of specific heats
t	Thickness
$W_p$	Propellant requirement

# INTRODUCTION

The on-board propulsion requirements for JOVE consist of the primary requirements for orbit insertion, trajectory correction and orbit trim (TC/OT) and the secondary requirements for Attitude Control and Stabilization (AC/S). These are treated separately in the various sections of this chapter, starting with a discussion of the primary requirements and their treatment.

## PRIMARY ON-BOARD PROPULSION REQUIREMENTS

### Introduction

The primary propulsion subsystems must provide the flexibility and capability for trajectory correction, orbit insertion and orbit trim as prescribed by the mission profile. The synthesis and analysis of the subsystems are based on the following operations:

- a. An initial trajectory correction shortly after injection.
- b. One or more subsequent corrections before insertion.
- c. Orbital insertion maneuver.
- d. Orbit trim maneuver to adjust the planetary orbit.
- e. Orbital transfer maneuver.
- f. Orbit trim maneuver.

The energy requirements can be classified broadly as those for orbit insertion and those for correction and orbit trim. The requirement for trajectory correction is estimated to be 150 meters per second; for orbit trim purposes the requirement is estimated as 100 meters per second. This represents a total requirement of 250 meters per second for trajectory and orbit adjustment, and the requirement for orbit insertion has been estimated as an additional 2000 meters maximum per second for a 1978 launch opportunity. The 1978 launch opportunity corresponds to the maximum requirement for the 1975-1980 time period, and for other missions propellant off-loading is feasible.

The required midcourse maneuver accuracy is a minimum velocity increment of 1 meter per second with a maximum allowable error of 0.1 meter per second. It is desirable to execute a maneuver as small as 0.1 meter per second, with a  $3\sigma$  error of 0.01 meter per second.



Certain general constraints on the spacecraft and the propulsion subsystem configuration are recognized as necessary. For instance, a modular concept with simple electrical and mechanical interfaces offers distinct advantages. The volume, shape, height, and weight are restricted by both practical and necessary considerations. A reasonable thermal environment must be attained for which the exact limits depend upon final selection of the subsystem. Finally, the subsystem must withstand the loads and vibrations associated with launching; operation of the subsystem must not impose undue loads and vibrations on the spacecraft.

## Propellant Selection

The velocity requirement for orbit insertion is such that only a small percentage of the total propulsion weight is allocated to midcourse correction and orbit trim. From before, the mission requirement is estimated to be 2250 meters per second for all purposes.

In Figure VI-1 the performance potential of several propellants is indicated where lines of constant mass ratio have been plotted for velocity vs. specific impulse. The lowest values for mass ratio for a given velocity requirement correspond to nuclear propulsion, cryogenic propellant, and fluorine systems, respectively. Generally the state of development, ease of handling, overall experience level and long term storability aspects enhance the selection of either a solid propellant or a hydrazine blend bipropellant either of which provides the orbit insertion velocity requirement with a mass ratio of approximately 1.6.

The use of a solid propellant configuration for retropropulsion necessitates the consideration of a separate subsystem for trajectory correction and orbit maneuvers. Such a separate system can be used also in conjunction with a bipropellant configuration for retropropulsion. An alternative is the use of a single subsystem with multiple start capability for the combined mission requirements. With the separate subsystem for trajectory correction, etc., the relatively small velocity requirement can be achieved with a monopropellant system. A system of this type employing monopropellant hydrazine requires additional fuel to that required by a bipropellant system, but propellant acquisition and complexity are not as significant.

## Subsystem Synthesis

For a dual subsystem configuration employing a monopropellant system for correction and trim maneuvers, there are several methods of obtaining thrust vector control during retropropulsion, including gimbal operation with the bipropellant system or throttling the midcourse chambers with either the bipropellant or solid fuel system. Also, with

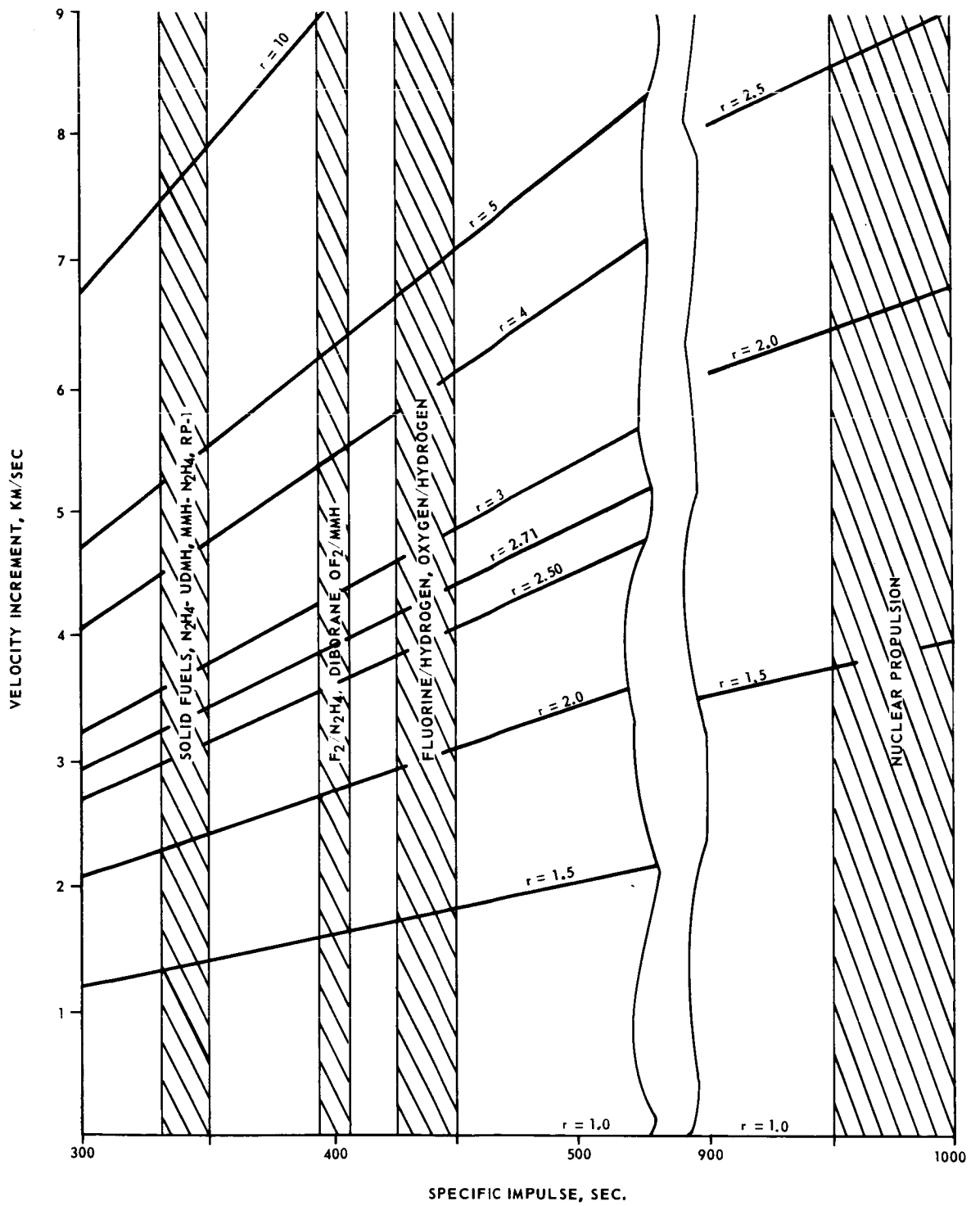


FIGURE VI-1. PROPELLANT CLASSIFICATIONS

the solid fuel configuration methods involving secondary fluid injection, a movable nozzle or a separate solid propellant gas generator can be considered. Secondary fluid injection has been successful in Minuteman and Polaris, but it requires additional propellant tanks and associated hardware. The solid propellant gas generator has been used in the roll control system developed for the Minuteman Wing VI third stage, but it, too, corresponds to the introduction of a third subsystem. The concept of a movable nozzle introduces additional complexity that is not offset, perhaps, by increased reliability or flexibility. For the solid propellant retropropulsion, it seems that throttling the midcourse thrust chambers is the least complex and most reliable method for thrust vector control. For bipropellant retropropulsion, either gimbaling or throttling of the midcourse thrust chambers is conceivable.

In a combined system for provision of the overall mission requirements consideration can be given to either a single bipropellant thrust chamber or multiple thrust chambers. Thrust vector control can be achieved by gimbaling, fluid injection, or, in the case of multiple thrust chambers, by throttling. The increase in system complexity and decrease in reliability accompanying multiple starts, however, is generally undesirable in connection with multiple thrust chamber configurations, so the single thrust chamber is considered as preferable. This configuration with stepped-thrust capability for flexibility and gimbal mounting for simplicity provides a desirable subsystem concept for the overall mission requirements.

In summary, three subsystems can be synthesized, each of which appears to be feasible for the propulsion requirements:

- a. Solid propellant retropropulsion with monopropellant TC/OT chamber throttling for thrust vector control.
- b. Bipropellant retropropulsion with monopropellant TC/OT provision, with gimbal mounting for thrust vector control.
- c. Single bipropellant thrust chamber with stepped thrust capability and gimbal mounting for combined retropropulsion and TC/OT provision.

## Subsystem Sizing

A design chart is shown in Figure VI-2 which relates velocity requirement ( $\Delta V$ ), mass ratio ( $r$ ), specific impulse ( $I_{sp}$ ) of the propellant, thrust ( $F_T$ ), propellant requirement ( $W_p$ ), gross capture weight ( $m_f$ ), and net injection weight ( $m_o$ ) for any particular mission.

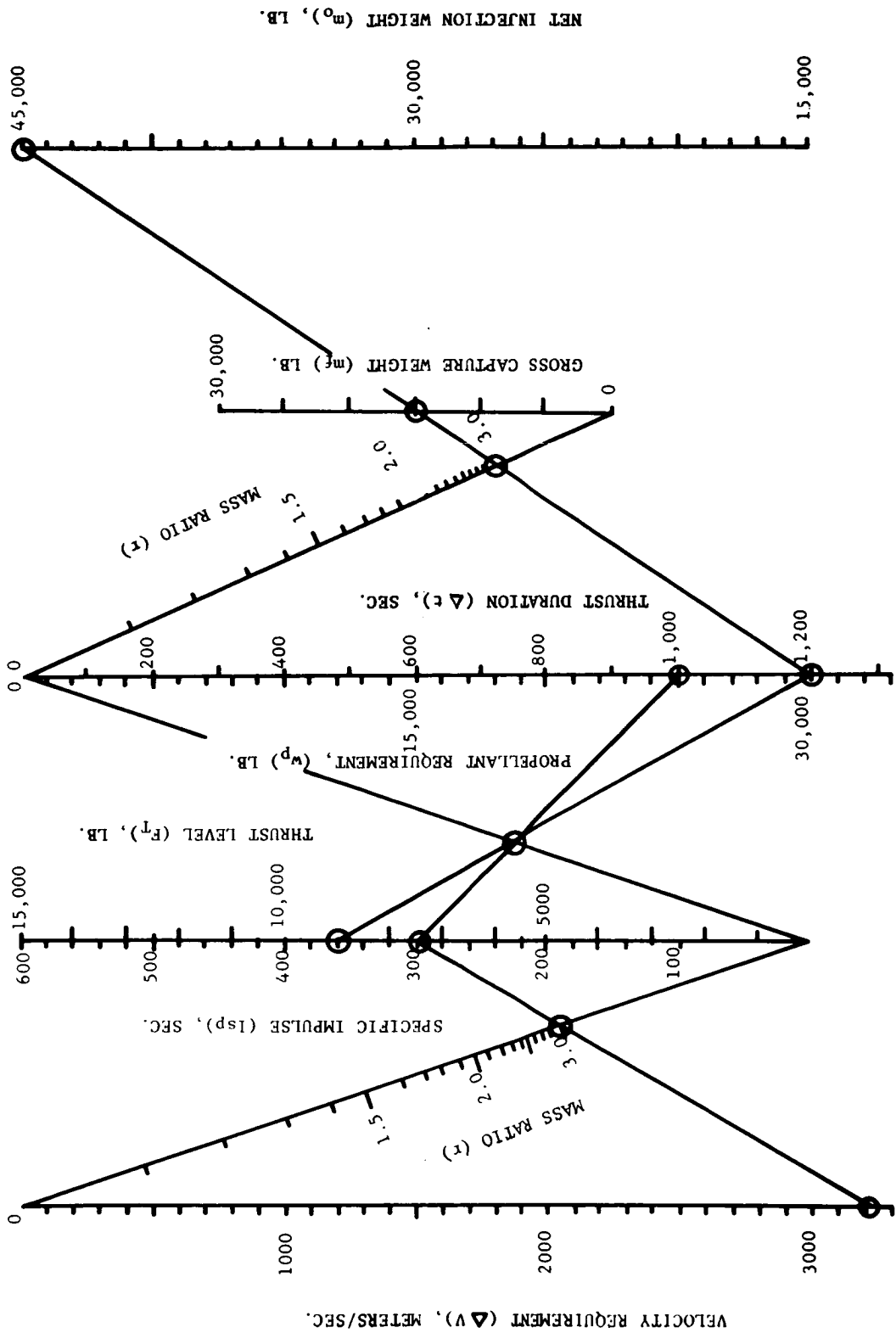


FIGURE VI-2. PROPULSION DESIGN CHART

For sizing of the retropropulsion system a net injection weight of 45 000 lb is selected as corresponding to near maximum capability of the Saturn V booster for an interplanetary mission. A gross capture weight or gross delivered payload of 15 000 lb is selected as a desirable maximum for propulsion sizing. With these constraints a maximum mass ratio of 3.0 and a maximum fuel requirement of 30 000 lb are derived from the chart.

A value of 1000 sec is selected as maximum thrust duration, corresponding to an approximate upper limit for ablative thrust chamber operation. This value, along with a typical value of 300 sec for specific impulse of the propellant, fixes a pivot point on the unmarked diagonal. This point along with the propellant requirement from above (30 000 lb) yields the solution for a minimum thrust requirement of 9000 lb.

For the same value of specific impulse and the maximum value 3.0 for a mass ratio, as found previously, the solution for maximum velocity contribution is found to be 3220 meters/second which represents a comfortable level for numerous interplanetary missions.

## Subsystem Solution

Typical Solid Propellant Retropropulsion Subsystem. In an earlier design study [Ref. VI-1] performance parameters and subsystem characteristics were reported for an Aerojet modified second-stage Minuteman Wing VI propulsion system. From the plots contained within that study the following data are extrapolated:

Expansion Ratio	70:1
Total Impulse	3 000 000 lb-sec
Propellant Weight	9900 lb
Total Motor Weight	11 320 lb
Effective Specific Impulse	294 sec
Effective Mass Fraction	0.899
Average Vacuum Thrust	33 000 lb
Throat Area	44.5 in. <sup>2</sup>
Nozzle Exit Diameter	63 in.
Overall Motor Length	155 in.

General Electric has reported also, for a monopropellant TC/OT subsystem, the percent error in velocity increment versus total thrust as supplied by the Propulsion Department of TRW/STL. For a minimum  $\Delta V$  trajectory correction of 0.1 meter/sec a

maximum error of 7 percent occurs with a total thrust of 115 lb. For a  $\Delta V$  correction of 1 meter/sec a maximum error of 7 percent is met easily for trajectory correction or orbit trim at this thrust level. The percent error for an orbit trim correction of 0.1 meter/sec at 115 lb thrust is approximately 15 percent.

To compute the amount of monopropellant required for thrust vector control accompanying a maneuver of 3 000 000 lb-sec it is necessary to make certain assumptions concerning the C. G. uncertainty during the maneuver. This is assumed to be 0.2 inch at the start of the maneuver and 0.4 inch at the end of the maneuver. The results of a typical calculation are tabulated below for the assumption shown:

Maximum Disturbing Torque	10 000 in. -lb
Thrust Chamber Radius	52 in.
Duty Cycle	100%
Duration	90 sec
Specific Impulse (Hydraxine)	230 sec
Propellant Requirement	75.4 lb
Thrust (Minimum Per Chamber)	25.0 lb
Thrust (Maximum Per Chamber)	210.0 lb

For the solid propellant subsystem the weight requirement for orbit insertion (3 000 000 lb-sec) may then be estimated as:

Engine Weight	11 320 lb
Thrust Vector Control	<u>100 lb</u>
Total	11 420 lb

For weight comparison purposes it is considered that the TC/OT monopropellant subsystem will be on-board with either the bipropellant or the solid propellant subsystem, so its weight will not be included in orbit insertion estimates, although with the solid propellant the TC/OT subsystem may be slightly heavier. The above values do not include necessary structural weight which is estimated at 300 lb.

Liquid Bipropellant Retropropulsion Subsystem. For applications of 9000 pounds thrust requirement (preceding section) in the 1975-1980 period the Lunar Excursion Module Descent Engine (LEMDE) will be a functional system that can be modified for particular needs. Studies have been made to determine its applicability as a propulsion subsystem for interplanetary spacecraft.

For weight comparison purposes, the results of a study by General Electric is shown here for a modified 4-tank LEMDE system:

Thrust Chamber ( Complete)	399 lb
Propellant Feed System	
Propellant Tank	376 lb
Plumbing	57 lb
Trapped Propellant	474 lb
Pressurization System	
Pressurant Tanks	380 lb
Plumbing	36 lb
Helium	35 lb
Miscellaneous Hardware	21 lb
Structural Weight	<u>206 lb</u>
Total Propulsion Inert Weight	1984 lb

Additionally, for a total retropropulsion impulse of 3 000 000 lb-sec with the modified LEMDE system the propellant usage is estimated as 10 000 lb. For a comparison with the solid propellant subsystem the following weight breakdown is obtained:

Inert System Weight	1984 lb
Propellant Requirement	<u>10 000 lb</u>
Total	11 984 lb

Since this subsystem incorporates gimbaling the thrust vector control ( TVC) it is not necessary to include a monopropellant requirement as for the solid propellant engine.

Single Bipropellant Thrust Chamber for Combined Propulsion Requirements. The modified LEMDE subsystem discussed above has the capability of two-thrust level operation, i. e. , 10 500 lb and 1050 lb. For retropropulsion with this subsystem the weight estimates in the preceding section are the same, so only the desirability of the 1050 lb thrust level for TC/OT utilization need be considered here.

For a spacecraft weight of 20 000 lb and a desirable  $\Delta V$  trajectory correction of 1 meter/sec with a maximum allowable error of 0. 1 meter/sec it is necessary to provide an impulse of approximately 2000 lb-sec minimum with a maximum allowable deviation of 200 lb-sec. For a trajectory correction of 0. 1 meter/sec with a maximum allowable

deviation of 0.01 meter/sec the impulse requirement is 200 lb-sec minimum with a maximum allowable deviation of 20 lb-sec. The modified LEMDE system can probably achieve the 1 meter/second maneuver keeping well within the allowable deviation, but information is not complete concerning minimum impulse bit, etc., for complete evaluation.

Discussion and Selection. Obviously, each subsystem described above offers certain advantages as a candidate for selection. Other subsystems exist which could be evaluated also for the JOVE vehicle.

The modified LEMDE subsystem with separate TC/OT provision has been shown to be favorably comparable with the modified Minuteman solid propellant subsystem from the standpoint of weight. It has a distinct advantage since midcourse chamber throttling is not required for TVC since the modified Minuteman could require a significant increase in the size of the TC/OT subsystem for TVC purposes. The modified LEMDE provides the minimum thrust level prescribed for JOVE (9000 lb) without the very high initial thrust accompanying the operation of a solid propellant engine.

The combined system consisting of the modified LEMDE would afford a weight reduction in TC/OT provision, assumed to be small. This subsystem provides no redundancy for trajectory correction and orbit trim maneuvers. Propellant acquisition could be a serious problem with this configuration.

With the modified LEMDE and a separate TC/OT subsystem, use of the main thrust chamber represents a desirable back-up mode for TC/OT. This configuration allows the main retropropulsion thrust chamber to be sealed off until it is prepared for the orbit insertion maneuver. Operation of the TC/OT subsystem can be used to settle the propellant before retropropulsion and thereby reduce the acquisition problem.

For the reasons above, along with the fact that the LEMDE has been designed to be man-rated, implying a very high reliability goal, the initial concept of JOVE will incorporate a modified LEMDE subsystem with a separate subsystem for TC/OT.

## RETROPROPULSION SUBSYSTEM CALCULATIONS

### Propellant Requirements

For the subsystem selected in the previous section the propellant consumption depends upon the required velocity increment for the mission and the net injection weight of the spacecraft. Propellant storage design is based on the attractive capability of the modified LEMDE, with tank sizing to permit a mass ratio of 2.5 maximum corresponding to a velocity increment of 2690 meters/sec. For a net injection weight of 18 500 lb this



corresponds to a propellant consumption of 11 000 lb for a typical specific impulse of 300 sec as seen in Figure VI-3.

The weight of hydrazine blend fuel required is obtained from the mixture ratio as

$$W_H = \frac{W_p}{1+R}$$

and the weight of oxidizer required is

$$W_o = \frac{RW_p}{1+R} .$$

## Bipropellant Storage Calculations

The hydrazine and oxidizer volumes are given by

$$V_H = \frac{W_p}{\rho_H (1+R)}$$

$$V_o = \frac{RW_p}{\rho_o (1+R)} .$$

The fuel and oxidizer tank requirements must include, additionally, screens to minimize sloshing, an ullage allowance, and an allowance for trapped fluids. If the additional volume is expressed as a fraction of the expelled fluid volume, then the required tank volumes are

$$V_{HT} = \frac{(1+V_H^*)}{\rho_H (1+R)} W_p$$

$$V_{OT} = \frac{(1+V_o^*) R}{\rho_o (1+R)} W_p .$$

The basic JOVE spacecraft provides 91.8 ft<sup>3</sup> for oxidizer storage and 79.2 ft<sup>3</sup> for hydrazine storage. Considering 50-50 hydrazine-UDMH and nitrogen tetroxide, a typical set of retropropulsion parameters are specified as

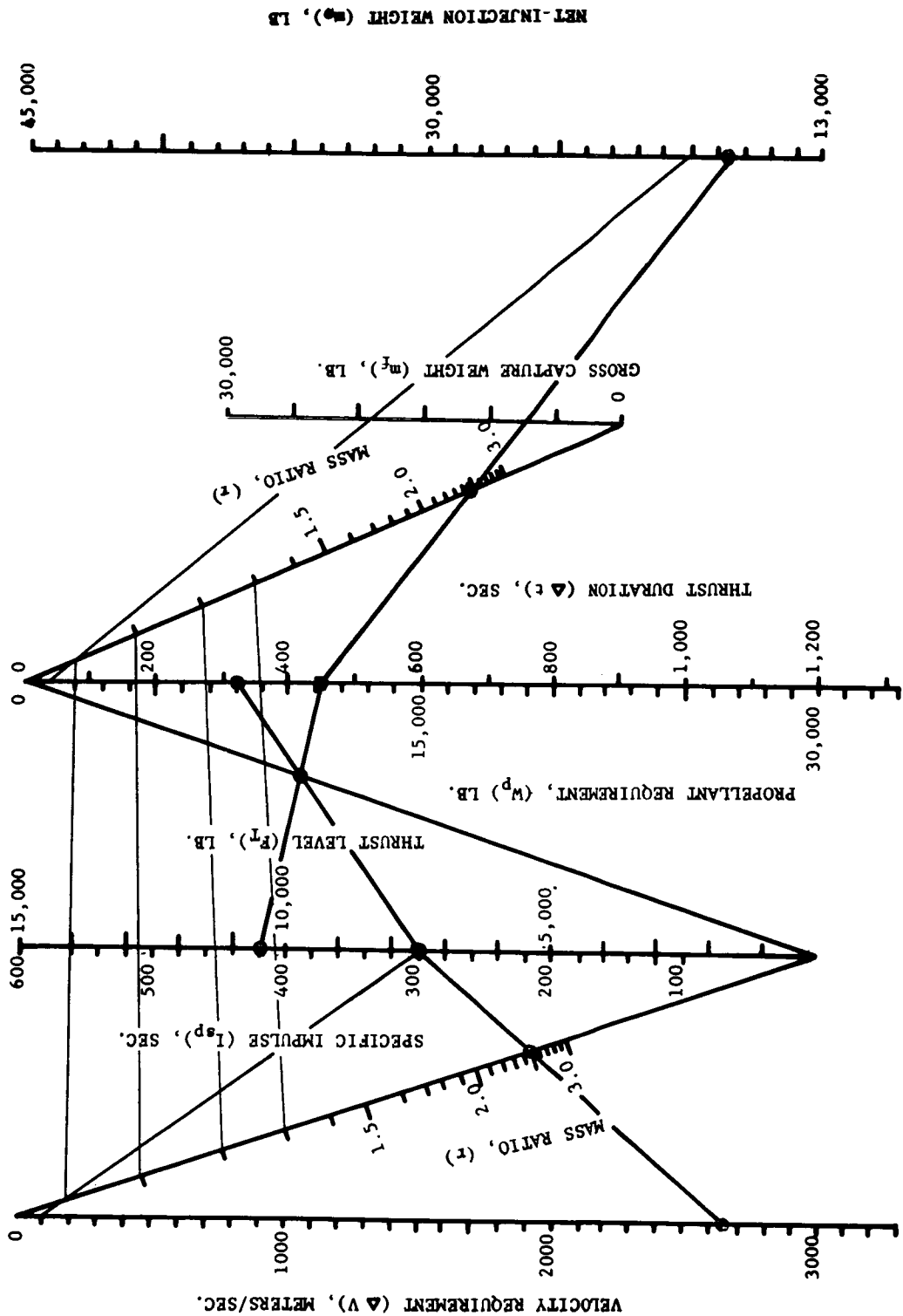


FIGURE VI-3. PROPELLANT REQUIREMENTS - TANK SIZING ANALYSIS

$$W_p = 11\ 100\ \text{lb}$$

$$R = 2.0$$

$$\rho_o = 85.5\ \text{lb/ft}^3$$

$$\rho_H = 49.8\ \text{lb/ft}^3$$

The volumes and weights of expelled hydrazine and oxidizer are

$$V_H = \frac{11\ 100}{(49.8)(3.0)} = 74.2\ \text{ft}^3$$

$$V_o = \frac{(11\ 100)(2)}{(85.5)(3.0)} = 86.5\ \text{ft}^3$$

$$W_H = \frac{11\ 100}{3} = 3700\ \text{lb}$$

$$W_o = \frac{(11\ 100)(2)}{3} = 7400\ \text{lb}$$

From these values the tank factors  $V^*$  are calculated as

$$V^* = 0.0675$$

$$V_o^* = 0.0615$$

Although typical values are not known for these factors, they probably should exceed 0.10 for consideration of ullage as well as trapped propellant. This is not explored since there is growth potential present in the basic design, and the possibility exists also for reduction in tank size and weight for lesser mission requirements than those specified in the sizing study.

## Pressurant Requirements

The operating pressure of the LEMDE thrust chamber is 220 psia. Common storage is used for both LEMDE and TC/OT pressurant. The selected pressurant is helium, stored at 3500 psia. For the LEMDE subsystem the weight of pressurant gas required, assuming adiabatic expansion, is

$$W_{PG} = \frac{(V_{HT} + V_{OT}) P_2}{R T_1} \left( \frac{k}{1 - \frac{P_2}{P_1}} \right)$$

and the required tank volume is

$$V_{PG} = W_{PG} \frac{R T_1}{P_1} = \frac{\frac{P_2}{P_1}}{1 - \frac{P_2}{P_1}} (V_{HT} + V_{OT})$$

For the following typical values,

$$P_2 = 220 \text{ psia}$$

$$P_1 = 3500 \text{ psia}$$

$$R = 386 \frac{\text{ft-lb}}{\text{lb} \cdot \text{R}}$$

$$k = 1.66$$

$$V_{HT} + V_{OT} = 171 \text{ ft}^3 \text{ (calculated previously)}$$

The weight and required volume are calculated for the pressurant

$$W_{PG} = \frac{220(171)(144)(1.66)}{386(530)(0.9372)} = 46.9 \text{ lb}$$

$$V_{PG} = \frac{1.66(0.0628)}{0.9372} = (171) = 19.05 \text{ ft}^3$$

The size and weight of two pressurant tanks, two feet in diameter, cylindrical, with hemispherical ends, based on the above volume is calculated from

$$W_{PGT} = \frac{2\rho_s t}{r} [V_{PGT} + \frac{2}{3}\pi r^3]$$

For  $\rho_s = 0.16 \text{ lb/ft}^3$ ,  $t = 0.66 \text{ in.}$ ,

$$W_{\text{PGT}} = \frac{2(0.16)(1728)(0.66)}{12(1)} \left[ 19.05 + \frac{2(3.14)}{3} \right] = 643 \text{ lb}$$

Considering common pressurant storage a small amount of this weight should be contributed to the TC/OT subsystem, but the difference is negligible.

## Subsystem Weight

In the preliminary design study mentioned previously, General Electric estimated the inert weight breakdown for a LEMDE configuration similar to the one selected as the preferred configuration for JOVE. These estimates, where applicable (thrust chamber, plumbing, etc.), are used to obtain an estimate for the basic retropropulsion subsystem discussed in the preceding sections.

### ESTIMATED INERT WEIGHT BREAKDOWN-JOVE RETROPROPULSION

Thrust Chamber (GE)	399 lb
Propellant Feed System	
Propellant Tanks	580 lb
Plumbing (GE)	57 lb
Trapped Propellant (GE)	474 lb
Pressurization System	
Pressurant Tanks (with fittings)	700 lb
Plumbing (GE)	36 lb
Helium	47 lb
Miscellaneous Hardware	25 lb
Structure (GE)	<u>206 lb</u>
TOTAL PROPULSION INERT WEIGHT	2524 lb

# TRAJECTORY CORRECTION/ORBIT TRIM (TC/OT) PROPULSION SUBSYSTEM DESIGN

## Introduction

The TC/OT propulsion subsystem synthesis, selection and design is based on the general requirements discussed previously, as well as on considerations introduced by the selection of the modified LEMDE subsystem for orbit insertion. Without the additional requirement of TVC the subsystem is required to provide only the trajectory correction and orbit trim functions, except for possible utilization for propellant acquisition purposes.

## Subsystem Synthesis

Either a monopropellant or a bipropellant system is considered to be the best choice for the TC/OT subsystem. Since positive propellant acquisition is essential for this subsystem, the use of bladders must be considered. The Mariner vehicles have used butyl rubber bladders in the case of monopropellants for several months duration, while bipropellant applications of bladders have been of limited duration. The indication is that a monopropellant subsystem lends itself better to the JOVE design, although a bipropellant subsystem would provide a weight savings. The most practical arrangement is to pair the monopropellant thrusters for symmetrical orientation about one or another of the major control axes. Two symmetrical pairs (4) provide an attractive back-up mode of operation for engine-out capability.

## Subsystem Sizing and Selection

The sizing of the TC/OT subsystem involves a trade-off of thrust level, thrust duration, and  $\Delta V$  capability, subject to practical hardware constraints.

It is desirable to avoid extremely long durations of thrust because of time dependent errors in guidance accuracy and propulsion operation. It is necessary to limit the thrust level since there exists a minimum possible thrust duration which controls the minimum impulse and therefore the minimum  $\Delta V$  provision.

The thrust duration for the TC/OT subsystem for a given maneuver is given by

$$\Delta t = \frac{m_o \Delta V}{g_e F_T}$$

This equation can be solved for maximum or minimum thrust level corresponding to minimum or maximum  $\Delta t$ , respectively.

$$(F_T)_{\min.} = \frac{(m_o)_{\max.} (\Delta V)_{\max.}}{g_c (\Delta t)_{\max.}}$$

$$(F_T)_{\max.} = \frac{(m_o)_{\min.} (\Delta V)_{\min.}}{g_c (\Delta t)_{\min.}}$$

For subsystem sizing the following ranges were assumed for spacecraft weight, velocity increment, and thrust duration.

$$5000 < m_o < 40\,000 \text{ lb}$$

$$0.1 < \Delta V < 150 \text{ meters/sec}$$

$$0.025 < \Delta t < 1000 \text{ sec}$$

Subsystem thrust range corresponding to these values is found to be

$$602 < F_T < 2040 \text{ lb}$$

Practical consideration of existing hardware and subsystem weight lead to the choice of the lower thrust level of 602 lb. This is equivalent to four (4) 150 lb thrusters in a symmetrical arrangement as described previously.

## Subsystem Design and Analysis

In the design and analysis of the TC<OT subsystem the mission and system parameters, thrust, spacecraft weight, velocity requirement, thrust duration, propellant requirement, and specific impulse of the propellant, are related through the relations:

$$F_T = \frac{m_o \Delta V}{g_c \Delta t}$$

and

$$W_P = \frac{m_o \Delta V}{g_c I_{sp}}$$

The total subsystem weight is considered to be the sum of the weights of propellant loaded, propellant tanks, pressurant, pressurant tanks, bladder configuration and combined fixed hardware as given by

$$W_{\text{system}} = W_H + W_{\text{HT}} + W_{\text{PG}} W_{\text{PGT}} + W_B + W_{\text{COM}}$$

Hydrazine and Hydrazine Storage Weights. The total required weight of hydrazine will include the weights of the expected consumption, specific impulse degradation contingency,  $\Delta V$  reserve contingency and an explosion efficiency contingency. The total weight is expressed as

$$W_H = \left( \frac{1 + \alpha_H + \frac{\delta \Delta V}{\Delta V}}{\epsilon} \right) W_P$$

The hydrazine storage volume must accommodate the bladder and the required hydrazine and must include an ullage factor. The total required volume is

$$V_{\text{HT}} = \left( 1 + \frac{V_B}{V_H} + \frac{V_{\text{ull}}}{V_H} \right) V_H$$

where  $V_H$  is obtained from the hydrazine weight as

$$V_H = \frac{W_H}{\rho_H} = \left( \frac{1 + \alpha_H + \frac{\delta \Delta V}{\Delta V}}{\epsilon} \right) \frac{W_P}{\rho_H}$$

So, expressing  $W_H$  and  $V_{\text{HT}}$  in terms of the net injection weight and  $\Delta V$  requirement

$$W_H = \left( \frac{1 + \alpha_H + \frac{\delta \Delta V}{\Delta V}}{\epsilon} \right) \frac{m_o \Delta V}{I_{\text{sp}} g_c}$$

$$V_{\text{HT}} = \left( 1 + \frac{V_B}{V_H} + \frac{V_{\text{ull}}}{V_H} \right) \left( \frac{1 + \alpha_H + \frac{\delta \Delta V}{\Delta V}}{\epsilon} \right) \frac{m_o \Delta V}{\rho_H I_{\text{sp}} g_c}$$

For the basic JOVE design a storage configuration for the monopropellant was selected as two cylindrical tanks, two feet in diameter with hemispherical ends. The weight of this configuration is



$$W_{HT} = \frac{2\rho_s t}{r} \left[ V_{HT} + \frac{2}{3} \pi r^3 \right]$$

or, in terms of the basic parameters

$$W_{HT} = \frac{2\rho_s t}{r} \left[ \left( 1 + \frac{V_B + V_{ull}}{V_H} \right) \left( \frac{1 + \alpha_H + \frac{\delta\Delta V}{\Delta V}}{\epsilon} \right) \frac{m_o \Delta V}{\rho_H I_{sp} g_c} + \frac{2}{3} \pi r^3 \right]$$

Pressurant and Pressurant Storage Weights. The weight of the pressurant gas required, assuming adiabatic expansion, is

$$W_{PG} = \frac{P_2 V_{HT}}{R T} \left( \frac{k}{1 - \frac{P_2}{P_1}} \right)$$

The corresponding storage volume required is

$$V_{PG} = \frac{P_2/P_1}{1 - \frac{P_2}{P_1}} k V_{HT}$$

For common storage of LEMDE and TC/OT pressurant, the additional tank weight for TC/OT is considered to be

$$W_{PGT} = \frac{2\rho_s t'}{r'} V_{PG}$$

Hence, in terms of system and mission requirements

$$W_{PG} = \left( \frac{k}{1 - \frac{P_2}{P_1}} \right) \left( \frac{P_2}{R T} \right) \left( 1 + \frac{V_B}{V_H} + \frac{V_{ull}}{V_H} \right) \left( \frac{1 + \alpha_H + \frac{\delta\Delta V}{\Delta V}}{\epsilon} \right) \frac{m_o \Delta V}{\rho_H I_{sp} g_c}$$

$$W_{PGT} = \left( \frac{k}{1 - \frac{P_2}{P_1}} \right) \left( \frac{P_2}{P_1} \right) \left( \frac{2\rho_s t'}{r'} \right) \left( 1 + \frac{V_B}{V_H} + \frac{V_{ull}}{V_H} \right) \left( \frac{1 + \alpha_H + \frac{\delta\Delta V}{\Delta V}}{\epsilon} \right) \frac{m_o \Delta V}{\rho_H I_{sp} g_c}$$

Bladder and Hardware Weights. The weight of the bladder material is expressed

as

$$W_B = \rho_B \left( \frac{V_B}{V_H} \right) \left( \frac{1 + \alpha_H + \frac{\delta \Delta V}{\Delta V}}{\epsilon} \right) \frac{m_o \Delta V}{\rho_H I_{sp} g_c}$$

The weight of the combined hardware consists of structure, engine and plumbing weights.

Inert Subsystem Weight. The inert subsystem weight includes the weights of the tanks for hydrazine and pressurant along with the bladder and hardware weights. This is expressed as

$$W_{inert} = \left( \frac{1 + \alpha_H + \frac{\delta \Delta V}{\Delta V}}{\epsilon} \right) \frac{m_o \Delta V}{\rho_H I_{sp} g_c} \left\{ 2\rho_s \left( 1 + \frac{V_B}{V_H} + \frac{V_{ull}}{V_H} \right) \left( \frac{t}{r} + \frac{k \frac{P_2}{P_1} \frac{t'}{r'}}{1 - \frac{P_2}{P_1}} \right) + \rho_B \left( \frac{V_B}{V_H} \right) \right\} + \frac{4}{3} \pi \rho_s t r^2 + W_{COM}$$

The following values for JOVE are selected for the parameters involved in the inert subsystem weight:

$$\alpha_H = 0.01$$

$$\frac{V_B}{V_H} = 0.02$$

$$\frac{\delta \Delta V}{\Delta V} = 0.05$$

$$\frac{V_{ull}}{V_H} = 0.01$$

$$\epsilon = 0.95$$

$$\frac{P_2}{P_1} = 0.0625$$

$$m_o = 18\,500 \text{ lb}$$

$$\rho_H = 50 \text{ lb/ft}^3$$

$$\Delta V = 250 \text{ meters/sec}$$

$$\rho_s = 0.16 \text{ lb/in}^3$$

$$I_{sp} = 235 \text{ sec}$$

$$\rho_B = 70 \text{ lb/ft}^3$$

$$t = 0.05 \text{ in.}$$

$$W_{COM} = 0.1 W_{inert}$$

$$t' = 0.66 \text{ in.}$$

$$r = 24 \text{ in.}$$

$$r' = 12 \text{ in.}$$

Then

$$\begin{aligned}
 W_{\text{inert}} &= \frac{(1.15)(18500)(250)(3.281)}{(0.95)(0.90)(50)(32.2)(235)} \left\{ 2(0.16)(1728)(1.12) \right. \\
 &\quad \times \left. \frac{0.05}{24} + \frac{1.67(0.0625)(0.66)}{(0.09375)} + 70(0.02) \right\} \\
 &\quad + \frac{\frac{4}{3}(3.14)(0.16)(0.05)(24)^2}{0.9} = 54.2(5.08 + 1.4) + 21.4 = 372.4 \text{ lb}
 \end{aligned}$$

## ATTITUDE CONTROL PROPULSION SUBSYSTEM CALCULATIONS

### Thrust Level Requirements

The thrust level requirement for the attitude control system is determined by pertinent constraints on expected response. For JOVE the selected constraint is the maximum excursion angle through which the spacecraft is permitted to travel following a micrometeoroid impact.

The maximum disturbance torque, corresponding to a micrometeoroid collision, is

$$T_{\text{max.}} = \frac{M^2 \bar{V}^2 b^2}{2I \theta_f} .$$

The torque developed by the attitude control system is

$$T = \frac{\Delta t}{t} F_T \ell .$$

After substituting for maximum torque, the minimum thrust level may be obtained as

$$F_T = \frac{M^2 \bar{V}^2 b^2}{2I \theta_f \ell} \left( \frac{t}{\Delta t} \right) .$$

For sizing, typical values for JOVE are selected for the parameters as

$$M = 6.85 \times 10^{-6} \text{ slugs (0.1 gm)}$$

$$\left( \frac{t}{\Delta t} \right) = 3$$

$$\bar{V} = 6.562 \times 10^4 \text{ ft/sec}$$

$$b = 25 \text{ ft}$$

$$l = 20 \text{ ft}$$

$$I = 3\,000 \text{ slugs-ft}^2$$

$$\theta_f = 0.0349 \text{ rad}$$

Then, the minimum thrust level is calculated as

$$F_T = \frac{(6.85)^2 \times 10^{-12} \times (6.562)^2 \times 10^8 \times (6.25) \times 10^2 \times 3}{2(3000) (3.49) \times 10^{-2} \times 20}$$

## Impulse Requirements

The minimum total impulse requirement corresponds to use of the minimum possible pulse width in the limit cycle operation.

For limit cycling the angular rate is computed as

$$\dot{\theta} = \frac{\Delta I \ell}{2I} = \frac{F_T \Delta t \ell}{2I} \quad .$$

The pulse spacing is

$$t_1 = \frac{4\theta_E I}{F_T \Delta t \ell} \quad .$$

The impulse per axis is

$$J = \frac{(\Delta I)^2 \ell P}{2I \theta_E} = \frac{F_T^2 (\Delta t)^2 \ell P}{2I \theta_E}$$

and the total impulse requirement for three axes is

$$I_T = \frac{3}{2} \frac{(\Delta I)^2 \ell P}{I \theta_E} = \frac{3}{2} \frac{F_T^2 (\Delta t)^2 \ell P}{I \theta_E} \quad .$$

Typical values for JOVE of the parameters associated with normal limit cycle operation are selected as

$$F_T = 0.0905 \text{ lb}$$

$$\Delta t = 0.025 \text{ sec}$$

$$\theta_E = 0.00349 \text{ rad}$$

$$P = 7.8 \times 10^7 \text{ sec}$$

The following values are calculated for angular rate, pulse spacing and total impulse

$$\dot{\theta} = \frac{0.0905(0.025)(20)}{2(3000)} = 7.55 \times 10^{-6} \text{ rad/sec}$$

$$t_1 = \frac{4(0.00349)(3000)}{0.0905(0.025)(20)} = 9.27 \times 10^2 \text{ sec}$$

$$I_T = \frac{3}{2} \frac{(9.05)^2 \times (2.5)^2 \times 20 \times 7.8}{(3000)(0.0349)} = 1142 \text{ lb-sec}$$

## Propellant Requirements

The amount of high pressure  $N_2$  that is discharged in limit cycle operation is  $I_T/I_{sp}$ . The value of specific impulse depends upon the degree of expansion and is limited by the saturation temperature of the pressurant. Allowing for specific impulse degradation, total impulse requirements, and residual gas the weight of high pressure  $N_2$  is

$$W_{N_2} = \beta_P \frac{I_T}{I_{sp}} \left( \frac{1 + \alpha_P}{1 - \frac{P_f T_i}{P_i T_f}} \right)$$

The required storage volume is

$$V_{N_2} = \frac{R T}{P_i} W_{N_2}$$

The required storage volume is

$$V_{N_2} = \frac{RT}{P_i} W_{N_2}$$

Typical values for JOVE are selected for the redundant storage, specific impulse, degradation, temperatures, and pressures as

$$\beta_P = 2.0$$

$$I_{sp} = 56 \text{ sec}$$

$$\alpha_P = 0.10$$

$$P_f = 150 \text{ psia}$$

$$P_i = 3000 \text{ psia}$$

$$T_i = T_f = 530^\circ \text{ R}$$

The storage requirements are calculated from these as

$$W_{N_2} = 2 \frac{(1142) (1.10)}{(56) (0.95)} = 47.2 \text{ lb}$$

$$V_{N_2} = \frac{(55.15) (530)}{(144) (3000)} (47.2) = 3.18 \text{ ft}^3$$

## Discussion

The calculations in the preceding sections do not consider the impulse requirements corresponding to acquisition modes, disturbance torques, etc., but are typical for normal limit cycle operation. The basic design incorporates additional AC/S storage capacity (7.2 ft<sup>3</sup>) which should provide amply for all requirements.

## SUMMARY

The retropropulsion subsystem is designed to provide a total impulse of up to  $3.25 \times 10^6$  lb-sec with 50-50 N<sub>2</sub>H<sub>4</sub>/UDMH and N<sub>2</sub>O<sub>4</sub> as fuel and oxidizer. The inert weight of the subsystem is estimated as 2524 lb for this impulse requirement. The design incorporates a growth potential of approximately 15-20 percent.

The TC/OT subsystem is designed to provide a total impulse of up to  $4.2 \times 10^5$  lb-sec with hydrazine as monopropellant. The inert weight of the subsystem is estimated as 372 lb for this impulse requirement. There is a possibility for growth potential.

The AC/S subsystem is designed to provide a total limit cycle impulse of 1142 lb-sec with high pressure  $N_2$ . The existing design permits considerably greater storage.

## REFERENCE


1. Propulsion System Analysis. Voyager Spacecraft System Phase 1A Task B Preliminary Design, vol. C, General Electric, January 1966.

## BIBLIOGRAPHY

Alternate Designs Considered. Voyager Spacecraft System Preliminary Design, vol. B. General Electric, July 1965.

A Study of Jupiter Flyby Missions. Final Technical Report, General Dynamics, May 1966.





**CHAPTER VII**

**GUIDANCE AND CONTROL SYSTEM**

## CHAPTER VII. GUIDANCE AND CONTROL SYSTEM

### DEFINITION OF SYMBOLS

$\dot{\phi}_n$	Angular search rate in pitch and yaw
a	Acceleration in degrees/sec <sup>2</sup>
T	Torque in ft-lb
I	Moment of inertia in slug-ft <sup>2</sup>
t	Time in seconds
$\dot{\phi}_r$	Angular roll search rate
ACS	Attitude Control System

# INTRODUCTION

The functions of interest in this section are: (1) estimation of the position and velocity of the spacecraft, (2) prediction of terminal errors and steering, and (3) attitude determination and control. The implementation of these functions can be divided up in many ways between "on board" systems and Earth-based tracking and data processing facilities. Practical considerations based on the present state-of-the-art result in the decision that the attitude sensing and vehicle maneuvering associated with guidance corrections or steering operations can be performed by on board components while the position and velocity of the spacecraft and the nature of the required vehicle maneuvers are determined by Earth-based facilities.

Using these constraints, a basic control concept has been worked out for the JOVE mission which makes use of previously developed concepts from the Mariner and Voyager projects. It is characterized by several pertinent features. Optical sensors on board the spacecraft are used to provide attitude reference. The Deep Space Instrumentation Facility (DSIF) is used to track the spacecraft and guidance corrections are determined by an Earth-based computer making use of the tracking information. A central computer and sequencer (CC&S) on the spacecraft provides master timing for all spacecraft systems and translates guidance commands into control signals for the attitude control actuators, the mid-course propulsion system, and the primary propulsion system. Possible variations in the design of the guidance and control system are discussed briefly.

Specific functions to be performed by the guidance and control system are:

1. Acquisition of external references.
2. Pointing of the spacecraft such that the fixed high-gain antenna points toward Earth.
3. Midcourse corrections.
4. Orbital injection control.
5. Orbit trim maneuvers.
6. Orientation of scientific scan platform.

The guidance and attitude control functions cannot be performed independently. Attitude control, however, is mainly concerned with controlling the spacecraft with respect to the three-degrees-of-freedom that determine the motion of the body around its center of mass. The guidance system controls the spacecraft with respect to the other three degrees-of-freedom which locate the center of the mass. The main difference between the two is that the attitude sensors are airborne while the location and velocity of the spacecraft are determined from Earth-based equipment.

## GUIDANCE SYSTEM

### Introduction

The term "guidance system" as used here includes two functions: a. the determination of the vehicle's position and velocity, and b. the computation of maneuvers required to achieve the desired end conditions. The implementation of these maneuvers is also discussed here. Alternate means of carrying out the guidance function using on-board sensors and computers are discussed in Appendix G, Volume II.

### Determination of Vehicle's Velocity and Position (Navigation)

The tracking and orbit determination of the spacecraft can be accomplished with the Earth-based DSIF system and an Earth-based computer, with on-board sensors and an Earth-based computer, or with a complete on-board system. The use of an on-board computer for trajectory determination and corrections does not appear feasible at the present time caused by a reliability problem over the long time period involved and because weight and power considerations for on-board computer make it impossible to provide a capability equal to that of an Earth-based computer. Consideration was given to an on-board guidance system in the vicinity of Jupiter because of the errors associated with tracking by the DSIF increase as the spacecraft moves away from Earth. It was decided, however, on the basis of previous studies [Ref. VII-1, VII-2] that the use of the DSIF for tracking purposes would result in a terminal error of less than 4000 to 5000 km. Since this error is satisfactory for a mission such as JOVE, it was decided that the position and velocity of the spacecraft should be determined by tracking with the DSIF. This information

is fed into the computer which is programmed to determine the best estimate of the actual trajectory and compare this with the nominal trajectory. On the basis of this comparison, the  $\Delta V$  required to correct the trajectory is computed. This is the same approach that has been used on the Mariner missions.

For more complicated missions which require greater accuracy than can be provided by DSIF, some form of on-board guidance will be required. A possibility for increasing the contribution of JOVE to the space effort would be to take advantage of the mission to test sensors or other instruments proposed for use on an on-board guidance system. For example, it has been suggested that the spacecraft position might be determined by multiple star tracking, or pattern recognition of groups of stars. Such a device might be placed on JOVE to determine its capabilities.

## Implementation of the Guidance Function

Based on the  $\Delta V$  requirements determined by the computer, commands are relayed to the spacecraft and stored in the Central Computer and Sequencer (CC&S). At the designated time, these commands are sent to the attitude control system, which switches automatically to the maneuver mode discussed in the previous section, and the spacecraft is realigned so that the thrust vector points in the direction of the required  $\Delta V$ . With the spacecraft oriented in this manner, the appropriate engine (TC/OT engines for mid-course and orbit trim maneuvers and the LEMDE for orbit insertion) is fired and continues to burn until the output of an integrator connected to an accelerometer indicates that the desired magnitude of  $\Delta V$  has been achieved. At this time the engine is automatically shut off and the spacecraft returns to its normal cruise mode.

## ATTITUDE CONTROL SYSTEM

### Introduction

The term "attitude control system" refers to the group of actuation devices and associated electronics which are employed to generate torques about the spacecraft axes for controlling the orientation to some desired condition. In this section, design criteria associated with the problem of achieving the desired attitude control of the spacecraft are considered. The resulting attitude control

system is quite similar to those proposed for Voyager, which in turn will use the same basic control concepts successfully flown on Mariner. The principal improvements required for a Jupiter mission appear to be in the area of reliability for the much longer time periods involved. It is anticipated that state-of-the-art advances in control system components will provide the required degree of reliability.

## Attitude Control Concepts

Attitude control concepts can generally be classified as passive, semi-passive, or active. Passive control systems make use of either spin-stabilization techniques or environmental fields such as gravity, solar radiation pressure, or magnetic fields. Active control systems use either external control moments or momentum storage devices, or both. Semipassive control systems make use of both passive and active control techniques. Such a system combines the utilization of the torques available from an environmental field (or spin-stabilization) with the improved performance in terms of response time and maneuver capability of an active system. An example of this type system is on Mariner IV [Ref. VII-3] where a semipassive technique made use of solar radiation pressure in conjunction with an active attitude control system using cold gas jets.

Spin-stabilization is the only passive method that has been extensively implemented as a primary means of spacecraft control. The utilization of environmental fields as a primary means of spacecraft control is severely limited because of the resulting extremely low speed of response and limited acceleration capability. Furthermore, for a deep space mission such as JOVE, solar pressure is the only environmental effect of any appreciable significance except in the vicinity of Jupiter, and it decreases rapidly as the spacecraft travels away from the sun. The nature of the spacecraft's orbit about Jupiter precludes any worthwhile utilization of the gravity or magnetic fields of Jupiter for passive control purposes.

In light of the remarks above, the basic choice among attitude control concepts is between spin-stabilization and three-axis stabilization with an active attitude control system. Spin-stabilization is attractive in those cases where the scientific mission is limited and low-accuracy inertial orientation of only one spacecraft axis is sufficient to meet the system requirements. On a deep space mission with the capability proposed for JOVE, three-axis stabilization provides more precise midcourse and orbit control, simpler implementation in pointing the high-gain, narrow beamwidth antenna towards Earth, improved TV resolution, and more flexibility. For these reasons, a three-axis stabilized spacecraft is chosen.

A system of active attitude control using cold gas jets is the best known technique, and it has been used extensively in a wide variety of spacecraft. Reaction wheels are momentum storage devices which might, for example, be used to provide a continuous control capability with a gas jet system being used to supply the relatively large torques required during spacecraft maneuvers and to backup the reaction wheels in case of large disturbances such as meteoroid impact or gimbaling of the planet scan platform. The advantages of such a system arise from the decreased amount of cold gas required and the increased reliability of the cold gas jet system caused by fewer operations required of the valves. Reaction wheels, however, are not suitable on a mission such as JOVE because of the long operating time involved. For this reason a cold gas jet system was chosen as the means of implementing the attitude control of the spacecraft.

Other systems which were considered to provide thrust for the attitude control system included monopropellant and bipropellant systems. Both these systems require a high degree of temperature control which is not required for cold gas systems. In addition, both systems must be operated at a higher minimum thrust level than cold gas if safe, reliable, and stable operation is to be achieved.

Electric propulsion systems have also been suggested to provide thrust for attitude control. The high electrical power requirements, however, and the lack of hardware development preclude the serious consideration of such systems for JOVE.

In the interests of a simple and conservative design, a cold gas jet system was chosen. A design option would be to use heat from the RTG's to heat the gas and thereby increase the specific impulse.

## Celestial References

The stabilization of the three-axis stabilized spacecraft will require suitably selected celestial bodies so that inertial directions are continuously known with respect to the vehicle. A Sun-Canopus reference system has been selected. The sun's brightness makes recognition easy and allows simple sensors to be used. Canopus is the brightest star in its area and has no undesirable near neighbors. Canopus is located approximately at right angles to the spacecraft trajectory so that the sun and Canopus provide orthogonal references.

## Operating Modes

The ACS must operate in three distinct modes in controlling the angular orientation of the spacecraft. These three modes are the acquisition mode, the cruise mode, and the maneuver mode. Based on information received from the three control loops, the sun gate sensors, the Command Decoder, and the Central Computer and Sequencer, the logic control unit switches the ACS to the proper operating mode.

Acquisition Mode. In this mode, the ACS rotates the spacecraft from any arbitrary attitude in order to accomplish acquisition of the sun and Canopus references. This is accomplished in the following sequence:

1. Gyros are on and operating in their rate mode.
2. Roll star sensors are initially locked out, with signals from the roll gyro used to limit roll rotation rates.
3. 360° acquisition sun sensors are used in pitch and yaw gyros.
4. When the sun is within the field of view of the cruise sun sensors, the acquisition sun sensors are switched out.
5. After acquisition of the sun, the spacecraft rolls about the roll axis in search of Canopus, with rate signals provided by the roll gyro.
6. With the sun and Canopus acquired, the gyros are switched off and the ACS switched to the cruise mode.

A simplified block diagram of the pitch and yaw acquisition and cruise modes with the switching required to switch between the two is shown in Figure VII-1. The coarse sun gate is used to implement switching from the acquisition sun sensors to the cruise sun sensor. The logic control unit switches the gyros out and the derived rate feedback network in when  $\Theta_r$  and  $\dot{\Theta}_r$  nulls indicate that Canopus has been acquired.



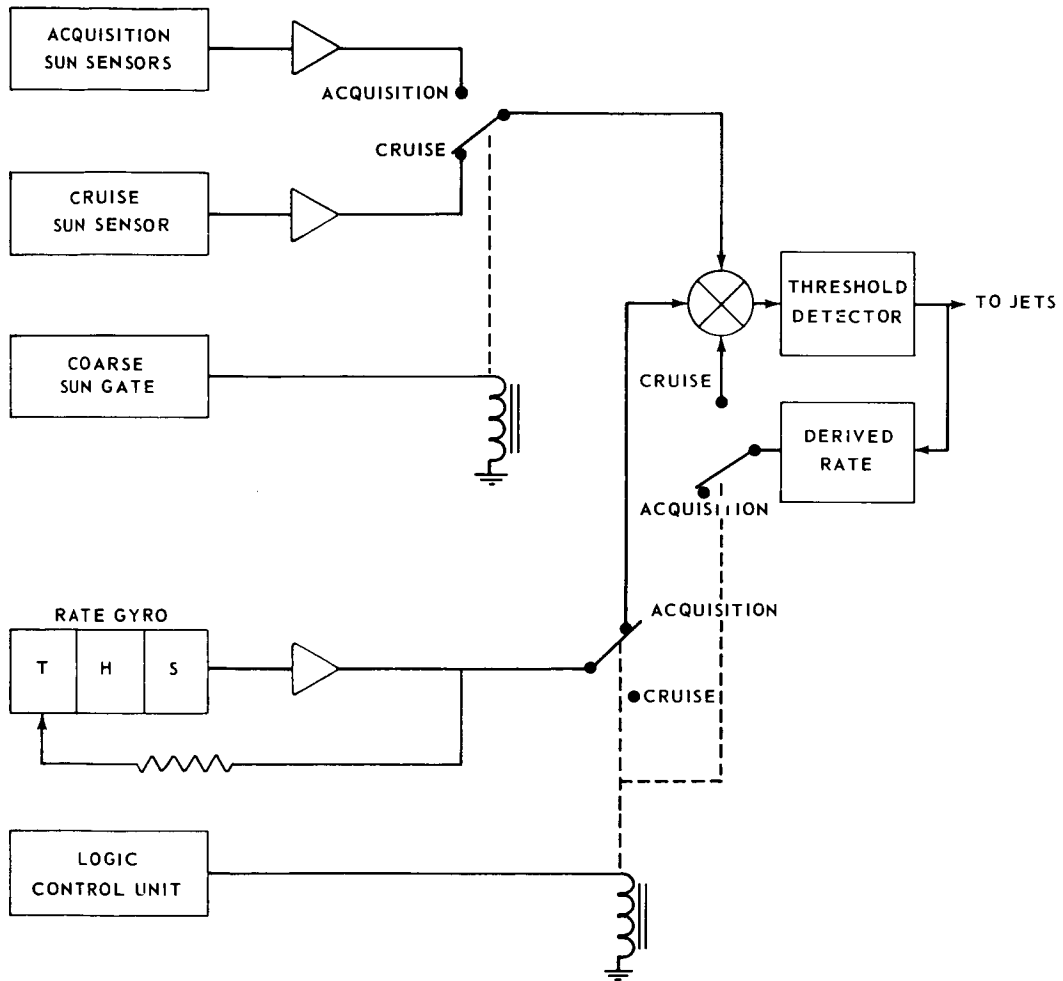


FIGURE VII-1. PITCH OR YAW ACQUISITION AND CRUISE MODES - SIMPLIFIED BLOCK DIAGRAM

Initial angular rates as high as 3 degrees/second about each axis are assumed for initial acquisition. Following a midcourse maneuver, the initial rates are approximately zero. Searching rates of 0.2 deg/sec in pitch and yaw and 0.1 deg/sec in roll are used. Sun acquisition time is the time spent in thrusting to the search rate ( $\dot{\phi}_n$ ) plus the time spent in coasting at this rate and decelerating to zero rate. The longest possible thrusting time for initial acquisition is the time required to decelerate from 3 deg/sec to 0 and then to  $\dot{\phi}_n$  and back to 0. The acceleration is given by

$$a = \frac{T}{I}$$

Substituting the values  $T = 0.603$  ft-lb and  $I = 3000$  slug-ft<sup>2</sup> gives a maximum thrusting time of  $t \approx 261 + 174 \left| \dot{\phi}_n \right|$  seconds ( $\dot{\phi}_n$  must be expressed in deg/sec). The sign of  $\dot{\phi}_n$  is chosen so that coasting will always be  $\leq 180$  degrees. This gives a maximum coasting time of  $180/\left| \dot{\phi}_n \right|$ . The maximum initial sun acquisition time is then

$$t_{\max.} = 261 + 174 \left| \dot{\phi}_n \right| + 180/\left| \dot{\phi}_n \right|$$

For  $\dot{\phi}_n = 0.2$  deg/sec, this time is approximately 19.9 minutes. For subsequent reacquisitions this time will be decreased by about 4.35 minutes since the initial rates will be zero.

The initial roll rates are reduced to zero during sun acquisition. The spacecraft may be required to roll almost a full 360° in order to locate Canopus. The maximum time involved (based on  $I_r = 3000$  slug-ft)<sup>2</sup> is

$$t_{\max.} = 87 \left| \dot{\phi}_r \right| + 360/\left| \dot{\phi}_r \right|, \text{ [where } \dot{\phi}_r \text{ is expressed in}$$

deg/sec]

Since  $\dot{\phi}_r = 0.1$  deg/sec, this maximum time is approximately 60 minutes.

Cruise Mode. Following acquisition of the sun and Canopus, the spacecraft operates in the cruise mode. The cruise mode pertains to normal operations of the spacecraft in orbit about Jupiter as well as during the interplanetary cruise, and is the mode in which the ACS will operate throughout most of the mission. This mode is characterized by the following:

1. The gyros are off.
2. The cruise sun sensor controls the pitch and yaw axes and the Canopus sensor controls the roll axis.
3. The ACS operates in a limit cycle mode with a deadband of  $\pm 2$  degrees for the first 270 days and  $\pm 0.2$  degree for the remainder of the mission.
4. Damping is provided by derived rate feedback around an on-off electronic switching amplifier which has a threshold equal to the deadband.
5. The nominal limit cycle rate is 0.0048 deg/sec.
6. The disturbance free fuel consumption is approximately 55 pounds (see Chapter VI).
7. Any non-catastrophic disturbance that results in the loss of either the sun or Canopus will cause the system to switch automatically to the acquisition mode.

Two possible orientations of the spacecraft during the cruise mode were considered. In one case the spacecraft roll axis would be pointed toward the sun and in the other case toward Earth. Some of the factors considered in the final decision are indicated in Table VII-1.

The primary consideration involved in the decision of how the spacecraft should be oriented was whether to gimbal the large, high-gain antenna or the sun sensor. On previous missions the sun sensor has been fixed due to the high degree of accuracy required for a primary reference. Because of the advantages in fixing the high-gain antenna, however, and on the assumption that it will be possible to gimbal the sun sensor with the required accuracy, it was decided to orient the spacecraft in the following manner.

During the first 270 days of the mission, the medium-gain antenna will be used and the limit cycle deadband limited to  $\pm 0.2$  degree in order to satisfy pointing requirements of the high-gain antenna. By orienting the spacecraft toward the sun for the first 270 days, the angle through which the sun sensor must be gimballed in the yaw axis is limited to  $\pm 15$  degrees (Fig. VII-2). If the sun sensor is also gimballed by about  $\pm 5$  degrees in the pitch axis, it will not be necessary to gimbal the Canopus sensor in the roll axis [Ref. VII-1].

TABLE VII-1. FACTORS CONSIDERED IN DETERMINING  
DESIRED ORIENTATION OF THE SPACECRAFT

<u>SUN-POINTING</u>	<u>EARTH-POINTING</u>
High-gain antenna must be gimballed	High-gain antenna can be fixed
Sun sensor can be fixed	Sun sensor must be gimballed
Flexible waveguide is required between the antenna and transponder	Rigid waveguide can be used between the antenna and transponder
Solar scan platform can be fixed	Solar scan platform must be gimballed

Consideration was also given to pointing the spacecraft toward the sun with a fixed antenna using electronic gimbaling. This concept was not adopted because of the complexity and lack of experience with such antennas for deep space communication. The concept is discussed in Volume II, Appendix E.

Maneuver Mode. In this mode the gyros are used to provide an inertial reference for controlling the spacecraft's attitude. This operating mode is used for:

1. Attitude reorientation for the midcourse velocity correction and orbit insertion.
2. Maintaining the desired attitude during thrusting.
3. Maintaining the spacecraft's attitude during sun or Canopus occultation.

For a midcourse velocity correction or orbit insertion maneuver, the attitude control functions are performed in the following manner:

1. The desired spacecraft attitude is determined by ground computation, transmitted to the spacecraft, and stored in the Central Computer and Sequencer prior to initiating the maneuver.

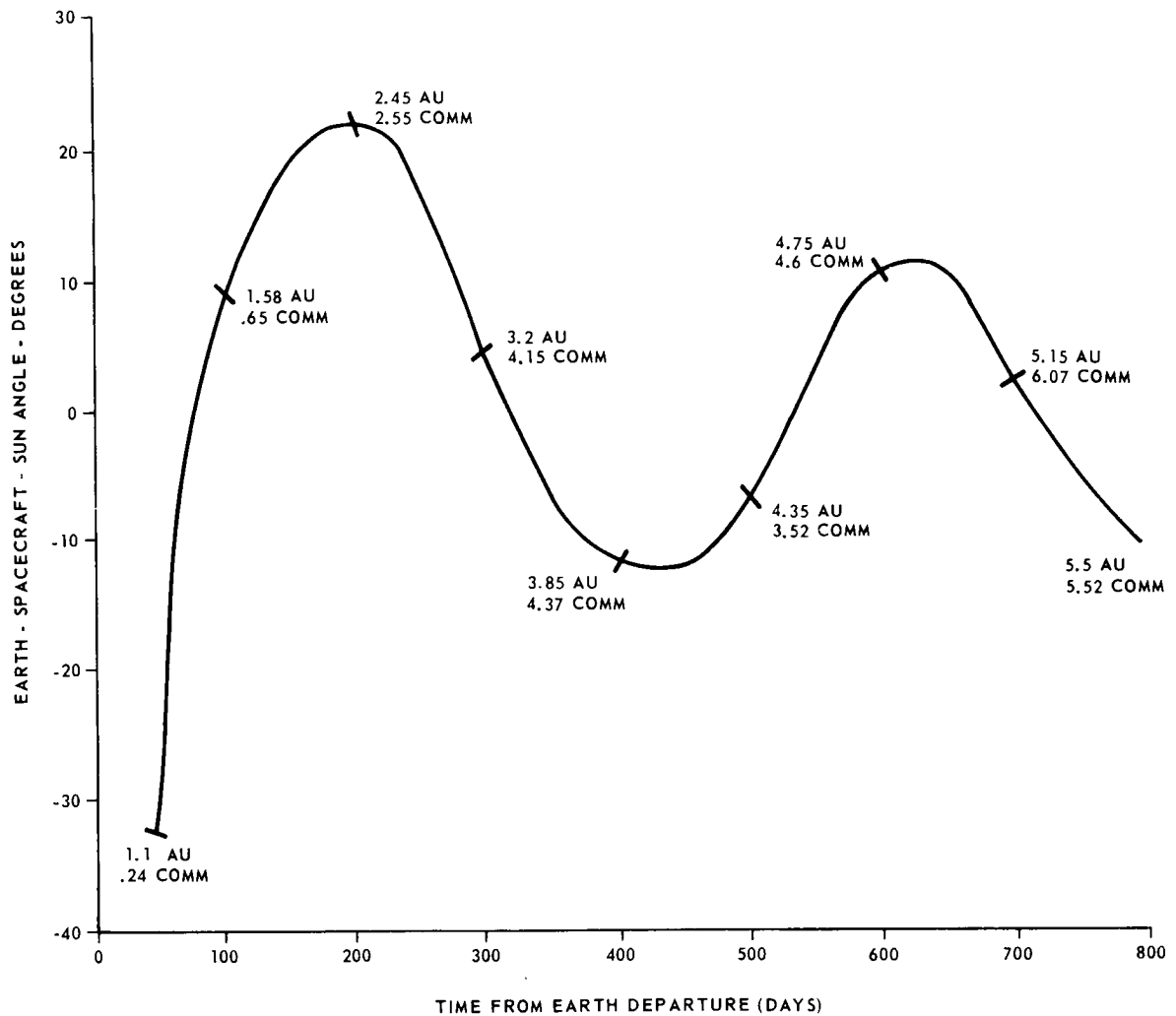


FIGURE VII-2. VARIATION OF EARTH-SPACECRAFT-SUN ANGLE WITH ELAPSED MISSION

2. The gyros are turned on before initiating the maneuver.
3. Based on information stored in the Central Computer and Sequencer, gyro torquing current generators produce a precision current to command the desired reorientation attitude.
4. The gyros operating in position mode provide the inertial reference for maintaining the spacecraft in the desired attitude until thrusting is completed.
5. During thrusting, the orientation of the spacecraft is controlled by gimbaling the engine providing the thrust.
6. When the required  $\Delta V$  is achieved, the engine is cut-off.
7. Upon completion of the desired maneuver, the ACS is switched to the acquisition mode for reacquisition of the sun and Canopus.

In case of occultation of the sun or Canopus, the gyros are turned on before the beginning of the occultation period. Command sequences are stored in the Central Computer and Sequencer for this period. During sun occultation the logic control unit automatically switches the pitch and yaw loops to inertial position control when the output of the sun sensors indicate the start of occultation. When the logic control unit determines that the sun is present, it switches the pitch and yaw loops back into the cruise mode configuration. For a Canopus occultation, the roll axis is switched to inertial reference for a period of time which includes the occultation period.

The operation of the ACS can be summarized with the aid of Figure VII-3. In the acquisition mode, the gyros provide rate signals which control the cold gas jet system as the spacecraft is oriented in the proper attitude with respect to the sun and Canopus. In the cruise mode, the gyros are turned off and the sun and Canopus sensors provide signals which provide control for the cold gas jets. In case of sun or Canopus occultation, the affected sensor is replaced by gyros operating in position mode. In the maneuver mode, the gyros operate in the rate mode while the spacecraft is being oriented to point the thrust vector in the desired correction. During the remainder of the maneuver, the gyros operate in position mode to provide an inertial reference for the ACS. During thrusting, the attitude is maintained by gimbaling the engine.

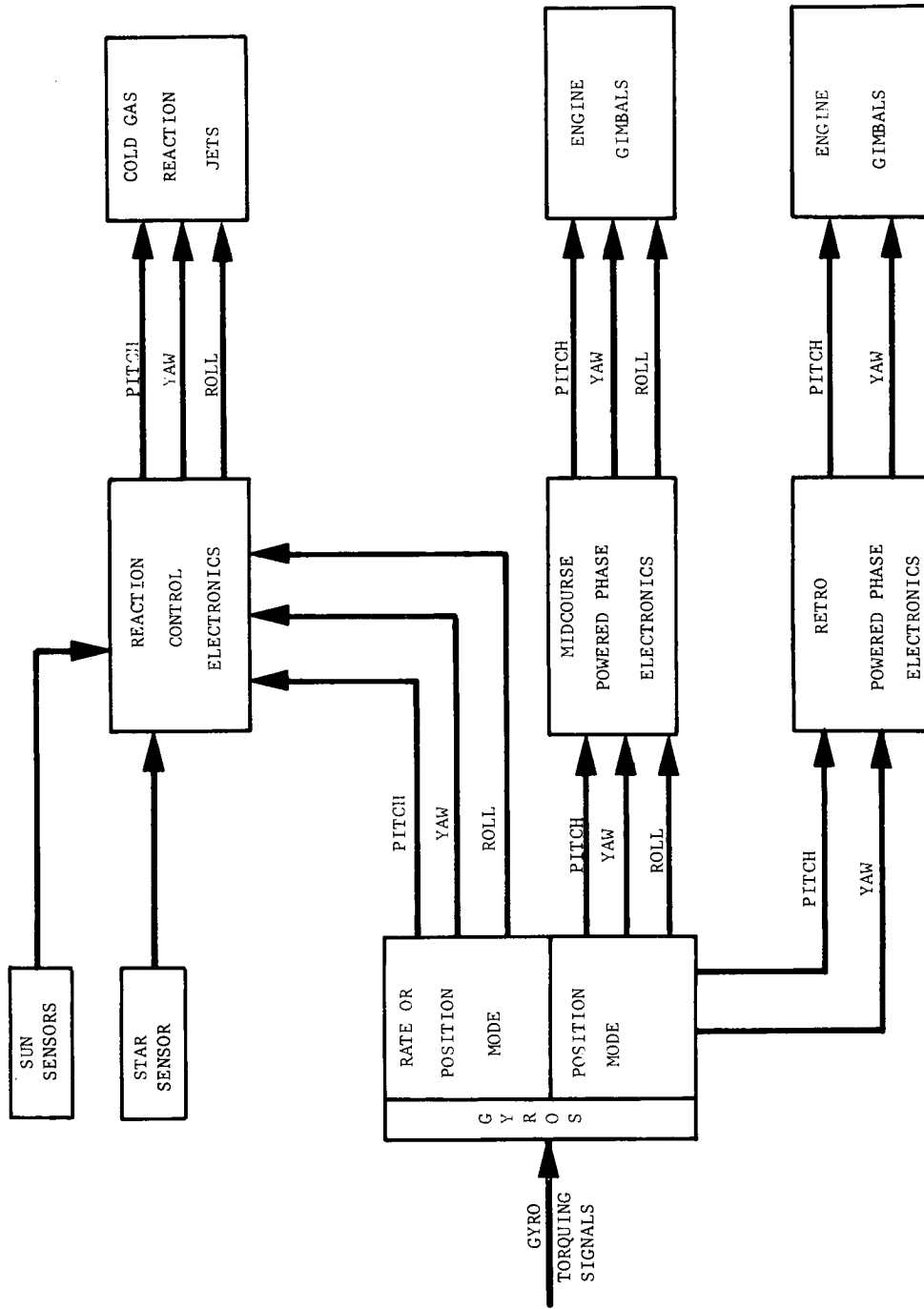


FIGURE VII-3. ON-BOARD CONTROL SYSTEM

## Cold Gas Jet System

The cold gas jet system contains two separate, identical gas systems similar to that used on Mariner IV. A typical arrangement of attitude control nozzles consists of four nozzles on each of the three axes (Fig. VII-4). Torques generated by the gas jet system are nominally applied to the vehicle as pure couples. With twelve nozzles, there are a total of six possible couples, one plus and one minus about each of the three control axes. A couple is generated by actuating a pair of gas jet thrusters. One of these thrusters will be a part of one of the gas systems while the second thruster will be a part of the other gas system. In case of failure of either jet of a couple to operate, the remaining jet will provide torque, although at half the design value. In order to further increase the reliability of each gas jet system, two solenoid valves are used in series with each nozzle to minimize the effect of excessive seat leakage or the failure of one of the solenoid valves to close. Each gas system will be charged with two times the mass required to overcome the effects of catastrophic leakage in one system.

Other systems considered to provide thrust for the attitude control system included monopropellant and bipropellant systems. Both these systems have the disadvantage of requiring a high degree of temperature control that is not necessary for cold gas. This is particularly important when the length of pipe required to connect the thrusters to the fuel tanks is considered. In addition, the minimum thrust level of both systems must be restricted to higher values than for cold gas if safe, reliable, and stable operation is to be achieved.

Electronic propulsion has also been suggested as a possible means of supplying torque for the ACS. However, the high electrical power requirements and lack of hardware development preclude the serious consideration of such systems for JOVE.

In view of the above discussion, a cold gas jet system was chosen in the interest of a simple and conservative design. Considerable experience with such systems on previous missions is a significant advantage. A design option would be to use the heat from the RTG's to heat the cold gas and thereby increase its specific impulse.



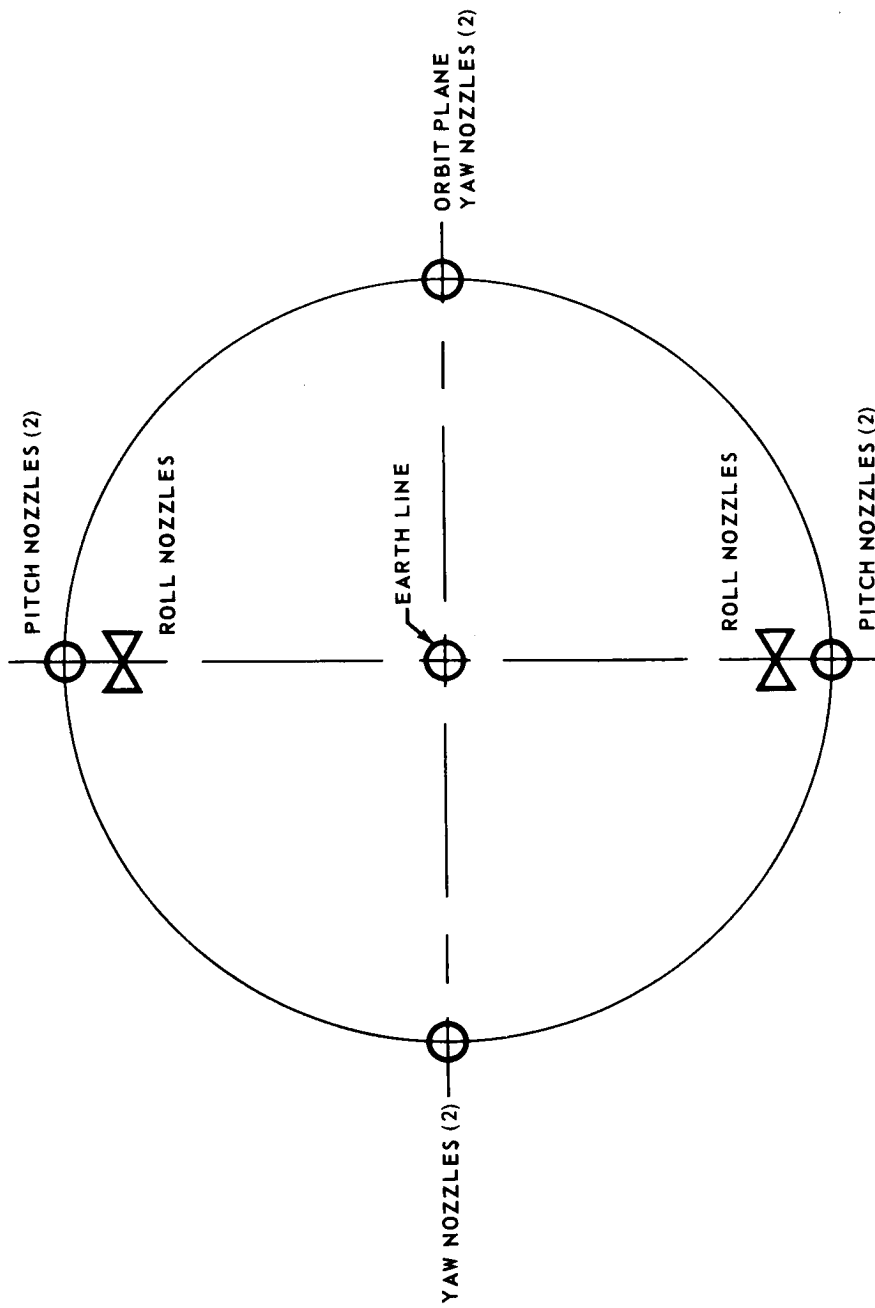


FIGURE VII-4. ARRANGEMENT OF ATTITUDE CONTROL NOZZLES

## Sensors

In this section, the sensors that will be carried on JOVE for guidance and control purposes are listed and their purpose explained briefly.

- a. Acquisition sun sensor - This sensor must have a 360° field of view in both the pitch and yaw axes. It is used in the acquisition mode to provide signals to the ACS until the fine sun sensor is acquired. For redundancy and to provide the required field of view, four of these are placed around the rim of the high-gain antenna.
- b. Cruise Sun sensor - The cruise sun sensor is locked on the sun during the time the spacecraft is operating in the cruise mode. On JOVE this sensor must be gimballed up to  $\pm 15$  degrees in the yaw axis and  $\pm 5$  degrees in the pitch axis. One method which has been proposed for orienting a spacecraft precisely at some offset angle with respect to the sun makes use of a rotatable optical slab which is placed in the field of view of the detector elements. The optical slab is rotated to a prescribed angle relative to the optical axis to displace the light bundle at the detectors. In order to null the output, the spacecraft is oriented at an offset angle. An accuracy of better than 2 seconds of arc is reported for this sensor [Ref. VII-5]. Two cruise sun sensors are supplied for redundancy.
- c. Canopus sensor - The Canopus sensor is locked on Canopus during the time the spacecraft operates in the cruise mode. Two sensors will be provided for redundancy.
- d. Earth sensor - An earth sensor will be used during the early part of the mission to verify Canopus acquisition.
- e. Gyros - Two complete gyro packages will be included for redundancy. Each package will contain three single axis gyros, an accelerometer, and the associated electronics.

## ARTICULATION

The systems which must be articulated include: the medium-gain antenna, the solar scan platform, the planet scan platform, and the cruise sun sensor. The only item that will require development is the gimbaling of the sun sensor.

## SUMMARY

The guidance and control system proposed for JOVE is similar to those which have been proposed for Voyager and which have been successfully flown on Mariner. The principal features of the system are shown below:

1. Three-axis stabilized spacecraft.
2. Sun-Canopus reference frame.
3. Gyros provide inertial reference during acquisition, maneuvers, and Sun or Canopus occultation.
4. Spacecraft is tracked by the radio system.
5. Fixed high-gain antenna.
6. Cold gas jets to provide thrust for attitude control.
7. Trajectory Control/Orbit Trim engines and LEMDE gimballed to provide attitude control during thrusting.
8. Science scan platform, sun sensor, medium-gain antenna, and the solar scan platform must be articulated.

A comparison of these features with the proposed Voyager guidance and control system indicates that the principal differences are in the much longer mission time of JOVE and in the fact that the high-gain antenna is fixed and the sun sensor gimballed.

## REFERENCES

1. Advanced Planetary Probe Study Final Technical Report. Report No. 4547-6006-ROOOO, vol. 3, Contract 951311. TRW Systems, July 27, 1966.
2. A Study of Jupiter Flyby Missions. Report No. FZM-4625, JPL Contract 951285. General Dynamics, May 17, 1966.
3. Mariner Mars 1964 Project Report. Technical Report Number 32-740, JPL, 1966.
4. Voyager Spacecraft System Phase 1A Task B Preliminary Design, Spacecraft Functional Description. General Electric, January 31, 1966.
6. Hatcher, Norman W.: A Survey of Attitude Sensors for Spacecraft. NASA SP-145, 1967.

## BIBLIOGRAPHY

Application of the Saturn V Launch Vehicle to Unmanned Scientific Exploration of the Solar System. Report No. TR-292/3-6-075, Contract NASA-20082, Northrop Space Laboratories, September 1966.

Heitchue, R. D.: Space Age Fundamentals. Douglas Missile and Space Systems Division, 1964.

Kendrick, J. B.: TRW Space Data, TRW Systems Group, 1967.

Phase 1A Study Report, Voyager Spacecraft, Alternate Designs Subsystems Considerations. Vol. 5, Appendixes E-F-G-J-K-L, Report No. 5410-0005-RU-002, Contract No. 951113, TRW Systems, July 30, 1965.

Report from Mars-Mariner IV - 1964-65. Government Printing Office.

Voyager Spacecraft System. Final Technical Reports, Task B, The Boeing Company, January 1966.

Voyager Spacecraft System. Final Technical Reports, Task B, TRW Systems Group, January 1966.

**CHAPTER VIII**  
**POWER SUPPLY SYSTEM**

## CHAPTER VIII. POWER SUPPLY SYSTEM

### DEFINITION OF SYMBOLS

$W_e$	Watts, electrical
$W_{th}, W$	Watts, thermal
TWT	Traveling Wave Tube
AU	Astronomical Unit
R	Distance from the sun in AU
SNAP	Systems for Nuclear Auxiliary Power
$\alpha$	Alpha particle, thermal diffusivity, Seebeck coefficient
$\beta, \beta^-$	Beta particle
$\gamma$	Gamma radiation
$\sigma_f$	Fission cross section
$\sigma_a$	Absorption cross section
n	Neutron
n, f	A fission reaction
$T_m$	Average temperature $\frac{(T_1 + T_2)}{2}$
$\Delta T$	A temperature difference
T	Temperature
$\nabla^2$	Laplacian operator

## DEFINITION OF SYMBOLS (Continued)

$q^{\text{in}}$	Volumetric heat generation (Btu/hr ft <sup>3</sup> )
$k_f$	Thermal conductivity of fuel
$k_{fc}$	Thermal conductivity of fuel capsule
$k$	Thermal conductivity
$t$	Time
$r$	Radial parameter (length)
$b$	Barns
$l$	Length
$Z$	Figure of merit
$\rho$	Electrical resistivity
$\theta_m$	Temperature weighted figure of merit
$V_{oc}$	Open circuit voltage
$A_n, A_p$	Cross sectional area for thermoelement
$A$	Surface area
$T_h$	Hot junction temperature
$T_c$	Cold junction temperature
$q_r$	Radiation heat transfer
$\sigma$	Stefan Boltzmann Constant
$\epsilon$	Emissivity
RTG	Radioisotopic thermoelectric generator



## DEFINITION OF SYMBOLS (Concluded)

$\phi$	Neutron flux
nvt	Flux time
AEC	Atomic Energy Commission
VAB	Vertical Assembly Building

### SUBSCRIPTS

n	n type semiconductor
p	p type semiconductor

## INTRODUCTION

The JOVE mission, like all other space ventures, would not be possible without an electric power source. Power is required for telecommunication with Earth, for recording of data from scientific and engineering instrumentation, for thermal control of the spacecraft and for a myriad of other functions.

JOVE has a  $640 W_e$  power supply system consisting of eight  $80 W_e$  radio-isotopic thermoelectric generator (RTG) units. Each RTG is fueled by  $Pu^{238}$  in the form of  $PuO_2$  and has a two staged thermoelectric generator section consisting of both SiGe and PbTe thermoelements. Each unit has ten beryllium fins with approximately 20 feet of radiator surface area. In addition, there is an ablative shield for intact reentry for each of the eight RTG's in case of a mission abort condition. The total RTG power supply weighs 645 pounds and the estimated cost is \$12 800 000.

In the following sections of this chapter, the details and facts concerning the decisions on the JOVE power supply system will be examined and some of the ramifications resulting from those decisions will be considered.

### MISSION POWER REQUIREMENTS AND POWER ALLOTMENT

The spacecraft will be provided with a  $640 W_e$  power supply. The maximum power required during any phase of the JOVE mission is approximately 600 electrical watts. Thus, with a rated power of  $640 W_e$  the JOVE craft will have  $40 W_e$  for a margin of safety in case a malfunction would occur in any part of the power supply system.

The  $600 W_e$  power estimate was made by dividing the JOVE mission into phases. There are five different power phases for project JOVE distinct because of the characteristic environmental or mission conditions imposing various power requirements on the spacecraft during these flight phases. These five phases are designated the pre-launch (ground) phase, the launch phase, the heliocentric coast phase, the propulsion maneuver phase and the Jovian orbit phase. Each of these phases is broken down further into the four separate categories of communications, experiments, guidance and attitude control, and thermal control (Table VIII-1). An elaboration on the power allotments, as

shown in Table VIII-1, by listing major power requiring components of the communications system helps to verify some of the estimates listed. Power requirements for the instruments in the experiment package are listed in detail in Chapter III and will not be repeated. The other system requirements are normally small and thus will remain unspecified.

The pre-launch phase is principally a check-out phase. Since the RTG's are operating constantly after the active fuel capsules are put in place (page 8-22) this power can be used. The power required would be due to the check-out and operation of three transponders ( $48 W_e$ ), the two  $50 W_e$  Traveling Wave Tubes (TWT) amplifiers and power supply ( $296 W_e$ ), the command module ( $20 W_e$ ), and the computer and sequencer ( $20 W_e$ ). The operation of other units would be checked as some of these were shut off.

The launch phase operation would require that power be supplied for the three magnetic tape recorders ( $10 W_e$ ) since there will be recording only. The other communication equipment, as specified above with the exception of the  $50 W_e$  TWT's, would also be operating.

Two different size Traveling Wave Tubes will be used during the heliocentric coast phase of the JOVE mission. A  $20 W_e$  TWT ( $57 W_e$ ) will be used with the medium-gain antenna out to a distance of approximately 2 AU from the sun. Since the medium-gain antenna is 2-axis gimballed,  $25 W_e$  are required for its operation. At 2 AU from the sun, in order to insure a sufficient communications bit rate, the spacecraft will be oriented so that the fixed high-gain antenna will point to the earth and the two  $50 W_e$  TWT's ( $296 W_e$ ) will take over. The three transponders ( $48 W_e$ ), the command module ( $20 W_e$ ), the computer and sequencer ( $20 W_e$ ), and the telemetry and recording system ( $20 W_e$ ) make up the rest of the communications package for this phase of the JOVE mission.

## COMPARISON OF POWER SUPPLIES

The attributes of potential spacecraft electrical power supplies such as batteries, fuel cells, solar cells, and radioisotopic thermoelectric generators were compared in a study for the JOVE mission. Spacecraft have already been powered electrically by each of these units. The selection of a particular power system was made on the basis of payload requirements, costs, and reliability over a 900-1000 day mission.

TABLE VIII-1. POWER ALLOTMENT

<u>MISSION PHASE</u>		<u>POWER REQUIREMENT (W<sub>e</sub>)</u>
I.	PRE-LAUNCH	
	Communications	
	Experiments	
	Guidance and Control	(System
	Thermal Control	Checkout)
	TOTAL	385 (Periodically)
II.	LAUNCH	
	Communications	98
	Experiments	0
	Guidance and Control	32.6
	Thermal Control	<u>0</u>
	TOTAL	130.6
III.	HELIOCENTRIC COAST	
A.	For JOVE out to a distance of approximately 2 AU from the sun	
	Communications	190
	Experiments	21.6
	Guidance and Control	11.0
	Thermal Control	<u>50.0</u>
	TOTAL	272.6
B.	For JOVE at a distance greater than approximately 2 AU from the sun	
	Communications	404
	Experiments	21.6
	Guidance and Control	11.0
	Thermal Control	<u>50.0</u>
	TOTAL	486.6
IV.	PROPULSION MANEUVER	
	Communications	404
	Experiments	21.6
	Guidance and Control (Peak)	123
	Thermal Control	<u>50</u>
	TOTAL	598.6
V.	JOVIAN ORBIT	
	Communications	404
	Experiments	84.6
	Guidance and Control (Peak)	45.2
	Thermal Control	<u>50</u>
	TOTAL	583.8

Nuclear reactor-based power systems were ruled out for consideration because of the low mission power requirements involved. They would be unrealistic because the weight of the reactor itself makes comparison practical only for systems above 10 kW. The reactor has a minimum critical size and weight (250 lb [Ref. VIII-1]) required to maintain a controlled nuclear reaction. Then, more weight must be added for shielding because of the great magnitude of reactor radiation effects before output power is even considered.

As one part of the evaluation, a parametric analysis (Table VIII-2) was carried out for the respective weights of power systems over a mission trip duration up to 1000 days. This table was prepared simply by extrapolation of data given in Reference VIII-2. It will provide one parameter, weight, as a criterion for choice of one power system over another. Large weight penalties are sufficient grounds for rejection of a particular system. The weights of the fuel cells, batteries, and solar cells are functions of the mission power requirement (specified) and the mission length whereas the weight of the isotopic power supply (for a long half-life power supply) is just dependent on a specification of the power requirements. The solar cell power system weight will be further dependent on the distance one travels from its energy source, the sun.

The fuel cell considered was a hydrogen-oxygen type with a specific reactant consumption rate of 0.9 lb/kW-hr (0.4 kg/kW-hr). Fuel cells have proved extremely useful for short time missions especially those that are manned since the production of water is a direct by-product of their operation. Since a 1000 watt<sub>e</sub> fuel cell with its associated controls, valves, etc., weighs approximately 40 lb (18.1 kg), this weight is neglected compared to the tank and fuel requirements on a "long" mission such as the envisioned JOVE mission. For this reason, only the effect of mission length and power level on the tank and fuel requirements for a fuel cell is considered in the parametric analysis.

The Nickel-Cadmium batteries considered in the Table VIII-2 have a specific weight of 22 lb/kW-hr (10 kg/kW-hr) [Ref. VIII-2] and are thus found to be an unfavorable source of primary power on long term missions. During peak load periods, however, they are frequently considered as an auxiliary source of power and could be used for project JOVE on that basis.

Solar cells have been used very successfully for many satellite space missions. The apparent difficulty with using them for a Jupiter mission is that Jupiter is located approximately 5 AU from the solar cells' energy source,

TABLE VIII-2. PARAMETRIC COMPARISON OF SEVERAL POWER SYSTEMS  
 [Reference VIII-2]

POWER LEVEL (Watts <sub>e</sub> )	SYSTEM	400 days		800 days		1000 days	
		lb	kg	lb	kg	lb	kg
100	Fuel Cell	1104	503	2208	1006	2760	1258
	Isotopic	100	45	100	45	100	45
	Battery (Ni-Cd)	21 120	9630	42 240	19 260	52 800	24 050
	Solar Cell (2.6 AU av)	675	306	675	306	675	306
300	Fuel Cell	3312	1509	6624	3018	8270	3770
	Isotopic	300	135	300	135	300	135
	Battery (Ni-Cd)	--	--	--	--	--	--
	Solar Cell (2.6 AU av)	2025	918	2025	918	2025	918
600	Fuel Cell	6624	3018	13 248	6036	16 540	7540
	Isotopic	600	270	600	270	600	270
	Battery (Ni-Cd)	--	--	--	--	--	--
	Solar Cell (2.6 AU av)	4050	1836	4050	1836	4050	1836

the sun. This does have an advantage for the cell in that the temperature gradient that it sees is not as severe as it would be in an Earth orbit, but the distance places a strong geometry attenuation on the cell's energy utilization. Intensity of solar radiation at 1 AU is 134 watts<sub>th</sub>/ft<sup>2</sup> whereas in the vicinity of Jupiter the solar radiation is cut to 5.8 watts<sub>th</sub>/ft<sup>2</sup> [Ref. VIII-1]. This is a result of the intensity being cut down by a factor of almost  $R^2$  (where R is the distance from the sun in AU). This fact must be considered when evaluating solar cells as a power system.

For the parametric study (Table VIII-2) an average value of 2.6 AU from the sun was used as a basis for calculating solar cell weights. This is satisfactory for a comparison, but actually a major portion of the JOVE mission is spent at distances farther from the sun than this, and 5 AU is where the power requirements will be greatest.

The fuel used to specify the RTG as a basis for comparison in the parametric evaluation of the power system was Pu<sup>238</sup>. This is the only fuel that has been used in space missions at the present time and is attractive, for example, because of its long half-life. (Other advantages and disadvantages to fuels will be discussed later in the report.) As a result of this long half-life, 97 percent of the power available at launch is still available at the end of the mission if all the components are operating properly. This is the reason it was previously stated that the weight of the RTG's on-board the spacecraft is simply specified by the power level required for the mission and it is not basically a function of mission length. This fact is obvious in Table VIII-2.

With this background the weight comparison of power supplies (Table VIII-2) can be seen to indicate that with power requirements of 600 W<sub>e</sub> and a 900-1000 day mission time (including time for orbiting Jupiter) the isotopic power supply is the best choice.

On such a basis, the fuel cell and the Nickel-Cadmium batteries can be ruled out as primary sources of power because of the excessive weight of these systems. As was mentioned previously, a battery is frequently an auxiliary power source which can be charged during periods when little power is required. Because of the long duration of the JOVE mission, however, the unreliability of a battery operating for this time period under space environmental conditions rules out the use of it even in this manner. It should be pointed out that Shair, et al., would not agree with this statement on reliability [Ref. VIII-3].

The solar cell power supply is heavier than the isotopic supply on the basis of the comparison made in Table VIII-2. Some comments are necessary, however, before such a reliable power source is ruled out for the JOVE mission. It is estimated that a solar radiator area of  $5 W_e / ft^2$  [Refs. VIII-2 and VIII-4] ( $53.8 W_e / m^2$ ) is required for a sun-oriented solar cell system in a near-Earth orbit (1 AU). This amounts to a specific weight of approximately 1 - lb (0.45 kg) per watt<sub>e</sub>. Such a value varies as an inverse function of  $R^2$  (AU) as one moves away from 1 AU.

The Mariner solar cell system produced about  $680 W_e$  with  $9.6 W_e / lb$  ( $55^\circ C$ ) at 1 AU [Ref. VIII-5]. This system, as well as most other solar cell powered space missions, was sun-oriented. Based on approximately  $300 ft^2$  of sun-oriented solar panels required for the Voyager spacecraft, approximately  $3000 ft^2$  would be needed for the power requirements of JOVE. If it is desired that the solar cells be sun-oriented, either they must be gimballed or the craft should be oriented properly to the sun at all times. With a large number of deployed cells, gimbaling would be extremely difficult if not impossible. If a sun-oriented craft is chosen, the possibility of fixed Earth oriented antenna is precluded and the antenna would have to be articulated. That is not only difficult, if a large antenna is used, but also costly in terms of power and reliability of the JOVE mission. If the solar cells are unoriented, however, an Earth oriented antenna could be used but the solar panel area would become larger by a factor of perhaps five or six. This would then become a prohibitive alternative because of the size of these panels.

Another important criterion in considering the solar cell is the devastating effect of radiation on the cell during the entire JOVE mission including the time that the craft spends in the Jovian trapped radiation belt. Radiation, especially high energy electrons and protons can damage a large number of cells during the JOVE trip. This factor affects the reliability of the solar cell system and, of course, degrades its power producing potential. Power degradation would become a maximum during the Jupiter orbiting phase of the mission when power requirements are greatest.

Radioisotopic thermoelectric generators (RTG's) are compact and reliable. They are a source of constant operating power and need not be articulated in any manner on the spacecraft though they are fixed on the craft so that they will primarily face black space. This is so that the fins may reject heat to as low a temperature or heat sink as possible.



The main disadvantage of RTG's is that they emit nuclear radiation constantly. Thus, components that are affected by such radiation must be kept as far from the RTG locations as possible.

After considering all factors, RTG's were chosen to supply the 640  $W_e$  of power for project JOVE. Eight 80  $W_e$  RTG units will make up the power system. This size unit was chosen for several reasons. An 80  $W_e$  unit may be passively cooled rather than actively cooled. (An active coolant is required in a large RTG unit.) That means that fins may be used to dissipate the heat from the system rather than a fluid which is pumped through the system to actively cool it. (An alternative power supply using an active cooling system is considered in Appendix D, Volume II.)

A second reason for choosing an 80  $W_e$  unit rather than a larger unit is related to the unit's specific power. There is no great increase in specific power for a unit of size greater than 100  $W_e$  [Ref. VIII-6]. Thus, an 80  $W_e$  unit has realized about as high a gain in specific power as can be potentially achieved.

Redundancy in components over a three year mission is very important. There is redundancy within the 80  $W_e$  RTG aboard JOVE with series-parallel circuits for thermoelectric elements and the like (page 8-22 ). Eight 80  $W_e$  units, however, provide redundancy also since a failure of one or two units does not ruin an entire mission. With one RTG unit lost, project JOVE could still be carried out with little change and even the loss of two units would cause very little sacrifice of mission objectives. With larger RTG units, such a statement would not be possible.

The conclusion then is that JOVE will have eight 80  $W_e$  RTG units as its power supply system.

## SNAP SYSTEMS AVAILABLE

The first notable RTG's used in the space program were SNAP3B7 and SNAP3B8 which were installed in Transit 4 navigation satellites. The first was on Transit 4A and the following on Transit 4B, both producing 2.7  $W_e$  with 5.2

percent efficiency and both were launched in 1961. SNAP3B7 continues to produce power to transmit signals to Earth but a capacitor shorted the power conditioning equipment on SNAP3B8 about seven months after launch and the RTG no longer operated. It is interesting to note that one month later, Transit 4B's power supplies failed shortly after a high altitude nuclear test.

An item of current interest is the SNAP-19 generator which will be launched this fall as part of the Nimbus B weather satellite. Two SNAP-19 generators are being flown together, producing about  $50 W_e$  and weighing approximately 50 lb. Their purpose on this mission is primarily as part of a test sequence to allay fears and build up confidence in their performance.

Another NASA radioisotopic powered mission is the SNAP-27 generator under development by the AEC for the Apollo Lunar Surface Experiment Package. The generator is specifically intended to provide power for scientific experiments left on the moon by the Apollo astronauts. It is thus in contrast to the Nimbus B generator which was retrofitted to a solar power design. For this reason, it is more efficient and weighs less than does SNAP-19. It weighs 46 lb and produces  $56 W_e$  for a one year period on the surface of the moon after two years of storage on Earth. Its fuel is  $Pu^{238}$  as was SNAP-19 and other space-tested SNAP systems. A short summary of interesting SNAP units is shown in Table VIII-3.

## RTG FUEL CONSIDERATIONS

There are a number of fuels which could be and have been chosen for use in radioisotope thermoelectric generators (Table VIII-4). There are advantages and disadvantages to each fuel considered. If an abundant, relatively inexpensive fuel were desired, a  $\beta$  emitter, such as Strontium 90, could be offered. Most  $\beta$  emitters, however,  $Sr^{90}$  included, require a great deal of shielding and they also normally have a low power density. The latter is because  $\beta$  emissions from a radioisotope occur over a spectrum of energy and not at one particular energy as do  $\alpha$  emissions. Beta emissions are more difficult to shield because they lead to bremsstrahlung as well as to subsequent  $\gamma$  radiation, both of which are highly penetrating forms of electromagnetic radiation.

A more expensive, much less abundant form of fuel is an  $\alpha$  emitter which has a relatively high specific power (w/g) or power density (w/cc). Since specific power is inversely related to the half-life of the isotope, one might immediately assume that a short half-life is the optimum. This, however, is not

TABLE VIII-3. SYSTEMS FOR NUCLEAR AUXILIARY POWER (SNAP) UNITS  
(TYPICAL SPACE APPLICATION UNITS)

<u>SNAP</u>	<u>USE</u>	<u>POWER</u> (W <sub>e</sub> )	<u>FUEL</u>	<u>DESIGN LIFE</u> (years)	<u>STATUS</u>
3B7	Navigation Satellite Transit 4A	2.7	Pu <sup>238</sup>	5	In orbit (1961) - operating
3B8	Navigation Satellite Transit 4B	2.7	Pu <sup>238</sup>	5	In orbit (1961) - not operating
19	Weather Satellite Nimbus B	25	Pu <sup>238</sup>	5	To be launched (1967)
27	Apollo Lunar Surface Experiment Package	50	Pu <sup>238</sup>	1	Under development
29	Department of Defense	500	Po <sup>210</sup>	0.25	Under development

TABLE VIII-4. CHARACTERISTICS OF ATTRACTIVE RADIOISOTOPIC HEAT SOURCES  
[ Ref. VIII-7 ]

	Cobalt <sup>60</sup>	Strontium <sup>90</sup>	Cesium <sup>137</sup>	Promethium <sup>147</sup>	Polonium <sup>210</sup>	Plutonium <sup>240</sup>	Americium <sup>241</sup>	Curium <sup>242</sup>	Curium <sup>244</sup>
Specific Power, W/g	17.4	0.95	0.42	0.33	141	0.56	0.11	120	2.8
Half-Life, years	5.3	28	30	2.7	0.38	89	458	0.45	18
Isotopic Purity, %	10	50	35	95	95	80	90	90	90
Compound Form	Metal	SrTiO <sub>3</sub>	Glass	Pm <sub>2</sub> O <sub>3</sub>	Metal	PuO <sub>2</sub>	Metal	Cm <sub>2</sub> O <sub>3</sub>	Cm <sub>2</sub> O <sub>3</sub>
Density of Compound g/cc	8.9	4.6	3.2	6.6	9.3	10	11.7	11.75	11.75
Active Isotope in Compound, %	10	24	16	82	95	70	90	82	82
Specific Power of Compound, W/g	1.7	0.23	0.067	0.27	134	0.39	0.1	98	2.3
Power Density, W/cc of Compound	15.5	1.16	0.215	2.22	1210	3.9	1.17	1150	27
Volume for 2 kW Heat cc	129	1840	9300	1120	1.65	513	1710	1.74	74
Availability	Available	Available	Available	Available	Available	Limited	Limited	Potentially	Potentially
annual kW-(1967- <sup>(a)</sup> )	(67 kW)	(67 kW)	(48 kW)	(11 kW)		Available	Production	Available	Available
Shielding Requirement	Heavy	Heavy	Heavy	Minor	Minor	Minor	Minor	Minor	Minor
Biological Hazard	3x10 <sup>-9</sup>	3x10 <sup>-10</sup>	5x10 <sup>-9</sup>	2x10 <sup>-8</sup>	2x10 <sup>-9</sup>	7x10 <sup>-13</sup>	2x10 <sup>-12</sup>	4x10 <sup>-11</sup>	3x10 <sup>-12</sup>
Estimated Cost, \$/W <sup>(a)</sup>	33	19 <sup>(a)</sup>	21 <sup>(a)</sup>	91 <sup>(a)</sup>	26 500 <sup>(c)</sup>	894	200	17	357
Estimated Cost, \$/g	570	18 <sup>(a)</sup>	9 <sup>(a)</sup>	30 <sup>(a)</sup>	188	500 <sup>(c)</sup>	1820	2000	1000
Curies per gram	1130	142	87	914	4500	17	3.25	3310	84
Curies per watt	65	150	207	2770	32	30	30	28	30
Spontaneous Fission Half- life, Years						4.9x10 <sup>(10)</sup>	1.4x10 <sup>38</sup>	7.2x10 <sup>6</sup>	1.4x10 <sup>7</sup>

(a) From proposed Hanford Isotope Plant, Hw-77770 (kW<sub>t</sub> = thermal kilowatts).

(b) Except for shielding against neutrons.

(c) From AEC data; also "Nucleonics": March 1963, Table I, page 63 ("projected" costs)

the case since one desires a long half-life as well as a high specific power. The high specific power indicates that the isotope will supply a great amount of heat for a small amount (mass) of fuel present. The long half-life is desirable so that the power does not drop considerably during the lifetime of the mission (Figure VIII-1). Thus, the problems related to power flattening can be avoided.

$\text{Pu}^{238}$  is an  $\alpha$  emitter which has a relatively long half-life (89 years) and yet a high specific power (Table VIII-3). The principal  $\alpha$  particles it emits are 5.50 MeV and 5.46 MeV in energy, while the accompanying gamma radiation is primarily 0.444 MeV and thus does not present a great hazard. As a result of its long  $\alpha$  emission half-life, it does not require power flattening during a five-year mission, nor does it greatly degrade in power production during that period (less than 4 percent). It is available, though in limited quantities. For these reasons and because of the experience gained using it in previous RTG power supplies, it has been designated as the preferred fuel for use in JOVE RTG's.

Since  $\text{Pu}^{238}$  as a metal has a relatively low melting point of 913°K, another fuel form must be used. The density and melting points of several potential fuel forms are listed in the brief table below.

---

TABLE VIII-5.  $\text{Pu}^{238}$  FUEL FORMS

<u>Fuel Form</u>	<u>Density (g/cm<sup>3</sup>)</u>	<u>Melting Point (°K)</u>
Pu metal (pure)	16.5	913
$\text{Pu}_2\text{C}_3$	12.7	2173
PuC	13.6	1923
$\text{PuO}_2$	11.46	2950
$\text{Pu}_2\text{O}_3$		2523

---

$\text{PuO}_2$  is used in both SNAP-19 and SNAP-27 generators for space and is the fuel form designated for the JOVE spacecraft. Its melting point is sufficiently high so that there is no danger of the fuel meltdown even during an abortive reentry. The only disadvantage encountered by using it is that  $\text{O}^{18}$  has a ( $\alpha$ , n) cross section which leads to an increase in the nuclear radiation emitted from the RTG (See page 8-36).

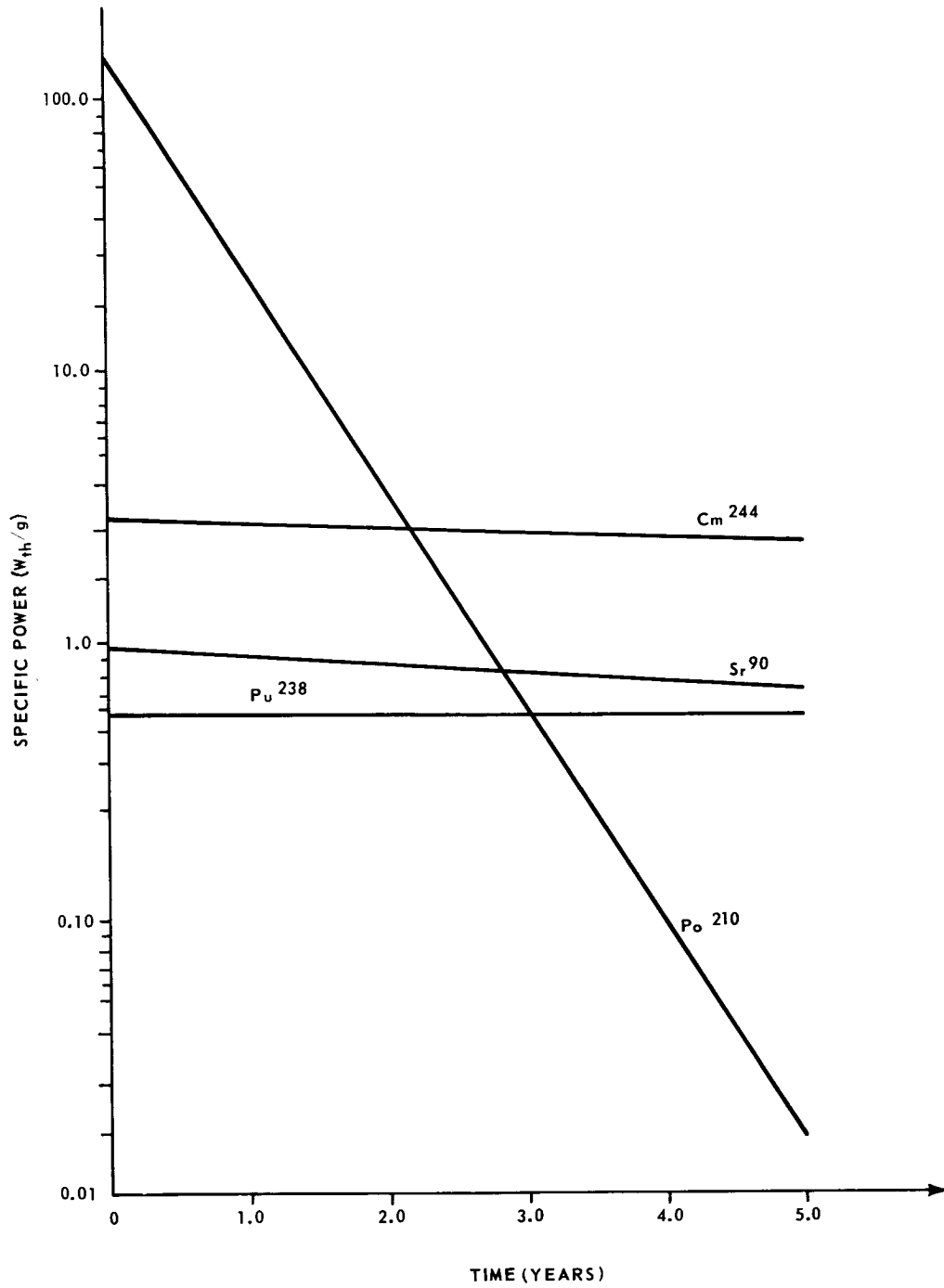
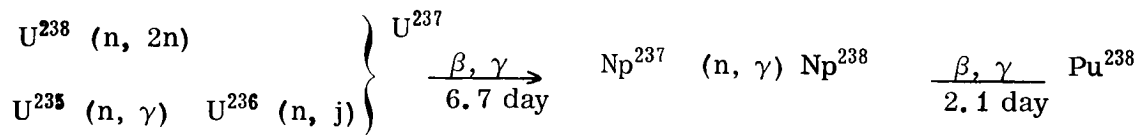


FIGURE VIII-1. ISOTOPIC POWER VARIATION WITH TIME

$\text{Pu}^{238}$  is expensive and also rather difficult to obtain in any large quantities. It is normally produced from  $\text{Np}^{237}$  by bombardment in a reactor. In other words, it is not a common fission product. It can be produced by the following reactions:



As one can see from these reactions, the key to the production of  $\text{Pu}^{238}$  is  $\text{Np}^{237}$ , a relatively stable isotope with a half-life of  $2.14 \times 10^6$  years. The first reaction to form  $\text{Np}^{237}$  is an (n,  $\gamma$ ) reaction ( $\sigma_a$   $\text{Np}^{237} = 170\text{b}$ ) in  $\text{U}^{235}$  leading to  $\text{U}^{236}$  and then to  $\text{U}^{237}$  though  $\text{U}^{236}$  has an absorption cross section of only 6 barns. As a result of this low cross section, the fuel is normally recycled several times and upgraded (keeping the percentage of  $\text{U}^{236}$  high) to improve the  $\text{U}^{237}$  yield. When  $\text{U}^{237}$  emits a beta particle,  $\text{Np}^{237}$  is formed and can be chemically separated. The second reaction to produce  $\text{Pu}^{238}$  is the (n, 2n) reaction in  $\text{U}^{238}$  to product  $\text{U}^{237}$  which then continues on the same path as was seen earlier to form  $\text{Pu}^{238}$ . The  $\text{Np}^{237}$  placed in a reactor to undergo the neutron capture reaction forms a reasonably pure (85 percent)  $\text{Pu}^{238}$ , the contamination being due to the new  $\text{Pu}^{238}$  absorbing a neutron and forming some  $\text{Pu}^{239}$  during the irradiation of the remaining  $\text{Np}^{237}$ . If the  $\text{Np}^{237}$  is not separated from the  $\text{U}^{238}$  in the slightly enriched uranium fuel, the  $\text{U}^{238}$  will form so much  $\text{Pu}^{239}$  that the specific heat of the  $\text{Pu}^{238} - \text{Pu}^{239}$  mixture will be tremendously reduced (about 99 percent) from that of the reasonable pure  $\text{Pu}^{238}$ .

It should also be noted that for each reactor cycle only approximately 10 to 20 percent of the  $\text{Np}^{237}$  can be converted to  $\text{Pu}^{238}$ . Increasing the neutron flux or irradiation time does not increase the yield either because the  $\text{Np}^{238}$  and  $\text{Pu}^{238}$  already formed have very high fission and neutron absorption cross sections respectively, ( $\sigma_f$ )  $\text{Np}^{238} = 1600\text{b}$  and ( $\sigma_a$ )  $\text{Pu}^{238} = 597\text{b}$  and are easily burned out.

There is another way in which  $\text{Pu}^{238}$  can be formed that requires only that  $\text{Am}^{241}$  capture a neutron to form  $\text{Cm}^{242}$  which alpha decays to  $\text{Pu}^{238}$ .  $\text{Am}^{241}$  is obtained from the decay of  $\text{Pu}^{241}$ , either inside or outside a reactor. If the  $\text{Pu}^{241}$ , however, is separated and allowed to decay outside the reactor, it will form pure  $\text{Am}^{241}$ , whereas inside the reactor during irradiation it will form a mixture of  $\text{Am}^{241}$  and  $\text{Am}^{243}$  and this mixture will contain less  $\text{Am}^{241}$  because of neutron capture by  $\text{Am}^{241}$ . The rate at which  $\text{Pu}^{238}$  is formed from  $\text{Am}^{241}$  is limited by the 13 year half-life of  $\text{Pu}^{241}$  and by the small amount (0.46 percent) of  $\text{Pu}^{241}$  present in plutonium. These two facts severely inhibit this means of production of  $\text{Pu}^{238}$ .

Note that Figure VIII-2 provides a detailed decay scheme for the reactions just considered in the production of  $\text{Pu}^{238}$ .

Because of the large increase in the last three years in the number of civilian thermal nuclear reactors which are now contracted to be built, the potential for recovery of isotopes has increased considerably. Schulman [Ref. VIII-8] indicates that if proper steps are taken, approximately 1 thermal kilowatt of  $\text{Pu}^{238}$  can be obtained for every 1000 megawatts of installed power in the industry. Note the flow scheme (Fig. VIII-3) which must, however, be followed in its production. For this reason, only minor amounts of  $\text{Pu}^{238}$  can become available until the late 70's when it is estimated that 100 thermal kilowatts could be produced annually by civilian means.

Since it takes 7 years to complete a  $\text{Pu}^{238}$  production cycle, the AEC may have to ensure that a sufficient amount of  $\text{Pu}^{238}$  is available. There may be competing demands on reactors for purposes other than optimum  $\text{Np}^{237}$  yields. Schulman [Ref. VIII-8] has estimated amounts of  $\text{Np}^{237}$  that might be produced in various types of civilian power reactors (Table VIII-6). The yield of  $\text{Np}^{237}$  increases rapidly with burnup so that the economy of the fuel cycle itself will greatly influence results.

TABLE VIII-6. PRODUCTION OF  $\text{Np}^{237}$  IN SPECIFIC REACTORS  
[Ref. VIII-8]

Reactor	Type	Thermal Power MWth	Initial Enrichment %	$\text{Np}^{237}$ Production $\text{k}_{\text{g}}/\text{yr}$
Yankee	pressurized-water	485	3.40	1.4
Dresden I	boiling water	626	1.50	2.3
Douglas Point	heavy water cooled	693	0.71	1.8
Hinkley Point	gas cooled	954	0.71	2.5
Oak Ridge Nat'l Lab GCR-3	advanced	1908	3.00	4.7
Saline Water Reactor	advanced	8300	0.71	24.0



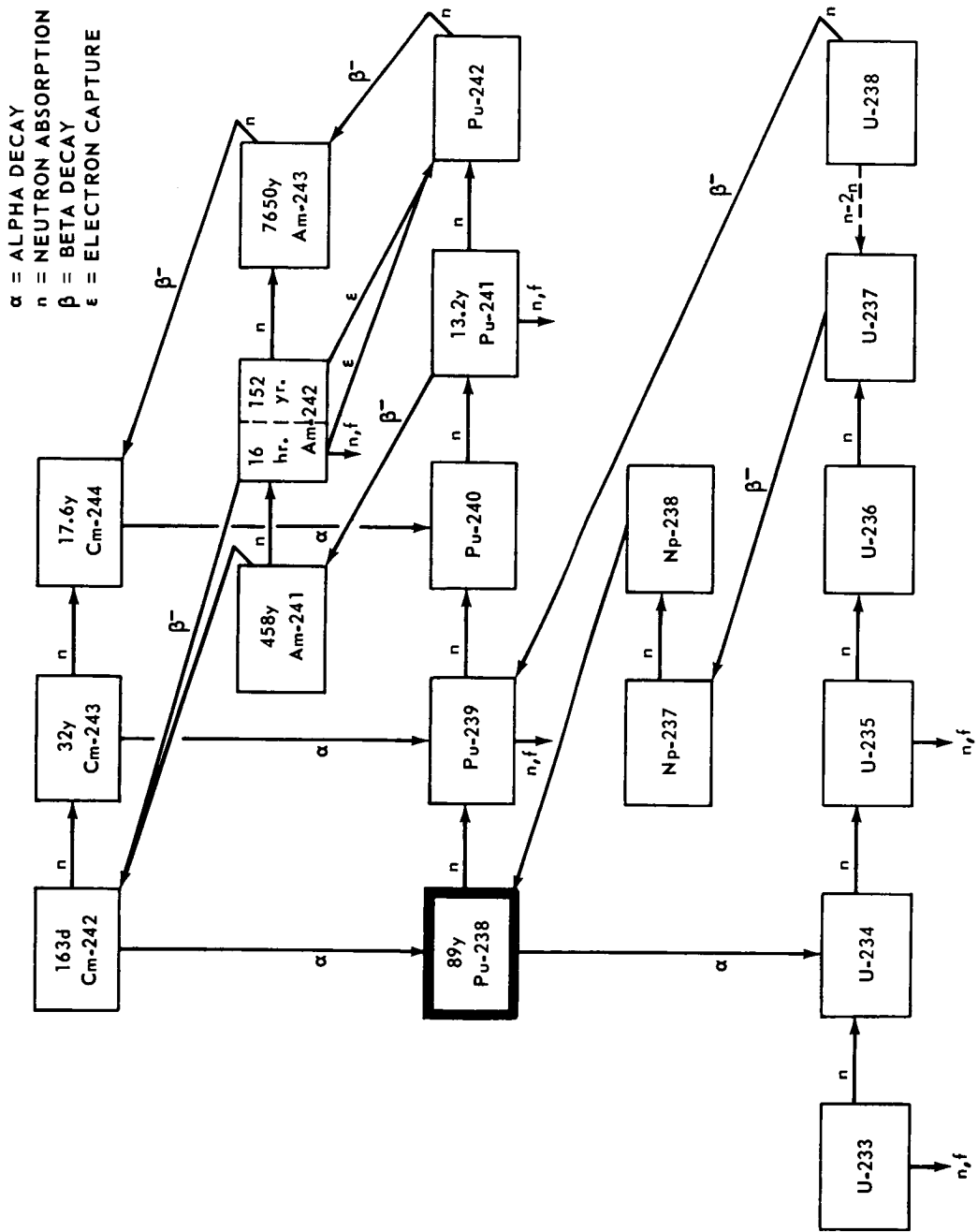
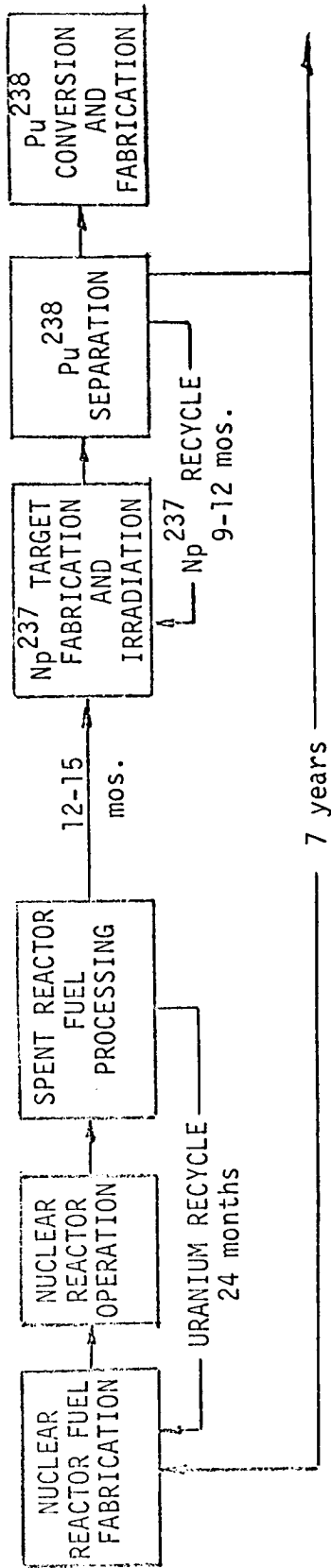


FIGURE VIII-2. PRODUCTION OF Pu<sup>238</sup>



SPECIFIC POWER

Pu <sup>238</sup>	0.56 W <sub>th</sub> /g	RTG	=	FUEL COST = (\$900/W <sub>th</sub> )	x	( $\frac{80\text{We}}{\text{Unit}}$ )	= \$1,600,000
PuO <sub>2</sub>	0.39 W <sub>th</sub> /g	UNIT COST				EFFICIENCY ( $\frac{\text{Me}}{\text{W}_{\text{th}}}$ )	= (0.045)

TOTAL RTG UNIT = 1 We/1b

TOTAL POWER SUPPLY COST = \$12,800,000

FIGURE VIII-3. FLOWSHEET FOR PRODUCTION OF Pu<sup>238</sup>

Schulman also estimated that the AEC could produce between 200 and 400 thermal kilowatts of  $\text{Pu}^{238}$  between now and 1980. The mid-1970's would be the only years when there would be a key problem resulting from the lack of sufficient civilian reactors that would be operational soon enough to produce  $\text{Pu}^{238}$  for that period.

## NUCLEAR SAFETY WITH AN RTG POWER SUPPLY

The entire nuclear safety problem with an RTG power supply is centered around being certain that no radiation escapes from the fuel capsule of an RTG either during the JOVE mission or before launch from the pad at Cape Kennedy. The only way that nuclear safety criteria will be met for each of these cases is if the fuel is encapsulated properly in a fuel capsule. First, consider what would happen in an abort condition if the RTG were aborted from the JOVE spacecraft in case of a launch accident. There are two approaches which may be followed in such a consideration. The first approach requires complete burn-up of the encapsulating RTG material while reentering Earth's atmosphere with a wide dispersion of an inert refractory fuel form. In this case, the fuel form will be an oxide, specifically  $\text{PuO}_2$ . This fuel has a high melting point. For this reason it is normally not burned into very fine particles.  $\text{PuO}_2$  is also fabricated in large sizes (approximately 150 microns). Thus  $\text{PuO}_2$  will probably neither melt, nor will it break up into very fine atmospheric dust after release from its fuel capsule during aerodynamic burn-up and, therefore, inhalation of fall-out radiation at sea level will not be a problem. However, this is only the first approach to the problem.

The second approach, and the one which seems to be more prevalent and more stressed by the AEC at the present time, is that of considering the complete containment of the radioisotope under all mission abort conditions. This implies that the fuel capsule, in fact that the entire RTG, is aborted from the spacecraft with an ablative shield so that it can reenter Earth's atmosphere completely intact. The ablative shield acts as a nose cone and a heat shield and thus allows reentry without any subsequent damage incurred to the RTG. Of course, on impact, the fuel capsule itself must remain intact and this is very difficult to achieve without a very thick fuel capsule wall. One can assume that the fuel capsule might even achieve velocities up to 300 or 400 feet per second during this reentry phase. To withstand the pressure on impact at such a velocity, the fuel capsule, primarily Haynes 25, must be approximately 0.8 inch in wall thickness.

It is significant to note that the AEC in their most recent memoranda, have specified the use of an inert fuel form and complete interact reentry of the encapsulating system. Thus, some of the safety ultimatums of both approaches are seen in these memoranda.

The problem of nuclear safety on the launch pad is an entirely different one. Here there is a condition of high nuclear radiation which can present a hazard. (This is considered later in this report). But there is also a greater problem involved in case of a launch pad conflagration. This would mean that once again the RTG and its fuel capsule would have to stay completely intact with the temperatures involved in such a holocaust. . It is fortunate in our spacecraft preferred design that the reentry ablative shield is at the bottom of the RTG and that this shield would be facing any sort of conflagration that would occur. Thus, the fuel capsule would probably contain all of the radioactive material intact in the case of such an accident. Only a more detailed study could more exactly determine what would happen in such an event.

## DESCRIPTION OF THE RTG UNIT

### General Description

The preliminary design of an RTG power system must consider at least the general characteristics of the major components of the system. These major components can be defined as four distinct parts of an RTG power system:

- a. The isotopic heat source including the capsule that contains it.
- b. The thermoelectric conversion section where the heat is converted to electricity.
- c. The heat dissipation system where the heat is rejected to the environment.
- d. The ablative shield reentry portion.

In a general description of the RTG, the isotopic heat source will be the first portion considered. It was mentioned previously that plutonium is the only type of RTG fuel that has ever been used in a satellite. This is primarily because of the advantageous characteristics of  $\text{Pu}^{238}$ . The  $\text{Pu}^{238}$  long half-life,

the high specific power, the operating experience and the relatively low radiation emission characteristics are offset only by its high cost and its limited availability. One other disadvantage to using  $\text{Pu}^{238}$ , at least in its metallic form, is that it has a very low melting point. This was the primary reason for selecting  $\text{PuO}_2$ .  $\text{PuO}_2$  has a melting point very close to  $3000^\circ\text{K}$ . This is some  $2300^\circ$  higher than the melting point of plutonium metal. Using  $\text{PuO}_2$ , however, leads to the problem of contending with the alpha-neutron nuclear reaction in  $\text{O}^{18}$ , as was previously mentioned. One other important factor that must be considered is the fact that  $\text{Pu}^{238}$  emits alpha particles, which being helium nuclei, cause a terrific gaseous pressure to be built up in the fuel capsule holding the plutonium fuel during a three year mission. Calculations indicate that the helium pressure might go as high as 107 atmospheres, or higher, if the fuel capsule has no way of letting the gaseous helium out through the capsule wall. A one-way porous material would be a solution to this problem and it is at present being developed but is not yet on the market. Also, since plutonium is a very corrosive material, it cannot be used directly with Haynes 25 which is normally considered for fuel capsule material and either tantalum or platinum-rhodium matrix must be considered to encapsulate the fuel body. Then between the fuel body and the fuel capsule would be put a liquid metal for thermal contact purposes. Out from this would come the cylindrical fuel capsule itself and then one moves into the thermoelectric conversion section of the device. In this section is contained the thermoelectric elements which will convert the thermal heat of the fuel to electricity which will be used as power on JOVE.

Two types of thermoelectric materials are being considered as candidates for the RTG thermoelectric conversion section. They are lead-telluride ( $\text{PbTe}$ ) and silicon-germanium ( $\text{SiGe}$ ).  $\text{PbTe}$  thermoelements have been commonly used in RTG's and thus there is a great deal of operating experience with these. Although lead-telluride thermoelements would have been superior conversion properties at the same  $\Delta T$  as compared to silicon-germanium, they cannot operate at as high a temperature as the silicon germanium elements can. Thus, the Carnot efficiency attainable from the lead-telluride system is lower than the  $\text{SiGe}$  system. The product of the Carnot efficiency and the thermoelectric conversion efficiency is equal to the thermal efficiency of the RTG. Thus, the Carnot efficiency plays an important role in the overall efficiency of the system. The lead-telluride thermoelements, because they operate at a lower temperature, require more radiator fin surface for heat rejection and thus cause one to increase the overall weight of the RTG.

Another important consideration to make is related to the magnetic field generated by the RTG. This is the result of two specific conditions, one being the current flow from the RTG, the other being the use of ferromagnetic materials. Lead-telluride systems use iron in the hot and cold shoes to which the thermoelectric elements are attached. Though the JOVE spacecraft has magnetometers

out on booms rather than as an integral part of the spacecraft surface, they will still be affected by any magnetic field on the craft. Thus, any reduction in the magnetic field, accomplished by minimizing the ferromagnetic material used, or carefully designing a circuit, will help reduce this condition. Silicon-germanium systems are, on the whole, magnetically clean compared to lead-telluride system, since no ferromagnetic materials are used in their construction. Thus, SiGe thermoelectric elements have another advantage. A third consideration that must be made is that lead-telluride thermoelectric elements must be hermetically sealed in a compartment with an inert atmosphere; otherwise the elements would degrade rapidly. The SNAP 27 system used argon gas for this purpose. Any leakage of this gas would rapidly degrade the performance of the system. Fortunately silicon-germanium thermoelements operate well in either air or vacuum. It should be mentioned, however, that PbTe thermoelectric elements that can operate in a vacuum are being developed at the present time, though they seem suitable only at very low temperatures. Proper development should lead to their use at high temperatures very shortly.

The major disadvantage to the use of SiGe thermoelements has been the requirement that they be used at very high temperatures where they have the highest figure of merit. This leads to the development of a fuel capsule which can operate in the temperature range close to 1300°K. Since a solution to the problem of high temperature creep because of high helium pressure in the fuel capsule has not been solved, deformation of the fuel capsule over a three year period may cause rupture of the capsule and thus failure of the RTG power supply. The one way porous material mentioned earlier in this report could be a solution to this problem. Also, development of refractory materials with better characteristics at higher temperatures may help in the solution of the problem.

In the design for the JOVE RTG units both SiGe and PbTe thermoelements are used in a multi-staging type of thermoelectric generator. This type of generator uses the optimum operating conditions of both type of thermoelements in their best temperature range and thus produces a more efficient type of RTG.

Although only preliminary calculations have been carried out, it seems quite feasible that a system using this type of design can be developed. The preliminary design calculations will be considered in this report later in this same section.

To complete this thermoelectric-generator portion of the RTG it should be mentioned that the load is attached to each of the thermoelements and each of the thermoelements is separated by a mica strip which is an electrical insulator. The hot fuel capsule is also separated from the thermoelements and from the

hot shoe plate by an electrical insulator. Spring type load connectors are used to take the load to the primary conditioning unit. From the cold junction at the outside portion of the RTG there is a connection to the shell and radiator section of the RTG. This section is called the heat dissipation system for the RTG and will now be considered.

The heat dissipation system consists primarily of the fins by which the heat is rejected from the RTG. This essentially completes the cycle of power production and the power supply, since heat was produced in the fuel section and now is dissipated to the environment through the fins. The environment, of course, will be different depending on where your spacecraft is located. Hopefully, most of the time, the fins of the RTG will see black space and thus be able to dissipate the heat most effectively by radiation. This is the way the spacecraft configuration has been designed, with the fins pointing to space as much as possible. The fins will be of beryllium with an emissivity of 0.9. They will be of trapezoidal shape, approximately 10 inches in width and 14 inches in length. They will be required to dissipate 6070 BTU's per hour or 1780 thermal watts for each RTG. This is the amount of heat that is produced by the fuel in the RTG power supply. The fourth section of the RTG's is not really considered an integral part of the power supply, but it is important in the considerations of nuclear safety. It is the ablative shield in reentry section. It is over the edge of this particular shield that the power connector on its cord goes and thus attaches to the spacecraft to supply power. The ablative shield is connected to the spacecraft at eight locations. These locations are equipped with a squib device and a spring with which to reject the total ablative shield and RTG in case of an abort. The general configuration of these RTG's is shown in Figures VIII-4, VIII-5, and VIII-6.

## Sample Preliminary Calculations

The first calculations to be considered are those concerned with the heat transfer from the fuel through the fuel capsule to the thermal electric converters. To do this, the first equation will be written for the fuel body itself. Note Figure VIII-6.

$$\nabla^2 T + q^{\text{in}}/k_f = \frac{1}{\alpha} \frac{\delta T}{\delta t} \quad (1)$$

or

$$\nabla^2 T + q^{\text{in}}/k_f = 0 \quad \text{for steady state} \quad (2)$$

POWER - 640 ELECTRICAL WATTS

POWER SUPPLY - RADIOISOTOPIC THERMOELECTRIC GENERATORS

SIZE - 80 We

NUMBER - 8

FUEL -  $\text{Pu}^{238}$

FUEL FORM -  $\text{PuO}_2$

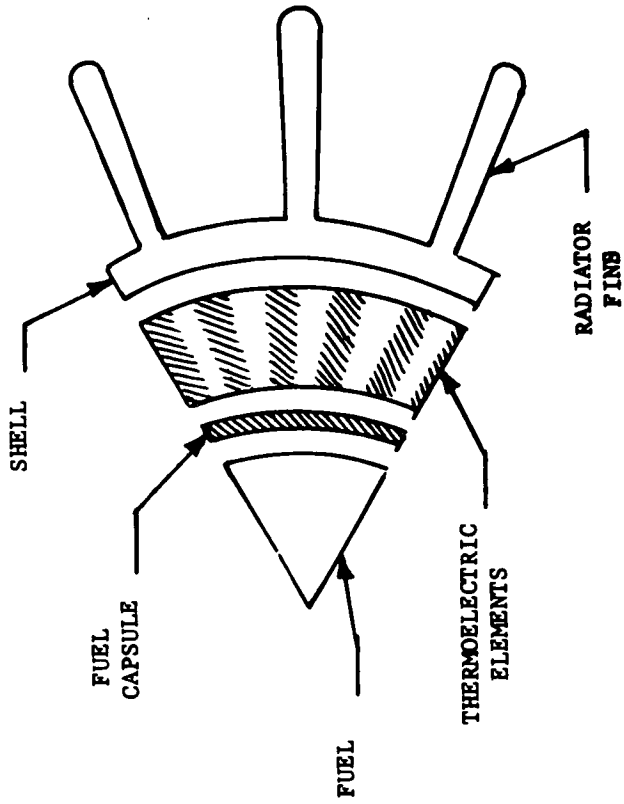


FIGURE VIII-4. JOVE MISSION POWER SUPPLY



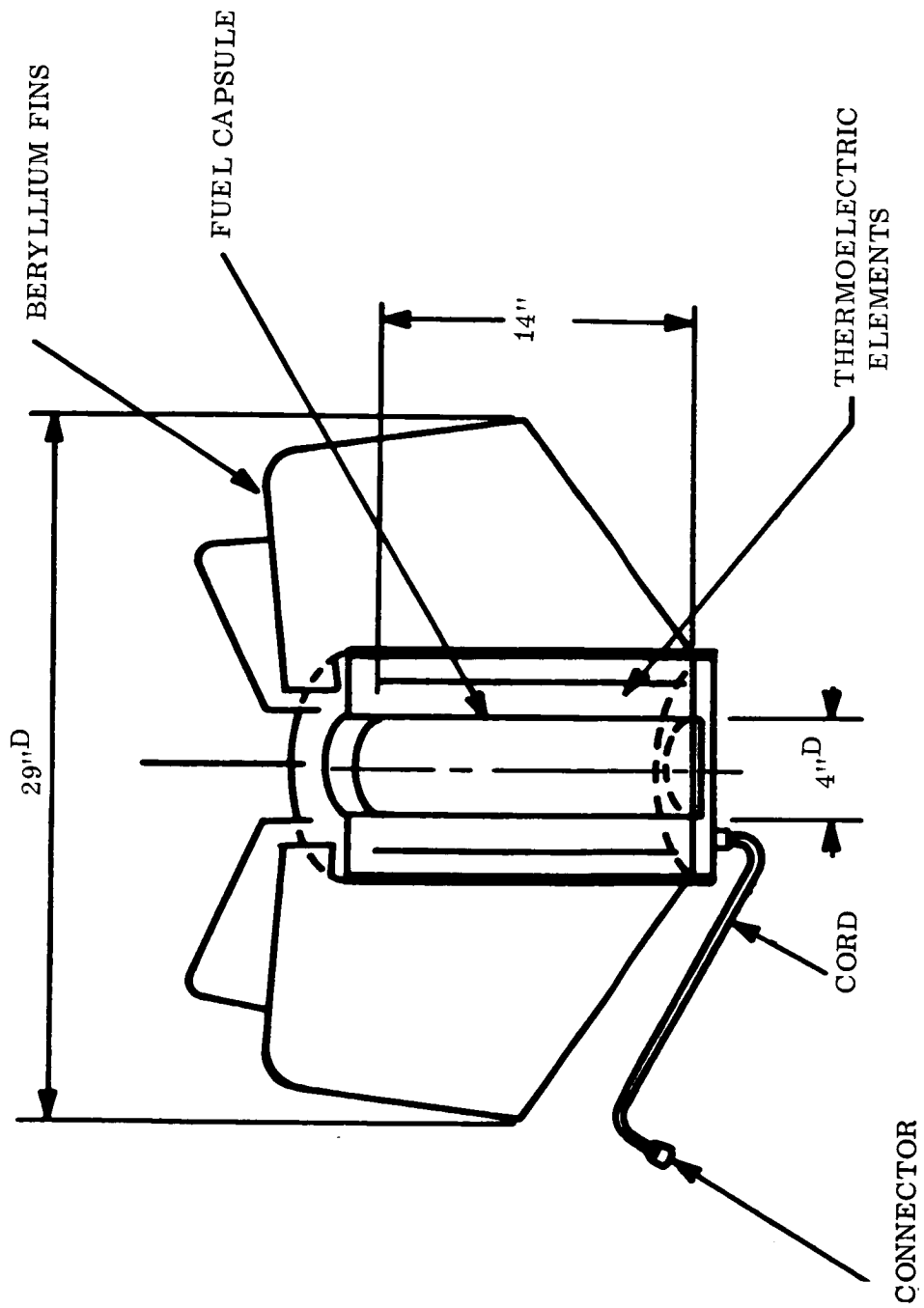
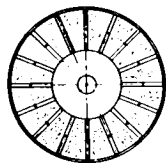
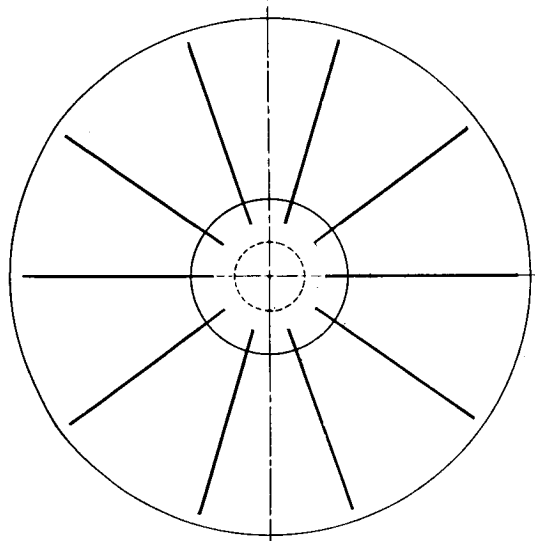


FIGURE VIII-5. 80 W<sub>e</sub> PICTORIAL VIEW



SECTION AA

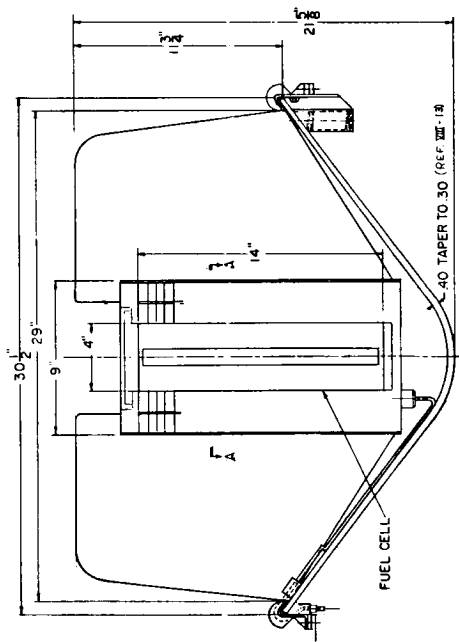


FIGURE VII-6. SCHEMATIC VIEW - JOVE'S 80 W<sub>e</sub> RTG

The boundary conditions that are set at this fuel surface, which has a boundary of a fuel void on one side and the fuel capsule on the other are a bit difficult to describe. The first one is that there is no heat flow across the maximum fuel temperature boundary ( $\frac{\delta T}{\delta r} = 0$  at  $T = T_{im}$ ). This maximum temperature can be assumed to be directly at the void surface. Normally there would be heat flow in this direction, but since there is no place for the heat to go, this must be the maximum temperature, and all heat flow must go out from this point. Of course, we have assumed that there is only radial flow of heat for this problem, and that we have a steady state condition. The second boundary condition is simply stated that  $T = T_2$  at  $r = R_2$  (Fig. VIII-7). Solving equation (1) with its boundary conditions gives

$$T_1 - T_2 = \frac{q_{in}}{4 k_f} [R_2^2 - r^2] + \frac{q_{in} R_1^2}{2k_f} [\ln r/R_2]. \quad (3)$$

Now the temperature distribution in the fuel capsule is considered. There are also two boundary conditions in this problem. The first is that  $T = T_2$  at  $r = R_2$ . This assumes, for these preliminary calculations, that there is no fuel body container of tantalum, that there is no liquid metal contact, and that the temperature is the same at the fuel wall as it is in the fuel capsule. This is a good assumption. The second boundary condition is that all the heat that flows through the fuel wall must flow into the fuel capsule. Since this amount of heat is known, this can be equated to Fourier's law of conduction.

$$6070 \text{ BTU/hr} = - k_{fc} (2\pi) R_2 l \left. \frac{\delta T}{\delta r} \right|_{r = R_2} \quad (4)$$

Solving  $\nabla^2 T = 0$  for the fuel capsule and using the specified boundary conditions gives

$$T_2 - T_1 = (31.1^\circ \text{ F}) \ln r/R_2 \quad (5)$$

Assume

$k_{fc} = 30 \text{ Btu/hr-ft-}^\circ \text{ F.}$	$k_f = 2 \text{ Btu/hr-ft-}^\circ \text{ F.}$
$R_1 = 0.85 \text{ inch}$	$R_2 = 2 \text{ inches}$
$R_3 = 1.20 \text{ inches}$	$l = 12.4 \text{ inches}$

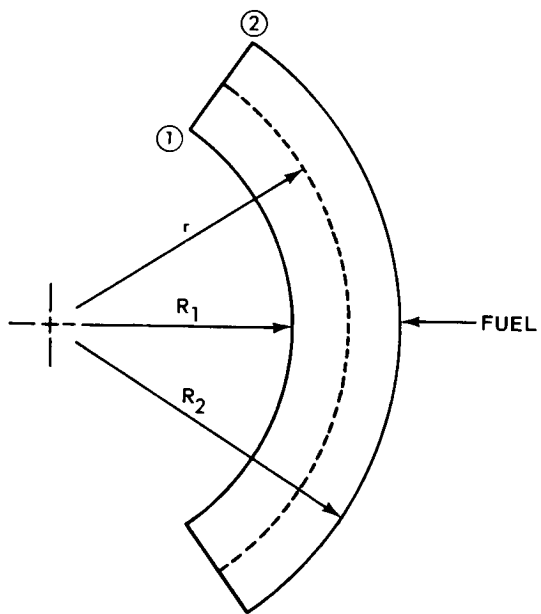


FIGURE VIII-7. FUEL BODY CROSS SECTION

A preliminary calculation using a hot junction temperature of 1300° K yields a fuel body maximum temperature of only 1759° F. Since the melting point of plutonium dioxide is given as 2240° K (3572° F) by Corliss and Harvey [Ref. VIII-6], and 2960° K (4872° F) by Levedahl [Ref. VIII-4], the 1759° F is certainly a safe figure and the fuel would be in no danger of melting. Of course, if the fuel capsule thermal conductivity were only 3 Btu/hr-ft-° F, down by a factor of 10 from the 30 Btu/hr-ft-° F assumed, there would be a difference of 159° instead of 15.9°. This is not significant enough to cause fuel capsule meltdown. The thermal conductivity of PuO<sub>2</sub> may also be lower than was estimated. It would have to be a significantly lower figure, however, to make any considerable difference in the value just calculated. The worst condition, of course, would be if there were a launch pad conflagration which would cause the hot junction temperature to become very high.

No temperature drop was assumed across the hot shoe because of the shoe material's high thermal conductivity. Putting a mica strip of aluminum oxide, Boron-nitride, or some other coating in - before the hot shoe - as an electrical insulator would cut down on the hot shoe temperature because radiation would be the only mechanism of heat transfer. Temporell-1500 or some other thermal insulating material that can tolerate a high maximum surface temperature and still have a very low thermal conductivity is used as a thermal insulator between thermoelements. Min-K2000 can tolerate 1365° K but its thermal conductivity in air is 1.9 watts/cm<sup>2</sup> - °K and in vacuum 1.6 watts/cm<sup>2</sup> - °K.

Thermal conductivities lower than this would be very desirable. Mica strips would be placed along the sides of the SiGe and PbTe elements between the insulation and the element.

The hot junction temperature has been assumed as 1300° K (hotter than any present concept allows) for the SiGe thermoelements going to a cold junction temperature at 700° K. Placing a lead-telluride thermoelement in series with the SiGe couple will then help to take advantage of the better PbTe efficiency at lower temperatures (assume a cold temperature of 400° K). A mica sheet for electrical insulation will be placed between the SiGe element and the PbTe element. Spring loading contacts take the power from the two different couples. An optimum length to area ratio for the elements is a paramount parameter to consider as is the temperature drop across the element. Since this type of thermoelement pattern cannot be found on present RTG concepts, development must take place to prove it out in actual operation. Other thermoelements may also be considered, but this concept does seem feasible. Preliminary calculation will only indicate some of the parameters and their relationship to the temperature drops for each thermoelectric element system separately. More precise calculations would be undertaken in a subsequent, more detailed study.

Of course, much more is known about PbTe thermoelements than about SiGe elements and the JOVE mission may have to rely on the use of these converter elements only. Development should soon be to the level, however, where higher temperatures can be withstood by an operating RTG.

Lead-telluride is an intermetallic compound that oxidizes easily at elevated temperatures. In its pure form it contains 38.113 w/o tellurium and melts at 1195°K. Its density is 8 g/cm<sup>3</sup>. Both Pb and Te are soluble in PbTe to several hundredths of a percent with excess lead resulting in an n-type material and excess Te producing p-type properties. Many dopants have been analyzed with PbTe in order to improve the figure of merit and one of these has been chosen for preliminary calculations on the JOVE RTG's. Note the properties of the n and p type PbTe and SiGe thermoelements listed in Table VIII-7. The values are taken at an average temperature ( $T_m$ ) of  $550^\circ\text{K} = \frac{(700+400)}{2}^\circ\text{K}$  respectively.

The preliminary calculations are carried out on the two thermoelectric materials separately. The procedure for making these preliminary calculations can be found in books by Anquist [ Ref. VIII-10] or Chang [ Ref. VIII-11]. The figure of merit for the lead-telluride and the silicon-germanium thermoelements is known for both n and p type materials at the average temperature considered, along with the other properties of electrical resistivity, Seebeck coefficient, thermal conductivity, and the figure of merit times its average temperature. Calculations will thus proceed by finding an optimal figure of merit with respect to geometry adjustments for the combination of n and p elements.

The optimal figure of merit is

$$\theta_m = \frac{T_m (\alpha_n + \alpha_p)^2}{\left( \sqrt{\rho_n k_n} + \sqrt{\rho_p k_p} \right)^2} = 1.1 \quad (6)$$

The optimum resistance ratio can be found. This is just the ratio of the external resistance to the internal resistance. This will be an optimum only when the temperature weighted figure of merit is a maximum and thus, the thermal conductivity-electrical resistivity term in the denominator of equation (6) must be a minimum. Knowing the optimum resistance ratio, the voltage per couple can be calculated. This is the voltage, not open circuit, but with the resistance as given by the optimum ratio for external resistance to internal resistance. Thus, knowing that there is a constant load (which will be mentioned later) one can calculate the number of couples in series required to give 28 volts DC power. A series-parallel setup, however, will be used for redundancy in the JOVE

TABLE VIII-7. PROPERTIES OF THERMOELECTRIC ELEMENTS

PbTe thermoelements [ Ref. VIII-9]

n type with 0.055% PbI<sub>2</sub> (mol %)

$$Z = 1.4 \times 10^{-3} (\text{°K})^{-1}$$

$$\rho = 1.1 \times 10^{-3} \text{ ohm-cm}$$

$$\alpha = 220 \times 10^{-6} \text{ volts/°K}$$

$$k = 2.0 \times 10^{-2} \text{ watts/cm°K}$$

$$\theta_m = ZT_m = 0.77$$

p type with 1.0 Na (a/o)

$$Z = 1.3 \times 10^{-3} (\text{°K})^{-1}$$

$$\rho = 1.8 \times 10^{-3} \text{ ohm-cm}$$

$$\alpha = +230 \times 10^{-6} \text{ volts/°K}$$

$$k = 1.6 \times 10^{-2} \text{ watts/cm°K}$$

$$\theta_m = ZT_m = 0.72$$

SiGe thermoelements [ Ref. VIII-9]

n type

$$Z = 0.85 \times 10^{-3} (\text{°K})^{-1}$$

$$\rho = 2.0 \times 10^{-3} \text{ ohm-cm}$$

$$\alpha = 250 \times 10^{-6} \text{ volts/°K}$$

$$k = 4.2 \times 10^{-2} \text{ watts/cm°K}$$

$$\theta_m = ZT_m = 0.85$$

p type

$$Z = 0.7 \times 10^{-3} (\text{°K})^{-1}$$

$$\rho = 2.5 \times 10^{-3} \text{ ohm-cm}$$

$$\alpha = 250 \times 10^{-6} \text{ volts/°K}$$

$$k = 4.2 \times 10^{-2} \text{ watts/cm°K}$$

$$\theta_m = ZT_m = 0.7$$

system, though a plain series circuit would give 28 volts DC with the least number of thermocouples. The open circuit voltage is simply the Seebeck coefficient for both legs combined times the temperature difference across the legs.

$$V_{oc} = (\alpha_n + \alpha_p) \Delta T = (450 \times 10^{-6} \frac{\text{volts}}{^\circ\text{K}}) (300^\circ\text{K}) = 0.135 \text{ volts.} \quad (7)$$

The ratio of areas to lengths which minimizes the resistance-conductivity product for the thermocouples is found to be

$$r = (\rho_n k_p / \rho_p k_n)^{\frac{1}{2}} = \frac{(1.1 \times 10^{-3} \text{ ohm-cm}) (1.6 \times 10^{-2} \frac{\text{watts}}{\text{cm-}^\circ\text{K}})}{(1.8 \times 10^{-3} \text{ ohm-cm}) (2.0 \times 10^{-2} \frac{\text{watts}}{\text{cm-}^\circ\text{K}})} = 0.699 \quad (8)$$

It was assumed that both n and p legs of this PbTe thermoelectric couple are 1 cm in length and that the ratio of the area to length for the n type element is 1 cm. (Actually, a parametric study should be carried out to optimize this ratio in a second phase thermoelectric generator design.) Boman [Ref. VIII-12] also has carried out a study on the effect of the length of a thermoelectric element on the RTG design.

$$\frac{A_n}{l_n} = 1 \text{ cm, and since } r = 0.7$$

$$A_p = \frac{l_p}{r(l_n/A_n)} = \frac{1 \text{ cm}}{0.7(1) \text{ cm}^{-1}} = 1.43 \text{ cm}^2$$

Thus, the thermal conductance for the thermocouple is

$$k = k_n \frac{A_n}{l_n} + k_p \frac{A_p}{l_p} = 4.29 \times 10^{-2} \frac{\text{watts}}{^\circ\text{K}} \quad (9)$$

The internal resistance may be calculated and is shown to be  $r + 3.7 \times 10^{-3}$  ohms. Thus, the optimum efficiency external system resistance for maximum power occurs; then the load resistance is equal to the internal resistance. The current can thus be found. The power delivered per couple is  $1.23 W_e$ . For maximum power, the lead-telluride portion of the generator would have a thermal efficiency of 9.21 percent.



$$\eta_{th} = \frac{\Delta T/T_h}{4/\left(\frac{\theta_m T_h}{T_m}\right) + 2 - \frac{1}{2}\left(\frac{\Delta T}{T_h}\right)} = 9.21\% \quad (10)$$

The same type of calculation can be carried out for the silicon-germanium elements.

Implicit in the JOVE/RTG system is the power conditioning equipment that must accompany this power source. One of the design constraints is that the RTG power source must operate continuously into its rated load if Peltier cooling of its hot junction is to be properly maintained. It is desirable to keep the hot shoe temperature close to the rated temperature to enable the largest temperature difference between hot and cold shoes to be reached. By having open circuit operation which would result if a constant external load is not present. Peltier cooling is removed and the hot shoe temperature will increase to perhaps above the safe rated temperature. Thus, the fuel capsule and fuel temperatures will correspondingly increase and perhaps compromise the integrity of the RTG fuel capsule. Hot shoe temperature, output power and output voltage each should be plotted as a function of output current in a more complete study to assure that this condition will not occur. To be certain that such a condition does not arise, however, a shunt regulator which maintains a constant load on the source in the presence of active load variations will be used in the power conditioning section of the power system. Other power conditioning for loads grouped by their specific power profiles will then follow this unit and supply specific requirements.

For the radiator section of the RTG, preliminary calculations were made simply using beryllium fins,  $\epsilon = 0.9$  [Ref. VIII-12] and assuming radiation to black space.

$$q_r = \sigma \epsilon A [T_{fin}^4 - 0] = 1780 \text{ watts} \quad (11)$$

Thus, it was found that 10 fins as shown in Figure VIII-5 will provide sufficient radiating area.

No calculations were done on the ablative heat shield but the RTG system as seen in Reference VIII-13 was adopted along with its squib device and spring loading.

## RADIATION LEVELS CAUSED BY THE RTG UNITS

In order to account for the nuclear radiation emitted from each 80 W<sub>e</sub> RTG unit, the mass of Pu<sup>238</sup>, in the form of PuO<sub>2</sub> is calculated for each unit. At 4.5 percent efficiency, 1780W<sub>th</sub> are required for each RTG. Since the specific power for PuO<sub>2</sub> is 0.39 W<sub>th/g</sub> of PuO<sub>2</sub>, 4570 grams of PuO<sub>2</sub> are required per RTG. Since Stoddard and Albenesius [ Ref. VIII-14] give the activity per gram caused by PuO<sub>2</sub>, the activity for each 80 W<sub>e</sub> RTG unit can easily be calculated (Table VIII-8). It should be noted that the PuO<sub>2</sub> is not entirely Pu<sup>238</sup> and a table listing its composition is thus included (Table VIII-9). This is provided so that a comparison of isotopic compositions for the actual RTG fuel can be made later in order to revise theoretical RTG radiation estimates.

With a fuel capsule wall thickness of 0.8 inch, the gamma radiation will be cut down to a level such that only neutron radiation must be considered to be a hazard to the JOVE mission.

The neutron radiation level at 1 meter from the RTG, considering the fuel as a point source, neglecting self-shielding and other shielding effects is

$$\begin{aligned} \phi &= \frac{9.5 \times 10^7 \text{ neutrons}}{\text{sec } (4\pi) (100)^2 \text{ cm}^2} = (7.6 \times 10^2 \frac{\text{neutrons}}{\text{cm}^2\text{-sec}}) \\ &= 760 \frac{\text{neutrons}}{\text{cm}^2\text{-sec}} \end{aligned}$$

Thus, over the JOVE 900-day mission,

$$\begin{aligned} \eta \nu t = \phi t &= \left[ 760 \frac{\text{neutrons}}{\text{cm}^2\text{-sec}} \right] [900 \text{ days}] \left[ \frac{24 \text{ hrs}}{\text{day}} \right] \left[ \frac{3600 \text{ sec}}{\text{hr}} \right] \\ &= 5.9 \times 10^{10} \frac{\text{neutrons}}{\text{cm}^2} \end{aligned}$$

This figure can be converted to an absorbed dose using an assumed conversion of 1 n/cm<sup>2</sup> ≈ 3.0x10<sup>-7</sup> ergs/gram.

TABLE VIII-8. ACTIVITY OF AN 80 W<sub>e</sub> RTG

(a) Alpha activity:  $2.33 \times 10^{15}$  disintegrations/sec

(b) Gamma activity

Energy MeV	Abundance (protons/sec)			
	t = 1 day	t = 1 year	t = 2.5 years	t = 5.0 years
0.04-0.5	$9.6 \times 10^{11}$	$9.6 \times 10^{11}$	$9.6 \times 10^{11}$	$9.1 \times 10^{11}$
0.5-1.0	$1.5 \times 10^9$	$1.6 \times 10^9$	$1.8 \times 10^9$	$2.2 \times 10^9$
1.0-2.0	$2.2 \times 10^7$	$2.3 \times 10^7$	$3.1 \times 10^7$	$4.5 \times 10^7$
2.0-3.0	$6.9 \times 10^6$	$4.3 \times 10^7$	$2.1 \times 10^8$	$5.5 \times 10^8$
3.0-5.0	$6.4 \times 10^5$	$6.4 \times 10^5$	$6.4 \times 10^5$	$5.9 \times 10^5$
5.0-7.0	$1.1 \times 10^5$	$1.1 \times 10^5$	$1.1 \times 10^5$	$1.1 \times 10^5$

t = time since separation of decay products

(c) Neutron activity

Energy MeV	Abundance neutrons/sec
0.0-0.5	$1.6 \times 10^6$
0.5-1.0	$3.2 \times 10^6$
1.0-2.0	$2.5 \times 10^7$
2.0-3.0	$4.4 \times 10^7$
3.0-4.0	$2.0 \times 10^7$
4.0-5.0	$2.1 \times 10^6$
5.0-6.0	$3.3 \times 10^5$
6.0-7.0	$1.1 \times 10^5$
7.0-8.0	$7.8 \times 10^4$
8.0-10.0	$2.9 \times 10^4$
10.0-13.0	$1.4 \times 10^4$

Total =  $9.5 \times 10^7$  neutrons/sec

TABLE VIII-9. ISOTOPIC COMPOSITION OF Pu IN  
PuO<sub>2</sub> [ Ref. VIII-14]

Pu <sup>236</sup>	=	0.00012%	Np <sup>237</sup>	=	0.5%
Pu <sup>238</sup>	=	81%	Th	=	0.01%
Pu <sup>239</sup>	=	15%	U	=	0.3%
Pu <sup>240</sup>	=	2.9%			
Pu <sup>241</sup>	=	0.8%			
Pu <sup>242</sup>	=	0.1%			

$$nvt = (5.9 \times 10^{10}) (3.0 \times 10^{-7}) \frac{\text{ergs}}{\text{gram}} = 1.8 \times 10^4 \text{ ergs/gram.}$$

The value is well below the threshold of damage from radiation effects for items located 1 meter from an RTG unit. Most of the electronics and scientific instruments are 7-10 feet from the RTG's and thus will not be adversely affected by RTG radiation.

## GROUND OPERATIONS FOR THE RTG POWER SUPPLY

One of the most important phases to consider of the entire JOVE mission encompasses all the ground operations before launch. The scheduling alone of such operations would require a detailed study. Certain cursory observations, however, related to ground operations affecting the RTG's will be made.

To set up a basis for the analysis there are certain ground rules that must be followed concerning the RTG's as received from the AEC (or from a contractor). First of all, let the RTG be characterized by two basic parts: The generator assembly (which will include the generator, shell, and fin sections along with the re-entry vehicle, separation device, and mounting brackets), and the fuel capsule. These two components will be shipped to the launch area separately but in a fully tested condition. There will be one set of eight generator assemblies and fuel capsules for the spacecraft. Also it is well known that a fuel capsule can be simulated within two percent of its actual performance by an electrical simulator.

For flight acceptance, the fuel capsule and the generator assembly will proceed through totally different checkout phases. The fuel capsule itself will remain stored after inspection except for various tests where an active fuel capsule is required. Thus, the fuel capsule simulator will be primarily used for testing since such a procedure minimizes the nuclear radiation exposure of any inspection worker.

After arriving at the test area, the generator assembly will be given incoming acceptance tests and will immediately be coupled with its active fuel capsule for performance tests. Following this step, the fuel capsules will be stored while the same performance test is carried out with the electric fuel capsule simulator for a comparison. After acceptance of these results, the generator assembly will proceed to the spacecraft assembly area where it will be installed in JOVE along with safety devices, radiation monitoring devices, and proper cooling facilities. With the fuel capsule simulator in place, performance tests can once again be carried out. Having replaced the fuel simulators by the active capsules, both radiation and magnetic mapping of the spacecraft will take place. With the completion of these tests the fuel capsules will be sent to Cape Kennedy. Meanwhile, the spacecraft must be checked for residual radiation and then sent on to the Cape along with the fuel simulator. Upon arrival at the Cape the active fuel capsules will be inspected and stored until it is time to place them on JOVE for launch. When the spacecraft arrives, it too will be inspected and the fuel capsule simulator will be installed for systems testing, compatibility testing, and dummy runs. Of course, active cooling of the power system will be necessary here also. With final systems flight acceptance tests completed, radiation safeguards will be set up and the active fuel capsules will be installed in place of the fuel simulators. Magnetic and radiation mapping will be carried out on the integrated spacecraft system. The spacecraft performance will be tested next with the actual RTG units in place as a final check before the shroud cooling system can be initiated and just before the spacecraft can be housed inside its shroud. The total vehicle assembly with shroud in place will now be transported to the launch pad on an eight hour trip. On the pad, pre-launch checkout and monitoring will begin. Presently it is estimated that such tests will be of 6- to 8-week duration but eventually reduced to 2 weeks by the late 1970's. Shroud cooling will be continuous during this period and will terminate only upon umbilical separation just before launch. From that time on, active cooling of the RTG's can be stopped and radiation heat transfer becomes the primary mechanism of cooling. New thermal problems will arise during this flight phase and they will be considered later in the report ( see page 8-41).

A general description of the procedure involved with handling the RTG's and integrating them with the spacecraft has been given to provide a feeling for some of the problems inherent in such a system. Two of the more specific ones

become relatively obvious from such an analysis, i. e. , the nuclear radiation problem and the active cooling difficulty which arises. Both of these problems will be briefly discussed in order to indicate that there is an awareness of them. An indication of the precautions that will be taken to minimize the potential hazard because of the presence of the RTG's will also be given.

For ground measurements of nuclear radiation when the active fuel capsule is present, neutrons and gamma rays must both be detected. Since both thermal and fast neutrons must be detected, fission chambers as well as a Hurst fast dosimeter and a semi-conductor detector must be present. For gamma radiation, a scintillation detector, a Geiger-Müller counter and a semi-conductor detector would probably be sufficient.

The maximum accumulated absorbed dose permitted for any worker is 3 rems/quarter (3 months) or .230 rems/week. Such a dose should not be absorbed by an individual in a short period of time, even though it would not be exceeded, nor should key personnel ever exceed this limit. By using an estimate of the radiation from the RTG's (see page 8-36), along with this limiting dose, one can calculate the number of trained personnel required to perform operations on the actively fueled spacecraft. Neglecting the gamma radiation (a small value compared to the total dosage) a man would be exposed to a flux of 760 neutrons/cm<sup>2</sup>-sec at a distance of one meter from any one RTG. This value is relatively high, and a worker could be available for, at best, a few hours.

It is unique to an RTG power source that once it is energized with active fuel capsules, no other external power supply is required. This has advantages, such as readily available power, but it also has its disadvantages. One of those disadvantages is that cooling provisions must be made during ground handling operations to dissipate the heat produced by the RTG's

The total power of the RTG's is  $640 W_e$  or approximately 48 500 Btu/hr at 4.5 percent efficiency. Thus, 48 500 Btu/hr must be dissipated in some fashion. One technique would be to develop a cooler which could be easily removed (Refer to Chapter V, page 5-35 ). This would allow for degassing of superinsulation at the same time. Another possibility, if the degassing problem were solved, would be to use convective heat transfer. With a 20° F,  $\Delta T$ , a mass flow of air (or nitrogen) of approximately 200 lb/min would be required to dissipate the total RTG heat. This may seem like a stringent condition, especially for the launch pad; however, the projected air conditioning of stage compartments of the Apollo/Saturn space vehicle are listed below [ Ref. VIII-13].

<u>STAGE</u>	<u>FLOW RATE (lb/min)</u>
S-IC	185
S-II	500
S-IVB	300
I. U.	150/200
<u>CSM</u>	<u>140</u>
TOTAL for SPACE VEHICLE	1400

Launch Pad 39A has a design of approximately 2000 lb/min of air cooled to 33-35° F at the Mobile Launcher base.

It is further stated that for the Voyager/Saturn space vehicle, the environmental conditioning capacity potentially available for the spacecraft is in the order of 700-800 lb/min. This is sufficient for the JOVE mission.

Facilities for air conditioning inside the Vertical Assembly Building (VAB) are more adequate than they are on the launch pad. Air or nitrogen cooling conditions (200 lb/min) must also be assured for the trip on the transporter from the VAB to the launch pad.

## RTG TEMPERATURES DURING FLIGHT PHASES

Twenty square feet of radiator fin surface area is found to be sufficient to reject to space the heat produced by the RTG fuel. It must be certain, however, that these fins can "see" space as the environment to which they dissipate heat. There are two periods during the JOVE mission when the RTG's will not "see" space but rather some other environment. One of these periods is during the launch of JOVE, until the time when the nose cone is jettisoned from the spacecraft. The inside of the nose cone is all that the RTG's will see during this period. The second occurrence is when the retropropulsion system is operative and the RTG's "look" partially at space and in part at the plume from the LEMDE engine. The temperatures of the RTG's during each of these periods have been theoretically considered (see page 8-21 ) and found not to be excessive.

## COST ESTIMATES FOR THE POWER SUPPLY SYSTEM

By far the major portion of the RTG power supply system cost is caused by the cost of the fuel itself. Schulman [ Ref. VIII-8] estimates that the radioisotope,  $\text{Pu}^{238}$ , will cost \$500/watt<sub>th</sub> in the near future. Deonigi [ Ref. VIII-7] lists values of \$894/watt<sub>th</sub> and \$500/g which he found from two different sources. An earlier (1961) source referred to by Rohrman [ Ref. VIII-15] lists the estimated cost of  $\text{Pu}^{238}$  to be \$1600/watt<sub>th</sub> and the cost per gram as \$880/g. A representative of Martin-Marietta, in a private communication, said \$1000/watt<sub>th</sub> would be a highly conservative estimate. Another Jupiter study [ Ref. VII-1] listed the RTG fuel cost at \$1500/watt<sub>th</sub> in 1965 dollars. A study for the Voyager program [ Ref. VIII-16] indicated that the isotope cost for the RTG's amounted to \$22 500 per electrical watt. Assuming, in this case, 4.25 percent efficiency, this would mean \$965/watt<sub>th</sub>. Thus, a whole spectrum of values is available from which one can choose an estimate. The graph shown in (Fig. VIII-8) is an attempt to estimate a value which can be used this year. Choosing what appears to be a very conservative value of \$900/watt<sub>th</sub> for the RTG fuel cost and assuming an efficiency of 4.5 percent for the system, an estimate of 1.6 million dollars is established for each 80 W<sub>e</sub> RTG. Thus, for a 640 W<sub>e</sub> total power supply system on the JOVE mission, the cost will amount to approximately \$12 800 000.



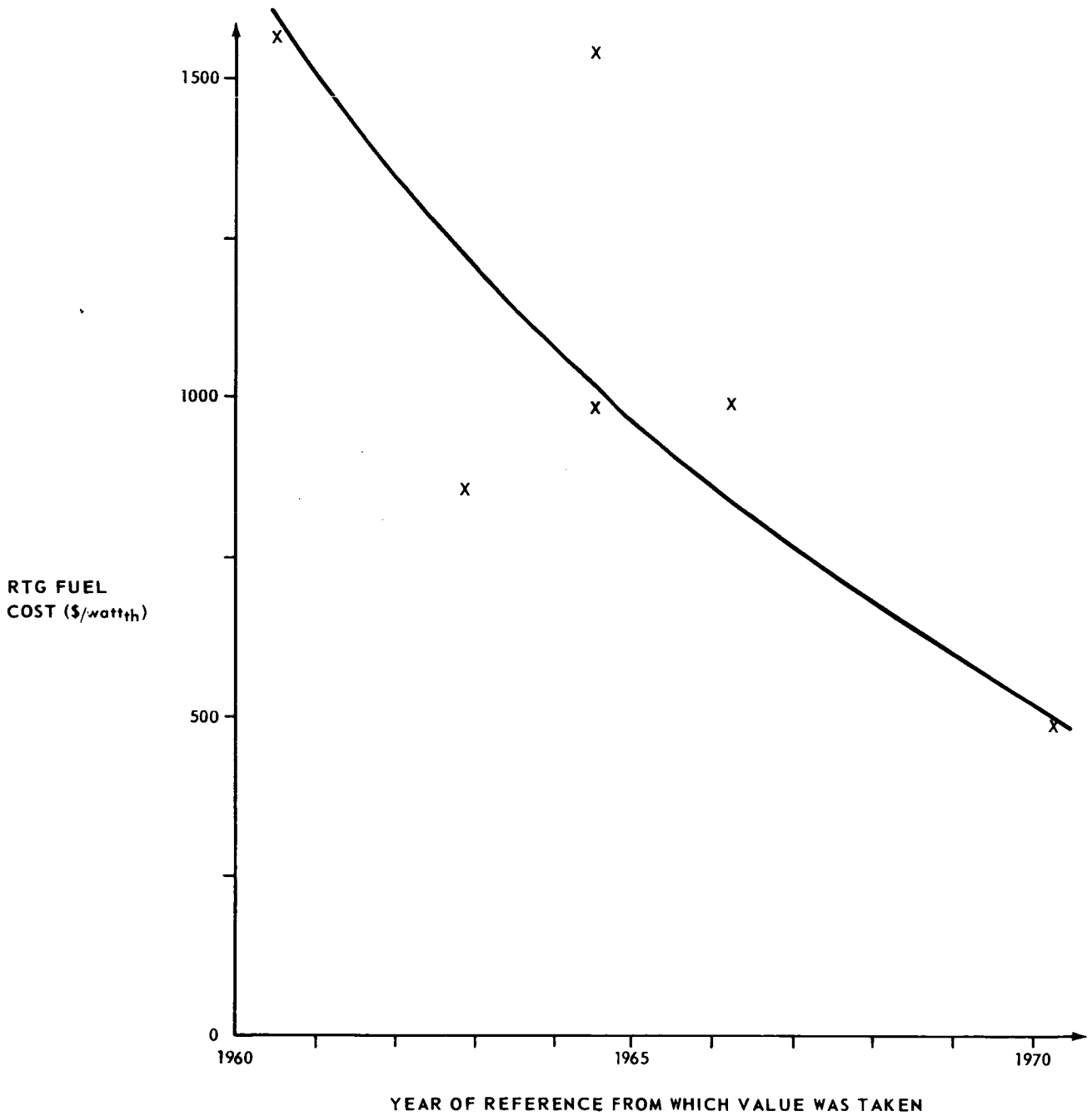


FIGURE VIII-8. RTG FUEL COST

## REFERENCES

1. A Study of Jupiter Flyby Missions (Final Technical Report). Report No. FZM-4627. General Dynamics, Fort Worth Division, May 17, 1966.
2. Application of the Saturn/Apollo Hardware to Unmanned Scientific Exploration of the Solar System. Report No. TM-292/3-6-003, Northrop Space Laboratories, Huntsville, Alabama, April 1966.
3. Shair, R. C.; Lerner, S. R.; Joyner, P. A. and Evans, G. E.: A Review of Batteries and Fuel Cells for Space Power Systems. Journal of Spacecraft and Rockets. vol. 4, no. 7, pp. 833-838, July 1967.
4. Levedahl, W. J.: Private Communication. Unpublished 1967.
5. Rappaport, P.: Photovoltaic Power. Journal of Spacecraft and Rockets, vol. 4, no. 7, pp. 838-841, July 1967.
6. Corliss, William R. and Harvey, Douglas G.: Radioisotope Power Generation. Prentice-Hall, Inc., 1964.
7. Deonigi, D. E. and Eschbach, E. A.: Production and Indifference Pricing of Transuranium Isotopes. Proceedings of the ANS National Topical Meeting, Augusta, Georgia, March 1966.
8. Schulman, Fred: Isotopes and Isotope Thermoelectric Generators. Advanced Technology Conference. NASA SP-131, August 1966, pp. 73-93.
9. Sutton, G. W.: Direct Energy Conversion. Interuniversity Electronics Series, McGraw-Hill Book Company, 1966.
10. Anquist, S.: Direct Energy Conversion. Allyn and Bacon, Inc., 1965.
11. Chang, Sheldon S.: Energy Conversion. Prentice Hall, Englewood Cliffs, New Jersey, 1963.
12. Boman, L. H.: Application of a Radioisotope Heat Source Interior to a Tubular Thermoelectric Generator. Proceedings of the ANS National Topical Meeting, Augusta, Georgia, March 1966.

## REFERENCES (Concluded)

13. Voyager RTG Spacecraft Design Definition RTG Study - Voyager Task C. Report No. VOY-C1-TR16. General Electric Missile and Space Division, Philadelphia, Pennsylvania, March 1, 1967.
14. Stoddard, D. H. and Albenesius, E. L.: Radiation Properties of Pu<sup>238</sup> Produced for Isotopic Power Generators, DP-984, E. I. Dupont De Nemours and Co., July 1965.
15. Rohrmann, C. A.: Radioisotopic Heat Sources, HW-76323. Hanford Atomic Products Operation, Richland, Washington, February 1963.
16. Voyager Spacecraft System Preliminary Design, Alternate Designs Considered, System Alternates, Volume B (Book 1 of 3). Report No. DIN: 65SD4388. General Electric, Spacecraft Department, July 30, 1965.

## BIBLIOGRAPHY

Advanced Planetary Probe Study, Final Technical Report, vol. 2. Report No. 4547-6005-ROOOO. Spin-Stabilized Spacecraft for the Basic Mission, TRW Systems, July 27, 1966.

Application of the Saturn V Launch Vehicle to Unmanned Scientific Exploration of the Solar System. Report No. TR-292/3-6-075, Jupiter Orbiter/Solar Probe Mission Study Advanced Mission Investigations, Northrop Space Laboratories, Huntsville, Alabama, September 1966.

Deverall, J. E. and Kemme, J. E.: Satellite Heat Pipe, LA-3278-MS. Los Alamos Scientific Laboratory of the University of California, April 20, 1965.

Frank, S.; Smith, J. T. and Taylor, K. M.: Heat Pipe Design Manual, MND-3288. Martin Nuclear, February 1967.

Hofman, F. E. and Johnson, G. W. S. and Simonsen, L. H.: Development of Cost Estimating Techniques and Relationships for Unmanned Space Exploration Missions PRC R-870. Planned Research Corporation, Los Angeles, California, October 28, 1966.

Kick Stage Electrical Power Selection. Report No. TN-AE-66-147, Space Division, Chrysler Corporation, New Orleans, Louisiana, July 1, 1966.

Marcus, B. D.: On the Operation of Heat Pipes, 9895-6001-TU-000. Physical Electronics Laboratory, TRW Space Technology Laboratories, May 1965.

Voyager Spacecraft System, Preliminary Design, Flight Spacecraft Preferred Design, Telecommunications, Volume A (Book 2 of 4). Report No. DIN: 65SD4388, General Electric, Spacecraft Department, July 30, 1965.

Wood, W. D. and Dean, H. W.: Thermal Properties of High-Temperature Materials. RSIC-202, U. S. Army Missile Command, Redstone Arsenal, Alabama, June 1964.

CHAPTER IX  
COST AND RELIABILITY



## CHAPTER IX. COST AND RELIABILITY

### DEFINITION OF SYMBOLS

CER	Cost Estimating Relationships
AGE	Aerospace Ground Equipment
JPL	Jet Propulsion Laboratory
TTC	Tracking, Telemetry, and Command
PRC	Planning Research Corporation
P/V TPC	Planetary Vehicle Total Program Cost
$P_x$	Probability of success using method x
$P_y$	Probability of success using method y
$P_i$	Probability of failure of individual subsystem i
$P_x^{(K)}$	$P_x$ for K channel redundancy
$P_y^{(K)}$	$P_y$ for K channel redundancy
R	$P_y/P_x$

## SPACECRAFT PROGRAM AND COST ESTIMATING RELATIONSHIPS

The true cost of a spacecraft system and a support system must be broken down into a number of categories that consider every possible item of the total expense. Basically one considers the spacecraft system to consist of the planetary vehicle and the launch vehicle. The support system consists of all the necessary facilities and all of the manpower involved in the proper functioning of these facilities. When plans have been made to integrate these systems and tentative launch dates are set, one has a space program.

The necessary support system facilities are those in which any function pertaining to conception, design, management, fabrication, transportation, testing, assembling, launch, and other operations will be performed. These facilities will need to be inherited or constructed. The manpower will either be inherited by transfer from some other branch within an organization or will need to be recruited. All of this will need to be costed before funding can be obtained for any space program.

Presented here is a breakdown on the estimated cost of the JOVE planetary vehicle which was obtained through the use of graphs prepared for a report published in October 1966 by the Planning Research Corporation (PRC), under contract to the Jet Propulsion Laboratory (JPL). A detailed breakdown on the estimated cost of an entire space program may be obtained from the PCR graphs and tables in the same report. Since the JOVE report is a conceptual systems engineering design of a planetary reconnaissance vehicle, however, it is presumptuous to include a detailed breakdown estimate for an entire space program at this time. Nevertheless, it would not be too far wrong to double the cost of the JOVE Planetary Vehicle to obtain the price of a complete JOVE Space Program. Since the cost will escalate with respect to time a three percent per annum increase in cost must be added to estimates made in this chapter, with escalations to begin after the year 1965 when the Cost Estimating Relationships (CER's) were prepared.

## JOVE Planetary Vehicle

The JOVE planetary vehicle as conceived will need to be made into a functional design. A complete set of working drawings consisting of all the detail drawings, assembly drawings, and parts lists will be necessary. Mock-ups for fitting of subsystems, wind-tunnel models, and "boiler plate" models for other testing will need to be fabricated. JOVE planetary vehicles and spare parts will need to be manufactured. The cost for all of this will be chargeable to the total JOVE Space Program.

## Saturn V Launch Vehicle

Saturn V, now considered to be the standard-heavyweight interplanetary launch vehicle for at least the 1970 decade, will be developed and operational in 1978 when the first attractive opportunity will occur for launching JOVE. At that time, Saturn V will possibly be uprated to develop more than the presently designed seven and one half million pounds of thrust on liftoff. Improvements in the performance and the efficiency of the F1 engines, the development of more powerful and more efficient propellants, and additional strap-on boosters probably will, either singly or in combination, contribute appreciable to liftoff capabilities. It is within the realm of possibilities that the Saturn final stage will be a nuclear powered system when JOVE is launched during the more favorable payload year, 1980. The cost of a Saturn V as of the given launch year will be chargeable to the JOVE Space Program.

## Support System

The support system for the advanced planetary exploration programs already planned will be in operation by 1978. The system may need additional sophistication tailored to suit the JOVE program, but it is also possible that the state of the art may be advanced enough by then to fit the requirements of JOVE. Certainly it will be by 1980. The cost then of the support system chargeable to the JOVE program will be the operating manpower and the use of all the necessary transportation, assembling, launching, and tracking facilities. It may be concluded from the above that growth improvements in the launch vehicle and the support system, properly chargeable to some of the other



advanced planetary programs, may reduce the previous estimation factor for these two items in the JOVE Space Program. Perhaps, only an increase of fifty percent will need to be added to the cost of the JOVE planetary vehicles to get a realistic cost for estimating the JOVE Space Program.

## ALLOCATION OF SUBSYSTEM WEIGHTS TO COST CATEGORIES

In order to allocate the weights of subsystems as developed in Table V-2 to the appropriate cost categories for using the PRC graphs and tables, Table IX-1 has been prepared for "Planetary Vehicle" and Table IX-2 for "Propulsion Module." In most instances the method of distribution is obvious; however, some clarification will make the cost categories even more understandable.

1. Cabling - The cabling was distributed almost equally to all cost categories except the electrical power which is the terminal point for this cost item.

2. Contingency - The weight allowed for contingencies was allocated in proportion to the subtotal weight for all cost categories.

3. Navigation and Guidance - Computing and sequencing is most applicable to this cost category because this subsystem contains the command processing and storing devices, the planetary vehicle time reference sensors, and the sequence command devices.

4. Communications, T T and C - Because they are of a similar electronic nature, radio, telemetry, and command were grouped under this cost category.

5. Stabilization and Control - Guidance and control is most applicable to this cost category because it contains the attitude control system, the autopilot, and the cold gas jet system.

6. Structure - Pyrotechnic mechanisms and controls, temperature control, and the planetary vehicle adapter are more closely related to structure than to any of the other cost categories.

TABLE IX-1. DISTRIBUTION OF JOVE MISSIONS WEIGHTS TO COST CATEGORIES,  
PLANETARY VEHICLE WEIGHTS (Wt = 4652 lb)

Items	Cost Categories	JOVE Weights	Experiments or Mission Sensors	Navigation and Guidance	Communications T T and C	Data Management	Stabilization and Control	Structure	Electrical Power
Structural and Mechanical		1383						1383	
Pyrotechnics		24						24	
Temperature Control		260						260	
Radio		272			272				
Data Storage		52				52			
Telemetry		16			16				
Command		15			15				
Computing and Sequencing		35		35					
Cabling		200	33	33	33	34		33	
Power		645							645
Guidance and Control		430					430		
Science Instruments		150	150						
Planetary Vehicle Adapter		520						520	
Contingency		650	40	10	40	15	100	315	130
TOTALS		4652	223	78	376	101	564	2535	775

TABLE IX-2. DISTRIBUTION OF JOVE MISSIONS WEIGHTS TO COST CATEGORIES,  
 PROPULSION MODULE (Wt = 15 194 lb)

Items	Cost Categories	JOVE Weights	Propulsion Module Structure	Propulsion Liquid Rocket
Structure		1637	1637	
Engines		449		449
Totals		2086	1637	449

## COST OF THE JOVE PLANETARY VEHICLE

The following tables which show the cost breakdown of the various planetary vehicle subsystems and other related expense items are after those shown in the previously mentioned Planning Research Corporation's report. The graphs from which the cost estimating relationships were obtained were developed for the PRC cost model from "The Space Planner's Guide," USAF Report, July 1, 1965. This informative source was updated with information from aerospace contractors, NASA reports, and NASA officials.

Table IX-3 shows the total hardware cost of four planetary vehicles to be \$125 970 000. Table IX-4 shows the total hardware cost of four planetary vehicle propulsion modules to be \$63 270 000. Table IX-5 shows the cost for integrating the planetary vehicle module and the planetary vehicle propulsion module. It further shows that the integration of the eight planetary vehicle modules into the four planetary vehicle systems amounts to a total planetary vehicle program cost of \$422 340 000. This does not include the cost of the Saturn V launch vehicle or the support system. The dollar value is for 1965, without using the escalation factor, because there are too many variables which might invalidate straight line escalating of the dollar.

## DISCUSSION

A detailed explanation of how to use the tables and graphs would be lengthy and would not enhance the value of this study. It is believed that the reader who is interested in estimated cost determinations will find the method self-explanatory after studying the table notations with reference to the Cost Estimating Relationships (CER's).

No attempt will be made to defend the selection of the PRC cost model for this estimate. There are other valid methods which could have been used with equal success. It is not implied here that this is the best cost model to be used in estimating the cost of future unmanned interplanetary reconnaissance missions.

Time will tell whether one cost estimating model is superior to another method. One thing that can be said with certainty -- when the national space program has grown from the infancy of space exploration to full aerospace technological stature the necessary experience required to predict with accuracy the price of interplanetary travel will have been accumulated.



TABLE IX-4. PLANETARY VEHICLE PROPULSION MODULE COST  
(DOLLARS X 10<sup>6</sup>)

Cost Categories	Qualifying Parameters	Parameter Input	CER Ref. Fig.	Design Dev. Cost	CER Ref. Fig.	Parameter Output	First Unit Cost	No. Test Articles	Cost Test Articles	No. Flight Articles	Cost of Flight Articles	Total HDW. Cost
Propulsion Module Structure	Weight (lb)	1637	IX-3	33.0	IX-4	4000 \$/lb	6.55	5	32.75	4	26.20	58.95
Retropropulsion (LEMDE) (Liquid)	Thrust (lb)	10 500	IX-5	6.0	IX-6	15 \$/lb	0.16	5	0.80	4	0.64	1.44
Propulsion (TC/OT) (Liquid)	Thrust (lb)	600	IX-5	2.4	IX-6	90 \$/lb	0.05	20	1.00	16	0.80	1.80
Propulsion (AC/S) (Gas)	Thrust (lb)	12	IX-5	1.0	IX-6	1000 \$/lb	0.01	60	0.60	48	0.48	1.08
Age	P/V Dry Wt (lb)	2086	IX-19	15.0								
Tooling and Sp. Test Equipment	P/V Dry Wt (lb)	2086	IX-19	6.6								
Totals			Σ†	64.0	①				35.15	②	28.12	63.27
Systems Integration		① + ② 99.15x10 <sup>6</sup>	IX-20	6.2								

TABLE IX-5. PLANETARY VEHICLE TOTAL PROGRAM COST (P/V TPC)  
(DOLLARS X 10<sup>6</sup>)

ITEM	(1) Design Development Cost	(2) Cost of Test Articles	(3) D/D Plus Test Articles	(4) Integration	(5) Cost of Flight Articles	(6) Total Cost
			(1) + (2)	(3) & CER (IX-20)	Dollars x 10 <sup>6</sup>	(3) + (4) + (5)
JOVE Plan. Vehic. Module	136.1	63.33	199.43	10.0	62.64	272.07
JOVE P/V Propul. Module	64.0	35.15	99.15	5.0	28.12	132.27
		+ Σ	298.58		+ Σ	404.34
P/V Systems Integration Increment Ref: (7) & CER (IX-20)		(7)			(8)	18.00
			---	P/V TPC		422.34

(Mission support and space flight operations, including the Saturn V launch vehicle would cost as much as the P/V TPC per mission based on the PRC model. The P/V TPC is based on the 1965 dollar-escalate at 3 percent per annum after 1965)

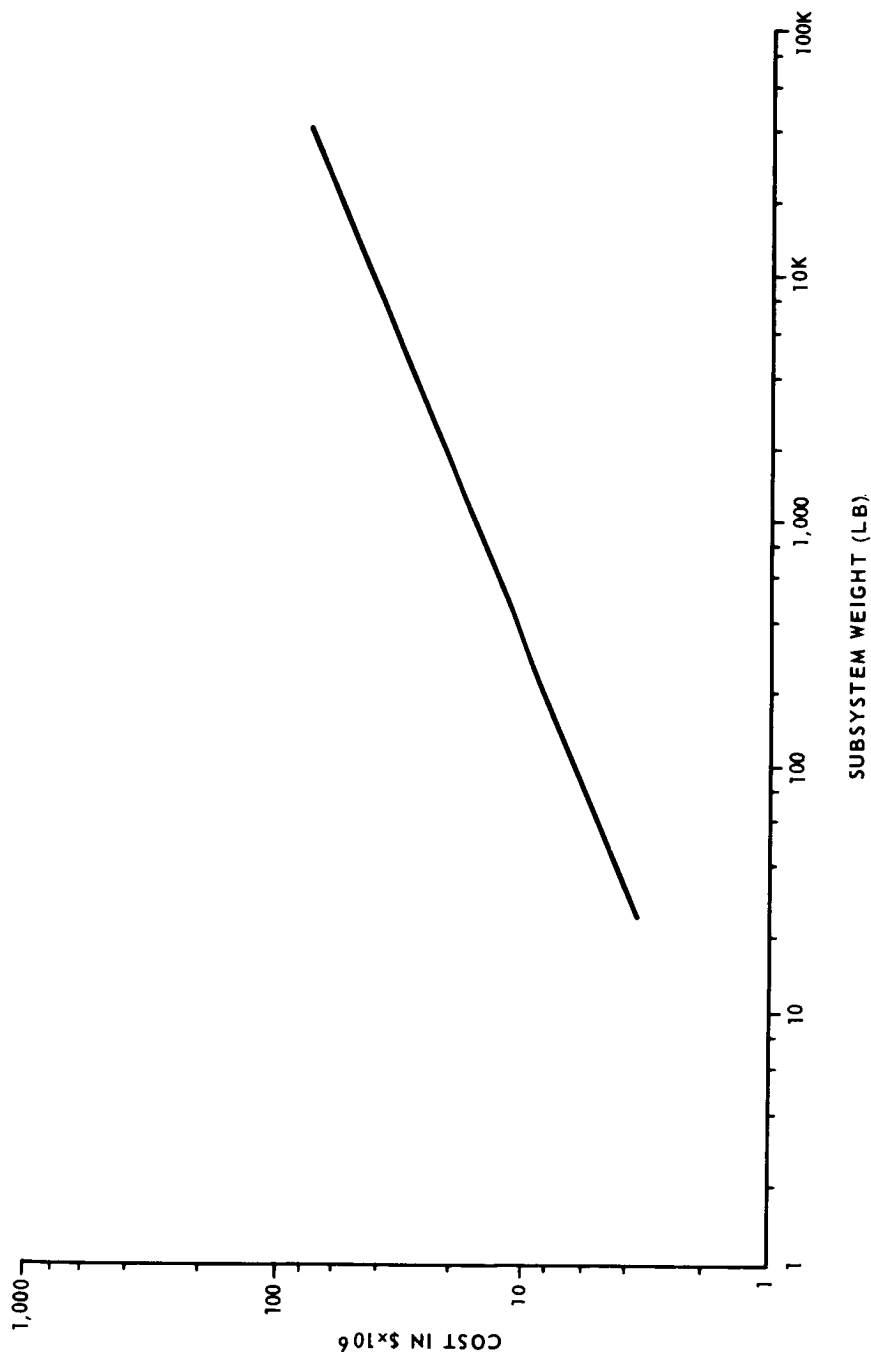


FIGURE IX-1. PLANETARY VEHICLE STRUCTURE DESIGN/DEVELOPMENT COSTS



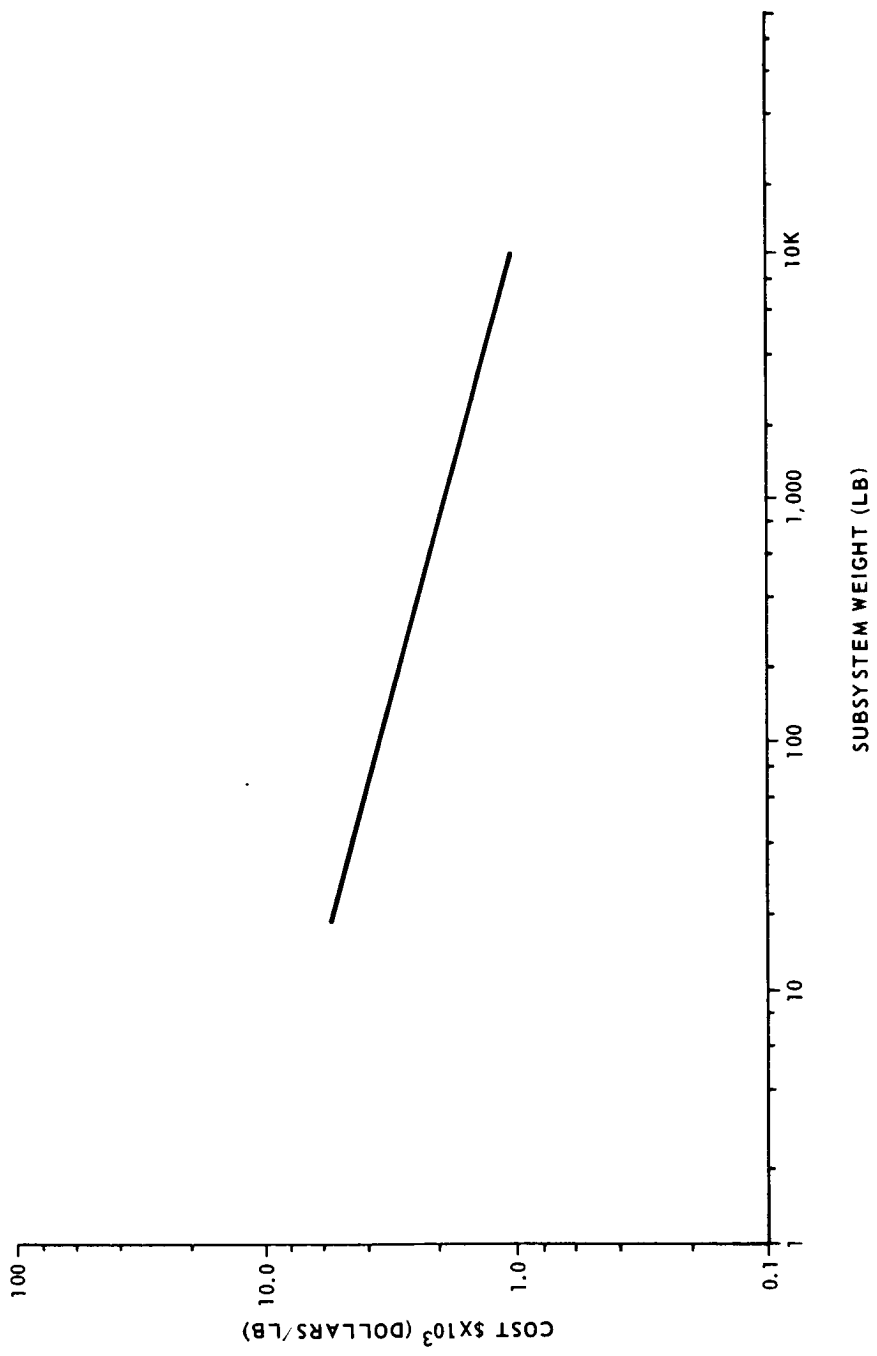


FIGURE IX-2. PLANETARY VEHICLE STRUCTURE FIRST UNIT COST

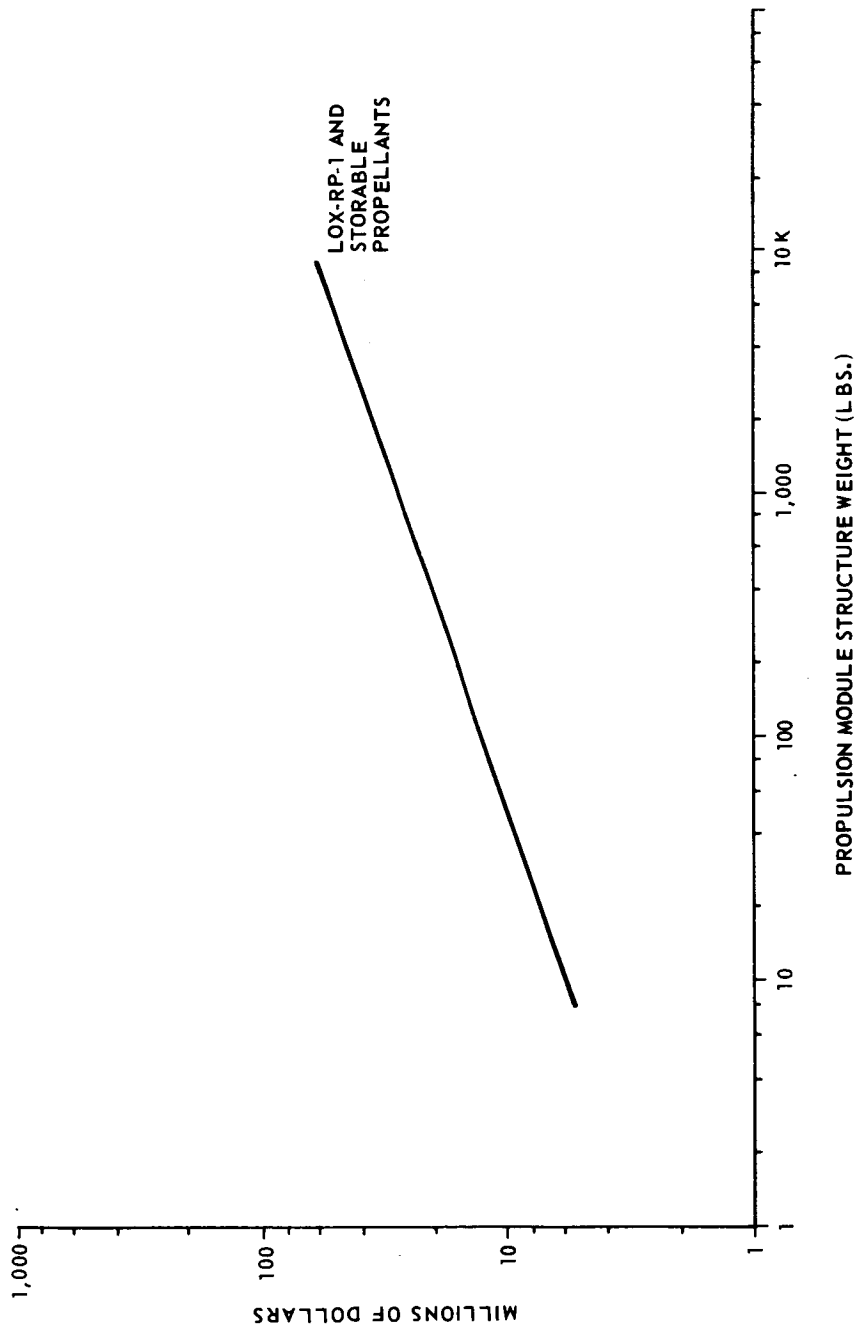


FIGURE IX-3. PROPULSION MODULE STRUCTURE DESIGN/DEVELOPMENT COST

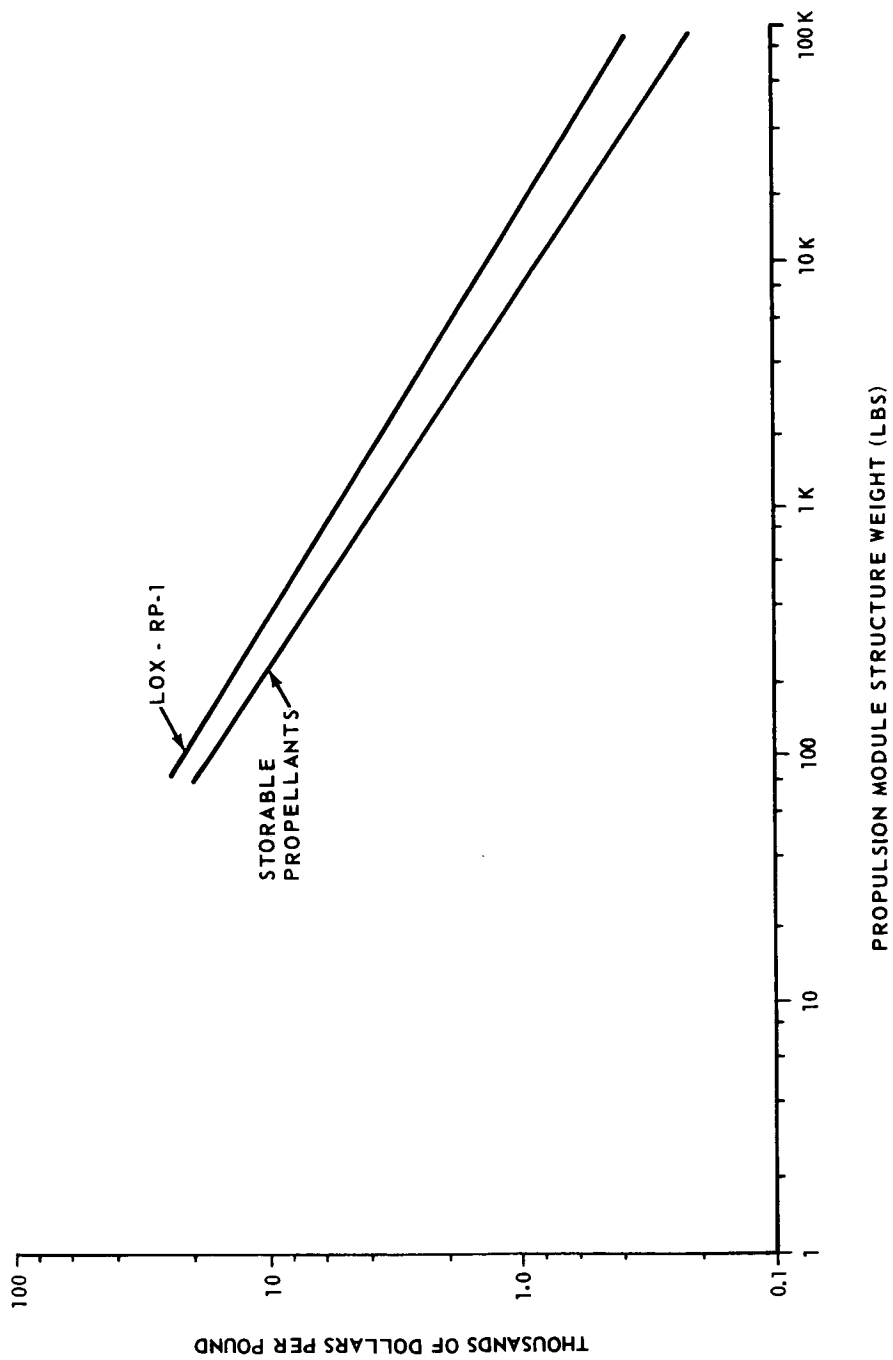


FIGURE IX-4. PROPULSION MODULE STRUCTURE FIRST UNIT COST

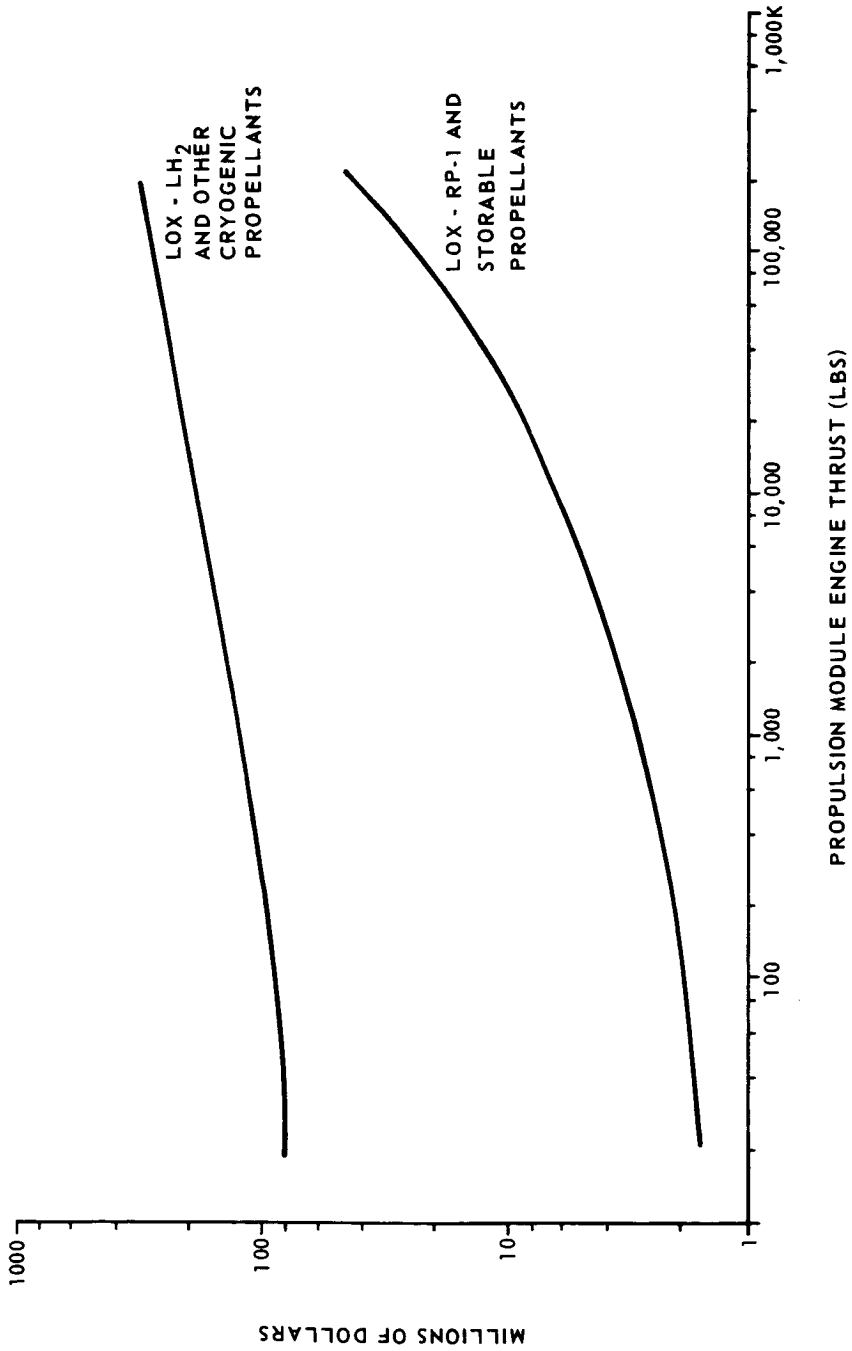


FIGURE IX-5. PROPULSION MODULE ENGINE (LIQUID PROPELLANT) DESIGN-DEVELOPMENT COST

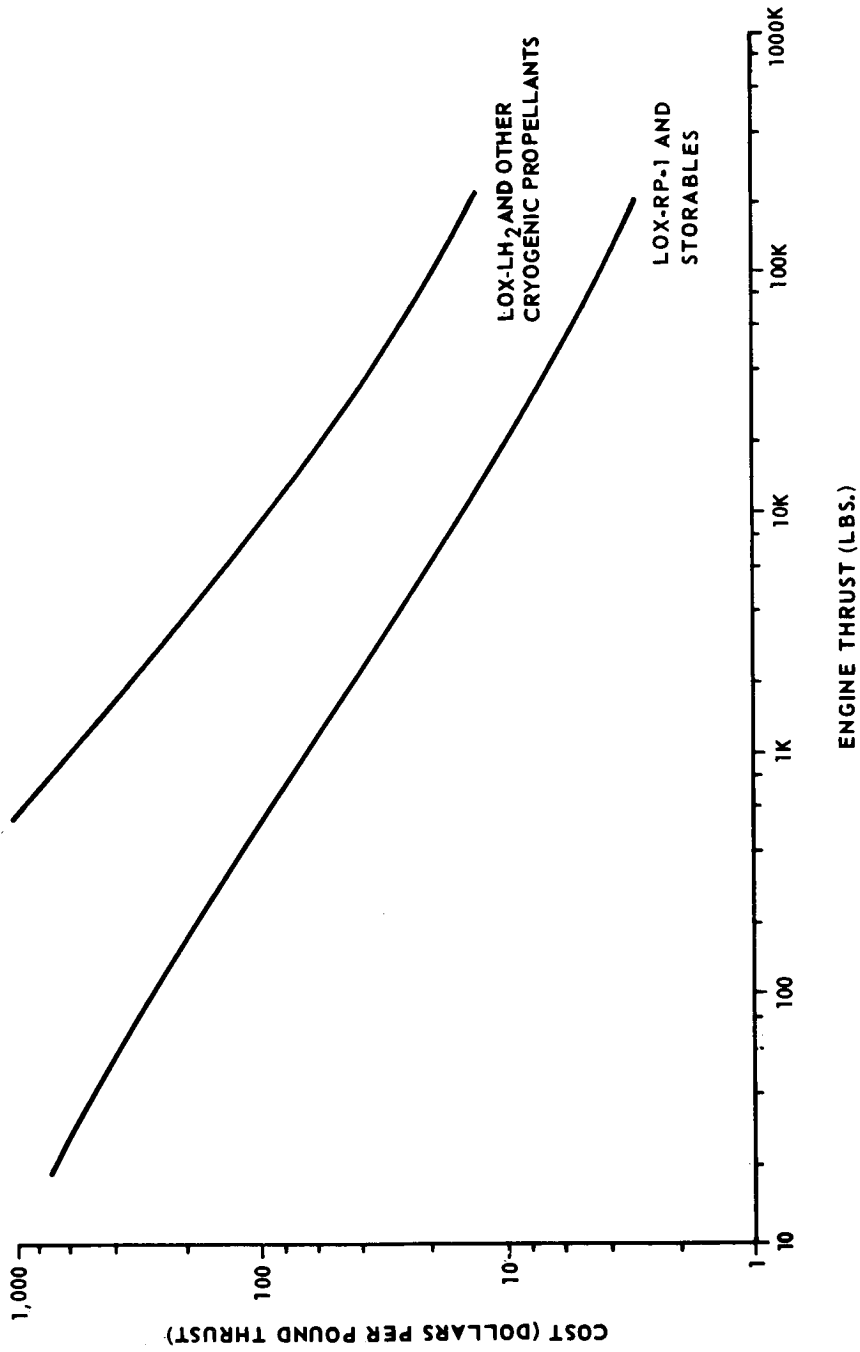


FIGURE IX-6. PROPULSION UNIT ENGINE FIRST UNIT COST

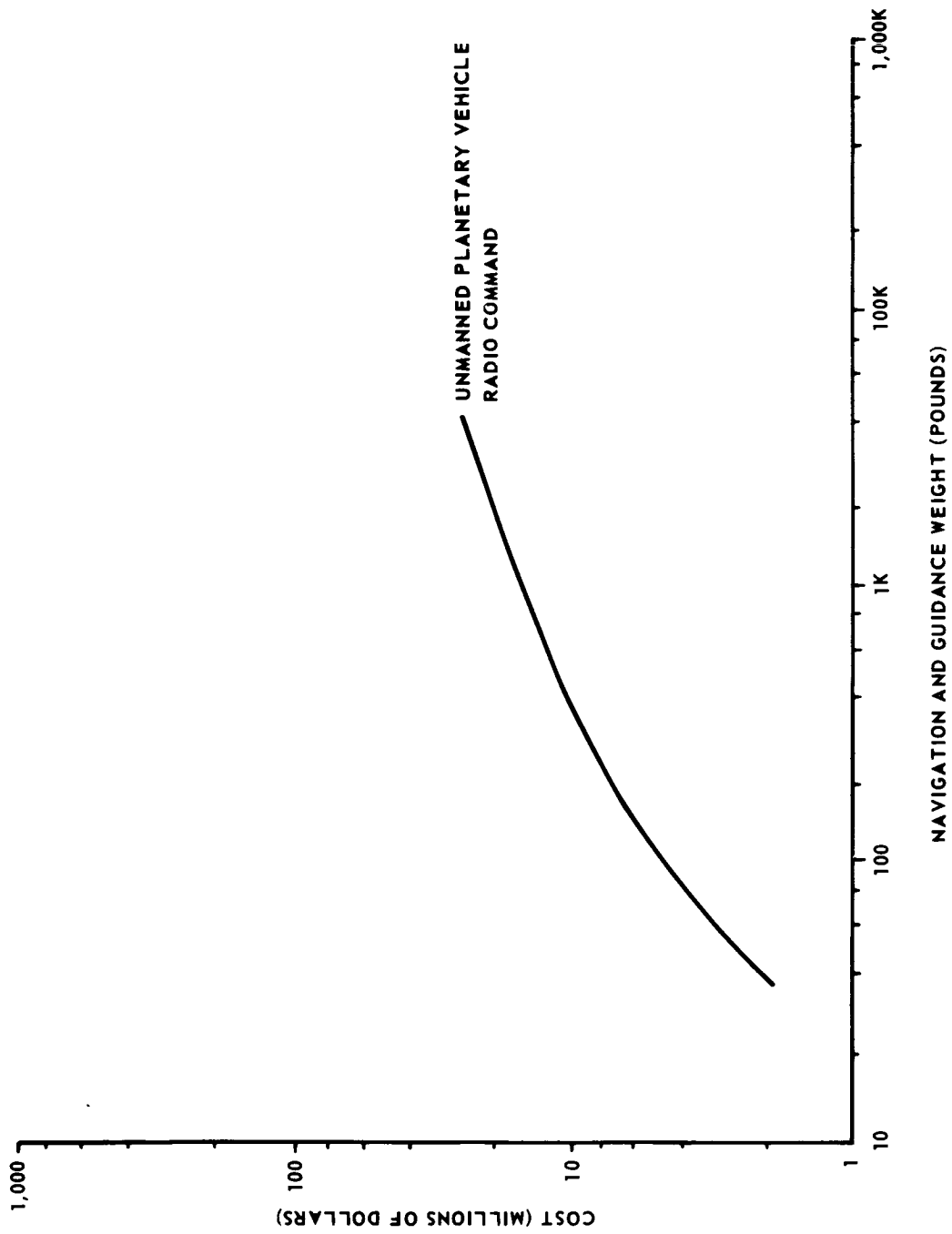
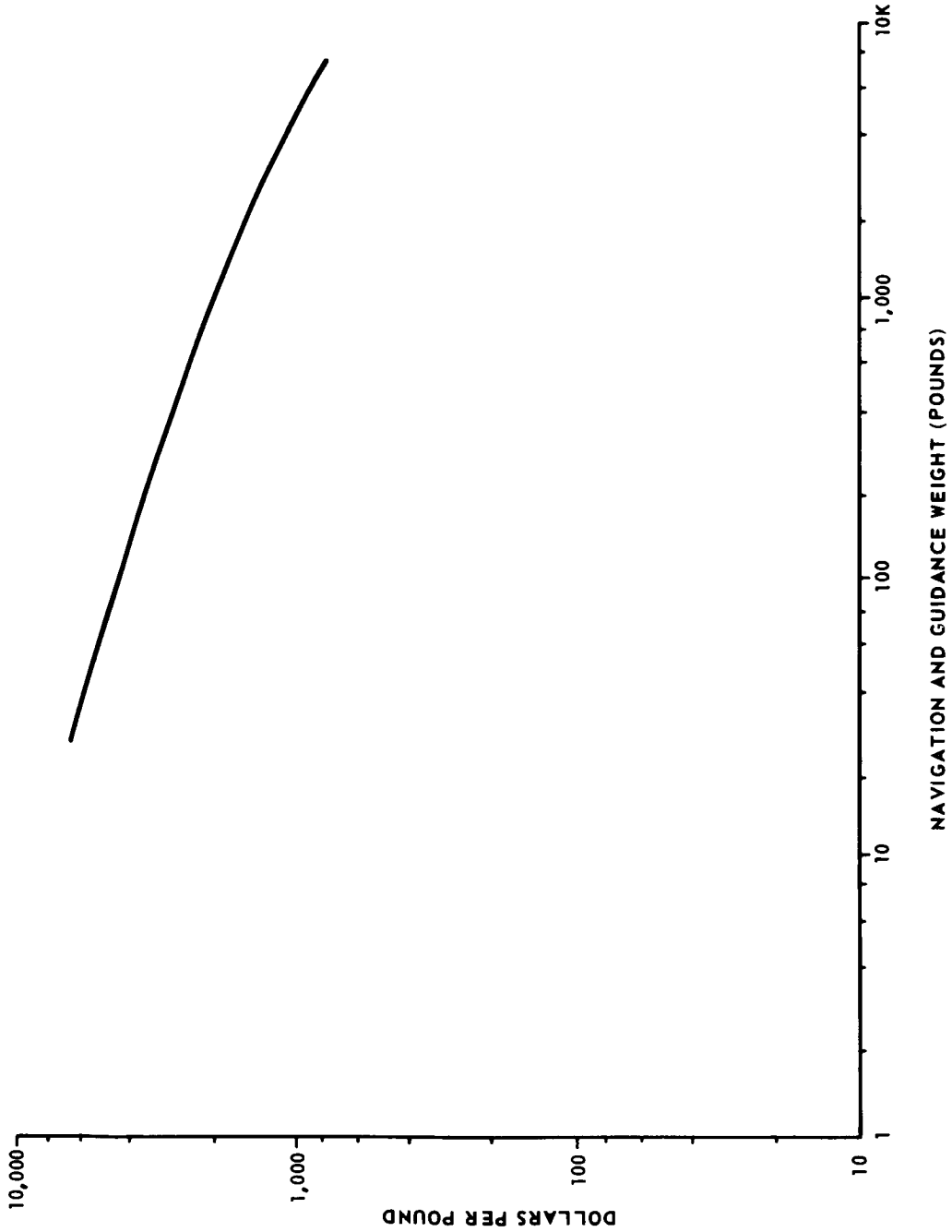


FIGURE IX-7. NAVIGATION AND GUIDANCE DESIGN/DEVELOPMENT COST VERSUS WEIGHT



9-18

FIGURE IX-8. NAVIGATION AND GUIDANCE FIRST UNIT COST

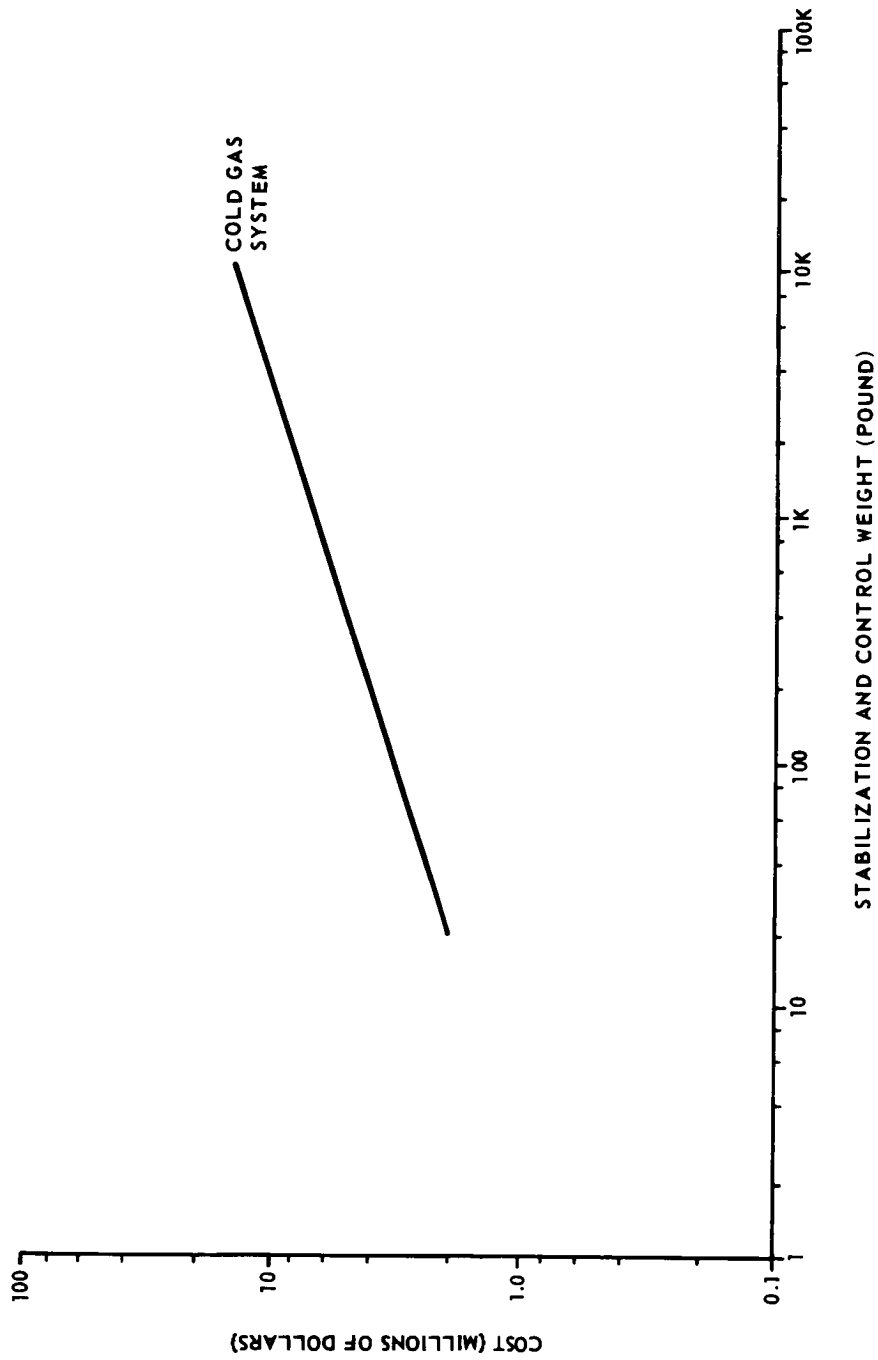


FIGURE IX-9. STABILIZATION AND CONTROL SYSTEM DESIGN/DEVELOPMENT COST



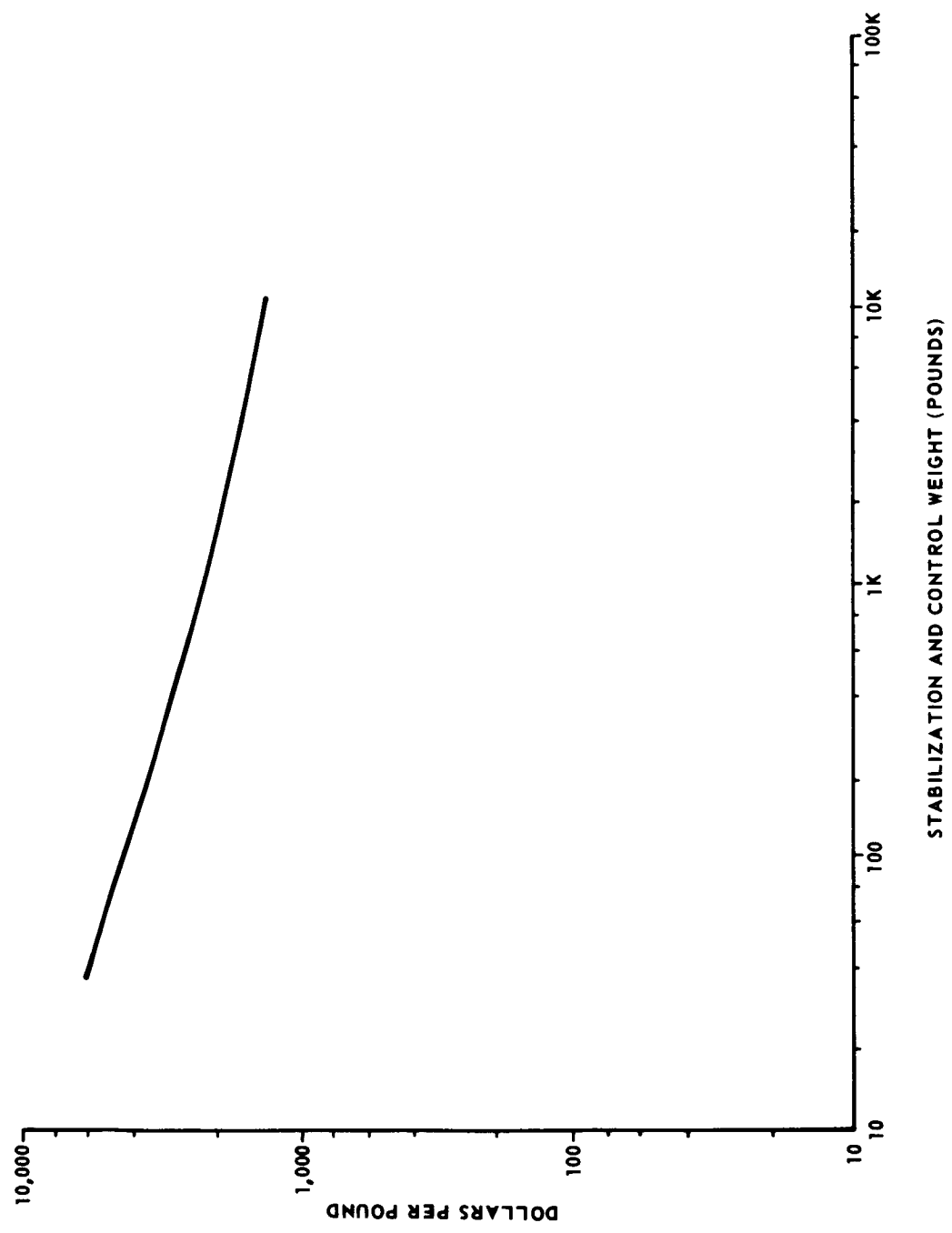


FIGURE IX-10. STABILIZATION AND CONTROL FIRST UNIT COST

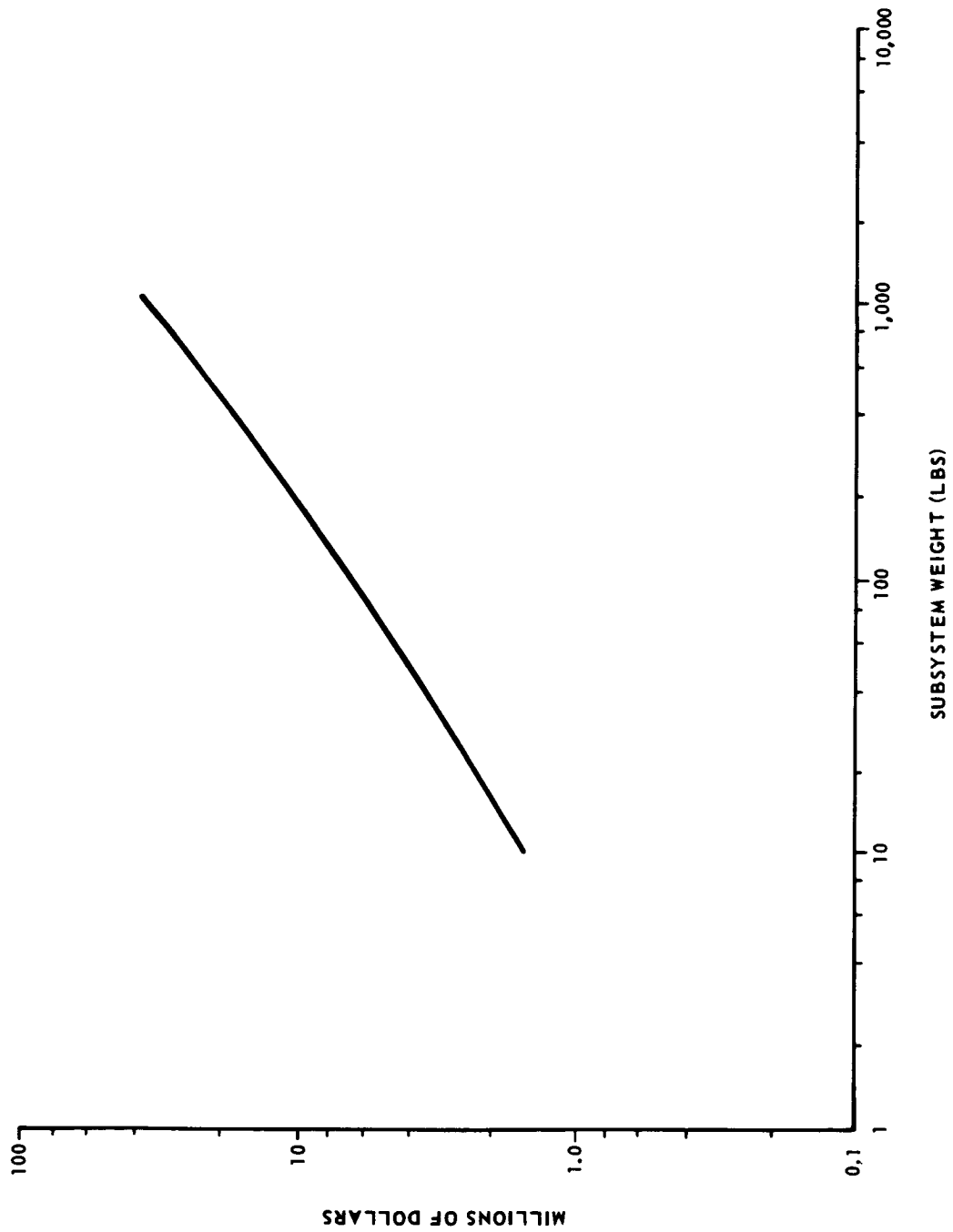


FIGURE IX-11. COMMUNICATIONS DESIGN/DEVELOPMENT COST

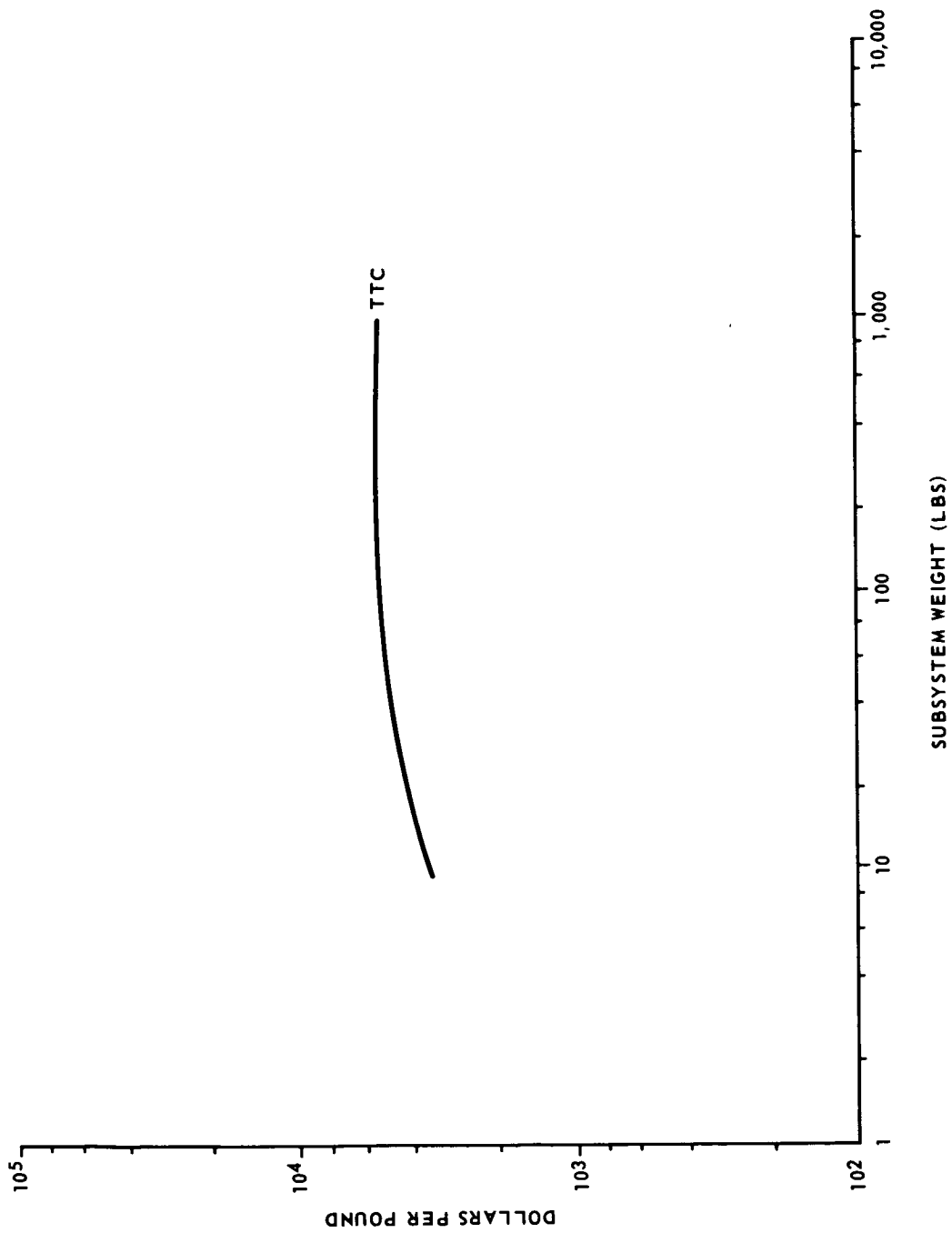


FIGURE IX-12. COMMUNICATIONS FIRST UNIT COST

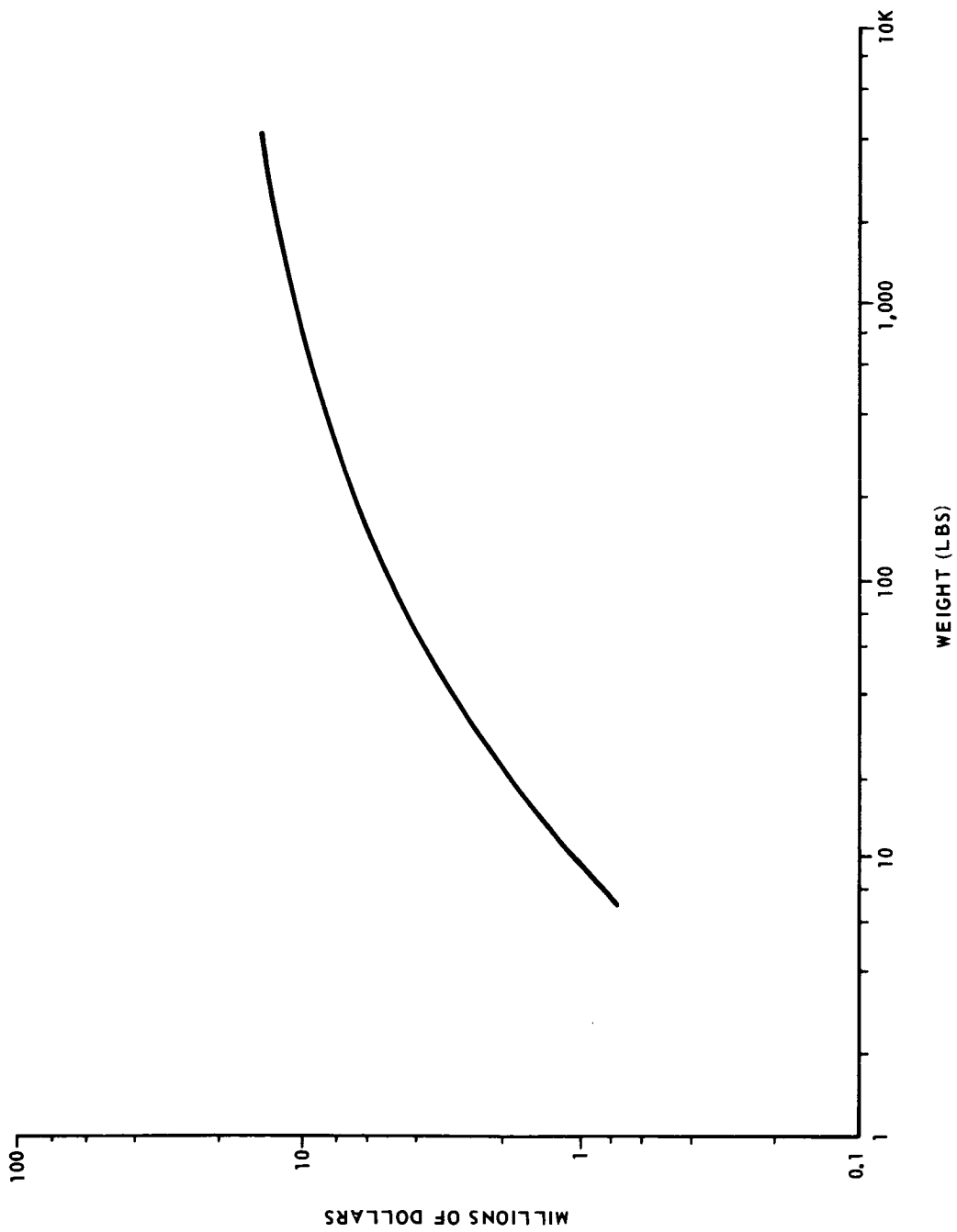


FIGURE IX-13. DATA MANAGEMENT DESIGN/DEVELOPMENT COST

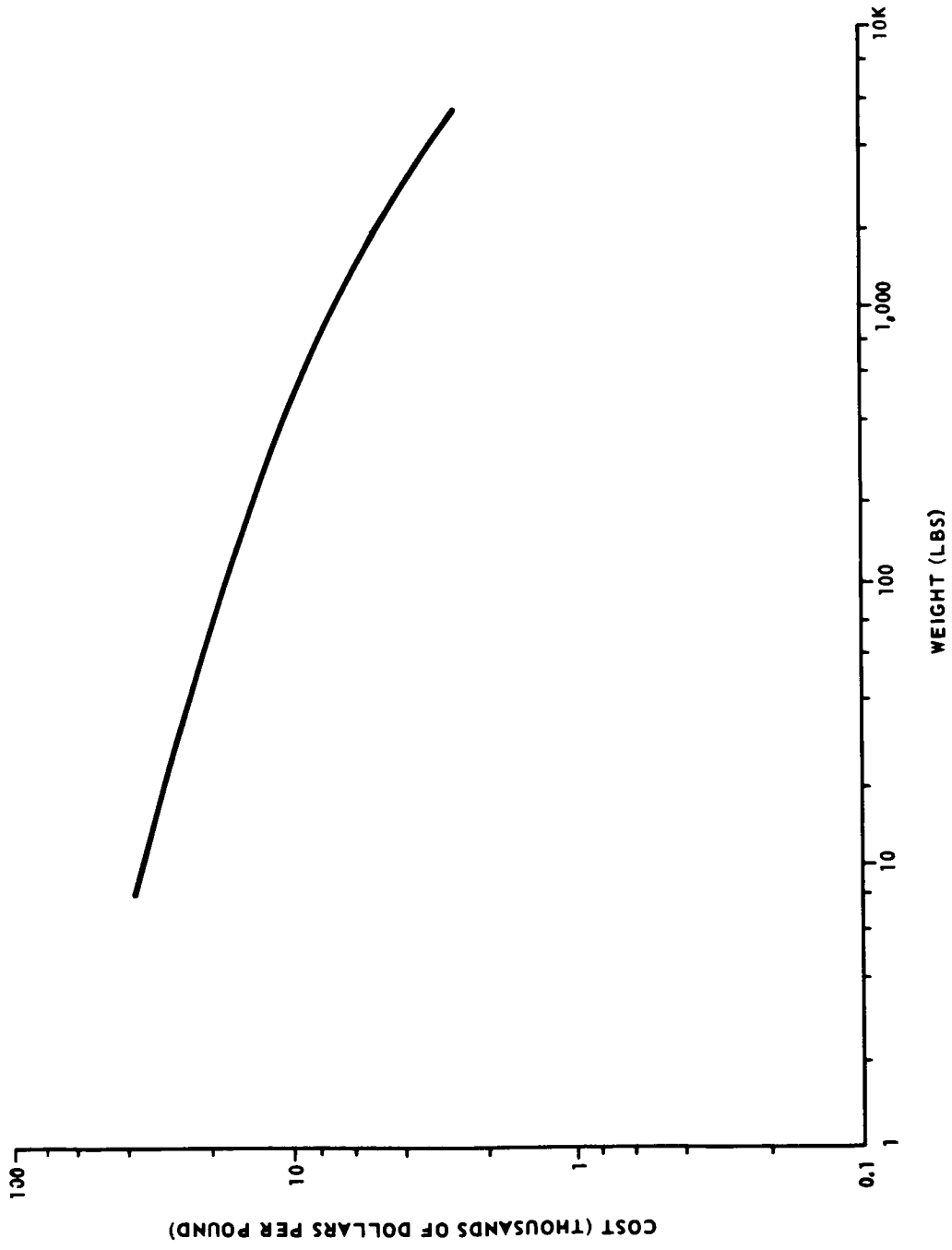


FIGURE IX-14. DATA MANAGEMENT FIRST UNIT COST

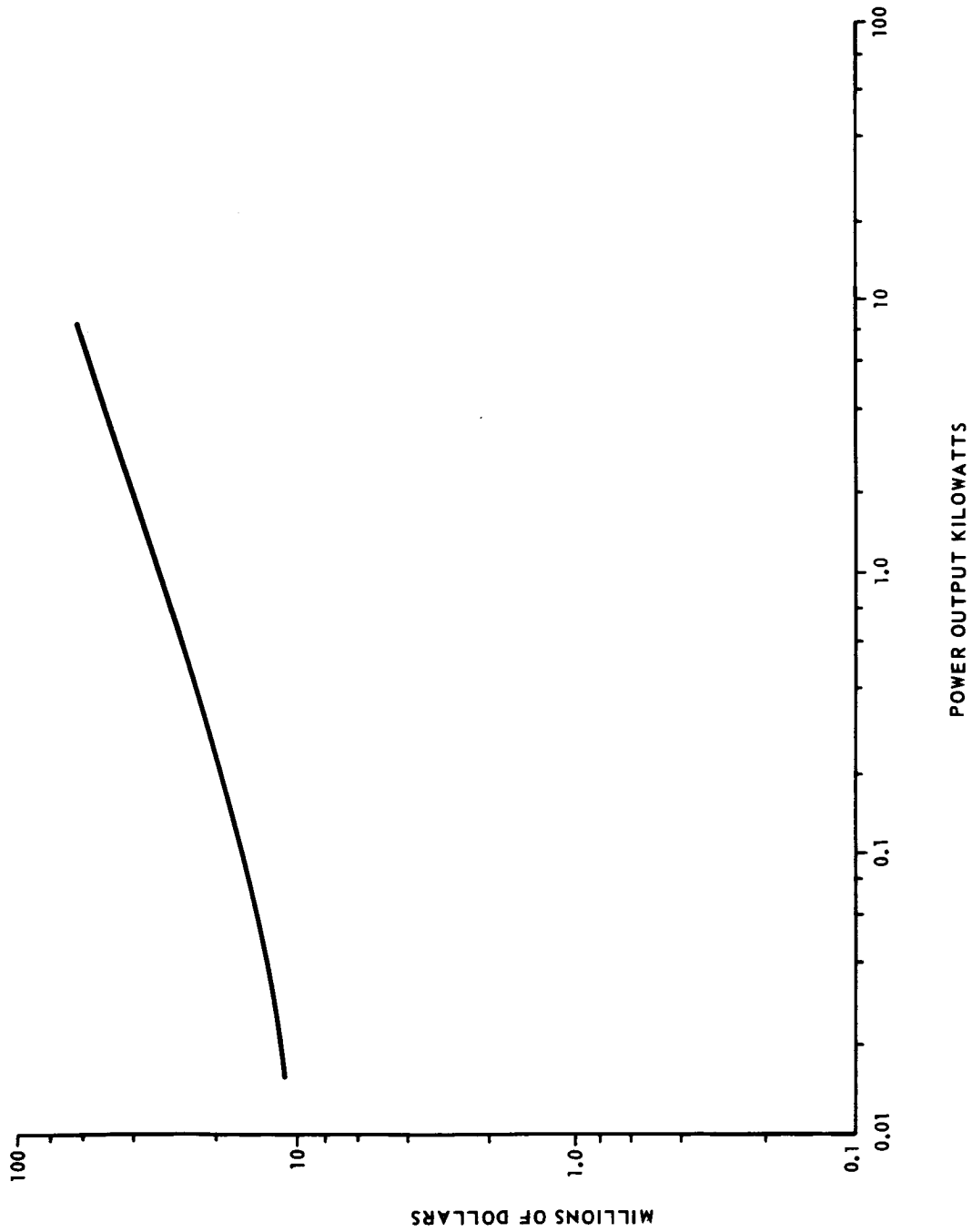


FIGURE IX-15. RADIOISOTOPE THERMOELECTRIC GENERATOR POWER SUPPLY DESIGN/DEVELOPMENT COST

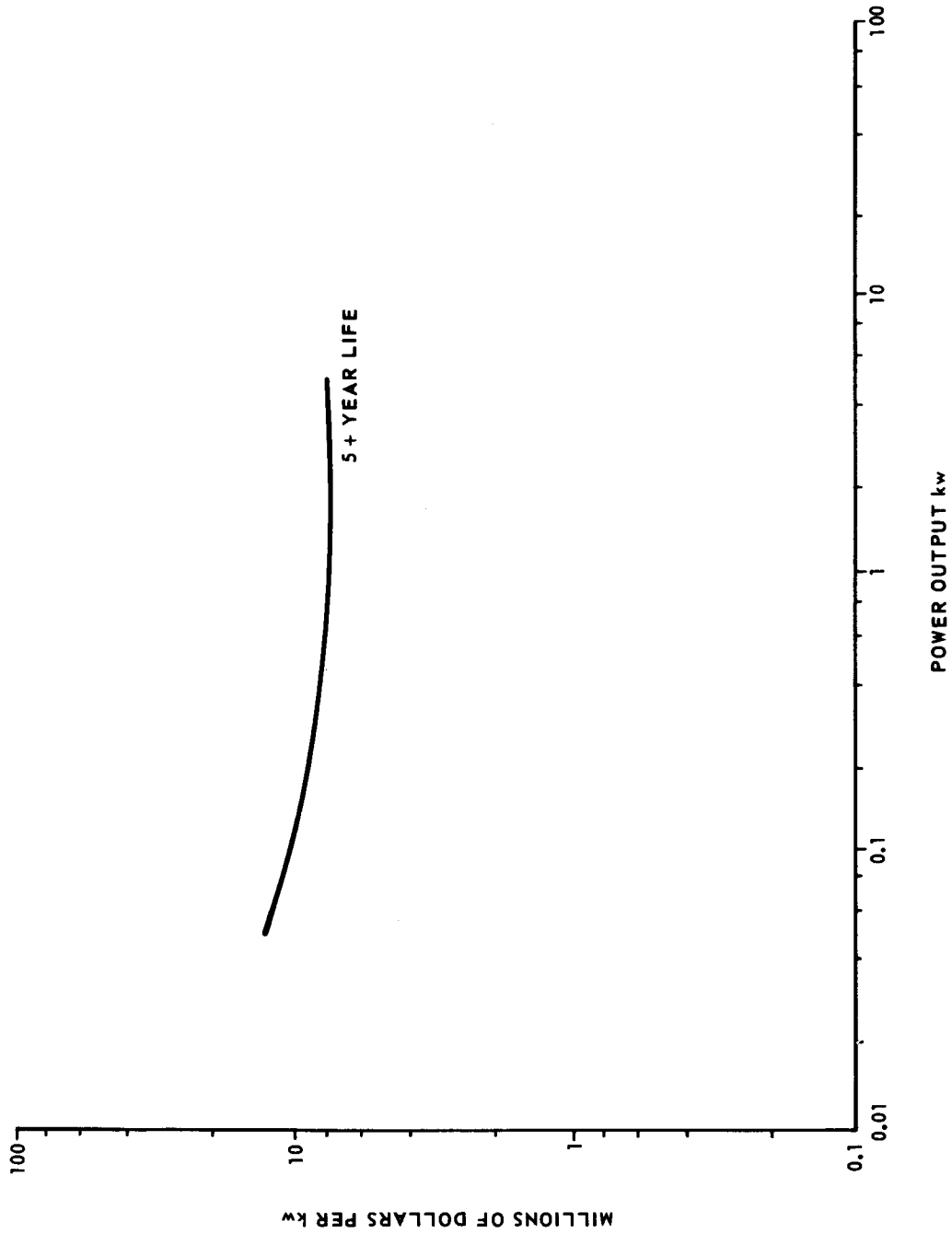


FIGURE IX-16. RADIOISOTOPE THERMOELECTRIC GENERATOR POWER SUPPLY  
FIRST UNIT COST

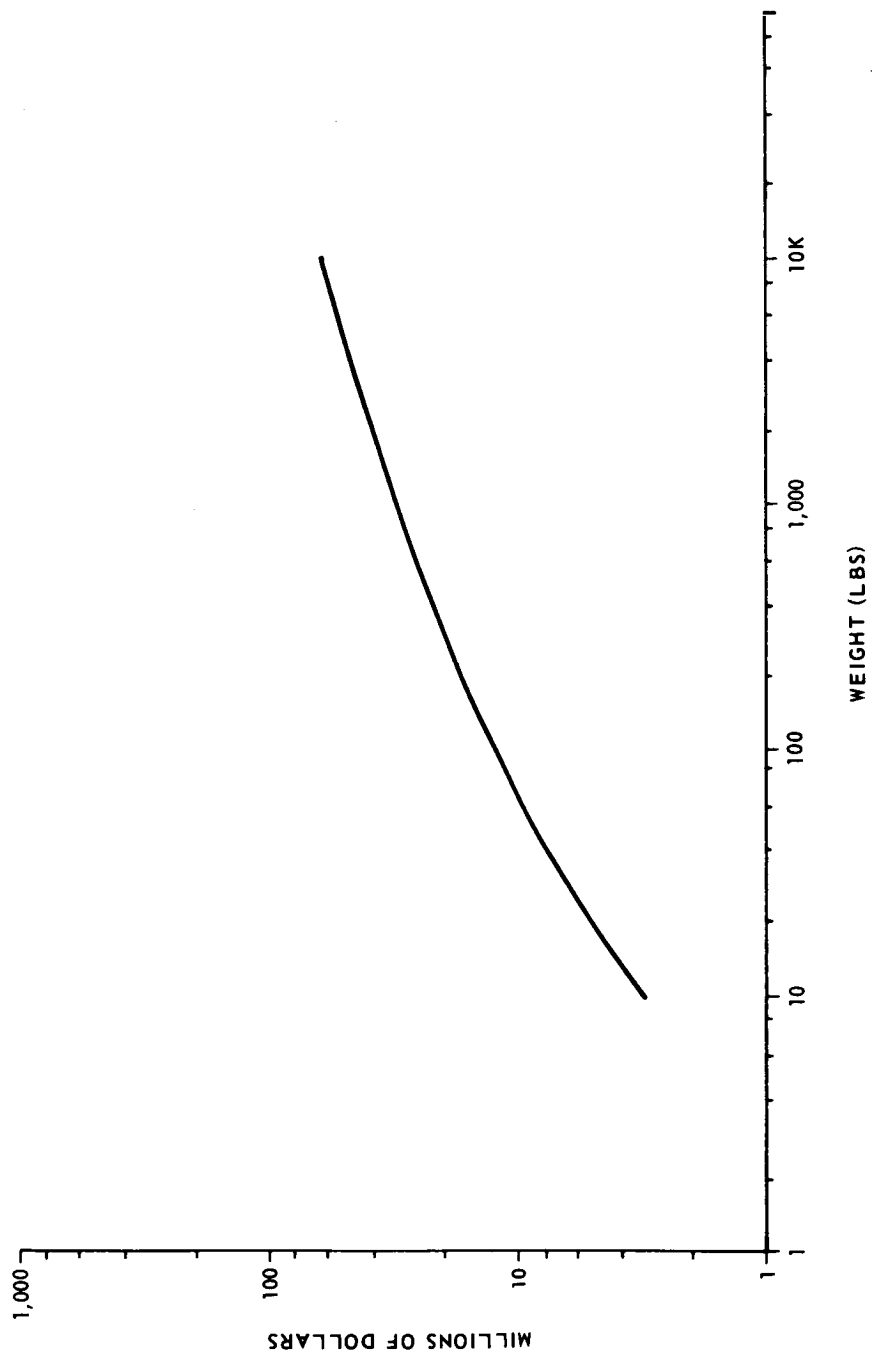


FIGURE IX-17. SCIENTIFIC INSTRUMENTS (EXPERIMENTAL AND MISSION SENSORS)  
DESIGN/DEVELOPMENT COST



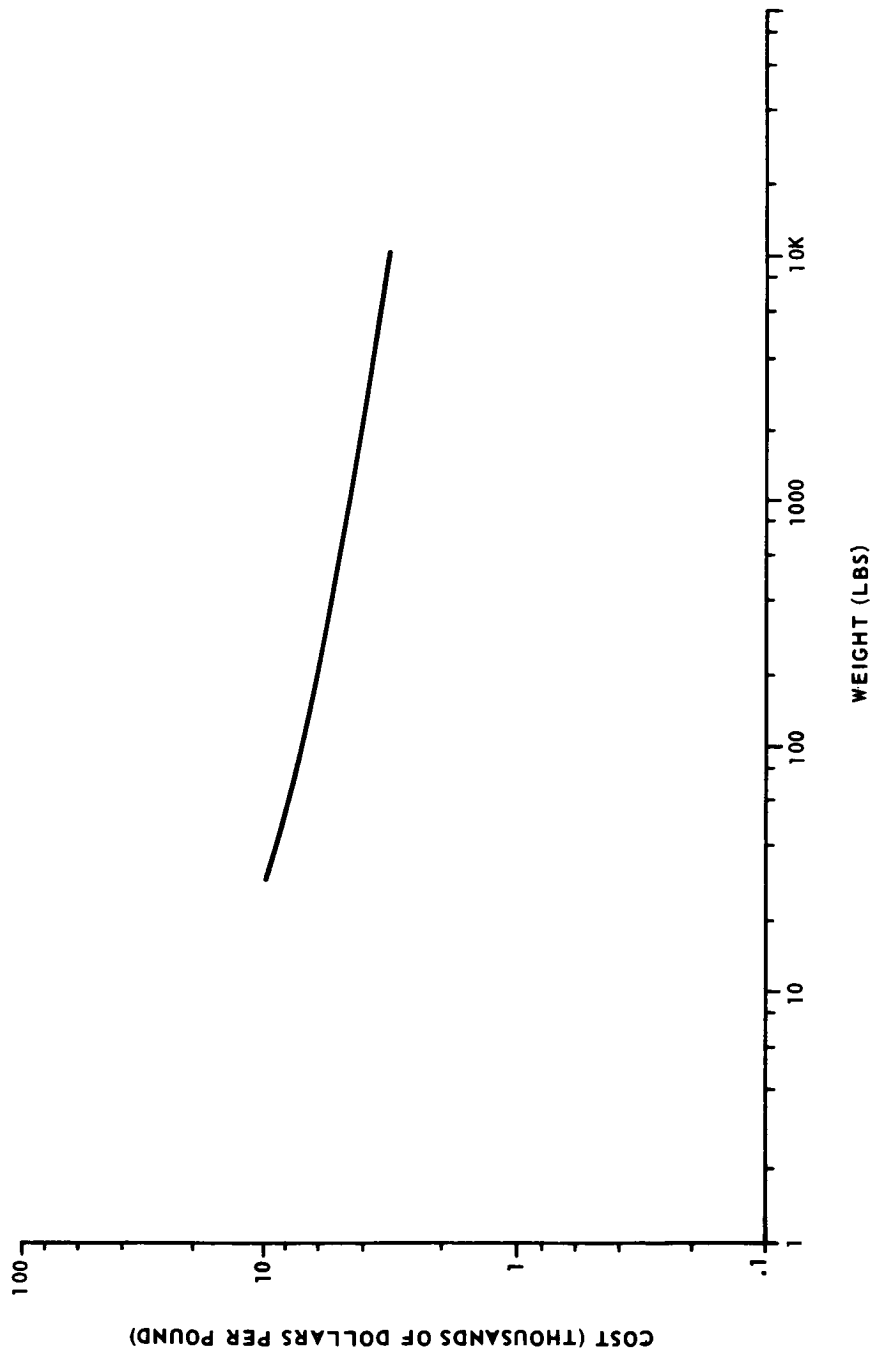


FIGURE IX-18. SCIENTIFIC INSTRUMENTS FIRST UNIT COST PAYLOAD  
(EXPERIMENTS AND MISSION SENSORS)

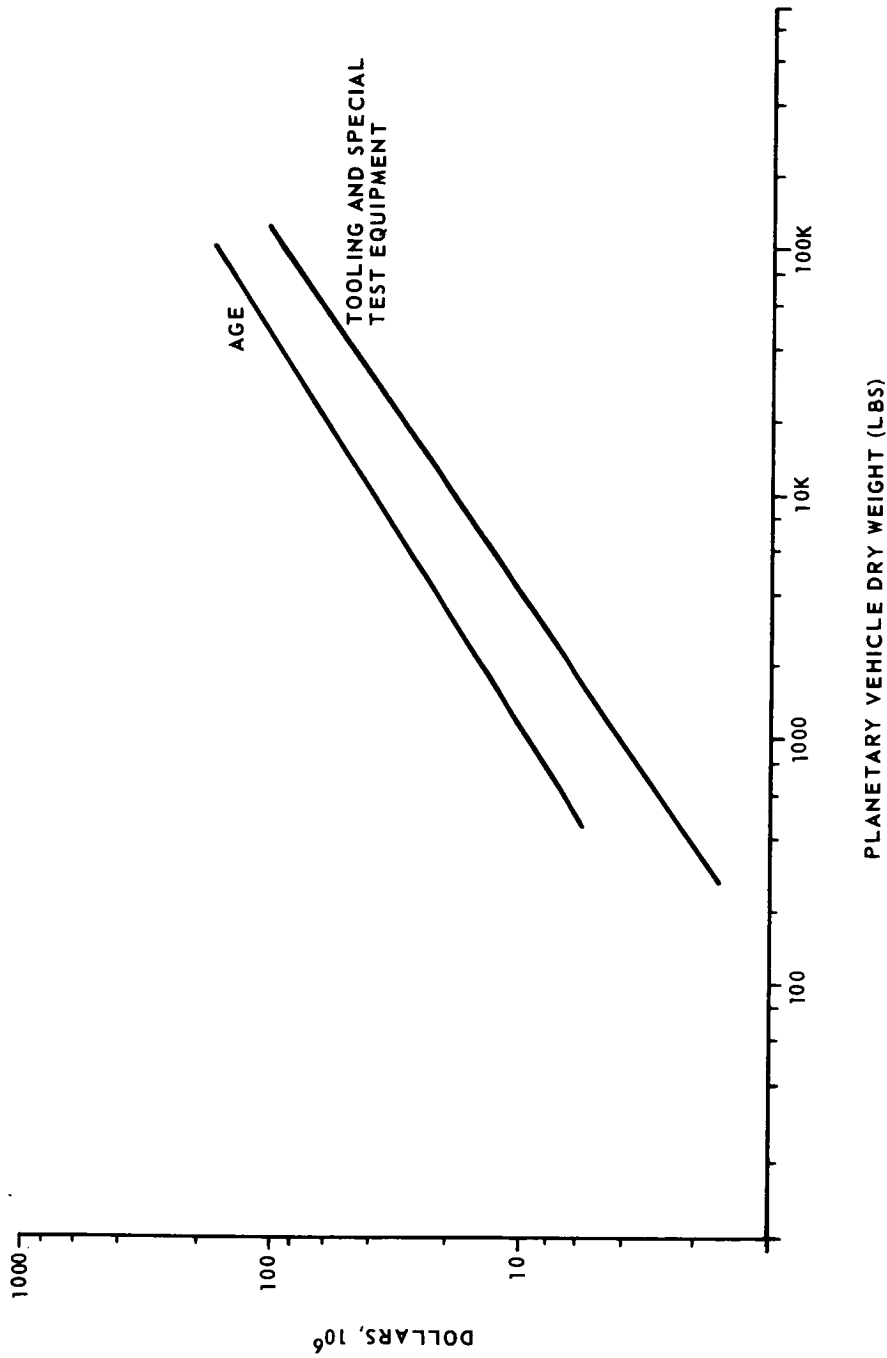


FIGURE IX-19. COST OF AGE, TOOLING, AND SPECIFIC TEST EQUIPMENT

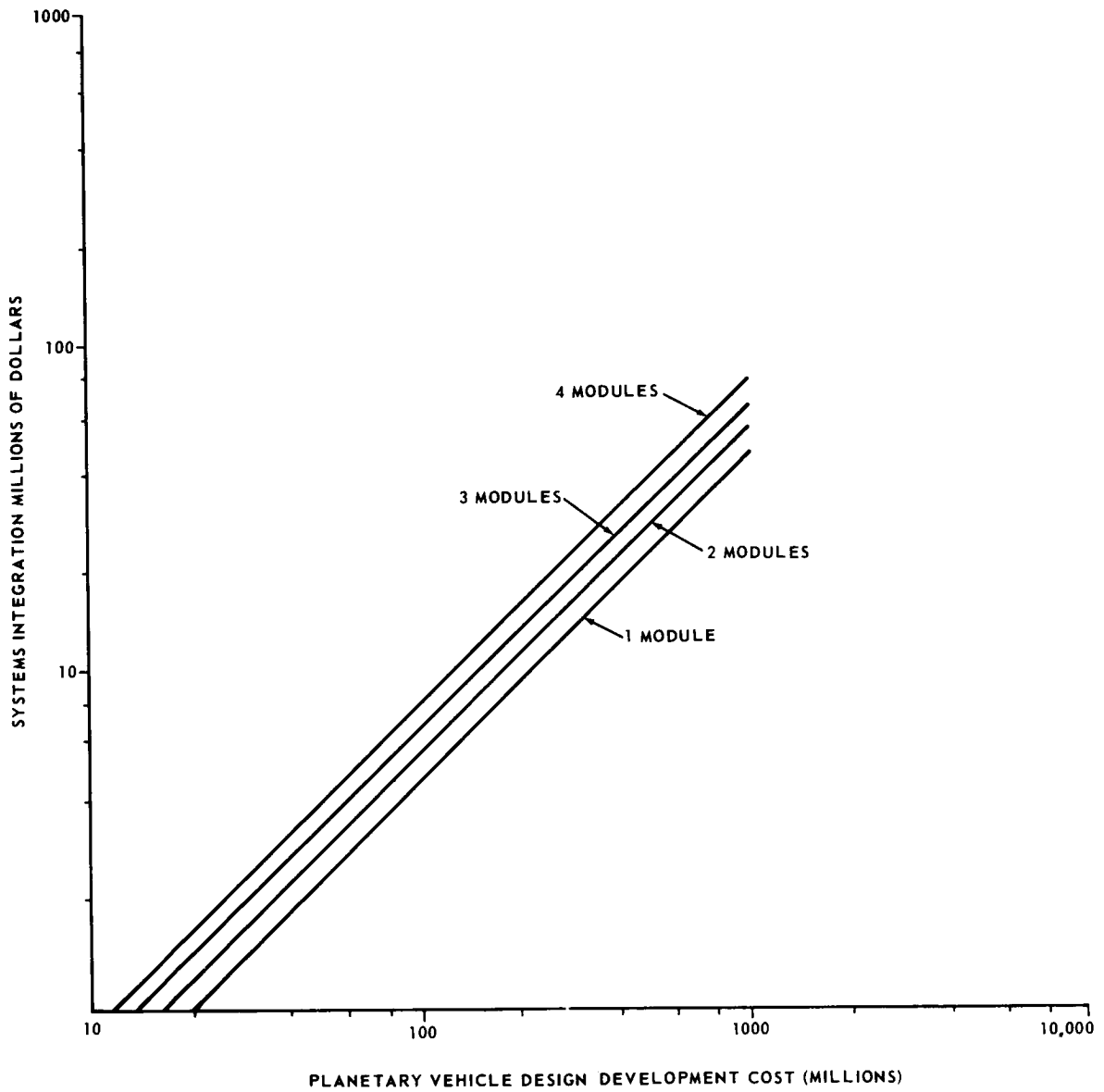


FIGURE IX-20. COST OF SYSTEMS INTEGRATION

# RELIABILITY

## Introduction

There are three basic techniques available for maximizing the reliability of any mission. They are manufacturing, testing, and redundancy. Most components should be required to undergo many hundreds of hours of pre-launch testing to test them well beyond the region of infant mortality. It is obvious that not all parts should be tested this way because it consumes part of their known, limited lifetime. There is a compromise to be made here in testing for infant mortality versus long range effects since the test is absolutely essential. Tests must be performed on most parts to assure that their mean lifetime and its variance are such that they can operate with high reliability for at least 1000 days. Techniques of construction in the large (e. g., spacecraft) and the small (e. g., transistors) must be carefully developed to improve reliability.

JOVE is designed with state-of-the-art materials and components which have not all been tested for the length of time required for this mission nor have they been tested in the space environment around Jupiter (vacuum, radiation). Development of testing programs will remedy this before actual flight and development of new products such as radiation insensitive transistors will greatly increase mission reliability.

A typical JPL screening process for transistors is:

- a. Visual 20 power inspection for cracked glass to metal seals, tarnished leads, corroded leads, broken leads, etc.
- b. Operating parameters at 25° C.
- c. Storage capability 168 hours at 200° C.
- d. Repetition of b.
- e. Operate 168 hours at 100° C with 280 mW power dissipated.
- f. Repetition of b.

This is an expensive but necessary procedure which really saves money in the long run because of the greatly increased reliability of these components.

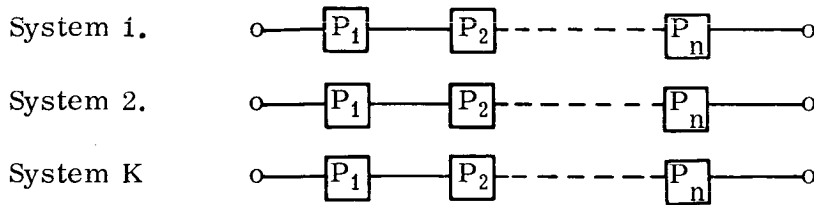
JOVE will have provisions for a last minute operational check on all subsystems while on the launching pad.

## Redundancy

After manufacturing and testing, the best tool for reliability is redundancy. There are two basic types of redundancy, active and passive. Active redundancy consists of having two units operating at the same time. In passive redundancy only one unit operates while the other one waits to be substituted in the case of failure of the first. There are many units on the mission whose failure would render the mission completely useless. Some of these, such as the antenna, do not allow for redundancy because of their size and weight, whereas items like the transmitter, data processing system, and data storage system allow for multiple redundancy. Power requirements suggest the use of passive redundancy, although active redundancy is preferred for the data storage system. Throughout this discussion it is tacitly assumed that the mechanism for changing from one unit to another has a higher order reliability than the unit itself so that perfect reliability is assumed for these switching operations.

The greatest cause of failure for electronic parts on this mission will be from the radiation environment; all other causes will be negligible compared to this. Multiple redundancy of these electronic parts, particularly the transmitter and data processing system, is strongly recommended. The following work investigates and compares two methods of substitution for passive redundancy. The first method will be to replace the entire unit when it fails. The second method is to divide the unit into several subsystems replacing only the particular subsystem that fails. This latter method obviously gives a higher reliability but one needs to investigate whether the improvement is worth the added complexity.

System Replacement. First look at a general system broken into subsystems with K distinct entire units for redundancy. Method x consists of replacing the entire system. Method y consists of replacing only a particular subsystem.



For method y 
$$P_y^{(K)} = \prod_{i=1}^n (1 - P_i^K)$$

For method x the value of  $P_x^{(K)}$  must be found by solving an iterative equation

$$P_x^{(K)} = \prod_{i=1}^n (1 - P_i) + \left[ 1 - \prod_{i=1}^n (1 - P_i) \right] P_x^{(K-1)} .$$

Let  $Q_x^{(K)} = P_x^{(K)} - 1$       Let  $A = \prod_{i=1}^n (1 - P_i) .$

Then  $Q_x^{(K)} + 1 = A + [1 - A] [Q_x^{(K-1)} + 1]$

Then  $Q_x^{(K)} = [1 - A] Q_x^{(K-1)} = [1 - A]^2 Q_x^{(K-2)}$  etc.

Therefore  $Q_x^{(K)} = [1 - A]^{K-1} Q_x^1$

But  $Q_x^{(1)} = P_x^{(1)} - 1 = A - 1 .$

Therefore  $Q_x^{(K)} = - [1 - A]^K$

And 
$$P_x^{(K)} = 1 - \left[ 1 - \prod_{i=1}^n (1 - P_i) \right]^K$$

$$R_k = \frac{P_y^{(K)}}{P_x^{(K)}} = \frac{\prod_{i=1}^n (1 - P_i^K)}{1 - \left[ 1 - \prod_{i=1}^n (1 - P_i) \right]^K} .$$

Theorem:  $R_k \geq 1$  meaning that method y is better than method x.

The proof of this is obvious using an argument based on sets. If B is the set of all the ways the system can fail by method x and C is the set of all ways the system can fail by method y then C is a subset of B and  $P(B) \leq P(A)$ .

Subsystem Replacement. Now consider redundancy with  $K=2$  (in most instances); therefore, the following theorem is proven for this case.

$$\text{For } K=2 \quad R_2 = \frac{\prod_{i=1}^n (1 + P_i)}{2 - \prod_{i=1}^n (1 - P_i)} .$$

$$\text{Consider } F = \prod_{i=1}^n (1 + P_i) + \prod_{i=1}^n (1 - P_i) - 2 .$$

Minimize F with respect to the  $P_i$  values

$$\frac{2F}{2P_i} = 0 = \frac{\prod_{i=1}^n (1 + P_i)}{(1 + P_i)} - \frac{\prod_{i=1}^n (1 - P_i)}{(1 - P_i)} .$$

$$\text{Solving: } \prod_{i=1}^n \frac{(1 + P_i)}{(1 - P_i)} = \frac{1 + P_i}{1 - P_i} = \frac{1 + P_m}{1 - P_m} \quad \text{For all } 1 \leq j, m \leq n .$$

Therefore  $P_j = P_i$  for all  $1 \leq i, j \leq n$

$$\prod_{i \neq j} \frac{(1 + P_i)}{(1 - P_i)} = 1 .$$

Since all factors are equal they must all equal 1.

Therefore  $P_i = 0$  for all  $1 \leq i \leq n$

This is the only extremum; hence it gives the unique minimum for F.  $F \geq 0$

Therefore  $\prod_{i=1}^n (1 + P_i) \geq 2 - \prod_{i=1}^n (1 - P_i)$  and  $R_2 \geq 1$ .

$$\lim_{P_i \rightarrow 1} R_2 = 2^{n-1}$$

Preferred Method. It appears that as long as  $P_i$  is very low there is not enough difference in the two systems to justify use of system  $y$  but when  $P_i$  is larger, the latter method becomes many times superior. This point will be illustrated with a particular case,  $n=4$ .

Symmetry considerations indicate that maximum reliability is obtained in the  $n$  subsystems if they have equal probabilities of failure. It is therefore recommended that the entire system be broken down into the desired number of subsystems,  $n$ , such that the probabilities of failure of each subsystem are roughly equal. In electronic systems this can be done to a first approximation by having an equal number of transistors and diodes in each subsystem. Now assume that

$$p_1 = p_2 = p_3 = \dots = p_n = p$$

$$p_x^{(2)} = (1 - p)^4 \left[ 2 - (1 - p)^4 \right]$$

$$p_y^{(2)} = (1 - p)^4 (1 + p)^4$$

$$R_2 = \frac{(1 + p)^4}{2 - (1 - p)^4}$$

$p$	1.0	0.5	0.4	0.3	0.2	0.1	0.05	0.01	0
$p_x^{(2)}$	0	0.122	0.233	0.422	0.652	0.879	0.970	0.998	1
$p_y^{(2)}$	0	0.319	0.491	0.686	0.849	0.960	0.986	0.998	1
$R_2$	8	2.61	2.10	1.63	1.30	1.08	1.02	1.00	1

These results are graphed on Figure IX-21 and IX-22.

Conclusions and Results. From the graphs it is obvious that method  $y$  is substantially superior to method  $x$  even if the probability of an individual subsystem's failing is as low as 0.2. In the radiation environment encountered, the transistor degradation or failure rate would be high enough to warrant use of method  $y$  with a ten or twenty percent increase in overall system reliability. It is therefore recommended that in the critical electronic systems such as the transmitter and data processing system method  $y$  should be used as the optimal method for passive redundancy.



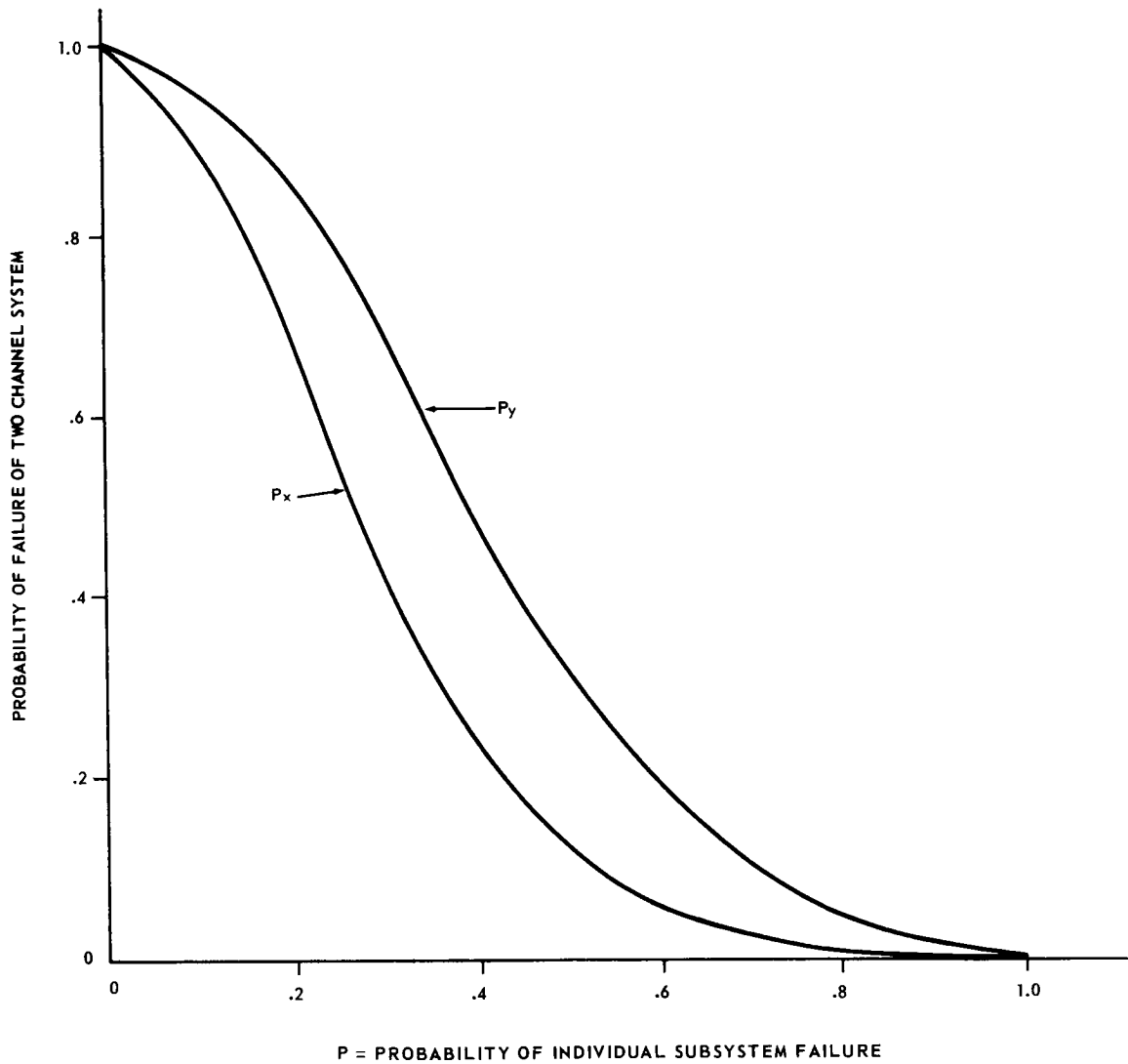
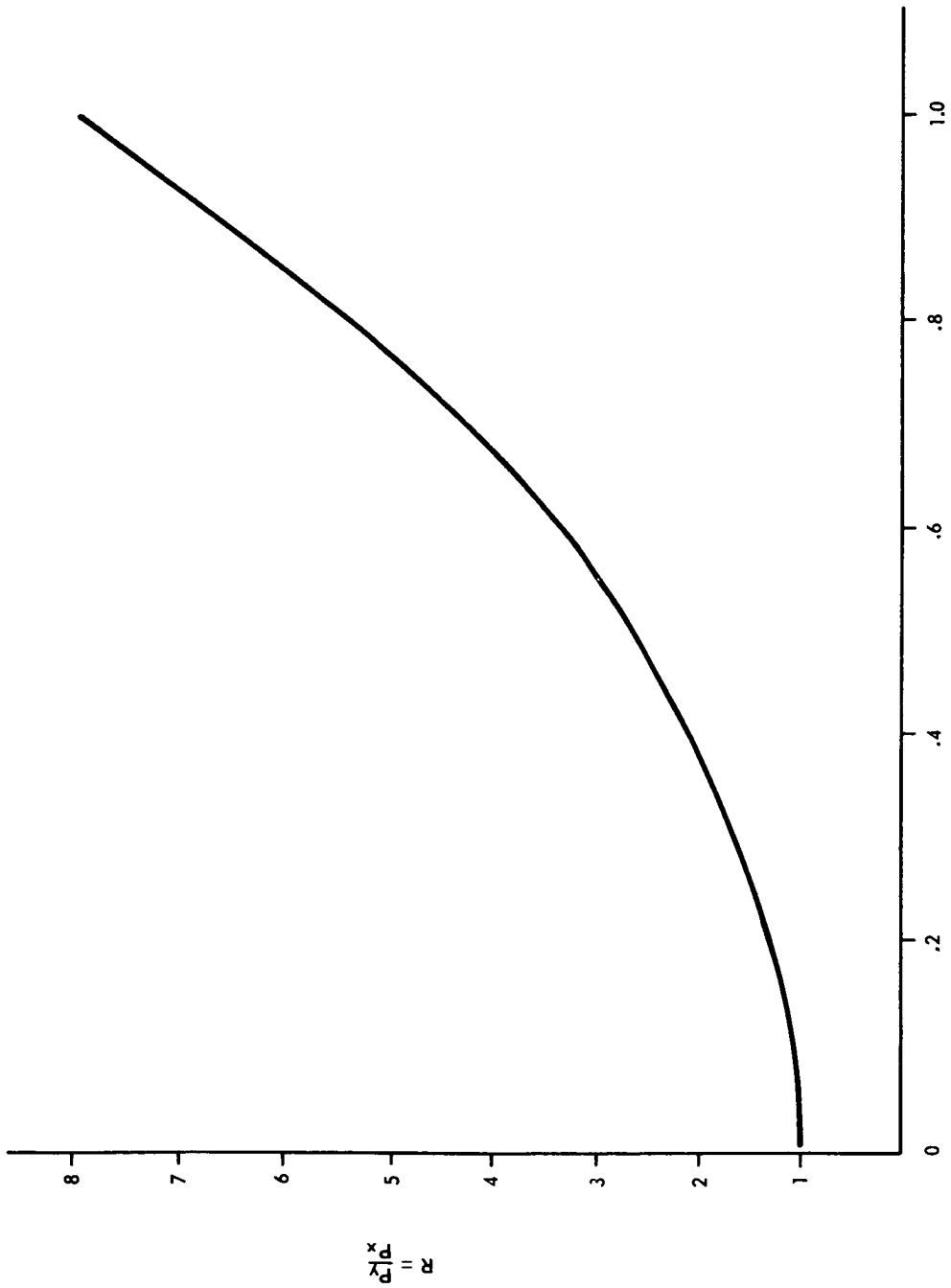


FIGURE IX-21. COMPARISON OF RELIABILITIES FOR ENTIRE SYSTEM REPLACEMENT (METHOD x) AND SUBSYSTEM REPLACEMENT (METHOD y) FOR A SYSTEM CONTAINING FOUR SUBSYSTEMS



P = PROBABILITY OF SUBSYSTEM FAILURE

FIGURE IX-22. RATIO OF  $P_y$  TO  $P_x$  VS. P

## BIBLIOGRAPHY

Easterday, Bowman, Gahm, and Spradlen: Reliability of Integrated Circuits Used in Missile Systems. Report No. RSIC-330, October 1964.

Klapheke, Spradlin, and Easterday: Preindications of Failure in Electronic Components. Report No. RSIC-445, July 1965.

Lusser, R.: Planning and Conducting Reliability Test Programs for Guided Missiles. U. S. Army Ordnance Missile Command, June 1952.

Lusser, R.: Production Environmental Testing. Redstone Arsenal, Huntsville, Alabama, November 1957.

Lusser, R.: Reliability of Guided Missiles. Redstone Arsenal, Huntsville, Alabama, January 1959.

Lusser, R.: Testing to Specified Limits Versus Testing to Failure. Redstone Arsenal, Huntsville, Alabama, October 1958.

Lusser, R.: The Notorious Unreliability of Complex Equipment. U. S. Army Ordnance Missile Command, September 1956.

Lusser, R.: The Reliability Program at Redstone Arsenal. Redstone Arsenal, Huntsville, Alabama, October 1954.

Lusser, R.: Unreliability of Electronics - Cause and Cure. Redstone Arsenal, Huntsville, Alabama, November 1957.

Masubucki: Nondestructive Measurement of Residual Stresses in Metals and Metal Structures. Report No. RSIC-410, April 1965.

Pieruschka, Erick: Optimum Allocations of Funds for Reliability Programs of Guided Missiles. U. S. Army Ordnance Missile Command, January 1955.

Schutz et. al.: Mariner-Mars Science Subsystem. Report No. JPL TR 32-813.

Space Environmental Effects on Materials and Components, Vols. I and II. Battelle Memorial Institute. Report Nos. RSIC-150, RSIC-151.

Survey of a Jovian Mission, I. I. T. Research Institute Report on Contract NASA-65 (06).